Transcriptional Control of Tissue Resident Macrophage Phenotype

Mark Jonathan Gurney

Thesis presentation for the degree of

Doctor of Philosophy (Medicine)

January 2022

Acknowledgments

Firstly I would like to thank my primary supervisor Prof. Philip R. Taylor for providing me with the opportunity to undertake this PhD, and the releasing from my research assistant role for a period to complete the write up of this thesis. His help with writing this thesis has been invaluable.

Special acknowledgement must go to Dr. Magdalena Czubala, who has been a constant support throughout my PhD, as my assistant supervisor. Thanks for keeping me sane through the months of the COVID-19 pandemic when we were the sole occupiers of the laboratories, for being the ever-present sounding board for ideas, planning of experiments and overall being the best colleague and friend I could ask for.

I am grateful to Dr. Robert Andrews who has provided me with training in bioinformatics in the analysis of genomic data. These invaluable skills and knowledge have shaped this thesis and will continue to shape me as a scientist going forward.

There are many members, past and present, of the Myeloid Cell Biology Group, who have helped me over the past 4 years. Thank you all for the office chats, pub excursions and meals out.

Dr. Ruth Jones (no not one from Gavin and Stacey), thank you for the never-ending supply of baked goods. You have been an invaluable colleague and friend the past 4 years; however my waistline does not thank you for it. Elena Simonazzi, my fellow long suffering PhD student. We finally made it! Thank you for dragging me out of my hobbit hole and the obscene number of dinners and nights out with friends. The last four years would haven't of been nearly as enjoyable without you!

To my friends, those near and far, you have been a saving grace the past few years and thank you for all the adventures and never-ending friendship. Lastly to my family, who have been a constant source of support, in particular my mother, for your endless encouragement, Thank You.

Summary

Background

Tissue-resident macrophages take residence in tissues during early embryogenesis, developing independently in within their final tissue resulting in tissue-specific transcriptomes. Tissue-specific transcription factor expression, such as GATA-binding-protein-6 (GATA6) in peritoneal cavity macrophages and Spalt-like-1 (SAL1) in microglia have previously been identified.

Musculoaponeurotic-fibrosarcoma oncogene homolog (*Maf*) transcription factor family is enriched in several tissue-resident macrophage enhancer-genes. Previously identified as important for macrophage terminal differentiation, *Maf* is a potent activator of interleukin-10 (*Il10*), with overexpression of *Maf* suggested to suppress interleukin-12 (*Il12*) transcription in macrophages.

Rationale

The role of *Maf* in tissue-resident macrophages, and what impact loss of *Maf* has on the transcriptome of tissue-resident populations has yet to be investigated.

Experimental Approach

To investigate the role of *Maf*, specific lentiviral overexpression constructs were generated and validated. These constructs were utilised to validate the characterisation of conditional and constitutive CX3C-chemokine receptor 1 (*Cx3cr1*)-restricted knockout mouse lines.

The role of *Maf* was investigated in two populations: microglia and peritoneal tissue-resident macrophages ($CD11b^{high}$,$F4/80^{high}$,$Tim4^{+}$).

Results

Maf was demonstrated to exhibit differential phenotypic control of these populations. Microgliosis was observed in $Maf^{fl/fl}Cx3cr1^{Cre/+}$ compared to $Maf^{fl/fl}Cx3cr1^{+/+}$ mice, together with loss of $MHCII^{+}CD206^{low}$ border-associated macrophage (BAM) population. Interestingly, no significant changes in homeostatic phenotype and development were observed in peritoneal tissue-resident macrophages.

Transcriptomic analysis of $Maf^{fl/fl}Cx3cr1^{Cre/+}$ and $Maf^{fl/fl}Cx3cr1^{+/+}$ mice revealed a more proinflammatory-primed transcriptome under naïve conditions, which correlated with the reduction in Il-10 expression. Whilst Maf-deficiency had little effect on naïve

peritoneal tissue-resident macrophages, it appeared to play an important role in regulation of the inflammatory monocyte-derived macrophage transcriptome in zymosan-induced peritonitis.

Implications

Across multiple transcriptomic analyses several genes associated with alternative-activation of macrophages were demonstrated to be downregulated in *Maf*$^{fl/fl}$*Cx3cr1*$^{Cre/+}$ mice. Suggestive of *Maf* influencing an alternative-activated macrophage phenotype and transcriptome across distinct macrophage populations of different ontogenies.

Table of Contents

Chapter 2

List of Figures

List of Tables

Chapter 1

General Introduction

1.1. Overview of Tissue Resident Macrophages

1.1.1. Brief History of Macrophages

Macrophages are myeloid immune cells first identified by Elie (Ilya) Metchnikoff, who discovered the process of phagocytosis and the cells responsible for it in 1892 (1). However macrophages are responsible for far more than just being "big-eaters" as their name suggests. Macrophages are located throughout the body's tissues and have been demonstrated to be key in the removal of apoptotic cells and debris, antigen presentation to adaptive immune cells, producers of both pro- and anti-inflammatory mediators, injury repair and responsible for maintaining tissue homeostasis.

Ralph van Furth and Zanvil Cohn demonstrated that the majority of macrophages were replenished from bone marrow derived monocytes, and later established the mononuclear phagocyte system (MPS) (2). Where macrophages, circulating monocytes and their precursor cells in the bone marrow were grouped together based on similarities in their morphology, function, origin and their ability to phagocytose (2).

This theory was further expanded with the discovery of macrophage-dendritic cell precursors (MDPs) (3), and the discovery of common myeloid progenitor (CMPs), a bone marrow monocyte-restricted precursor (4). This dogma however began to be disputed following the presence of primitive macrophages in the yolk sac (5), indicating the monocyte-to-macrophage differentiation did not apply to all adult macrophage populations. Early fate mapping experiments (6,7) and evidence of tissue resident macrophage local proliferation within tissues (8,9), ultimately indicating an alternative origin for tissue resident macrophages.

1.1.2. Haematopoiesis and Early Macrophage Development

Three successive, but overlapping, waves of haematopoietic progenitor development have been identified (10). Defined as primitive, pro-definitive/erytho-myeloid progenitors (EMPs), and definitive/hematopoietic stem cells (HSCs) . Macrophages from these waves can be defined by the expression of three key genes, Runt-related transcription factor 1 (*Runx1*), V-Myb avian myeloblastosis viral oncogene homolog/transcriptional activator (*Myb*) and Neurogenic locus notch homolog protein 1 (*Notch1*) (11).

Primitive haematopoiesis occurs in the absence of all three transcription factors (11). Primitive macrophages are considered immature but displaying macrophage morphology.

Primitive macrophages are present in blood islands of the yolk sac at embryonic day 9 (E9) (12) and in the foetal liver from E10 to E17 (12,13), originally thought to derived from the mesoderm. Foetal liver macrophages from E17 demonstrate more differentiation with similar features to those in adult tissue resident macrophages (14). As immature monocytes are not detected until E12 onwards and present in the foetal liver at E16, this disputed the MPS theory as being the sole source of all macrophages (11).

EMPs in the yolk sac of mouse embryos at E8.25, are distinguishable from HSCs by their lack of Lymphocyte antigen 6A-2/6E-1 (Ly-6A.2/Ly-6E.1) surface expression (15). EMPs are *Runx1* dependent for emergence, however *Myb* and *Notch1* independent (16). EMPs can differentiate into macrophages within the yolk sac with embryonic-derived immature macrophages detectable at E9.0 (12,13), and mature macrophages can be found in the yolk sac and brain from E9.5, and in the foetal liver by E10.5 (17). EMPs colonise the foetal liver from E9.0 onwards where they have been demonstrated to play a significant role in hematopoietic cell production including macrophages (18).

HSCs emerge from the aorto-gonado-mesonephros (AGM) region on E10.5 (19), where they migrate to colonise the foetal liver until E12.5 (19) and begin to expand rapidly before subsequently colonising the bone marrow for maintenance throughout adulthood. HSCs are *Runx1* dependent and require *Notch1* for emergence from the AGM (15,20). Foetal and adult HSCs also require *Myb* expression for self-renewal and maintenance (21). All three waves have been determined to generate tissue resident macrophages either directly or indirectly in the case of monocyte derived macrophages.

1.1.3. Tissue Resident Macrophages Transcriptional Control

Tissue resident macrophages are a heterogeneous population of immune cells with tissue specific functions, however stem from a core pre-macrophage stage before developing into their tissue specific niche fulfilling populations. Pre-macrophages are established by lineage determining transcription factors, with the most notable of these being CCAAT/enhancer-binding proteins (C/EBPs) and PU.1 (22,23).

PU.1 (encoded by *Spi-1*) is an essential transcription factor for the development of all macrophages, where it acts as a scaffold for histone modifiers (24), ultimately establishing an enhancer landscape where several other transcription factors perform their function through interactions with PU.1. Additionally PU.1 regulates a large number of myeloid genes including colony stimulating factor receptor (*Csf1r*) (25). CSFR1 can act as the

receptor for both interleukin-34 (IL-34) and monocyte colony-stimulating factor (M-CSF). M-CSF is required for the survival and proliferation of most macrophages populations(26), whereas IL-34 has been identified to be specifically required for the development of microglia (27) and Langerhans cells (28).

However tissue resident macrophage populations are specialised to the tissue they reside in, through a combination of tissue specific growth factors and specific transcription factors. This thesis will concentrate on two tissue resident macrophage populations, microglia and peritoneal tissue resident macrophages, with their respective development discussed below. In brief other tissue resident macrophages have been summarised in Table 1.1.1 (based on 28–30).

Tissue	Resident Macrophage	Tissue Specific Factors	CSFR1 ligand	Transcription Factors
Brain	Microglia	TGF-b	IL-34 and M-CSF	SALL1, IRF8, SMAD2/3
Bone	Osteoclast	RANKL	M-CSF	NFATC1, NFkB, MITF, c-FOS, C/EBPa
Heart	Cardiac Macrophages	Unknown	M-CSF	Unknown
Peritoneal Cavity	Large Peritoneal Macrophages	Retinoic Acid	M-CSF	GATA6, C/EBPb
Liver	Kupffer Cells		M-CSF	ID3, IRF8
Lung	Alveolar Macrophages	GM-CSF	M-CSF	PPARy, BACH2, C/EBPb
Skin	Langerhans Cells	TGF-b	IL-34	RUNX3, ID2
Spleen	Marginal Zone Macrophages	Heme	M-CSF	LXRa
	Red Pulp Macrophages	Heme	M-CSF	SPI-C, IRF8/4

Table 1.1.1 Summary table of tissue resident macrophages and their respective tissue specific factors and transcription factors

1.1.4. Role of Tissue Resident Macrophages

Tissue resident macrophages sense the microenvironment, maintaining tissue homeostasis and have been demonstrated to be critical during mouse development, just as through clearance of senescent and apoptotic cells during organogenesis (31,32), and have been shown to be critical in regulating vessel morphogenesis and maturation during development.

Whilst tissue resident macrophages share many of these properties across different tissues, they also have highly tissue specific functions. For example osteoclasts, Kupffer cells or alveolar macrophages are highly adapted to their tissue with specific purposes. Osteoclasts continuously reabsorb and restructuring bone mass (33,34), Kupffer cells take up dying red blood cells from the circulation and recycling iron (35), whilst alveolar macrophages have been demonstrated to be critical for the removal of particles form the alveoli and pulmonary surfactant (36,37).

Tissue macrophages perform an essential role in the identification of pathogens, and are considered at the frontline of host defense utilising their phagocytic mechanism clearance (38). Following recognition of microbial challenge, tissue resident macrophages initiate an influx of other inflammatory immune cells including leukocytes, neutrophils and also monocytes which act as a source for inflammatory macrophages. The significance of resident macrophages in initiating inflammatory immune responses has been demonstrated when depletion studies result in impaired chemokine production and neutrophil influx in experimental inflammation (39–41). However it is important to note that in these depletion studies multiple populations of macrophages will likely be deleted.

1.2. Microglia

1.2.1. Origin of Microglia

Microglia were first described by Nissl in 1899 (42), however del Rio-Hortega was the first to refer to these cells as microglia in 1932 (43). Compared to other tissue resident macrophages microglia ontogeny has been heavily investigated, particularly in recent years, and has been demonstrated to be yolk sac derived from EMPs between E7-8 (10), before infiltrating the brain at E9 (7). Additionally a subpopulation of *Hoxb8+* microglia have been suggested to enter the brain at E12.5 from a latter wave of yolk sac haematopoiesis (44). This early colonisation is before the establishment of the blood brain barrier at E13.5 (45).

Runx1-Mer-Cre-Mer fate mapping models and utilisation of tamoxifen administration at E7.0 illustrated that macrophages derived from these primitive macrophages infiltrate the whole embryo (6), contributing to almost all tissue resident macrophages. However labelled microglia persist into adulthood, whereas most other tissue resident macrophages are unlabelled in adult tissues (6). This has suggested local self-renewal, without significant peripheral contribution.

However, whilst microglia were believed to be solely derived from E7.5 *Runx1+* yolk sac progenitors with little contribution from other haematopoiesis stages, competing theories of reestablishment of microglia following ablation suggests that the original dogma of microglia homogony and ontogeny may not as straightforward as first thought. When adult mice are ablated with diphtheria toxin or a CSF-1 receptor kinase inhibitor microglia can self-restore (46–48). Three main theories have been considered, firstly if peripheral bone marrow derived macrophages infiltrate the brain and differentiate into microglia (46,47,49). Secondly if a small population of local progenitors remain after depletion (50), ultimately resulting in generation of replacement microglia, or alternatively a small number of microglia remain following ablation, proliferate rapidly and expand.

In microglial development transforming growth factor beta (TGF-b) (51) has been identified as a tissue specific factor. Mice which lack TGF-b have been shown to result in significantly reduced number of microglia (52), and TGF-b has been demonstrated to be required to upregulate several microglial genes *in vitro*. Additionally combination of both M-CSF and TGF-b result in upregulation of more microglial genes than M-CSF alone in *ex vitro* cultures, indicating that both signals are essential for microglial development (52).

Although it has been shown that TGF-b signalling actually maintain microglia an inactivated state rather than providing survival signal, which is regulated by SMAD2/3 through TGF-b (53).

CSF1R signalling has been proposed to be a more important signal in the adult, as deletion results in a rapid loss of microglia. In *Csf1*$^{op/op}$ mice however only a moderate reduction in the microglia population was demonstrated in distinct regions of the brain (54). This indicated that an absence of M-CSF can be compensated for through an alternative mechanism. Deletion of IL-34 considerably impairs microglia development in specific brain regions which do not overlap with those of the *Csf1*$^{op/op}$ model, suggestive of distinct spatial expression of M-CSF and IL-34 resulting in spatial loss of microglia (27).

Sal-like 1 (*Sall1*), a zinc finger transcription factor, has been identified as a key microglia-specific transcription factor (53). Microglia deficient in *Sall1* have demonstrated upregulation of genes associated with other macrophage populations and reduced expression of microglia signature genes (53). Monocyte derived microglia-like cells have been shown to not express *Sall1*, suggesting it to be a specific marker for embryonically-derived microglia (53). Furthermore this suggests that both ontogeny and microenvironment influence the tissue resident macrophage profile.

Between human and mouse microglia there some important differences, with portmortum and surgical tissues indicating a number of significant transcriptional differences (55,56). However several important core microglia genes are conserved including *Spi-1*, *Sall1* and interferon regulatory factor 8 (*Irf8*), which have all been identified as a key tissue specific transcription factors for microglia (Table 1.1.1) (55,56).

1.2.2. Microglial Function

The functions of microglia are wide and varied. In naïve steady state conditions microglia are highly ramified cells, with multiple branches and processes. These ramification have been shown to be in continuous motion, protruding or retracting to cover long distances surveying the brain (57,58). Microglial processes come in contact with other cells of the brain including neurons and astrocytes (59–61).

Microglia have been demonstrated to be key in early development of the central nervous system (CNS). As with all macrophages, microglia phagocytose apoptotic cells such as neural stem cells generated during neurogenesis through TYRO3, AXL and MER (62,63). Mice which are deficient for *Axl,* or *Mer* demonstrate accumulation of apoptotic neurons,

but also result in an increased number of active neurons suggesting microglia also play a role in maintaining the number of viable neurons (62).

During postnatal development microglia continue to maintain the CNS. Whether through elimination of redundant neurons as discussed above or shaping the neuronal synapses through synaptic pruning (64). Synaptic pruning occurs through a number of mechanisms including two components of the complement cascade, complement component 1q (C1q) and complement component 3 (C3) (65).

Astrocytes produce the majority of transforming growth factor beta (TGF-b) in the brain, with astrocyte-derived TGF-b demonstrated to results in neurons to upregulate C1q and C3 expression, which acts as a tag on synapses for recognition through complement receptor 3 (CR3) on microglia or in direct engulfment utilising the opsonisation of the complement cascade (66). Mice which lack either CR3 or C3 have been demonstrated to be unable to effectively prune synapses (65). Microglia also mediate synaptic pruning via C-X3-C motif chemokine receptor 1 (CX3CR1), which is exclusively expressed on microglia in the CNS (64). CX3CR1 interacts with its sole ligand C-X3-C motif chemokine ligand 1 (CX3CL1) is predominantly expressed on neuronal cell surface (67), ultimately resulting in phagocytosis.

Upon injury to the brain, such as laser-induced microlesions, have shown to stimulate microglia directing the microglial processes toward the site of injury to form a “ball-and-chain” structures that phagocytose the damaged tissue (68). Systemic inflammatory stimuli or larger injuries also induce microglia to change their shape from a highly ramified cell to a more amoeboid shape, with an enlarged cell body and shortened processes limiting coverage area (69).

Microglia secrete several chemokines, cytokines, and neurotropic factors that contribute to the immune response. Microglia as the most prevalent immune cell in the brain is believed to be the principal source of proinflammatory cytokines such as IL-1, IL-6 and TNF, as well as regulatory cytokines such as IL-12 and IL-18 (70). Whilst the majority of studies have focused on the proinflammatory response of microglia, anti-inflammatory cytokines including IL-10 are encoded by microglia (71), indicating their importance in not only initiating but also regulating inflammation within the brain and maintaining homeostasis.

Due to microglia being the largest population of immune cells in the brain, their ability to release both proinflammatory and anti-inflammatory factors, and demonstrated to be key in early and postnatal development of the CNS, microglia have been heavily investigated in neurodegenerative diseases.

1.3. Peritoneal Tissues Resident Macrophages

1.3.1. Origin of Peritoneal Tissue Resident Macrophages

It is fair to say that peritoneal macrophages are probably the most well studied of all mouse macrophage populations, in terms of cell biology, development, and inflammatory responses. However the exact ontogeny of peritoneal tissue resident macrophages is not entirely clear.

Macrophages of the peritoneal cavity have been defined into two macrophage subsets that coexist in peritoneal cavity in adult mice. These two population are often referred to as large peritoneal macrophages (LPM) and small peritoneal macrophages (SPM) according to their size (72). LPMs account for approximately ~90% of peritoneal cavity macrophages under naïve steady state conditions and express high levels of CD11b and F4/80 (72). Whereas SPMs expresses lower levels of F4/80, but also express high levels of major histocompatibility complex II (MHCII), which is not expressed on LPMs (72). High F4/80 expression on macrophages has previously been correlated with being derived from the yolk sac or foetal liver, and not of bone marrow origin (7).

Many studies have tried to determine if these CD11b^{high} F4/80^{high} LMPs are peritoneal tissue resident macrophages, and whether they are EMP derived from the yolk sack or foetal liver, or alternatively HSC/monocyte derived. However due to the presence of these two macrophage populations in the peritoneal cavity, this resulted in conflicting results. Several early studies indicated that CD11b^{high} F4/80^{high} peritoneal tissue resident macrophages are maintained locally through self-renewal in adult life (73,74). However later studies suggested that whilst tissue resident macrophages such as those of the liver, lung or kidney were EMP derived, that peritoneal tissue resident macrophages did not (16,75). This was further supported with chimeric C57BL/6-CD45.1 mice, where the majority of both peritoneal macrophage populations expressed CD45.1, indicated that both subsets differentiate from bone marrow-derived monocytes following ablation by irradiation (76).

Within the same study however, CCAAT/enhancer binding protein b (C/EBPb) deficient mice (*Cebpb*$^{-/-}$) demonstrated loss of the CD11b^{high} F4/80^{high} tissue resident macrophage population in the peritoneal cavity and increased numbers of the SPM population (76). This was suggestive of alternative transcriptional control and therefore possibly distinct ontogenies for the two peritoneal macrophage population. It was demonstrated that SPMs from wildtype mice adoptively transferred into these *Cebpb*$^{-/-}$ mice could differentiate into CD11b^{high} F4/80^{high} tissue resident macrophage population (76). Therefore it is believed that under naïve steady state conditions SPMs could contribute to generate CD11b^{high} F4/80^{high} tissue resident macrophage.

Cx3cr1 expression has been utilised for the investigation of SPM and LPM populations, and shows active expression on SPMs and indicated past expression of CX3CR1 on LPMs through GFP expression in *Cx3cr1*$^{CreRosa26R\text{-}FGFP}$ mice (76). This data indicated that SPMs to be recent descendants of CX3CR1 expressing precursors and therefore are short-lived cell. In comparison LPMs are indicated to have a more distant ontogeny to the progenitor cell, corroborating they originate from the yolk sac or foetal liver (76).

Additionally fate mapping studies have utilised *Cx3cr1* mice with a GFP reporter or conditional/constitutive active Cre recombinase, to further elucidate macrophage populations, including those of the peritoneal cavity (9). Ultimately demonstrating that tissue resident macrophage populations in the liver, spleen, lung and peritoneal cavity are established are established during embryonic development, and are maintained through adulthood in naïve steady state conditions independent of replenishment from bone marrow-derived (9).

Longevity and proliferation of peritoneal macrophage populations have been studied utilising bromodeoxyuridine (BrdU)-labelling. Labelled CD11b^{high} F4/80^{high} peritoneal tissue resident macrophages demonstrated continued presence after 14 days, suggesting that they are a long-lived population, and therefore suggestive of being maintained through proliferation (76). SPMs however were conversely detected at low number after 6–10 days, suggests that these cells have a low proliferation rate and are short-lived cells (76).

Analysis of nuclear protein Ki67 and phosphorylated histone H3 (pHH3) staining, an indicator of a discrete stage of mitosis, revealed the number of proliferating CD11b^{high} F4/80^{high} macrophages decreases in 12-week-old mice compared with proliferation capacity in 2 week old mice (77). After 12–16 weeks, the number of

CD11b^{high} F4/80^{high} macrophages in the peritoneal cavity is self-maintained through a low rate of proliferation (77). CD11b^{high} F4/80^{high} LPMs are therefore considered to be tissue resident macrophages either derived from yolk sac or foetal liver, due their long life and ability to self-renew through local proliferation, and to be predominantly independent of bone marrow-derived monocytes (8).

Whereas lymphocyte antigen 6 complex (Ly6C) expressing monocytes recruited to the peritoneal cavity have been demonstrated to give rise to SPMs during inflammatory conditions (9,72). Ly6C^{+} monocytes are thought to migrates through a C-C chemokine receptor type 2 (CCR2)-dependent pathway, whilst Ly6C^{-} monocytes have been indicated to migrate in response to CX3CR1 signalling (78). Under naïve steady state conditions monocytes have been shown to not contribute to the CD11b^{high} F4/80^{high} tissue resident macrophage pool in the peritoneal cavity (79).

Following identification of specific transcriptional control of peritoneal tissue resident macrophages through the zinc finger transcription factor GATA-binding protein 6 (*Gata6*), which has been described to be key for maturation and function (80). *Gata6* was shown to be selectively expressed by CD11b^{high} F4/80^{high} LPMs, with the number of CD11b^{high} F4/80^{high} LPMs reduced in the peritoneal cavity in *Gata6*-deficient mice (81). Transcriptional activation of *Gata6* has been shown to be regulated in a two-step process through environmental factors. Retinoic acid, present in the omentum, binds the retinoic acid receptor which in turn binds the poised *Gata6* promotor.

Ex-vivo cultured peritoneal tissue resident macrophages lose their expression of *Gata6*; however this can be restored by supplementing culture media with retinoic acid, suggestive of its importance as an tissue specific environmental factor in peritoneal tissue resident macrophages (81). Additionally mice fed a vitamin A-deficient diet demonstrated a reduction in *Gata6* expression and a reduced number of peritoneal tissue resident macrophages (82). Essentially illustrating retinoic acid as a omentum derived factor necessary to drive expression of *Gata6*, which in turn activates peritoneal tissue resident macrophage specific genes. In addition to the regulation of gene expression in CD11b^{high} F4/80^{high} peritoneal macrophages, *Gata6* has been demonstrated to be involved in the control of the proliferation, survival, and metabolism of CD11b^{high} F4/80^{high} LPMs (80).

Few studies have been undertaken on human peritoneal tissue resident macrophage ontogeny and transcriptional control in comparison to those from mice, however CD14^{high} CD16^{high} macrophages are believed to be the homologous human population of CD11b^{high}

F4/80^{high} murine tissue resident macrophages due to their high levels of GATA6 expression (83).

1.3.2. Peritoneal Tissue Resident Macrophage in Inflammation

Under steady state conditions the peritoneal cavity comprises of the previously discussed two populations of macrophages (LPMs and SPMs), B-cells, T-cells, natural killer cells, dendritic cells and eosinophils, with macrophages represent 30–35% of total peritoneal cavity cells (84). Following stimuli such as infection, or inflammatory signals, results in a dramatic alteration in cell numbers and frequencies of the peritoneal cavity macrophage populations.

Commonly referred to as the "disappearance reaction", CD11b^{high} F4/80^{high} tissue resident macrophage numbers are rapidly lost upon infection or inflammatory stimuli (85). CD11b^{high} F4/80^{high} tissue resident macrophage disappearance from peritoneal cavity is not attributed to cell death, but rather to their migration to the omentum, in a retinoic acid and *Gata-6*-dependent response (72,81). CD11b^{high} F4/80^{high} tissue resident macrophages basal number return after stimulation, suggesting that LPMs can return to peritoneal cavity from the omentum to resolve an infectious or inflammatory process (72,77,80,81,84).

Meanwhile there is an increase in frequency and cell number of SPMs, through recruitment of bone marrow-derived inflammatory Ly6C^{+} monocytes as discussed above (9,72,76,77,84). To add further complication, following inflammation in the peritoneal cavity, monocyte-derived SPMs have been suggested to contribute to CD11b^{high} F4/80^{high} tissue resident peritoneal macrophages, however this has demonstrated to be sexually dimorphic with more SPMs contributing in males than in females (86). The extent to which SPMs contribute to the replacement of CD11b^{high} F4/80^{high} LPMs is believed to depend on the magnitude of initial CD11b^{high} F4/80^{high} tissue resident macrophage disappearance (87,88).

Inflammation-recruited monocyte derived SPMs which survive following mild inflammation exhibited striking long-term differences to the incumbent CD11b^{high} F4/80^{high} tissue resident macrophages including high MHCII and low *Gata6* expression (88). However they rapidly adopted a GATA6^{+} MHCII^{low} peritoneal tissue resident-like phenotype, including TIM4 and VSIG4 expression, following transfer into naïve macrophage-depleted mice (88).

1.4. v-Maf musculoaponeurotic fibrosarcoma oncogene homolog (*Maf*)

1.4.1. Maf Gene in Mus Musculus

v-Maf musculoaponeurotic fibrosarcoma oncogene homolog (*Maf*) is located on Chromosome 8:qE1 of the mouse genome. The *Maf* gene encodes two isoforms generated through alternative splicing (89). These two isoforms are referred to as *Maf* short form (ENSMUST00000109104) and *Maf* long form (ENSMUST00000069009). The *Maf* short form is encoded by one exon constituted of 370 amino acids, while the long form is encoded by two exons (Figure 1.4.1A), forming consensus coding sequences (CCDC) of 1113bp for the short form or 1133bp for long form.

The two encoded proteins differ in their carboxy terminal, with the long form containing an additional 10 amino acids. Since the short form is expressed at higher levels (as determined by fragments per kilobase of transcript per million (FPKM) values of 6.93054 for *Maf* short form and 3.22905 *Maf* long form) in naïve peritoneal tissue resident macrophages of C57BL/6 mice (unpublished data), the efforts of this thesis will be founded on the short classical isoform.

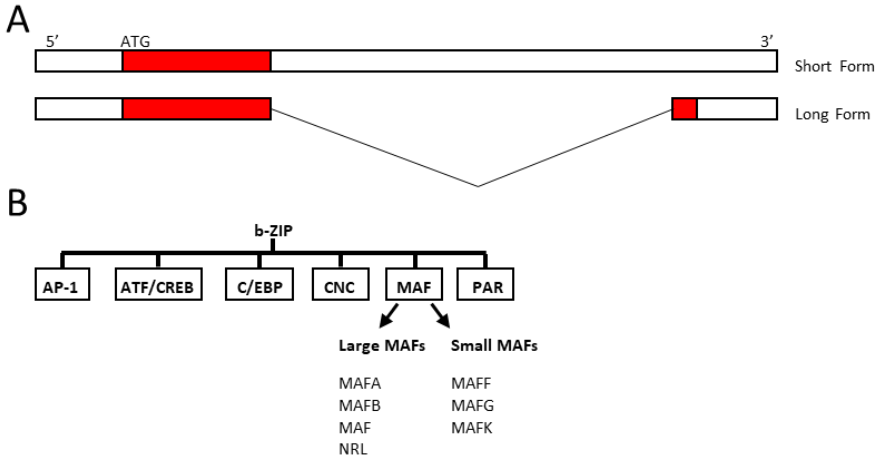

Figure 1.4.1: v-Maf musculoaponeurotic fibrosarcoma oncogene homolog (*Maf*)

A) Schematic of v-Maf musculoaponeurotic fibrosarcoma oncogene homolog (*Maf*) splice variants of long and short form, with exons (red), untranslated regions (white) and introns (black line) highlighted. B) Basic leucine zipper (b-ZIP) super-family, and the two subfamilies: large and small MAF proteins. Adapted from (90).

1.4.2. MAF Protein

In the mouse embryo, MAF is dynamically expressed in multiple tissues with different onsets of expression. MAF is widely expressed in regions such as the eye, spinal cord, cartilage, spleen, kidney, heart, lung, intestine, muscle, uterus, and liver (91,92)

The MAF family was identified in 1989 in an AS42 transforming retrovirus, from a naturally occurring musculoaponeurotic fibrosarcoma of a chicken (93), with the gene being named after musculoaponeurotic fibrosarcoma. The MAF oncoproteins are basic leucine zipper (b-ZIP) transcription factors that belong to the b-ZIP super-family, that includes activator protein 1 (AP-1), activating transcription factors/cAMP response element binding proteins (ATF/CREB), enhancer binding proteins (C/EBP), cap'n'collar (CNC), proline and acidic amino acid-rich (PAR) families (Figure 1.4.1B). The MAF family can be subdivided into two subfamilies: large and small MAF proteins (6). Small MAF proteins include MAFF, MAFG and MAFK, whilst the large MAF proteins are MAFA, MAFB, MAF and NRL (Figure 1.4.1B).

The protein encoded by *Maf* possesses a b-ZIP domain close to its C-terminus. Large MAFs share an N-terminal transcriptional domain, approximately 100 amino acid, rich in serine, proline and tyrosine. *Maf* contains a linker between the transactivation domain and the ancillary DNA-binding domain composed of histidine repeats and rich in glycine residues (94). b-ZIP domains are characterised by a series of leucines spaced 7 residues apart along an α-helix, resulting in adjacent leucine residues to occur on every second turn on the same side of the helical structure. Long side chains of leucine residues interact with other leucine residue side chains on another compatible b-ZIP proteins, allowing formation of homodimers and heterodimers (95).

MAF family members recognise DNA sequences 13-14bp in length, almost twice as long as other b-ZIP proteins (96). MAF binding sites, called Maf recognition elements (MAREs), are derivatives of sites recognised by AP-1 and ATF/CREB proteins. The addition of an ancillary binding region in MAF family members, compared to other b-ZIP proteins, results in unusual DNA recognition specificity with exceptionally stable complexes. Cooperative binding mediated by the basic and ancillary regions is thought to adopt a helix-turn-helix structural-recognition motif (97).

1.4.3. Role of MAF in Macrophages

The ontogeny and functional diversity of tissue resident macrophages has been well studied (98), including specific transcription factors first proposed by Lavin et al. (30). However the role of *Maf* in macrophage subtypes and tissue resident macrophages has not yet been fully analysed (20). Previous studies have demonstrated *Maf* is expressed constitutively by resting monocytes and macrophages (100), however expression varies with low expression in alveolar macrophages (99), and high expression in microglia (101,102). Compared to monocytes, macrophage enhancers are enriched for MAF binding motifs (30), suggesting that MAF may also act in concert with other transcription factors such as PU.1 to specify a general macrophage phenotype (101).

Foetal liver cells demonstrated that the mature erythroid compartments were significantly reduced in *Maf*-knockout ($Maf^{-/-}$) embryos compared with $Maf^{+/+}$ littermates (103). Furthermore the number of erythroblasts surrounding the macrophages in erythroblastic islands were also significantly reduced in $Maf^{-/-}$ embryos (103). *Maf* has been demonstrated to be required for the expression of F4/80 in foetal liver macrophages, and that *Maf* directly regulates the expression of F4/80 by binding to the half-MARE of the F4/80 promoter in foetal liver macrophages (104), a key marker used for the identification of macrophages.

It has been demonstrated that *Maf* is a potent activator of interleukin-10 (*Il10*) gene expression in monocytes and macrophages, furthermore overexpression of *Maf* has been suggested to suppress IL-12 p40 and p35 gene transcription (105). IL-10 is an essential anti-inflammatory cytokine whilst IL-12 is proinflammatory, ultimately indicating *Maf* has a role in modulating inflammation. *Maf* has been shown to be important for macrophage terminal differentiation, and macrophages that lack *Maf* are suggested to be immortalised and proliferate indefinitely in the presence of macrophage colony stimulating factor 1 (M-CSF) (106).

Thus *Maf* expression may provide insights into the transcriptional regulation underlying macrophage heterogeneity. In *Maf*-null mice, disruption of the *Maf* gene affected both prenatal and postnatal survival (107), therefore *Maf* is both an immunologically and developmentally important gene. *Maf* displayed a +7.9-fold change between *Gata6* knockout and wildtype counterpart in bioinformatic analysis of GeneChip array from peritoneal tissue resident macrophages (unpublished data).

1.5. Myeloid Leukaemia Factor 1 (*Mlf1*)

1.5.1. *Mlf1* Gene in Mus Musculus

Located on Chromosome 3:qE1, *Mlf1* gene can encode four splice variants. *Mlf1 A* (ENSMUST00000061322) is composed of 8 exons constituted of 282 amino acids, whilst *Mlf1 B* (ENSMUST00000077916) is encoded by 7 exons, the third exon being excluded, constituted of 267 amino acids (108) (Figure 1.5.1). The two other splice variants do not result in protein coding (ENSMUST00000126628 and ENSMUST00000142538).

All 4 splice variants were detected in naïve peritoneal tissue resident macrophages of C57BL/6 mice (unpublished data). *Mlf1 B* isoform is expressed at the highest levels (as determined by FPKM values of 3.53228 for *Mlf1 B*, 2.94764 E-6 for *Mlf1 A*, 1.0183 E-19 for ENSMUST00000126628 and 3.56907 E-67 for ENSMUST00000142538), the efforts of this thesis will be founded on this isoform.

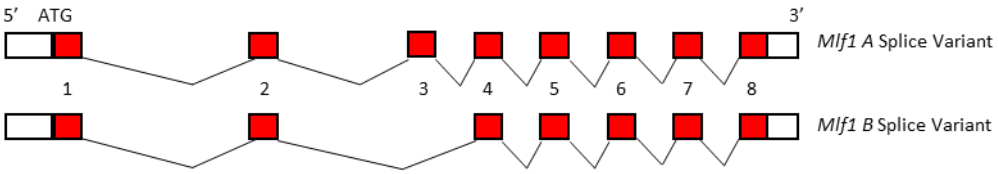

Figure 1.5.1: Myeloid leukaemia factor 1 (*Mlf1*)

Schematic of myeloid leukaemia factor 1 (*Mlf1*) protein coding splice variants *Mlf1 A* and *Mlf1 B*, with exons (red), untranslated regions (white) and introns (black line) highlighted.

1.5.2. MLF1 Protein

Myeloid leukaemia factor 1 (MLF1) was originally identified as a carboxyl-terminal component of the leukemic fusion protein NPM-MLF1 generated by the t(3;5)(q25.1;q34) chromosomal translocation in patients with acute myeloid leukaemia (AML) (109). In clinical studies MLF1 has been shown to be overexpressed in >25% of myelodysplastic syndrome associated AML and the malignant transformation phase of myelodysplastic syndrome (MDS) (110). Information on the physiological function of MLF1 is limited and is derived mostly from studies identifying MLF1 interaction partners.

The 14-3-3 binding site is one of the only known functional features of the MLF1 sequence, along with one nuclear export sequence (NES, 89-98aa) and two nuclear localisation sequences (NLS, 168-174aa and 232-236aa) (111). The presence of NES and NLS sequences

indicate MLF1 is a cytoplasmic–nuclear-shuttling protein. The majority of MLF1 is located in the cytoplasm, and has been reported to interact with several proteins including CSN3 (111), 14-3-3 (112), MLF1 adaptor molecule (MADM) (113), and MLF1-interacting protein (MLFIP) (114). MAF nuclear accumulation in mice has been shown to be dependent on 14-3-3 proteins (112).

It has been strongly suggested that MLF1 is involved in lineage determination, as MLF1 has been isolated as one of the genes involved in lineage switching from erythroleukemic cells to morphological and biochemical features of a macrophage phenotype (115). These findings along with the role of MLF1 in AML and MDS imply that MLF1 normally regulates the development of primitive hematopoietic cells, and its deregulation leads to hematopoietic dysplasia and leukemogenesis.

Bioinformatic analysis of GeneChip array from peritoneal tissue resident macrophages deficient of *Gata6* when compared to their wild type counterparts indicate a -4.2-fold change in *Mlf1* expression (unpublished data).

1.5.3. Role of MLF1 in Macrophages

The exact role of *Mlf1* in mice has not been well characterised. Originally named hematopoietic lineage switch 7 (*Hls7*), due to overexpression of *Mlf1* having been demonstrated to result in inhibition of erythroid differentiation in the erythroleukemic J2E cell line, and promoted M1 monoblastoid cell line to differentiate into myeloid cells (115). *Mlf1*-knockout mice have been shown to result in no discernible abnormalities under naïve conditions, however demonstrated increase splenic B-cell and T-cell number when compared to wildtype mice, however no difference in myeloid cell number was detected (116).

Murine MLF1 shares ~80% homology with human MLF1 at protein level, and therefore what little is known regarding *Mlf1* in humans and drosophila have provided suggestions for its role. The role of murine *Mlf1* has been demonstrated to regulate the hematopoietic switch by promoting the degradation of the cyclin-dependent kinase inhibitor ($p27^{Kip1}$), a cell cycle inhibitor preventing cell cycle exit (117). Whereas human *MLF1* overexpression induces p53 in primary mouse fibroblasts (111), another major component of cell cycle arrest.

Mlf1 in drosophila has been suggested to protect RUNX transcription factors from degradation through the proteasome (118), however the exact mechanism for this is not

understood. It has been suggest that MLF1 protein could favour the interaction between RUNX1 and core-binding factor subunit beta (PEBP2-β), which is required to prevent RUNX1 degradation by the proteasome (119). Human *MLF1* has been observed to be expressed in HSCs and CMPs (discussed above), with weaker expression during cell differentiation (110), further suggesting its role in haematopoiesis. Ultimately the exact role of *Mlf1* in macrophages is unclear, and as of yet the role of *Mlf1* in tissue resident macrophages has not previously been explored.

1.6. Hypothesis and Aims

It is hypothesised that the transcription factors *Maf* and *Mlf1* are responsible for sculpting the resident macrophage phenotype, and that manipulation of expression will modulate their homeostatic and inflammatory properties.

Therefore the aims of these thesis are…

- Develop and validate a method to explore the role of *Mlf1* and *Maf* in tissue resident macrophages.
- Assess effect on generation or retention of tissue resident macrophages and modified phenotype in $Maf^{fl/fl}Cx3cr1^{Cre/+}$ and $Maf^{fl/fl}Cx3cr1^{+/+}$ mice.
- Ascertain whether *Maf*-deficiency has a significant impact on tissue resident macrophage transcriptome in naïve conditions and following mild immune challenge.

Chapter 2

Materials and Methods

2.1. Buffers and Solutions

Solution/Buffer	Ingredients
Mammalian Cell Lysis Buffer	100 mM Tris pH 8.5 5 mM EDTA 200 mM NaCl 0.2 % (v/v) SDS Nuclease free water
MUSE Staining Solution	625 ng/mL Propidium Iodide (PI) 500 ng/mL Live Dead Stain 751 (Fisher) 1X DPBS
Freezing Media	10 % (v/v) DMSO 90 % (v/v) Heat-Inactivated filtered FBS (Gibco)
2 % Formaldehyde	36.5-38 % Formaldehyde solution in water 1X DPBS
FACS Block	5 % (v/v) filtered Rabbit Serum 4 µg/mL rat anti-mouse FcγRII/III (2.4G2 clone) FACS Wash
FACS Wash	0.5 % (w/v) BSA 5 mM EDTA 1X DPBS
MACS Buffer	0.5 % (w/v) BSA 1X DPBS
0.5 % Saponin FACS Block	5 % (v/v) filtered Rabbit Serum 4 µg/mL rat anti-mouse FcγRII/III (2.4G2 clone) 0.5 % Saponin FACS Wash
0.5 % Saponin FACS Wash	0.5 % (w/v) Saponin 0.5 % (w/v) BSA 5 mM EDTA 1X DPBS

Ammonium-Chloride-Potassium (ACK) Lysis Solution	150nM NH_4Cl 10mM $KHCO_3$ 0.1 mM Na_2EDTA
Lavage Fluid	5 mM EDTA 10% FBS 1X DPBS
Immunofluorescence Permeabilization and Block Solution	1X Tris-buffered saline (TBS) 0.5 % Triton X-100 1 % BSA 0.3 M Glycine
Immunofluorescence Staining Solution	1X Tris-buffered saline (TBS) 0.5 % Triton X-100 1 % BSA

Table 2.1.1 Common Buffers and Solutions.

2.2. Mice

All animal work in this thesis was conducted in accordance with UK Home Office Guidelines and Animal [Scientific Procedures] Act 1986 which encompasses EU Directive 2010/63/EU on the protection of animals used for scientific purposes. Animal work was undertaken by trained staff under a Home Office approved establishment licence, project licences (PO5D6A456 and P92CA01DA) and individual's personal licences at Cardiff University's Biological Services (BIOSERV) Unit, in a specific pathogen free (SPF) unit which undergoes quarterly bespoke health screens.

Animals were housed in either open top ventilated cages in racks with shaded tops or scantainers, exceeding the minimum space allocations set out in Annex III of Directive 2010/63/EU and Appendix A to the Council of Europe Convention ETS 123, with a maximum of 5 mice under 30 g in weight per cage. Solid floor polycarbonate cages with an adequate depth of dust-free softwood bedding substrate, in a humid 20-24°C environment, on a 12-hour light/dark cycle where chow and water were provided *ad libitum*, with sunflower seeds for variation and foraging when animals were not undergoing procedure. Nesting material consisting solely of dust-free virgin kraft paper

which was provided in a compacted form that requires shredding, along with 50mm Ø polycarbonate or recycled fibreboard tunnels and 30mm Ø aspen balls for added cage complexity and as gnawing material.

Cages were regularly cleaned and replaced with fresh bedding substrate, chow and water, whilst scent-marked nesting material was transferred between cages to reduce stress and refreshed as required. Welfare-related assessments and interventions, if required, were performed by the Named Animal Care and Welfare Officers (NACWOs) and the Named Veterinary Surgeon (NVS).

Details of the age, sex and number of mice used in each experiment or experimental group can be found in the figure legends throughout this thesis. The transgenic mice strains used in this thesis, listed in

Table 2.2.1, B6J.B6N(Cg)-Maf$^{tm2.1Cbm}$ mice were kindly provided from Dan Littman's Laboratory (New York University) in collaboration with Carmen Birchmeier (Max Delbrück Center, Berlin), B6J.B6N(Cg)-Cx3cr1$^{tm1.1(cre)Jung}$ and B6J.129P2(C)-Cx3cr1$^{tm2.1(cre/ERT2)Jung}$ were originally purchased from The Jackson Laboratory, and all lines were bred inhouse.

Official Strain Name	Thesis Abbreviation
B6J.B6N(Cg)-*Maf*$^{tm2.1Cbm}$	Maf^{fl}
B6J.B6N(Cg)-*Cx3cr1*$^{tm1.1(cre)Jung}$	Cx3cr1^{CONST}
B6J.129P2(C)-*Cx3cr1*$^{tm2.1(cre/ERT2)Jung}$	Cx3cr1^{ERT}

Table 2.2.1 Official and abbreviated names of the transgenic mice strains used in this thesis.

2.3. Genotyping

Genomic DNA (gDNA) was isolated from ear-punch biopsies taken by BIOSEV staff for animal identification. Biopsies were digested with 50 µl of mammalian lysis buffer and 100 µg/ml of proteinase K (from Tritirachium album, Sigma P4850) in 1.5 ml microcentrifuge tubes (Starlab) at 52 °C for 1 hour, being shaken at 800 rpm in a Thermoshaker (Grant-bio, PSC24N). Proteinase K was inactivated at 72 °C for 30 minutes at 800 rpm. Tubes were cooled to room temperature before 400 µl of nuclease free water (ThermoFisher Scientific) was added to each sample and thoroughly vortexed. GoTaq® Green Mastermix (Promega) was used for genotyping as per manufacturer's instructions. Specific DNA primer sequences for targets of interest listed in Table 2.3, provided by The Jackson

Laboratory and Dan Littman's Laboratory, were purchased through Sigma Aldrich. Each reaction was conducted in a 0.2 ml PCR tube or 0.2 ml PCR 96-well plate (Starlab) with the addition of 1 µl of gDNA.

Target Primer	Forward Primer (5'-3')	Reverse Primer (5'-3')
Cx3cr1^{CONST}	GCAGGGAAATCTGATGCAAG	GCAGGGAAATCTGATGCAAG
Cx3cr1$^{CONST\ WT}$	CCTCAGTGTGACGGAGACAG	
Cx3cr1$^{ERT\ Cre}$	GTTAATGACCTGCAGCCAAG	ACGCCCAGACTAATGGTGAC
Cx3cr1$^{ERT\ WT}$	AGCTCACGACTGCCTTCTTC	
Maf$^{flox/WT}$	CGCACCCTGACAACGTG	ATGATCAGGCTCAGGCTTAAA

Table 2.3.1 PCR primers used for genotyping of transgenic mice strains used in this thesis.

Tubes were placed in a Mastercycler® Nexus Gradient (Eppendorf) PCR machine and the PCR reaction was electrophoresed on a 2% agarose gel. Agarose powder (Fisher Scientific) was dissolved in 1X Tris-Acetate-EDTA (TAE) buffer (from a 50X stock solution (Fisher Scientific).

To visualise the DNA 1:20,000 dilution SYBR™ Safe (ThermoFisher Scientific) was added to the dissolved agarose and gently mixed before being poured into an appropriately sized Fisherbrand™ gel mould, with the addition of a comb (Fisher Scientific) to form individual wells. The samples were then loaded alongside 100 base pair (bp) DNA ladder (Promega) and run using the Biorad PowerPac™ HC High-Current Power Supply at 120 V for ~25 minutes. The gels were then transferred to a UV transilluminator where they were imaged.

2.3.1. *Maf* Floxed Genotyping

Maf$^{fl/fl}$ mice were originally generated by Carmen Birchmeier (120), however before being provided to us from Dan Littman's Laboratory at New York University, the strain had been backcrossed with C57BL/6 for several generations to generate the B6J.B6N(Cg)-Maf$^{tm2.1Cbm}$ background. To summarise the generation of the Maf$^{fl/fl}$ mice, one loxP site was introduced 1547 bp upstream of the start codon of the CCDS of Maf, and the second together with an FRT flanked neomycin resistance cassette 411bp downstream of the

termination codon. This results in expected genotyping band sizes of 417bp for wildtype or 547bp for floxed mice.

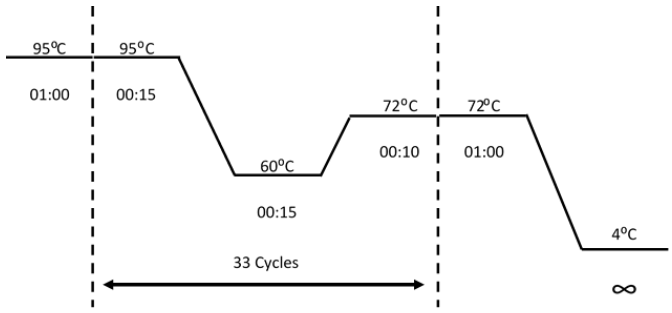

Figure 2.3.1 Schematic of *Maf* Flox/WT genotyping PCR reaction

2.3.2. Cx3cr1 Cre Genotyping

Originally developed by Steffen Jung (9), in the Cx3cr1^{CONST} mice a Cre recombinase cassette gene replaced the Cx3cr1 coding exon. In generation of the Cx3cr1^{ERT} mice the CreERT2 cassette gene replaced the first 390 bp of the Cx3cr1 CCDS. Both Cx3cr1^{CONST} and Cx3cr1^{ERT} strains were backcrossed for multiple generations onto the C57BL/6 background. For Cx3cr1^{CONST} this results in expected genotyping band size of 302 bp for wildtype and 380 bp of Cre recombinase, and for Cx3cr1^{ERT} 151 bp wildtype and 230 bp for CreERT2 cassette.

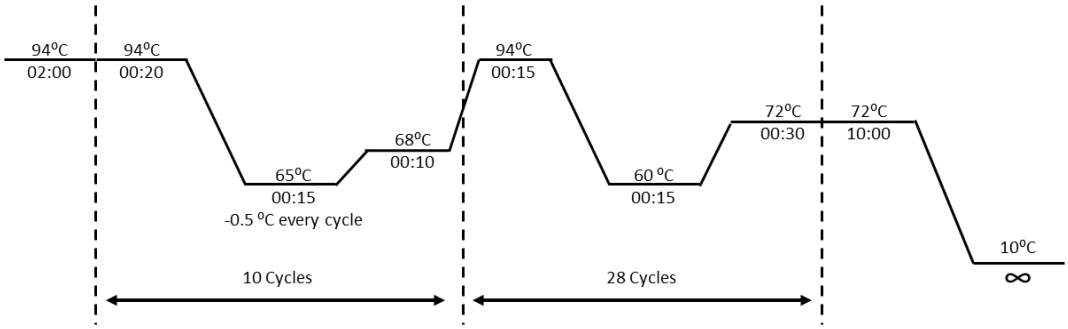

Figure 2.3.2 Schematic of *Cx3cr1* Cre/WT genotyping PCR reaction

2.4. Cell Culture

All cells were incubated at 37°C in a humid incubator with 5% CO2 unless otherwise stated. Dulbecco's Modified Eagle Medium (DMEM) and Roswell Park Memorial Institute 1640 (RPMI) were supplemented with heat-inactivated Foetal Bovine Serum (FBS) and Penicillin-Streptomycin antibiotics (100X) (ThermoFisher Scientific). Unless stated otherwise the cell were maintained in multiwell plates, T75cm^2 or T175 cm^2 flasks with filter caps (Greiner Bio One).

2.4.1. Cryopreservation and Thawing

Cells were centrifuged at 350 *x g* for 5 minutes; the supernatant was aspirated, and the cell pellet resuspended in 1 ml of freezing media per 3-5 x 10^6 cells. The suspension was divided into 1 ml aliquots and frozen down in either a Mr. Frosty™ (Thermofisher) or a CoolCell® LX (Biocision) overnight at -80 °C in a New Brunswick ULT freezer. Cryopreserved cells were then moved into liquid nitrogen for longer term storage.

Cells were thawed by warming to room temperature until the ice crystals disappeared. Defrosted aliquots were quickly transferred into 10 ml of the corresponding media and centrifuged at 350 *x g* for 5 minutes to dilute freezing medium. Supernatant was aspirated and the cells resuspended in the appropriate fresh culture media.

2.4.2. Cell Counting and Viability

Muse® Cell Analyzer (Luminex) was utilised to count cell number and measure viability. Samples were prepared by diluting cells 1:20 with Muse staining solution and following a 5-minute incubation at room temperature these samples were run on the Muse® Cell Analyzer as per manufacturer's instructions. Muse staining solution contains both LDS 751 and propidium iodine. LDS 751 is a fluorescent cell-permeant nucleic acid dye allowing for counting of all nucleated cells, PI is a membrane impermeant nucleic acid dye which can therefore be used to exclude non-viable cells.

2.4.3. Jurkat Cell Line

The Jurkat cell line is an immortalised human T-lymphocyte line which was established from the peripheral blood of an acute T-cell Leukaemia patient (121). These non-adherent cells were maintained in standard RPMI media and passaged twice-weekly at a 1:20-1:40

dilution, following centrifugation at 350 *x g* for 5 minutes of the cell suspension and resuspended in fresh RPMI.

2.4.4. Human Embryonic Kidney (HEK) 293T Cell Line

Human Embryonic Kidney 293T cell line (HEK 293T) was originally derived from human embryonic kidney cells that were virally transformed to stably express the SV40 large T-antigen (122). HEK 293T cells were cultured in standard DMEM media and passaged every 3-4 days at a 1:3 dilution. Media was aspirated and the cell monolayer was gently washed with Dulbecco's Phosphate Buffered Saline (DPBS) prior to addition of 0.05 % Trypsin-EDTA (Thermofisher) and incubated at 37 °C for 5 minutes to detach the cells. The cells suspension was then collected into a 50 ml falcon tube and 10 ml of standard DMEM was added to neutralise the Trypsin-EDTA. The cell suspension was then centrifuged at 350 *x g* for 5 minutes, the supernatant was removed before the cells were resuspended in fresh DMEM.

2.4.5. Macrophage Precursor (MØP) Cell Line

Conditionally immortalised Macrophage Precursor (MØP) cell lines were derived from transfecting CD117+ murine bone marrow cells with a retrovirus carrying an oestrogen inducible HoxB8 gene, as previously described (123). MØP cells were maintained in standard RPMI media supplemented with 1 µM oestrogen (10 mM β-estradiol (w/v) in absolute ethanol; Sigma) and 10 ng/ml recombinant murine Granulocyte-Macrophage Colony Stimulating Factor (GM-CSF; Peprotech) and were passaged every 3-4 days at a 1:20-40 dilution.

2.4.5.1. Differentiation of MØP Cells

Oestrogen was depleted from the MØP cultures by washing the cells in 10 ml standard RPMI media three times, centrifuged at 350 *x g* for 5 minutes in-between washes. After the final wash cells were counted as previously described and resuspended in RPMI media containing 20 ng/ml Macrophage Colony Stimulating Factor (M-CSF). Differentiating MØP cells were incubated for 4 days, with additional M-CSF supplemented RPMI media added on day 2.

The differentiated MØP cells were harvested using Lidocaine-EDTA. The media was discarded, and cells were washed with DPBS before sufficient Lidocaine-EDTA was added

to cover the bottom of the well. Following 3-4 minutes of incubation at 37 °C before the addition of double the volume of RPMI media to inactivate the Lidocaine-EDTA. The cell suspension was then transferred to a 50 ml falcon tube and centrifuged at 350 *x g* for 5 minutes to pellet the cells before downstream applications.

2.4.6. Bone-Marrow Derived Macrophages (BMDMs)

Femur and tibia bones were harvested from sacrificed mice and placed into 50 ml falcon tube containing ice-cold DPBS. The epiphyses of each bone were removed, and marrow was flushed out of the medullary cavity using a 27-gauge (G) needle on a 10 ml syringe containing perfusion buffer, directly into a 70 µM strainer placed on a 50 ml falcon tube.

The plunger of a 5 ml syringe was used to assist with the passing of any cells through the strainer. Cells were centrifuged at 350 *x g* for 5 minutes, after which either cells were cryopreserved, as described in Section 2.4 or underwent a red-blood-cell (RBC) lysis using 1 ml of Ammonium-Chloride-Potassium (ACK) lysis solution and incubated for 1 minute before 9 ml of DPBS was added. Frozen bone-marrow aliquots did not require this step as freeze/thawing results in lysis of RBCs.

Bone-marrow cells were resuspended in 10 ml of standard DMEM and counted as described in Section 2.4.2. Cells were plated in 145 mm x 20 mm (diameter x height) culture dish (Greiner Bio One) at $1x10^7$ per plate in 25 ml of DMEM with 20 ng/ml of M-CSF and incubated for 7 days at 37 °C. Differentiation media was refreshed every 2 days before being harvested with Lidocaine-EDTA buffer as mentioned above.

2.4.7. Functional Macrophage Assays

Functional assays were performed on fully differentiated MØP. Following harvest with Lidocaine-EDTA, as described above, cells were counted (Section 2.4.2) and replated at seeding density of $4x10^5$ per well in Corning® Costar® Ultra-Low Attachment 24 Well Plates and cells were incubated to adhere for a minimum of 5 hours in 20 ng/ml of M-CSF media. Prior to treatment the supernatant was removed and briefly washed with media before treatment with 20 ng/ml M-CSF with 100 ng/ml *E. coli 0111:B4 l*ipopolysaccharides (LPS) for the time specified in each experiment as indicated in the appropriate figure legends.

2.5. *In Vivo* Experiments and Cell Isolation

2.5.1. Peritoneal Lavage

Mice were sacrificed as per Schedule 1. The abdominal skin was lifted with forceps and a small incision made in the abdominal skin using scissors. This enables the skin to be torn by hand, exposing the abdominal wall. Using a 10 ml syringe 6 ml of ice-cold Lavage Buffer was injected into the peritoneal cavity using a 21G hypodermic needle (BD Bioscience). The mice were then gently rocked to ensure a maximum cell harvest and the needle re-inserted to withdraw cell-containing fluid. Following recovery the needle was removed and the fluid was transferred to a 15 ml falcon tube and placed on ice.

2.5.2. Intraperitoneal (I.P.) Injections of Zymosan Particles

Zymosan particles were counted on the Muse at a 1:40 dilution as described in section 2.4.2. Mice were injected intraperitoneally with a 29 G 0.5 ml insulin needle (Fisher Scientific) containing $2x10^6$ zymosan particles in 100 µl DPBS. Mice were sacrificed as per Schedule 1, 48 hrs after injection.

2.5.3. I.P. Injection of Tamoxifen

Prior to injection 1 g Tamoxifen powder was resuspended in pre-warmed (70°C) ethanol and placed at 70 °C until fully dissolved, resulting in a concentration of 200 mg/ml, aliquoted and stored at -20 °C. On the day of injection, corn oil (Sigma) was pre-warmed (70°C) and combined with the Tamoxifen-ethanol stock solution resulting in a final concentration of 20 mg/ml. The mice were weighed and dosed at either 100 mg/kg or 200 mg/kg with a 25 G needle (BD Bioscience) on a 1 ml syringe (Fisher Scientific) every 24 hours up to 5 days. Number of injections are specified in each experiment and can be found in the figure legends. Mice were sacrificed 7 days after final injection.

2.5.4. Microglia Isolation

Bijou tubes were filled with 2 ml of Hank's Balanced Salt Solution without Ca^{2+} and Mg^{2+} (HBSS w/o; ThermoFisher Scientific) and weighed. Brains were harvested following schedule 1 and stored on ice in the HBSS w/o bijou tubes. Tubes containing whole brain were weighted to calculate brain weight for enzymatic digestion, which was performed

using the Adult Brain Dissociation Kit, mouse and rat (ABDK; Miltenyi Biotec) as per manufacturer's instructions.

The specific contents of these kits are proprietary knowledge, however all enzymes and buffers were calculated according to brain weight and added to a GentleMACS™ C-tube (Miltenyi) followed by the brain and 1 ml HBSS w/o. The C-tubes were then placed in the GentleMACS^{TM} OctoDissociator with heaters (Miltenyi Biotec) and run on the program "37C_ABDK". Exact details of GentleMACS^{TM} OctoDissociator programs are proprietary, however manufacturer literature states the C-tube are heated to 37 °C for 30 minutes whilst being rotated at 840 rpm. The resulting cell suspension was passed through a 70 µM strainer into a 50 ml falcon tube containing 10 ml HBSS with Ca^{2+} and Mg2+, before being centrifuged at 300 *x g* for 7 min.

Supernatant was removed, and cell suspension was resuspended in 3.1 ml of DPBS with Ca^{2+} and Mg^{2} ($DPBS^{+/+}$) and transfer to 15 ml tube. The addition of 900 µl Debris Removal Solution was well mixed by inversion of the tube. Very gently 4 ml ice-cold $DPBS^{+/+}$ was overlaid on top of the cell suspension, and then centrifuged for 10 min at 3,000 *x g* at 4°C (with partially reduced acceleration and brake (setting 6 on Sorvall Legend RT)).

This results in three phases being formed: a top clear layer, a myelin debris layer, and a cloudy cellular layer at the bottom of the tube. The myelin debris was removed with a P1000, carefully trying to not disturb the bottom cellular layer. Following the removal of the myelin the clear top phase was removed with a fresh P1000 tip.

To remove any remaining debris removal solution the cells were washed with 12 ml of cold $DPBS^{+/+}$ and centrifuged at 4°C for 10 min at 1,000 *x g*. Supernatant was discarded and 1ml of diluted Red Blood Cell Removal Solution (1x, diluted in ddH_2O) was combined with the cell pellet by pipetting up and down, and incubated for 10 min on ice, before being centrifuged at 4°C at 300 *x g* for 7 min. Supernatant was discarded and cell pellet was washed with 10 ml of cold MACS buffer.

2.6. Flow Cytometry

Samples were run on the Attune NxT Flow Cytometer (Thermo Fisher Scientific). Each experiment used single colour controls and where possible photo multiplier tube (PMT) voltage settings were kept consistent between experiments.

2.6.5. Cell Staining

Chapter 3 assesses different fixatives and permeabilisation methods for antibodies. Ultimately in the method used, cells were counted (Section 2.4.2) and fixed with 2 % formaldehyde for 20 minutes at on ice. Fixative was removed by centrifuging at 350 *x g* for 5 min and the supernatant was discarded. Cells were resuspended in 1 ml sort buffer and 3 $x10^5$ cells were transferred to one well of a V-bottom 96 well plate (Greiner). The plate was then centrifuged at 350 *x g* for 5 minutes and the supernatant discarded.

Where intra-cellular/intra-nuclear staining was required, additional steps were conducted. Cells were resuspended in 100 µl of 1X Permeabilization Reagent resuspended in Permeabilization Diluent, both from eBioscience™ Foxp3 / Transcription Factor Staining Buffer Set (Thermofisher). The plate was then centrifuged at 350 *x g* for 5 minutes and the supernatant discarded and repeated for a second time as per the buffer set instructions.

Following discarding of the supernatant 100 µl of flow block buffer was added and incubated at 4 °C for 20 minutes. During this incubation desired antibodies were diluted in flow block buffer to form a mastermix (Table 2.6.1). The plate was then centrifuged at 350 *x g* for 5 minutes and the supernatant discarded and replaced with 100 µl of the antibody mastermix. For unstained samples 100 µl of FACS block was added per well and incubated at 4 °C for 20 minutes.

The plate was then centrifuged at 350 *x g* for 5 minutes and washed with flow wash buffer and centrifuged at 350 *x g* for 5 minutes twice. Cells were resuspended in 100 µl focussing fluid (Thermofisher) and transferred to 5ml flow tubes (Greiner) and resuspended in an additional 350 µl focussing fluid.

Target	Fluorophore	Clone	Isotype	Supplier	Catalogue Number
Anti-Rabbit IgG (H+L)	APC	Polyclonal	Donkey	Jackson Immuno	711-136-152
CD11b	APC-Cyanine7	M1/70	Rat IgG2a, κ	Biolegend	101226
CD11c	Alexa Fluor® 488	N418	Armenian Hamster IgG	Biolegend	117313
CD16/32	BD Horizon™ V450	2.4G2	Rat IgG2b, κ	BD Bioscience	560539
CD16/32 (Fc Block)	Purified	2.4G2	Rat IgG2b, κ	BD Bioscience	553142
CD206 (MMR)	Brilliant Violet 785™	C068C2	Rat IgG2a, κ	Biolegend	141729
CD38	PE	90	Rat IgG2a, κ	Biolegend	102707
CD40	APC-Fire™ 750	Mar-23	Rat IgG2a, κ	Biolegend	124631
CD45	Pacific Blue™	30-F11	Rat IgG2a, κ	Biolegend	103125
CD68	APC-Cyanine7	FA-11	Rat IgG2a, κ	Biolegend	137023
CD80	APC	16-10A1	Armenian Hamster IgG	Biolegend	104713
CD86	Alexa Fluor® 488	GL-1	Rat IgG2a, κ	Biolegend	105017
Cx3cr1	Alexa Fluor® 488	SA011F11	Mouse IgG2a, κ	Biolegend	149021
Cx3cr1	PE	SA011F11	Mouse IgG2a, κ	Biolegend	149005
F4/80	Pacific Blue™	BM8	Rat IgG2a, κ	Biolegend	123124
Folate Receptor β	PE	10/FR2	Rat IgG2a, κ	Biolegend	153303
GFP	Alexa Fluor® 488	FM264G	Rat IgG2a, κ	Biolegend	338008
HSP70	Alexa Fluor® 488	W27	Mouse IgG2a, λ	Biolegend	648003
I-A/I-E (MHC-II)	PerCP/Cy-5.5	M5/114.15.2	Rat IgG2b, κ	Biolegend	107626

Isotype Control	PE	eBM2a	Mouse IgG2a, κ	Thermo Fisher	12-4724-41
Isotype Control	PE	MOPC-21	Mouse IgG1, κ	Biolegend	400111
Isotype Control	Alexa Fluor® 488	MOPC-173	Mouse IgG2a, κ	Biolegend	400233
Isotype Control	eFluor® 660	eBMG2b	Mouse IgG2b, κ	Thermo Fisher	50-4732-82
Isotype Control	Alexa Fluor® 488	HTK888	Armenian Hamster IgG	Biolegend	400923
Isotype Control	APC-Cyanine7	RTK2758	Rat IgG2a, κ	Biolegend	400523
Isotype Control	APC-Fire™ 750	RTK2758	Rat IgG2a, κ	Biolegend	400567
Isotype Control	Brilliant Violet 785™	RTK2758	Rat IgG2a, κ	Biolegend	400545
Ly-6C	APC-Cyanine7	HK1.4	Rat IgG2c, κ	Biolegend	128026
Ly-6G	FITC	1A8	Rat IgG2a, κ	Biolegend	127606
LYVE-1	PE	ALY7	Rat IgG1, κ	Thermo Fisher	12-0443-80
MAF	Unconjugated	Polyclonal	Rabbit IgG	Abcam	ab203885
MAF	PE	T54-856	Mouse IgG2a, κ	BD Bioscience	565795
MAF	eFluor® 660	sym0F1	Mouse IgG2b, κ	Thermo Fisher	50-9855-82
MAIR-V	PE	TX70	Rat IgG2a, κ	Biolegend	132704
Major Histocompatibility Complex (MHC) H-2	PE	M1/42	Rat IgG2a, κ	Biolegend	125505
MRVI-1	Unconjugated	Polyclonal	Rabbit IgG	Thermo Fisher	PA3-851
P2RY12	APC	S16007D	Rat IgG2b, κ	Biolegend	848005
Rat CD2	Alexa Fluor® 488	OX-34	Mouse IgG2a	Bio-Rad	MCA154A488

S1P1/EDG-1	PE	713412	Rat IgG2a	R&D Systems	FAB7089P-100UG
Siglec H	PE	551	Rat IgG1, κ	Biolegend	129605
SPI-1 (PU.1)	Alexa Fluor® 488	7C2C34	Rat IgG2a, κ	Biolegend	681305
Tim-4	PE	RMT4-54	Rat IgG2a, κ	Thermo Fisher	12-5866-82
TLR2	PE	QA16A01	Mouse IgG1, κ	Biolegend	153003
VSIG-4	APC	NLA14	Rat IgG2a, κ	Thermo Fisher	17-5752-80

Table 2.6.1 List of flow cytometry antibodies used throughout this thesis.

2.6.6. Fluorescence-Activated Cell Sorting (FACS)

Cell sorting was performed on the FACS Aria III (BD Bioscience), by trained flow cytometry specialists in Central Biotechnology Services (CBS) at Cardiff University. Samples were stained as described above and kept of ice prior and post sorting. Cell sorts for RNA were performed with a pre-cooled sample injection and collection chamber at 4 °C.

2.6.6.1. DSP (dithiobis(succinimidyl propionate))/Lomant's Reagent Crosslinking of Microglia for FACS

To preserve microglia for FACS and to prevent clumping of samples we determined the requirement for a N-hydroxysuccimide ester (NHS ester) crosslinker such as DSP (Thermofisher). A 50X stock solution of DSP (50 mg/ml) was generated by dissolving 1g of DSP in 100% anhydrous DMSO, aliquoted and store at −80 °C. Immediately before use the 50X stock was diluted to its working concentration (1 mg/ml) with DPBS in a 15 ml Falcon tube, by dropwise adding DPBS using a 1000 µl pipette whilst vortexing. The solution was filtered using a 30 µm filter (Miltenyi) and kept on ice.

Following the isolation of microglia as described in section 2.5.4, 1 ml of 1X DSP was added for every 1 x10^6 cells and left on ice for 30 minutes. Excess DSP was chemically quenched through adding 60 µl of 1 M Tris HCl pH 7.5 (final concentration 20 mM) per 1ml of 1X DSP used and mi*x* *g*ently by pipetting. Microglia were then centrifuged at 4°C at 300 *x g* for 7 min and resuspended in DSPS prior to staining as discussed above.

2.6.7. Imaging Cytometry

Amnis Imagestream®X Mark II (Luminex) imaging cytometer is an advanced flow cytometer acquiring both integrated fluorescence signals as well as high quality fluorescence images, allowing for visual assessment combined with flow cytometry. Samples were stained as described in 2.6.5, and prior to running samples were resuspended in a small volume of 20 µl DPBS in a 1.5 ml microcentrifuge tubes (Starlab). The magnification in each experiment can be found in the figure legends throughout this thesis.

2.7. Quantitative PCR (qPCR)

2.7.1. Ribonucleic Acid (RNA) Extraction

RNA isolation from cell culture where it is possible to obtain cell numbers exceeding $1x10^6$ cells were extracted as described in section 2.8.2 using RNeasy Mini Kit (Qiagen) and spin columns were eluted in 30 µl nuclease free water. RNA extractions from less than $5x10^5$, such as *in vivo* cells which have undergone FACS or those from functional macrophage assays in section 2.4.7, were extracted using either the RNeasy Micro Kit (Qiagen) or miRNeasy Micro Kit (Qiagen) and eluted in 15 µl nuclease free water.

2.7.2. Reverse Transcription

Isolated RNA was measured using the Nanodrop 2000 providing concentration of nucleic acid and 260:280 ratio as a determination of purity of nucleic acid to protein. Samples were normalised based on concentration of nucleic acid and as per manufactures instruction of High-Capacity cDNA Reverse Transcription Kit (Thermofisher Scientific) to generate complementary DNA (cDNA) for qPCR (Figure 2.7.1).

No template controls (NTC), where nuclease free water was used to replace the RNA, and reverse transcription controls (RTC), where the MultiScribe™ Reverse Transcriptase was replaced with nuclease free water, were utilised in all qPCR reactions to control of RNA and genomic DNA contamination respectively.

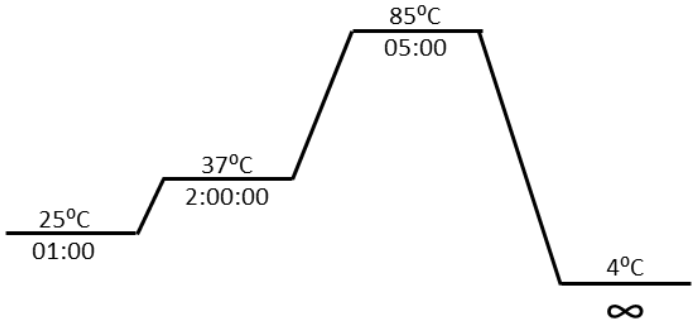

Figure 2.7.1 Schematic of High-Capacity cDNA Reverse Transcription Kit

2.7.3. qPCR Reaction

All qPCR reactions utilised PowerUp™ SYBR™ Green Master Mix (Thermofisher Scientific) as per manufacturer's instructions. qPCR reactions were conducted either in a 96 well plate format with a 20 µl reaction on the ViiA 7 Real-Time PCR System (Thermofisher Scientific), or in a 384 well plate format with a 10 µl reaction on the QuantStudio 12K Flex Real-Time PCR System (Thermofisher Scientific). Both instruments used a standard 2 step PCR reaction with the addition of a melt curve analysis after the final cycle (Figure 2.7.2).

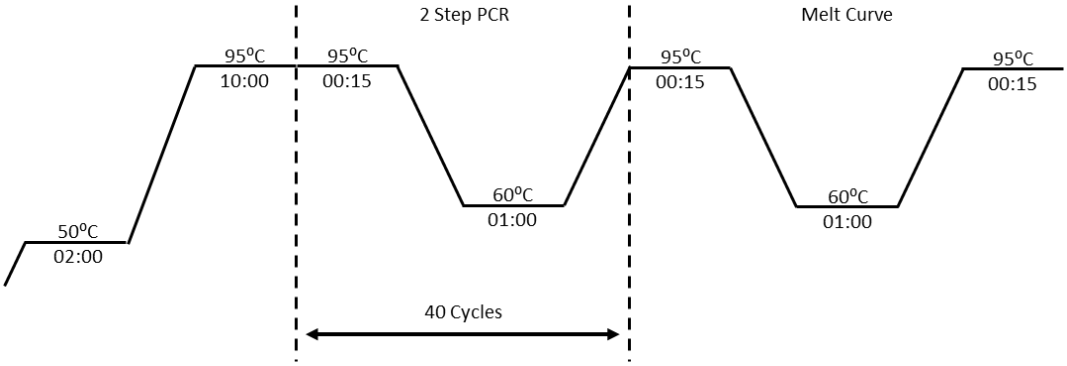

Figure 2.7.2 Schematic of Standard 2-Step PCR and Melt Curve.

All qPCR primers were designed, where possible, to be intron spanning (Figure 2.7.1), were checked using NCBI Primer-BLAST, and generated by Sigma Aldrich. *Ywhaz* was used as the endogenous control in all assays.

Target	Forward Primer (5'-3')	Reverse Primer (5'-3')
Maf	AGAGGCGGACCCTGAAAAAC	GTTTTCTCGGAAGCCGTTGC
Maf Codon Opt	AACAGCGTCATGTCCTGGAA	TCACATAAAGAACTCGGGGCTG
Per3	ACTGCTCCAACTCAGCTTCC	TCTGTCTCCACCTCCACAGA
Creb5	CGTTTCCCAACAGAGGACCA	TGCTCAAAGGAGCAGTCCAG
Cd300lf	CATTGGCCCAGCAATCCAA	CATCTTCACCACCGCCACT
Mrvi1	CATCGCCGTCTTGCATC	CGTGGCCTTTGACATGC
Dnm1	GCAGAAGGTCCTCAATCAGC	TCGAAGTCCACTGCAAACTG
Ptprm	AGGCGACGGCCAACTAACA	CTTCTTGGCCAGTTTCCTCTTC
Dbp	AGCCTTCTGCAGGGAAACAG	TGAGGGCAGAGTTGCCTTG
Lyve1	TGGTGTTACTCCTCGCCTCT	TTCTGCGCTGACTCTACCTG
Tgfbr3	CAGGATCTAGGCTGGAAATGG	GGGTTCAGGGTGTTGTATAGTC
H2-Q6	TGTCCTTGTAGCTTGGCCATC	AAGGTCACACTGGCTGTCACT
Klf12	GCTAATGCTTGATGGAATGCC	AGTTGTGGACGTTTGGAGAC
Vsig4	ATGGGACTGGAAAACTTGAGGAG	CTGCAGCGGAACAAGATATAAGG

S1pr1	TTGAGCGAGGCTGCTGTTTC	GGGGTGGTATTTCTCCAGGC
Cd38	ACTGGAGAGCCTACCACGAA	AGTGGGGCGTAGTCTTCTCT
Clec7a	TGGGTGCCCTAGGAGGTTTT	CGGTGAGACGATGTTTGGCT
Hspa1a/Hspa1b	ATGGACAAGGCGCAGATCC	CTCCGACTTGTCCCCCAT
Folr2	GGAGCCTGCCTGTAAGAGTC	TTACGCCAACTCTGGTCCAC
Cd5l	GTTGGATCGTGTTTTTCAGA	TCCCACTCGCTGCACTTTGGT
Ywhaz	TTGAGCAGAAGACGGAAGGT	GAAGCATTGGGGATCAAGAA
Il-1ß	CAACCAACAAGTGATATTCTCCATG	GATCCACACTCTCCAGCTGCA
Il-6	AGATAAGCTGGAGTCACAGAAGGAG	CGCACTAGGTTTGCCGAGTA
Il-10	ATTTGAATTCCCTGGGTGAGAAG	CACAGGGGAGAAATCGATGACA
Il-12	CACCCTTGCCCTCCTAAAC	CACCTGGCAGGTCCAGAG
Tnf	GTCCCCAAAGGGATGAGAAGTT	GTTTGCTACGACGTGGGCTACA
Bhlhe40	GATGTTCGGGTAGGAGATCCTTC	CGGAGCGAAGACAGCAAG
Cxcl13	CGGATTCAAGTTACGCCCC	CCATTTGGCACGAGGATTCAC
Pilra	CTGGATCTGCAAACCACAGTTG	CTCTCTTCTGGGGTTTTTAATCTC
Cd22	CAGGCTTCCAACGACATAGGC	GGGAGACTTTAGGGATGCGG
Tlr5	GATGGATGCTGAGTTCCCCC	GGCTATCCTGCCGTCTGAAG
Tlr8	GGCTACAGGACTTCATCCACA	CACTCTCTTCAAGGTGGTAGC
Cd209a	CAGTTGAAGGCTGGCGTAGA	ACAAGTTGAGCCCCCACATT
Xist	CCAGGGGAATAGCTCACC	GCCACTATTGCAGCAGCTTT
Cd93	CGGAGAATCAGTACAGCCCA	GTGGCTTCCCCCTCATCTAAG
Cd163	TGCCTCTGCTGTCACTAACG	TTCATTCATGCTCCAGCCGT
Cd276	ATCCAAGACAGCTCTACGGC	CTCAACACTGCCAGAGGGTG
Ccr2	GTTCAGCTGCCTGCAAAGAC	ATGCCGTGGATGAACTGAGG
Cd72	ACTGGCAGCATTCGATGAAC	TCAGAGTCCTGCCTCCACTT
Fcgr4	TCTGCTTCAGCAGCATGTGG	GGTCACGCTGTCTTCCTCAA

Table 2.7.1 List of qPCR primers used throughout this thesis.

2.8. Cloning

2.8.1. Cloning Plasmids

2.8.1.1. Overexpression Vector Layouts

Cloning vectors previously established in the lab were utilised for overexpression (80). Both vectors share the same backbone containing the coding sequence for ampicillin resistance, simian virus 40 (SV40) promoter and respective reporter genes under the control of the spleen focus forming virus (SFFV) promoter and the woodchuck hepatitis virus posttranscriptional regulatory element (WPRE) (Figure 2.8.1). A T2A peptide sequence, originally derived from *Thosea asigna* virus 2A (124) (Figure 2.8.1), allows for the generation of multiple separate proteins from a single mRNA sequence, transcribed from a single promoter (125). *XhoI* restriction enzyme cut site, located between the SFFV promotor and T2A peptide sequence, was utilised for gene insertion.

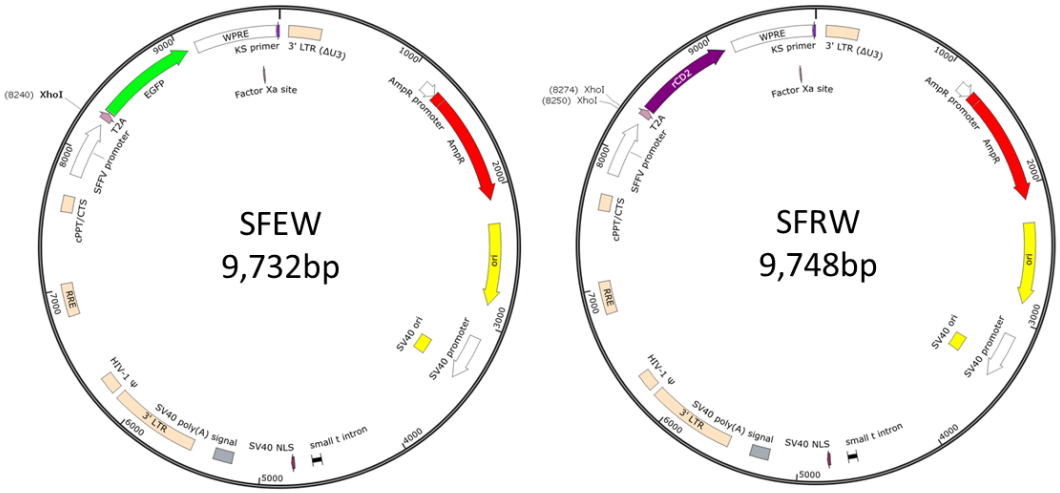

Figure 2.8.1: Plasmid maps of vectors utilised for overexpression cloning.

Both plasmids have the same backbone containing ampicillin resistance, SV40 promoter and respective reporter gene under the control of the SFFV promoter and WPRE. Restriction enzyme binding site for *XhoI* is indicated in both plasmids at between the SFFV promoter and T2A peptide sequence. SFEW plasmid's eGFP reporter is highlighted in green, and truncated rat-CD2 (rCD2) reporter in purple in the SFRW plasmid.

SFEW vector contains an enhanced green fluorescent protein (eGFP) reporter (Figure 2.8.1), a green fluorescent protein variant which contains chromophore mutations that make the protein 35 times brighter than wild-type GFP, originally derived from the jellyfish

Aequorea victoria, greatly increasing the sensitivity of the reporter (126). SFRW contains a truncated sequence for rat-CD2 (rCD2) reporter (Figure 2.8.1), where deletion of the cytoplasmic tail sequence prevents the ability to activate downstream kinases, whilst maintaining the extracellular portion of the rat CD2 protein allowing detection with a monoclonal antibody (127).

2.8.1.2. Lentivirus Vector Layout

Lentiviruses are enveloped retroviruses, derived from human immunodeficiency virus (HIV) (128). To increase the safety of lentivirus production, the components necessary for infectious viral particles are divided among multiple plasmids, referred to as a 2nd generation lentivirus (129). The HIV-1 packaging plasmid pCMV-Δ8.91, encodes viral capsid components of group antigens (gag), reverse transcriptase-polymerase (pol), trans-activator of transcription (tat) and regulator of expression of viron particles (rev), whilst the pMD2.G plasmid encodes the vesicular stomatitis virus G (VSV-G) envelope (130). Both plasmids are under a cytomegalovirus (CMV) enhancer and promotor (Figure 2.8.2).

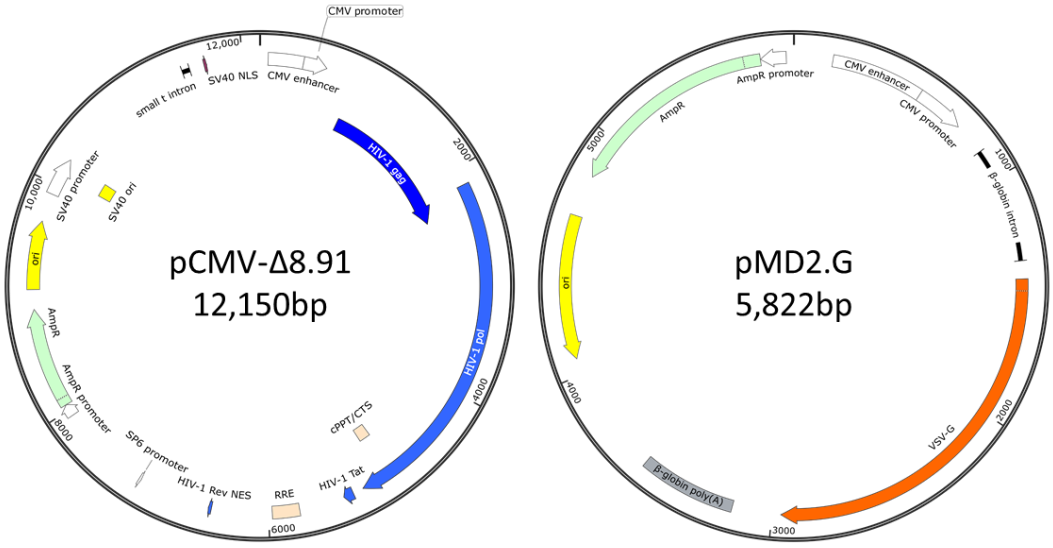

Figure 2.8.2: Plasmid maps for 2nd generation lentivirus production

HIV-1 viral capsid components of gag, pol, tat and rev (blue) are encoded in a single plasmid pCMV-Δ8.91. The VSV-G envelope (orange) is encoded by the pMD2.G plasmid, separating the necessary components to form infection viral particles and therefore a 2nd generation lentivirus. Cytomegalovirus (CMV) enhancer and promotor (white).

2.8.1.3. Preparation of Plasmid Stocks

In a 250 ml Erlenmeyer flask, 50 ml of sterile Luria Bertani (LB) broth (Sigma) containing 100 µg/ml of Ampicillin (Sigma) was prepared in a laminar flow cabinet. A clean pipette tip was used to scrape a small amount of the pre-existing plasmid glycerol stock into the flask, loosely covered with foil and incubated overnight at 37 °C at 225 rpm in a SI500 orbital shaking incubator (Stuart).

The next morning plasmid were extracted from the broth using the Plasmid Maxi Kit (Qiagen) as per manufacturer's direction utilising the QIAvac vacuum manifold (Qiagen). Plasmids were eluted in nuclease-free water (Thermofisher) and stored at -20 °C until required.

2.8.1.4. Linearisation of Plasmids

Plasmids were linearised by restriction enzyme *Xho*I (NEB) in 1X CutSmart® buffer (NEB). Where 3 µg of plasmid with excess *Xho*I (100 units), resulting in final reaction volume of 50 µl as per manufacturer's instructions in a 0.2 ml PCR tube (Starlab). The reaction was incubated at 37 °C for 1 hour before the enzyme was heat inactivated at 65 °C for 20 min in a Mastercycler® Nexus Gradient PCR machine (Eppendorf), alongside a no enzyme control reaction.

Linearisation was confirmed on 1% agarose gel as described in section 2.3, and linearised plasmid was extracted from the gel with a scalpel and purified using the NucleoSpin™ PCR clean-up kit (Macherey-Nagel) and eluted in nuclease-free water. The linearised vector was then stored at -20 °C until required.

2.8.2. Insert Preparations

RNA was obtained from whole peritoneal lavage and isolated as described in 2.7. Complementary DNA (cDNA) was generated using the Precision™ Reverse-Transcription Premix 2 kit (PrimerDesign), as per manufacturer's instructions. 20 µl of the Premix was added to a 0.2 ml PCR reaction tube (Starlab) along with 1 µg RNA. These samples were then heated in the Mastercycler® Nexus Gradient (Eppendorf) as described in Figure 2.8.3.

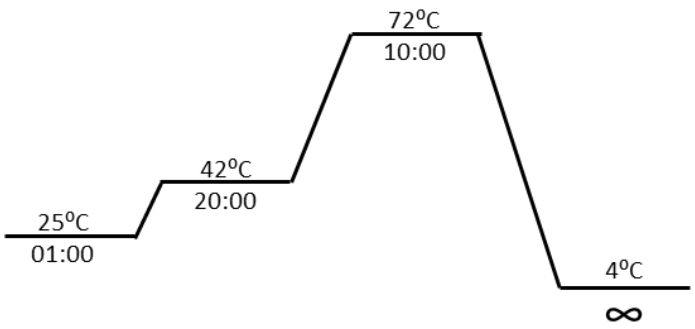

Figure 2.8.3 Schematic of Precision™ Reverse-Transcription Premix 2 kit PCR

2.8.4. Cloning PCR

Primers were designed for In-Fusion® cloning system (Takara Bio) (Figure 2.8.4A), where gene specific primers contain a 15bp overhang correspond to vector specific sequence. The forward primer included insertion of a Kozak sequence (131), between the preserved *XhoI* cut site and gene complementary DNA (cDNA) sequence (Figure 2.8.4B). The Kozak sequence is required to improve translation through ribosome binding (132).

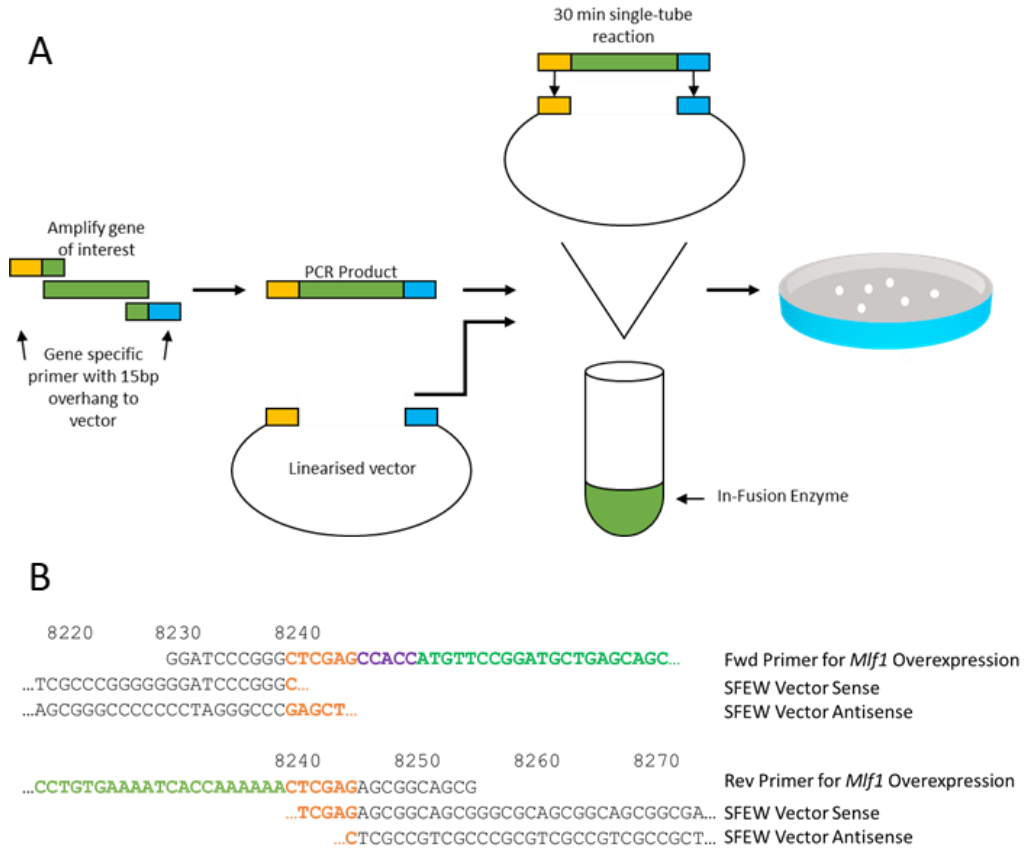

Figure 2.8.4. Schematic diagram of In-Fusion® cloning workflow.

A) From Left to Right: Amplification of PCR product with specific primers for cDNA target with 15bp overlap at the termini of the cloning insert and linearized cloning vector. Linearized vector combined with PCR product and In-Fusion® enzyme, where overhangs are annealed at the sites of complementarity, and the recombinant circular construct is rescued in *E. coli*. Bacterial transformation and colony plating. Image adapted from Takara Bio. B) Design of In-Fusion® cloning system primers for *Mlf1* overexpression in SFEW Vector, *Xho1* cut site (orange), insertion of Kozak sequence (purple) and *Mlf1* CCDS (green), demonstrating preservation of vector reading frame.

2.8.5. Transformation and Colony Selection

In-Fusion® (Takara) enzyme was combined with amplified gene PCR product and 200ng linerised cloning vector at a molar ratio of 2:1 respectively and underwent a single 30 min reaction at 50°C (Figure 2.8.4).

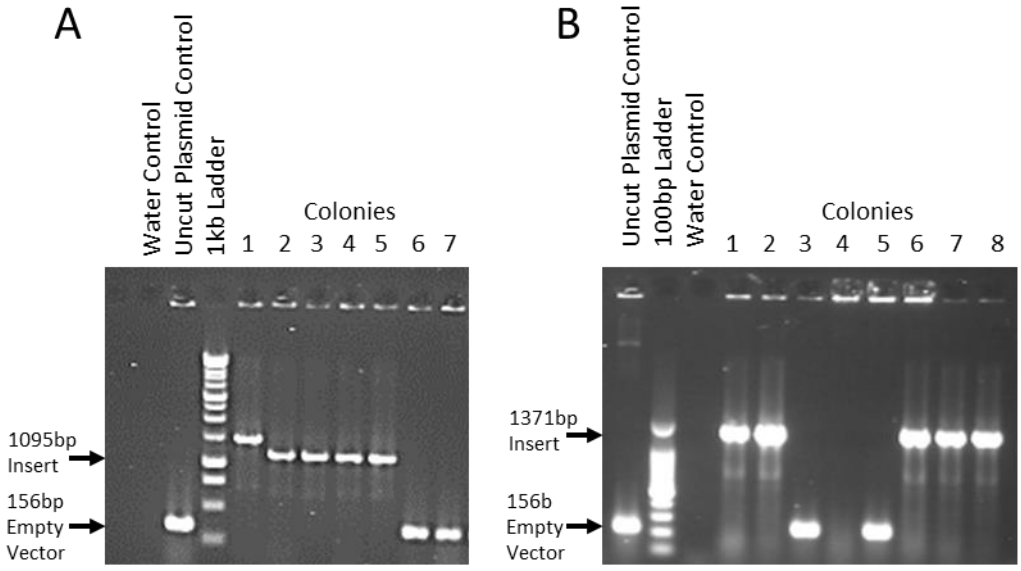

Figure 2.8.5: Colony PCR of picked colonies from *Mlf1* and *Maf* in SFEW vector, transformed in Stellar™ competent cells.

A) Colony PCR analysis of *Mlf1* clones in SFEW vector. Colony PCRs were run on a 1% (w/v) agarose gel with water control, an uncut plasmid transformed colony control and 1kb DNA ladder (Promega). Colonies 2-5 indicated a colony of predicted size, whilst colony 1 demonstrates a colony with larger than expected insert, and possibly a splice variant. Colonies 6 and 7 indicate colonies containing reannealed or uncut vector. B) Colony PCR analysis of codon optimised *Maf* clones in SFEW vector. Colonies shown are run on a 1% (w/v) agarose gel with water control, an uncut plasmid transformed colony control and 100bp DNA ladder (Promega). Colonies 1,2 and 6-8 demonstrate colonies of predicted size. Colonies 3 and 5 demonstrate reannealed or uncut vector colonies, along with a failed PCR reaction in colony 4.

Stellar™ competent cells (an *E. coli* HST08 strain) have a high transformation efficiency and were employed for bacteria transformation. Transformed bacteria were grown overnight on agar plates containing ampicillin as a selection pressure. Colonies were picked with a 10 µl pipette tip and added to PCR reaction mix. Primers were designed to match vector sequence on either side of *XhoI* cut site, permitting the production of a band of 156bp on a 1% (w/v) agarose if no insert was present (Figure 2.8.5). The addition of the

Mlf1 and *Maf* cDNA accompanied with the inserted Kozak sequence and preserved *XhoI* cut sites at both the 5' and 3' ends of the cDNA results in bands of 1095bp (Figure 2.8.5A) and 1371bp (Figure 2.8.5B) for each respective gene.

For each plasmid 2-3 colonies matching expected band size were cultured in LB broth with 100 µg/ml ampicillin selection (Sigma) pressure overnight in a shaking incubator. Midiprep (Sigma) isolated plasmids were sent to an external company for DNA sanger sequencing. Colonies containing the correct DNA sequence were then taken forward to produce lentiviruses.

2.9. Lentivirus Production

2.9.1. Transfection of Lentiviruses

Effectene® transfection reagent is a cationic non-liposomal lipid reagent (Qiagen). In conjunction with an enhancer buffer and a DNA-condensation buffer, plasmid DNA is condensed and coated with Effectene® micelle structures, allowing transfer of DNA into eukaryotic cells (133). The two lentiviral plasmids, pCMV-Δ8.91 and pMD2.G, with the transfer plasmid containing the gene of interest were combined at a ratio of 1.5:1:2 respectively with Effectene® transfection buffers. This was added to HEK 293T cells (134) for 48hrs.

2.9.2. Virus Purification by Sucrose Density

Media was removed from transfected HEK 293T flask after 48hrs and passed through a 0.45 µm syringe filter (Sartorius). Fresh media was added to the transfected HEK 293T cell, and an additional collection was made after 24hrs. The supernatant was transferred into a 31.5 ml thin-walled polypropylene konical tube (Beckman Coulter) and 3 ml of 20 % (w/v) sucrose solution was underlaid. The tubes were then centrifuged at 26,000 rpm for 90 minutes at 4 °C in a SW28Ti ultracentrifuge rotor in an Optima XPN-80 Ultracentrifuge (Beckman Coulter). Following ultracentrifugation media was removed and the tubes were inverted for 10 minutes to remove remaining liquid. Viral pellet was resuspended in 1 ml Aim V™ media (Thermofisher) and then aliquoted and stored at -80 °C (135).

2.9.3. Lentivirus Titres

Early studies demonstrated that a recombinant HIV-1 vector could efficiently introduce genes of interest into cultured human Jurkat leukemic T-cell line (136). Viral titres were performed to allow comparison between viral preparations. Flow cytometry was utilised to quantify viral infection through GFP mean fluorescent intensity (MFI) and percentage of GFP+ cells (Figure 2.9.1).

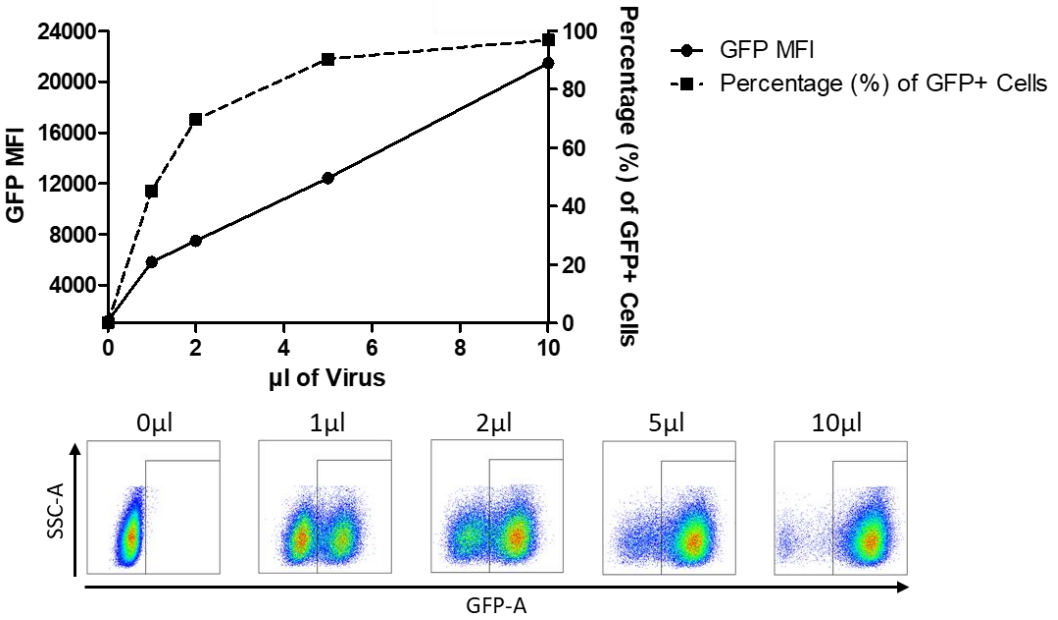

Figure 2.9.1: Lentiviral titre in Jurkat leukemic T-cell line.

Quantification of viral infection through GFP mean fluorescent intensity (MFI) and percentage of GFP+ cells. Example of flow cytometry plots of GFP expression obtained with in increasing dosage of lentivirus. Data displayed here is typical of all viral vector preparations produced in this thesis.

2.10. RNA Sequencing

2.10.1. Quality Control of RNA of Naïve Microglia

Prior to RNA-Sequencing library preparation the nucleic acid concentration and RNA Integrity Number (RIN) was calculated on a Bioanalyzer 2010 pico chip (Agilent Technologies) by CBS (Table 2.10.1). RIN is an algorithm for assigning integrity values to RNA measurements, from 1 (highly degraded) to 10 (highest integrity) (137). Library preparation was undertaken by Wales Gene Park.

	Genotype	Age	Sex	Nucleic Acid Conc.(ng/µl)	RIN
Sample 1	$Maf^{fl/fl}$ $Cx3cr1^{Cre/+}$	6.3 wks	Female	12.54	9.1
Sample 2	$Maf^{fl/fl}$ $Cx3cr1^{Cre/+}$	6.3 wks	Female	13.4	8.5
Sample 3	$Maf^{fl/fl}$ $Cx3cr1^{+/+}$	5.9 wks	Female	3.66	7.9
Sample 4	$Maf^{fl/fl}$ $Cx3cr1^{+/+}$	7.0 wks	Female	2.97	8.0

Table 2.10.1 Quality control of RNA obtained from Microglia for RNA-sequencing.

Prior to library construction samples were run on a on a Bioanalyzer 2010 pico chip to determine Nucleic Acid concentration (ng/µl) and RNA Integrity Number (RIN) for each sample before proceeding. Age, genotype, and sex of each sample are listed in the table.

2.10.2. Quality Control of Sequencing of Naïve Microglia

Raw sequencing sample FASTQ files were processed using Supercomputing Wales (SCW) to index, trim adapters, map reads, mark duplicates and generate feature counts. Quality control of samples were analysed at multiple stages throughout these processes. Single samples were split across two lanes to increase read counts and depth of sequencing, resulting in two raw files for each sample (Table 2.10.2) which were ultimately combined in the processing pipeline.

Illumina adapters are often found in RNA-sequencing data, and trimmed during analysis to increase the quality and reliability of downstream analysis (138). Trimming can also remove low quality bases, leading to a decrease in the number of reads, but an increase the proportion of mappable reads (138). Illumina adapters were removed prior to mapping, amounting to less than 0.1% of total basepairs removed (Table 2.10.3).

Marked duplicates are computationally defined by their mapping position, which does not distinguish between PCR-duplicates or biological duplicates. Computational removal of duplicates does not improve accuracy or precision in the analysis, and has been demonstrated to worsen statistical power and the False Discovery Rate (FDR/Adjusted P-value) for differential gene expression analysis (139) (Table 2.10.3).

Trimming	Sample1	(%)	Sample1_2	(%)	Sample2	(%)	Sample2_2	(%)
Total Reads Processed	53,585,197	NA	53,585,197	NA	38,356,744	NA	38,356,744	NA
Reads with Adapters	19,433,092	36.3	17,836,536	33.3	14,742,192	38.4	13,433,881	35
Reads Written (Passing Filters)	53,585,197	100	53,585,197	100	38,356,744	100	38,356,744	100
Total Basepairs Processed	5,412,104,897	NA	5,412,104,897	NA	3,874,031,144	NA	3,874,031,144	NA
Quality-Trimmed	2,557,972	0	5,853,106	0.1	1,676,108	0	5,278,470	0.1

Trimming	Sample3	(%)	Sample3_2	(%)	Sample4	(%)	Sample4_2	(%)
Total Reads Processed	42,636,747	NA	42,636,747	NA	41,317,941	NA	41,317,941	NA
Reads with Adapters	15,051,447	35.3	14,431,526	33.8	15,989,893	38.7	15,270,971	37
Reads Written (Passing Filters)	42,636,747	100	42,636,747	100	41,317,941	100	41,317,941	100
Total Basepairs Processed	4,306,311,447	NA	4,306,311,447	NA	4,173,112,041	NA	4,173,112,041	NA
Quality-Trimmed	2,126,227	0	5,514,040	0.1	1,604,602	0	4,535,462	0.1

Table 2.10.2 Quality Control of raw RNA-sequencing sample reads following trimming of adapter sequences.

Mapping	Sample1	(%)	Sample2	(%)	Sample3	(%)	Sample4	(%)
Total Reads	105,994,938		75,364,264		85,005,957		81,987,015	
Mapped Reads	98,238,200	92.68	69,934,194	92.80	80,258,346	94.42	75,978,033	92.67
Forward Strand	56,875,625	53.66	40,396,915	53.60	44,876,646	52.79	43,997,753	53.66
Reverse Strand	49,119,313	46.34	34,967,349	46.40	40,129,311	47.21	37,989,262	46.34
Failed QC	0	0	0	0	0	0	0	0
Duplicates	53,755,494	50.72	30,717,448	40.76	46,347,958	54.52	37,275,664	45.47
Paired-end Reads	105,994,938	100	75,364,264	100	85,005,957	100	81,987,015	100
'Proper-pairs'	98231694	92.68	69,927,586	92.79	80,250,344	94.41	75,972,956	92.67
Singletons	6,506	0.00	6,608	0.01	8,002	0.01	5,077	0.01

Table 2.10.3 Quality control of processed RNA-sequencing samples following marked duplicates and mapping.

2.10.3. Quality Control of RNA of Naïve Tissue Resident Macrophages

Prior to RNA-Sequencing library preparation the nucleic acid concentration, 260/280 ratio and RNA Integrity Number (RIN) was calculated on 4200 TapeStation (Agilent Technologies) (Table 2.10.4). RIN calculation and library preparation was undertaken by Wales Gene Park.

	Genotype	Age	Sex	Nucleic Acid Conc.(ng/µl)	260/280 Ratio	RIN
Sample 1	$Maf^{fl/fl}$ $Cx3cr1^{Cre/+}$	8.4wks	Female	39.0	1.95	9.0
Sample 2	$Maf^{fl/fl}$ $Cx3cr1^{+/+}$	8.4wks	Female	57.0	2.03	9.3
Sample 3	$Maf^{fl/fl}$ $Cx3cr1^{+/+}$	7.4wks	Female	147.2	1.94	9.3
Sample 4	$Maf^{fl/fl}$ $Cx3cr1^{Cre/+}$	7.4wks	Female	138.3	1.99	9.5
Sample 5	$Maf^{fl/fl}$ $Cx3cr1^{+/+}$	7.4wks	Male	120.5	1.95	9.7
Sample 6	$Maf^{fl/fl}$ $Cx3cr1^{Cre/+}$	7.4wks	Male	219.0	2.04	9.6

Table 2.10.4 Quality control of RNA obtained from peritoneal tissue resident macrophages for RNA-sequencing.

Prior to library construction samples were run on a 4200 TapeStation to determine Nucleic Acid concentration (ng/µl), 260/280 ratio (as indication of purity), RNA Integrity Number (RIN) for each sample before proceeding. Age, genotype, and sex of each sample are listed in the table.

2.10.4. Quality Control of Sequencing of Naïve Tissue Resident Macrophages

As described previously in 2.10.2, Illumina adapters were removed prior to mapping, amounting to less than 0.1% of total basepairs removed (Table 2.10.5). The two raw files for each sample (Table 2.10.5) were ultimately combined in the processing pipeline. Across the six samples marked duplicates were identified but not removed from the analysis (Table 2.10.6).

Trimming	Sample1	(%)	Sample1_2	(%)	Sample2	(%)	Sample2_2	(%)	Sample3	(%)	Sample3_2	(%)
Total Reads Processed	33,559,787		33,559,787		40,539,659		40,539,659		37,185,382		37,185,382	
Reads with Adapters	11,543,746	34.40	10,582,944	31.50	14,024,853	34.60	12,959,145	32.00	13,056,251	35.10	12,163,945	32.70
Reads Written (Passing Filters)	33,559,787	100.00	33,559,787	100.00	40,539,659	100.00	40,539,659	100.00	37,185,382	100.00	37,185,382	100.00
Total Basepairs Processed	3,389,538,487		3,389,538,487		4,094,505,559		4,094,505,559		3,755,723,582		3,755,723,582	
Quality-Trimmed	2,326,553	0.10	4,003,481	0.10	3,130,531	0.10	4,142,351	0.10	2,881,323	0.10	3,638,884	0.10

Trimming	Sample4	(%)	Sample4_2	(%)	Sample5	(%)	Sample5_2	(%)	Sample6	(%)	Sample6_2	(%)
Total Reads Processed	33,273,112		33,273,112		39,353,265		39,353,265		37,759,159		37,759,159	
Reads with Adapters	11,553,575	34.70	10,904,994	32.80	13,950,260	35.40	13,139,501	33.40	13,055,040	34.60	12,142,516	32.20
Reads Written (Passing Filters)	33,273,112	100.00	33,273,112	100.00	39,353,265	100.00	39,353,265	100.00	37,759,159	100.00	37,759,159	100.00
Total Basepairs Processed	3,360,584,312		3,360,584,312		3,974,679,765		3,974,679,765		3,813,675,059		3,813,675,059	
Quality-Trimmed	3,124,966	0.10	3,596,565	0.10	2,744,977	0.10	4,252,697	0.10	2,732,823	0.10	4,223,778	0.10

Table 2.10.5 Quality Control of raw RNA-sequencing sample reads following trimming of adapter sequences.

Mapping	Sample1	(%)	Sample2	(%)	Sample3	(%)	Sample4	(%)	Sample5	(%)	Sample6	(%)
Total Reads	66,372,698		80,918,604		74,029,332		66,459,420		78,287,218		75,055,771	
Mapped Reads	57,238,120	86.24	66,914,761	82.69	61,373,761	82.90	55,954,822	84.19	66,573,175	85.04	63,517,645	84.63
Forward Strand	37,753,531	56.88	47,461,033	58.65	43,342,363	58.55	38,481,867	57.90	45,000,526	57.48	432,967,42	57.69
Reverse Strand	28,619,167	43.12	33,457,571	41.35	30,686,969	41.45	27,977,553	42.10	33,286,692	42.52	31,759,029	42.31
Failed QC	0	0.00	0	0.00	0	0.00	0	0.00	0	0.00	0	0.00
Duplicates	19,457,856	29.32	25,048,535	30.96	19,802,700	26.75	17,252,402	25.96	21,108,170	26.96	21,266,703	28.33
Paired-end Reads	66,372,698	100.00	80,918,604	100.00	74,029,332	100.00	66,459,420	100.00	78,287,218	100.00	75,055,771	100.00
'Proper-pairs'	57,234,436	86.23	66,910,820	82.69	61,370,540	82.90	55,951.238	84.19	66,568,850	85.03	63,513,206	84.62
Singletons	3,684	0.01	3,941	0.00	3,221	0.00	3,584	0.01	4,325	0.01	4,439	0.01

Table 2.10.6 Quality Control of processed RNA-sequencing samples following marked duplicates and mapping.

2.10.5. Quality Control of RNA from Zymosan Treated Resident Peritoneal Macrophages

Prior to RNA-Sequencing library preparation the nucleic acid concentration, 260/280 nm ratio and RNA Integrity Number (RIN) was calculated on 4200 TapeStation (Agilent Technologies) (Table 2.10.7).

	Genotype	Age	Sex	Nucleic Acid Conc.(ng/µl)	260/280 Ratio	RIN
Sample 1	$Maf^{fl/fl}$ $Cx3cr1^{Cre/+}$	7.7wks	Female	146	2.0	9.6
Sample 2	$Maf^{fl/fl}$ $Cx3cr1^{Cre/+}$	7.7wks	Female	81.9	2.0	9.5
Sample 3	$Maf^{fl/fl}$ $Cx3cr1^{+/+}$	6.9wks	Female	102	2.0	9.7
Sample 4	$Maf^{fl/fl}$ $Cx3cr1^{+/+}$	6.9wks	Female	142	2.5	9.7
Sample 5	$Maf^{fl/fl}$ $Cx3cr1^{+/+}$	6.9wks	Female	31.4	1.8	8.7
Sample 6	$Maf^{fl/fl}$ $Cx3cr1^{+/+}$	6.9wks	Female	42.2	1.9	9.4

Table 2.10.7 Quality Control of RNA obtained from peritoneal tissue resident macrophages for RNA-sequencing.

Prior to library construction samples were run on a 4200 TapeStation to determine Nucleic Acid concentration (ng/µl), 260/280 ratio (as indication of purity), RNA Integrity Number (RIN) for each sample before proceeding. Age, genotype, and sex of each sample are listed in the table.

2.10.6. Quality Control of Sequencing of Zymosan Treated Tissue Resident Macrophages

As described previously in 2.10.2, Illumina adapters were removed prior to mapping, amounting to less than 0.1% of total basepairs removed (Table 2.10.8). The two raw files for each sample (Table 2.10.8) were ultimately combined in the processing pipeline. Across the six samples marked duplicates were identified but not removed from the analysis (Table 2.10.9).

Trimming	Sample1	(%)	Sample1_2	(%)	Sample2	(%)	Sample2_2	(%)	Sample3	(%)	Sample3_2	(%)
Total Reads Processed	43,538,249		43,538,249		41,220,132		41,220,132		77,213,878		77,213,878	
Reads with Adapters	16,999,354	39	15,700,892	36.1	14,855,546	36	14,362,495	34.8	28,290,094	36.6	26,983,077	34.9
Reads Written (Passing Filters)	43,538,249	100	43,538,249	100	41,220,132	100	41,220,132	100	77,213,878	100	77,213,878	100
Total Basepairs Processed	4,397,363,149		4,397,363,149		4,163,233,332		4,163,233,332		7,798,601,678		7,798,601,678	
Quality-Trimmed	3,263,753	0.1	4,647,485	0.1	2,183,573	0.1	4,174,171	0.1	4,615,080	0.1	7,052,938	0.1

Trimming	Sample4	(%)	Sample4_2	(%)	Sample5	(%)	Sample5_2	(%)	Sample6	(%)	Sample6_2	(%)
Total Reads Processed	61,680,575		61,680,575		53,252,605		53,252,605		65,485,130		65,485,130	
Reads with Adapters	23,281,519	37.7	22,594,895	36.6	20,333,434	38.2	19,638,652	36.9	23,630,128	36.1	22,716,978	34.7
Reads Written (Passing Filters)	61,680,575	100	61,680,575	100	53,252,605	100	53,252,605	100	65,485,130	100	65,485,130	100
Total Basepairs Processed	6,229,738,075		6,229,738,075		5,378,513,105		5,378,513,105		6,613,998,130		6,613,998,130	
Quality-Trimmed	3,168,772	0.1	6,470,451	0.1	3,055,341	0.1	5,517,576	0.1	3,366,588	0.1	7,099,237	0.1

Table 2.10.8 Quality Control of raw RNA-sequencing sample reads following trimming of adapter sequences.

Mapping	Sample1	(%)	Sample2	(%)	Sample3	(%)	Sample4	(%)	Sample5	(%)	Sample6	(%)
Total Reads	86,646,574		82,283,072		154,119,261		122,976,080		106,229,711		130,524,724	
Mapped Reads	67,352,774	77.73	72,431,394	88.03	131,826,635	85.54	108,756,012	88.44	94,938,017	89.37	114,670,600	87.85
Forward Strand	52,969,843	61.13	46,067,217	55.99	88,205,679	57.23	68,597,788	55.78	58,760,564	55.31	73,189,087	56.07
Reverse Strand	33,676,731	38.87	36,215,855	44.01	65,913,582	42.77	54,378,292	44.22	47,469,147	44.69	57,335,637	43.93
Failed QC	0	0.00	0	0.00	0	0.00	0	0.00	0	0.00	0	0.00
Duplicates	30,642,486	35.36	25,206,449	30.63	56,575,904	36.71	39,935,640	32.47	32,579,521	30.67	43,484,242	33.31
Paired-end Reads	86,646,574	100.00	82,283,072	100.00	154,119,261	100.00	122,976,080	100.00	106,229,711	100.00	130,524,724	100.00
'Proper-pairs'	67,349,512	77.73	72,427,330	88.02	131,821,158	85.53	108,750,134	88.43	94,932,292	89.37	114,663,034	87.85
Singletons	3,262	0.00	4,064	0.00	5,477	0.00	5,878	0.00	5,725	0.01	7,566	0.01

Table 2.10.9 Quality Control of processed RNA-sequencing samples following marked duplicates and mapping.

2.10.7. Quality Control of RNA from Zymosan Treated Peritoneal Inflammatory Macrophages

RNA extractions were performed from matched inflammatory macrophages of the same mice as those in 2.10.5, prior to RNA-Sequencing library preparation the nucleic acid concentration, 260/280 nm ratio and RNA Integrity Number (RIN) was calculated on 4200 TapeStation (Agilent Technologies) (Table 2.10.10).

	Genotype	Age	Sex	Nucleic Acid Conc.(ng/µl)	260/280 Ratio	RIN
Sample 1	$Maf^{fl/fl}$ $Cx3cr1^{Cre/+}$	7.7wks	Female	23.9	1.6	9.0
Sample 2	$Maf^{fl/fl}$ $Cx3cr1^{Cre/+}$	7.7wks	Female	11.3	2.6	7.1
Sample 3	$Maf^{fl/fl}$ $Cx3cr1^{+/+}$	6.9wks	Female	41.8	2.6	9.3
Sample 4	$Maf^{fl/fl}$ $Cx3cr1^{+/+}$	6.9wks	Female	16.4	2.5	8.4
Sample 5	$Maf^{fl/fl}$ $Cx3cr1^{+/+}$	6.9wks	Female	13.3	1.9	8.0
Sample 6	$Maf^{fl/fl}$ $Cx3cr1^{+/+}$	6.9wks	Female	15.6	1.6	7.9

Table 2.10.10 Quality Control of RNA obtained from peritoneal inflammatory macrophages for RNA-sequencing.

Prior to library construction samples were run on a 4200 TapeStation to determine Nucleic Acid concentration (ng/µl), 260/280 ratio (as indication of purity), RNA Integrity Number (RIN) for each sample before proceeding. Age, genotype, and sex of each sample are listed in the table.

2.10.8. Quality Control of Sequencing of Zymosan Treated Inflammatory Macrophages

Across the twelve reads on average 33.12 ± 0.53% (Mean ± SEM) contained Illumina adapters, and these were removed prior to mapping, amounting to less than 0.1% of total basepairs removed (Table 2.10.11).

The two raw files for each sample (Table 2.10.11) were ultimately combined in the processing pipeline. Across the six samples on average 32.16 ± 1.09% (Mean ± SEM) displayed marked duplicates but were not removed from the analysis (Table 2.10.11).

Trimming	Sample1	(%)	Sample1_2	(%)	Sample2	(%)	Sample2_2	(%)	Sample3	(%)	Sample3_2	(%)
Total Reads Processed	48,787,621	NA	48,787,621	NA	51,649,739	NA	51,649,739	NA	49,964,242	NA	48,787,621	NA
Reads with Adapters	17,431,646	35.7	16,659,523	34.1	19,586,827	37.9	18,394,468	35.6	19,752,013	39.5	17,431,646	35.7
Reads Written (Passing Filters)	48,787,621	100	48,787,621	100	51,649,739	100	51,649,739	100	49,964,242	100	48,787,621	100
Total Basepairs Processed	4,927,549,721	NA	4,927,549,721	NA	5,216,623,639	NA	5,216,623,639	NA	5,046,388,442	NA	4,927,549,721	NA
Quality-Trimmed	3,991,290	0.1	7,047,919	0.1	2,478,043	0	7,423,584	0.1	2,515,331	0	3,991,290	0.1

Trimming	Sample4	(%)	Sample4_2	(%)	Sample5	(%)	Sample5_2	(%)	Sample6	(%)	Sample6_2	(%)
Total Reads Processed	49,964,242	NA	49,885,259	NA	49,885,259	NA	50,077,775	NA	50,077,775	NA	66,169,789	NA
Reads with Adapters	18,736,425	37.5	19,210,515	38.5	17,646,673	35.4	19,692,054	39.3	18,216,169	36.4	22,807,296	34.5
Reads Written (Passing Filters)	49,964,242	100	49,885,259	100	49,885,259	100	50,077,775	100	50,077,775	100	66,169,789	100
Total Basepairs Processed	5,046,388,442	NA	5,038,411,159	NA	5,038,411,159	NA	5,057,855,275	NA	5,057,855,275	NA	6,683,148,689	NA
Quality-Trimmed	6,280,667	0.1	2,345,710	0	7,783,876	0.2	2,399,827	0	6,052,343	0.1	3,964,394	0.1

Table 2.10.11 Quality Control of raw RNA-sequencing sample reads following trimming of adapter sequences.

Mapping	Sample1	(%)	Sample2	(%)	Sample3	(%)	Sample4	(%)	Sample5	(%)	Sample6	(%)
Total Reads	97,234,142		102,684,051		99,026,084		98,180,780		98,535,209		132,065,786	
Mapped Reads	83,307,650	85.68	92,878,805	90.45	88,600,032	89.47	87,006,942	88.62	88,206,041	89.52	112,796,984	85.41
Forward Strand	55,580,022	57.16	56,244,383	54.77	54,725,861	55.26	54,676,740	55.69	54,432,014	55.24	75,666,786	57.29
Reverse Strand	41,654,120	42.84	46,439,668	45.23	44,300,223	44.74	43,504,040	44.31	44,103,195	44.76	56,399,000	42.71
Failed QC	0	0.00	0	0.00	0	0.00	0	0.00	0	0.00	0	0.00
Duplicates	27,178,514	27.95	31,230,897	30.41	30,930,880	31.24	32,365,639	32.97	32,291,903	32.77	47,334,369	35.84
Paired-end Reads	97,234,142	100.00	102,684,051	100.00	99,026,084	100.00	98,180,780	100.00	98,535,209	100.00	132,065,786	100.00
'Proper-pairs'	83,296,238	85.67	92,869,764	90.44	88,593,252	89.46	86,997,774	88.61	88,200,588	89.51	112,789,572	85.40
Singletons	11,412	0.01	9,041	0.01	6,780	0.01	9,168	0.01	5,453	0.01	7,412	0.01

Table 2.10.12 Quality Control of processed RNA-sequencing samples following marked duplicates and mapping.

2.11. Immunofluorescence and Morphological Analysis

2.11.1. Brain Extraction and Sectioning

Animals were euthanised with an overdose of Euthatal® Solution (Merial Animal Health Ltd) administered by I.P., followed by intracardial perfusion-fixation with 50 ml ice cold 4 % PFA. Brains were removed from the skull and stored in a bijou containing 2 ml of 4 % PFA at 4 °C for 48 hr. Subsequently brains were transferred and stored in DPBS with 0.1 % Sodium Azide (Sigma) at 4 °C until further processing. Each brain was sectioned using Leica VT1200S Vibratome (Leica Biosystems) into 50 µm-thick free-floating coronal sections and stored at 4 °C in DPBS with 0.1 % Sodium Azide.

2.11.2. Immunofluorescence Staining and Acquisition

Coronal sections from regions of interest were selected for each mouse utilising images from the Allen Mouse Brain Atlas (140) as a visual reference. Sections were washed with 1X Tris-buffered saline (TBS) (Fisher Scientific), then gently mixed on an orbital shaker for 1 hour at room temperature in Immunofluorescence Permeabilization and Block solution. Sections were washed with 1X TBS and transferred into Immunofluorescence Staining Solution containing primary antibodies (
Table 2.11.1) overnight at 4°C on an orbital shaker.

Target	Fluorophore	Dilution	Clone	Isotype	Supplier	Catalogue Number
GFAP	Unconjugated	1:1000	Polyclonal	Chicken IgY	Abcam	ab4674
Iba1	AF635	1:1000	Polyclonal	Rabbit	Wako	013-26471
NuEN	AF555	1:300	A60	Rat	Millipore	MAB377A5
Chicken IgY	FITC	1:200	Polyclonal	Goat	Abcam	ab46969

Table 2.11.1 List of Antibodies used for Immunoflourecence staining of coronal brain sections.

Sections were washed 3 times with 1X TBS and incubated for 2 hr at room temperature on an orbital shaker with secondary antibody in Immunofluorescence Staining Solution. Sections were washed with 1X TBS and counterstained for 10 minutes at room temperature with 500 ng/ml DAPI in DPBS. Sections were transferred to Menzel Gläser SuperFrost® Plus slides, and mounted with ProLong® Gold, prior to addition of a Menzel-Gläser #1 coverslip (0.13-0.16 mm) (all of the above Thermo Fisher Scientific). Slides were stored in the dark at 4 °C prior to imaging. Brain sections were imaged using a Cell

Observer Spinning Disk (Carl Zeiss Microscopy GmbH) confocal microscope with a 20x objective, and 0.49 µm Z-stacks were acquired.

2.12. Statistics and Analysis Software

2.12.1. Flow Cytometry and Imaging Flow Cytometry

All flow cytometry files were analysed using Flow Jo software (version 10.8.0; Beckton Dickinson). Data generated through imaging cytometry was analysed using IDEAS® software (version 6.3; Luminex), with inbuilt analysis wizards (Figure 2.12.1).

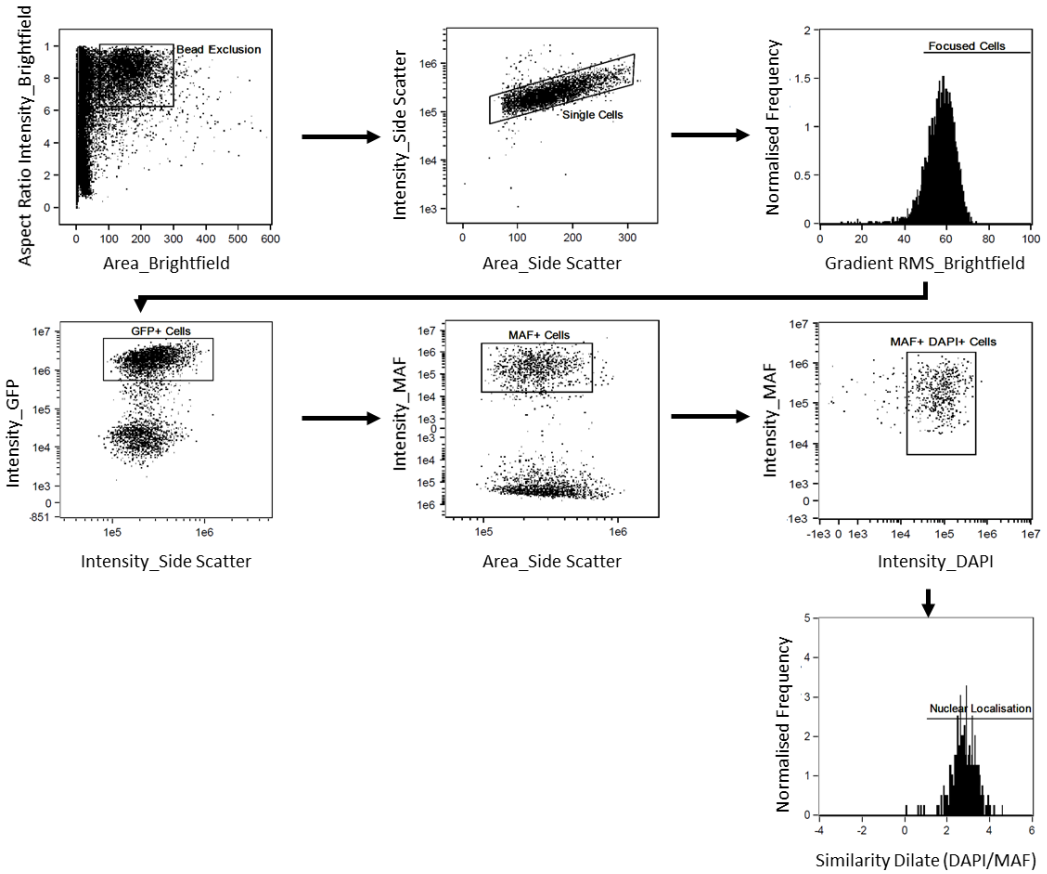

Figure 2.12.1 Gating strategy for the nuclear localization similarity wizard in Amnis ImageStreamX Mark II imaging flow cytometer IDEAS® software.

2.12.2. qPCR Analysis

40-ΔCT is calculated as 40 (the number of cycles) minus the difference in cycle threshold (delta-CT (ΔCT)) values, which is defined as the number of cycles required for the fluorescent signal to exceed background level, between that of the target gene and the CT value of the endogenous control (*Ywhaz*).

Relative quantification of fold change gene expression utilised the average ΔCT values of the biological replicates of the control group to create a 'Control Average', which is subtracted from the individual ΔCT to generate relative delta-delta CT (ΔΔCT), which is further converted to a log fold change (2^-(ΔΔCt)). Snap Gene version 5.3.2 was utilised for generation of plasmid maps.

2.12.3. Immunofluorescence Morphological Analyses

The central 30 optical sections of each z-stack were transformed into a frontal maximum-intensity orthogonal projection and used for the following analyses with Fiji Software (Fiji is just ImageJ).

2.12.3.1. Count and Area

After utilising the inbuilt "Background Subtraction" tool, Iba1 positive cells were manually counted using the "Cell Counter" plugin. Cell bodies partially outside the edges of the image were not included in the count analysis. Each image was subsequently converted to 8-bit format and Iba1 positive pixels were selected by applying a threshold to generate a binary image. The inbuilt "Measure" tool allowed the evaluation of area percentage covered by Iba1+ pixels.

2.12.3.2. Nearest Neighbour Distance

The 8-bit image was further analysed to obtain Nearest Neighbour Distance (NND) values. Two MorphoLibJ (141) plugin filters applied to the images. "Gray Scale Attribute" opening filter (Operation = "Opening", Attribute = "Area", Minimum Value = 25 pixels, Connectivity = 8) was utilised to isolate cells from background, followed by an opening "Morphological Filter" (Operation = "Opening", Element = "Octagon", Radius = 1 pixel) to separate the cell body from their ramifications.

Centroids were calculated for each cell body selecting a 30µm minimum size filter in the inbuilt "Analyse Particles" tool. Finally, the "NND" plugin was used to calculate the relative

values for all the identified cell bodies. All images were performed blinded to avoid any operator bias.

2.12.4. RNA-Sequencing Analyses

Pre-processing of raw sequencing sample FASTQ files was undertaken utilising the Supercomputing Wales (SCW) project, which is part-funded by the European Regional Development Fund (ERDF) via Welsh Government. A list of packages employed can be found in Table 2.12.1A.

A

Module	Version
STAR (25)	2.7.0e
Trim Galore (26)	0.6.4
Java	1.8
FastQC (27)	0.11.8
Picard	2.20.2
Java	1.8
Samtools	1.9
Bamtools	3.2.10
Subread	2.0.0

B

Module	Version
BiocParallel	1.24.1
biomaRt (28)	2.46.3
DESeq2 (29)	1.30.1
DEXSeq (30)	1.36.0
dplyr	1.0.7
edgeR (31)	3.32.1
Enhanced Volcano	1.8.0
ggplot2	3.3.5
pcaExplorer (32)	2.16.0
stringr	1.4.0
tidyr	1.1.4
tidyverse	1.3.1
VennDiagram	1.6.20
BiocParallel	1.24.1

Table 2.12.1 List of Modules and Packages used for RNA Sequencing data analysis.

A) List of modules employed on the Supercomputing Wales (SCW) platform for pre-processing of RNA Sequencing. B) List of packages employed in R for differential gene expression analysis and generation of graphical data from RNA Sequencing.

Differential gene expression analysis, subsequent analyses, and generation of graphical data from RNA Sequencing was undertaken in R version 4.0.5 (2021-03-31, “Shake and Throw”) programming language in RStudio (2021.09.0, build 351 "Ghost Orchid"). A list of packages employed can be found in Table 2.12.1B. DEXSeq required pre-analysis of FASTQ files on SCW utilising Python 3.6 and the inbuilt Python scripts of DEXSeq package.

Canonical pathway analysis and upstream pathway analysis was conducted on Ingenuity pathway analysis (IPA) (Qiagen).

2.12.5. Graphs and Statistics

Other than RNA Sequencing (2.12.4), all other graphs and statistical analyses were performed using GraphPad Prism (version 9.0.0). P-values of >0.05 were taken as non-significant (NS). P-values of <0.05 will be denoted with a single asterisk (*), P-values of <0.01 will be written as **, P-values of <0.001 as *** and p-value of <0.0001 as ****.

Chapter 3

Generation of Lentiviruses to Manipulate Expression of *Maf* and *Mlf1*

3.1. Introduction

3.1.1. Knockdown and Overexpression of *Maf* and *Mlf1* in *Mus Musculus*

Knockdown constructs have previously been published to study the role of *Maf* and *Mlf1* in several types of murine macrophage cell lines, predominately utilising small interfering RNAs (siRNAs) and short hairpins (shRNAs). Both siRNA and shRNA employ the same cellular mechanisms for the degradation of messenger RNA (mRNA) as endogenous micro-RNA (miRNA) (150).

siRNAs are a type of short non-coding, regulatory RNA involved in sequence-specific degradation of target mRNA in the RNA interference (RNAi) pathway. siRNAs are transiently expressed in the cytoplasm of transfected cells (151) and use endogenous RNA processing, either through loading into RNA-interfering silencing complex (RISC) directly or utilise a Dicer mediated process (152). Following RISC loading, siRNAs commence the RNAi process through targeting of mRNA cleavage and degradation (2). This in turn blocks further expression or accumulation of the target protein, leading to a decrease in its levels, and knockdown.

shRNAs have a hairpin structure that consist of a stem region of paired antisense and sense strands, connected by an unpaired nucleotide sequence that forms a hairpin loop. shRNAs can be stably integrated through virus-mediated transduction (153). The shRNA is transcribed by either RNA polymerase II or III (153) and the hairpin loop of the shRNA undergoes primary processing in the nucleus, before being transported to the cytoplasm, where the loop of the hairpin is processed off to form a double-stranded siRNA which can function as described above (154).

siRNAs have been exploited rather than shRNAs in the study of *Maf* in the RAW264.7 macrophage cell line (155,156), cultured peritoneal macrophages (155), tumour-associated macrophages (157) and bone marrow derived macrophages (BMDMs) (155,157). Overexpression constructs of *Maf* have been less well exploited and have utilised truncated sequences of *Maf* in RAW264.7 (100,158,159) and BMDMs (157). Whereas the opposite is true for *Mlf1*, with studies investigating the effects of overexpression constructs in NIH3T3 fibroblast (160), J2E murine erythroleukemia and M1 myeloblast cell lines (112), BMDMs (161), although as of yet has not been investigated by siRNA or shRNA knockdown approaches (162).

3.2. Chapter Aims

Commercial vectors for overexpression of either *Maf* or *Mlf1* were not available at the time of this study. Knockdown short hairpin (shRNA) plasmids for *Maf* and *Mlf1* were previously designed and validated in house by Dr. Natacha Ipseiz and by Dr. Magdalena Czubala respectively. Consequently the aims of this thesis chapter were…

- Generation of overexpression constructs for *Maf* and *Mlf1*.
- Knockdown and overexpression of *Maf* and *Mlf1* in Hoxb8 conditionally immortalised macrophage precursor (MØPs) cell lines and BMDMs using lentivirus delivery system.
- Validation of these constructs by mRNA expression analysis through quantitative PCR (qPCR) in MØP and BMDMs.
- Validate commercial antibodies and establish specific staining conditions for protein detection.
- Confirm manipulation of protein expression through flow cytometry in MØP and BMDMs.

3.3. Results

3.3.1. Cloning of *Maf* and *Mlf1* Overexpression Constructs

Overexpression constructs were utilised to validate *Maf* and *Mlf1* identification by mRNA and protein expression, with the possibility of use in functional studies. *Maf* and *Mlf1* coding sequence were initially amplified using the Phusion high-fidelity Taq polymerase, however this generated several nonspecific bands (Figure 3.3.1B). Combination of Phusion® at a ratio of 1:1 with lower fidelity Gotaq® (1–20 $\times 10^{-5}$ mutations/bp/template duplication) (20) resulted in loss of many of these nonspecific bands and enabled greater product yield of expected size at lower annealing temperatures (Figure 3.3.1B). However this combination of DNA polymerases would likely result in an increase in error rate, even though final plasmids are sequenced.

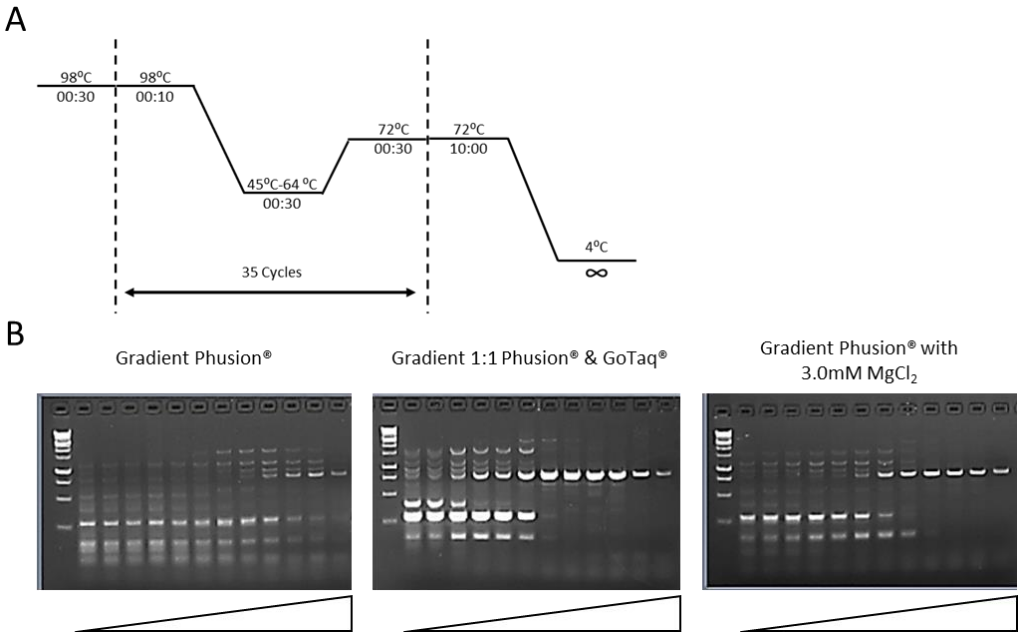

Figure 3.3.1: Optimisation of Phusion® high-fidelity DNA polymerase PCR for overexpression of *Mlf1* primers.

A) Thermocycler conditions for Phusion® high-fidelity DNA polymerase gradient PCR. B) Phusion® high-fidelity DNA polymerase gradient PCR (annealing temperature ranging from 45-64°C across 12 wells) on 2% (w/v) agarose gel *Mlf1* (expected band size 854 bp) with 1 kb DNA ladder (Promega), either as per manufacturer's instruction, with the addition of lower fidelity Gotaq® at a ratio of 1:1 or Phusion® high-fidelity DNA polymerase, or with an increased concentration of $MgCl_2$ to 3.0mM.

To preserve the low error rate of Phusion®, the concentration of $MgCl_2$ was increased to 3.0mM from the original 1.5mM provided in the Phusion® HF Buffer. Magnesium ions (Mg^{2+}) function as cofactors for DNA polymerases, enabling incorporation of deoxyribonucleotide triphosphates (dNTPs) (163). In addition, Mg^{2+} facilitate formation of the complex between the primers and cDNA template through stabilising the negative charges on the phosphate backbone. However high Mg^{2+} concentrations can result in nonspecific bands from this enhanced stability, including increased errors from misincorporation of dNTPs. The addition of $MgCl_2$ also reduced nonspecific bands and increased the strength of the expected size band at lower annealing temperatures when compared to that of 1.5mM $MgCl_2$ Phusion® HF Buffer mastermix (Figure 3.3.1B).

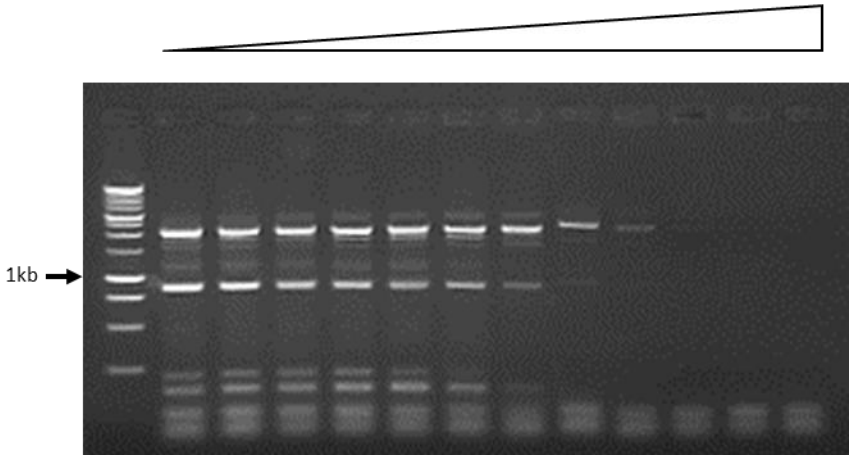

Figure 3.3.2: Phusion® high-fidelity DNA polymerase PCR for overexpression of *Maf* primers.

Analysis of Phusion® high-fidelity DNA polymerase gradient PCR with 3.0mM of $MgCl_2$ on 2% (w/v) agarose gel for *Maf* with 1kb DNA ladder (Promega), annealing temperature ranging from 45-64^{o}C across 12 wells (left to right).

Attempts to clone *Maf* under these optimised conditions concluded with a band below the expected size (1113 bp) and a band roughly twice the size (Figure 3.3.2). A faint band was observed of the correct size (Figure 3.3.2), however was insufficient to proceed with cloning. Ultimately it was decided to purchase the *Maf* sequence with the manufactured sequence was codon optimised (Appendix I). The purchased *Maf* sequence was used as a template and amplified from the supplied vector with Phusion® High-Fidelity DNA Polymerase as described above.

3.3.2. Validation of Constructs by Quantitative PCR (qPCR)

3.3.2.1. Short Hairpin (shRNA) Knockdown of *Maf*

Hoxb8 conditionally immortalised macrophage precursor (MØPs) cell lines offer an approach for *in vitro* generation of large numbers of mouse macrophages. MØPs are a macrophage precursor cell line, which when differentiated with either GM-CSF or M-CSF display a highly similar phenotype to dendritic-like cells or macrophages respectively (123). Many tissue resident macrophages resemble an M-CSF programmed macrophage, therefore M-CSF treated MOPs differentiated to macrophages and BMDMs were determined to be more a closely related macrophage phenotype than undifferentiated MØPs for this thesis.

To validate the constructs MØPs were stably transfected with the lentiviruses for overexpression of *Mlf1* and *Maf*, or with empty overexpression vector controls (135), shRNA sequences specific for *Mlf1* and *Maf*, or a non-silencing shRNA sequence control lentivirus. Vectors utilised for overexpression either encoded an enhanced GFP or truncated rat-CD2 (Figure 2.8.1). Cells were sorted using fluorescence-activated cell sorting (FACS Aria III) following infection through GFP+ cells or anti-Rat CD2 antibody labelling, to achieve a ≥95% infected cell line.

Maf shRNA lentiviral infected MØPs and the non-silencing shRNA control showed no significant difference in *Maf* expression to non-infected MØPs (Figure 3.3.3A), when using a one-way ANOVA analysis. *Maf* shRNA lentiviral infected M-CSF differentiated MØPs and the non-silencing shRNA control indicated no significant difference in *Maf* expression to non-infected in M-CSF differentiated MØPs (Figure 3.3.3B), when using a one-way ANOVA.

Bone marrow was obtained from C57BL/6 female mice aged 6-8 weeks and cultured with M-CSF for 7 days to obtain BMDMs (as described in Section 2.4.6), before infection with lentiviruses for 6 days whilst being maintained with M-CSF. Transfection efficiency was determined by confirmation of GPF or rCD2 by flow cytometry. Lentiviral transfected BMDMs derived from three C57BL/6 mice were combined for FACS, to obtain enough RNA for downstream qPCR. No significant differences were seen between the BMDM expressing *Maf* shRNA, non-silencing shRNA control or non-infected BMDMs (Figure 3.3.3C), when using a one-way ANOVA.

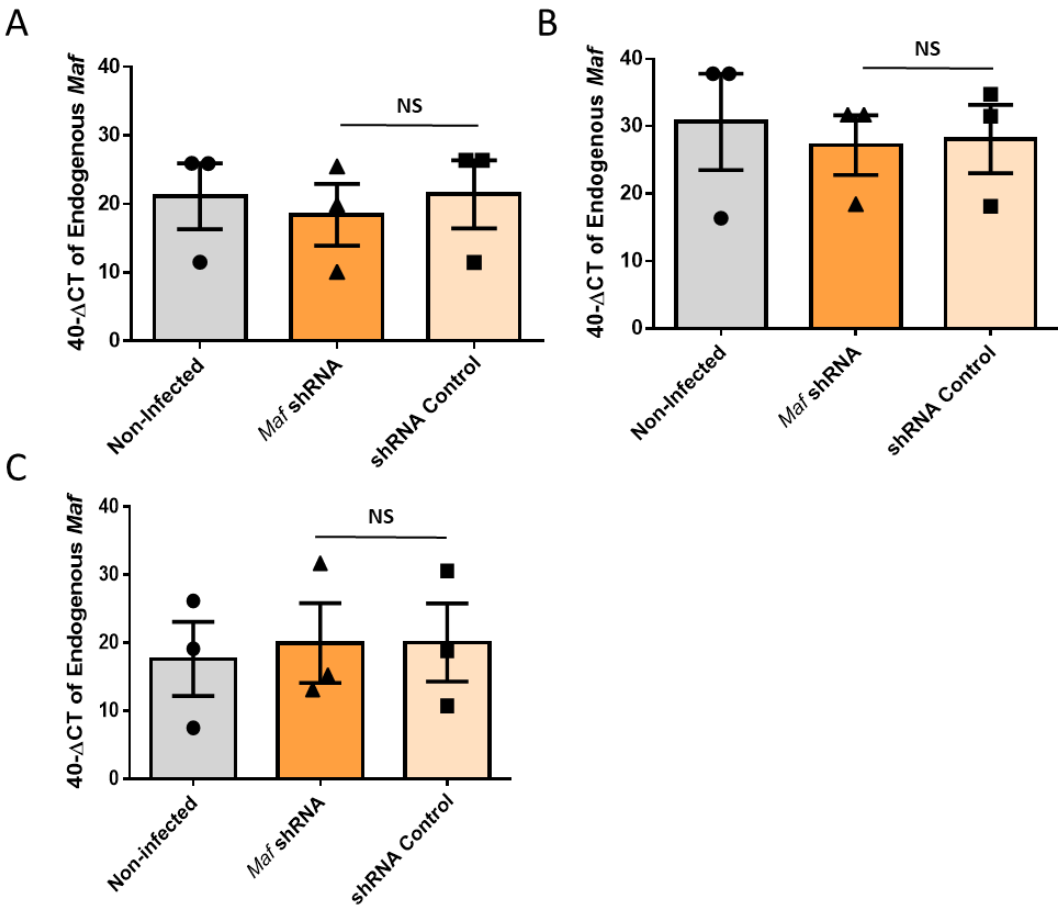

Figure 3.3.3: qPCR analysis of *Maf* shRNA and non-silencing shRNA control lentivirus in MØP, MCSF differentiated MØP and BMDM.

40-ΔCT values of genomic *Maf* expression when using lentiviral vectors expressing *Maf* shRNA, non-infected and non-silencing shRNA control viruses. A) MØP, B) MCSF differentiated MØP, and C) BMDM. In all cases, bars represent the means and error bars indicate ±SEM. Data represents 3 independent experiments (cells in C were pooled from 3 mice). All data was analysed using two-way ANOVA, with Sidak's multiple comparison test when significance in the ANOVA test was reached.

3.3.2.2. Overexpression of *Maf*

To validate generated overexpression constructs MØPs, MCSF differentiated MØPs and BMDMs were transfected with *Maf* overexpressing vectors or corresponding empty control vectors. *Maf* sequence for the overexpression vectors were codon-optimised during development, therefore different qPCR primers used for these transfected cells were specific to the codon optimised *Maf* compared to shRNA *Maf* transfected cells which utilised qPCR primers to genomic *Maf* sequence.

Two-way ANOVA of *Maf* overexpression and control virus in lentiviral infected MØPs indicated statistically significant difference (p-value = 0.0189, *) (Figure 3.3.4A). However no significant difference was detected between GFP or rCD2 reporters, nor interaction of the reporter with the viruses (Figure 3.3.4A). *Maf* overexpression GFP with overexpression GFP control and *Maf* overexpression rCD2 with overexpression rCD2 control through Sidak's multiple comparison test indicated no statistically significant differences (Figure 3.3.4A). 40-ΔCT of *Maf* overexpression GFP was 42.30 (±SEM 3.610) compared to overexpression GFP control 23.82 (±SEM 1.006), whilst *Maf* overexpression rCD2 39.74 (±SEM 6.750) in comparison to overexpression rCD2 control 27.54 (±SEM 2.260) in lentiviral infected MØPs.

M-CSF differentiated MØPs displayed no statistically significant difference with two-way ANOVA by any factor (Figure 3.3.4B), with little differences observed in 40-ΔCT values between *Maf* overexpression vectors and their overexpression control M-CSF differentiated lentiviral infected MØPs (Figure 3.3.4B).

In lentiviral infected BMDMs *Maf* expression was significantly increased between overexpression and overexpression control viruses (p-value = 0.0009, ***)(Figure 3.3.4C). In both GFP and rCD2 overexpression lentiviral infected BMDMs when using Sidak's multiple comparison test demonstrated to be statistically significant when compared to empty vector controls (p-value = 0.0087 ** and p-value = 0.0211 * respectively) (Figure 3.3.4C). Mean 40-ΔCT of *Maf* overexpression GFP was 45.67 (±SEM 1.773) compared to overexpression GFP control 30.95 (±SEM 2.784), with Sidak's multiple comparisons test indicating significance (p-value = 0.0096, **), and *Maf* overexpression rCD2 41.86 (±SEM 1.647) in comparison to overexpression rCD2 control 29.43 (±SEM 3.809) with Sidak's multiple comparisons test indicating significance (p-value = 0.0206, *) (Figure 3.3.4C).

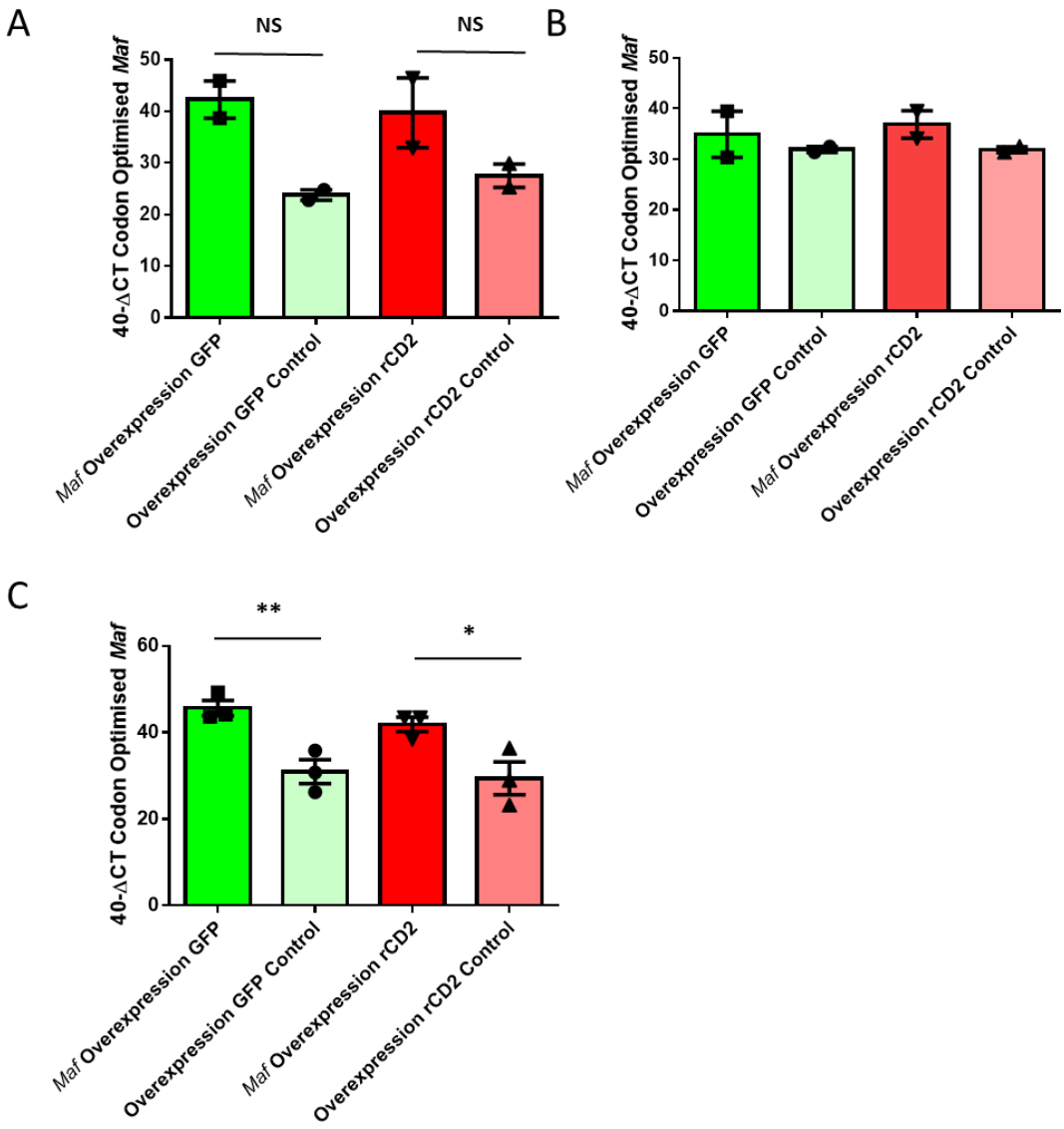

Figure 3.3.4: qPCR analysis of *Maf* overexpression in MØP, MCSF differentiated MØP and BMDM

40-ΔCT values of codon optimised *Maf* expression when using lentiviral vectors expressing *Maf* as a T2A fusion with either GFP or rCD2 and control viruses that lack the *Maf* coding sequence in A) MØP, B) MCSF differentiated MØP, and C) BMDM. In all cases, bars represent the means and error bars indicate ±SEM. Data represents 2 (A and B) or 3 (C) independent experiments (cells in C were pooled from 3 mice). All data was analysed using two-way ANOVA, with Sidak's multiple comparison test when significance in the ANOVA test was reached (NS = non-significant, * p-value = <0.05, ** p-value = <0.01).

3.3.2.3. *Mlf1* shRNA and Overexpression Lentiviruses

MØPs infected with *Mlf1* shRNA and overexpression lentiviruses as discussed in section 3.3.2.1, and were analysed by qPCR and one-way ANOVA, demonstrated to be statistically significant (p-value = 0.0006, ***) (Figure 3.3.5A). Mean 40-ΔCT of *Mlf1* shRNA expressing cells was 25.32 (±SEM 3.299) when compared to the non-silencing shRNA control 40-ΔCT value of 30.16 (±SEM 0.9415) (Figure 3.3.5A). Both GFP and rCD2 *Mlf1* overexpression lentiviral infected MØPs demonstrated increases in *Mlf1* expression in comparison to their respective empty vector control infected MØPs when analysed with Sidak's multiple comparison test (p-value = 0.004 *** and p-value = 0.046 ** respectively) (Figure 3.3.5A). However *Mlf1* shRNA when compared to its control virus was not statistically significant (Figure 3.3.5A).

Following differentiation of MØPs with M-CSF to macrophage phenotype, one-way ANOVA determined statistical significance (p-value = <0.0001, ***) (Figure 3.3.5B). Both GFP and rCD2 *Mlf1* overexpression lentiviruses displayed significant differences compared to respective controls with Sidak's multiple comparison test for both reporters (Figure 3.3.5B). *Mlf1* shRNA when compared to its control virus was not statistically significant (Figure 3.3.5B).

Lentiviral infected BMDMs (n=1) demonstrated an increased in *Mlf1* gene expression when compared to their respective empty control vector (Figure 3.3.5C), with *Mlf1* overexpression GFP 40-ΔCT value of 38.81 and *Mlf1* overexpression rCD2 value of 36.85 when compared to overexpression GFP control 26.42 and overexpression rCD2 26.46.

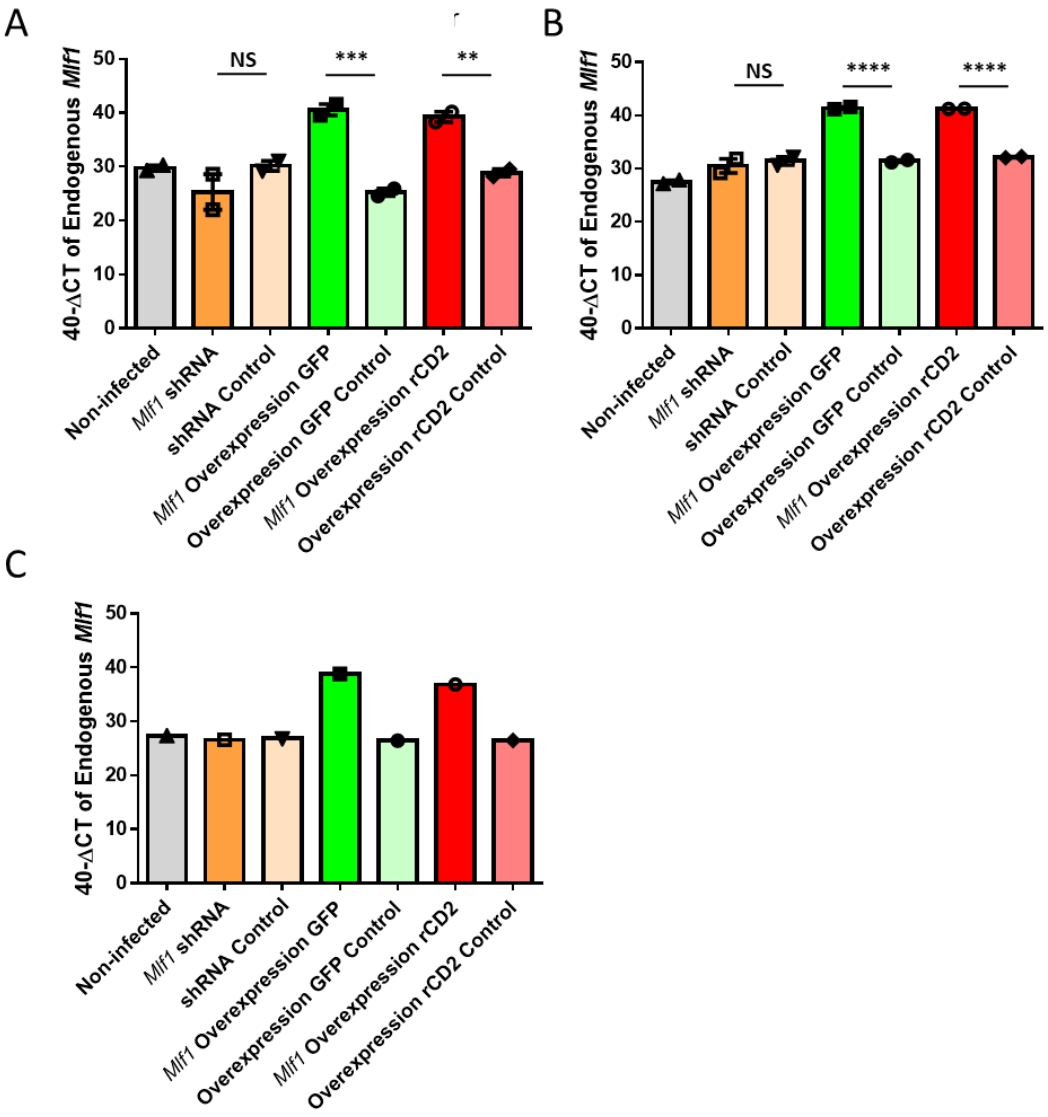

Figure 3.3.5: qPCR analysis of *Mlf1* in MØP, MCSF differentiated MØP and BMDM.

40-ΔCT values of genomic *Mlf1* expression when using lentiviral vectors expressing *Mlf1* shRNA, lentiviral vectors expressing *Mlf1* as a T2A fusion with either GFP or rCD2, with non-infected control and control non-silencing shRNA or viruses which lack the *Mlf1* coding sequence. In all cases, bars represent the means and error bars indicate ±SEM. Data represents 2 (A and B) or 1 (C) independent experiments (cells in C were pooled from 3 mice). All data was analysed using two-way ANOVA, with Sidak's multiple comparison test when significance in the ANOVA test was reached (NS = non-significant, ** p-value = <0.01, *** p-value = <0.001, **** p-value = <0.0001).

3.3.3. Validation of Constructs by Flow Cytometry

3.3.3.1. Comparison of Commercially Available MAF Antibodies

To further validate successful modulation of *Maf* expression in cell models, expression was investigated at protein level. More often detected by western blot (104,105) with the most commonly published antibody produced by Santa Cruz Biotechnology (Cat# sc-7866, Clone# M-153) no longer available, the use of three different anti-mouse MAF antibodies, obtained from Abcam, BD Biosciences and Thermofisher Scientific (originally developed by eBioscience) to be utilised in flow cytometry.

Three cell fixation/permeabilization methods were compared for each antibody to determine best conditions for flow cytometry. Specifically formaldehyde fixation followed by either cold methanol or 0.5% saponin for permeabilization, or a commercially available "FoxP3/Transcription Factor Fixation/Permeabilization" kit developed by eBioscience. A secondary antibody (DyLight™ 405 AffiniPure Goat Anti-Rabbit IgG, Jackson Immunoresearch) was utilised for detection of the unconjugated Abcam antibody, whilst the BD Bioscience antibody was already conjugated to R-phycoerythrin (PE) and the Thermofisher Scientific antibody to eFluor660. Each antibody was used to detect MAF expression under the three fixation/permeabilization. MAF detection was compared to unstained cells, with isotype matched controls used at same concentration as the MAF antibodies and, in the case of the Abcam antibody, a secondary antibody alone control staining (Figure 3.3.6).

Initial tests on non-infected MØPs showed small shifts with the Abcam antibody (Figure 3.3.6), when compared to its isotype matched control, with methanol and the eBioscience kit. However when treated with the eBioscience kit the forward scatter profile shifted significantly (Figure 3.3.6), making it impossible to separate out dead cells by forward and side scatter alone.

The BD antibody showed a good shift under methanol and saponin permeabilization , with the saponin generating a clearer shift from the isotype and unstained cells. However when using the eBioscience kit there was a larger shift in the isotype compared to unstained cells (Figure 3.3.6), resulting in very little difference between the MAF antibody and the isotype.

The Thermofisher Scientific antibody showed little shift when treated with methanol and only broadening of the peak with saponin when compared to unstained cells, however

when compared to the isotype this shift was lost. As the Thermofisher Scientific antibody was originally developed by eBioscience, it is little surprise that the shift was far more apparent when compared to the unstained cells when using the eBioscience kit, however once again the isotype resulted in the shift being lost in the MAF antibody (Figure 3.3.6).

To confirm specificity of these antibodies lentiviral infected MØPs with MAF overexpression GFP and overexpression GFP control viruses were utilised as described previously (Figure 3.3.6). The Abcam antibody showed an increased shift in the MAF overexpression GFP cell line under all three fixation/permeabilization conditions, whereas the Thermofisher scientific antibody showed little change across the three cell lines or the three fixation/permeabilization methods. Only the BD antibody in MØPs permeabilised with saponin showed a clear shift between the non-infected and overexpression GFP control, when compared to the MAF overexpression GFP cells (Figure 3.3.6).

Both the BD antibody under 0.5% saponin permeabilization conditions and the Thermo antibody using the "FoxP3/Transcription Factor Fixation/Permeabilization" kit showed a clear separation from unstained MØPs (Figure 3.3.6). Therefore both antibodies were taken forward. However the fixation/permeabilization for the eBioscience kit required optimisation to prevent the disruption of the forward scatter and investigate whether this would affect the isotype matched control in non-infected MØPs. All further experiments using the Thermofisher Scientific (henceforth referred to as Thermo) were fixed with formaldehyde and utilising the eBioscience kit permeabilization buffer only.

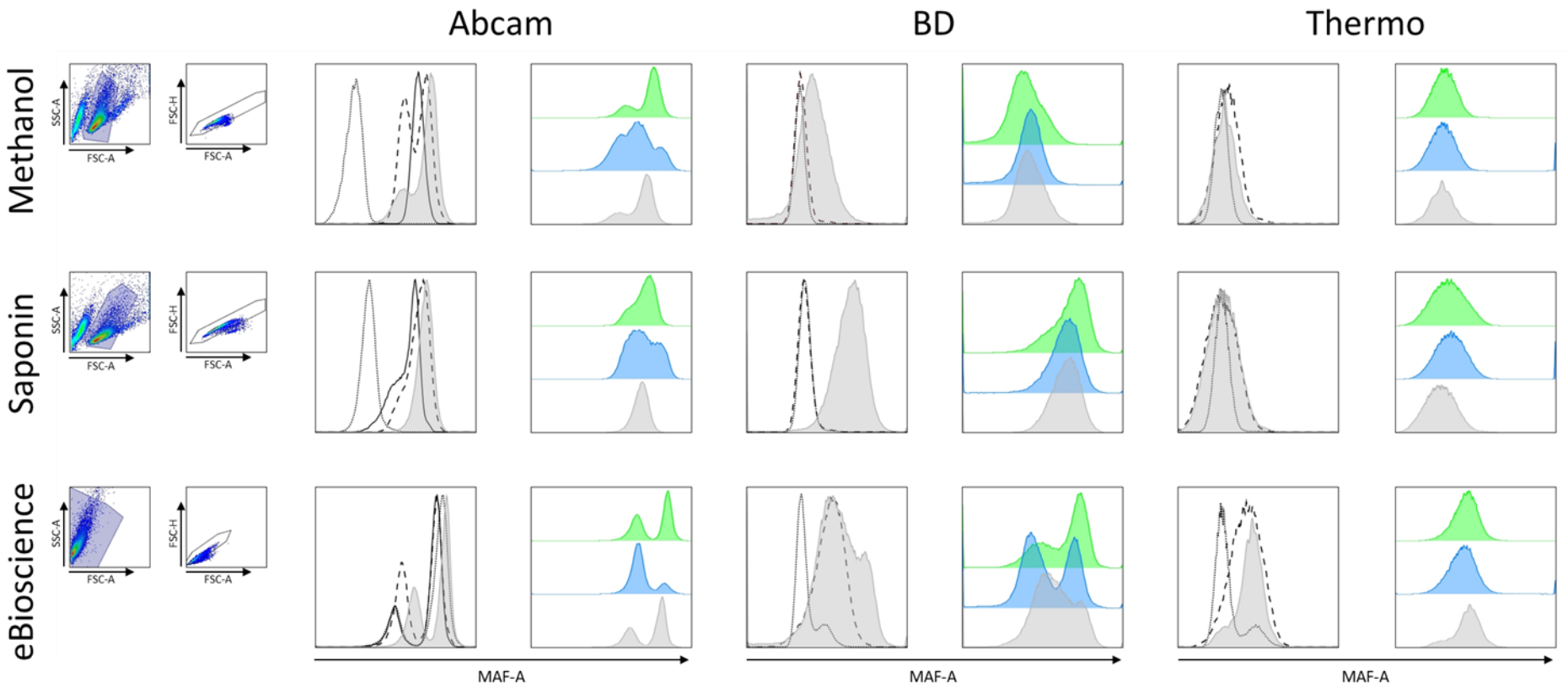
Abcam
BD
Thermo
Methanol
Saponin
eBioscience
SSC-A
FSC-A
FSC-H
FSC-A
MAF-A
MAF-A
MAF-A
Unstained MØPs
Isotype Matched Control
2° Antibody Only
Non-infected MØPs
Maf Overexpression GFP
Overexpression GFP Control

Figure 3.3.6: Comparison of commercially available MAF antibodies and different fixation and permeabilization buffers on lentivirally infected MØP.

Three different anti-mouse MAF antibodies were obtained from Abcam, BD Biosciences and Thermofisher Scientific. Formaldehyde with methanol or saponin along with commercially available "FoxP3/Transcription Factor Fixation/Permeabilization" kit by eBioscience were compared for fixation/permeabilization. Each antibody was tested using the three fixation/permeabilization buffers on non-infected MØP cells (grey) with appropriate isotype (dash line), secondary only (solid line) where required and unstained MØP cells (dotted line). *Maf* overexpression GFP MØP cells (green) and overexpression GFP control (blue) were also stained to determine target specificity. (n= 1).

3.3.3.2. MAF Expression in Transfected MØP Cell Lines

MØPs were infected with all *Maf* lentiviruses and vector controls and stained with either the BD Bioscience MAF antibody or an appropriate isotype control (Figure 3.3.7A). Flow cytometry was employed to obtain mean fluorescent intensity (MFI) of an isotype matched control, which was subtracted from MAF BD Bioscience antibody MFI, to exclude non-specific antibody binding, generating delta mean fluorescent intensity (ΔMFI) values. No statistically significant changes were detected in MAF expression across any of the lentiviral infected MØPs, when using the BD Bioscience antibody using one-way ANOVA analysis (Figure 3.3.7B).

The same MØPs were stained with Thermo Fisher antibody and appropriate isotype control (Figure 3.3.8A). One-way ANOVA of ΔMFI MAF expression indicated to be statistically significant (p-value = <0.0001, ****) (Figure 3.3.8B). Both GFP and rCD2 overexpression infected MØPs displayed an increase in ΔMFI MAF expression, which was deemed statistically significant by Sidak's multiple comparisons test when compared to overexpression control infected MØPs (p-value = <0.0001 **** and p-value = 0.0349 * respectively) (Figure 3.3.8B). Maf shRNA when compared to its control however was not significant (Figure 3.3.8B).

A

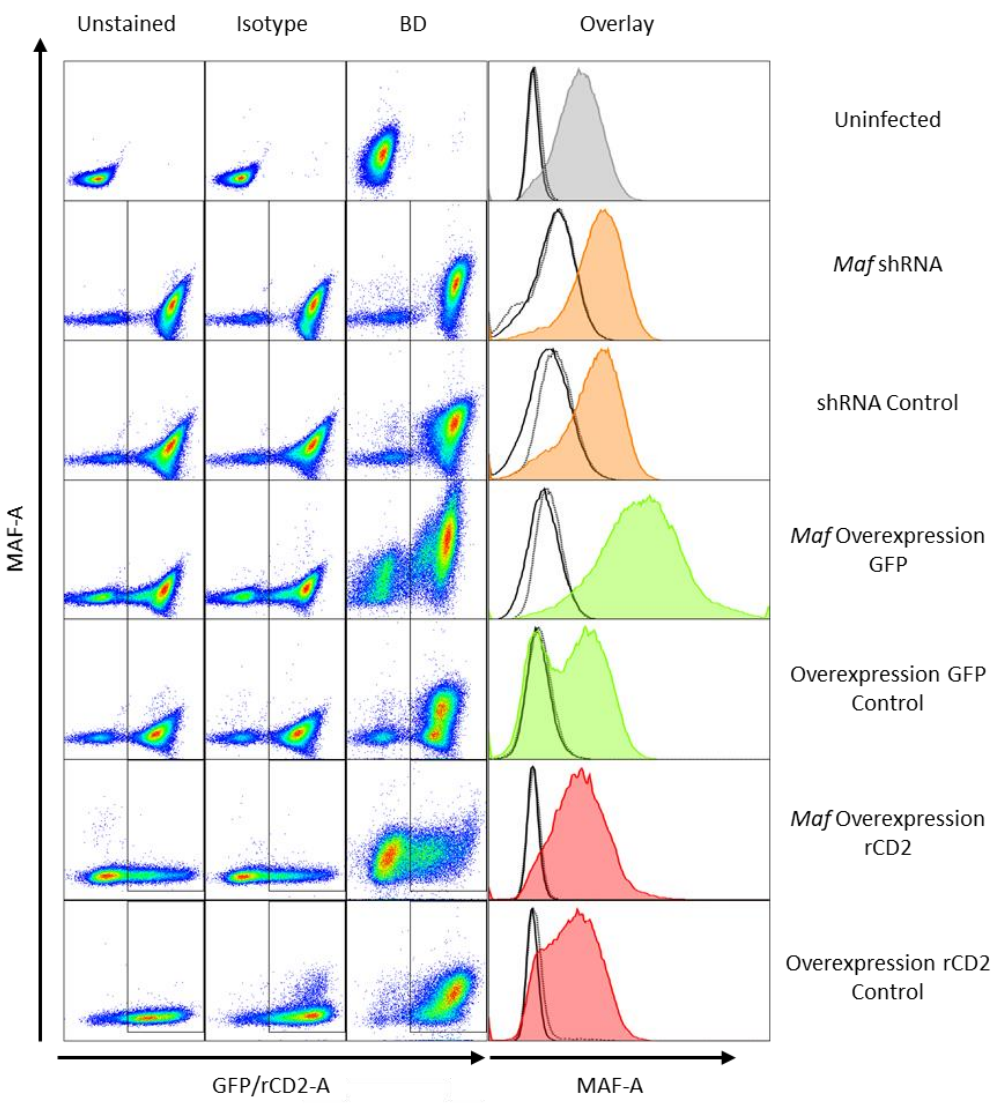
Unstained
Isotype
BD
Overlay
Uninfected
Maf shRNA
shRNA Control
Maf Overexpression GFP
Overexpression GFP Control
Maf Overexpression rCD2
Overexpression rCD2 Control
MAF-A
GFP/rCD2-A
MAF-A

B

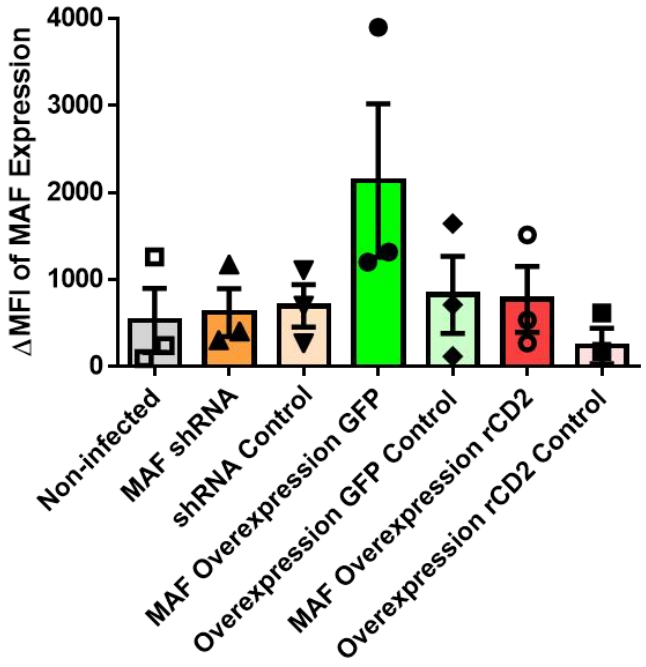
ΔMFI of MAF Expression
4000
3000
2000
1000
0
Non-infected
MAF shRNA
shRNA Control
MAF Overexpression GFP
Overexpression GFP Control
MAF Overexpression rCD2
Overexpression rCD2 Control

Figure 3.3.7: Validation of MAF detection by the BD Bioscience antibody in MØP cells infected with *Maf* shRNA and *Maf* overexpression lentiviral vectors.

Flow cytometry plots of MAF against GFP or rCD2 expression with unstained and isotype controls in A) non-infected MØPs, and MØPs lentivirally infected with *Maf* shRNA, non-silencing control, GFP *Maf* overexpression, GFP empty vector control, rCD2 *Maf* overexpression or rCD2 empty vector control. Histogram of MAF expression (detected with BD Bioscience antibody) overlaid with matched isotype control (dotted line) and unstained (solid line). B) Delta mean fluorescent intensity (ΔMFI) of MAF expression in GFP+/rCD2+ MØP cells using BD Bioscience MAF antibody. Data shown represents mean ΔMFI ±SEM (n=3 independent experiments), analysed with one-way ANOVA, with Sidak's multiple comparisons.

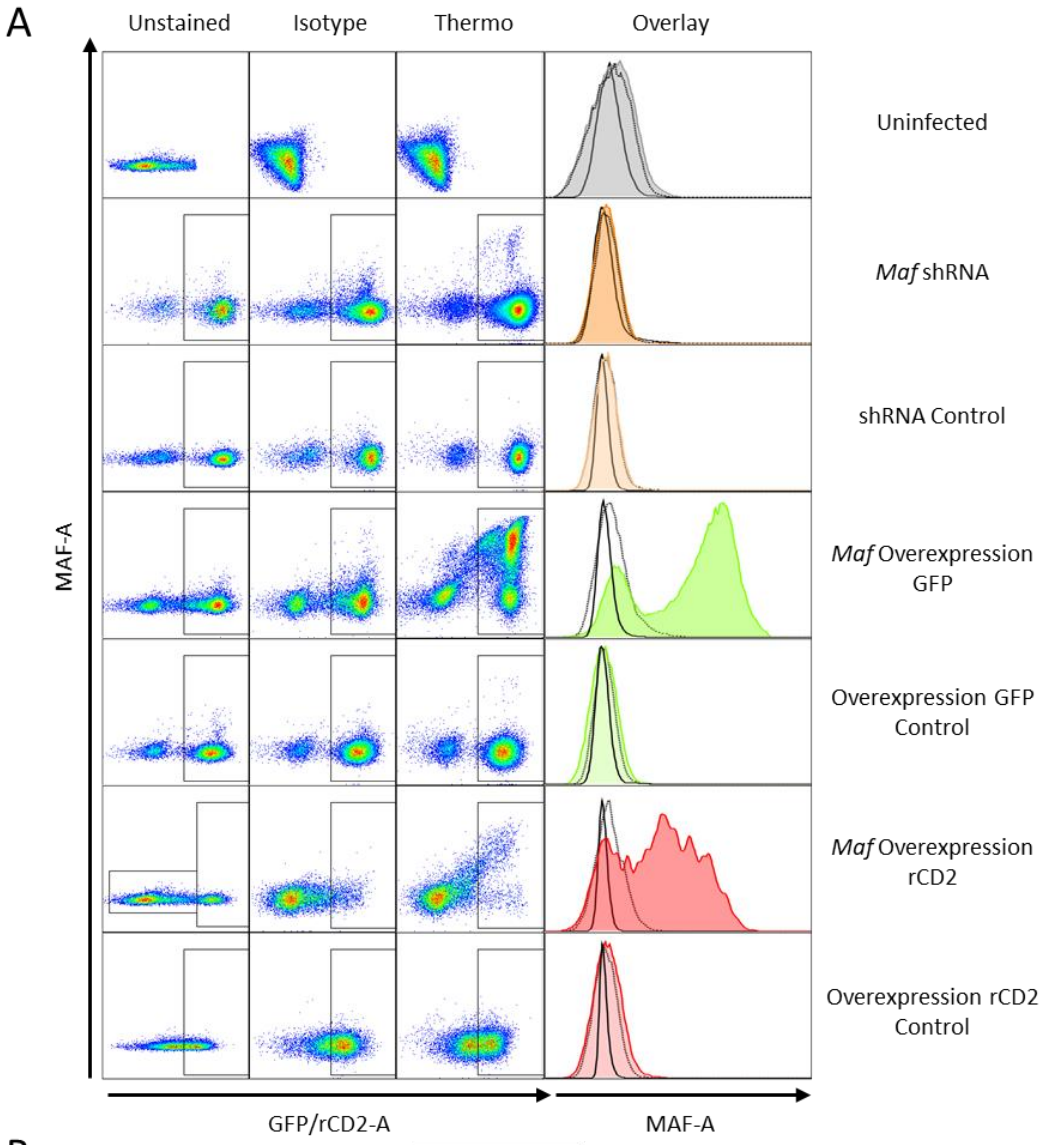
A
Unstained
Isotype
Thermo
Overlay
MAF-A
Uninfected
Maf shRNA
shRNA Control
Maf Overexpression GFP
Overexpression GFP Control
Maf Overexpression rCD2
Overexpression rCD2 Control
GFP/rCD2-A
MAF-A

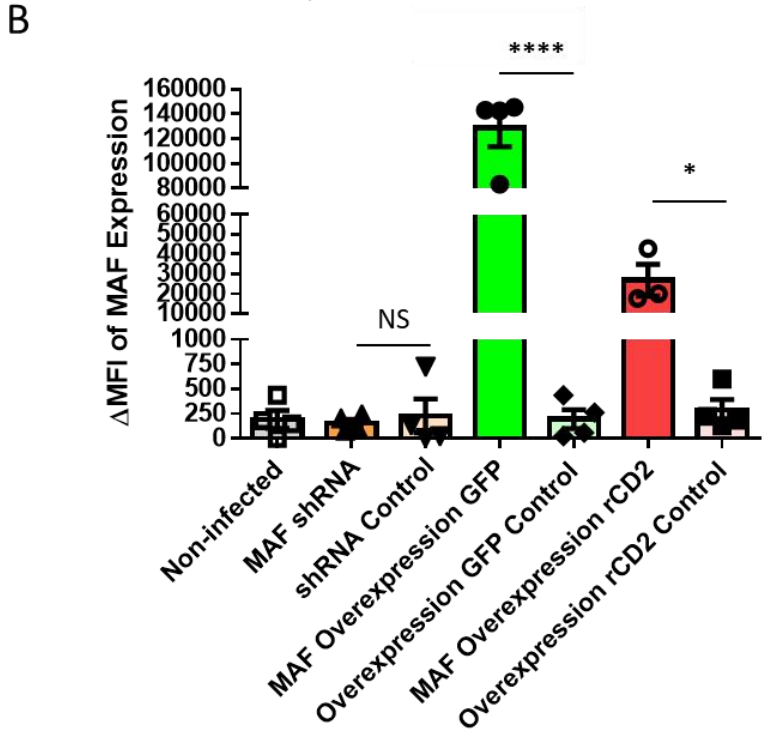
B
****
*
NS
ΔMFI of MAF Expression
160000
140000
120000
100000
80000
60000
50000
40000
30000
20000
10000
1000
750
500
250
0
Non-infected
MAF shRNA
shRNA Control
MAF Overexpression GFP
Overexpression GFP Control
MAF Overexpression rCD2
Overexpression rCD2 Control

Figure 3.3.8: Validation of MAF detection by the Thermo Fisher antibody in MØP cells infected with *Maf* shRNA and *Maf* overexpression lentiviral vectors.

Flow cytometry plots of MAF against GFP or rCD2 expression with unstained and isotype controls in A) non-infected MØPs, and MØPs lentivirally infected with *Maf* shRNA, non-silencing control, GFP *Maf* overexpression, GFP empty vector control, rCD2 *Maf* overexpression or rCD2 empty vector control. Histogram of MAF expression (detected with Thermo Fisher antibody) overlaid with matched isotype control (dotted line) and unstained (solid line). B) Delta mean fluorescent intensity (ΔMFI) of MAF expression in GFP+/rCD2+ MØP cells using Thermo Fisher MAF antibody. Data shown represents mean ΔMFI ±SEM (n=4 independent experiments), analysed with one-way ANOVA, with Sidak's multiple comparisons test (NS = non-significant, * p-value = <0.05, **** p-value = <0.0001).

3.3.3.3. MAF Expression in M-CSF Treated MØP Cell Lines

Lentiviral infected MØPs were differentiated to macrophages after 4 days of treatment with M-CSF and stained with BD Bioscience MAF antibody and appropriate isotype (Figure 3.3.9A). All lentiviral infected differentiated MØPs displayed increased expression in comparison to non-infected differentiated MØPs (Figure 3.3.9B), however with no statistically significant difference observed when using a one-way ANOVA.

The same differentiated MØPs were stained with Thermo Fisher antibody and appropriate isotype control (Figure 3.3.10A), with one-way ANOVA indicating statistical significance (p-value = <0.0001, ****) (Figure 3.3.10B). Both GFP and rCD2 overexpression infected MØPs displayed an increase in ΔMFI MAF expression, with only *Maf* overexpression GFP infected MØPs being statistically significant when compared to overexpression GFP control infected MØPs with Sidak's multiple comparisons test (p-value = <0.0001, ****) (Figure 3.3.10B).

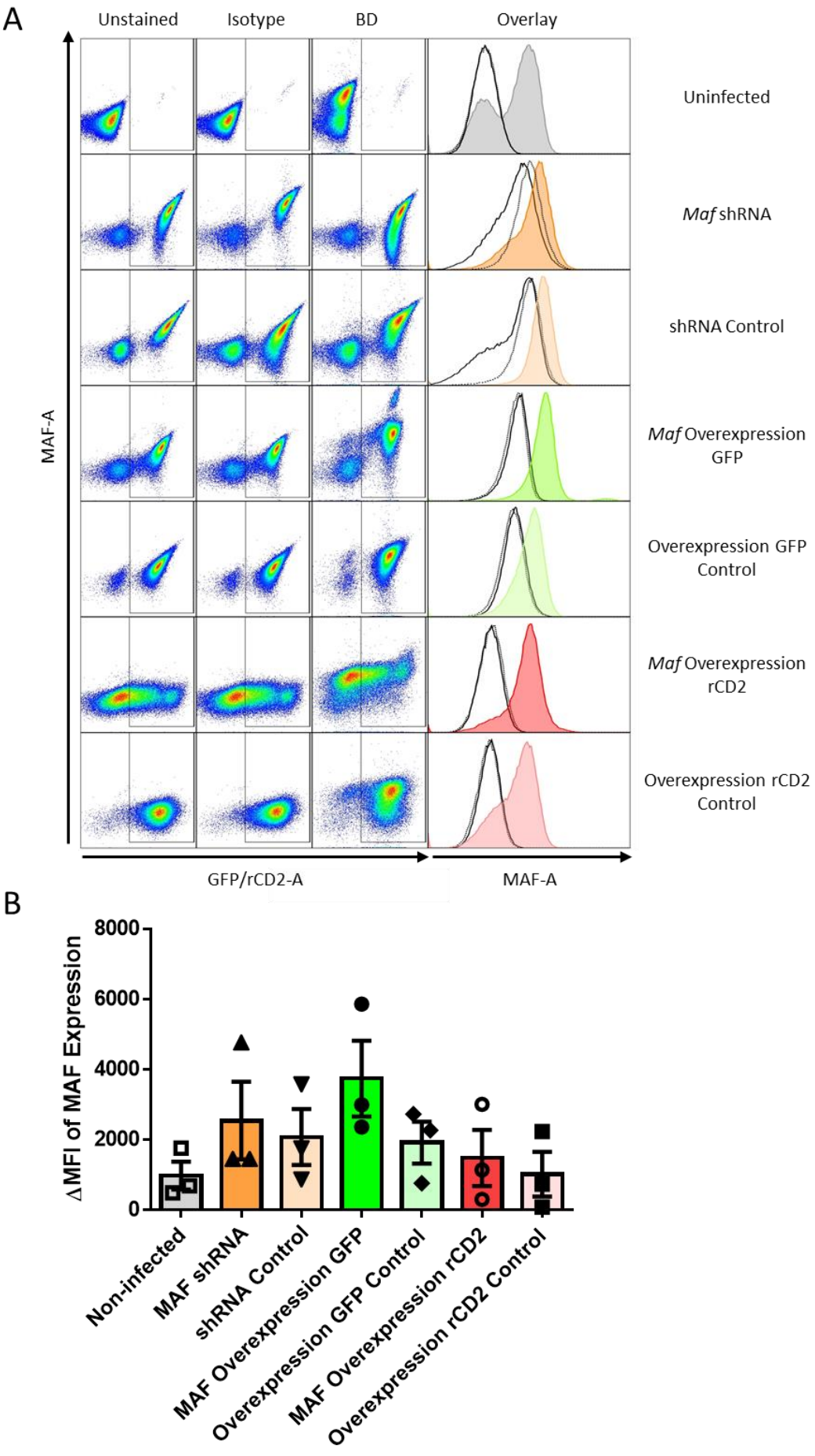
A
Unstained
Isotype
BD
Overlay
MAF-A
Uninfected
Maf shRNA
shRNA Control
Maf Overexpression GFP
Overexpression GFP Control
Maf Overexpression rCD2
Overexpression rCD2 Control
GFP/rCD2-A
MAF-A
B
ΔMFI of MAF Expression
8000
6000
4000
2000
0
Non-infected
MAF shRNA
shRNA Control
MAF Overexpression GFP
Overexpression GFP Control
MAF Overexpression rCD2
Overexpression rCD2 Control

Figure 3.3.9: Validation of MAF detection by the BD Bioscience antibody in M-CSF differentiated MØPs *Maf* shRNA and *Maf* overexpression lentiviral vectors.

Flow cytometry plots of MAF against GFP or rCD2 expression with unstained and isotype controls in A) non-infected MCSF differentiated MØPs, and MCSF differentiated MØPs lentivirally infected with *Maf* shRNA, non-silencing control, GFP *Maf* overexpression, GFP empty vector control, rCD2 *Maf* overexpression or rCD2 empty vector control. Histogram of MAF expression (detected with BD Bioscience antibody) overlaid with matched isotype control (dotted line) and unstained (solid line). B) Delta mean fluorescent intensity (ΔMFI) of MAF expression in GFP+/rCD2+ MCSF differentiated MØP cells using BD Bioscience MAF antibody. Data shown represents mean ΔMFI ±SEM (n=3 independent experiments), analysed with one-way ANOVA, with Sidak's multiple comparisons.

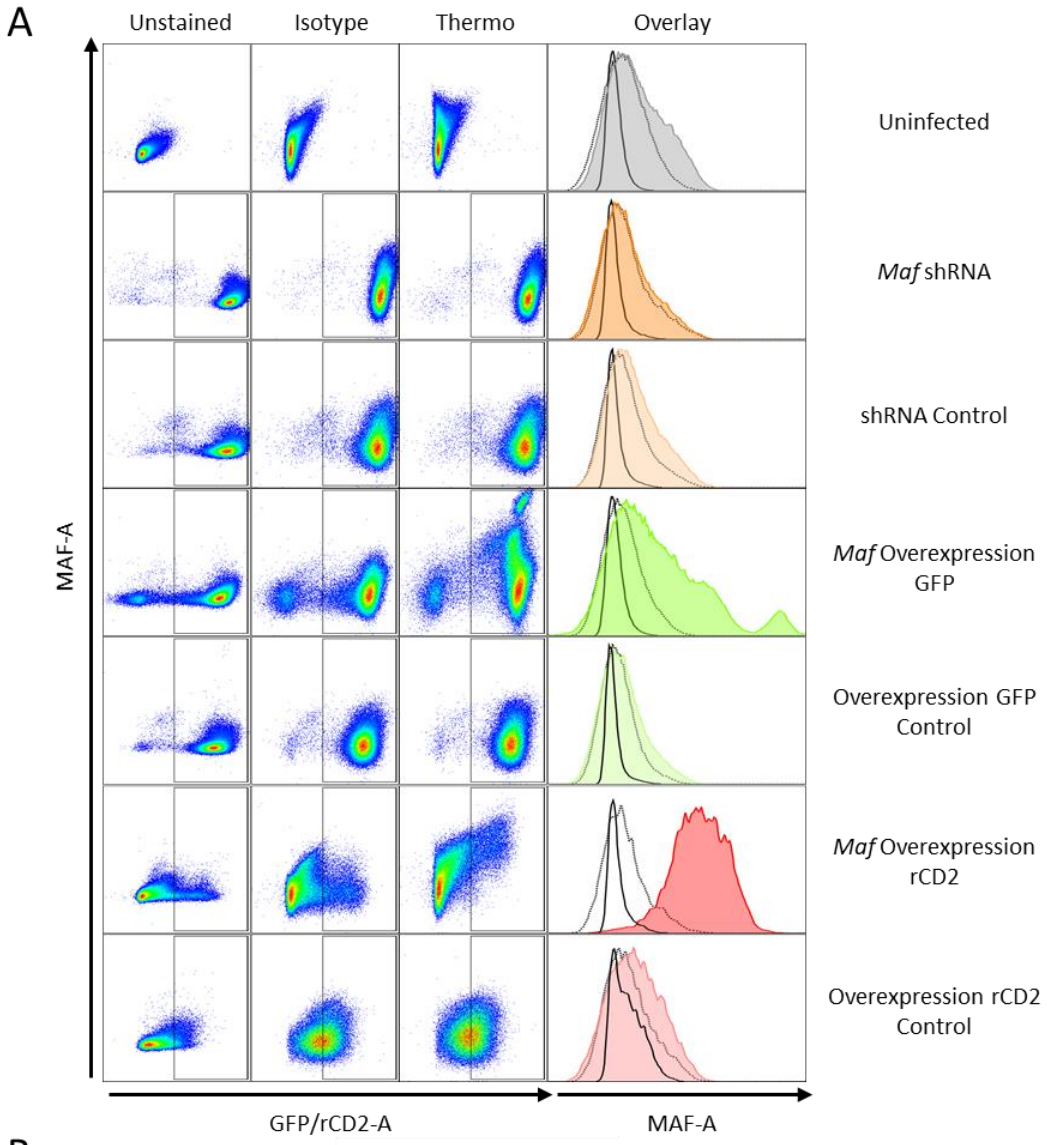
A
Unstained
Isotype
Thermo
Overlay
Uninfected
Maf shRNA
shRNA Control
Maf Overexpression GFP
Overexpression GFP Control
Maf Overexpression rCD2
Overexpression rCD2 Control
MAF-A
GFP/rCD2-A
MAF-A

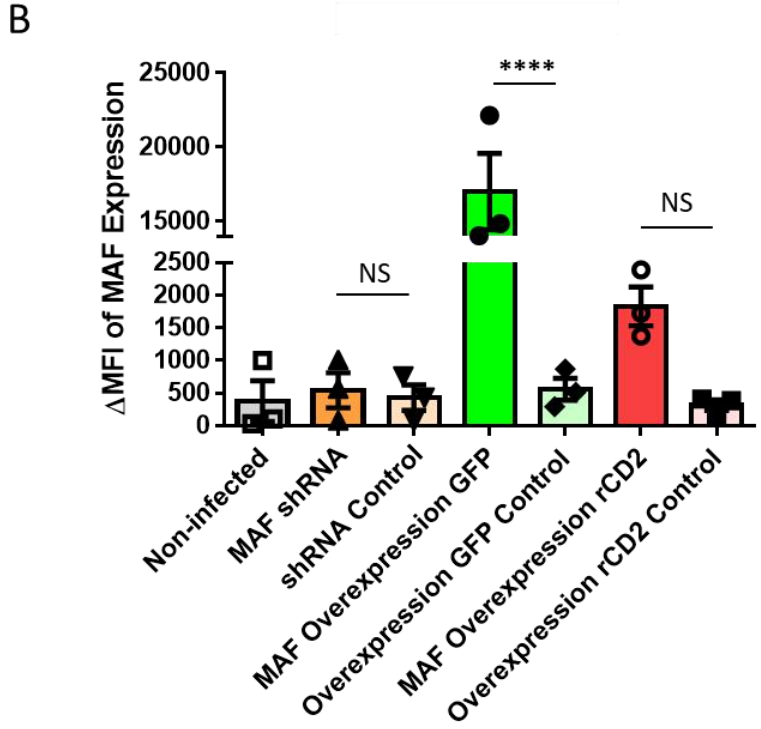
B
ΔMFI of MAF Expression
25000
20000
15000
2500
2000
1500
1000
500
0
****
NS
NS
Non-infected
MAF shRNA
shRNA Control
MAF Overexpression GFP
Overexpression GFP Control
MAF Overexpression rCD2
Overexpression rCD2 Control

Figure 3.3.10: Validation of MAF detection by the Thermo Fisher antibody M-CSF differentiated MØP cells infected with *Maf* shRNA and *Maf* overexpression lentiviral vectors.

Flow cytometry plots of MAF against GFP or rCD2 expression with unstained and isotype controls in A) non-infected MCSF differentiated MØPs, and MCSF differentiated MØPs lentivirally infected with *Maf* shRNA, non-silencing control, GFP *Maf* overexpression, GFP empty vector control, rCD2 *Maf* overexpression or rCD2 empty vector control. Histogram of MAF expression (detected with Thermo Fisher antibody) overlaid with matched isotype control (dotted line) and unstained (solid line). B) Delta mean fluorescent intensity (ΔMFI) of MAF expression in GFP+/rCD2+ MCSF differentiated MØP cells using Thermo Fisher MAF antibody. Data shown represents mean ΔMFI ±SEM (n=3 independent experiments), analysed with one-way ANOVA, with Sidak's multiple comparisons test (NS = non-significant, **** p-value= <0.0001).

3.3.3.4. MAF Expression in Transfected BMDMs

BMDMs were generated as described above (1.1.1). Lentivirus infected BMDMs were stained with BD Bioscience MAF antibody and appropriate isotype (A) with ΔMFI MAF expression deemed to be statistically significant by one-way ANOVA (p-value = <0.0001, ****) (B). GFP *Maf* overexpression virus displayed increased ΔMFI MAF expression in comparison to its corresponding control lentivirus infected BMDMs when analysed with Sidak's multiple comparisons test (p-value = <0.0001, ****) (Figure 3.3.11B).

rCD2 overexpression control infected BMDMs displayed similar levels of ΔMFI MAF expression to *Maf* rCD2 overexpression infected BMDMs and were not statistically significant (B). shRNA infected lentiviral infected BMDMs were also deemed statistically significant with Sidak's multiple comparisons test (p-value = 0.0139, *), when compared to the non-silencing shRNA sequence control lentivirus (Figure 3.3.11B).

Lentivirus transfected BMDMs were stained with Thermo Fisher antibody and appropriate isotype control (Figure 3.3.12A) and analysed with one-way ANOVA (p-value = 0.0010, ***) (Figure 3.3.12B). Sidak's multiple comparisons test indicated increases in ΔMFI MAF expression in both GFP and rCD2 overexpression transfected BMDMs to be statistically significant when compared to their respective overexpression controls (p-value = 0.0114 * and p-value = 0.0013 ** respectively) (Figure 3.3.12B). Whilst *Maf* shRNA and both displayed non-significant reductions in ΔMFI MAF expression compared to non-infected BMDMs (Figure 3.3.12B).

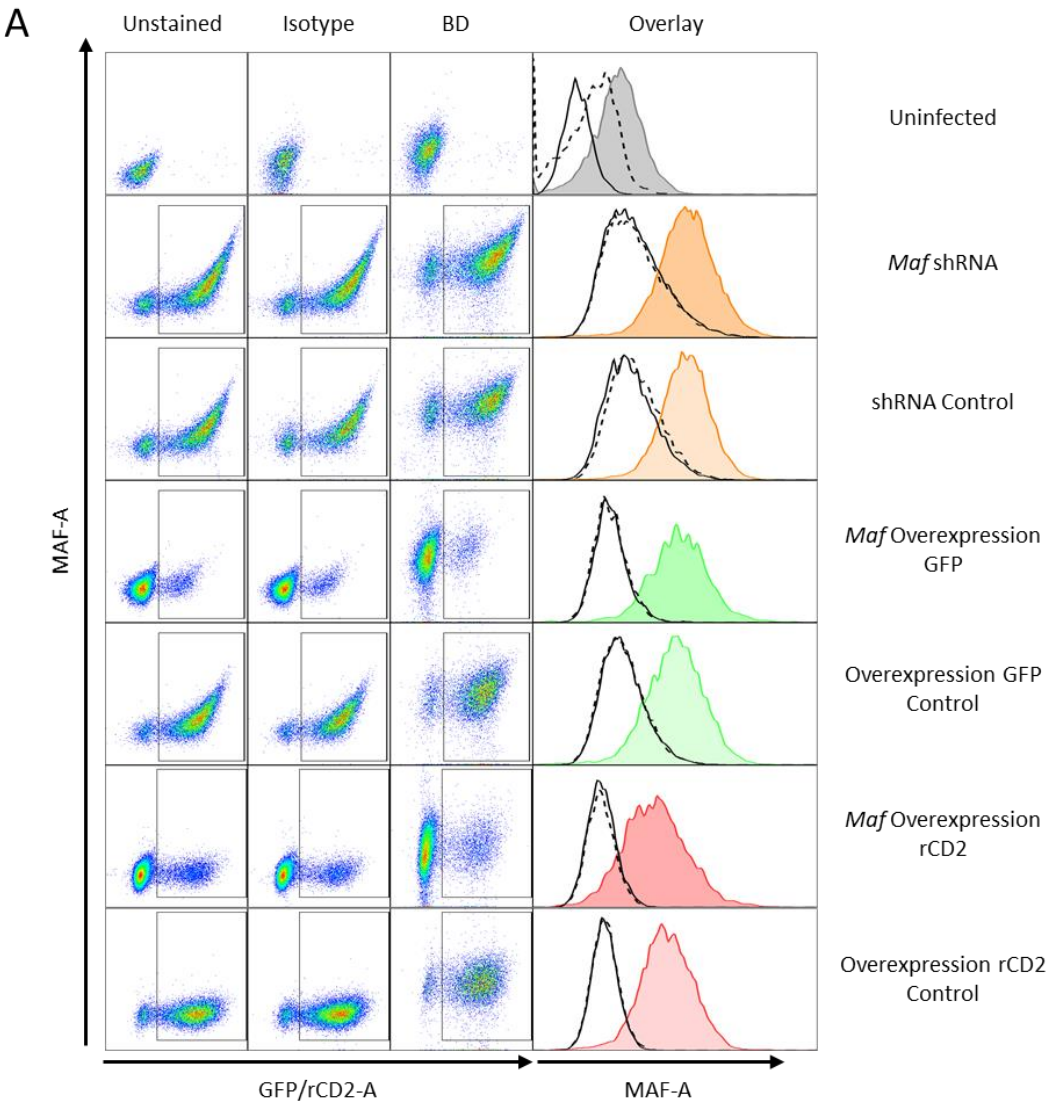
A
Unstained
Isotype
BD
Overlay
Uninfected
Maf shRNA
shRNA Control
Maf Overexpression GFP
Overexpression GFP Control
Maf Overexpression rCD2
Overexpression rCD2 Control
MAF-A
GFP/rCD2-A
MAF-A

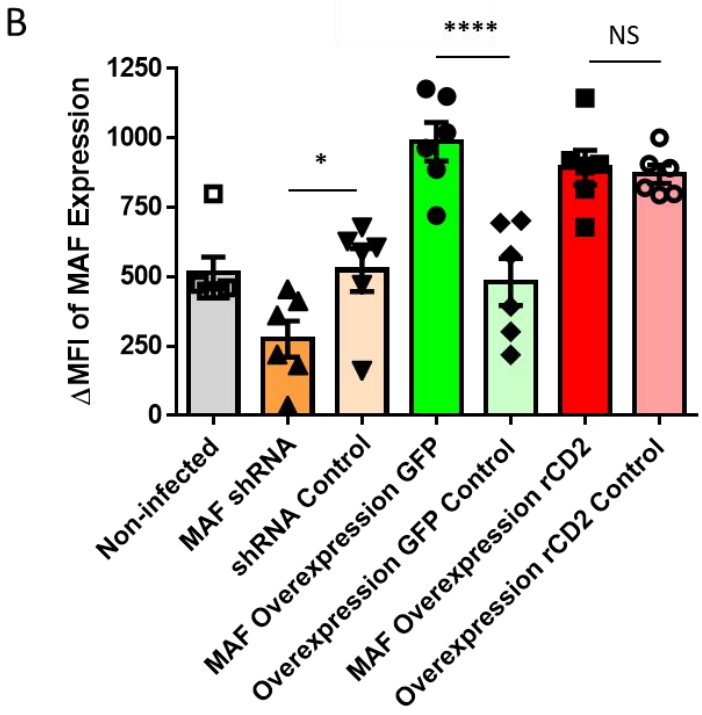
B
****
NS
*
ΔMFI of MAF Expression
1250
1000
750
500
250
0
Non-infected
MAF shRNA
shRNA Control
MAF Overexpression GFP
Overexpression GFP Control
MAF Overexpression rCD2
Overexpression rCD2 Control

Figure 3.3.11: Validation of MAF detection by the BD Bioscience antibody in BMDMs infected with *Maf* shRNA and *Maf* overexpression lentiviral vectors.

Flow cytometry plots of MAF against GFP or rCD2 expression with unstained and isotype controls in A) non-infected BMDMs, and BMDMs lentivirally infected with *Maf* shRNA, non-silencing control, GFP *Maf* overexpression, GFP empty vector control, rCD2 *Maf* overexpression or rCD2 empty vector control. Histogram of MAF expression (detected with BD Bioscience antibody) overlaid with matched isotype control (dotted line) and unstained (solid line). The data is representative of results from BMDMs cells derived from C57BL/6 female mice aged 6-8 weeks. B) Delta mean fluorescent intensity (ΔMFI) of MAF expression in GFP+/rCD2+ BMDMs using BD Bioscience MAF antibody. Data shown represents mean ΔMFI ±SEM (n=6 independent experiments), analysed with one-way ANOVA, with Sidak's multiple comparisons (NS = non-significant, * p-value = <0.05 and **** p-value = <0.0001).

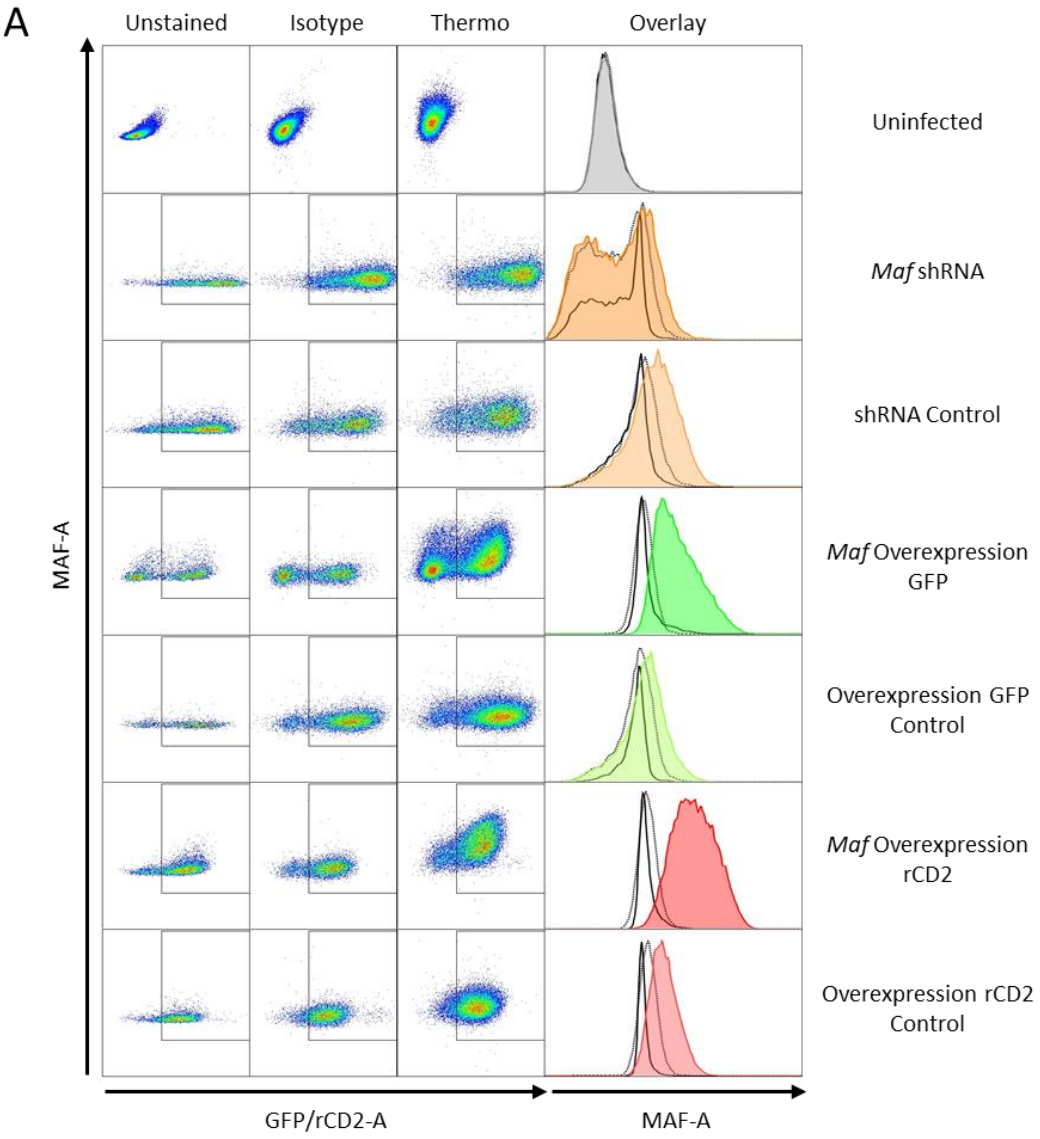
A
Unstained
Isotype
Thermo
Overlay
Uninfected
Maf shRNA
shRNA Control
Maf Overexpression GFP
Overexpression GFP Control
Maf Overexpression rCD2
Overexpression rCD2 Control
MAF-A
GFP/rCD2-A
MAF-A

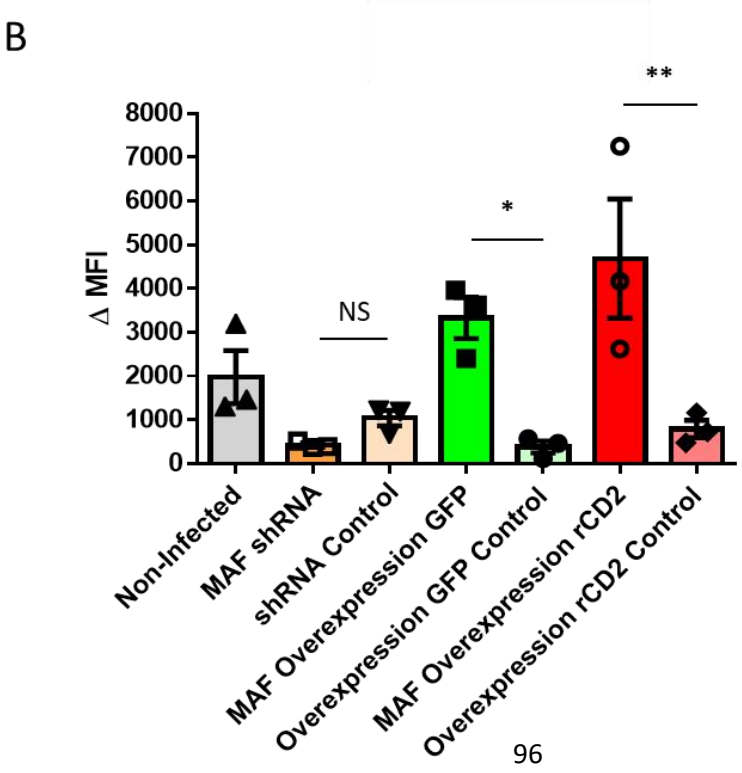
B
**
*
NS
Δ MFI
8000
7000
6000
5000
4000
3000
2000
1000
0
Non-Infected
MAF shRNA
shRNA Control
MAF Overexpression GFP
Overexpression GFP Control
MAF Overexpression rCD2
Overexpression rCD2 Control

Figure 3.3.12: Validation of MAF detection by the Thermo Fisher antibody in BMDMs infected with *Maf* shRNA and *Maf* overexpression lentiviral vectors.

Flow cytometry plots of MAF against GFP or rCD2 expression with unstained and isotype controls in A) non-infected BMDMs, and BMDMs lentivirally infected with *Maf* shRNA, non-silencing control, GFP *Maf* overexpression, GFP empty vector control, rCD2 *Maf* overexpression or rCD2 empty vector control. Histogram of MAF expression (detected with Thermo Fisher antibody) overlaid with matched isotype control (dotted line) and unstained (solid line). The data is representative of results from BMDMs cells derived from C57BL/6 female mice aged 6-8 weeks. B) Delta mean fluorescent intensity (ΔMFI) of MAF expression in GFP+/rCD2+ BMDMs using Thermo Fisher MAF antibody. Data shown represents mean ΔMFI ±SEM (n=6 independent experiments), analysed with one-way ANOVA, with Sidak's multiple comparisons (NS = non-significant, * p-value = <0.05 and ** p-value = <0.01).

3.3.4. Determination of MAF Antibodies Nuclear Localisation

To identify sub-cellular localisation of MAF signal from selected antibodies under their specific fixation and permeabilization conditions, M-CSF differentiated MØPs were assessed on the Amnis ImageStreamX Mark II imaging flow cytometer.

MAF antibody staining along with 4',6-diamidino-2-phenylindole (DAPI), a fluorescent DNA marker, allowed nuclear localisation analysis using the IDEAS® software. Nuclear localization similarity wizard uses the log transformed Pearson's correlation coefficient and is a measure of the degree to which two images are linearly correlated. This generates a similarity value for these cells, with positive values indicating a high degree of similarity, based on gating strategy (Figure 2.12.1).

Overlay images of BD Bioscience MAF staining and DAPI indicated a diffuse staining of MAF with some overlap with DAPI (Figure 3.3.13A). Nuclear co-localisation wizard for MAF using the BD Bioscience antibody in *Maf* overexpression GFP lentiviral infected M-CSF differentiated MØPs indicated a 12.00 % nuclear localised MAF+DAPI+ cells, with a similarity dilate value of 1.469 (Figure 3.3.13B). *Maf* overexpression rCD2 displayed a similar percentage of 12.21% overlap with a similarity dilate value of 1.328 (Figure 3.3.13C).

The same analysis was performed on *Maf* overexpression GFP lentiviral infected M-CSF differentiated MØPs with the Thermo MAF antibody, where overlay images suggested MAF staining being limited to the DAPI stained nucleus and its nearby surroundings (Figure 3.3.14A). This was substantiated with a similarity dilate mean value of 1.865 and 79.54% of nuclear localised MAF+DAPI+ cells (Figure 3.3.14B), indicating a very high degree of similarity. *Maf* overexpression rCD2 displayed an even higher percentage of 97.63% nuclear localised cells with a higher similarity dilate mean value of 2.849 (Figure 3.3.14C).

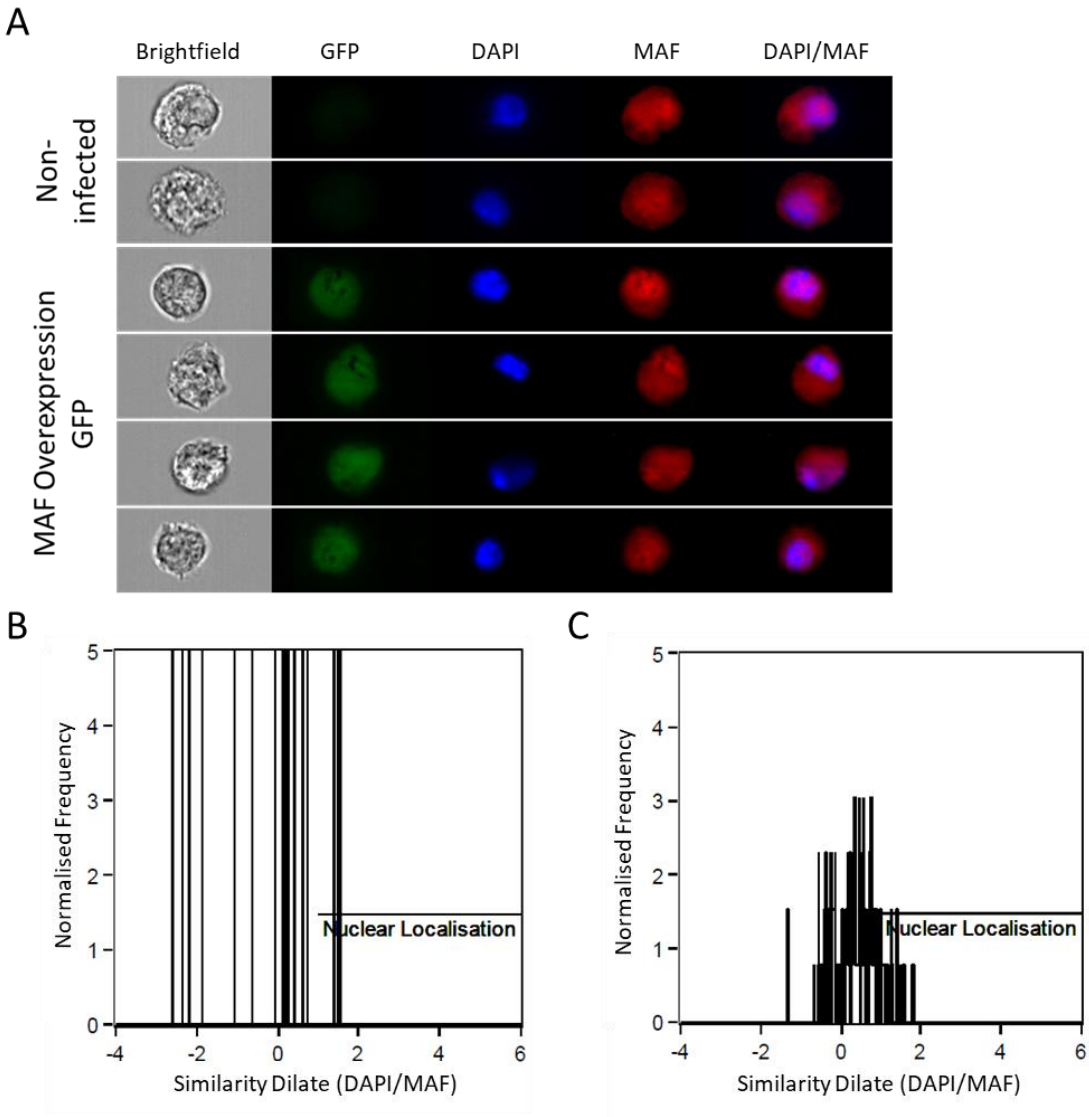

Figure 3.3.13: Imagestream analysis of MAF expression in lentivirus infected M-CSF differentiated MØPs with BD Bioscience antibody.

A) A composite image collected on ImageStreamX Mark II (Amnis, part of Millipore-Sigma) at 60x magnification of differentiated MØPs, displaying brightfield, GFP (green), DAPI (Blue) and MAF (red), with a merged image of DAPI and Maf with overlay. B) Similarity dilate of DAPI and MAF, in lentivirus infected Maf overexpression GFP M-CSF differentiated MOPs. C) Similarity dilate of DAPI and MAF, in lentivirus infected Maf overexpression rCD2 M-CSF differentiated MOPs. (n=1)

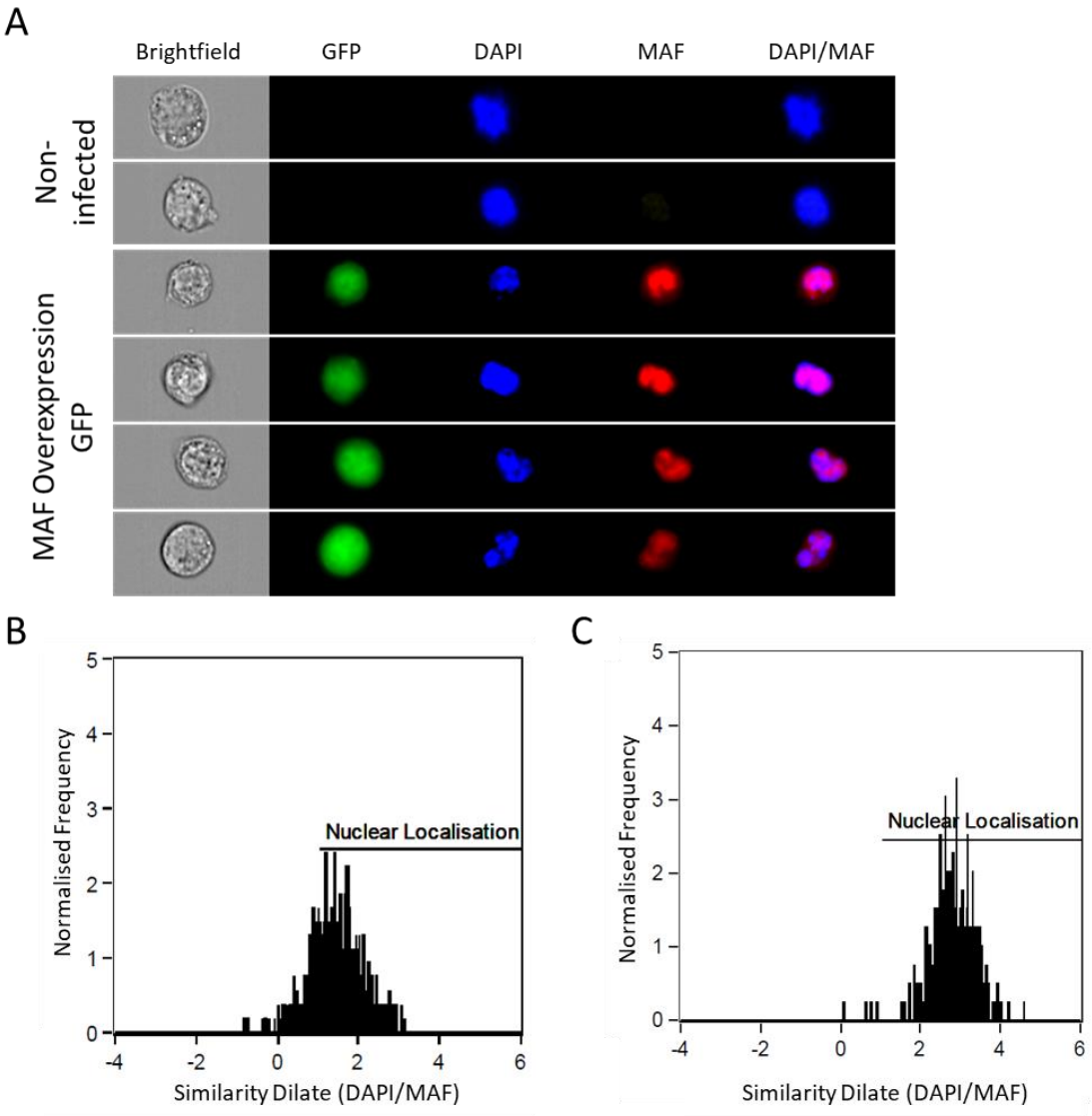

Figure 3.3.14: Imagestream analysis of MAF expression in lentivirus infected M-CSF differentiated MØPs with Thermo Fisher antibody.

A) A composite image collected on ImageStreamX Mark II at 60x magnification of M-CSF differentiated MØPs, displaying brightfield, GFP (green), DAPI (Blue) and MAF (red), with a merged image of DAPI and Maf with overlay. B) Similarity dilate of DAPI and MAF, in lentivirus infected Maf overexpression GFP M-CSF differentiated MOPs. C) Similarity dilate of DAPI and MAF, in lentivirus infected Maf overexpression rCD2 M-CSF differentiated MOPs. (n=1)

3.4. Discussion

3.4.1. Cloning of Overexpression Vectors

Overexpression vectors for *Mlf1* were successfully generated, however due to complexities of the *Maf* gene it was necessary for the sequence to be purchased and undergo codon optimisation. Lentiviruses were successfully developed for these overexpression vectors and their empty vector controls.

Maf overexpression cloning generated a band below expected size (Figure 3.3.2), which could be due to several possible reasons. The *Maf* CCDS contains several regions of 70bp and 150bp long with a GC content of <90%, resulting in *Maf* overall having a GC content of 68.9%, with the first 800bp having a GC content of 72.6%. Upon manufacture, the sequence was codon optimised, removing many of the GC rich regions, reducing the overall GC content to 58.7% (Appendix I). Using the online tool provided by Integrated DNA Technologies (https://www.idtdna.com/CodonOpt) the CCDS for *Maf* contains hairpins with GC content of 100% of "CCCCGCCGCCGCC" at position 474 bp and 691 bp. Secondary structures such as hairpins and loops are known to cause polymerase enzymes to abruptly stop (164), this hairpin was eliminated following codon optimisation.

3.4.2. Validation of shRNAs of *Maf* and *Mlf1*

Validation of these shRNA lentiviruses by mRNA expression was conducted in MØPs, M-CSF treated MØPs differentiated to a macrophage phenotype and BMDMs using qPCR. *Mlf1* shRNA infected MØPs, M-CSF treated MØPs and BMDMs displayed no significant difference in expression of *Mlf1* when compared to its non-silencing control (Figure 3.3.5). *Maf* shRNA infected MØPs, M-CSF treated MØPs and BMDMs demonstrated no statistical difference in genomic *Maf* expression to non-silencing shRNA sequence control infected cells (Figure 3.3.3).

Unfortunately due the lack of a commercially available anti-mouse MLF1 antibody which was validated for flow cytometry, and unlike with MAF where there is a 97% identical amino acid sequence between human and mouse MAF, allowing the use of anti-human antibodies, there is only 80% similarity between human and mouse MLF1 amino acids sequence when investigated with Needleman-Wunsch global alignment analysis (165).

Flow cytometric analysis of MAF protein expression of *Maf* shRNA lentivirus was conducted with two commercial antibodies. Of the commercially available MAF antibodies validated for flow cytometry, both the BD Bioscience and Thermo antibodies showed promise under different fixation/permeabilization protocols (Figure 3.3.6). BD Bioscience MAF antibody was not significantly different in MØPs (Figure 3.3.7), or M-CSF treated MØPs (Figure 3.3.9), however in BMDMs demonstrated a statistically significant reduction in MAF ΔMFI when compared to non-silencing control (Figure 3.3.11). Whilst Thermo MAF antibody demonstrated general statistical significance by one-way ANOVA analysis, in none of the three infected cell types was the *Maf* shRNA lentiviral infected cells deemed significantly different to non-silencing shRNA sequence control infected cells (Figure 3.3.8, Figure 3.3.10 and Figure 3.3.12).

Ultimately this indicated that the *Mlf1* shRNA had no effect on genomic *Mlf1* expression by qPCR, nor did the *Maf* shRNA on *Maf* expression determined by both qPCR and flow cytometry across all cell types. Several alternative shRNAs were investigated prior to the start of this PhD, and initial infection of MØPs had suggested significance knockdown of both *Mlf1* and *Maf* with their respective shRNAs. As we were unable to validate *Mlf1* by flow cytometry and alternatives for knockdown of *Maf* in MØPs and BMDMs could be generated from *Maf* knockout mice, further shRNA generation was abandoned.

3.4.3. Validations of Overexpression Vectors of *Maf* and *Mlf1*

GFP and rCD2 packaging vectors were utilised for both *Mlf1* and *Maf* overexpression lentiviruses (in methods section 2.8). *Mlf1* overexpression lentiviruses were validated by qPCR in MØPs, M-CSF treated MØPs and BMDMs (Figure 3.3.5). *Mlf1* overexpression GFP and rCD2 lentiviruses in all three cells indicated increases in *Mlf1* expression in comparison to their respective controls and non-infected cells, with both GFP and rCD2 viruses indicating statistical significance in MØPs and M-CSF differentiated MØPs (Figure 3.3.5A and Figure 3.3.5B respectively). BMDMs suggest similar overexpression in both GFP and rCD2 lentiviruses to that in MØPs and M-CSF differentiated MØPs, however require increased sample number to generate statistical significance (Figure 3.3.5C).

Consistently, *Maf* overexpression GFP and rCD2 lentiviruses displayed increases in codon optimised *Maf* expression across all three cell types when compared to respective controls, with two-way ANOVA analysis demonstrating overall statistical significance (Figure 3.3.4). However Sidak's multiple comparison test did not indicate statistical

significance between *Maf* overexpression GFP and overexpression GFP control nor between *Maf* overexpression rCD2 and overexpression rCD2 control in MØPs and M-CSF differentiated MØPs (Figure 3.3.4). Whereas in BMDM infected cells both *Maf* overexpression GFP and rCD2 reporter lentivirus indicated statistical significance when compared to their controls by Sidak's multiple comparison test (Figure 3.3.4C). This is likely due to low sample number in MØPs, and M-CSF differentiated MØPs, with additional samples possibly elucidating this further.

Protein expression for MAF was confirmed in MØPs, M-CSF treated MØPs differentiated to a macrophage phenotype and BMDMs with both BD Biosciences and Thermo Fisher MAF antibodies. BD Bioscience staining consistently showed an increase in MAF ΔMFI in *Maf* overexpression GFP lentiviral infected MØPs, M-CSF differentiated MØPs and infected BMDMs, whereas *Maf* overexpression rCD2 infected cells indicated no apparent difference in any of the three cell types, when compared their respective overexpression control (Figure 3.3.7, Figure 3.3.9 and Figure 3.3.11). However only BMDMs were statistically significant by one-way ANOVA with Sidak's multiple comparisons indicating *Maf* overexpression GFP to be statistically significant to the overexpression GFP control (Figure 3.3.11B).

In contrast the Thermo Fisher antibody consistently demonstrated the same *Maf* overexpression GFP infected cells to be statistically significant in all three cell types, when compared to overexpression GFP control infected cells with one-way ANOVA and Sidak's multiple comparisons (Figure 3.3.8B, Figure 3.3.10B, Figure 3.3.12B). Furthermore *Maf* overexpression rCD2 infected MØPs, differentiated MØPs and BMDM also displayed an increase in expression, however only infected MØPs and BMDMs resulted in a statistically significant increase in MAF ΔMFI expression, when analysed with a one-way ANOVA and Sidak's multiple comparisons (Figure 3.3.8B and Figure 3.3.12B).

3.4.4. Nuclear Localisation of *Maf* Antibodies

Utilising the ImageStreamX Mark II imaging flow cytometry allowed investigation of nucleus localisation of the two MAF antibodies. As MAF had previously been identified to be localised predominantly in the nucleus (166) it became clear of the chosen antibodies BD Bioscience was not wholly target specific, with diffuse staining throughout the cytoplasm (Figure 3.3.13A), whereas Thermo Fisher antibody displayed a high percentage

of overlap with DAPI nuclear staining (Figure 3.3.14A), and a higher degree of similarity dilate value with both *Maf* overexpression GFP and rCD2 vectors (Figure 3.3.14B/C).

3.4.5. Summary of Main Findings

The ultimate aim of this thesis is to determine the role of key transcription factors in tissue resident macrophages. Therefore it is fundamental to establish overexpression and knockdown/knockout models of the genes of interest, through a lentiviral delivery system, and to validate their expression.

Three commercially available antibodies for MAF were tested for optimal fixation/permeabilization for intra-nuclear staining by flow cytometry. Two antibodies, both previously validated for flow cytometry and published, indicated they were viable options for MAF protein validation.

Ultimately whilst both the GFP and rCD2 overexpression lentiviruses were validated as overexpressing *Maf* by qPCR in infected MØPs and BMDMs, when the BD Bioscience antibody was used to detect MAF protein, neither overexpression reporter was deemed statistically significantly different to their respective controls in infected MØPs, however the GFP overexpression lentivirus in BMDMs did demonstrate a significant increase.

Whereas with the Thermo Fisher MAF antibody the GFP overexpression lentivirus was demonstrated to consistently be statistically significant in all three cell types. Additionally following co-localisation determination of MAF antibody staining with DNA marker DAPI, it became clear that the Thermo Fisher antibody was more specific to MAF compared with that of the BD Bioscience antibody. However without a validated genomic knockdown of *Maf* for comparison it is possible that the Thermo Fisher antibody is only partially specific.

With this validation, the antibodies can now be employed for the study of *Maf* in knockout mice. Bone marrow isolated from these mice can be used as a source to generate *Maf* knockout MØPs, as an alternative to the *Maf* shRNA construct. The generation of stable MØP *Maf* overexpression cell lines can be used as tools for exploring expected effects in these mice. Future chapters will concentrate on the primary macrophages from two *Maf* knockout mouse strains and the effects on tissue resident macrophage phenotype, and their homeostatic and inflammatory properties.

Chapter 4

Microglia in *Maf*$^{fl/fl}$*Cx3cr1*$^{ERT/+}$ and *Maf*$^{fl/fl}$*Cx3cr1*$^{Cre/+}$ Transgenic Mice

4.1. Introduction

4.1.1. *Maf* Knockout Mice

There are few studies which have undertaken work in adult *Maf* knockout mice, as ubiquitous deletion of *Maf* results in embryonic lethality on the C57BL/6 genetic background (103). It is suggested that the absence of *Maf* effects the hematopoietic microenvironment resulting in impairment of erythroblastic island formation in the foetal liver (103). However knockout *Maf* mice ($Maf^{-/-}$) have been demonstrated to be produced in other backgrounds (107,167).

$Maf^{-/-}$ bred in the 129/SvJ background exhibit survival to full gestation, however experienced a lower rate than expected by mendelian inheritance, with post/perinatal lethality meant no pups survived beyond 4 weeks (167). $Maf^{-/-}$ mice on a BALB/c background also display postnatal survival, again with lower mendelian ratio than when compared to heterozygous ($Maf^{+/-}$) litter mates (107). Serial timed mating revealed intrauterine death of $Maf^{-/-}$ embryos between embryonic day (E)17.5-18.5 (107). Of the $Maf^{-/-}$ pups which did survive gestation only one third survived past weaning age. Surviving $Maf^{-/-}$ were visually separable from their littermates due to their runted size and development of microphthalmia (a genetic eye deformity) (107). Therefore the majority of previous studies of $Maf^{-/-}$ has been conducted on embryos between E12.5-18.5 (103,104,107,167).

Lately published alternatives include utilising CRISPR-Cas9 in *LysM-Cre* mice to generate myeloid specific deletion of *Maf* (157) have been developed. However the majority of new publications have employed the Cre-Lox system utilising the *Maf* floxed mice developed by Carmen Birchmeier, at the Max Delbrück Center, Berlin, Germany (120,168–172). These B6J.B6N(Cg)-$Maf^{tm2.1Cbm}$ (henceforth referred to as $Maf^{fl/fl}$) mice obtained for the work undertaken in this thesis were kindly provided, with Carmen Birchmeier's consent, by Dan Littman's laboratory (New York University) after multiple generations of backcrossing to C57BL/6 mice (168).

4.1.2. $Cx3cr1^{Cre}$ and $Cx3cr1^{CreERT}$ Mice

Chemokine (C-X3-C) motif receptor 1 (*Cx3cr1*) is widely expressed in mononuclear phagocytes including monocytes, macrophages and dendritic cells (9). It is important to note that *Cx3cr1* expression is not entirely limited to myeloid cells including monocytes,

macrophages and neutrophils as well as expressed on natural killer (NK) cells during maturation (173–175). However due to the broad expression of *Cx3cr1* within mononuclear phagocytes it was identified as a suitable candidate for targeting myeloid cells for further study (9).

In adult mice, many tissue resident macrophages including microglia and renal macrophages express *Cx3cr1* (174), whilst other macrophages cease expression of the chemokine receptor but originate from *Cx3cr1*$^{+}$ precursors, these include peritoneal tissue resident macrophages, splenic and alveolar macrophages (9,174).

Two mouse strains were selected for crossing with the *Maf*$^{fl/fl}$ mice: i) B6J.B6N(Cg)-*Cx3cr1*$^{tm1.1(cre)Jung}$ (henceforth referred to as *Cx3cr1*^{Cre}) where the *Cx3cr1* gene is replaced with a gene encoding a constitutively active Cre recombinase; ii) B6J.129P2(C)-*Cx3cr1*$^{tm2.1(cre/ERT2)Jung}$ (henceforth referred to as *Cx3cr1*^{CreERT}), where *Cx3cr1* is replaced with a conditionally activated Cre recombinase is fused to a mutant oestrogen ligand-binding domain (CreERT2), which requires the presence of the oestrogen antagonist tamoxifen for activation (9). As both transgenes disrupt the endogenous *Cx3cr1* expression, the experimental mice used are heterozygous, to partially maintain endogenous *Cx3cr1* expression.

Microglia are characterised by particularly high expression of *Cx3cr1* compared to other myeloid cells (174,176). Validation of the Jung *Cx3cr1*^{Cre} and *Cx3cr1*^{CreERT} murine lines indicated Cre expression was mainly restricted to microglia (177) in adult mouse brain, and therefore both lines were chosen for investigating the role of *Maf* in microglia.

In *Cx3cr1*^{Cre} mice the Cre recombinase is constitutively expressed, and Cre activation in low expressing *Cx3cr1* peritoneal tissue resident macrophages is believed to be associated with the precursors established in prenatal development (7,16,174). The tamoxifen-inducible *Cx3cr1*^{CreERT} strain allows for control of *Maf* deletion, either at specific developmental stages or after normal development in adult mice, whereas the constitutive *Cx3cr1*^{Cre} line could possibly be detrimental with the deletion of *Maf* during development stages.

Cx3cr1^{CreERT} mice treated with tamoxifen by oral gavage have been shown to have no impact on the peritoneal tissue resident macrophage population (9). Therefore the *Cx3cr1*^{Cre} line was preferred for investigating the role of *Maf* in adult peritoneal macrophages.

4.2. Chapter Aims

The aims of the chapter were…

- Investigate the usefulness of an inducible Cre mouse line alongside that of constitutive Cre-Lox recombination system to restrict *Maf* knockout in microglia.
- Validate the loss of *Maf* in microglia by RNA and protein expression.
- Determine differences in proportion of Microglia and other myeloid cells in *Maf* knockout and floxed mice.
- Assess gross phenotype of microglia in the absence of *Maf* through study of common macrophage markers in naïve mice.
- Ascertain whether *Maf*-deficiency has a significant impact on the homeostatic transcriptome of the microglia.

4.3. Results

4.1.3. Validation of the Deletion of *Maf* from Maf$^{fl/fl}$Cx3cr1$^{CreERT/+}$ Mice

4.1.3.1. Protein Expression of MAF in Microglia

4-hydroxytamoxifen (OHT), a synthetic oestrogen receptor ligand, is required to activate the CreERT2 in Cx3cr1^{CreERT} mice (178). Treating mice with tamoxifen, which is metabolized to OHT, can be achieved via several delivery routes (179). To determine the best route of delivery for the Maf$^{fl/fl}$ Cx3cr1$^{CreERT/+}$ mice, intraperitoneal injection (IP) of tamoxifen in corn oil and tamoxifen-sucrose supplemented chow were tested in two pilot experiments.

As discussed in 4.1.2 tamoxifen treatment activation of CreERT2 only occurs in Cx3cr1^{+} cells such as microglia. Cx3cr1 was confirmed to be highly expressed on isolated microglia by flow cytometry and was utilised as a distinguishing surface marker along with common myeloid markers such as CD11b (Figure 4.3.1A).

Reports on dosage of tamoxifen through intraperitoneal injection as well as number of injections to activate CreERT2 recombination vary (180–183). Therefore two different doses of tamoxifen (100mg/kg or 200mg/kg in corn oil) were injected 3 or 5 times, where injections were spaced 24hrs apart in a pilot study to test efficacy. Microglia were isolated 7 days after the last injection. MAF expression in microglia was determined by flow cytometry (Figure 4.3.1B), and the delta mean fluorescent intensity (ΔMFI) (as discussed at length in Chapter 3) was calculated (Figure 4.3.1C).

Microglial MAF expression was reduced in Maf$^{fl/fl}$Cx3cr1$^{CreERT/+}$ when compared to those of *Maf*$^{fl/fl}$*Cx3cr1*$^{+/+}$mice in all three intraperitoneal tamoxifen treatments (Figure 4.3.1C). Two of the treatments, 3 injections of 200mg/kg and 5 injections of 100mg/kg, displayed higher levels of knockdown of MAF in microglia (63.79% and 65.61% respectively) compared with 3 injections of 100mg/kg (51.8%) (Figure 4.3.1C).

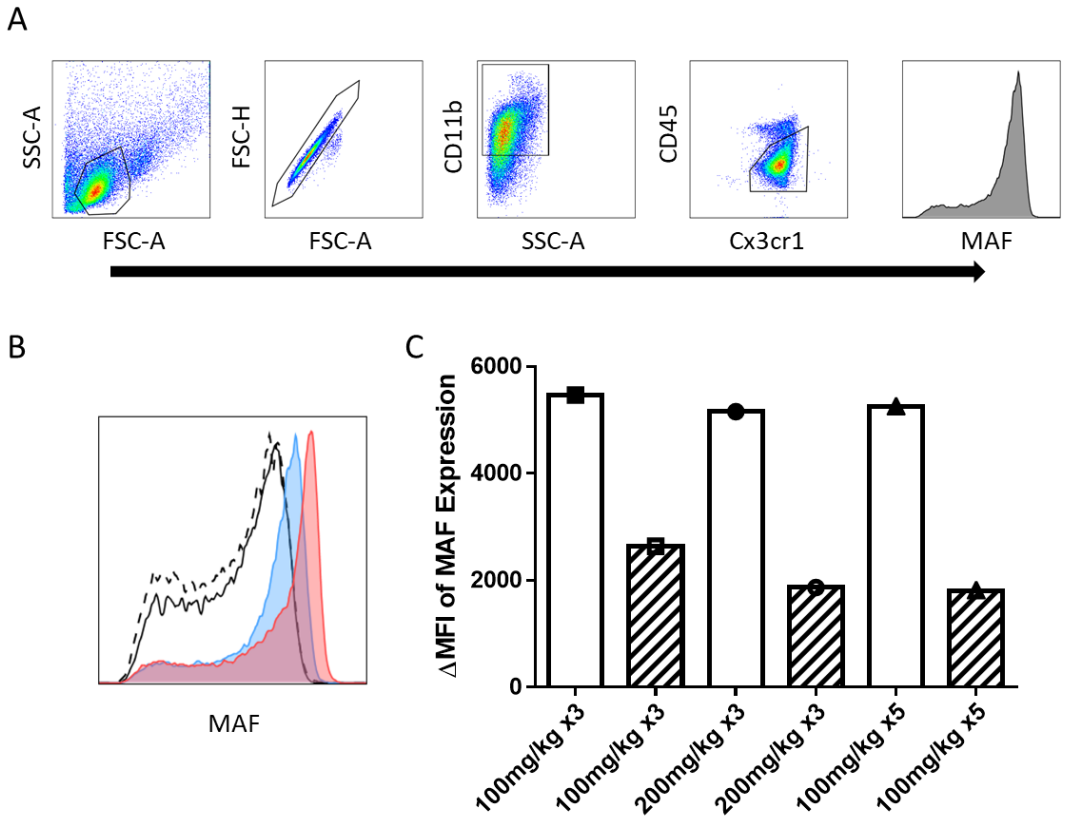

Figure 4.3.1 Determination of MAF protein expression in Maf$^{fl/fl}$Cx3cr1$^{CreERT/+}$ mice following intraperitoneal injection of tamoxifen.

Following treatment with intraperitoneal injections of tamoxifen protein expression of MAF with A) gating strategy of microglia with staining of common microglia markers and B) histogram of MAF expression by flow cytometry in *Maf$^{fl/fl}$Cx3cr1$^{+/+}$*(red) and Maf$^{fl/fl}$Cx3cr1$^{CreERT/+}$ (blue), with isotype controls (solid and dashed line respectively). C) Delta mean fluorescent intensity (ΔMFI) of MAF in microglia from *Maf$^{fl/fl}$Cx3cr1$^{+/+}$* (white) and Maf$^{fl/fl}$Cx3cr1$^{CreERT/+}$ (shaded) mice. Each bar represents a single mouse (n=1). All mice were male aged 6-8 weeks at the start of treatment.

An alternative delivery method of tamoxifen was tamoxifen-sucrose supplemented chow, which was investigated using Envigo Teklad diet TD.55125, containing 400mg/kg of tamoxifen citrate which is equivalent to 250mg/kg of tamoxifen (184). ΔMFI of MAF expression in microglia of Maf$^{fl/fl}$Cx3cr1$^{CreERT/+}$ when compared to *Maf$^{fl/fl}$Cx3cr1$^{+/+}$*mice display a 51.32 ± 2.16% (Mean ± SEM) reduction following treatment with tamoxifen-sucrose supplemented chow for 14 days prior to microglia isolation (Figure 4.3.2B). Weight loss was observed in all mice irrespective of genotype with 1:4 mice reaching the humane endpoint of 20% of initial weight loss (Figure 4.3.2C).

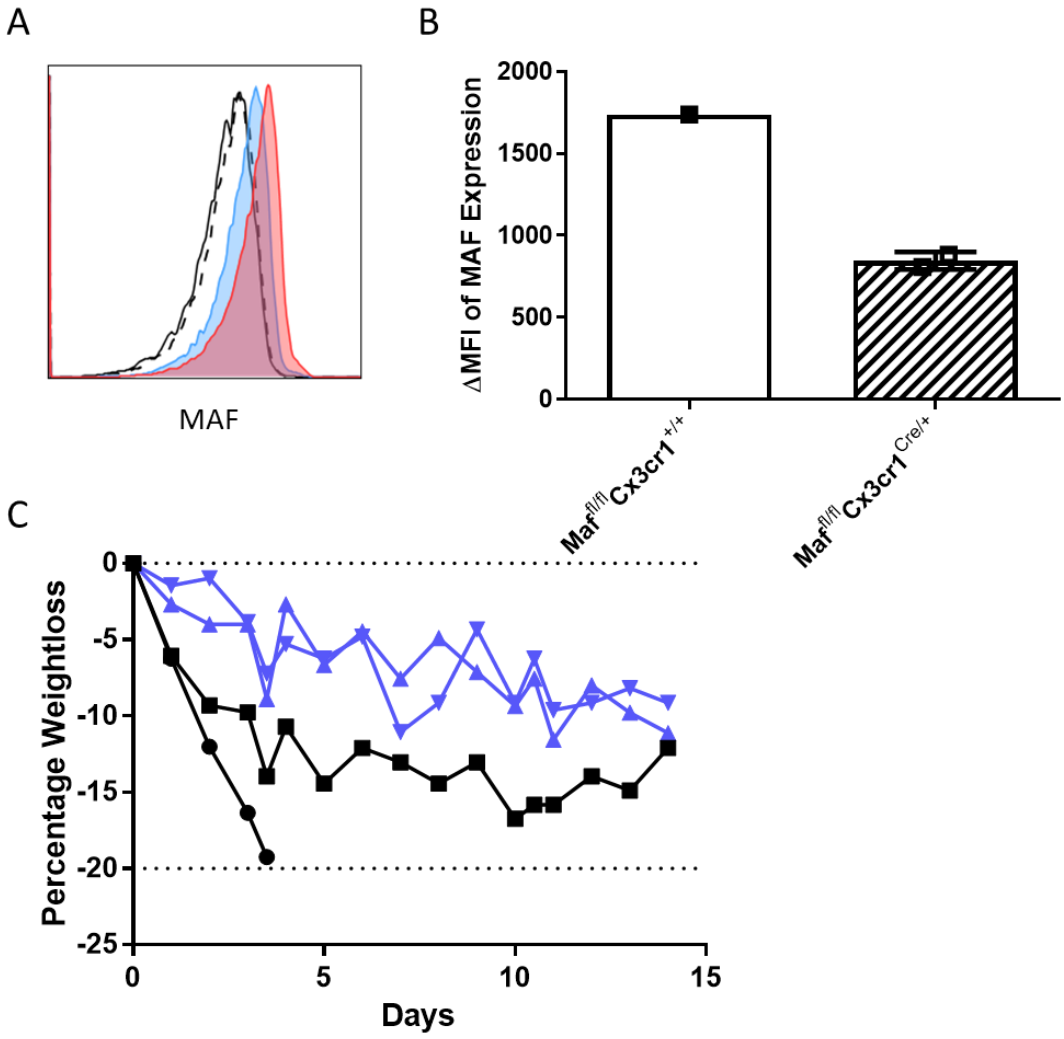

Figure 4.3.2 Determination of MAF protein expression in *Maf$^{fl/fl}$ Cx3cr1$^{CreERT/+}$* mice following tamoxifen-sucrose chow.

Following treatment for 14 days with tamoxifen-sucrose chow protein expression of MAF with A) histogram of MAF expression by flow cytometry in *Maf$^{fl/fl}$Cx3cr1$^{+/+}$* (red) and Maf$^{fl/fl}$Cx3cr1$^{CreERT/+}$ (blue) treated with tamoxifen-sucrose chow and isotype controls (solid and dashed line respectively). B) Delta mean fluorescent intensity (ΔMFI) of MAF in microglia in *Maf$^{fl/fl}$Cx3cr1$^{+/+}$* (white) and Maf$^{fl/fl}$Cx3cr1$^{CreERT/+}$ (shaded) mice. *Maf$^{fl/fl}$Cx3cr1$^{+/+}$*represents a single mouse (n=1), whilst Maf$^{fl/fl}$Cx3cr1$^{CreERT/+}$ and error bars indicate ±SEM (n=2). C) Daily weighing of *Maf$^{fl/fl}$Cx3cr1$^{+/+}$*and Maf$^{fl/fl}$Cx3cr1$^{CreERT/+}$ undergoing tamoxifen-sucrose supplemented chow treatments for 14 days, presented at percentage of weight lost from initial weight on day 0. Each line represents an individual mouse, *Maf$^{fl/fl}$Cx3cr1$^{+/+}$* (black) and Maf$^{fl/fl}$Cx3cr1$^{CreERT/+}$ (blue). Dotted lines represent initial weight and the humane end point of 20% of initial weight loss where mice were terminated. All mice were male aged 6-8 weeks at the start of treatment.

4.1.3.2. Quantitative PCR of *Maf* in Microglia

To verify genomic deletion of *Maf* in *Maf*$^{fl/fl}$*Cx3cr1*$^{CreERT/+}$ mice following treatment with 200mg/kg Tamoxifen I.P. for 3 consecutive days, microglia were isolated 7 days after the last injection, and sorted (using FACS Aria III) based on CD11b^{+}, CD45^{mid} expression (A). Microglia *Maf* expression was reduced significantly in *Maf*$^{fl/fl}$*Cx3cr1*$^{CreERT/+}$ mice by 40-ΔCT (B) and relative quantification of fold change gene expression (C) when analysed with two-way ANOVA, with genotype demonstrated as the only factor with significance (p-value = 0.0011 **, and p-value = 0.0033 ** respectively), when compared to *Maf*$^{fl/fl}$*Cx3cr1*$^{+/+}$ mice.

Mean 40-ΔCT of *Maf* in female *Maf*$^{fl/fl}$*Cx3cr1*$^{+/+}$ mice was 38.61 ± 0.0515 (Mean ± SEM) compared to *Maf*$^{fl/fl}$*Cx3cr1*$^{CreERT/+}$ females 36.99 ± 0.4915 (Mean ± SEM) (Figure 4.3.3B), with a mean difference of 1.617 ± 0.6192 (mean difference and standard error of difference (SE)), however was not deemed statistically significant by Šidák's multiple comparisons test (B).

In male mice the 40-ΔCT of *Maf* in *Maf*$^{fl/fl}$*Cx3cr1*$^{+/+}$ was 38.75 ± 0.3134 (Mean ± SEM) compared to Maf$^{fl/\ fl}$Cx3cr1$^{Cre ERT/+}$ 35.73 ± 0.4515 (Mean ± SEM) (Figure 4.3.3B), with a mean difference of 3.025 ± 0.5056 (mean difference and SE, p-value = 0.0020 **) by Šidák's multiple comparisons test.

Relative quantification of fold change gene expression of *Maf* expression in female *Maf*$^{fl/fl}$*Cx3cr1*$^{+/+}$ mice when compared to Maf$^{fl/fl}$Cx3cr1$^{Cre ERT/+}$ had a mean -2.002 $\log_2$ fold change, whilst male mice had a -2.078 $\log_2$ fold change (Figure 4.3.3C). When analysed with Šidák's multiple comparisons test relative quantification of fold change gene expression in both male and female were statistically significant (p-value = 0.0292 *, and p-value = 0.0321 *, respectively) between *Maf*$^{fl/fl}$*Cx3cr1*$^{+/+}$ and Maf$^{fl/fl}$Cx3cr1$^{Cre ERT/+}$ mice (Figure 4.3.3C).

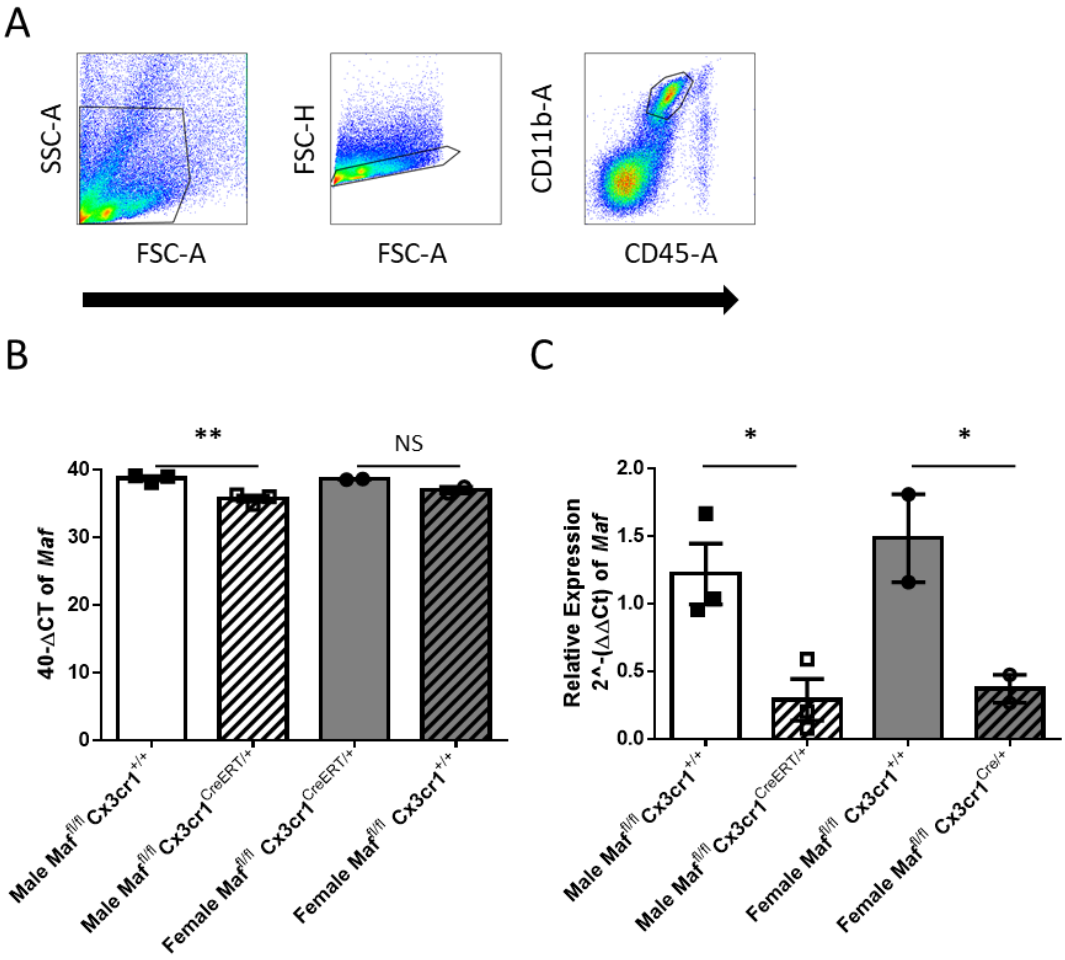

Figure 4.3.3 Verification of genomic deletion of *Maf* in Microglia from Maf$^{fl/fl}$Cx3cr1$^{CreERT/+}$ mice following three intraperitoneal injection of 200 mg/kg tamoxifen by qPCR.

Following treatment with intraperitoneal injections of following 200mg/kg tamoxifen A) gating strategy of microglia with staining of common microglia markerst. B) 40-ΔCT values and C) relative quantification of fold change gene expression of *Maf* in microglia from *Maf$^{fl/fl}$Cx3cr1$^{+/+}$* (male = white, female = grey) and Maf$^{fl/fl}$Cx3cr1$^{CreERT/+}$ (shaded) mice. All mice were 6-8 weeks of age. Error bars indicate ±SEM (female n=2, male n=3). Analysed with two-way ANOVA, with Šidák's multiple comparisons (NS = non-significant, * p-value = <0.05 and ** p-value = <0.01).

4.1.4. Validation of Deletion of Maf in Microglia in *Maf*$^{fl/fl}$*Cx3cr1*$^{Cre/+}$ Transgenic Mice

4.1.4.1. Protein Expression of MAF in Microglia

To determine if MAF expression was altered at a protein level in *Maf*$^{fl/fl}$*Cx3cr1*$^{Cre/+}$ mice ΔMFI of MAF in microglia was investigated. This demonstrated a reduction of 74.77% ± 9.54 % (Mean % difference ± SEM), when compared to those of *Maf*$^{fl/fl}$*Cx3cr1*$^{+/+}$mice (Figure 4.3.4), however was not statistically significant.

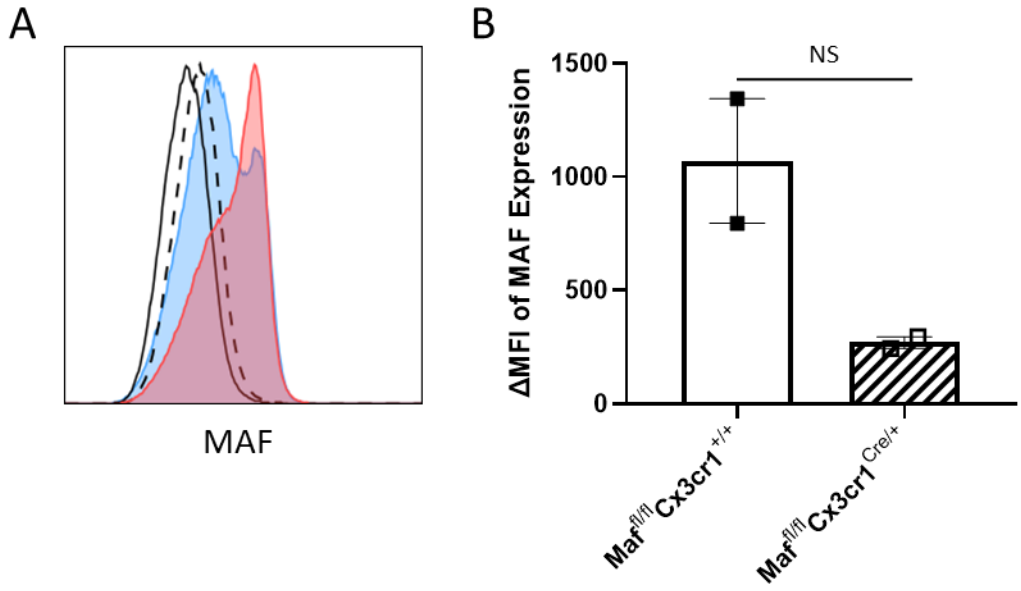

Figure 4.3.4 Determination of MAF protein expression in *Maf*$^{fl/fl}$*Cx3cr1*$^{Cre/+}$ mice

A) Histogram of MAF expression by flow cytometry in microglia from *Maf*$^{fl/f}$*Cx3cr1*$^{+/+}$ (red) and *Maf*$^{fl/f}$*Cx3cr1*$^{Cre/+}$ (blue) with isotype controls (solid and dashed line respectively). B) Delta mean fluorescent intensity (ΔMFI) of microglia in *Maf*$^{fl/fl}$*Cx3cr1*$^{+/+}$ (white) and *Maf*$^{fl/fl}$*Cx3cr1*$^{Cre/+}$ (shaded) mice. Error bars indicate ±SEM (n=2) with unpaired two-tailed T-test (p-value = 0.2246, NS = non-significant). All mice were male ages 6-8 weeks.

When investigating phenotypic differences of microglia in *Maf*$^{fl/fl}$*Cx3cr1*$^{Cre/+}$ and *Maf*$^{fl/fl}$*Cx3cr1*$^{+/+}$mice, common myeloid markers were studied using flow cytometry (Figure 4.3.5). Among the 16 myeloid markers only MAF and PU.1 displayed any clear differences in protein expression, with *Maf*$^{fl/fl}$*Cx3cr1*$^{+/+}$exhibiting higher expression than in *Maf*$^{fl/fl}$*Cx3cr1*$^{Cre/+}$ mice (Figure 4.3.5).

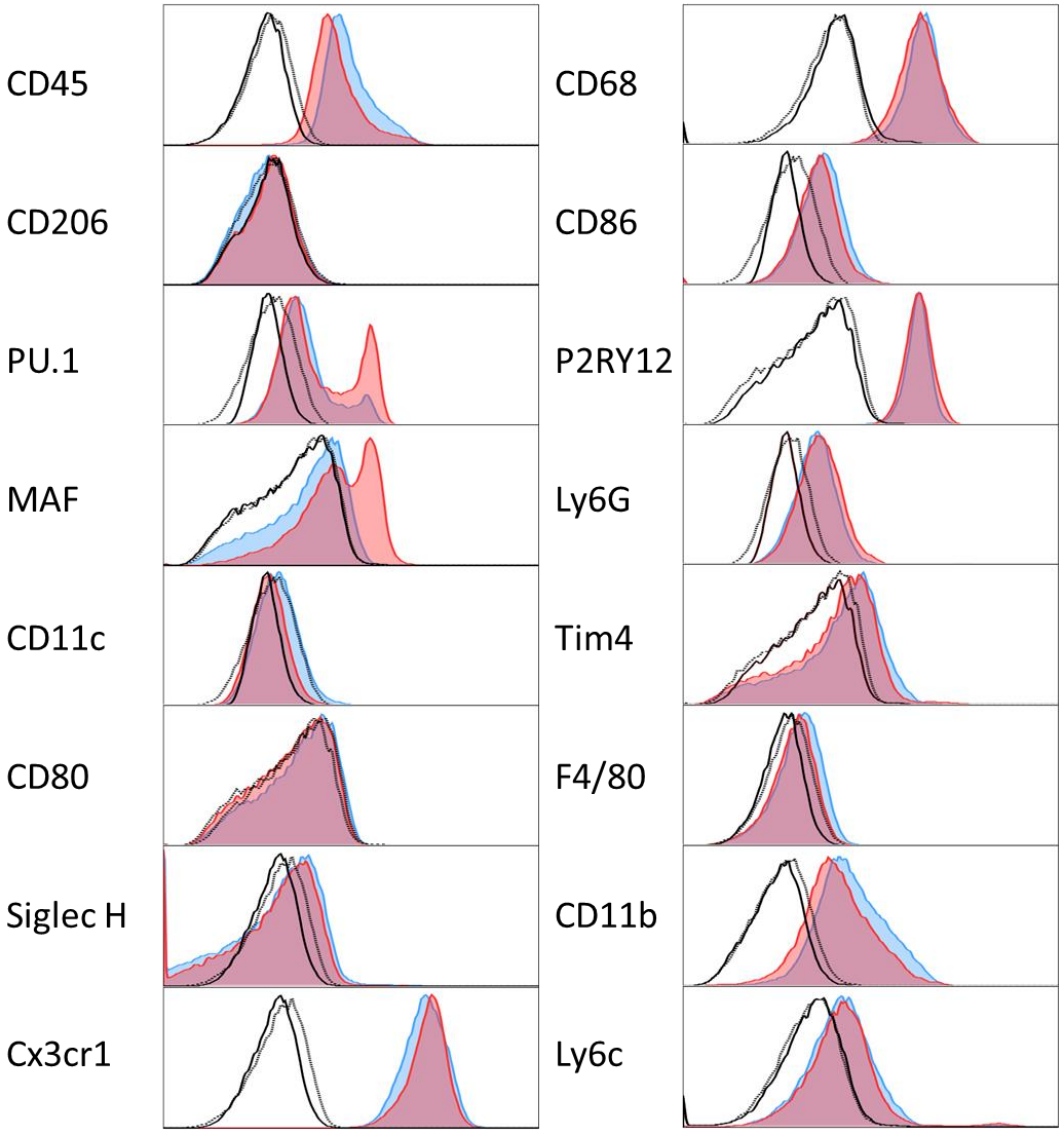

Figure 4.3.5 Expression of common myeloid markers on microglia of *Maf*$^{fl/fl}$*Cx3cr1*$^{Cre/+}$ and *Maf*$^{fl/fl}$*Cx3cr1*$^{+/+}$mice.

Flow cytometry histograms of common myeloid markers. *Maf*$^{fl/fl}$*Cx3cr1*$^{+/+}$(red), *Maf*$^{fl/fl}$*Cx3cr1*$^{Cre/+}$ (blue) with isotypes (solid black and dotted black respectively), representative of n=2. All mice were male and aged 6-8 weeks.

4.1.4.2. Quantitative PCR in Microglia

To confirm the constitutive knockout of *Maf* in microglia in *Maf*$^{fl/fl}$*Cx3cr1*$^{Cre/+}$ mice, microglia were isolated and sorted based on CD11b^{+}, CD45^{mid} expression as above (A). Microglia *Maf* expression was reduced significantly in *Maf*$^{fl/fl}$*Cx3cr1*$^{Cre/+}$ mice by 40-ΔCT (Figure 4.3.6A) and relative quantification of fold change gene expression (Figure 4.3.6B) by unpaired T-test (p-value = 0.0218 *, and p-value = 0.0253 * respectively), when compared to *Maf*$^{fl/fl}$*Cx3cr1*$^{+/+}$mice.

Mean 40-ΔCT of *Maf* in female *Maf*$^{fl/fl}$*Cx3cr1*$^{+/+}$ mice was 40.00 ± 0.5031 (Mean ± SEM) compared to *Maf*$^{fl/fl}$*Cx3cr1*$^{Cre/+}$ females 31.03 ± 2.406 (Mean ± SEM) (Figure 4.3.6A), with a mean difference of 8.973 ± 2.458 (mean difference and SE). Relative quantification of fold change gene expression of *Maf* expression in female *Maf*$^{fl/fl}$*Cx3cr1*$^{+/+}$mice when compared to *Maf*$^{fl/fl}$*Cx3cr1*$^{Cre/+}$ had a mean -6.800 $\log_2$ fold change (Figure 4.3.6B).

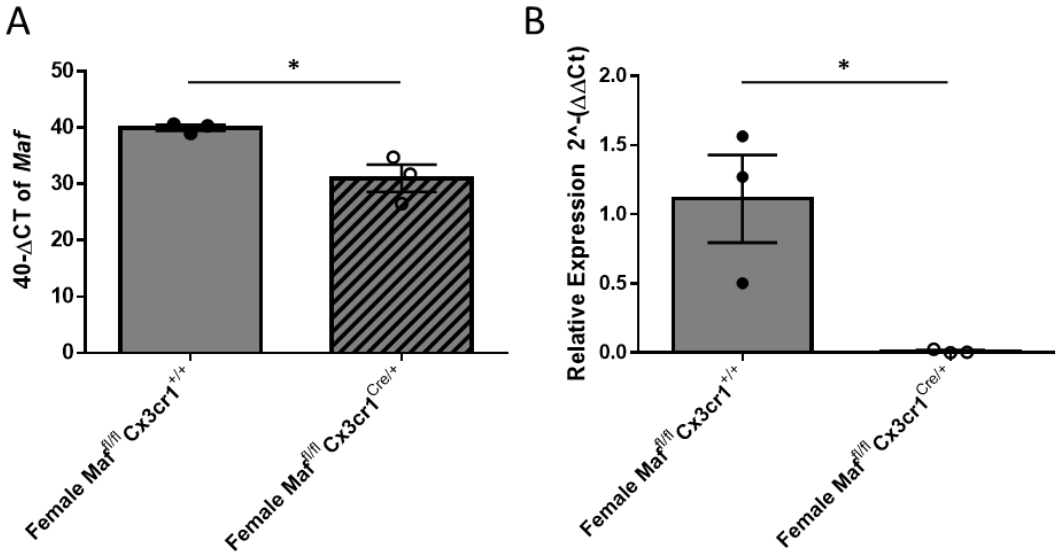

Figure 4.3.6 Determination of genomic deletion of *Maf* in microglia from *Maf*$^{fl/fl}$*Cx3cr1*$^{Cre/+}$ mice by qPCR.

A) 40-ΔCT values and B) relative quantification of fold change gene expression of *Maf* in Microglia from *Maf*$^{fl/fl}$*Cx3cr1*$^{+/+}$ and *Maf*$^{fl/fl}$*Cx3cr1*$^{Cre/+}$ (shaded) mice. All mice were female and 6-8 weeks of age. Error bars indicate ±SEM (n=3). Unpaired T-test displayed on graph (p-value = 0.05, *).

4.1.5. Border Associated Macrophages (BAMs) in *Maf*$^{fl/fl}$*Cx3cr1*$^{+/+}$ and *Maf*$^{fl/fl}$*Cx3cr1*$^{Cre/+}$ Mice

Whilst microglia are the most abundant and prominent macrophage population in the brain, border associated macrophages (BAMs) reside in the border regions of the brain such as the perivascular spaces of brain vessels, lining the meninges, and the choroid plexus. Investigation into two subpopulations of MHCII^{-} CD206^{high} and MHCII^{+} CD206^{low} BAMs between *Maf*$^{fl/fl}$*Cx3cr1*$^{+/+}$and *Maf*$^{fl/fl}$*Cx3cr1*$^{Cre/+}$ mice (Figure 4.3.7A) demonstrated the absence of the MHCII^{-} CD206^{high} BAM population. Backgating of the populations demonstrated BAM populations by CD11b and CD45 expression and distinction from microglia by their MHC and CD38 expression in *Maf*$^{fl/fl}$*Cx3cr1*$^{+/+}$(Figure 4.3.7B) and *Maf*$^{fl/fl}$*Cx3cr1*$^{Cre/+}$ mice (Figure 4.3.7C).

Two-way ANOVA of BAMs as percentage of all CD45^{+} CD11b^{+} cells, indicated population and interaction of population with genotype were statistically significant (p-value = 0.0058 ** and p-value = 0.0018 ** respectively) , but not by genotype alone (Figure 4.3.7D). The reduction in MHCII^{-} CD206^{high} BAMs was deemed statistically significant by Šidák's multiple comparison post-test (p-value = 0.0126, *), as was the increase in the percentage of MHCII^{+} CD206^{low} BAM population (p-value = 0.0469, *) (Figure 4.3.7D).

Absolute number of cells of BAM populations by two-way ANOVA with genotype and interaction of genotype with population were statistical significance (p-value = 0.0069 **, and p-value = 0.0019 **, respectively) (Figure 4.3.7E). Šidák's multiple comparison post-test indicated only MHCII^{-} CD206^{high} BAMs to be statistically significant (p-value = 0.0008, ***), whilst of MHCII^{+} CD206^{low} BAMs were not significant (Figure 4.3.7E).

When investigating the expression of MAF in BAM populations, MHCII^{-} CD206^{high} BAMs in *Maf*$^{fl/fl}$*Cx3cr1*$^{+/+}$ displayed very high MAF expression as determined by ΔMFI by flow cytometry (Figure 4.3.7F). In *Maf*$^{fl/fl}$*Cx3cr1*$^{Cre/+}$ mice MAF expression was reduced in both BAM populations, with two-way ANOVA indicating statistical significance by population, genotype and the interaction of the two factors (p-value = 0.0045 **, p-value = 0.0022 ** and p-value = 0.0194 * respectively) (Figure 4.3.7F). Post-test using Šidák's multiple comparison demonstrated the ΔMFI of MAF between *Maf*$^{fl/fl}$*Cx3cr1*$^{+/+}$and *Maf*$^{fl/fl}$*Cx3cr1*$^{Cre/+}$ mice to be statistically significant in MHCII^{-} CD206^{high} BAMs (p-value = 0.0017, **), however ΔMFI of MAF in MHCII^{+} CD206^{low} BAMs were not statistically significant (Figure 4.3.7F).

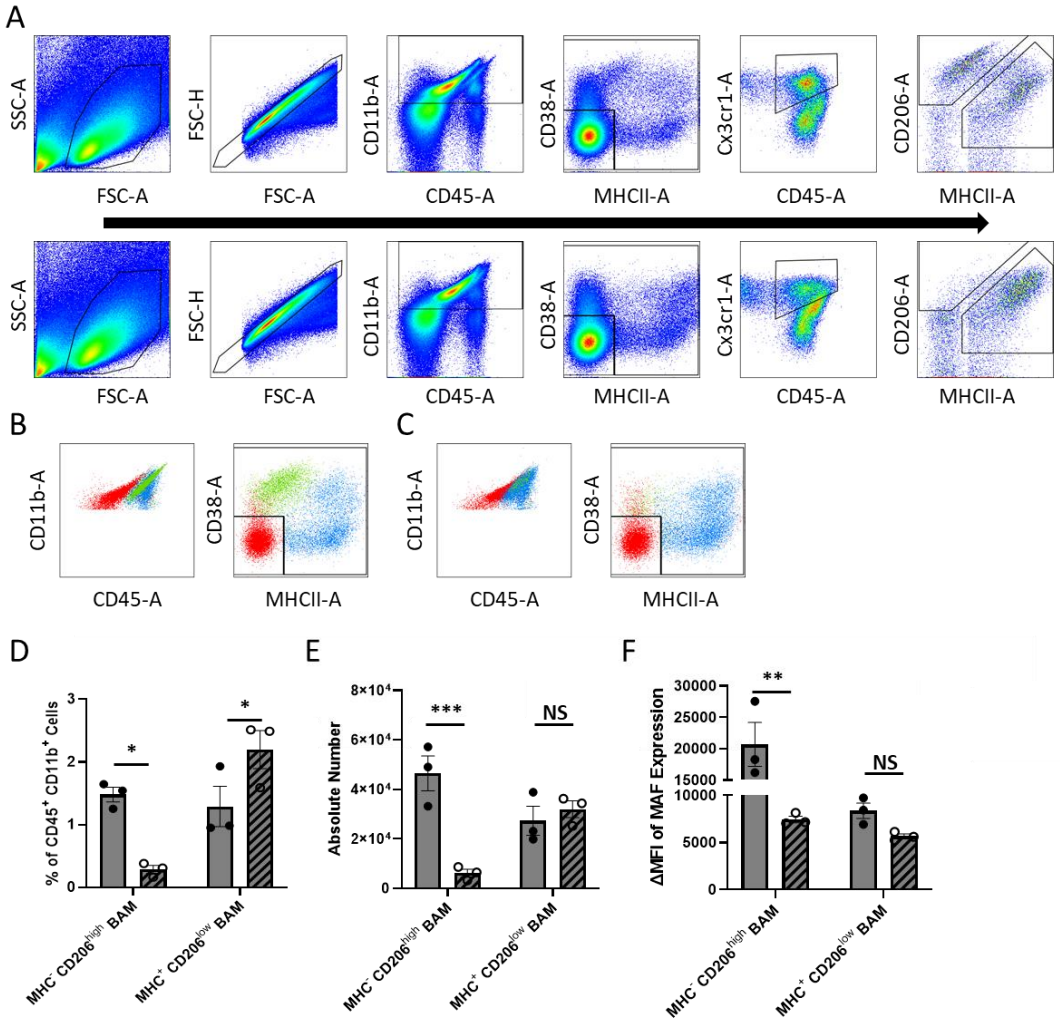

Figure 4.3.7 Border associated macrophages (BAMs) in *Maf*$^{fl/fl}$*Cx3cr1*$^{+/+}$ and *Maf*$^{fl/fl}$*Cx3cr1*$^{Cre/+}$ mice.

A) Flow cytometry gating strategy of Microglia and BAMs in *Maf*$^{fl/fl}$*Cx3cr1*$^{+/+}$and *Maf*$^{fl/fl}$*Cx3cr1*$^{Cre/+}$ mice. Backgating overlays of BAM populations and microglia by CD11b/CD45 expression and MHCII/CD38 expression in B) *Maf*$^{fl/fl}$*Cx3cr1*$^{+/+}$and C) *Maf*$^{fl/fl}$*Cx3cr1*$^{Cre/+}$ mice (microglia = red, MHCII^{-} CD206^{high} BAMs = green and MHCII^{+} CD206^{low} BAMs = blue). BAMs as D) percentage of cells of CD45^{+} and CD11b^{+} gating strategy and as E) absolute number. F) ΔMFI of MAF protein expression in BAM populations in *Maf*$^{fl/fl}$*Cx3cr1*$^{+/+}$ and *Maf*$^{fl/fl}$*Cx3cr1*$^{Cre/+}$ mice. All mice were female and aged 6-8 weeks. Šidák's multiple comparisons test on graphs (NS = non-significant, p-value = 0.05 *, p-value = 0.01 **, p-value = 0.001 *).**

4.1.6. Immunofluorescent Microscopy of *Maf*$^{fl/fl}$*Cx3cr1*$^{+/+}$and *Maf*$^{fl/fl}$*Cx3cr1*$^{Cre/+}$ Microglia

To investigate *in situ* differences in microglial number, area of coverage and proximity of microglia (nearest neighbour), the prefrontal cortex, cortex and two areas of the hippocampus, the dentate gyrus (DG) and cornu ammonis 3 (C3) region (Figure 4.3.8A) were analysed by immunofluorescent confocal microscopy in *Maf*$^{fl/fl}$*Cx3cr1*$^{+/+}$and *Maf*$^{fl/fl}$*Cx3cr1*$^{Cre/+}$ mice. Coronal sections were stained with neuronal nuclear protein (NuEN) for neurons, glial fibrillary acidic protein (GFAP) for astrocytes and ionized calcium binding adaptor molecule 1 (Iba1) to identify microglia with DAPI for nuclear colocalization of cell bodies (Figure 4.3.8B).

Two-way ANOVA of average cell body number per mm^3 was statistically significant by genotype (p-value = 0.0133, *) (Figure 4.3.8E) with *Maf*$^{fl/fl}$*Cx3cr1*$^{Cre/+}$ mice displaying increased number compared to *Maf*$^{fl/fl}$*Cx3cr1*$^{+/+}$mice. Whilst cell number was increased across all regions, Šidák's multiple comparison test did not determine any of the regions to be statistically significant (Figure 4.3.8E).

Iba1$^+$ staining with a threshold applied to select the total area covered by microglia soma and processes (Figure 4.3.8C), resulted in no statistically significant differences between *Maf*$^{fl/fl}$*Cx3cr1*$^{+/+}$and *Maf*$^{fl/fl}$*Cx3cr1*$^{Cre/+}$ mice (Figure 4.3.8F). Whereas proximity of microglial cell bodies through nearest neighbour analysis indicated genotype to be statistically significant by two-way ANOVA (p-value = 0.0018, **) (Figure 4.3.8G). Across all regions nearest neighbour distance was reduced, however following Šidák's multiple comparison post-test the C3 region of the hippocampus was the only region found to be statistically significant (p-value = 0.0459, *) (Figure 4.3.8G).

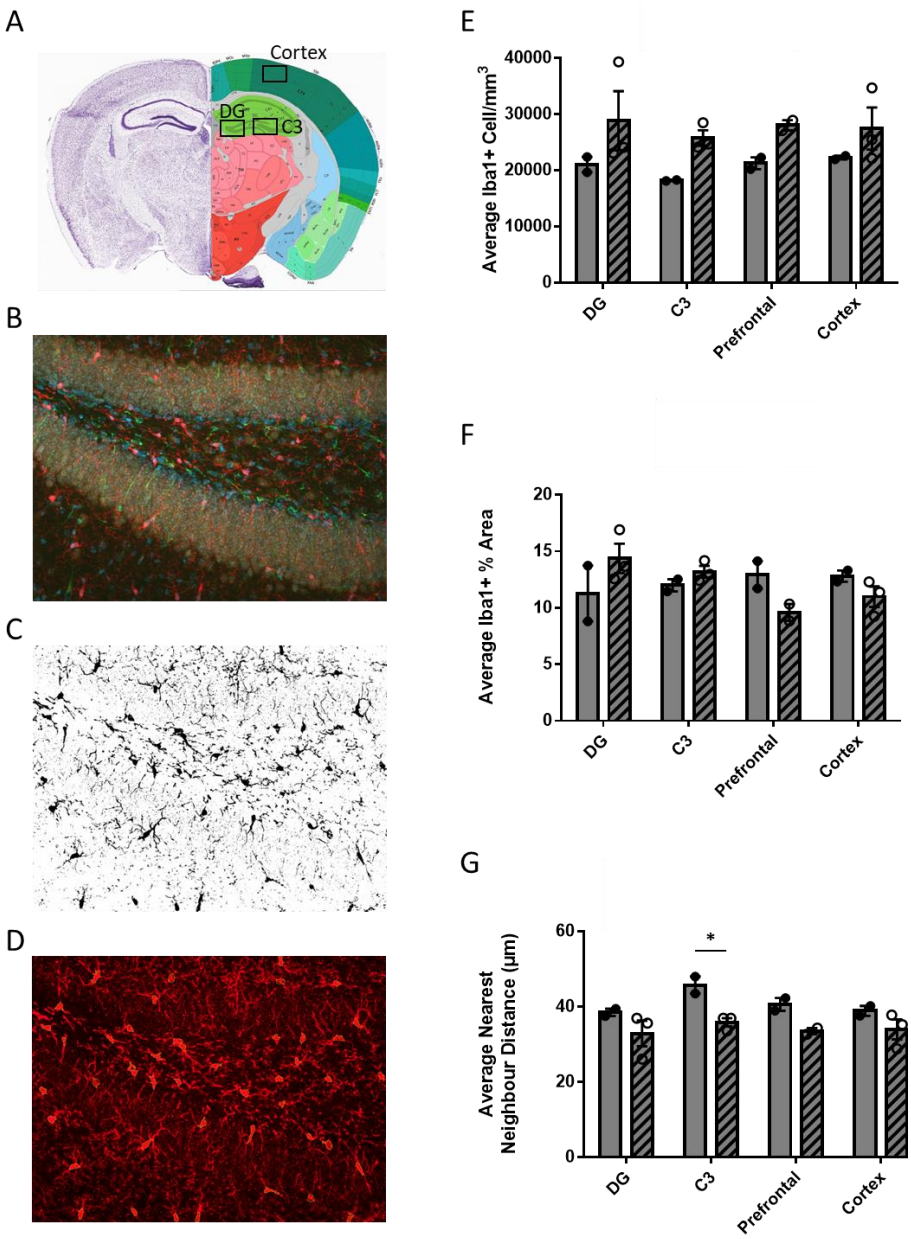

Figure 4.3.8 Immunofluorescent microscopy analysis of multiple regions of *Maf*$^{fl/fl}$*Cx3cr1*$^{+/+}$and *Maf*$^{fl/fl}$*Cx3cr1*$^{Cre/+}$ brains.

A) Regions of interest highlighted on coronal sections of mouse brain from Allen Mouse Brain Atlas (140). B) Representative staining of dente gyrus with NuEN (Yellow) for neurons, GFAP (green) for astrocytes, Iba1 (red) for microglia and DAPI (blue) for nuclei. C) Representative binary image of Iba1 staining for microglia stoma and processes for calculation of total area. D) Representative image of Iba1 staining for cell count and nearest neighbour analysis. E) Average microglia cell number, F) total area of Iba1+ staining and G) nearest neighbour analysis of microglia between *Maf*$^{fl/fl}$*Cx3cr1*$^{+/+}$ (n=2) and *Maf*$^{fl/fl}$*Cx3cr1*$^{Cre/+}$ (n=3) mice. All mice were female aged 6-8 weeks of age. Šidák's multiple comparisons test displayed on graphs (p-value = 0.05 *).

4.1.7. RNA Sequencing of Naïve Microglia from *Maf*$^{fl/fl}$*Cx3cr1*$^{+/+}$and *Maf*$^{fl/fl}$*Cx3cr1*$^{Cre/+}$ Mice

To investigate the consequences of the loss of *Maf* has on the transcriptome of microglia in *Maf*$^{fl/fl}$*Cx3cr1*$^{Cre/+}$ mice, microglia were isolated by FACS based on CD11b and CD45 expression (Figure 4.3.9A) for RNA sequencing. Raw sequencing FASTQ files were processed using Supercomputing Wales (SCW) to index, trim adapters, map reads, mark duplicates and generate feature counts (as detailed in section 2.10.2). The two most common RNA sequencing differential gene expression analyses DESeq2 and edgeR were utilised, with the combination of multiple methods thought to produce more reliable differential gene expression results (185).

DESeq2 and edgeR are based on negative binomial distribution (185) with both analyses normalising data initially via the calculation of size/normalisation factors, and both analyses hypothesise that the majority of genes are not differentially expressed. However DESeq2 uses a geometric mean normalisation strategy, whereas edgeR utilised a weighted mean of log ratios-based method. This difference in normalisation may capture different projections of differential expression.

Maf expression was determined by fragments per kilobase of transcript per million (FPKM) mapped reads indicated *Maf* in microglia to be on average 0.0409 ± 0.0327 (Mean and SEM) FPKM in *Maf*$^{fl/fl}$*Cx3cr1*$^{Cre/+}$ and average 40.59 ± 0.2625 (Mean and SEM) FPKM in *Maf*$^{fl/fl}$*Cx3cr1*$^{+/+}$mice (Figure 4.3.9B).

Exploratory data analysis of variance between samples and how they correlate through principal component analysis (PCA) indicated the *Maf*$^{fl/fl}$*Cx3cr1*$^{+/+}$ mice to have less variance than the *Maf*$^{fl/fl}$*Cx3cr1*$^{Cre/+}$ mice (Figure 4.3.10).

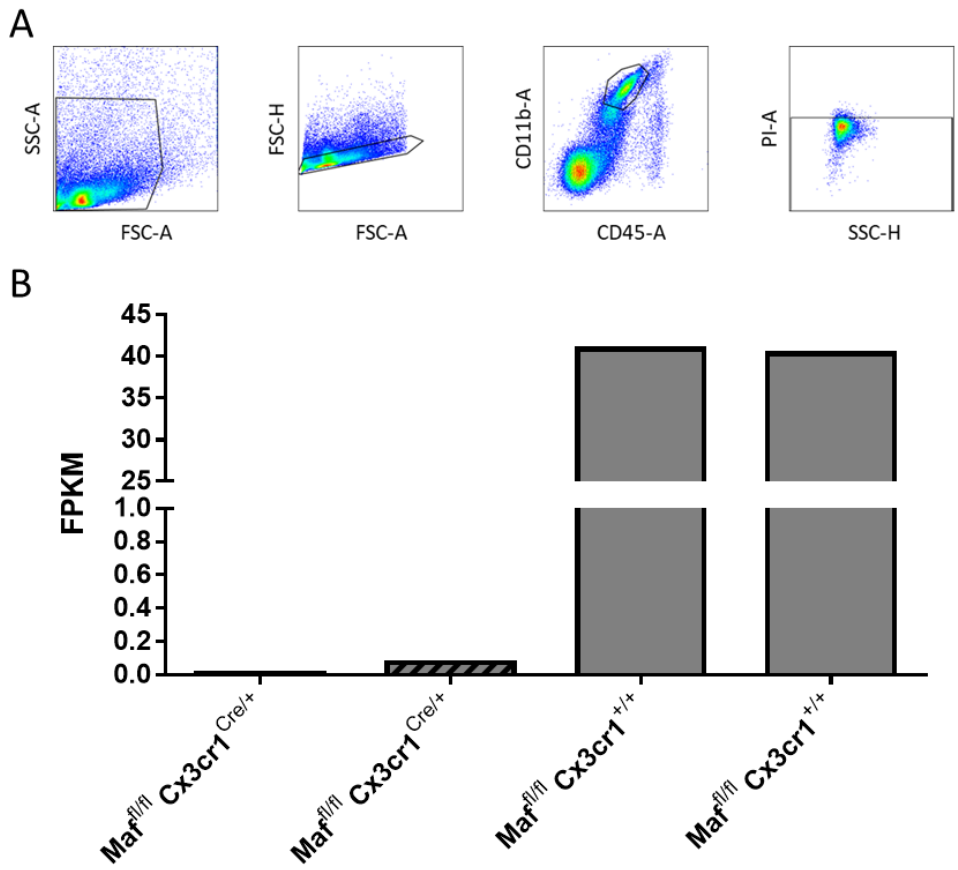

Figure 4.3.9 Fragments per kilobase of transcript per million (FPKM) mapped reads of *Maf* using DESeq2 differential expression method.

A) Gating strategy of microglia with staining of CD11b/CD45 and propidium iodine (PI) for viability. B) FPKM of *Maf* in Female *Maf*$^{fl/fl}$*Cx3cr1*$^{+/+}$(grey) and *Maf*$^{fl/fl}$*Cx3cr1*$^{Cre/+}$ (shaded) mice.

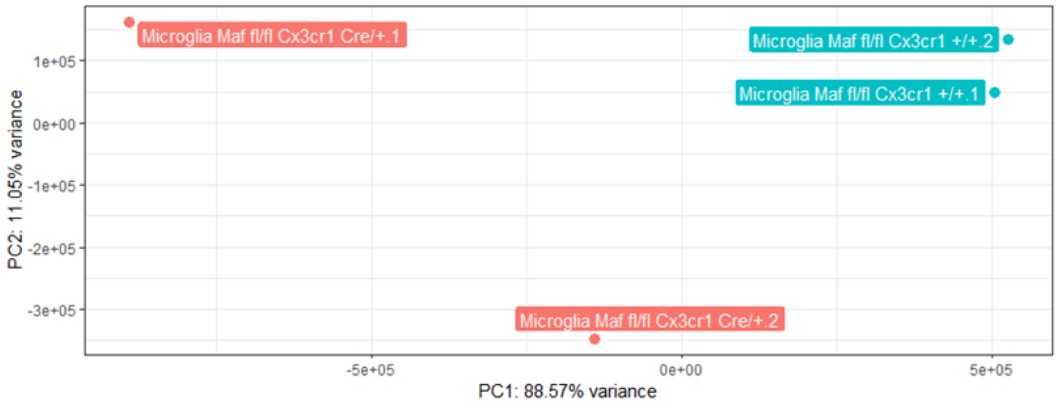

Figure 4.3.10 Principal component analysis (PCA) of RNA-sequencing samples.

Maf$^{fl/fl}$Cx3cr1$^{+/+}$mice (Teal) and Maf$^{fl/fl}$Cx3cr1$^{Cre/+}$ mice (Red).

Due to the proximity of microglia and MHCII^{-}CD206^{high} BAMs by CD11b and CD45 expression (Figure 4.3.7B/C), to check for contamination of BAMs in the microglia sorted population FPKM expression of cell specific genes were investigated alongside those of other common brain cells including astrocytes, neurons, oligodendrocytes, BAMs and blood derived monocytes (Figure 4.3.11). No obvious expression of the any of the non-microglial cell specific genes were discovered in the dataset, whereas all microglial genes were present in the dataset (Figure 4.3.11).

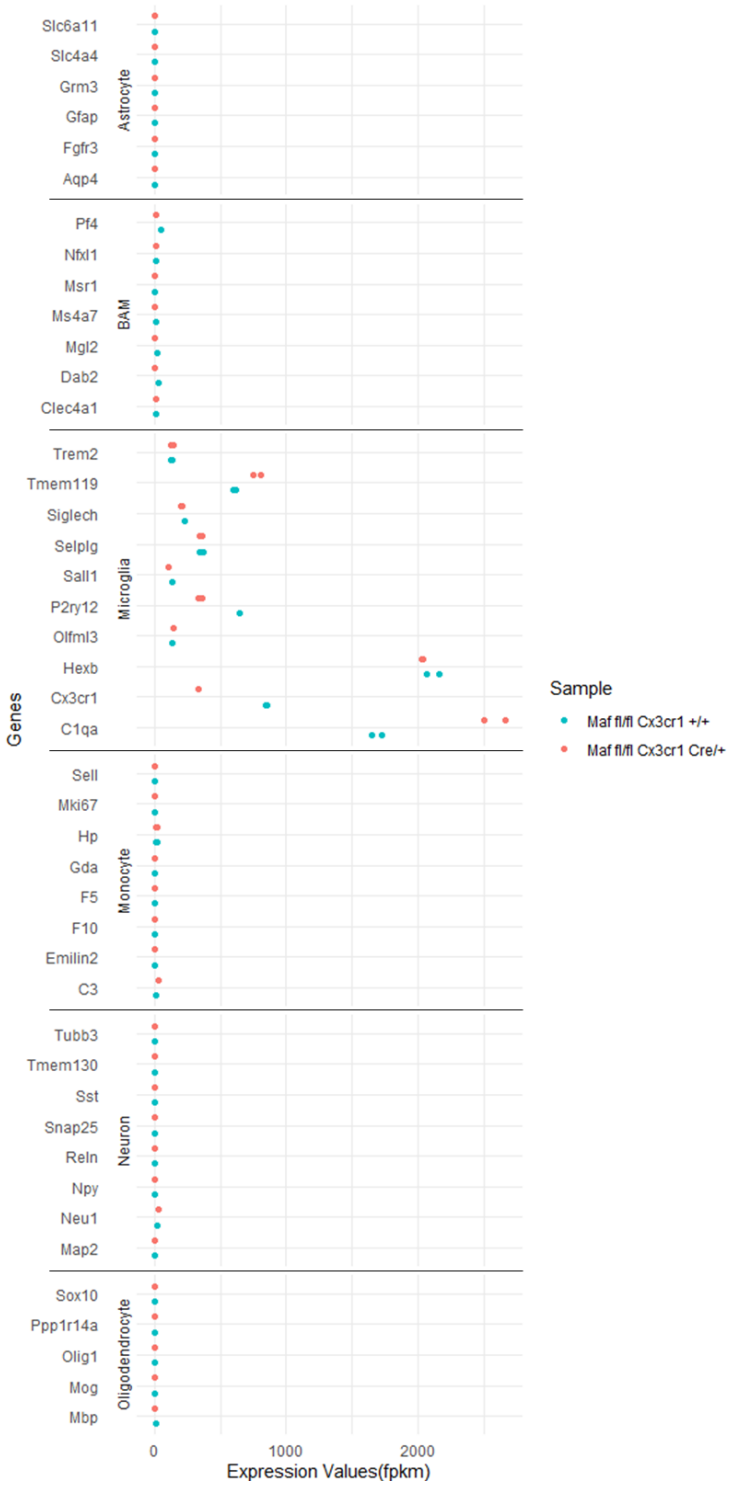

Figure 4.3.11 Fragments per kilobase of transcript per million (FPKM) of cell specific genes for common brain cells.

List of cell specific genes for astrocytes, neurons, oligodendrocytes, blood derived monocytes, border associated macrophages (BAM) and microglia, with FPKM values from dataset. *Maf*$^{fl/fl}$*Cx3cr1*$^{+/+}$mice (Teal) and *Maf*$^{fl/fl}$*Cx3cr1*$^{Cre/+}$ (Red).

4.1.7.1. Gene Expression across Multiple Differential Expression Methods

4.1.7.1.1. DESeq2 Differential Gene Expression Analysis

Maf was the most significantly reduced gene between *Maf*$^{fl/fl}$*Cx3cr1*$^{Cre/+}$ and *Maf*$^{fl/fl}$*Cx3cr1*$^{+/+}$microglia, with a -9.965 log2 fold change and an adjusted p-value of 3.10-14 (Figure 4.3.12A). Along with Maf, long non-coding RNA X-inactive specific transcript (Xist) was markedly increased by log_2 fold change, and several genes had extremely low adjusted p-values, with CUB and sushi multiple domains 3 (*Csmd3)* adjusted p-value beyond the limit of the smallest floating-point value in R (186). Therefore for visualisation and downstream analysis the maximum adjusted p-value of 1E-314 was manually applied to *Csmd3*.

Due to the wide spread of log fold changes and adjusted p-value this made the other gene changes difficult to visualise graphically, thereby setting a cut-off of adjusted p-value of 80 -log10 and a ±log2 fold change of 10 allowed visualisation of the other gene discoveries become clearer (Figure 4.3.12B).

DESeq2 differential gene analysis of *Maf*$^{fl/fl}$*Cx3cr1*$^{Cre/+}$ vs *Maf*$^{fl/fl}$*Cx3cr1*$^{+/+}$microglia generated 1,975 differential gene discoveries with an adjusted p-value <0.05 (Figure 4.3.18A) (the full list of genes can be found in Appendix II). Imposing a cut off ±1log_2 fold change resulted in 773 differential gene discoveries (Figure 4.3.18B).

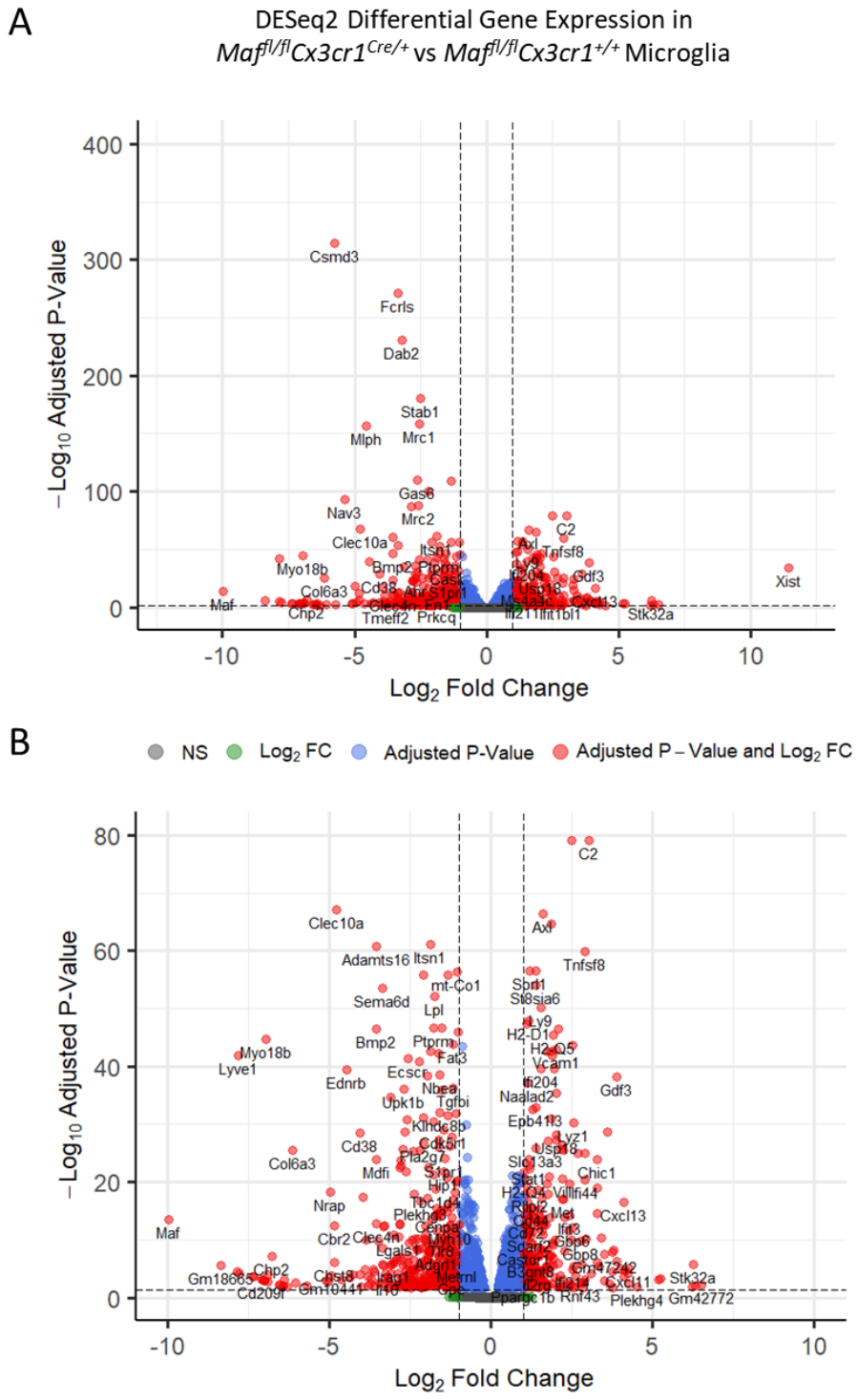

Figure 4.3.12 Differential gene expression discoveries utilising DESeq2 of *Maf*$^{fl/fl}$*Cx3cr1*$^{Cre/+}$ vs *Maf*$^{fl/fl}$*Cx3cr1*$^{+/+}$ Microglia.

RNA-Seq of naïve *Maf*$^{fl/fl}$*Cx3cr1*$^{Cre/+}$ and *Maf*$^{fl/fl}$*Cx3cr1*$^{+/+}$ microglia. A) Volcano plot of all gene discoveries using the DESeq2 differential gene expression method. B) Volcano plot with cut-off of adjusted p-value of 80 -log$_{10}$ and a 10 ±log$_2$ fold change on the graph to improve visualisation of other significant genes. Dashed lines representing cut off for adjusted p-value = 0.05 and ±log$_2$ fold change = 1 (n=2 mice of each genotype).

Canonical pathway analysis from Ingenuity pathway analysis (IPA) (Qiagen) of the DESeq2 discovered genes against those previously identified in all macrophages, identifying differentially expressed genes categorised to related canonical pathways. This resulted in 151 pathways with a p-value of overlap <0.05 (the full list of genes can be found in Appendix III).

The top 20 pathways indicated downregulation and upregulation within several canonical pathways including phagosome formation, pattern recognition receptors, Fcy receptor mediated phagocytosis, complement system and neuroinflammation signalling pathway (Figure 4.3.13).


Downregulated
No change
Upregulated
No overlap with dataset
-log(p-value)
Percentage
Phagosome Formation
Role of Pattern Recognition Receptors in Recognition of Bacteria and Viruses
Granulocyte Adhesion and Diapedesis
Role of Hypercytokinemia/hyperchemokinemia in the Pathogenesis of Influenza
Crosstalk between Dendritic Cells and Natural Killer Cells
Th1 and Th2 Activation Pathway
Agranulocyte Adhesion and Diapedesis
Fcγ Receptor-mediated Phagocytosis in Macrophages and Monocytes
Leukocyte Extravasation Signaling
Antigen Presentation Pathway
Breast Cancer Regulation by Stathmin1
Actin Cytoskeleton Signaling
Th2 Pathway
Complement System
Communication between Innate and Adaptive Immune Cells
Macropinocytosis Signaling
Th1 Pathway
Neuroinflammation Signaling Pathway
Osteoarthritis Pathway
CREB Signaling in Neurons
276
108
90
51
53
115
88
58
102
25
230
118
90
15
51
52
81
179
132
230
-log(p-value)

Figure 4.3.13 Top 20 Canonical pathways analysis of DESeq2 differential gene expression analysed genes as determined by p-value of overlap with pathways.

Canonical pathway analysis generated from Ingenuity Pathway Analysis (IPA) against those previously identified in all macrophages following DESeq2 differential gene expression method. Percentage of genes in the analysis overlap with pathway (green = downregulated, red = upregulated, white = no overlap). Numbers in bold are the total number of genes involved in the pathway, with-log p-value of overlap with each pathway indicated with orange line.

Upstream Regulators	DESeq2		
	Log_2 Fold Change	P-Value of Overlap	Targets in Dataset
Il10ra	0.45	3.57E-23	*Ankh, B3gnt7, Bmp2, C3, Ca2, Calhm6, Ccl5, Cd300lf, Cxcl9, Ednrb, F13a1, Fn1, Folr2, Gas6, Gbp2, Hcar2, Ifi16, Il12rb1, Il15ra, Il2rg, Irf7, Ly6a, Nlrc5, Olr1, Pf4, Plaat3, Reps2, Retnla, Rgs18, Rnf213, Rsad2, S1pr1, Slamf8, Stard8, Stat1, Tfec, Trpm2, Zc3h12c*
Ifng		3.03E-20	*C2, Ccl5, Ccl7, Ccr2, Cd44, Chst7, Clec10a, Cmpk2, Cxcl10, Cxcl2, Cxcl9, Fgf1, Fn1, Gbp2, Hcar2, Hip1, Hla-doa, Ifi16, Ifi44, Ifih1, Ifit1b, Ifit2, Ifit3, Ifnb1, Igf1, Il10, Itgal, Ldlr, Ly6a, Mrc1, Oas1, Oas3, Oasl, P2ry14, Pdgfc, Retnla, Rsad2, Stat1, Xaf1*
Cited2	-0.12	1.4E-16	*C3, Calhm6, Clec10a, Cmpk2, Cxcl10, Cxcl2, Cxcl3, Cxcl9, Fcgr3a/Fcgr3b, Gbp2, Hcar2, Ifi16, Ifi44, Ifih1, Ifit1b, Ifit2, Ifit3, Ifnb1, Kynu, Lpl, Mrc1, Oas1, Oas3, Oasl, P2ry14, Pdgfc, Plac8, Retnla, Rsad2, Slamf8, Xaf1*
Ptger4	-0.124	6.83E-14	*Ccl2, Ccl7, Cmpk2, Cxcl10, Cxcl9, Gbp2, Glis3, Hcar2, Ifi16, Ifih1, Ifit1b, Ifit2, Irf7, Olr1, Rnf213, Rsad2, S1pr1, Slamf8, Tbc1d4, Tlr8, Tnfsf10, Usp18, Xaf1*
Myd88	-0.035	8.97E-14	*Ccl5, Clec10a, Cmpk2, Cxcl10, Cxcl13, Cxcl2, Cxcl3, Cxcl9, Ednrb, Fpr1, Ifit1b, Ifit2, Ifnb1, Il10, Itgax, Jag1, Met, Mmp14, Mrc1, Oasl, Pilra, Rsad2, Tfec*
Mef2a	-0.067	8.25E-13	*Cxcl10, Cxcl9, Gbp2, Ifi44, Ifit1b, Ifit2, Ifit3, Ifnb1, Irf7, Nlrc5, Oas1, Rsad2*
Ifnb1	4.158	1.02E-12	*Ccl2, Ccl5, Cmpk2, Cxcl10, Cxcl2, Cxcl3, Ddx3y, Gbp2, Ifi16, Ifih1, Ifit1b, Ifit2, Ifit3, Il10, Irf7, Rsad2, Sqle, Stat1, Usp18*
Ticam1	0.25	6.72E-11	*Ccl5, Cmpk2, Cxcl10, Cxcl13, Cxcl2, Cxcl3, Ednrb, Fpr1, Ifit1b, Ifit2, Ifnb1, Jag1, Met, Oasl, Pilra, Rsad2, Tfec*
Nfat5	-0.064	8.17E-10	*Ccr3, Cxcl9, Ifi16, Ifit1b, Ifit2, Ifit3, Ifnb1, Rsad2, Stat1, Tnfsf10*
Sting1	-0.119	2.67E-09	*Ccl5, Cxcl10, Cxcl2, Cxcl9, Gas7, Ifi16, Ifit1b, Ifnb1, Il10, Oasl*

Nr1h3	-0.485	4.44E-09	*Ccl2, Ccl5, Ccl7, Ccr2, Ccr3, Cd4, Cx3cr1, Cxcl10, Fgl2, Fpr1, Gas6, Il10, Il12rb1, Irf7, Itgal, Itgb3, Lyz, Mmp9*
Tnf	-0.244	1.03E-08	*Acp5, Ca2, Ccl5, Cd44, Cxcl10, Cxcl13, Cxcl2, Cxcl3, Cxcl9, Fpr1, Gbp2, Il10, Mmp9*
Ldlr	-1.479	1.12E-08	*Ccl2, Ccl5, Ccl7, Ccr2, Ccr3, Cd4, Cx3cr1, Fgl2, Fpr1, Gas6, Il10, Il12rb1, Irf7, Itgb3, Lyz, Mmp14, Mmp9, Msr1*
Nr3c1	-0.181	2.25E-08	*Ccl5, Cxcl10, Cxcl9, Hcar2, Ifit1b, Ifit2, Ifnb1, Oasl*
Irf3	0.126	3.4E-08	*Ccl5, Cxcl10, Ifih1, Ifit1b, Ifit2, Ifnb1, Rsad2*
Cop1	0.035	7.96E-08	*C3, Ccl5, Cxcl10, Cxcl3, Fpr1, Gpnmb, Ifi16, Itgax*
Tbk1	0.164	8.18E-08	*Cxcl10, Ifi16, Ifnb1, Irf7, Rsad2, Usp18*
Csf1	-0.707	1.69E-07	*Axl, Capn2, Ccl2, Ccl7, Ccr2, Cd163, Gas7, Gpnmb, Gpr34, Il10, Itgax, Lpl, Retnla*
Il4	-0.787	4.84E-07	*Cd44, Chst7, Clec10a, Cxcl10, Igf1, Il10, Lpl, Mrc1, Retnla, Tfrc*
Stat1	1.178	8.43E-07	*C3, Ccl5, Cxcl10, Cxcl9, Gbp2, Ifit1b, Ifnb1, Igf1, Ppargc1b*

Figure 4.3.14 Top 20 Upstream regulators in DESeq2 differential gene expression analysis in microglia.

Upstream regulators identified in DESeq2 analysis with log2 fold change and p-value of overlap with each pathway. Genes with an adjusted p-value of <0.05 involved in each pathway are named.

In total 138 upstream regulators were identified through analysis with IPA in the DESeq2 dataset (Appendix IV), the top 20 pathway determined by p-value of overlap (Figure 4.3.14) indicated Interleukin 10 receptor subunit alpha (*Il10ra*) to have the lowest p-value of overlap of 3.57E-23 (Figure 4.3.14). Interferon gamma (*Ifng*) also demonstrated to be statistically significant with a p-value of overlap of 3.03E-20 however a $\log_2$ fold change could not be calculated. Several other cytokines were highlighted as the upstream regulators including *Ifnb1*, *Tnf*, and *Il4* along with key regulators of cytokine signalling such

as signal transducer and activator of transcription 1 (*Stat1*) and myeloid differentiation primary response 88 (*Myd88*) (Figure 4.3.14).

4.1.7.1.2. edgeR Differential Gene Expression Analysis

Comparison of $Maf^{fl/fl}Cx3cr1^{Cre/+}$ vs $Maf^{fl/fl}Cx3cr1^{+/+}$ microglia utilising edgeR generated 1,994 differential gene discoveries with an adjusted p-value <0.05 (Figure 4.3.18A) (the full list of genes can be found in Appendix V). Imposing a cut off ±1$\log_2$ fold change resulted in 1,088 differential gene discoveries (Figure 4.3.18B).

Maf was the significantly changed between $Maf^{fl/fl}Cx3cr1^{Cre/+}$ and $Maf^{fl/fl}Cx3cr1^{+/+}$ microglia, with a -10.11 $\log_2$ fold change and an adjusted p-value 6.65E-245 (A). Additionally several other genes including *Csmd3, mt-Rnr2* , *Ddx3y* and *Xist* were more significantly changed or had larger log fold changes (Figure 4.3.15A). As previously *Csmd3, mt-Rnr2* and *Ddx3y* adjusted p-value was beyond the limit of R (186) and the maximum adjusted p-value of 1E-314 was manually applied. Additionally due to such significant changes the other gene changes were difficult to visualise, and thereby setting a cut-off of adjusted p-value of 100 -$\log_{10}$ and a ±log fold change of 10 allowed visualisation allows other gene discoveries to become clearer (Figure 4.3.15B).

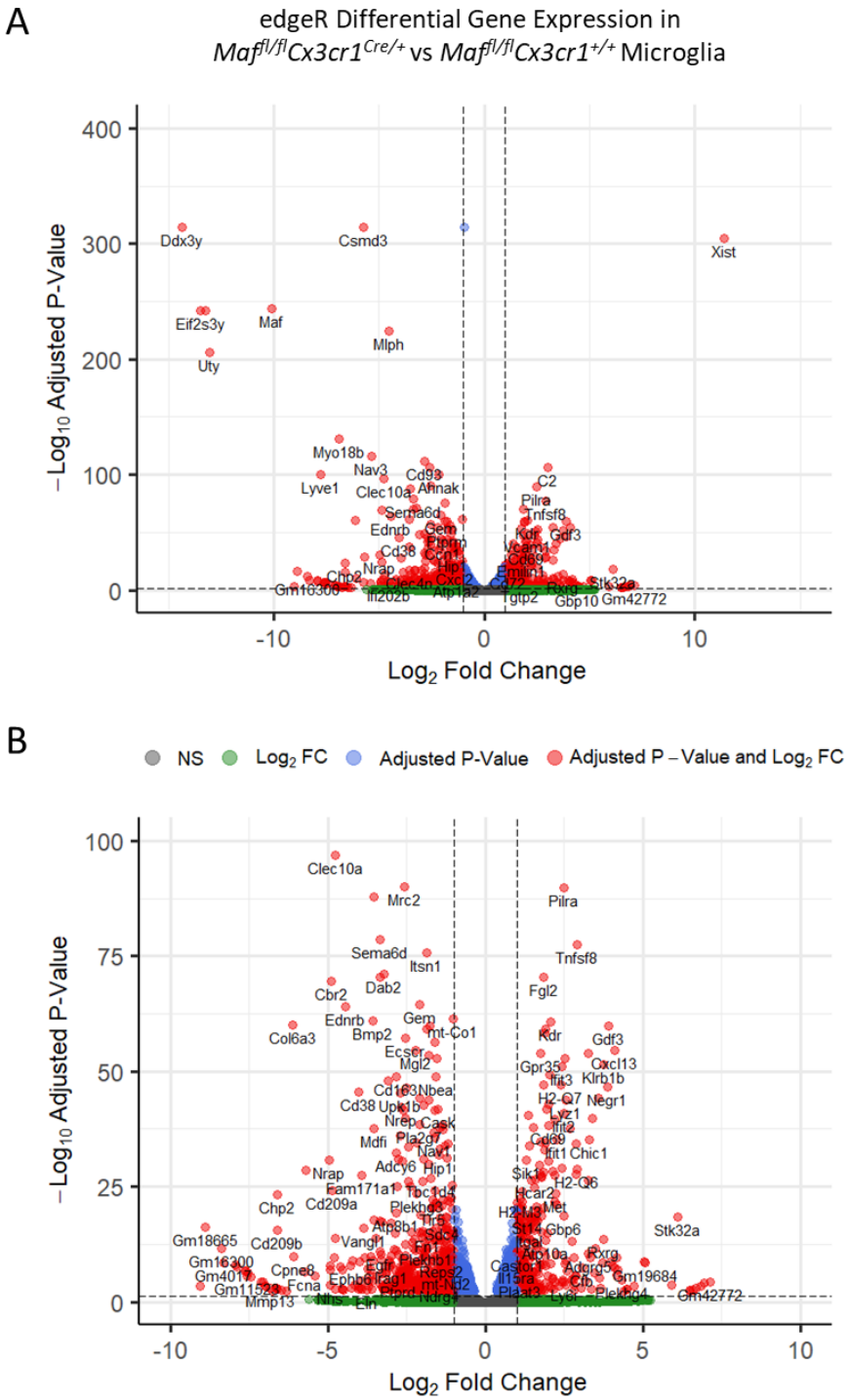

Figure 4.3.15 edgeR comparison of *Maf*$^{fl/fl}$*Cx3cr1*$^{Cre/+}$ vs *Maf*$^{fl/fl}$*Cx3cr1*$^{+/+}$Microglia.

RNA-Seq of naïve *Maf*$^{fl/fl}$*Cx3cr1*$^{Cre/+}$ and *Maf*$^{fl/fl}$*Cx3cr1*$^{+/+}$ microglia. A) Volcano plot of all gene discoveries using edgeR differential expression method. B) Volcano plot with cut-off of adjusted p-value of 100 -log10 and a 10 ±log fold change on the graph to improve visualisation of other significant genes. Dashed lines representing cut off for adjusted p-value = 0.05 and ±log$_2$ fold change = 1 (n=2 mice of each genotype).


Downregulated
No change
Upregulated
No overlap with dataset
-log(p-value)
Percentage
Phagosome Formation
Role of Hypercytokinemia/hyperchemokinemia in the Pathogenesis of Influenza
Role of Pattern Recognition Receptors in Recognition of Bacteria and Viruses
Granulocyte Adhesion and Diapedesis
Agranulocyte Adhesion and Diapedesis
Atherosclerosis Signaling
Breast Cancer Regulation by Stathmin1
Crosstalk between Dendritic Cells and Natural Killer Cells
Antigen Presentation Pathway
Communication between Innate and Adaptive Immune Cells
LXR/RXR Activation
IL-15 Production
Th1 and Th2 Activation Pathway
Altered T Cell and B Cell Signaling in Rheumatoid Arthritis
Hepatic Fibrosis / Hepatic Stellate Cell Activation
Th2 Pathway
Caveolar-mediated Endocytosis Signaling
CREB Signaling in Neurons
Dermatan Sulfate Biosynthesis (Late Stages)
Graft-versus-Host Disease Signaling
276
51
108
90
88
70
230
53
25
51
62
62
115
60
130
90
44
230
13
26
-log(p-value)

Figure 4.3.16 Top 20 Canonical pathways analysis of edgeR differential gene expression analysed genes as determined by p-value of overlap with pathways.

Canonical pathway analysis generated from Ingenuity Pathway Analysis (IPA) against those previously identified in all macrophages following edgeR differential gene expression method. Percentage of genes in the analysis overlap with pathway (green = downregulated, red = upregulated, grey = no change and white = no overlap). Numbers in bold are the total number of genes involved in the pathway, with -log p-value of overlap with each pathway indicated with orange line.

Canonical pathway analysis from IPA of the edgeR discovered genes against those previously identified in all macrophages, resulted in 111 pathways with a p-value of overlap <0.05 (the full list of genes can be found in Appendix VI). The top 20 pathway indicated downregulation and upregulation within several canonical pathways as in the DESeq2 dataset including phagosome formation, pattern recognition receptors and additional pathways including LXR/RXR activation and IL-15 production (Figure 4.3.16).

Upstream Regulators	edgeR		
	Log_2 Fold Change	P-Value of Overlap	Targets in Dataset
Il10ra	0.451	4.47E-21	*Ankh, B3gnt7, Bmp2, C3, Ca2, Calhm6, Ccl5, Cd300lf, Clec4m, Cxcl9, Ednrb, F13a1, Fn1, Folr2, Gas6, Gbp2, Hcar2, Ifi16, Il12rb1, Il15ra, Il2rg, Irf7, Ly6a (Includes Others), Nlrc5, Olr1, Pf4, Plaat3, Reps2, Retnla, Rgs18, Rnf213, Rsad2, S1pr1, Slamf8, Stard8, Stat1, Tfec, Trpm2, Zc3h12c*
Ifng	N/A	6.55E-19	*Adora2b, C2, Ccl5, Ccl7, Ccr2, Cd44, Chst3, Clec10a, Cmpk2, Cxcl10, Cxcl2, Cxcl9, Fgf1, Fn1, Gbp2, Hcar2, Hip1, Hla-doa, Ifi16, Ifi44, Ifih1, Ifit1b, Ifit2, Ifit3, Ifnb1, Igf1, Il10, Itgal, Ldlr, Ly6a (Includes Others), Mrc1, Oas1, Oas3, Oasl, P2ry14, Pdgfc, Retnla, Rsad2, Rtp4, Stat1, Xaf1*
Cited2	-0.12	4.81E-15	*C3, Calhm6, Clec10a, Cmpk2, Cxcl10, Cxcl2, Cxcl3, Cxcl9, Fcgr3a/Fcgr3b, Gbp2, Hcar2, Ifi16, Ifi44, Ifih1, Ifit1b, Ifit2, Ifit3, Ifnb1, Kynu, Lpl, Mrc1, Oas1, Oas3, Oasl, P2ry14, Pdgfc, Plac8, Retnla, Rsad2, Rtp4, Slamf8, Xaf1*
Ifnb1	4.101	3.1E-13	*Ccl2, Ccl5, Cmpk2, Cxcl10, Cxcl2, Cxcl3, Ddx3y, Gbp2, Ifi16, Ifih1, Ifit1b, Ifit2, Ifit3, Il10, Irf7, Nptx1, Rnd3, Rsad2, Sqle, Stat1, Usp18*
Ptger4	-0.122	5.07E-13	*Ccl2, Ccl7, Cmpk2, Cxcl10, Cxcl9, Gbp2, Glis3, Hcar2, Ifi16, Ifih1, Ifit1b, Ifit2, Irf7, Olr1, Rnf213, Rsad2, Rtp4, S1pr1, Slamf8, Tbc1d4, Tlr8, Tnfsf10, Usp18, Xaf1*
Myd88	-0.035	5.46E-12	*Ccl5, Clec10a, Cmpk2, Cxcl10, Cxcl13, Cxcl2, Cxcl3, Cxcl9, Ednrb, Fpr1, Ifit1b, Ifit2, Ifnb1, Il10, Itgax, Jag1, Met, Mmp14, Mrc1, Oasl, Pilra, Rsad2, Tfec*
Mef2a	-0.066	8.36E-12	*Cxcl10, Cxcl9, Gbp2, Ifi44, Ifit1b, Ifit2, Ifit3, Ifnb1, Irf7, Nlrc5, Oas1, Rsad2*
Sting1	-0.118	9.07E-10	*Ccl5, Cxcl10, Cxcl2, Cxcl9, Gas7, Ifi16, Ifit1b, Ifnb1, Il10, Il33, Oasl*
Ticam1	0.249	1.4E-09	*Ccl5, Cmpk2, Cxcl10, Cxcl13, Cxcl2, Cxcl3, Ednrb, Fpr1, Ifit1b, Ifit2, Ifnb1, Jag1, Met, Oasl, Pilra, Rsad2, Tfec*
Nfat5	-0.063	5.45E-09	*Ccr3, Cxcl9, Ifi16, Ifit1b, Ifit2, Ifit3, Ifnb1, Rsad2, Stat1, Tnfsf10*

Ldlr	-1.479	7.04E-09	*Ccl2, Ccl5, Ccl7, Ccr2, Ccr3, Cd4, Cx3cr1, Fgl2, Fpr1, Gas6, Il10, Il12rb1, Irf7, Itgb3, Lyz, Mmp14, Mmp9, Msr1, Scd, Tnfsf14*
Nr1h3	-0.476	1.58E-08	*Ccl2, Ccl5, Ccl7, Ccr2, Ccr3, Cd4, Cx3cr1, Cxcl10, Fgl2, Fpr1, Gas6, Il10, Il12rb1, Irf7, Itgal, Itgb3, Lyz, Mmp9, Scd*
Nr3c1	-0.18	1.03E-07	*Ccl5, Cxcl10, Cxcl9, Hcar2, Ifit1b, Ifit2, Ifnb1, Oasl*
Tnf	-0.246	1.05E-07	*Acp5, Ca2, Ccl5, Cd44, Cxcl10, Cxcl13, Cxcl2, Cxcl3, Cxcl9, Fpr1, Gbp2, Il10, Mmp9*
Irf3	0.127	1.31E-07	*Ccl5, Cxcl10, Ifih1, Ifit1b, Ifit2, Ifnb1, Rsad2*
Csf1	-0.706	2.33E-07	*Axl, Capn2, Ccl2, Ccl7, Ccr2, Cd163, Gas7, Gpnmb, Gpr34, Il10, Itgax, Lpl, Retnla, Spp1*
Tbk1	0.165	2.62E-07	*Cxcl10, Ifi16, Ifnb1, Irf7, Rsad2, Usp18*
Cop1	0.036	3.59E-07	*C3, Ccl5, Cxcl10, Cxcl3, Fpr1, Gpnmb, Ifi16, Itgax*
Il4	-0.799	2.88E-06	*Cd44, Chst3, Clec10a, Cxcl10, Igf1, Il10, Lpl, Mrc1, Retnla, Tfrc*
Mapkapk2	0.12	3.7E-06	*Cxcl2, Cxcl3, Ifnb1, Il10, Mrc1, Msr1, Retnla*

Figure 4.3.17 Top 20 Upstream regulators in edgeR differential gene expression analysis in microglia.

Upstream regulators identified in edgeR analysis with log_2 fold change and p-value of overlap with each pathway. Genes with an adjusted p-value of <0.05 involved in each pathway are named.

In total 130 upstream regulators were identified in IPA analysis of the edgeR dataset (Appendix VII), the top 20 pathway determined by p-value of overlap (Figure 4.3.17). Again *Il10ra* was identified to be significant upstream regulator with the lowest p-value of overlap of 4.47E-21 (Figure 4.3.17). The majority of the top 20 upstream regulators in DESeq2 analysis (Figure 4.3.14) were also found in the top 20 of the edgeR analysis dataset (Figure 4.3.17).

DESeq2 and edgeR differential gene expression methods resulted in 1,581 common genes with an adjusted p-value of <0.05 (Figure 4.3.18A), with edgeR identifying 413 distinct genes and DESeq2 generating 394 (Figure 4.3.18A). Of those gene discovories with an adjusted p-value of <0.05 and a ±1log_2 fold change 770 common genes were identified between the two differential expression methods (Figure 4.3.18B), edgeR generating 318 unique genes and DESeq2 generating 3 (Figure 4.3.18B).

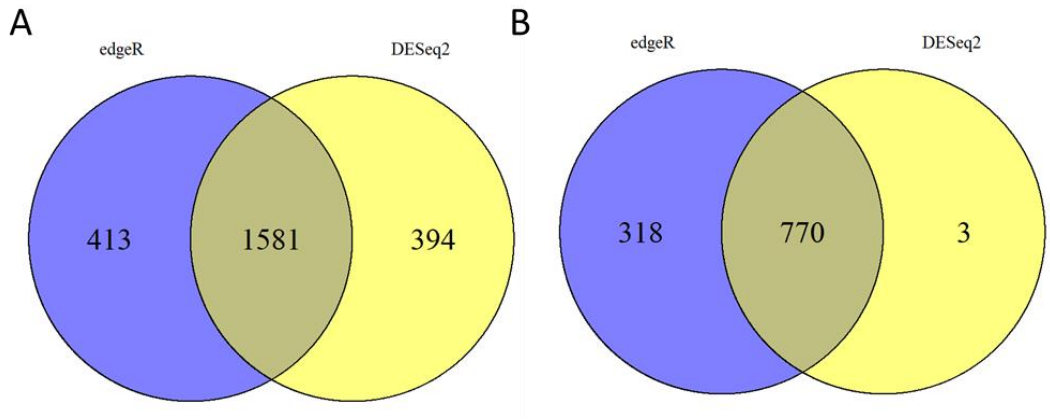

Figure 4.3.18 Venn diagram comparing between DESeq2 and edgeR differential expression methods.

A) Venn diagram comparing gene discoveries which are statistically significant (adjusted p-value <0.05) between DESeq2 and edgeR differential expression methods of naïve *Maf*$^{fl/fl}$*Cx3cr1*$^{Cre/+}$ and *Maf*$^{fl/fl}$*Cx3cr1*$^{+/+}$ microglia. B) Venn diagram comparing gene discoveries which are statistically significant (adjusted p-value <0.05) and have a ±1log_2 fold change between DESeq2 and edgeR differential expression methods of naïve *Maf*$^{fl/fl}$*Cx3cr1*$^{Cre/+}$ and *Maf*$^{fl/fl}$*Cx3cr1*$^{+/+}$ microglia.

4.1.7.2. Differential Exon Usage

Relative usage of exons was investigated using the DEXSeq (147,187) package from Bioconductor. Each exon of each sample is counted against the number of reads mapped to that exon and how many reads to any other exon of the same gene. This identifies differential expression of splice variants encoded by an individual genomic loci, leading to different functional gene products arising from a single genomic locus. Relative usage of exons between *Maf*$^{fl/fl}$*Cx3cr1*$^{Cre/+}$ and *Maf*$^{fl/fl}$*Cx3cr1*$^{+/+}$microglia generated 33 differential exons with an adjusted p-value <0.05 and a cut off ±1log$_2$ (Figure 4.3.19), which comprised of 29 unique genes.

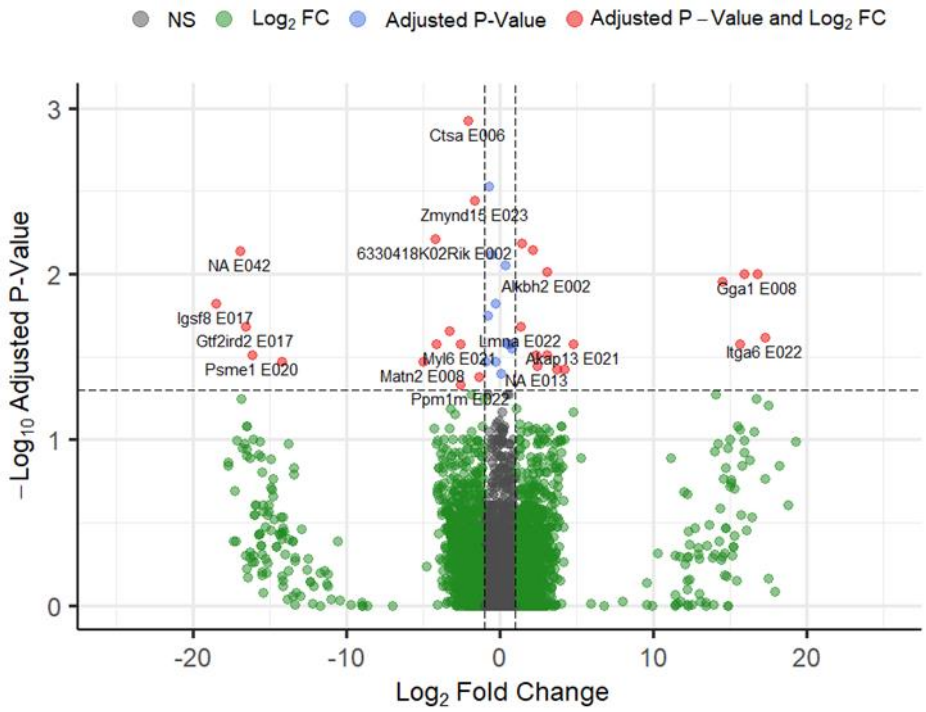

Figure 4.3.19 DEXSeq differential exon usage analysis of microglia in *Maf*$^{fl/fl}$*Cx3cr1*$^{Cre/+}$ vs *Maf*$^{fl/fl}$*Cx3cr1*$^{+/+}$mice

Volcano plot of DEXSeq differential exon usage analysis between *Maf*$^{fl/fl}$*Cx3cr1*$^{Cre/+}$ (n=2) and *Maf*$^{fl/fl}$*Cx3cr1*$^{+/+}$(n=2) mice, with dashed lines representing cut off for adjusted p-value = 0.05 and ±log$_2$ fold change = 1.

Gene	Exon	Log_2 Fold Change	Adjusted P-Value
Ctsa	E049	1.326647	0.000648
Cd47	E005	1.810041	0.000712
Abi3	E001	1.707745	0.000849
Ctsa	E006	-2.02159	0.001192
Zmynd15	E023	-1.59813	0.003627
Ctsa	E050	1.465658	0.006554
Alkbh2	E002	3.096859	0.009764
Gga1	E008	16.81873	0.00992
Tmed10	E008	14.49283	0.011177
Igsf8	E017	-18.4945	0.014988
Gtf2ird2	E017	-16.5407	0.020873
Lmna	E022	1.367213	0.020873
Wipf1	E022	-3.28931	0.02194
Itga6	E022	17.30169	0.024081
Myl6	E021	-2.52908	0.026289
Noc2l	E028	15.65274	0.026289
Rps14	E003	-4.14087	0.026602
Akap13	E021	4.79821	0.026602
Psme1	E020	-16.096	0.030821
Mtus1	E003	3.112634	0.030821
Matn2	E008	-4.95798	0.033559
Irgm1	E003	-14.1771	0.033559

Kdm1a	E007	3.725273	0.03771
Cables2	E005	4.23559	0.03771
Dnajb13	E008	-1.33601	0.04179
Ppm1m	E022	-2.56697	0.046658

Table 4.3.1 Summary of genes with relative exon usage in microglia *Maf*$^{fl/fl}$*Cx3cr1*$^{Cre/+}$ vs *Maf*$^{fl/fl}$*Cx3cr1*$^{+/+}$mice with adjusted p-value of <0.05 and ±1log$_2$ fold change

Genes with an adjusted p-value <0.05 and a cut off ±1log$_2$ are summarised in Table 4.3.1. Highlighted exons indicate a p-value of <0.05 (Figure 4.3.20, Figure 4.3.21 and Figure 4.3.22) and suggest a 16.82 log$_2$ fold change increase of differential transcript in golgi-localized gamma adaptin ear-containing ARF-binding (*Gga1*) exon 8 (ENSMUSG00000033128) (Figure 4.3.20).

Multiple exons in Cathepsin A (*Ctsa*) (ENSMUSG00000017760) (Figure 4.3.21) at E006, E049 and E050 display statistically significant differential exon usage (Table 4.3.1) between *Maf*$^{fl/fl}$*Cx3cr1*$^{Cre/+}$ compared to Maf$^{fl/fl}$Cx3cr1$^{+/+}$. Additionally exon E005 was statistically significant however did not meet the cut-off of 1 ± log$_2$ fold change (Figure 4.3.21).

Abi3 (ENSMUSG00000018381) demonstrated statistically significant changes in exon 1 (Figure 4.3.22), indicating an increase in *Abi3-201* transcript (ENSMUST00000059026.10) as E001 is only present in this transcript (Figure 4.3.22).

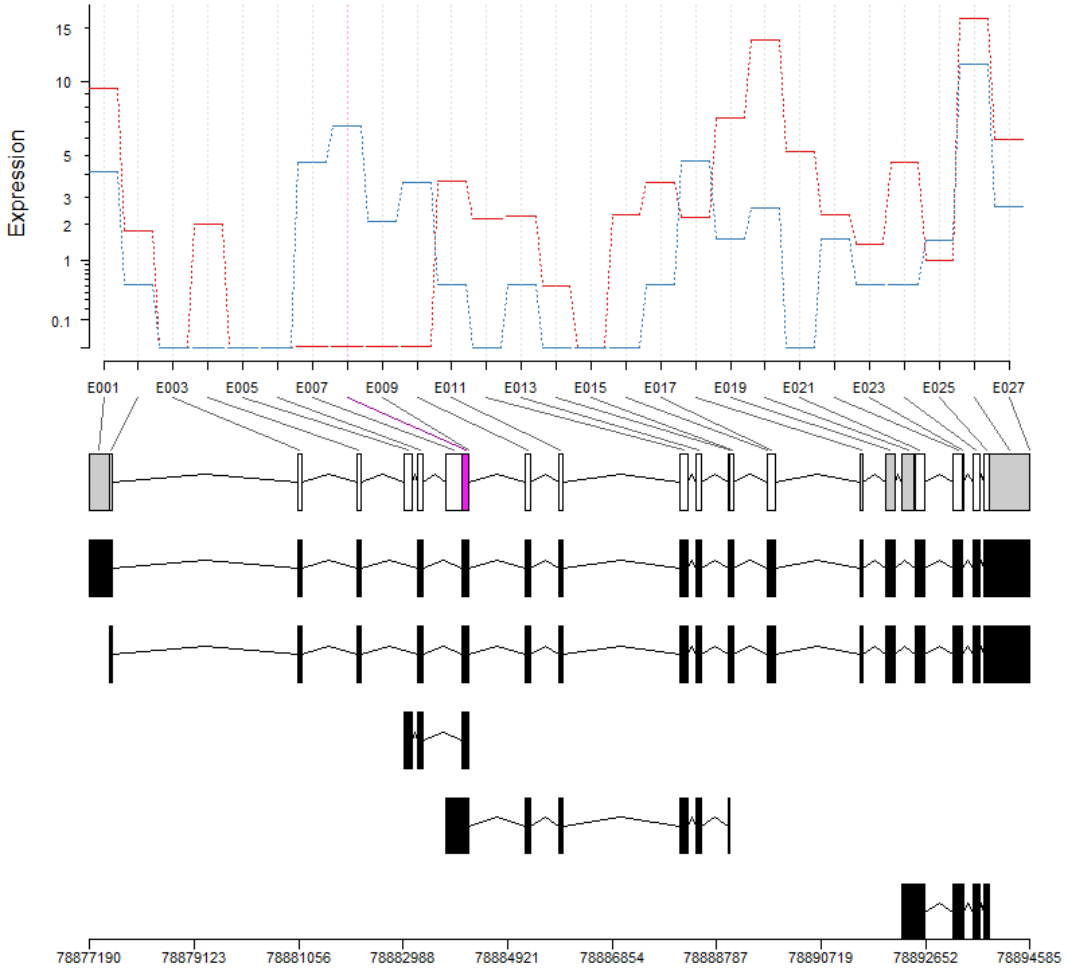

Figure 4.3.20 DEXSeq differential exon usage analysis of *Gga1* in microglia in *Maf*$^{fl/fl}$*Cx3cr1*$^{Cre/+}$ vs *Maf*$^{fl/fl}$*Cx3cr1*$^{+/+}$mice

DEXSeq plot of expression of exons in the *Gga1* gene in *Maf*$^{fl/fl}$*Cx3cr1*$^{Cre/+}$ (Blue line) (n=2) and *Maf*$^{fl/fl}$*Cx3cr1*$^{+/+}$(Red line) (n=2). Differential exons highlighted in pink (p-value <0.05) and transcripts of *Gga1* gene in black below.

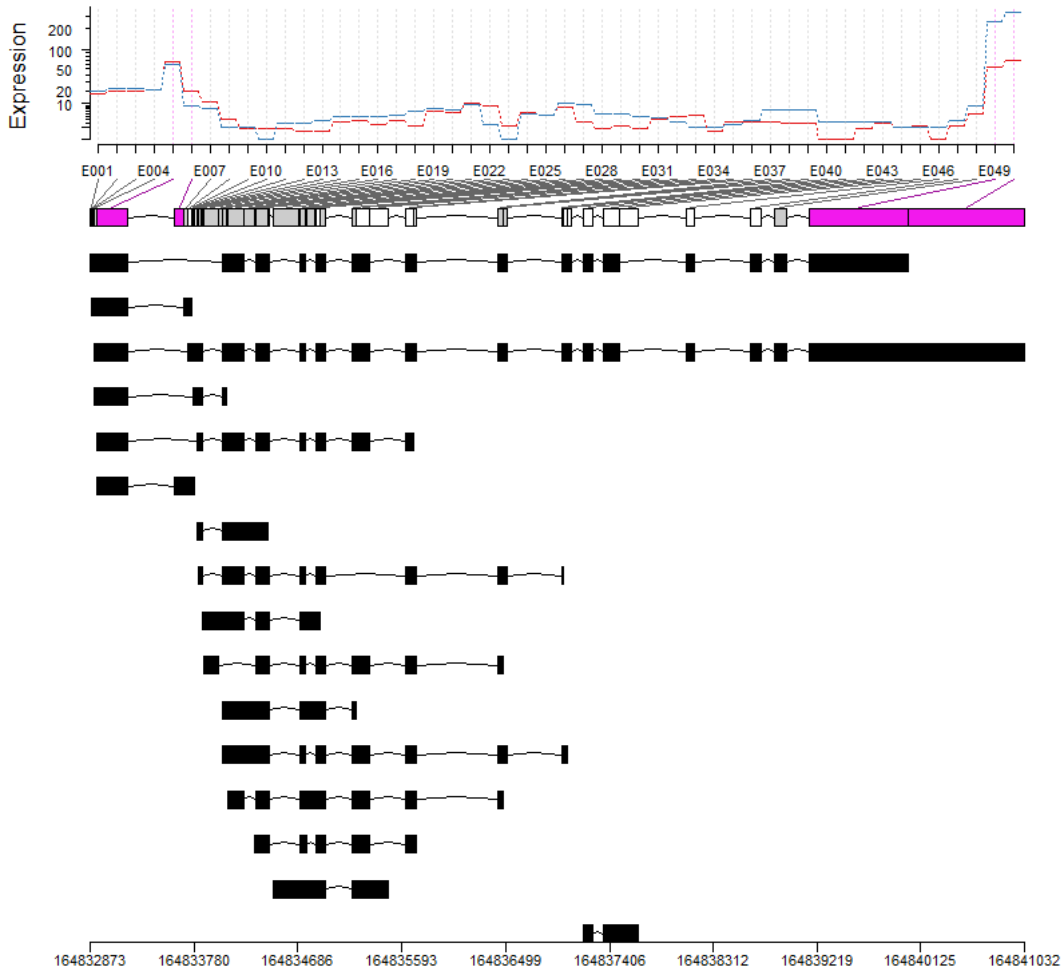

Figure 4.3.21 DEXSeq differential exon usage analysis of *Ctsa* in microglia in *Maf*$^{fl/fl}$*Cx3cr1*$^{Cre/+}$ vs *Maf*$^{fl/fl}$*Cx3cr1*$^{+/+}$mice

DEXSeq plot of expression of exons in the *Ctsa* gene in *Maf*$^{fl/fl}$*Cx3cr1*$^{Cre/+}$ (Blue line) (n=2) and *Maf*$^{fl/fl}$*Cx3cr1*$^{+/+}$(Red line) (n=2). Differential exons highlighted in pink (p-value <0.05) and transcripts of *Ctsa* gene in black below.

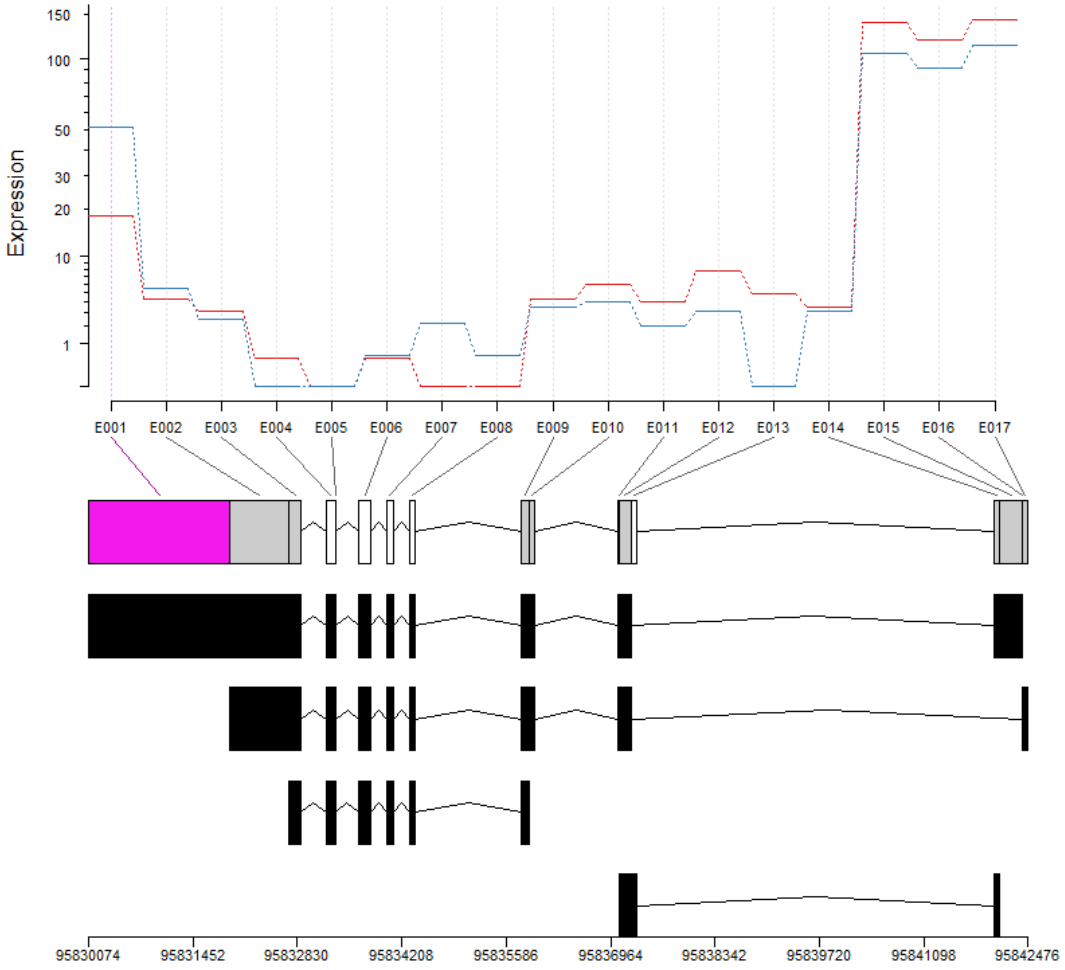

Figure 4.3.22 DEXSeq differential exon usage analysis of *Abi3* in microglia in *Maf*$^{fl/fl}$*Cx3cr1*$^{Cre/+}$ vs *Maf*$^{fl/fl}$*Cx3cr1*$^{+/+}$mice

DEXSeq plot of expression of exons in the *Abi3* gene in *Maf*$^{fl/fl}$*Cx3cr1*$^{Cre/+}$ (Blue line) (n=2) and *Maf*$^{fl/fl}$*Cx3cr1*$^{+/+}$(Red line) (n=2). Differential exons highlighted in pink (p-value <0.05) and transcripts of *Abi3* gene in black below.

4.1.8. Validation of RNA Sequencing of Naïve Microglia Gene Discoveries

Differential genes identified through DESeq2, and edgeR were selected for validation based on being protein coding, have an adjusted p-value of <0.05 and a ±1log_2 fold change in at least one of the differential expression methods, (summarised in Table 4.3.2).

Target	Microglia DESeq2		Microglia edgeR	
	Log_2 Fold Change	Adjusted P-Value	Log_2 Fold Change	Adjusted P-Value
Cd72	1.108483	3.62E-14	1.108039	1.25E-17
Cd22	1.77031	7.37E-28	1.769405	1.60E-35
Fcgr4	2.013017	4.94E-36	2.01384	1.15E-43
Cxcl13	4.101362	3.77E-17	4.095953	3.05E-55
Xist	11.41978	1.60E-34	11.37509	4.69E-305
Maf	-9.96517	3.10E-14	-10.1058	6.65E-245
Lyve1	-7.83762	1.37E-42	-7.79074	5.24E-101
Cd38	-4.04574	2.77E-29	-4.03766	2.56E-46
S1pr1	-1.43419	7.39E-25	-1.43281	7.31E-34
Tlr5	-1.67105	3.25E-16	-1.66675	2.92E-21
Tlr8	-1.52863	5.01E-11	-1.52233	4.57E-14
CD209a	NA	NA	-4.87018	5.76E-25
Cd93	-2.86671	3.07E-87	-2.8625	5.06E-112
Cd163	-2.8318	2.78E-13	-2.82462	1.65E-49
Cd276	-1.9445	2.83E-23	-1.94255	8.98E-32
Ccr2	-1.33258	0.015809	-1.32695	4.09E-09

Table 4.3.2 Summary of targets selected for validation of RNA sequencing data.

List of targets for validation by qPCR for validation with log_2 fold change and Adjusted p-value from DESeq2 and edgeR analyses. Genes which did not meet the cut off (adjusted p-value <0.05 and have a ±1log_2 fold change) in one of the analyses had an NA applied.

4.1.8.1. Validation of Gene Discoveries by qPCR

To validate the differential gene discovery analysis qPCR was conducted on *Maf*$^{fl/fl}$*Cx3cr1*$^{+/+}$and *Maf*$^{fl/fl}$*Cx3cr1*$^{Cre/+}$ microglia, isolated by FACS as above (Figure 4.3.9A). 40-ΔCT indicated overall significance by genotype, target and interaction of genotype x targets (p-value = 0.0004 ***, p-value = <0.0001 **** and p-value = <0.0001, **** respectively) when analysed by two-way ANOVA (Figure 4.3.23A). Šidák's multiple comparisons test indicated *Maf* and *Lyve1* to be statistically significant (p-value = <0.0001, **** for both) along with *Xist* (p-value = 0.0412, *) between *Maf*$^{fl/fl}$*Cx3cr1*$^{+/+}$and *Maf*$^{fl/fl}$*Cx3cr1*$^{Cre/+}$ mice (Figure 4.3.23A).

Whilst relative quantification of fold change gene expression indicated genotype, targets and the interaction of the two factors (p-value = 0.00357 *, p-value = <0.0001 **** and p-value = <0.0001 **** respectively) when analysed by two-way ANOVA (Figure 4.3.23B). Šidák's multiple comparisons test demonstrated *Cd22* (p-value = <0.0001, ****) and *Xist* (p-value = 0.0001,***) to be statistically significant (Figure 4.3.23B).

Some targets however did not validate log_2 fold change from Table 4.3.2. Therefore the correlation between the relative quantification of fold change against DESeq2 analysis (Figure 4.3.24A) and edgeR analysis (Figure 4.3.24B) log_2 fold change of *Maf*$^{fl/fl}$*Cx3cr1*$^{+/+}$and *Maf*$^{fl/fl}$*Cx3cr1*$^{Cre/+}$ microglia was investigated. DESeq2 analysis had a moderate-strong positive correlation coefficient of 0.6748365 (Figure 4.3.24A), and edgeR analysis had a moderate-strong positive correlation coefficient of 0.6781589 (Figure 4.3.24A), both of which were statistically significant (p-value = 0.004132 **, and p-value = 0.003884 ** respectively).

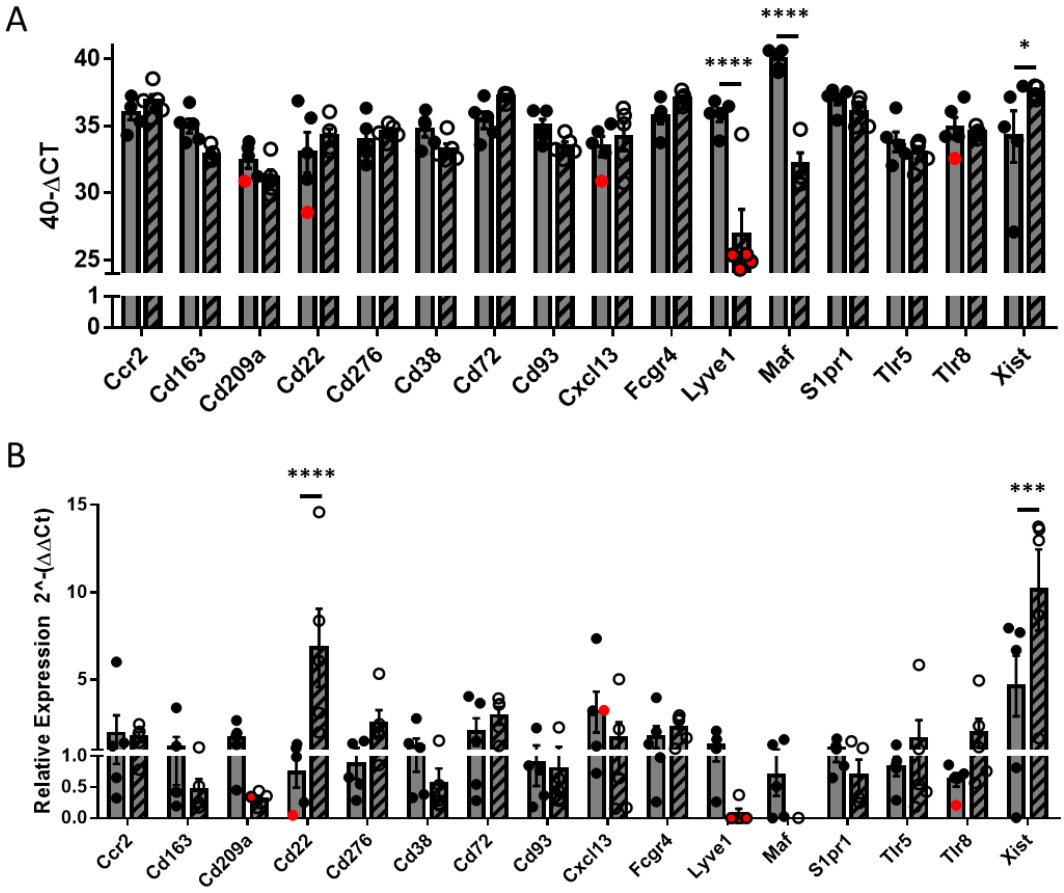

Figure 4.3.23 qPCR Validation of diffferential gene discoveries in microglia.

A) 40-ΔCT values and B) relative quantification of fold change gene expression in *Maf*$^{fl/fl}$*Cx3cr1*$^{+/+}$mice (grey) and *Maf*$^{fl/fl}$*Cx3cr1*$^{Cre/+}$ (shaded) mice microglia. Error bars indicate ±SEM (n=5). All mice were female and aged 6-8 weeks. Analysed with 2-way ANOVA with Šidák's multiple comparison test displayed on graphs (p-value = <0.05 *, p-value = <0.001, * and p-value = <0.0001, ****). Red points indicate manual CT of 40 where genes were undetectable by qPCR.**

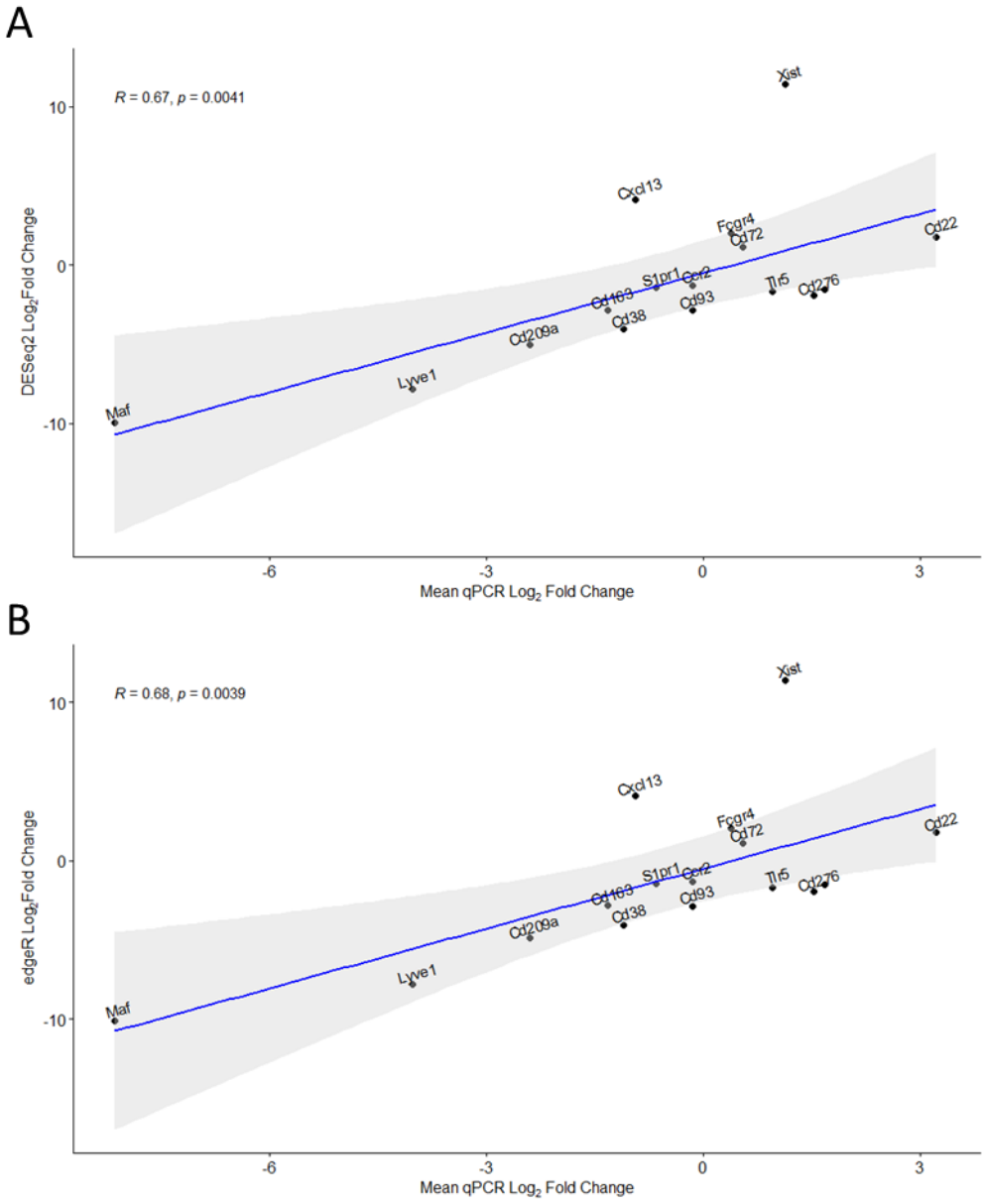

Figure 4.3.24 Pearson Correlation of RNA Sequencing log_2 Fold Change and qPCR log_2 Fold Change.

A) Correlation of DESeq2 analysis of *Maf*$^{fl/fl}$*Cx3cr1*$^{+/+}$and *Maf*$^{fl/fl}$*Cx3cr1*$^{Cre/+}$ microglia log_2 fold change against qPCR log_2 fold change based on relative quantification (2^(ΔΔCt). B) Correlation of edgeR analysis of *Maf*$^{fl/fl}$*Cx3cr1*$^{+/+}$ vs *Maf*$^{fl/fl}$*Cx3cr1*$^{Cre/+}$ microglia log_2 fold change against qPCR log_2 fold change based on relative quantification (2^(ΔΔCt)). Pearson correlation coefficient (R value and blue line) with coefficient interval (grey area) and p-value displayed on graph (p).

4.4. Discussion

4.4.1. Validation of *Maf* in *Cx3cr1*^{CreERT} and *Maf* in *Cx3cr1*^{Cre} Microglia

Generation of *Maf*$^{fl/fl}$*Cx3cr1*$^{Cre/+}$ and *Maf*$^{fl/fl}$*Cx3cr1*$^{CreERT/+}$ mice for this thesis through crossing of Maf$^{fl/fl}$ mice with the *Cx3cr1*^{Cre} and *Cx3cr1*^{CreERT} mice resulted in mice homozygous for *Maf* floxed allele and heterozygous for either *Cx3cr1*^{Cre} or *Cx3cr1*^{CreERT}. This breeding strategy allowed generation of both Cre animals and *Maf*$^{fl/fl}$*Cx3cr1*$^{+/+}$ genotypes in the same litter, making age and sex matching simpler for *in vivo* experiments, as well as minimising potential impact of the microbiome.

Pilot experiments to determine the efficacy of tamoxifen on knockdown of *Maf* in Maf$^{fl/fl}$Cx3cr1$^{CreERT/+}$ mice, either through intraperitoneal injection in corn oil (Figure 4.3.1) or tamoxifen-sucrose chow (Figure 4.3.2) were evaluated by flow cytometry. Intraperitoneal injection of either 200mg/kg 3x or 100mg/kg 5x, 24hrs apart, resulted in the greatest reduction in MAF protein expression in microglia (Figure 4.3.1). qPCR validation of *Maf* in Maf$^{fl/fl}$Cx3cr1$^{CreERT/+}$ following three intraperitoneal injection of 200 mg/kg tamoxifen demonstrated statistically significant reduction in *Maf* expression when compared to *Maf*$^{fl/fl}$*Cx3cr1*$^{+/+}$mice ()

Under the National Centre for the Replacement, Refinement and Reduction of Animals in Research (NC3Rs) guidelines, tamoxifen-sucrose chow could be deemed more refined than intraperitoneal injection with corn oil. However consistently mice receiving tamoxifen-sucrose chow resulted in 1:4 of mice having to be terminated before the end of the treatment due to reaching a humane end point (weight loss limit of -20%) (Figure 4.3.2C), which is likely due to neophobia or general distaste for the tamoxifen-sucrose chow.

Protein expression of MAF was reduced in microglia from *Maf*$^{fl/fl}$*Cx3cr1*$^{Cre/+}$ mice when compared to *Maf*$^{fl/fl}$*Cx3cr1*$^{+/+}$mice (Figure 4.3.4). qPCR validation of *Maf* in *Maf*$^{fl/fl}$*Cx3cr1*$^{Cre/+}$ demonstrated statistically significant reduction in *Maf* expression when compared to *Maf*$^{fl/fl}$*Cx3cr1*$^{+/+}$mice (Figure 4.3.6). Phenotyping of microglia indicated common myeloid markers displayed little change except for PU.1 (Figure 4.3.5) and indicated no overt abnormalities or phenotype under naïve conditions between *Maf*$^{fl/fl}$*Cx3cr1*$^{Cre/+}$ and *Maf*$^{fl/fl}$*Cx3cr1*$^{+/+}$ mice. Additionally qPCR analysis of Maf$^{fl/fl}$Cx3cr1$^{CreERT/+}$ mice indicated residual *Maf* expression following treatment with

tamoxifen (), compared to the complete loss in *Maf*$^{fl/fl}$*Cx3cr1*$^{Cre/+}$ mice (Figure 4.3.6) when compared to *Maf*$^{fl/fl}$*Cx3cr1*$^{+/+}$ mice. Therefore all further work in this thesis focused on *Maf*$^{fl/fl}$*Cx3cr1*$^{Cre/+}$ mice rather than in Maf$^{fl/fl}$Cx3cr1$^{CreERT/+}$ mice, removing any possible side effects of tamoxifen and allowing both microglia and peritoneal tissue resident macrophages to be studied in the same animal, reducing the number of animals required for this thesis.

4.4.2. BAMs in Maf$^{fl/fl}$Cx3cr1$^{+/+}$and Maf$^{fl/fl}$Cx3cr1$^{Cre/+}$ Mice

Non-parenchymal macrophages of the brain are collectively termed border-associated macrophages (BAMs) and are the second most abundant immune cell after microglia and represent about 10% of all brain macrophages (188). Two subpopulations of BAMs were investigated, MHCII^{-} CD206^{high} and MHCII^{+} CD206^{low} BAMs, and demonstrated the absence of the MHCII^{-} CD206^{high} BAM population in *Maf*$^{fl/fl}$*Cx3cr1*$^{Cre/+}$ mice (Figure 4.3.7A).

Backgating of the populations demonstrated BAM populations by CD11b and CD45 expression and distinction from microglia by their MHC and CD38 expression in *Maf*$^{fl/fl}$*Cx3cr1*$^{+/+}$(Figure 4.3.7B) and *Maf*$^{fl/fl}$*Cx3cr1*$^{Cre/+}$ mice (Figure 4.3.7C), concurrent with previous publications (172,189).

The reduction in MHCII^{-} CD206^{high} BAMs was deemed statistically significant by Šidák's multiple comparison post-test (p-value = 0.0126, *), as was the increase in the percentage of MHCII^{+} CD206^{low} BAM population (p-value = 0.0469, *) (Figure 4.3.7D). However absolute number of cells in BAM populations indicated only MHCII^{-} CD206^{high} BAMs to be statistically significant (p-value = 0.0008, ***), whilst of MHCII^{+} CD206^{low} BAMs were not significant (p-value = 0.7720, NS) (Figure 4.3.7E).

MAF expression in BAM populations indicated MHCII^{-} CD206^{high} BAMs displayed very high MAF expression as determined by ΔMFI by flow cytometry (Figure 4.3.7F), ultimately suggesting *Maf* is an essential transcription factor for MHCII^{-} CD206^{high} BAMs. This data was also recently confirmed in a publication in the same Maf$^{fl/fl}$ mice with multiple Cre strains including Lyve1$^{Cre/+}$, LySM$^{Cre/+}$ and Csf1r$^{Cre/+}$ mice(172), demonstrating the same loss of MHCII^{-} CD206^{high} BAM population and increase in MHCII^{+} CD206^{low} BAMs population (172).

The physiological functions of BAMs ultimately remain unknown; however a number of studies have suggested that BAMs support and maintain the blood brain barrier to control

the drainage of CNS (190). Additionally it is hypothesised that factors produced by BAMs could regulate or initiate many of the inflammation-associated changes in the CNS vasculature (191). Therefore the effects of ablation of the MHCII^{-} CD206^{high} BAM population in *Maf*$^{fl/fl}$*Cx3cr1*$^{Cre/+}$ mice during mild immune challenge requires further study.

4.4.3. Immunofluorescence Microscopy of Microglia

Whilst absolute number of microglia was previously determined by flow cytometry (Figure 4.3.4) indicated no statistically significant differences, however this does not consider the *in situ* 3D structure of the brain or any possible effects on cell number through isolation. Therefore determination of microglial cell number, area of coverage and nearest neighbour analysis was deemed a more accurate measurement, whilst providing additionally understanding of microglial ramifications.

Average microglial cell body number per mm^3 was statistically significant by genotype (p-value = 0.0133, *) (Figure 4.3.8E) with *Maf*$^{fl/fl}$*Cx3cr1*$^{Cre/+}$ mice displaying increased number compared to *Maf*$^{fl/fl}$*Cx3cr1*$^{+/+}$mice across all regions (Figure 4.3.8E). Additionally proximity of microglial cell bodies through nearest neighbour analysis indicated genotype to be statistically significant by two-way ANOVA (p-value = 0.0018, **) with all regions indicating a reduction in nearest neighbour distance (Figure 4.3.8G). Whereas Iba1^{+} staining of the total area covered by microglia soma and processes (Figure 4.3.8C), resulted in no statistically significant differences between *Maf*$^{fl/fl}$*Cx3cr1*$^{+/+}$and *Maf*$^{fl/fl}$*Cx3cr1*$^{Cre/+}$ mice (Figure 4.3.8F).

This overall suggests an increase in microglia number in *Maf*$^{fl/fl}$*Cx3cr1*$^{Cre/+}$ mice, and consequently a reduction in distance between cells. However with no apparent differences in area of coverage, alluding to *Maf*$^{fl/fl}$*Cx3cr1*$^{Cre/+}$ microglia having altered ramifications, which would require further investigation through morphological 3D analysis. As the C3 area of the hippocampus demonstrated statistical significance, increased study of additional hippocampal regions along with increased sample number could further elucidate these results.

4.4.4. RNA Sequencing of Naïve Microglia from *Maf*$^{fl/fl}$*Cx3cr1*$^{+/+}$and *Maf*$^{fl/fl}$*Cx3cr1*$^{Cre/+}$ Mice

Confirmation of contamination of other neural cell types in the dataset indicated no obvious expression of the any of the non-microglial cell specific genes, whereas all microglial genes were present in the dataset (Figure 4.3.11). This was encouraging that differential gene discoveries were microglia specific and not due to the overspill of MHCII^{-} CD206^{high} BAM or their ablation in Maf$^{fl/fl}$Cx3CR1$^{Cre/+}$ compared to *Maf*$^{fl/fl}$*Cx3cr1*$^{+/+}$.

However *Mrc1* (the gene which encodes CD206) and major histocompatibility (MHC) class II genes were identified as a differential gene discoveries with an adjusted p-value of <0.05 in both DESeq2 and edgeR analyses (and), possibly indicating some contamination of BAMs. This could be overcome with employing single cell sequencing instead of bulk RNA, however this would result in reduced sequencing depth, or additional staining when employing FACS to better separate the microglial and BAM populations.

DESeq2 differential gene analysis of *Maf*$^{fl/fl}$*Cx3cr1*$^{Cre/+}$ vs *Maf*$^{fl/fl}$*Cx3cr1*$^{+/+}$microglia generated 1,975 differential gene discoveries with an adjusted p-value <0.05 (Figure 4.3.18A) and imposing a cut off ±1log$_2$ fold change resulted in 773 differential gene discoveries (Figure 4.3.18B). edgeR analysis generated 1,994 differential gene discoveries with an adjusted p-value <0.05 (Figure 4.3.16A) and imposing a cut off ±1log$_2$ fold change resulted in 1,088 differential gene discoveries (Figure 4.3.16B).

Maf was the most significantly reduced gene as determined by log$_2$ fold change between *Maf*$^{fl/fl}$*Cx3cr1*$^{Cre/+}$ and *Maf*$^{fl/fl}$*Cx3cr1*$^{+/+}$microglia (A) in DESeq2 differential gene analysis, whilst *Xist* was markedly increased by log$_2$ fold change. *Xist* is a sex-associated gene, and has previously been indicated to play a role in cytokine control in BV-2 cells, a well-characterised and extensively employed model system for microglia, where knockdown of *Xist* resulted in reduced TNF-a, IL-1b, and IL-6 and enhanced IL-10 following lipopolysaccharides (LPS) activation (192). This has also been confirmed in primary microglia cells with consistent attenuation of TNF-α and IL-6 in LPS treated microglial cells when *Xist* has been deleted (193). Conversely overexpression of *Xist* enhanced the expression and release of pro-inflammatory TNF-a and IL-6 in microglia, promoting the proinflammatory polarisation of microglia (194).

edgeR analysis again *Maf* was significantly changed between *Maf*$^{fl/fl}$*Cx3cr1*$^{Cre/+}$ and *Maf*$^{fl/fl}$*Cx3cr1*$^{+/+}$microglia, with a -10.11 log$_2$ fold change and an adjusted p-value 6.65E-

245 (A). Additionally however several other genes including *Csmd3, mt-Rnr2*, *Ddx3y* and *Xist* were more significantly changed or had larger log_2 fold changes (A). As with *Xist*, other sex-associated genes *Ddx3y, Eif2s3y* (195) were highly significantly changed, with *Ddx3y* adjusted p-value beyond the limit of R.

Comparison of the two differential gene analyses DESeq2 and edgeR resulted in 1,581 common genes with an adjusted p-value of <0.05 (Figure 4.3.18A), with edgeR identifying 413 distinct genes and DESeq2 generating 394 (Figure 4.3.18A). Of those gene discoveries with an adjusted p-value of <0.05 and a $\pm 1 log_2$ fold change 770 common genes were identified between the two differential expression methods (Figure 4.3.18B), edgeR generating 318 unique genes and DESeq2 generating 3 (Figure 4.3.18B).

Of the unique differential gene discoveries in edgeR analysis, rearranged during transfection proto-oncogene (*Ret*) tyrosine kinase had an adjusted p-value of 0.0316 with a -4.1037 log_2 fold change (). RET has previously been demonstrated to be expression in monocytes and increase in expression in human macrophages (196). Moreover several proinflammatory genes encoding chemokines (*Ccl20*, *Ccl2*, *Ccl3*, *Ccl4*, *Ccl7*, *Cxcl1*) and cytokines (*Il1b*, *Il6* and *Il8*) have been shown to be upregulated by RET in human peripheral blood mononuclear cell (PBMCs), particularly in monocytes and macrophages (197).

Canonical pathway analysis in IPA of the DESeq2 discovered genes against those previously identified in all macrophages, resulted in 151 pathways with a p-value of overlap <0.05, whilst edgeR analysis resulted in 111 pathways with a p-value of overlap <0.05. Key macrophage pathways are highlighted in both analyses including phagosome formation, pattern recognition receptors, IL-12 signalling/production and neuroinflammation signalling pathway as examples (and Figure 4.3.16). However additional important macrophage pathways were identified in the DESeq2 dataset such as Fcγ receptor-mediated phagocytosis and IL-10 signalling ().

In total 138 upstream regulators were identified through IPA analysis of the DESeq2 dataset (Figure 4.3.14) and 130 upstream regulators were identified in the edgeR dataset (Figure 4.3.17), with a p-value of overlap >0.05, many of which key signalling and activation components of cytokine genes such as myeloid differentiation primary response 88 (*Myd88*) and members of the signal transducer and activator of transcription (STAT) protein family.

A considerable number of key immune related genes were evident within both DESeq2 and edgeR datasets with 3 chemokine receptors (*Cx3cr1*, *Cxcr4, Ccr2, Ccr3* and *Ccr5*), 2 chemokine receptor-like genes (*Ccrl2* in both analyses whilst *Cmklr1* only in DESeq2) and 10 chemokine ligands (*Ccl5*, *Ccl7*, *Ccl12*, *Ccl24*, *Cxcl1*, *Cxcl2*, *Cxcl9*, *Cxcl10*, *Cxcl11, Cxcl13* and *Cxcl16*) identified with an adjusted p-value of <0.05 (and). Furthermore the chemokine signalling pathway was identified in the canonical pathway analysis in both datasets (and Figure 4.3.16).

Reduction in *Cx3cr1* expression in $Maf^{fl/fl}Cx3cr1^{Cre/+}$ mice when compared to $Maf^{fl/fl}Cx3cr1^{+/+}$ mice is to be expected due to the genotype, where one of the *Cx3cr1* alleles is replaced with a gene encoding the constitutively active Cre recombinase (9). CCR2 is well established as crucial for monocyte recruitment (198), and in the brain CCR2 expression has been associated with Alzheimer's disease (AD) and was the first chemokine receptor shown to be associated with AD (199). Recent genome-wide association (GWAS)-by-familial-proxy of Alzheimer's disease has highlight *Maf* as a gene candidates in microglia to be implicated in AD pathogenesis (200).

Deficiency of CCR2 in the AD mouse model Tg2576 (which contains two "Swedish" mutations in amyloid beta precursor protein (APP)) accelerates early disease progression through impairing the accumulation of mononuclear phagocytes (199). Furthermore in the AD model the lack of CCR2 stimulated the expression of TGF-β receptors and CX3CR1 in plaque-associated microglia, implicating CX3CR1 as another chemokine receptor in AD pathology (201).

Cx3cr1 was identified as an upstream regulator with a reduction in differential expression in both DESeq2 and edgeR analyses (p-value = 0.00326 and p-value = 0.012 respectively) (and). Therefore it is possible that the loss of one of the *Cx3cr1* alleles in the $Maf^{fl/fl}Cx3cr1^{Cre/+}$ genotype may be responsible for some of the differential gene discoveries. Utilisation of a *Cx3cr1-GFP* crossed mouse as a control, such as $Maf^{fl/fl}Cx3cr1^{GFP/+}$ genotype, would account for the reduced *Cx3cr1* allele whilst maintaining *Maf* expression.

CCR3 binds to several chemokines and was notably described as a co-receptor for human immunodeficiency virus (HIV) entry into microglia (202). *Maf* has previously been linked with HIV infection in microglia through loss of p53 (203), however the exact mechanism is not understood. CCR3 in an AD mouse model has also been shown to play a role in

microglia activation, and CCR3 deficiency in an AD model resulted in reduced microgliosis (204).

Microgliosis can be defined as microglial activation that perpetuates further microglial activation, ultimately self-propelling in a progressive cycle of microglial activation (205). *Ccr3* was identified as an upstream regulator in the DESeq2 analysis with a differential expression ratio of -3.355 log_2 and a p-value = 0.00844 (Figure 4.3.14). Therefore CCR3 expression on microglia is believed to be involved in the immune response and microgliosis. This correlates with the findings from immunofluorescence microscopy of microglia discussed above in 4.4.3, indicating microgliosis in *Maf*$^{fl/fl}$*Cx3cr1*$^{Cre/+}$ mice when compared to *Maf*$^{fl/fl}$*Cx3cr1*$^{+/+}$mice.

Investigating cytokine and cytokine receptor genes highlighted *Il10* and *Il18* to have an adjusted p-value of <0.05, however only *Il10* had a ±1log_2 fold change in both DESeq2 and edgeR analysis (and). Additionally *Il33* was identified only in edgeR differential gene analysis with an adjusted p-value of <0.05 with a ±1log_2 fold change (). Several cytokine receptors had an adjusted p-value of <0.05 (*Il1r2*, *Il1rl1*, *Il2rg*, *Il6st*, *Il7r*, *Il15ra*, *Il10ra*, *Il12rb1, Il12rb2*, *Il18*) in both analyses (and), as did *Il10rb* and receptor kinases *Irak2* in DESeq2 analysis (), plus *Irak3* in edgeR differential gene analyses ().

However only *Il1r2*, *Il15ra*, *Il2rg*, *Il12rb1* had a ±1log_2 fold change in both analyses (and) with *Sigirr* and *Il17rd* discovered in the edgeR analysis with an adjusted p-value of <0.05 and a ±1log_2 fold change (). Furthermore several cytokines were identified as upstream regulators in both DESeq2 and edgeR analyses (*Csf1* (which encodes for M-CSF), *Il1A*, *Il2*, *Il4*, *Il6*, *Il13*, *Ifng, Ifnb1* and *Tnf*), with a p-value <0.05 (Figure 4.3.14 and Figure 4.3.17).

Canonical pathway analysis highlighted IL-15 production pathway in both analysis with a 4.58 -log(P-Value) and a Z-score of 1.528 indicating activation in the DESeq2 analysis (). Likewise IL-12 signalling and production pathway was identified through canonical pathway analysis, with IL-10 signalling pathway in DESeq2 analysis (), however did not indicate any significant Z score (defined as ±2 by IPA).

Maf has previously been identified in a key transcription factor for *Il10* regulation (100) and controlling the switch between anti-/proinflammatory cytokine release through IL-10 and IL-12 (206). *Il10ra* was identified as an upstream regulator and was significantly reduced in both DESeq2 and edgeR analysis with a Z-score of -6.823 and -6.605 respectively and a p-value of overlap of 4.71E-23 and 6.26E-25 respectively (Figure 4.3.14

and Figure 4.3.17). Therefore the statistically significant changes in IL-10 and its receptor subunits (*Il10ra* and *Il10rb*), and likewise IL-12 receptor subunits (*Il12rb1* and *Il12rb2*), align with the literature regarding the role of *Maf* in macrophages, however this has not been demonstrated previously in microglia.

IL-33 has been demonstrated to induces IL-10 production in foam cell macrophages (207), however the mechanism for this is not well understood. Additionally a relationship between *Maf* and *Il33* has been suggested in bone marrow-derived macrophages (BMDMs), where expression of *Maf* was upregulated by IL-33 stimulation (208,209). Therefore where loss of *Maf* resulted in a -2.413 $\log_2$ fold change of *Il*33 gene expression in the edgeR dataset suggests a direct relationship between *Maf* and *Il33* in the control of IL-10, however to fully determine this would require further study.

Classically activated signatures of proinflammatory macrophages include *Cxcl16*, *Cxcl9*, *Il15ra*, and *Il17ra* (210). In both differential gene analyses the loss of *Maf* resulted in an increase in *Cxcl9* and *Il15ra* gene expression indicating a more proinflammatory macrophage phenotype in $Maf^{fl/fl}Cx3cr1^{Cre/+}$ microglia when compared to those from $Maf^{fl/fl}Cx3cr1^{+/+}$mice.

Several genes belonging to the complement system had an adjusted p-value of <0.05 in both differential gene discoveries (*C1qa, C1qb, C1qc, C1rl, C2, C3, C3ar1, C4b, C5ar1. C5ar2, Cfh, Cfb*) with *Cfp* also identified in the edgeR analysis, however only *C2*, *C3* and *Cfb* had a ±1$\log_2$ fold change in either analysis (and). The complement system was highlighted in canonical pathway analysis with a 2.42 -log(P-Value) and a Z-score of 2.0 in edgeR and 5.58 -log(P-Value) and a Z-score of 1.633 in DESeq2 analysis (and Figure 4.3.16).

Additional a number of major histocompatibility genes (MHC) were increased in $Maf^{fl/fl}Cx3cr1^{Cre/+}$ microglia when compared to those from $Maf^{fl/fl}Cx3cr1^{+/+}$mice, included class Ia genes (*H2-D1* and *H2-K1*), several non-classical class Ib genes (*H2-Q5*, *H2-T10*, *H2-Q4*, *H2-M3*, *H2-T22*, *H2-Q7* and *H2-Q6*), as well as class II major histocompatibility (MHCII) gene (*H2-Oa*), all of which had an adjusted p-value of <0.05 and a ±1$\log_2$ fold change in both DESeq2 and edgeR analyses (and).

Class II histocompatibility gene *H2-Ob* was also increased in the both datasets, however whilst it had an adjusted p-value of <0.05 it had a 0.601 $\log_2$ fold change (and). Antigen presentation pathways was identified through canonical pathway analysis with a 5.37 and

6.28 -log(P-Value) in edgeR and DESeq2 respectively, however was unable to generate a Z-score for activation (and Figure 4.3.16).

In steady state conditions microglia lack MHCII expression (211) (Figure 4.3.7), however MHCII induction is associated with microglia activation (212) and during neurodegenerative disease the microglial population is the largest MHCII-expressing antigen presenting cells in the brain parenchyma. Furthermore alterations in MHCII expression on inflammatory macrophages has previously been indicated in IL-10 knockout mice (213). Ultimately the increase in MHCII expression in *Maf*$^{fl/fl}$*Cx3cr1*$^{Cre/+}$ microglia indicate these microglia may be more activated, when compared to those from *Maf*$^{fl/fl}$*Cx3cr1*$^{+/+}$mice and align to literature regarding reduction of IL-10.

The mitochondrial genome contains 37 genes that encode 13 proteins, 22 transfer RNAs (tRNAs), and 2 ribosomal RNAs (rRNAs) (214). Whilst rRNAs are removed prior to library preparation for RNA sequencing, tRNAs and protein encoding mitochondrial genes are still present in the library. Several of these genes were reduced in *Maf*$^{fl/fl}$*Cx3cr1*$^{Cre/+}$ microglia when compared to those from *Maf*$^{fl/fl}$*Cx3cr1*$^{+/+}$mice (*mt-Co1*, *mt-Cytb*, *mt-Nd1*, *mt-Nd2*, *mt-Nd4*, mt-*Nd5*, *mt-Rnr1*, *mt-Ta* and *mt-Tp*), and cytidine/uridine monophosphate kinase 2 (*Cmpk2*), a mitochondria-associated gene, was increased in expression, all with an adjusted p-value of <0.05 and a ±1log$_2$ fold change in both DESeq2 and edgeR differential gene analyses (and). Additionally two other mitochondrial genes (*mt-Tl1* and *mt-Tl2*) were reduced in expression with an adjusted p-value of <0.05 and a ±1log$_2$ fold change in the edgeR dataset only ().

Mitochondria, in addition to cellular energy production, are now being recognised as key regulators of the immune response of macrophages (215). *Cmpk2* overexpression has been previously indicated to result in enhanced expression of proinflammatory genes (*Il1b*, *Tnf* and *Il8*) and is associated with enhanced mitochondrial reactive oxygen species (ROS) in THP-1-derived macrophage (216).

The pattern recognition receptor family of toll-like receptors (TLRs) initiate several interferon regulatory factors (IRFs) upon activation, ultimately resulting in a type I interferon response. Interferon-stimulated genes following TLR4 activation In THP1-derived macrophages, demonstrated CMPK2 induction to be associated with type I IFN signalling (217), which ultimately act as activating ligands for the NLR family pyrin domain containing 3 (NLRP3) inflammasome complex in stimulated macrophages (218). Upstream regulators analysis highlighted type I interferon beta (*Ifnb1*) and the interferon alpha and

beta receptor subunit 1 (*Infar1*) along with *Nlrp3* in both DESeq2 and edgeR datasets (Figure 4.3.14 and Figure 4.3.17).

Several TLRs had an adjusted p-value <0.05 with *Tlr2*, *Tlr9* and *Tlr4* in the DESeq2 dataset only (), and *Tlr3*, *Tlr5*, *Tlr8* and *Tlr12* in both analyses (and). However only *Tlr5* and *Tlr8* had a ±1$\log_2$ fold change, with both reduced in $Maf^{fl/fl}Cx3cr1^{Cre/+}$ when compared to $Maf^{fl/fl}Cx3cr1^{+/+}$microglia (and). Additionally several IRFs were present in both analyses (*Irf1*, *Irf7* and *Irf9*) (and), with *Irf8* present in the DESeq2 analysis ().

Pattern recognition receptor pathway had a -log(P-Value) of 9.49 in DESeq2 and 7.53 in edgeR, with a Z-score of 3.024 and 2.683 respectively in canonical pathway analysis between $Maf^{fl/fl}Cx3cr1^{Cre/+}$ and $Maf^{fl/fl}Cx3cr1^{+/+}$microglia. Several upstream regulators relating to TLRs and IRFs were identified, with *Tlr2*, *Tlr3*, *Irf3*, *Irf8*, *Irf9* and *Myd88* with a p-value of overlap <0.05 in both DESeq2 and edgeR analysis (Figure 4.3.14 and Figure 4.3.17). The DESeq2 analysis also indicated *Tlr7* and *Irf2* (Figure 4.3.14), whilst edgeR demonstrated *Tlr9* and *Irf1* as upstream regulators (Figure 4.3.17).

Yolk sac primitive macrophages have been identified as the direct precursor of the definitive microglia population in the central nervous system (6). In the yolk sac *Irf8* and *Spi1* (the gene which encodes PU.1) have previously been identified as vital for the development of microglia (219). It has been well established that both PU.1 and IRF8 can act as heterodimers or as downstream targets of each other (220).

Furthermore deletion of *Spi1* in microglia has been demonstrated to result in consequential downregulation of *Irf8* (219). The expression of *Irf8* is restricted to microglia in the CNS (221), with a broad range of effects crucial to the transformation of microglia to a reactive state by regulating the expression of various genes involved in microglial innate responses, including *Tlr2* and *Tlr4* (222), chemotaxis through purinergic receptor P2Y12R (*P2ry12*) and *Cx3cr1* (221), and inflammatory cytokines such as interleukin-1b (*Il1b*) (221).

Relative usage of exons between $Maf^{fl/fl}Cx3cr1^{Cre/+}$ and $Maf^{fl/fl}Cx3cr1^{+/+}$microglia generated 33 differential exons with an adjusted p-value <0.05 and a cut off ±1$\log_2$ (Figure 4.3.19, and summarised in Table 4.3.1), which comprised of 29 unique genes. Of these the lysosomal gene *Ctsa* indicated numerous exon differences with an adjust p-value of <0.05 (Figure 4.3.21). *Ctsa* encode Cathepsin A, a lysosomal hydrolases cathepsin, and upregulation of *Ctsa* has previously been identified as a differential gene in disease-

associated microglia in AD (223). *Abi3* also demonstrated statistically significant changes in exon 1 (adjusted p-value = 0.00085) (Figure 4.3.22). A structural component of the WAVE2 complex (224), *Abi3* expression in microglia has been associated with AD (225,226). Additional microglia genes associated with AD were also identified as upstream regulators, with *Trem2* and *Syk* identified in both DESeq2 and edgeR analyses (226,227). Future work could include crossing of the *Maf*$^{fl/fl}$*Cx3cr1*$^{Cre/+}$ onto an AD mouse line, which could elucidate the role of *Maf* in microglia in this disease model.

To validate the RNA sequencing differential gene discoveries a panel of 16 genes were investigated by qPCR on *Maf*$^{fl/fl}$*Cx3cr1*$^{+/+}$and *Maf*$^{fl/fl}$*Cx3cr1*$^{Cre/+}$ microglia. Overall statistically significant differences were attributed to genotype, targets and interaction of genotype x targets (Figure 4.3.23). Correlation of the relative quantification of fold change with both DESeq2 and edgeR analyses indicated moderate-strong positive correlation and were statistically significant (Figure 4.3.24). Ultimately this indicated that the differential gene discoveries determined by DESeq2 and edgeR to be valid, however increased number of samples for qPCR would be required to confirm this.

4.4.5. Summary of Findings

In summary, *Maf* expression was determined to be reduced in both Maf$^{fl/fl}$Cx3cr1$^{Cre\mathit{ERT}/+}$ mice, either through intraperitoneal injection in corn oil or tamoxifen-sucrose chow, and *Maf*$^{fl/fl}$*Cx3cr1*$^{Cre/+}$ mice when compared to *Maf*$^{fl/fl}$*Cx3cr1*$^{+/+}$mice. Ultimately all further work in this thesis was conducted in *Maf*$^{fl/fl}$*Cx3cr1*$^{Cre/+}$ mice rather than in Maf$^{fl/fl}$Cx3cr1$^{Cre\mathit{ERT}/+}$ mice, removing any possible side effects of tamoxifen and allowing both microglia and peritoneal tissue resident macrophages to be studied in the same animal, reducing the number of animals required for this thesis. However this is at the expense of developmental study of the role of *Maf* in Maf$^{fl/fl}$Cx3cr1$^{Cre\mathit{ERT}/+}$ mice, and the possibility of *Maf* specific developmental abnormalities begin masked in *Maf*$^{fl/fl}$*Cx3cr1*$^{Cre/+}$ mice.

Ablation of the MHCII^{-} CD206^{high} BAM population in *Maf*$^{fl/fl}$*Cx3cr1*$^{Cre/+}$ which was demonstrated to have high MAF expression, suggesting *Maf* is an essential transcription factor for MHCII^{-} CD206^{high} BAMs, and was concurrent with a publication in the same Maf$^{fl/fl}$ mice (172). The effects of ablation of the MHCII^{-} CD206^{high} BAM population however requires further study.

Immunofluorescence of *Maf*$^{fl/fl}$*Cx3cr1*$^{Cre/+}$ mice indicated an increase in microglia number and consequently a reduction in distance between cells compared to *Maf*$^{fl/fl}$*Cx3cr1*$^{+/+}$ mice. However with no apparent differences in area of coverage, alluding to *Maf*$^{fl/fl}$*Cx3cr1*$^{Cre/+}$ microglia having altered ramifications, which would require further investigation through morphological 3D analysis.

RNA sequencing of *Maf*$^{fl/fl}$*Cx3cr1*$^{+/+}$and *Maf*$^{fl/fl}$*Cx3cr1*$^{Cre/+}$ microglia resulted in almost 2,000 differential gene expression discoveries by both DESeq2 and edgeR, with 1,581 common genes with an adjusted p-value of <0.05, and 770 common genes with a $\pm 1 \log_2$ fold change between the two differential expression methods. Overall a considerable number of key immune related genes were evident within both DESeq2 and edgeR datasets, with changes in chemokines, chemokine receptors, cytokines, the complement system, pattern recognition receptors and MHC expression, along with several upstream regulators indicating a proinflammatory polarisation of microglia in *Maf*$^{fl/fl}$*Cx3cr1*$^{Cre/+}$ mice when compared to *Maf*$^{fl/fl}$*Cx3cr1*$^{+/+}$mice. Therefore further study in the role of *Maf* in neuroinflammation would be of interest, such as systemic LPS stimulation, to elucidate how the proinflammatory transcriptome and loss of *Il10* effects microglial responses.

Additionally many pathways and genes aligned with those previously identified as key components of the role of microglia in Alzheimer's disease (AD), and this requires further investigation in an AD model to determine the possible role of *Maf* in microglia in AD.

4.4.5.1. Hypothesis of Findings

It is hypothesised that loss of the transcription factor *Maf* results in a more proinflammatory polarisation of microglia in *Maf*$^{fl/fl}$*Cx3cr1*$^{Cre/+}$ mice when compared to *Maf*$^{fl/fl}$*Cx3cr1*$^{+/+}$mice, and this could be through the reduction of *Il-10* and ablation of the MHCII^{-} CD206^{high} border associated macrophage population.

Chapter 5

Peritoneal Tissue Resident Macrophages in *Maf*$^{fl/fl}$*Cx3cr1*$^{Cre/+}$ Transgenic Mice

5.1. Introduction

5.1.1. Transcriptomic Analyses of *Maf* in Peritoneal Tissue Resident Macrophages

The role of *Maf* has been studied in several tissues at a transcriptomic level in *Maf* knockout mice. Mostly these have concentrated on chromatin immunoprecipitation sequencing (ChIP-Seq) (105,157,169,228,229) or Assay for Transposase-Accessible Chromatin using sequencing (ATAC-Seq) (169,229–231). Furthermore these previously published studies have investigated the role of *Maf* in lymphoid cells such as different subset of T-cells (169,228–233).

Those which have studied myeloid cells have been predominantly on bone marrow derived macrophages (105,157), and have indicated *Maf* to be a potent activator of interleukin 10 (*Il10*) gene expression in macrophages, and a suppressor if interleukin 12 (*Il12*) p40 and p35 gene transcription (105). Additionally that *Maf* has a direct binding sites in the colony-stimulating factor 1 receptor (*Csf1r*) gene and therefore is involved in regulating CSF1R expression on macrophages (157).

Recent publications have investigated the role of *Maf* in tissue resident macrophages (30,172,230,234), including peritoneal tissue resident macrophages which have highlighted the importance of *Maf* (30,234). Transcriptomic analysis of *Maf* and *Mafb* double knockout peritoneal tissue resident macrophages was utilised for assessing self-renewal gene networks in macrophages, revealing that *Maf*/*Mafb* expression resulted in negative expression for nearly all self-renewal genes, suggesting of a role of *Maf* in macrophage self-renewal (234). However these peritoneal macrophages were cultured and infected with short hairpin RNA (shRNA) for the deletion of the transcription factors.

The overall aim of this chapter was to address the role specifically of *Maf* in peritoneal resident macrophages, via transcriptomic study of a discrete myeloid *Maf* deficiency. Currently there are no published works containing RNA sequencing (RNA Seq) of *in situ* peritoneal tissue resident macrophages from *Maf* knockout mice.

5.2. Chapter Aims

The aims of the chapter were…

- Validate the loss of *Maf* in peritoneal tissue resident macrophages by RNA and protein expression in *Maf*$^{fl/fl}$*Cx3cr1*$^{Cre/+}$ and *Maf*$^{fl/fl}$*Cx3cr1*$^{+/+}$ mice.
- Determine if *Maf* deficiency alters generation or retention of peritoneal tissue resident macrophages in these mice.
- Evaluate whether *Maf* results in a modified phenotype, through studying expression of common macrophage markers on peritoneal tissue resident macrophages in naïve mice.
- Ascertain whether *Maf*-deficiency in peritoneal tissue resident macrophages has a significant impact on macrophage phenotype (transcriptome) in naïve conditions and following mild immune challenge.

5.3. Results

5.3.1. Validation of the Deletion of *Maf* in the Peritoneal Cavity of *Maf*$^{fl/fl}$*Cx3cr1*$^{Cre/+}$ Mice

5.3.1.1. Peritoneal Tissue Resident Macrophage Composition

Flow cytometry was utilised to investigate the proportion of tissue resident macrophages in peritoneal lavage, from *Maf*$^{fl/fl}$*Cx3cr1*$^{Cre/+}$ and *Maf*$^{fl/fl}$*Cx3cr1*$^{+/+}$ mice (Figure 5.3.1A). Peritoneal tissue resident macrophages were defined as CD11b^{high}, F4/80^{high} and Tim4^{+}.

To determine if the proportion of tissue resident macrophages were different between *Maf*$^{fl/fl}$*Cx3cr1*$^{Cre/+}$ and *Maf*$^{fl/fl}$*Cx3cr1*$^{+/+}$ mice, the percentage of CD11b^{high}, F4/80^{high} and Tim4^{+} cells based on single cells of FSC/SSC gating strategy (Figure 5.3.1A) were identified by flow cytometry (Figure 5.3.1B). In male and female *Maf*$^{fl/fl}$*Cx3cr1*$^{+/+}$ mice tissue resident macrophages represent 81.82 % ± 2.956 % (Mean ± SEM) and 86.40 % ± 2.570 % (Mean ± SEM) respectively of single cells based on FSC/SSC gating (Figure 5.3.1B). Whilst male and female *Maf*$^{fl/fl}$*Cx3cr1*$^{Cre/+}$ mice represent 81.97 % ± 3.002 % (Mean ± SEM) and 88.73 % ± 2.311 % (Mean ± SEM) (Figure 5.3.1B). However percentage of tissue resident macrophages in total lavage in *Maf*$^{fl/fl}$*Cx3cr1*$^{Cre/+}$ mice when compared to *Maf*$^{fl/fl}$*Cx3cr1*$^{+/+}$ mice in both sexes was not statistically significant when analysed by two-way ANOVA, by either genotype, sex or the interaction of the two factors (Figure 5.3.1B).

Additionally when investigating absolute number of tissue resident macrophages in peritoneal lavage of *Maf*$^{fl/fl}$*Cx3cr1*$^{+/+}$ and *Maf*$^{fl/fl}$*Cx3cr1*$^{Cre/+}$ mice, both male and female *Maf*$^{fl/fl}$*Cx3cr1*$^{Cre/+}$ indicated increase in number when compared to *Maf*$^{fl/fl}$*Cx3cr1*$^{+/+}$ mice (Figure 5.3.1C). However upon analysis with two-way ANOVA, neither genotype, sex or the interaction of the two factors were determined to be statistically significant (Figure 5.3.1C).

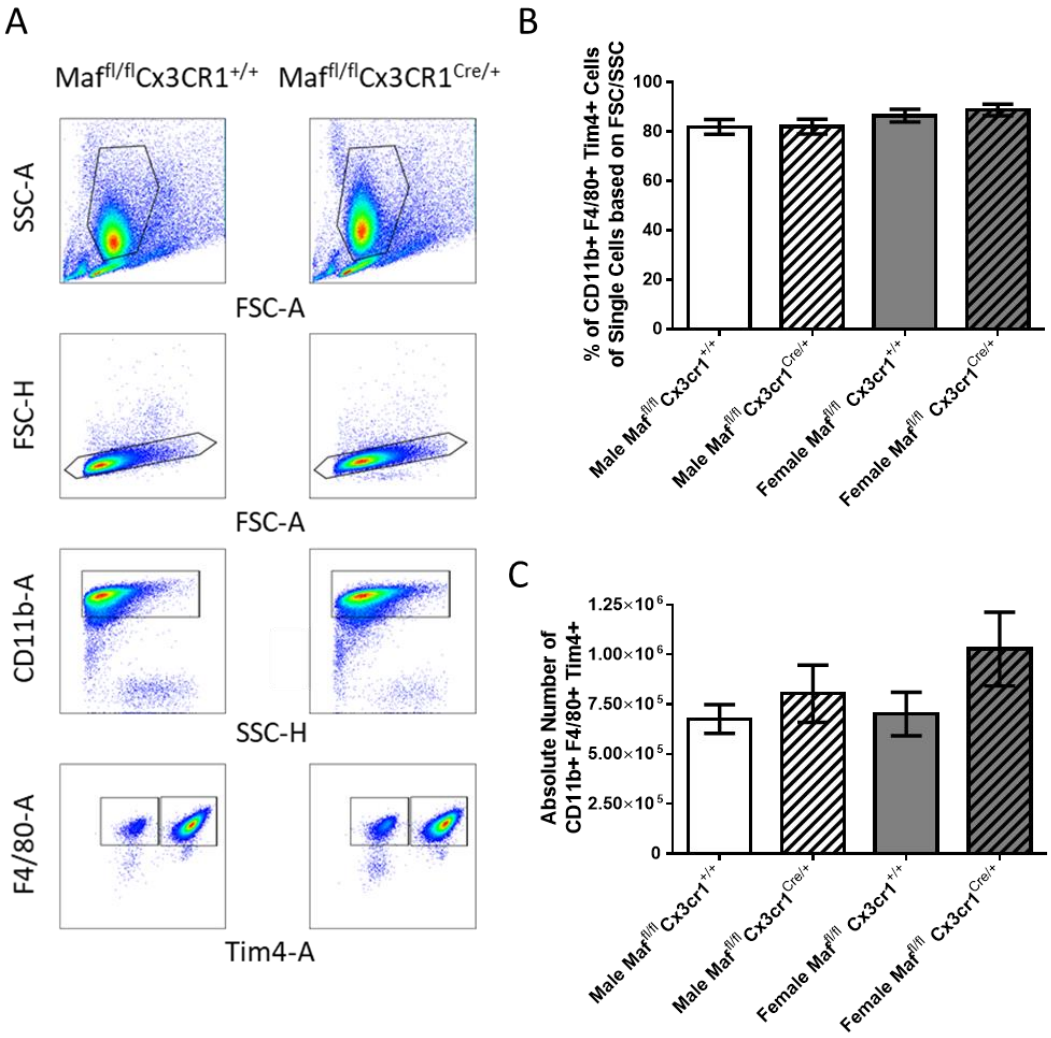

Figure 5.3.1 Proportion of tissue resident macrophages in *Maf*$^{fl/fl}$*Cx3cr1*$^{Cre/+}$ and *Maf*$^{fl/fl}$*Cx3cr1*$^{+/+}$ mice.

Flow cytometry of A) peritoneal lavage from *Maf*$^{fl/fl}$*Cx3cr1*$^{Cre/+}$ and *Maf*$^{fl/fl}$*Cx3cr1*$^{+/+}$ mice, indicating gating strategy for peritoneal tissue resident macrophages. B) Percentage of tissue resident macrophages in *Maf*$^{fl/fl}$*Cx3cr1*$^{Cre/+}$ and *Maf*$^{fl/fl}$*Cx3cr1*$^{+/+}$ mice, based on single cells of FSC/SSC gate. C) Absolute number of tissue resident macrophages in *Maf*$^{fl/fl}$*Cx3cr1*$^{Cre/+}$ and *Maf*$^{fl/fl}$*Cx3cr1*$^{+/+}$ mice. *Maf*$^{fl/fl}$*Cx3cr1*$^{+/+}$ (male = white, female = grey) and *Maf*$^{fl/fl}$*Cx3cr1*$^{Cre/+}$ (shaded) mice. All mice were aged 6-8 weeks. Error bars indicate ± SEM (n=11). All data was analysed using two-way ANOVA.

5.3.1.2. Protein Expression of Maf in Peritoneal Tissue Resident Macrophages

MAF protein expression in peritoneal tissue resident macrophages in *Maf*$^{fl/fl}$*Cx3cr1*$^{Cre/+}$ mice when compared with those of *Maf*$^{fl/fl}$*Cx3cr1*$^{+/+}$ mice (Figure 5.3.2), demonstrated a reduction in MAF expression of 63.23 % ± 7.498 % (Mean ± SEM) as determined by ΔMFI, which was statistically significant when analysed with an unpaired two-tailed t-test.

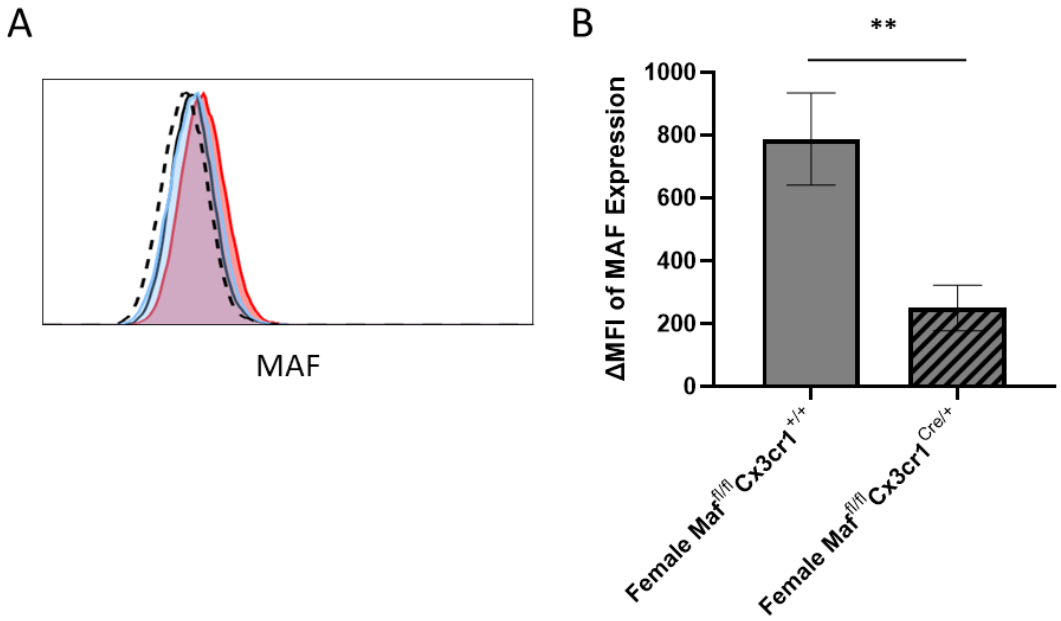

Figure 5.3.2 Determination of MAF protein expression in peritoneal tissue resident macrophages in *Maf*$^{fl/fl}$*Cx3cr1*$^{+/+}$and *Maf*$^{fl/fl}$*Cx3cr1*$^{Cre/+}$ mice

A) Histogram of MAF expression by flow cytometry of peritoneal tissue resident macrophages from *Maf*$^{fl/fl}$*Cx3cr1*$^{+/+}$ (red) and *Maf*$^{fl/fl}$*Cx3cr1*$^{Cre/+}$ (blue) mice with isotype controls (solid and dashed line respectively). B) Delta mean fluorescent intensity (ΔMFI) of peritoneal tissue resident macrophages in female *Maf*$^{fl/fl}$*Cx3cr1*$^{+/+}$ (grey) and *Maf*$^{fl/fl}$*Cx3cr1*$^{Cre/+}$ (shaded) mice. All mice were aged 6-8 weeks. Error bars indicate ± SEM (n=10). Unpaired two-tailed t-test on graph (p-value = 0.0042, **).

When investigating phenotypic differences of peritoneal tissue resident macrophages in *Maf*$^{fl/fl}$*Cx3cr1*$^{Cre/+}$ and *Maf*$^{fl/fl}$*Cx3cr1*$^{+/+}$ mice, common myeloid markers were studied using flow cytometry (Figure 5.3.3). Among the 16 myeloid markers only CX3CR1 displayed any clear differences in protein expression, with *Maf*$^{fl/fl}$*Cx3cr1*$^{+/+}$ exhibiting higher expression than in *Maf*$^{fl/fl}$*Cx3cr1*$^{Cre/+}$ mice (Figure 5.3.3).

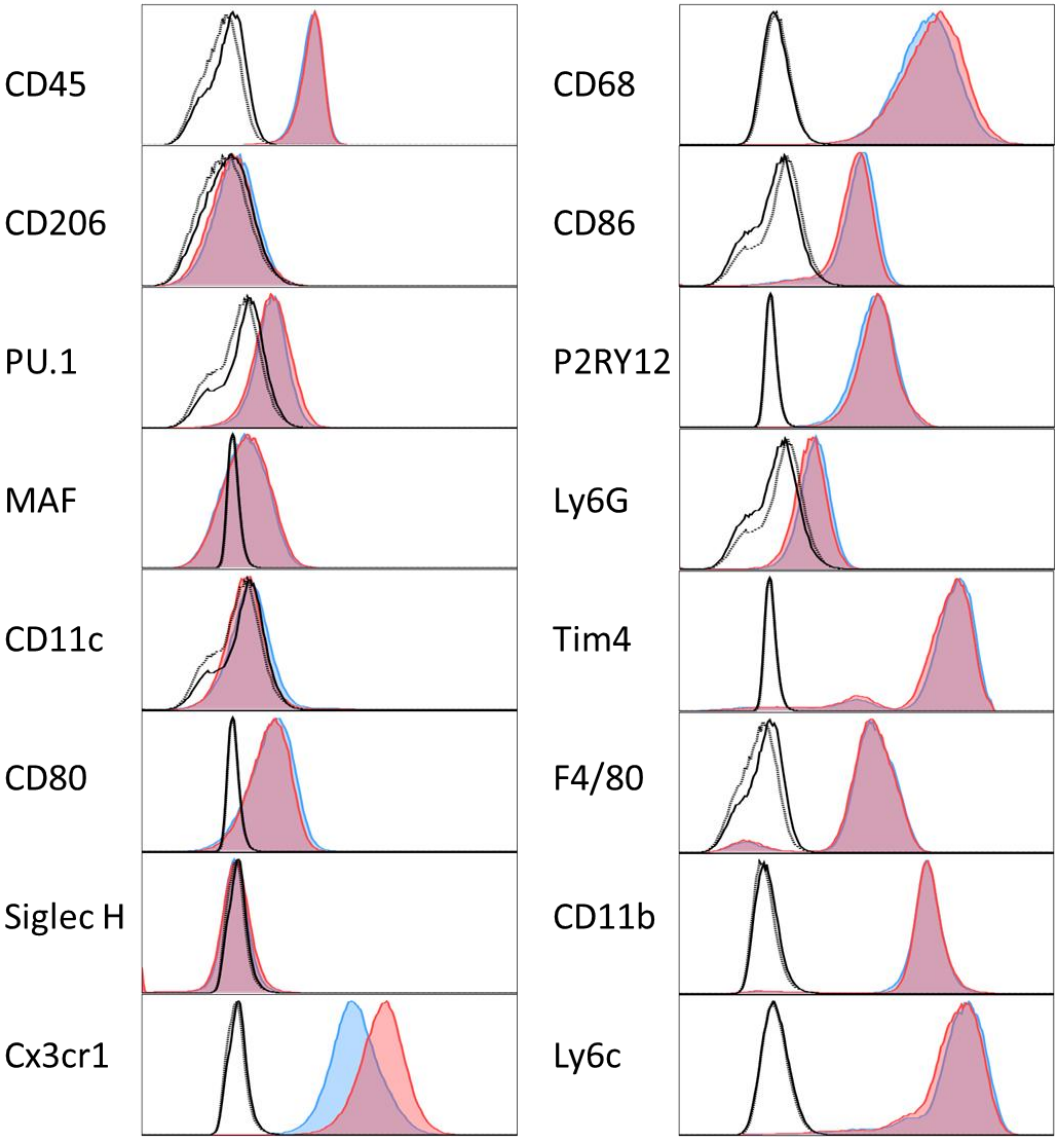

Figure 5.3.3 Expression of common myeloid markers in peritoneal tissue resident macrophages of in *Maf*$^{fl/fl}$*Cx3cr1*$^{Cre/+}$ and *Maf*$^{fl/fl}$*Cx3cr1*$^{+/+}$ mice.

Flow cytometry histograms of common myeloid markers. *Maf*$^{fl/fl}$*Cx3cr1*$^{+/+}$ (red), *Maf*$^{fl/fl}$*Cx3cr1*$^{Cre/+}$ (blue) and isotypes (solid black and dotted black respectively), representative of n=2. All mice were male and aged 6-8 weeks.

5.3.1.3. Quantitative PCR Deletion of *Maf* in Peritoneal Macrophages

To validate loss of *Maf* in *Maf*$^{fl/fl}$*Cx3cr1*$^{Cre/+}$ mice, peritoneal tissue resident macrophages were sorted (using FACS Aria III) based on CD11b^{high}, F4/80^{high} and Tim4^{+} expression (Figure 5.3.4A) following peritoneal lavage. Peritoneal tissue resident macrophage *Maf* expression was reduced significantly in *Maf*$^{fl/fl}$*Cx3cr1*$^{Cre/+}$ mice by 40-ΔCT (Figure 5.3.4B) and relative quantification of fold change gene expression (Figure 5.3.4C) by two-way ANOVA with genotype demonstrated as the only factor with significance (p-value = <0.0001 **** and p-value = 0.0005 *** respectively), when compared to *Maf*$^{fl/fl}$*Cx3cr1*$^{+/+}$ mice.

Mean 40-ΔCT of *Maf* in female *Maf*$^{fl/fl}$*Cx3cr1*$^{+/+}$ mice was 36.94 ± 0.4583 (Mean ± SEM) compared to *Maf*$^{fl/fl}$*Cx3cr1*$^{Cre/+}$ females 26.32 ± 0.9097 (Mean ± SEM) (Figure 5.3.4B), with a mean difference of 10.62 ± 0.9504 (mean difference and standard error of difference (SE), p-value = <0.0001 by Šidák's multiple comparisons test). In male mice the 40-ΔCT of *Maf* in *Maf*$^{fl/fl}$*Cx3cr1*$^{+/+}$ was 36.55 ± 0.8520 (Mean ± SEM) compared to *Maf*$^{fl/fl}$*Cx3cr1*$^{Cre/+}$ 36.55 ± 0.2073 (Mean ± SEM) (Figure 5.3.4B), with a mean difference of 9.617 ± 0.9504 (mean difference and SE, p-value = <0.0001 by Šidák's multiple comparisons test).

Relative quantification of fold change in peritoneal tissue resident macrophages *Maf* gene expression in female *Maf*$^{fl/fl}$*Cx3cr1*$^{+/+}$ mice when compared to *Maf*$^{fl/fl}$*Cx3cr1*$^{Cre/+}$ had a mean -10.0196 Log_2 fold change, whilst male mice had a -9.11201 Log_2 fold change (Figure 5.3.4C). When analysed with Šidák's multiple comparisons test relative quantification of fold change gene expression in both male and female were statistically significant between *Maf*$^{fl/fl}$*Cx3cr1*$^{+/+}$ and *Maf*$^{fl/fl}$*Cx3cr1*$^{Cre/+}$ mice (Figure 5.3.4C).

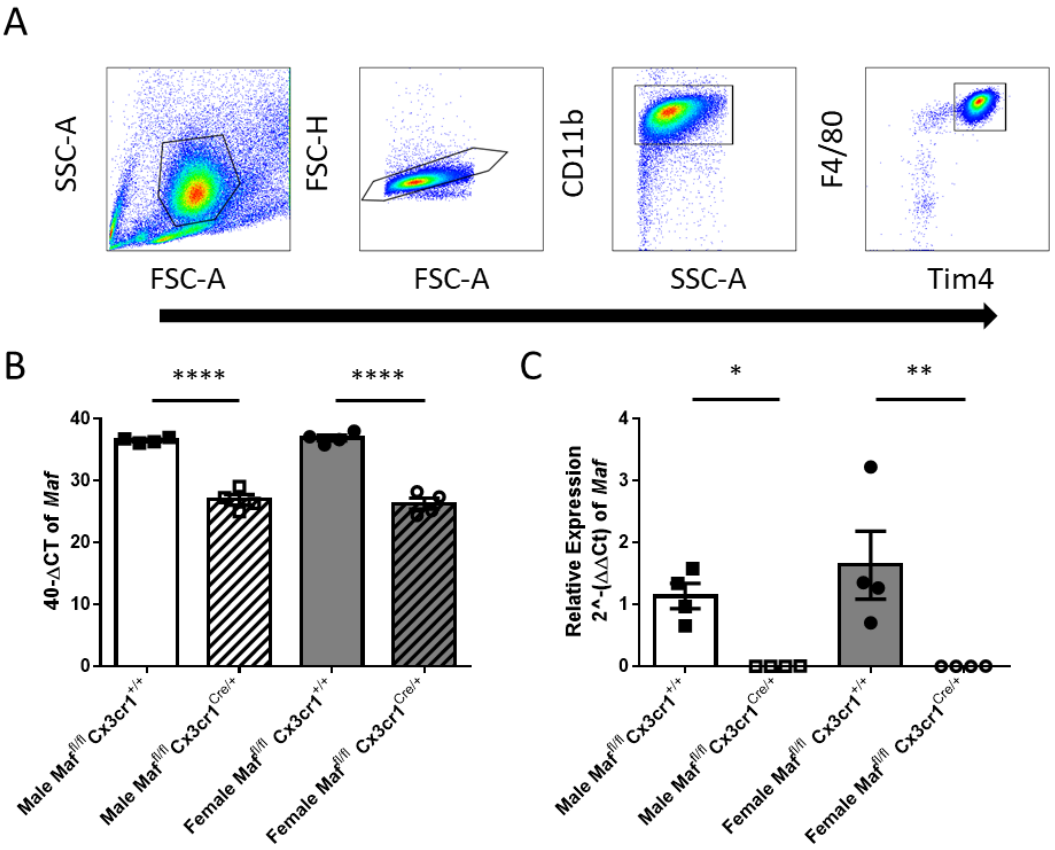

Figure 5.3.4 Determination *Maf* expression in peritoneal tissue resident macrophages in *Maf*$^{fl/fl}$*Cx3cr1*$^{+/+}$ and *Maf*$^{fl/fl}$*Cx3cr1*$^{Cre/+}$ mice by qPCR.

A) Gating strategy of peritoneal tissue resident macrophages with staining of CD11b, F4/80 and Tim-4. B) 40-ΔCT values and C) relative quantification of fold change gene expression of *Maf* in peritoneal tissue resident macrophages in *Maf*$^{fl/fl}$*Cx3cr1*$^{+/+}$ (Male = white, female = grey) and *Maf*$^{fl/fl}$*Cx3cr1*$^{Cre/+}$ (shaded) mice. All mice were 6-8 weeks of age. Error bars indicate ±SEM (n=4/group).

5.3.2. Generation and Validation of MΦP Cell Lines derived from *Maf*$^{fl/fl}$*Cx3cr1*$^{+/+}$ and *Maf*$^{fl/fl}$*Cx3cr1*$^{Cre/+}$ Mice

5.3.2.1. Protein Expression of MAF in *Maf*$^{fl/fl}$*Cx3cr1*$^{+/+}$ and *Maf*$^{fl/fl}$*Cx3cr1*$^{Cre/+}$ MΦPs

MΦPs were generated (as described in 2.4.5) from both male and female *Maf*$^{fl/fl}$*Cx3cr1*$^{+/+}$ and *Maf*$^{fl/fl}$*Cx3cr1*$^{Cre/+}$ mice aged 6-8 weeks of age. Protein expression of MAF was confirmed through flow cytometry (Figure 5.3.5). MAF expression by two-way ANOVA demonstrated genotype as the only factor with any significance (Figure 5.3.5).

Female *Maf*$^{fl/fl}$*Cx3cr1*$^{+/+}$ MΦPs when compared to female *Maf*$^{fl/fl}$*Cx3cr1*$^{Cre/+}$ MΦPs had a ΔMFI mean difference of 78.72 % ± 7.98 % (mean % difference and SEM, p-value = 0.0011 **, by Šidák's multiple comparisons test), whilst male MΦPs had a mean difference 72.30 % ± 0.998 % (mean % difference and SEM, p-value = 0.0019 **, by Šidák's multiple comparisons test) (Figure 5.3.5).

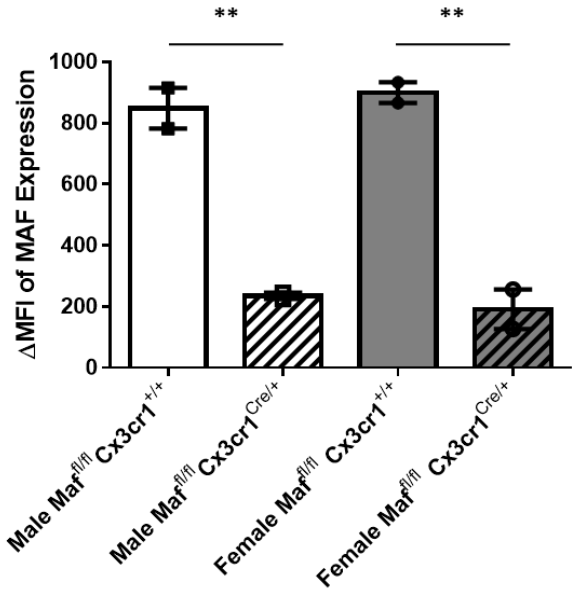

Figure 5.3.5 MAF protein expression in MΦPs generated from *Maf*$^{fl/fl}$*Cx3cr1*$^{+/+}$ and Maf$^{fl/fl}$Cx3cr1$^{Cre/+}$ mice.

Delta mean fluorescent intensity (ΔMFI) of MΦPs generated from *Maf*$^{fl/fl}$*Cx3cr1*$^{+/+}$ (male (white), female (grey)), *Maf*$^{fl/fl}$*Cx3cr1*$^{Cre/+}$ (shaded) mice (n=2 separate experiments). Error bars indicate ± SEM. 2-way ANOVA (Genotype p-value = 0.00102, **). Šidák's multiple comparison test is displayed on graphs. (p-value = <0.01, **).

5.3.2.2. qPCR of Maf in Maf$^{fl/fl}$Cx3cr1$^{+/+}$ and Maf$^{fl/fl}$Cx3cr1$^{Cre/+}$ MΦPs

Genomic loss of *Maf* was confirmed in the MΦP cell lines through qPCR. Mean 40-ΔCT of *Maf* in female *Maf$^{fl/fl}$Cx3cr1$^{+/+}$* MΦPs was 34.10 ± 0.8963 (Mean ± SEM) compared to *Maf$^{fl/fl}$Cx3cr1$^{Cre/+}$* females 21.99 ± 0.3825 (Mean ± SEM) (Figure 5.3.6A), with a mean difference of 12.11 ± 1.293 (mean difference and SE, p-value = <0.0001, ****, by Šidák's multiple comparisons test). In male MΦPs the 40-ΔCT of *Maf* in *Maf$^{fl/fl}$Cx3cr1$^{+/+}$* was 34.36 ± 0.3576 (Mean ± SEM) compared to *Maf$^{fl/fl}$Cx3cr1$^{Cre/+}$* 23.25 ± 0.1506 (Mean ± SEM) (Figure 5.3.6A), with a mean difference of 11.11 ± 1.293 (mean difference and SE, p-value = <0.0001, ****, by Šidák's multiple comparisons test).

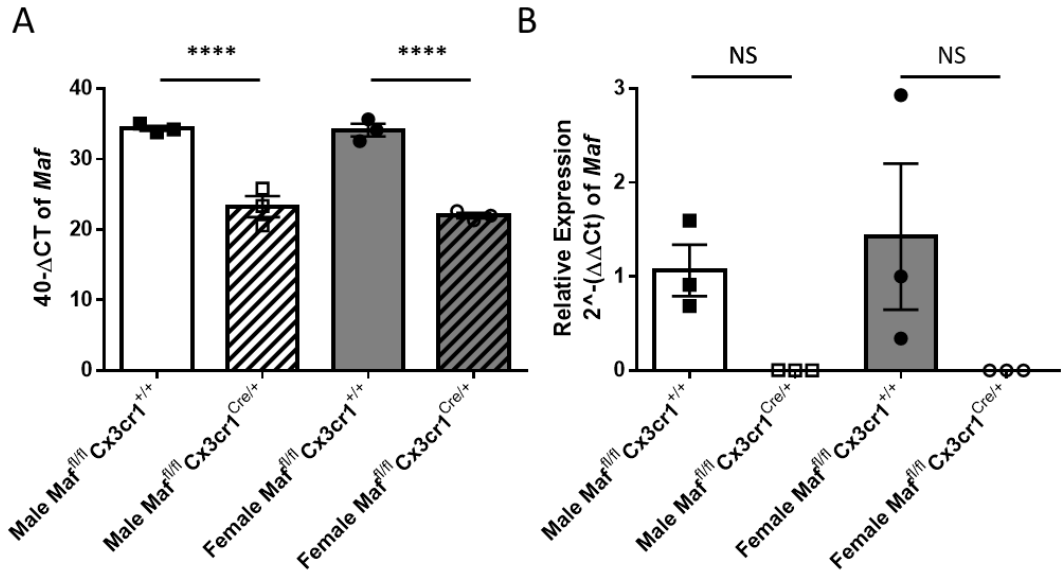

Figure 5.3.6 *Maf* expression in *Maf$^{fl/fl}$Cx3cr1$^{+/+}$* and *Maf$^{fl/fl}$Cx3cr1$^{Cre/+}$* MΦPs by qPCR.

A) 40-ΔCT values and B) relative quantification of fold change gene expression of *Maf* in *Maf$^{fl/fl}$Cx3cr1$^{+/+}$* (male white, female grey) and *Maf$^{fl/fl}$Cx3cr1$^{Cre/+}$* (shaded) MΦPs. Error bars indicate ± SEM (n=3). 2-way ANOVA (p-value = <0.0001, ** and p-value = 0.0166, *). Šidák's multiple comparison test is displayed on graphs. (p-value = <0.0001, ****).**

Relative quantification of fold change in *Maf* gene expression in female *Maf$^{fl/fl}$Cx3cr1$^{+/+}$* MΦPs when compared to *Maf$^{fl/fl}$Cx3cr1$^{Cre/+}$* MΦPs had a mean -12.2691 Log_2 fold change, whilst male mice had a -9.95633 Log_2 fold change (Figure 5.3.6B). When analysed with Šidák's multiple comparisons test relative quantification of fold change gene expression in both female and male were not deemed significant between *Maf$^{fl/fl}$Cx3cr1$^{+/+}$* and *Maf$^{fl/fl}$Cx3cr1$^{CreERT/+}$* mice (Figure 5.3.6B).

5.3.3. Immune Challenge of *Maf*$^{fl/fl}$*Cx3cr1*$^{+/+}$ and *Maf*$^{fl/fl}$*Cx3cr1*$^{Cre/+}$ MΦPs with *E. coli* Lipopolysaccharides (LPS)

To investigate the role of *Maf* in immune challenge M-CSF differentiated *Maf*$^{fl/fl}$*Cx3cr1*$^{+/+}$ and *Maf*$^{fl/fl}$*Cx3cr1*$^{Cre/+}$ MΦPs were utilised in a time course experiment, treated with 100 ng/ml *E. coli 0111:B4* lipopolysaccharides (LPS). *Maf* expression between *Maf*$^{fl/fl}$*Cx3cr1*$^{+/+}$ and *Maf*$^{fl/fl}$*Cx3cr1*$^{Cre/+}$ MΦPs was significantly different when analysed by three-way ANOVA (Genotype, p-value = 0.0005 ***) (Figure 5.3.7).This was consistent when time as a factor was included (Time x Genotype, p-value = 0.0004 ***). Expression of *Maf* peaked at 6 hr in both male and female *Maf*$^{fl/fl}$*Cx3cr1*$^{+/+}$ MΦPs (Figure 5.3.7).

Expression of *Bhlhe40* (Basic Helix-Loop-Helix Family Member E40), which has been previously identified as a possible repressor of *Maf* (229,235), was significantly reduced in expression in *Maf*$^{fl/fl}$*Cx3cr1*$^{Cre/+}$ MΦPs compared to the *Maf*$^{fl/fl}$*Cx3cr1*$^{+/+}$ MΦPs (Figure 5.3.7A) (Genotype, p-value = 0.0382 *). Sex and genotype across time were also identified as being significantly different (Time x Genotype, p-value = 0.0017 **; Time x Sex, p-value = 0.0210 *) (Figure 5.3.7B).

Expression of the cytokines *Il-1b*, *Il-6*, *Il-10*, *Il-12* and *Tnf* were investigated by qPCR. Time was the only significantly different factor between *Maf*$^{fl/fl}$*Cx3cr1*$^{+/+}$ and *Maf*$^{fl/fl}$*Cx3cr1*$^{Cre/+}$ MΦPs with regard to *Il-1b*, *Il-10* and *Tnf* expression (Figure 5.3.8) when analysed by three-way ANOVA (Time, p-value = <0.0001, ****; p-value = 0.0044, **; p-value = <0.0001, **** respectively). These three cytokines also peaked at 3 hr time point in both male and female *Maf*$^{fl/fl}$*Cx3cr1*$^{+/+}$ and *Maf*$^{fl/fl}$*Cx3cr1*$^{Cre/+}$ MΦPs, and then continued to reduce with time (Figure 5.3.8).

Il-6 expression demonstrated a significant difference by time (Time, p-value = <0.0001, ***), and additionally with time by genotype (Time x Genotype, p-value = 0.0010, ***) (Figure 5.3.8). *Il-6* expression peaked at 3 hr in male and female *Maf*$^{fl/fl}$*Cx3cr1*$^{+/+}$ MΦPs, whilst in both male and female *Maf*$^{fl/fl}$*Cx3cr1*$^{Cre/+}$ MΦPs *Il-6* expression peaked at 6 hr (Figure 5.3.8). *Il-12* expression was much lower than other cytokines, however a significant difference by time, and by genotype was evident between *Maf*$^{fl/fl}$*Cx3cr1*$^{+/+}$ and *Maf*$^{fl/fl}$*Cx3cr1*$^{Cre/+}$ MΦPs (Time, p-value = 0.0061, **; Genotype, p-value = 0.0325, *) (Figure 5.3.8) when analysed with three-way ANOVA, with *Maf*-deficient cells producing less.

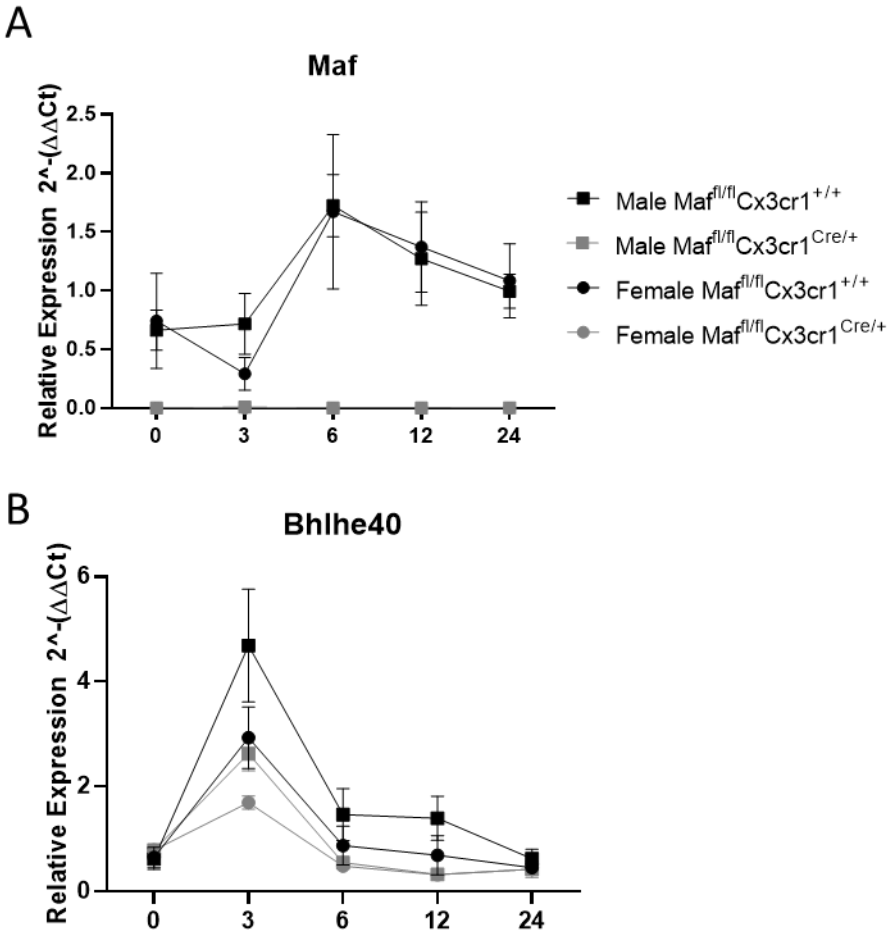

Figure 5.3.7 *Maf* and *Bhlhe40* expression by qPCR from *E. coli* LPS treated *Maf*$^{fl/fl}$*Cx3cr1*$^{+/+}$ and *Maf*$^{fl/fl}$*Cx3cr1*$^{Cre/+}$ MΦPs.

Relative quantification of fold change gene expression of A) *Maf* and B) *Bhlhe40* in *Maf*$^{fl/fl}$*Cx3cr1*$^{+/+}$ (male = black square; female = black circle) and *Maf*$^{fl/fl}$*Cx3cr1*$^{Cre/+}$ (male = grey square; female = grey circle) MΦPs. Error bars indicate ±SEM (n=3 independent experiments). All data was analysed using three-way ANOVA.

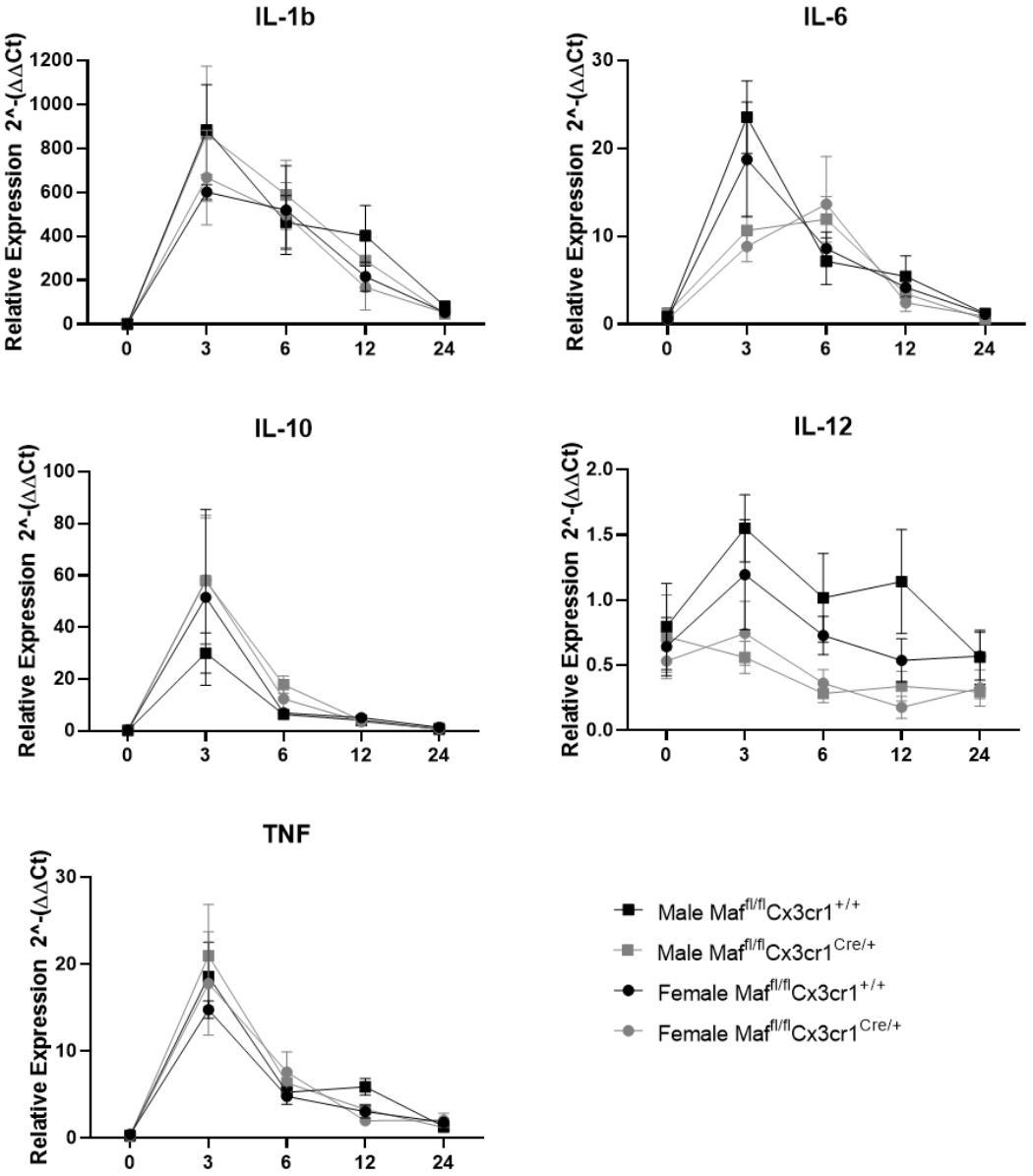

Figure 5.3.8 *Il-1b, Il-6, Il-10, Il-12 and Tnf* expression from *E. coli* LPS treated *Maf*$^{fl/fl}$*Cx3cr1*$^{+/+}$ and *Maf*$^{fl/fl}$*Cx3cr1*$^{Cre/+}$ MΦPs evaluated by qPCR.

Relative quantification of fold change gene expression of *Il-1b, Il-6, Il-10, Il-12 and Tnf* in *Maf*$^{fl/fl}$*Cx3cr1*$^{+/+}$ (male = black square; female = black circle) and *Maf*$^{fl/fl}$*Cx3cr1*$^{Cre/+}$ (male = grey square; female = grey circle) MΦPs. Error bars indicate ± SEM (n=3 independent experiments). All data was analysed using three-way ANOVA.

5.3.4. RNA Sequencing of Naïve Peritoneal Macrophage

5.3.4.1. Gene Expression across Multiple Differential Expression Methods

5.3.4.1.1. DESeq2 Differential Gene Expression Analysis

To confirm the loss of Maf in $Maf^{fl/fl}Cx3cr1^{Cre/+}$ mice, *Maf* expression was determined by fragments per kilobase of transcript per million (FPKM) mapped reads indicated *Maf* in peritoneal tissue resident macrophages to be below 0.047 FPKM in $Maf^{fl/fl}Cx3cr1^{Cre/+}$ compared to 4.43-4.71 FPKM in $Maf^{fl/fl}Cx3cr1^{+/+}$ mice (Figure 5.3.9).

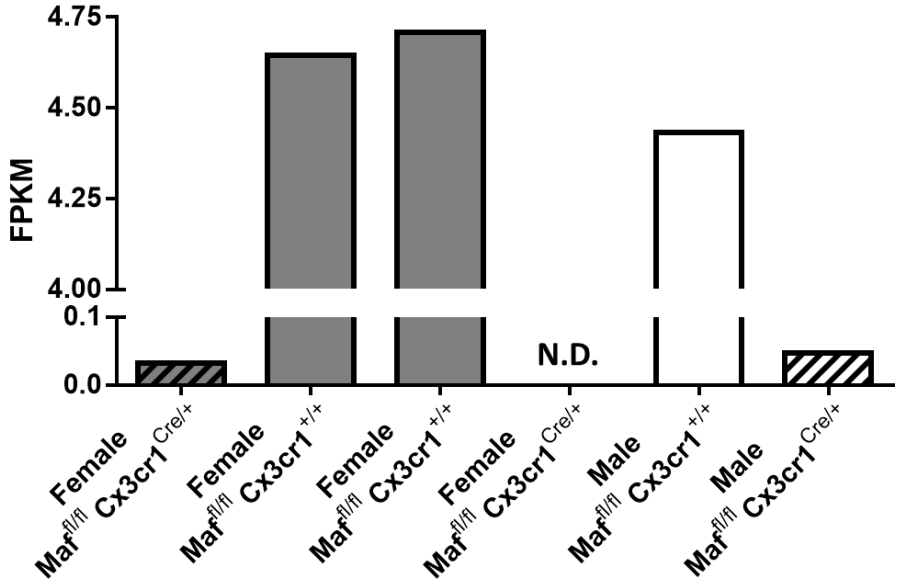

Figure 5.3.9 Fragments per kilobase of transcript per million (FPKM) mapped reads of *Maf* using DESeq2 differential expression method.

***Maf*$^{fl/fl}$*Cx3cr1*$^{+/+}$ mice (male = white, female = grey) and *Maf*$^{fl/fl}$*Cx3cr1*$^{Cre/+}$ (shaded) mice. Non-detected = N.D.**

Maf was the most significantly changed gene between $Maf^{fl/fl}Cx3cr1^{Cre/+}$ and $Maf^{fl/fl}Cx3cr1^{+/+}$ peritoneal tissue resident macrophages, with a -7.41 $\log_2$ fold change and an adjusted p-value of 1.74E-64 (Figure 5.3.10A). Due to *Maf* being so markedly changed the other gene changes are difficult to visualise graphically therefore by removing *Maf* from the visualisation the other gene discoveries become clearer (Figure 5.3.10B).

DESeq2 differential gene analysis of $Maf^{fl/fl}Cx3cr1^{Cre/+}$ vs $Maf^{fl/fl}Cx3cr1^{+/+}$ peritoneal tissue resident macrophages generated 98 differential expressed genes with an adjusted p-value <0.05 (the full list of genes can be found in Appendix VIII). Imposing a cut off ±1$\log_2$ fold change resulted in 29 differential gene discoveries.

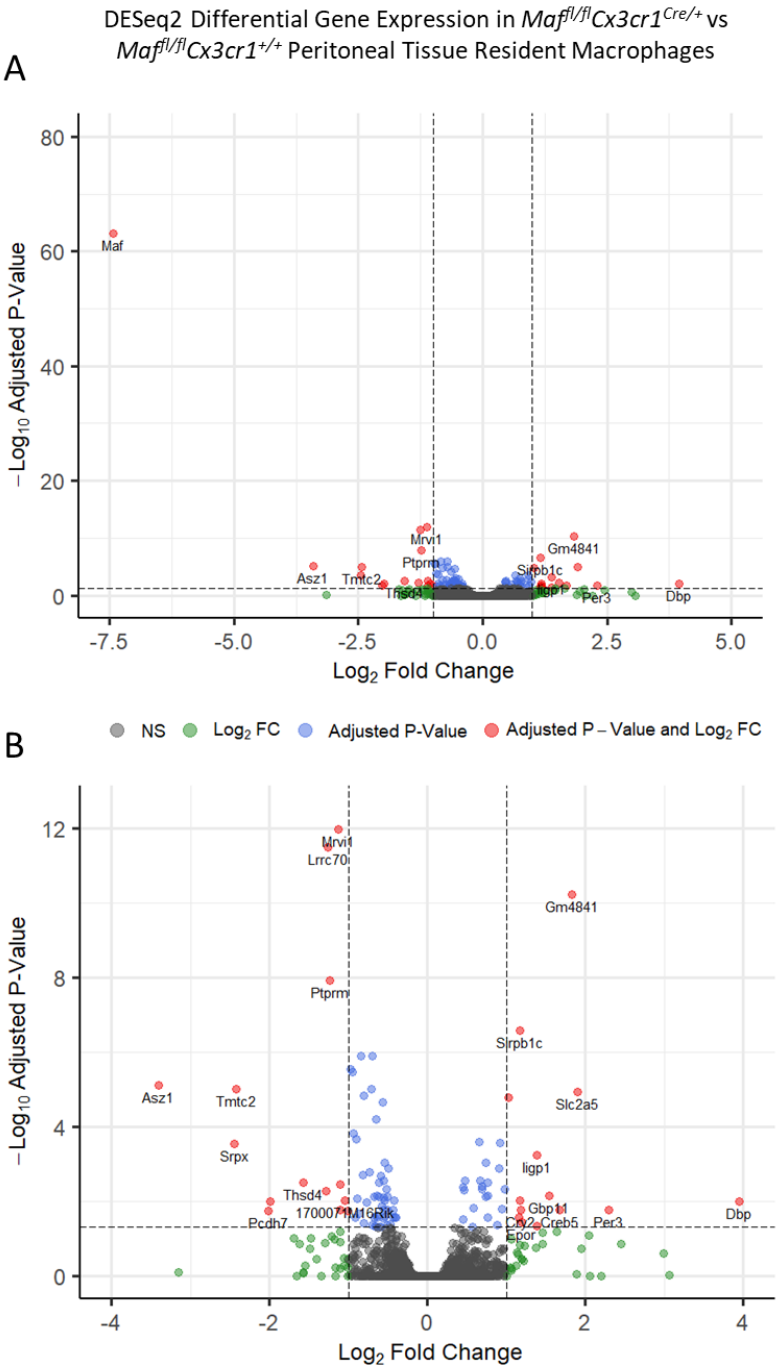

Figure 5.3.10 DESeq2 comparison of *Maf*$^{fl/fl}$*Cx3cr1*$^{Cre/+}$ vs *Maf*$^{fl/fl}$*Cx3cr1*$^{+/+}$ peritoneal tissue resident macrophages.

RNA-Seq of naïve *Maf*$^{fl/fl}$*Cx3cr1*$^{Cre/+}$ and *Maf*$^{fl/fl}$*Cx3cr1*$^{+/+}$ peritoneal tissue resident macrophages. A) Volcano plot of all gene discoveries using DESeq2 differential expression method. B) Volcano plot with *Maf* removed from the graph to improve visualisation of other significant genes. Dashed lines representing cut off for adjusted p-value = 0.05 and ±log$_2$ fold change = 1 (n=3 mice of each genotype).

Canonical pathway analysis from Ingenuity pathway analysis (IPA) (Qiagen) of the DESeq2 discovered genes against those previously identified in all macrophages, indicated downregulation and upregulation within several canonical pathways including phagosome formation, T-helper (Th) activation, notch signalling and sphingosine-1-phosphate signalling pathways (Figure 5.3.11).

Figure 5.3.11 Canonical pathway analysis of DESeq2 differential gene expression analysis.

Canonical pathway analysis generated from Ingenuity Pathway Analysis (IPA) against those previously identified in all macrophages following DESeq2 differential gene expression method. Percentage of genes in the analysis overlap with pathway (green = downregulated, red = upregulated, white = no overlap). Numbers in bold are the total number of genes involved in the pathway. Specific gene discoveries with adjusted p-value <0.05 involved in each pathway named, with-log p-value of each pathway indicated with orange line.

5.3.4.1.2. edgeR Differential Gene Expression Analysis

Comparison of *Maf*$^{fl/fl}$*Cx3cr1*$^{Cre/+}$ vs *Maf*$^{fl/fl}$*Cx3cr1*$^{+/+}$ peritoneal tissue resident macrophages utilising edgeR generated 95 differential gene discoveries with an adjusted p-value <0.05 (the full list of genes can be found in Appendix IX). Imposing a cut off ±1log_2 fold change resulted in 31 differential gene discoveries.

Maf was the most significantly changed gene between *Maf*$^{fl/fl}$*Cx3cr1*$^{Cre/+}$ and *Maf*$^{fl/fl}$*Cx3cr1*$^{+/+}$ peritoneal tissue resident macrophages, with a -7.43 log_2 fold change and an adjusted p-value 6.65E-64 (A). Again, due to *Maf* being so significantly changed the other genes are difficult to visualise, and the removal of *Maf* from the visualisation allows other gene discoveries to become clearer (B).

Canonical pathway analysis was then performed in IPA comparing the edgeR discovered genes against those previously identified in all macrophages. In addition to those detected in DESeq2 (Figure 5.3.11) differential expression analysis several pathways including retinoate biosynthesis, G-protein coupled receptor signalling, Wnt/Ca^+ and cAMP-mediated synthesis pathways displayed downregulation and upregulation (Figure 5.3.13). Furthermore only histamine degradation and fatty acid α-oxidation pathways were downregulated (Figure 5.3.13).

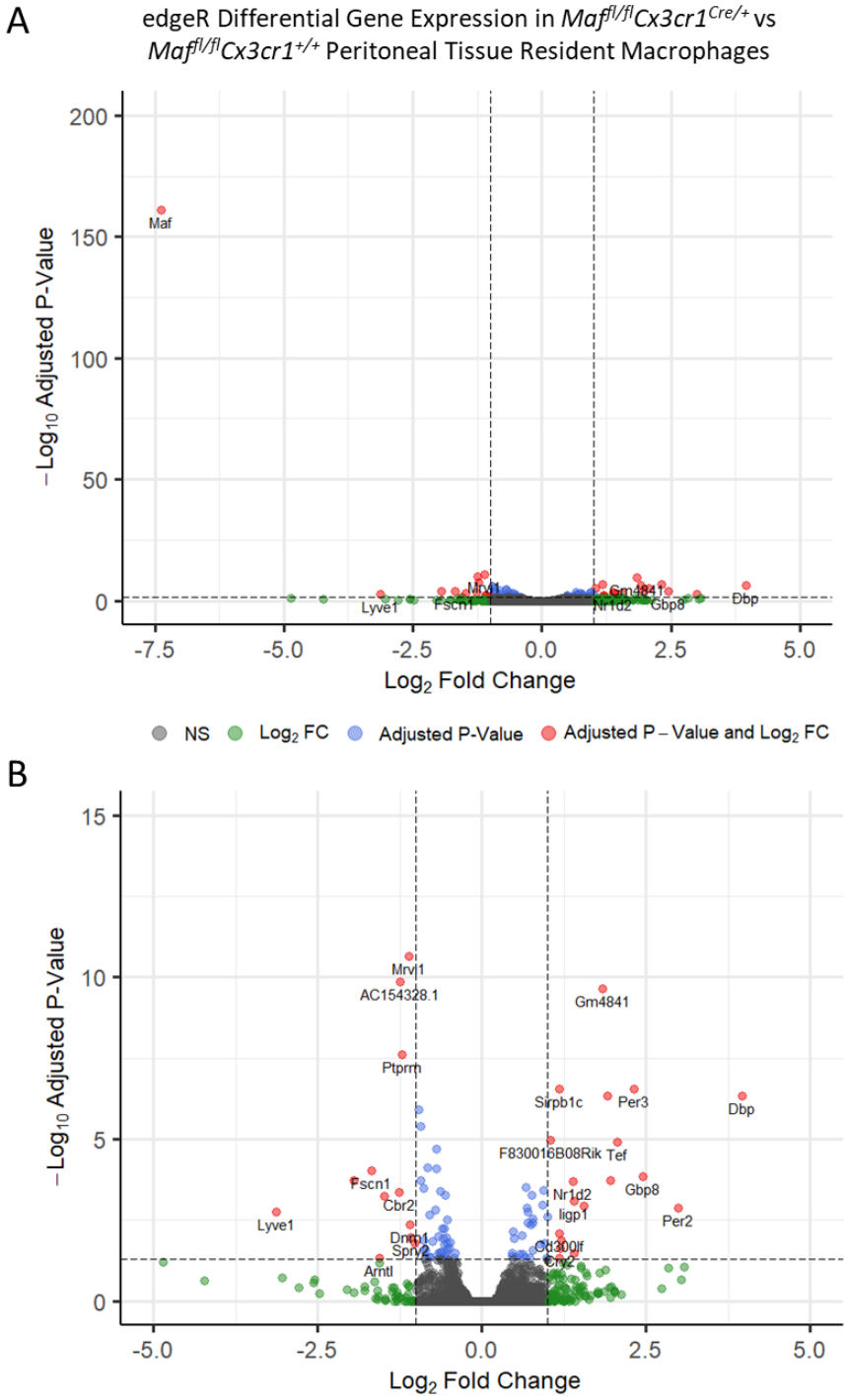

Figure 5.3.12 edgeR comparison of *Maf*$^{fl/fl}$*Cx3cr1*$^{Cre/+}$ vs *Maf*$^{fl/fl}$*Cx3cr1*$^{+/+}$ peritoneal tissue resident macrophages.

RNA-Seq of naïve *Maf*$^{fl/fl}$*Cx3cr1*$^{Cre/+}$ and *Maf*$^{fl/fl}$*Cx3cr1*$^{+/+}$ perionteal tissue resident macrophages. A) Volcano plot of all gene discoveries using edgeR differential expression method. B) Volcano plot with *Maf* removed from the data set to improve visualisation of other significant genes. Dashed lines representing cut off for adjusted p-value = 0.05 and ±log$_2$ fold change = 1 (n=3 mice of each genotype).

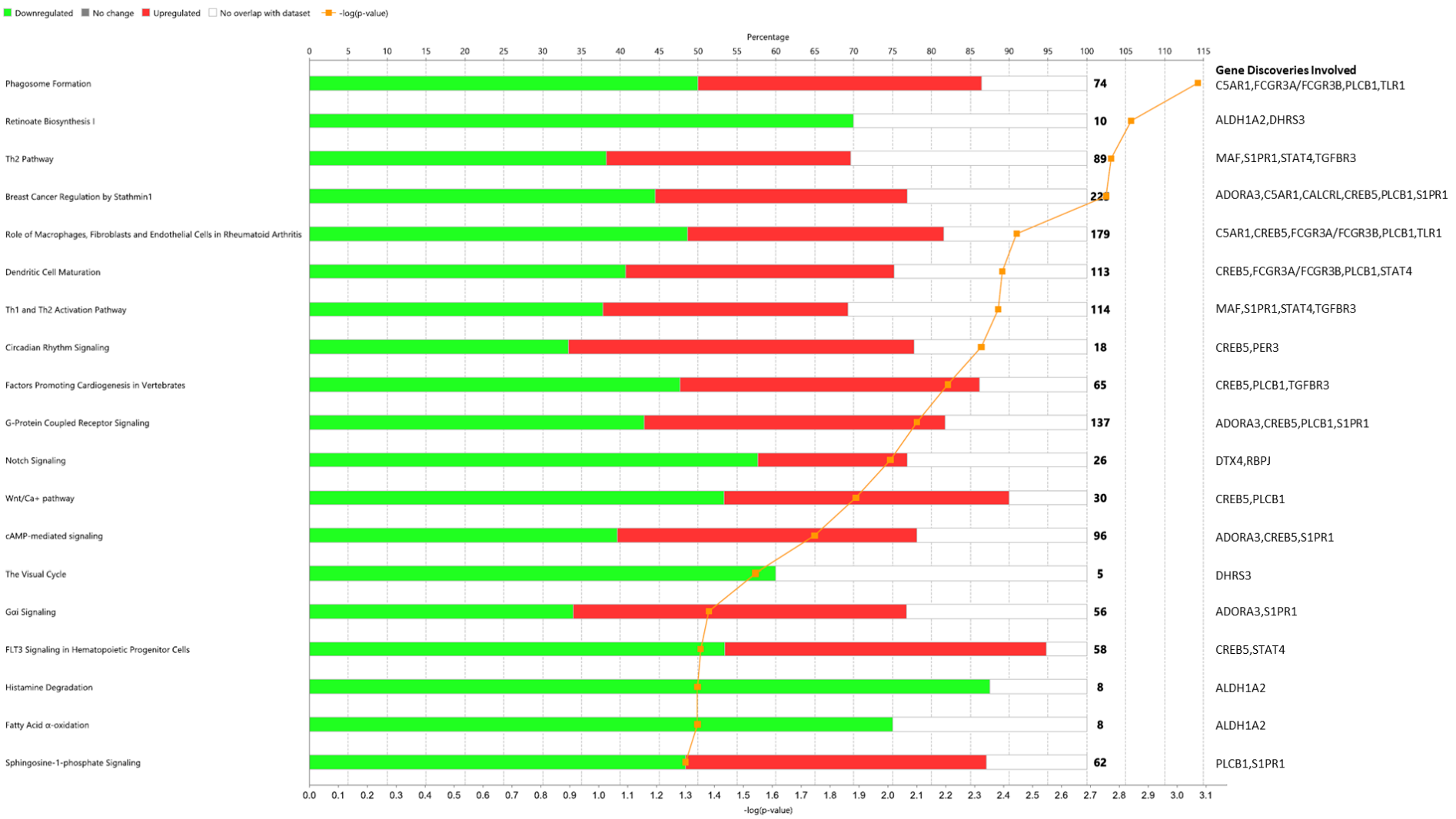
Downregulated
No change
Upregulated
No overlap with dataset
-log(p-value)
Percentage
0 5 10 15 20 25 30 35 40 45 50 55 60 65 70 75 80 85 90 95 100 105 110 115
Gene Discoveries Involved
Phagosome Formation 74 C5AR1,FCGR3A/FCGR3B,PLCB1,TLR1
Retinoate Biosynthesis I 10 ALDH1A2,DHRS3
Th2 Pathway 89 MAF,S1PR1,STAT4,TGFBR3
Breast Cancer Regulation by Stathmin1 22 ADORA3,C5AR1,CALCRL,CREB5,PLCB1,S1PR1
Role of Macrophages, Fibroblasts and Endothelial Cells in Rheumatoid Arthritis 179 C5AR1,CREB5,FCGR3A/FCGR3B,PLCB1,TLR1
Dendritic Cell Maturation 113 CREB5,FCGR3A/FCGR3B,PLCB1,STAT4
Th1 and Th2 Activation Pathway 114 MAF,S1PR1,STAT4,TGFBR3
Circadian Rhythm Signaling 18 CREB5,PER3
Factors Promoting Cardiogenesis in Vertebrates 65 CREB5,PLCB1,TGFBR3
G-Protein Coupled Receptor Signaling 137 ADORA3,CREB5,PLCB1,S1PR1
Notch Signaling 26 DTX4,RBPJ
Wnt/Ca+ pathway 30 CREB5,PLCB1
cAMP-mediated signaling 96 ADORA3,CREB5,S1PR1
The Visual Cycle 5 DHRS3
Gαi Signaling 56 ADORA3,S1PR1
FLT3 Signaling in Hematopoietic Progenitor Cells 58 CREB5,STAT4
Histamine Degradation 8 ALDH1A2
Fatty Acid α-oxidation 8 ALDH1A2
Sphingosine-1-phosphate Signaling 62 PLCB1,S1PR1
0.0 0.1 0.2 0.3 0.4 0.5 0.6 0.7 0.8 0.9 1.0 1.1 1.2 1.3 1.4 1.5 1.6 1.7 1.8 1.9 2.0 2.1 2.2 2.3 2.4 2.5 2.6 2.7 2.8 2.9 3.0 3.1
-log(p-value)

Figure 5.3.13 Canonical pathway analysis of edgeR differential gene expression analysis.

Canonical pathway analysis generated from Ingenuity Pathway Analysis (IPA) against those previously identified in all macrophages following edgeR differential gene expression method. Percentage of genes in the analysis overlap with pathway (green = downregulated, red = upregulated, white = no overlap). Numbers in bold are the total number of genes involved in the pathway. Specific gene discoveries with adjusted p-value <0.05 involved in each pathway named, with-log p-value of each pathway indicated with orange line.

DESeq2 and edgeR differential gene expression methods resulted in 76 common genes with an adjusted p-value of <0.05 (Figure 5.3.14A), with edgeR identifying 19 distinct genes and DESeq2 generating 22 (Figure 5.3.14A). Of those gene discovories with an adjusted p-value of <0.05 and a $\pm 1 \log_2$ fold change 19 common genes were identified between the two differential expression methods (Figure 5.3.14B), edgeR generating 12 unique genes and DESeq2 generating 10 (Figure 5.3.14B).

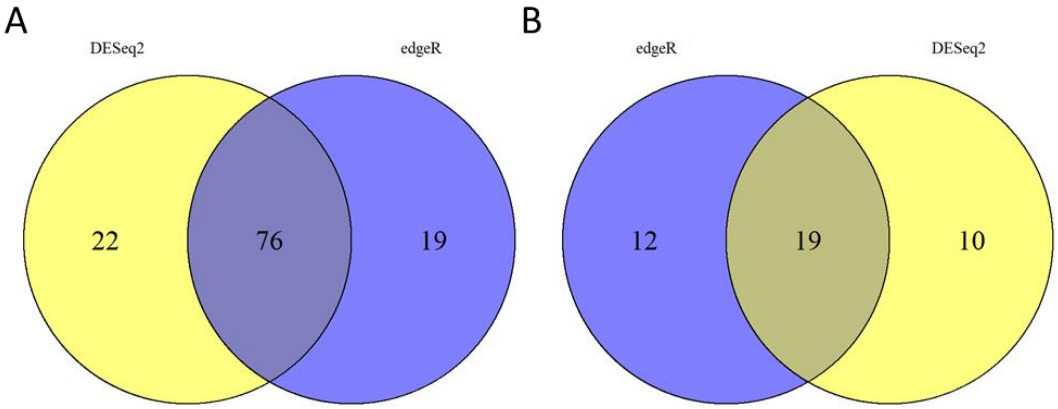

Figure 5.3.14 Venn diagram comparing between DESeq2 and edgeR differential expression methods.

A) Venn diagram comparing gene discoveries which are statistically significant (adjusted p-value <0.05) between DESeq2 and edgeR differential expression methods. B) Venn diagram comparing gene discoveries which are statistically significant (adjusted p-value <0.05) and have a $\pm 1 \log_2$ fold change between DESeq2 and edgeR differential expression methods.

5.3.4.1.3. Sex Variations in Peritoneal Tissue Resident Macrophages between *Maf*$^{fl/fl}$*Cx3cr1*$^{Cre/+}$ and *Maf*$^{fl/fl}$*Cx3cr1*$^{+/+}$ mice

Exploratory data analysis of variance between samples and how they correlate through principal component analysis (PCA) indicates the male *Maf*$^{fl/fl}$*Cx3cr1*$^{Cre/+}$ and *Maf*$^{fl/fl}$*Cx3cr1*$^{+/+}$ to have less variance than the female counterparts (Figure 5.3.15). Furthermore the male *Maf*$^{fl/fl}$*Cx3cr1*$^{+/+}$ mouse correlates closely with all three *Maf*$^{fl/fl}$*Cx3cr1*$^{+/+}$ when implementing confidence ellipses, suggesting a possible sex variant effect (Figure 5.3.15).

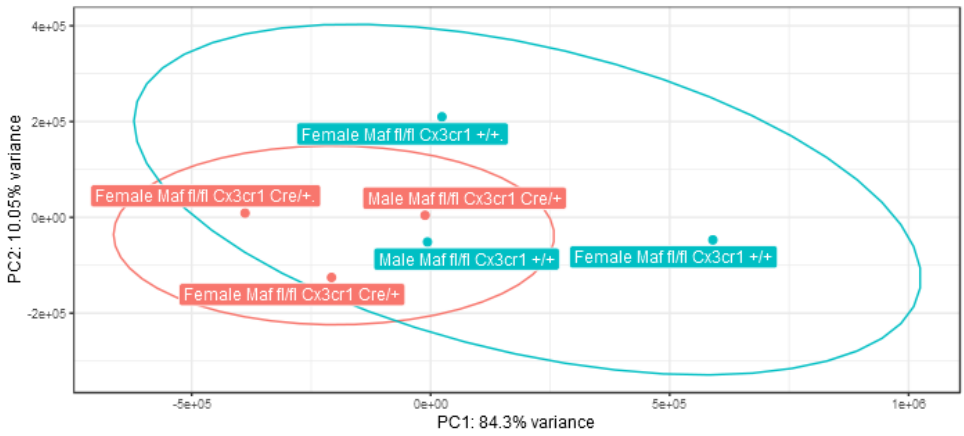

Figure 5.3.15 Principal component analysis (PCA) of RNA-sequencing samples.

***Maf*$^{fl/fl}$*Cx3cr1*$^{+/+}$ mice (Teal) and *Maf*$^{fl/fl}$*Cx3cr1*$^{Cre/+}$ (Red), with confidence ellipses for each genotype.**

To determine if there were sex specific differences between the two genotypes comparisons were done with edgeR of male *Maf*$^{fl/fl}$*Cx3cr1*$^{Cre/+}$ vs *Maf*$^{fl/fl}$*Cx3cr1*$^{+/+}$ (n=1 of each genotype) (A) and female *Maf*$^{fl/fl}$*Cx3cr1*$^{Cre/+}$ vs *Maf*$^{fl/fl}$*Cx3cr1*$^{+/+}$ (n=2 of each genotype) (B). Furthermore these differences were then compared to generate male vs female volcano plot (Figure 5.3.17).

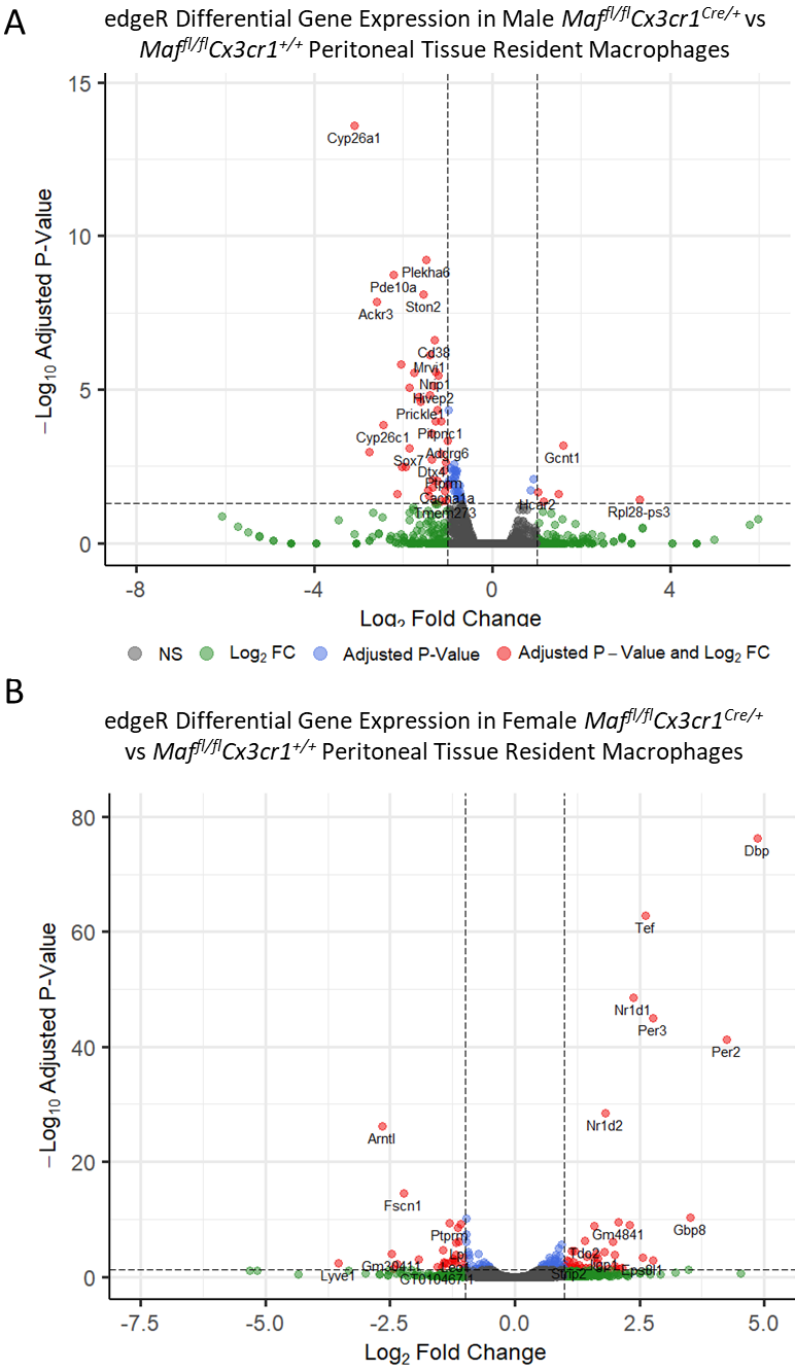

Figure 5.3.16 edgeR comparison of *Maf*$^{fl/fl}$*Cx3cr1*$^{Cre/+}$ vs *Maf*$^{fl/fl}$*Cx3cr1*$^{+/+}$ in Males and Females.

RNA-Seq of naïve *Maf*$^{fl/fl}$*Cx3cr1*$^{Cre/+}$ and *Maf*$^{fl/fl}$*Cx3cr1*$^{+/+}$ peritoneal tissue resident macrophages in male and female mice. A) Volcano plot with *Maf* removed from the data set to improve visualisation of other significant genes in male *Maf*$^{fl/fl}$*Cx3cr1*$^{Cre/+}$ (n=1) and *Maf*$^{fl/fl}$*Cx3cr1*$^{+/+}$ (n=1). B) Volcano plot with *Maf* removed from the data set to improve visualisation of other significant genes in female *Maf*$^{fl/fl}$*Cx3cr1*$^{Cre/+}$ (n=2) and *Maf*$^{fl/fl}$*Cx3cr1*$^{+/+}$ (n=2). Dashed lines representing cut off for adjusted p-value = 0.05 and ±log$_2$ fold change = 1.

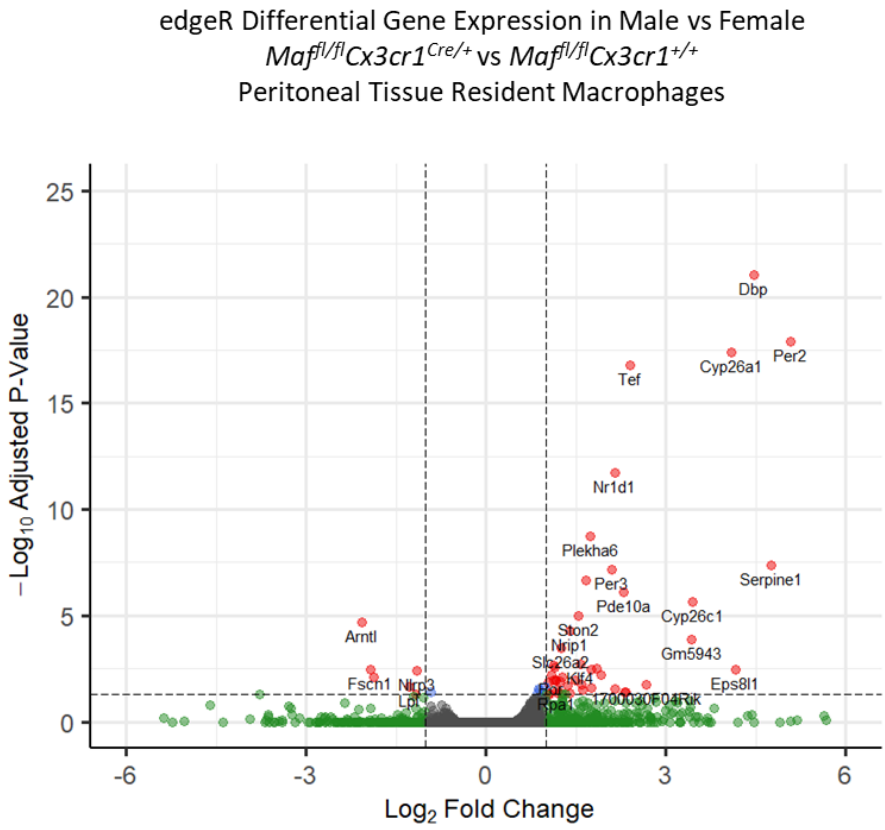

Figure 5.3.17 edgeR comparison between Male *Maf$^{fl/fl}$Cx3cr1$^{Cre/+}$* vs *Maf$^{fl/fl}$Cx3cr1$^{+/+}$* and Female *Maf$^{fl/fl}$Cx3cr1$^{Cre/+}$* vs *Maf$^{fl/fl}$Cx3cr1$^{+/+}$* mice.

Volcano plot between male Maf$^{fl/fl}$Cx3cr1$^{Cre/+}$ vs Maf$^{fl/fl}$Cx3cr1$^{+/+}$ and female Maf$^{fl/fl}$Cx3cr1$^{Cre/+}$ vs Maf$^{fl/fl}$Cx3cr1$^{+/+}$ mice. Female Maf$^{fl/fl}$Cx3cr1$^{Cre/+}$ (n=2) and Maf$^{fl/fl}$Cx3cr1$^{+/+}$ (n=2), male Maf$^{fl/fl}$Cx3cr1$^{Cre/+}$ (n=1) and Maf$^{fl/fl}$Cx3cr1$^{+/+}$ (n=1), with dashed lines representing cut off for adjusted p-value = 0.05 and ±log$_2$ fold change = 1.

Gene discoveries indicated that both male and female *Maf$^{fl/fl}$Cx3cr1$^{Cre/+}$* vs *Maf$^{fl/fl}$Cx3cr1$^{+/+}$* mice result in 15 common genes which have an adjusted p-value of <0.05 (Figure 5.3.18A), with female mice generating 122 unique genes and male mice 68 (Figure 5.3.18A). Of those gene discoveries with an adjusted p-value of <0.05 and a ±1log$_2$ fold change 6 common genes were identified between the two differential expression methods (Figure 5.3.18B), female mice generating 64 specific genes and male mice 42 (Figure 5.3.18B).

However when correlating the log$_2$ fold change of the 112 genes (as determined by p-value of <0.05 and a ±1log$_2$, in either sex, summarised in Figure 5.3.18B) between female and male mice, there was a moderate Pearson correlation of R=0.46 (p-value = 0.36E-6, ****), indicating a similar trend in expression of these genes (Figure 5.3.18C).

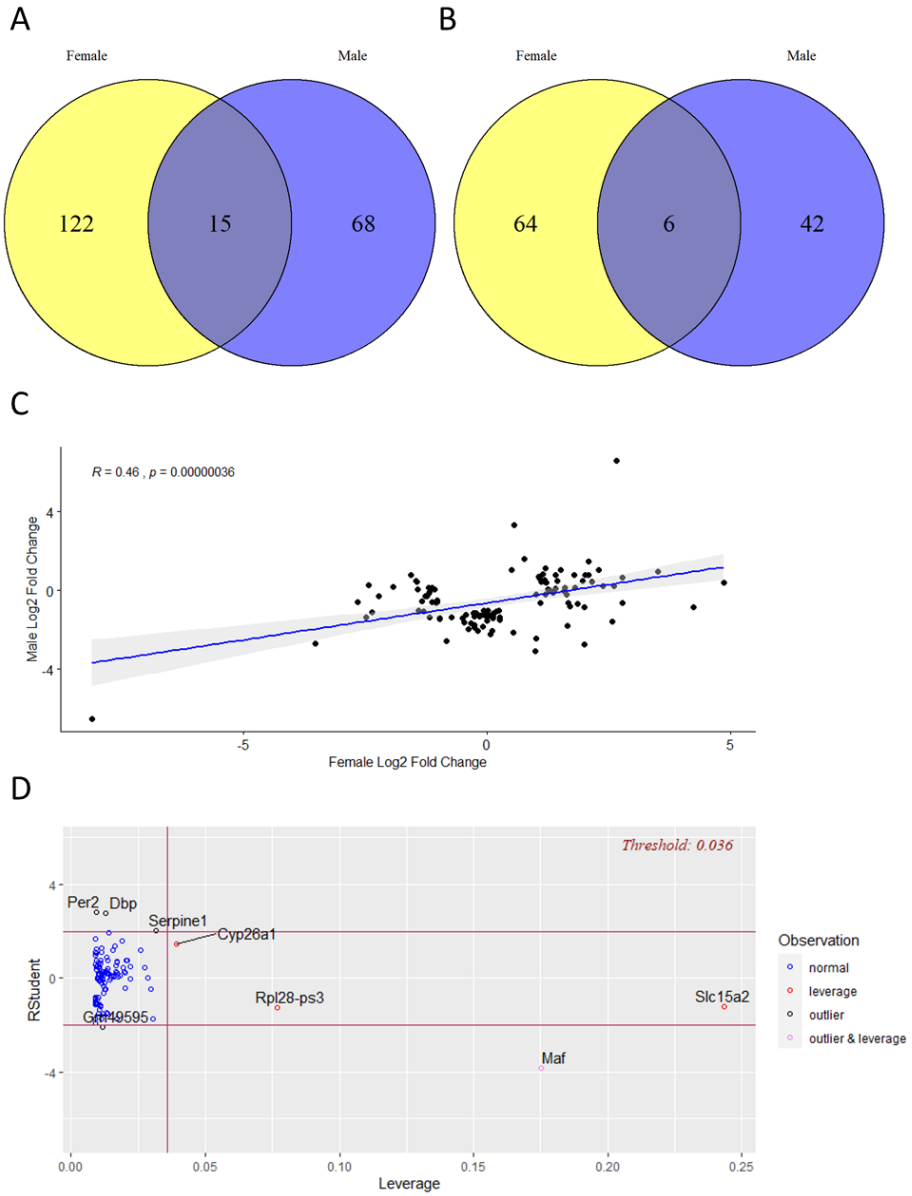

Figure 5.3.18 Correlation and regression analysis of Male *Maf*$^{fl/fl}$*Cx3cr1*$^{Cre/+}$ vs *Maf*$^{fl/fl}$*Cx3cr1*$^{+/+}$ and Female *Maf*$^{fl/fl}$*Cx3cr1*$^{Cre/+}$ vs *Maf*$^{fl/fl}$*Cx3cr1*$^{+/+}$ mice.

A) Venn diagram comparing gene discoveries which are statistically significant (adjusted p-value <0.05) between male and female mice. B) Venn diagram comparing gene discoveries which are statistically significant (adjusted p-value <0.05) and have a ±1log$_2$ fold change between male and female mice. C) Correlation of ±log$_2$ fold changes from between Male *Maf*$^{fl/fl}$*Cx3cr1*$^{Cre/+}$ vs *Maf*$^{fl/fl}$*Cx3cr1*$^{+/+}$ and Female *Maf*$^{fl/fl}$*Cx3cr1*$^{Cre/+}$ vs *Maf*$^{fl/fl}$*Cx3cr1*$^{+/+}$ mice, with Pearson correlation coefficient analysis (blue line). D) Studentized Residuals vs Leverage plot between Male *Maf*$^{fl/fl}$*Cx3cr1*$^{Cre/+}$ vs *Maf*$^{fl/fl}$*Cx3cr1*$^{+/+}$ and Female *Maf*$^{fl/fl}$*Cx3cr1*$^{Cre/+}$ vs *Maf*$^{fl/fl}$*Cx3cr1*$^{+/+}$ mice. Horizonal red line indicating Cook's distance threshold and vertical red line indicating leverage threshold of 0.036.

Regression analysis of the 112 gene discoveries visualised in a studentized residuals vs leverage plot (Figure 5.3.18D) identifies influential data points in the model. Utilising Cook's distance indicates several outliers including *Per2* (ENSMUSG00000055866), *Dbp* (ENSMUSG00000059824) and *Serpine1* (ENSMUSG00000037411) (Figure 5.3.18D). When combined with leverage (amount of influence) *Slc15a2* (ENSMUSG00000022899) is indicated to have the highest leverage however is not an outlier (Figure 5.3.18D), with only *Maf* being both an outlier based on Cook's distance and high leverage (Figure 5.3.18D).

When adding mouse sex to the model matrix for DESeq2 (Figure 5.3.19) or edgeR (Figure 5.3.20), edgeR generated 148 differential gene discoveries with an adjusted p-value <0.05 (the full list of genes can be found in Appendix X), and DESeq2 109 differential gene discoveries with an adjusted p-value <0.05 (the full list of genes can be found in Appendix XI).

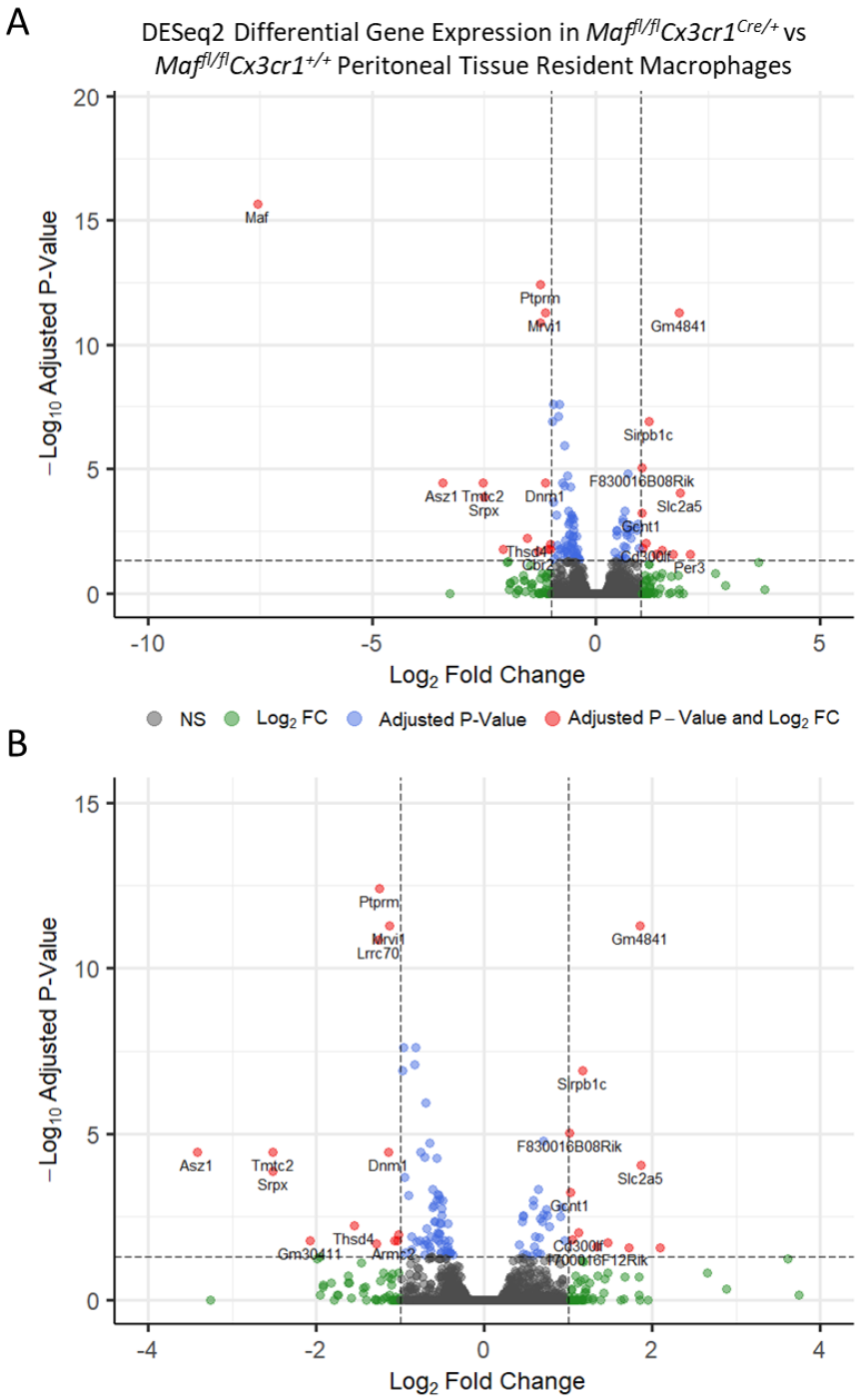

Figure 5.3.19 DESeq2 comparison of *Maf*$^{fl/fl}$*Cx3cr1*$^{Cre/+}$ vs *Maf*$^{fl/fl}$*Cx3cr1*$^{+/+}$ peritoneal tissue resident macrophages when including sex in the model matrix.

A) Volcano plot of all gene discoveries using DESeq2 differential expression method when including sex as a variable. B) Volcano plot with *Maf* removed from the data set to improve visualisation of other significant genes. *Maf*$^{fl/fl}$*Cx3cr1*$^{Cre/+}$ (n=3) and *Maf*$^{fl/fl}$*Cx3cr1*$^{+/+}$ (n=3), with dashed lines representing cut off for adjusted p-value = 0.05 and ±log$_2$ fold change = 1.

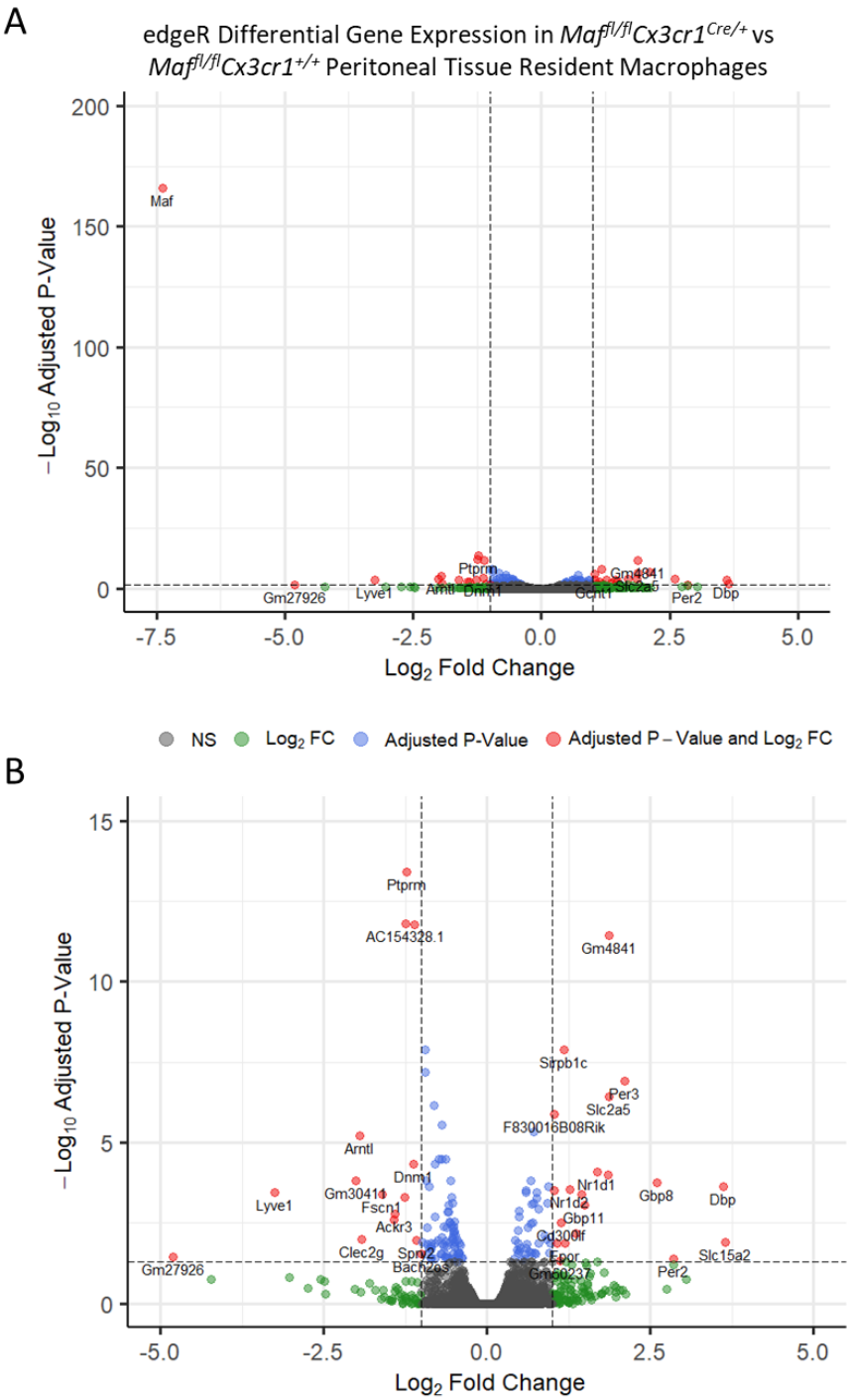

Figure 5.3.20 edgeR comparison of *Maf*$^{fl/fl}$*Cx3cr1*$^{Cre/+}$ vs *Maf*$^{fl/fl}$*Cx3cr1*$^{+/+}$ peritoneal tissue resident macrophages when including sex in the model matrix.

A) Volcano plot of all gene discoveries using edgeR differential expression method when including sex as a variable. B) Volcano plot with *Maf* removed from the data set to improve visualisation of other significant genes. *Maf*$^{fl/fl}$*Cx3cr1*$^{Cre/+}$ (n=3) and *Maf*$^{fl/fl}$*Cx3cr1*$^{+/+}$ (n=3), with dashed lines representing cut off for adjusted p-value = 0.05 and ±log$_2$ fold change = 1.

The two analyses resulted in 97 shared gene discoveries which have an adjusted p-value of <0.05, with edgeR generating 51 unique genes and DESeq2 generating 12 (Figure 5.3.21A). Of those gene discoveries with an adjusted p-value of <0.05 and a ±1log_2 fold change 16 common genes were identified between the two differential expression methods (Figure 5.3.21B), edgeR generating 20 distinct genes and DESeq2 9 (Figure 5.3.21B).

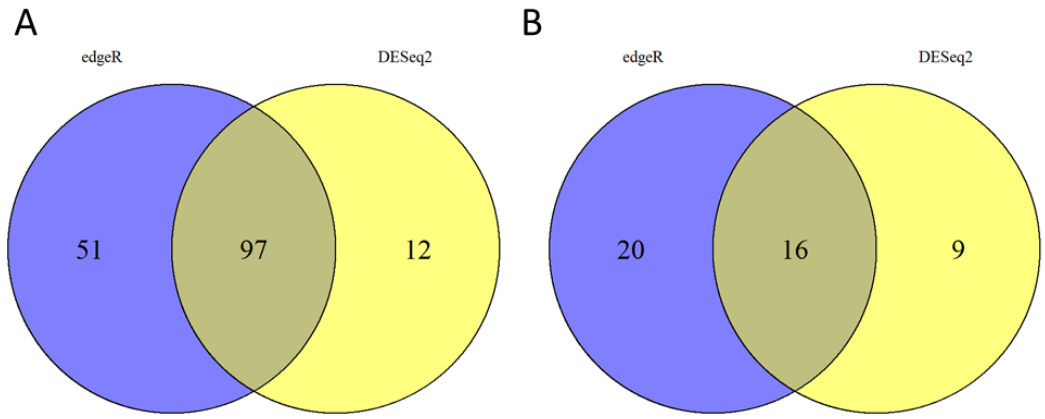

Figure 5.3.21 Venn diagram comparing between DESeq2 and edgeR differential expression methods when including sex into the model matrix.

A) Venn Diagram comparing gene discoveries which are statistically significant (adjusted p-value <0.05) between DESeq2 and edgeR differential expression methods when including sex into the comparison matrix. B) Venn diagram comparing gene discoveries which are statistically significant (adjusted p-value <0.05) and have a ±1log_2 fold change between DESeq2 and edgeR differential expression methods when including sex into the comparison matrix.

Canonical pathway analysis from IPA of the 109 gene discoveries from DESeq2 differential expression when sex is included in the model matrix, compared against those previously identified in all macrophages. Additional pathways of interest were elucidated including eicosanoid signalling, leukotriene signalling pathways (Figure 5.3.22).

Analysing the 148 edgeR differential gene discoveries with IPA when sex is included in the model matrix as above, as in the DESeq2 analysis, several additional pathways including eicosanoid signalling displayed downregulation and upregulation (Figure 5.3.23). Again histamine biosynthesis pathway was indicated to be upregulated, whilst arginine degradation I and Retinoate biosynthesis were only downregulated (Figure 5.3.23).

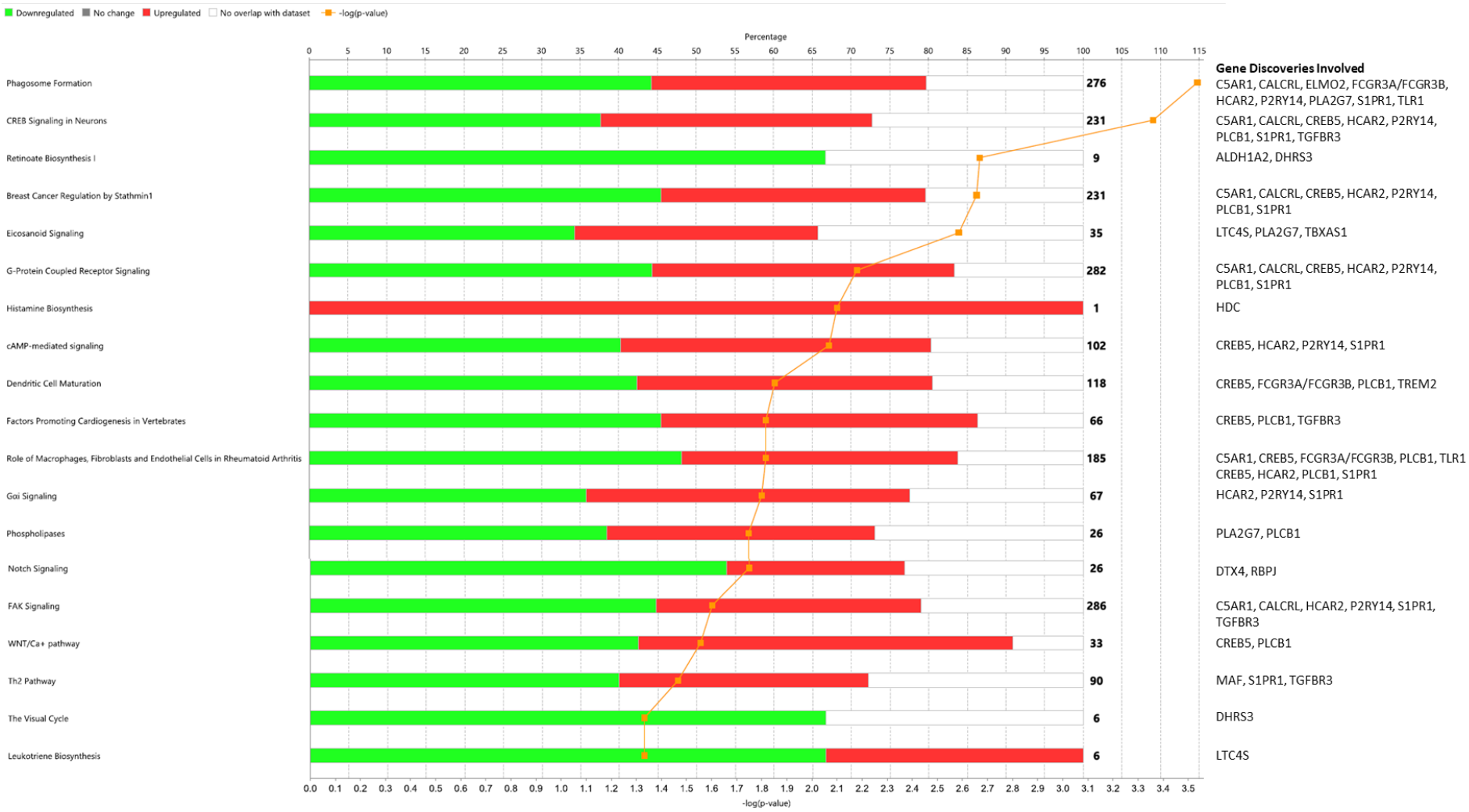
Downregulated
No change
Upregulated
No overlap with dataset
-log(p-value)
Percentage
0 5 10 15 20 25 30 35 40 45 50 55 60 65 70 75 80 85 90 95 100 105 110 115
Gene Discoveries Involved
Phagosome Formation
276
C5AR1, CALCRL, ELMO2, FCGR3A/FCGR3B, HCAR2, P2RY14, PLA2G7, S1PR1, TLR1
CREB Signaling in Neurons
231
C5AR1, CALCRL, CREB5, HCAR2, P2RY14, PLCB1, S1PR1, TGFBR3
Retinoate Biosynthesis I
9
ALDH1A2, DHRS3
Breast Cancer Regulation by Stathmin1
231
C5AR1, CALCRL, CREB5, HCAR2, P2RY14, PLCB1, S1PR1
Eicosanoid Signaling
35
LTC4S, PLA2G7, TBXAS1
G-Protein Coupled Receptor Signaling
282
C5AR1, CALCRL, CREB5, HCAR2, P2RY14, PLCB1, S1PR1
Histamine Biosynthesis
1
HDC
cAMP-mediated signaling
102
CREB5, HCAR2, P2RY14, S1PR1
Dendritic Cell Maturation
118
CREB5, FCGR3A/FCGR3B, PLCB1, TREM2
Factors Promoting Cardiogenesis in Vertebrates
66
CREB5, PLCB1, TGFBR3
Role of Macrophages, Fibroblasts and Endothelial Cells in Rheumatoid Arthritis
185
C5AR1, CREB5, FCGR3A/FCGR3B, PLCB1, TLR1 CREB5, HCAR2, PLCB1, S1PR1
Gαi Signaling
67
HCAR2, P2RY14, S1PR1
Phospholipases
26
PLA2G7, PLCB1
Notch Signaling
26
DTX4, RBPJ
FAK Signaling
286
C5AR1, CALCRL, HCAR2, P2RY14, S1PR1, TGFBR3
WNT/Ca+ pathway
33
CREB5, PLCB1
Th2 Pathway
90
MAF, S1PR1, TGFBR3
The Visual Cycle
6
DHRS3
Leukotriene Biosynthesis
6
LTC4S
0.0 0.1 0.2 0.3 0.4 0.5 0.6 0.7 0.8 0.9 1.0 1.1 1.2 1.3 1.4 1.5 1.6 1.7 1.8 1.9 2.0 2.1 2.2 2.3 2.4 2.5 2.6 2.7 2.8 2.9 3.0 3.1 3.2 3.3 3.4 3.5
-log(p-value)

Figure 5.3.22 Canonical pathway analysis of DESeq2 differential gene expression analysis when sex is included.

Canonical pathway analysis generated from Ingenuity Pathway Analysis (IPA) against those previously identified in all macrophages following DESeq2 differential gene expression method when sex is included in the model matrix. Percentage of genes in the analysis overlap with pathway (green = downregulated, red = upregulated, white = no overlap). Numbers in bold are the total number of genes involved in the pathway. Specific gene discoveries with adjusted p-value <0.05 involved in each pathway named, with-log p-value of each pathway indicated with orange line.


Downregulated
No change
Upregulated
No overlap with dataset
-log(p-value)
Percentage
0 5 10 15 20 25 30 35 40 45 50 55 60 65 70 75 80 85 90 95 100 105 110 115
Gene Discoveries Involved
Phagosome Formation 276 ACKR3, C5AR1, CALCRL, ELMO2, FCGR3A/FCGR3B, HCAR2, P2RY14, S1PR1, TLR1
CREB Signaling in Neurons 231 ACKR3, C5AR1, CALCRL, HCAR2, P2RY14, PLCB1, S1PR1, TGFBR3
Retinoate Biosynthesis I 9 ALDH1A2, DHRS3
Th1 and Th2 Activation Pathway 115 MAF, NFIL3, S1PR1, STAT4, TGFBR3
Dendritic Cell Maturation 118 FCGR3A/FCGR3B, FSCN1, PLCB1, STAT4, TREM2
Breast Cancer Regulation by Stathmin1 231 ACKR3, C5AR1, CALCRL, HCAR2, P2RY14, PLCB1, S1PR1
Circadian Rhythm Signaling 132 NFIL3, NR1D2, PER2, PER3, PLCB1
Histamine Biosynthesis 1 HDC
Th2 Pathway 90 MAF, S1PR1, STAT4, TGFBR3
G-Protein Coupled Receptor Signaling 282 ACKR3, C5AR1, CALCRL, HCAR2, P2RY14, PLCB1, S1PR1
FAK Signaling 286 ACKR3, C5AR1, CALCRL, HCAR2, P2RY14, S1PR1, TGFBR3
Notch Signaling 26 DTX4, RBPJ
Gαi Signaling 67 HCAR2, P2RY14, S1PR1
Urea Cycle 4 ARG1
Arginine Degradation VI (Arginase 2 Pathway) 4 ARG1
Arginine Degradation I (Arginase Pathway) 4 ARG1
Eicosanoid Signaling 35 LTC4S, TBXAS1
Calcium Transport I 5 ANXA5
Citrulline Biosynthesis 5 ARG1
0.0 0.1 0.2 0.3 0.4 0.5 0.6 0.7 0.8 0.9 1.0 1.1 1.2 1.3 1.4 1.5 1.6 1.7 1.8 1.9 2.0 2.1 2.2 2.3 2.4 2.5 2.6 2.7 2.8
-log(p-value)

Figure 5.3.23 Canonical pathway analysis of edgeR differential gene expression analysis when sex is included.

Canonical pathway analysis generated from Ingenuity Pathway Analysis (IPA) against those previously identified in all macrophages following edgeR differential gene expression method when sex is included in the model matrix. Percentage of genes in the analysis overlap with pathway (green = downregulated, red = upregulated, white = no overlap). Numbers in bold are the total number of genes involved in the pathway. Specific gene discoveries with adjusted p-value <0.05 involved in each pathway named, with-log p-value of each pathway indicated with orange line.

Upstream Regulators	DESeq2		
	Log_2 Fold Change	P-Value of Overlap	Targets in Dataset
Il10ra	-0.094	8.85E-06	*Cd300lf, Hcar2, Hpse, Ltc4s, Reps2, S1pr1, Sell, Sirpb1*
Cited2	0.227	0.0202	*C5ar1, Fcgr3a/Fcgr3b, Hcar2, P2ry14*

Table 5.3.1 Upstream regulators in DESeq2 differential gene expression analysis when sex is included.

Upstream regulators identified in DESeq2 analysis with log2 fold change and p-value of overlap with each pathway. Genes with an adjusted p-value of <0.05 involved in each pathway are named.

Upstream Regulators	edgeR		
	Log_2 Fold Change	P-Value of Overlap	Targets in Dataset
Il10ra	-0.077	6.11E-06	*Cd300lf, Hcar2, Hpse, Ltc4s, Reps2, S1pr1, Saa3, Sell, Sirpb1*
Gata6	0.096	2.74E-05	*Arg1, Cd163, Lyve1, Saa3, Vsig4*
Eif4ebp1	0.081	0.00693	*Arg1, Nfil3*
Eif4ebp2	0.021	0.00693	*Arg1, Nfil3*
Cited2	0.24	0.00942	*Arg1, C5ar1, Fcgr3a/Fcgr3b, Hcar2, P2ry14*
S1pr1	-0.494	0.00982	*Nlrp3*
P2rx7	-0.137	0.00982	*Nlrp3*
Csf1	0.271	0.0182	*Arg1, C5ar1, Cd163*
Fyn	-0.016	0.0196	*Nlrp3*
mir-10	1.537	0.0196	*Arg1*
Sting1	0.321	0.0211	*Arg1, Hdc*
Map3k8	0.052	0.0218	*Arg1, Dok2, Fscn1*
Taz	-0.089	0.0347	*Aldh1a2, Arg1*
Klf4	0.13	0.0387	*Arg1*
Prdx1	-0.04	0.0387	*Arg1*
Vasp	0.081	0.0482	*Arg1*
Pdcd1		0.0482	*Nlrp3*

Table 5.3.2 Upstream regulators in edgeR differential gene expression analysis when sex is included.

Upstream regulators identified in edgeR analysis with log2 fold change and p-value of overlap with each pathway. Genes with an adjusted p-value of <0.05 involved in each pathway are named.

Two upstream regulators were identified with IPA from the DESeq2 analysis, interleukin 10 receptor subunit A (*Il10ra*) identifying 8 genes which had an adjusted p-value of <0.05, and Cbp/p300-interacting transactivator (*Cited2*) which identified 4 genes (Table 5.3.1).

edgeR analysis highlighted 17 upstream regulators with a p-value of overlap <0.05 (Table 5.3.2). Additional to *Il10*ra and *Cited2*, GATA Binding Protein 6 (*Gata6*) displayed 5 genes and M-CSF encoding gene (*Csf1*) which highlighted 3 genes which had an adjusted p-value of <0.05 (Table 5.3.2). All majority of other upstream regulators had either only 1 or 2 gene discoveries with an adjusted p-value of <0.05 associated, predominantly *Arg1* or *Nlpr3* (Table 5.3.2).

5.3.4.2. Differential Exon Usage

When comparing *Maf*$^{fl/fl}$*Cx3cr1*$^{Cre/+}$ vs *Maf*$^{fl/fl}$*Cx3cr1*$^{+/+}$ peritoneal tissue resident macrophages generated 2 differential exons with an adjusted p-value <0.05 and a cut off ±1log$_2$ (Figure 5.3.24A).

Sphingosine Kinase 2 (*Sphk2*) (ENSMUSG00000057342) at exon 11 was identified as having statistically significantly changed usage (adjusted p-value = 1.59E-09, 2.393 log$_2$ fold change) between *Maf*$^{fl/fl}$*Cx3cr1*$^{Cre/+}$ and *Maf*$^{fl/fl}$*Cx3cr1*$^{+/+}$ peritoneal tissue resident macrophages (Figure 5.3.24B). The predicted gene *GM10602* (ENSMUSG00000073985) at exon 10 was also determined to be statistically significantly changed usage (adjusted p-value = 0.0072, 2.576 log$_2$ fold change) (Figure 5.3.24C).

Further investigation into only the female *Maf*$^{fl/fl}$*Cx3cr1*$^{Cre/+}$ and *Maf*$^{fl/fl}$*Cx3cr1*$^{+/+}$ peritoneal tissue resident macrophage elucidated two further differential exon usages in *SphK2*, at exon 10 (adjusted P-Values = 0. 0052, with a 2.177 log$_2$ fold change) and at exon 1 usage which even though had a -2.132 log$_2$ fold change was not deemed statistically significant (adjusted P-Values = 0.09171) (Figure 5.3.25B).

It was not possible to undertake exon usage analysis in male *Maf*$^{fl/fl}$*Cx3cr1*$^{Cre/+}$ and *Maf*$^{fl/fl}$*Cx3cr1*$^{+/+}$ (due to n=1), however examining individual samples normalised counts of the *Sphk2* exon usage elucidated the male *Maf*$^{fl/fl}$*Cx3cr1*$^{Cre/+}$ (n=1) had a more similar count to that of the *Maf*$^{fl/fl}$*Cx3cr1*$^{+/+}$ mice (n=3) across the first 6 exons (Figure 5.3.26).

A

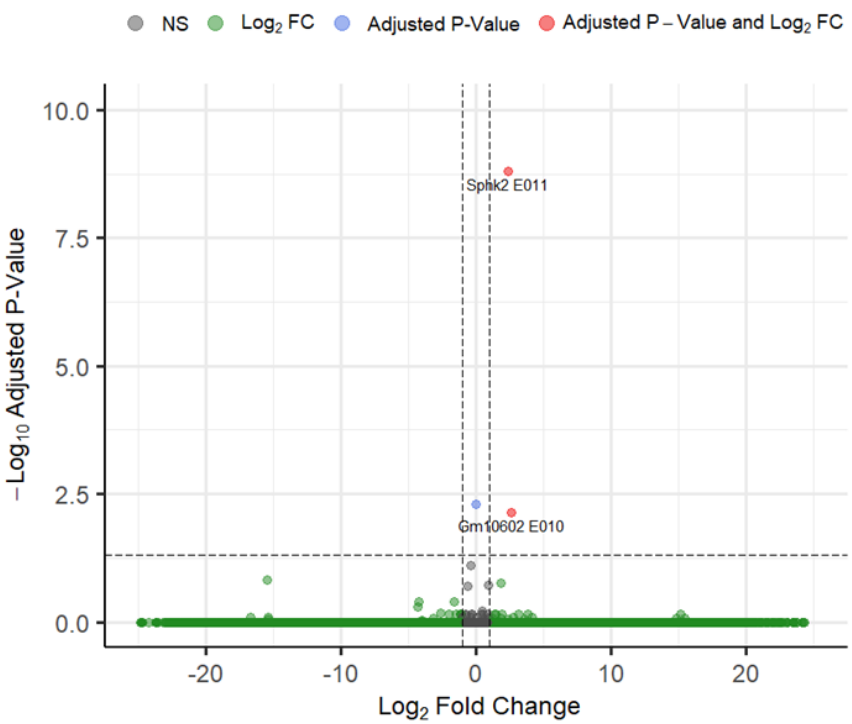
NS
Log2 FC
Adjusted P-Value
Adjusted P – Value and Log2 FC
Sphk2 E011
Gm10602 E010
−Log10 Adjusted P-Value
Log2 Fold Change
10.0
7.5
5.0
2.5
0.0
-20
-10
0
10
20

B

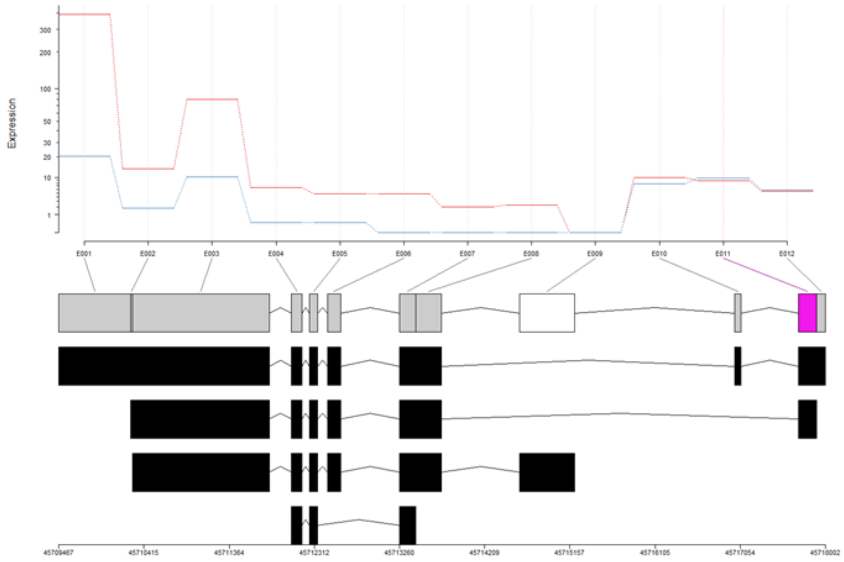
Expression

C

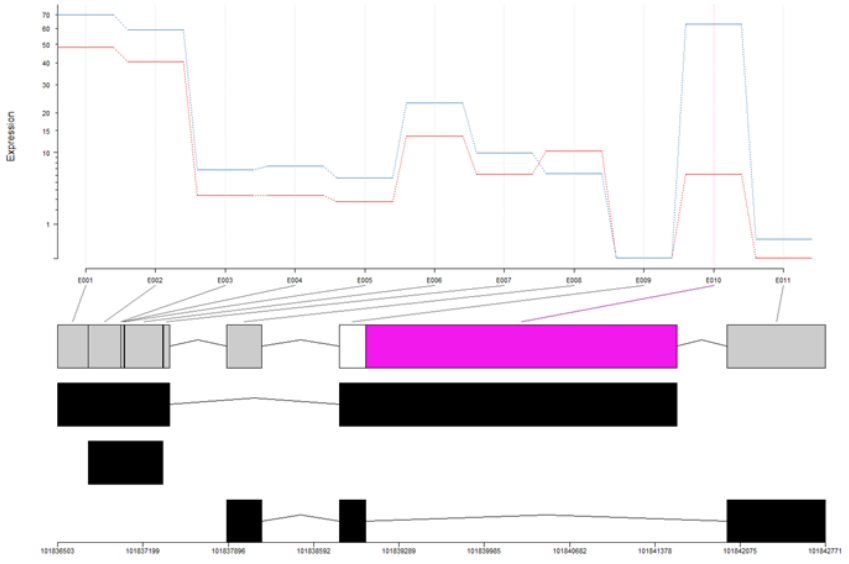
Expression

Figure 5.3.24 DEXSeq differential exon usage analysis of peritoneal tissue resident macrophages in *Maf*$^{fl/fl}$*Cx3cr1*$^{Cre/+}$ vs *Maf*$^{fl/fl}$*Cx3cr1*$^{+/+}$ mice.

A) Volcano plot of DEXSeq differential exon usage analysis between *Maf*$^{fl/fl}$*Cx3cr1*$^{Cre/+}$ (n=3) vs *Maf*$^{fl/fl}$*Cx3cr1*$^{+/+}$ (n=3) mice, with dashed lines representing cut off for adjusted p-value = 0.05 and ±log$_2$ fold change = 1. B) DEXSeq plot of expression of exons in the *Sphk2* gene in *Maf*$^{fl/fl}$*Cx3cr1*$^{Cre/+}$ (Blue line) (n=3) and *Maf*$^{fl/fl}$*Cx3cr1*$^{+/+}$ (Red line) (n=3). Differential exons highlighted in pink (p-value <0.05) and transcripts of *Sphk2* gene in black below. C) DEXSeq plot of expression of exons in the *Gm10602* gene in *Maf*$^{fl/fl}$*Cx3cr1*$^{Cre/+}$ (Blue line) (n=3) and *Maf*$^{fl/fl}$*Cx3cr1*$^{+/+}$ (Red line) (n=3). Differential exons highlighted in pink (p-value <0.05) and transcripts of *Gm10602* gene in black below.

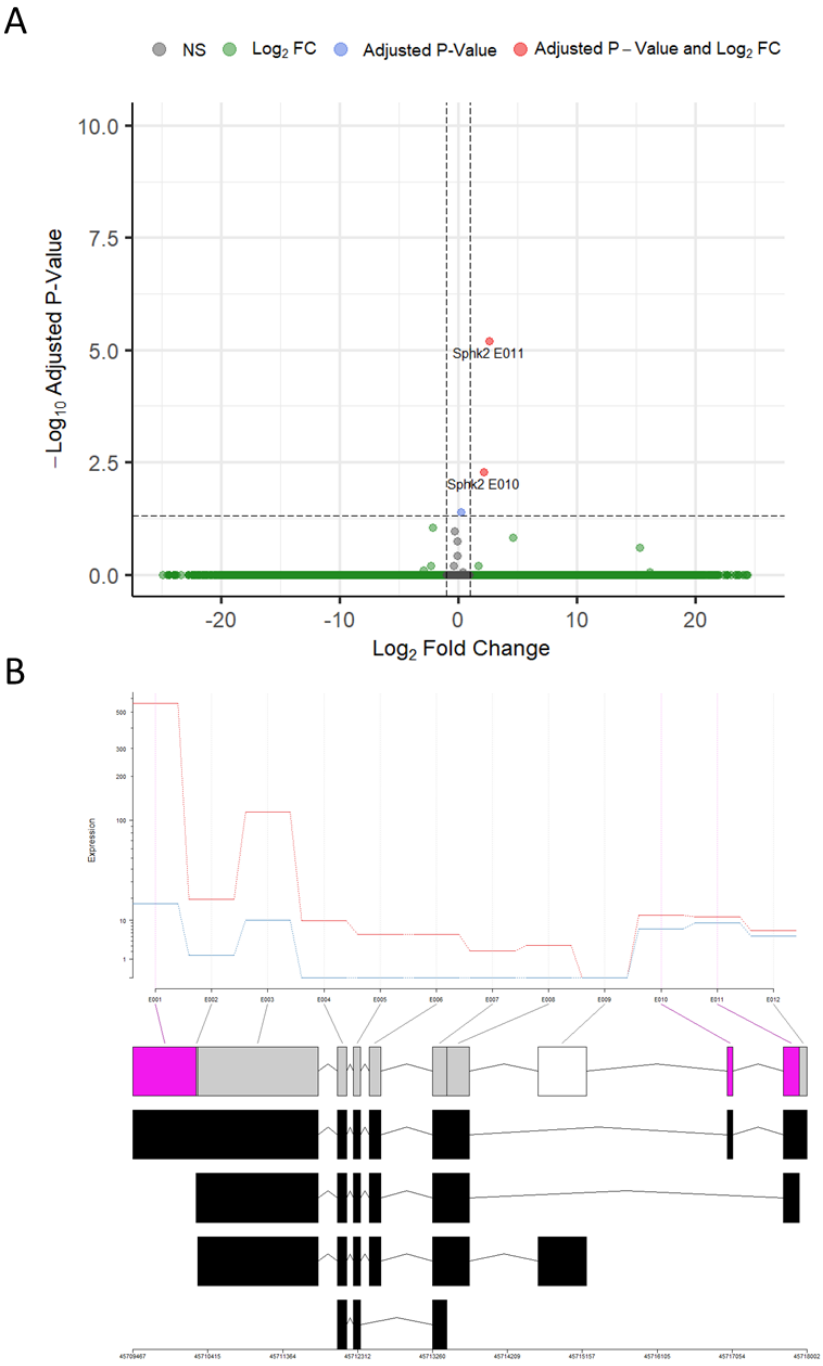

Figure 5.3.25 DEXSeq differential exon usage analysis of peritoneal tissue resident macrophages in female *Maf*$^{fl/fl}$*Cx3cr1*$^{Cre/+}$ vs *Maf*$^{fl/fl}$*Cx3cr1*$^{+/+}$ mice.

A) Volcano plot of DEXSeq differential exon usage analysis between *Maf*$^{fl/fl}$*Cx3cr1*$^{Cre/+}$ (n=2) vs *Maf*$^{fl/fl}$*Cx3cr1*$^{+/+}$ (n=2) mice, with dashed lines representing cut off for adjusted p-value = 0.05 and log$_2$ fold change = 1. B) DEXSeq plot of expression of exons in the *Sphk2* gene in female *Maf*$^{fl/fl}$*Cx3cr1*$^{Cre/+}$ (Blue line) (n=2) and *Maf*$^{fl/fl}$*Cx3cr1*$^{+/+}$ (Red line) (n=2). Differential exons highlighted in pink (p-value = 0.05) and transcripts of *Sphk2* gene in black below.

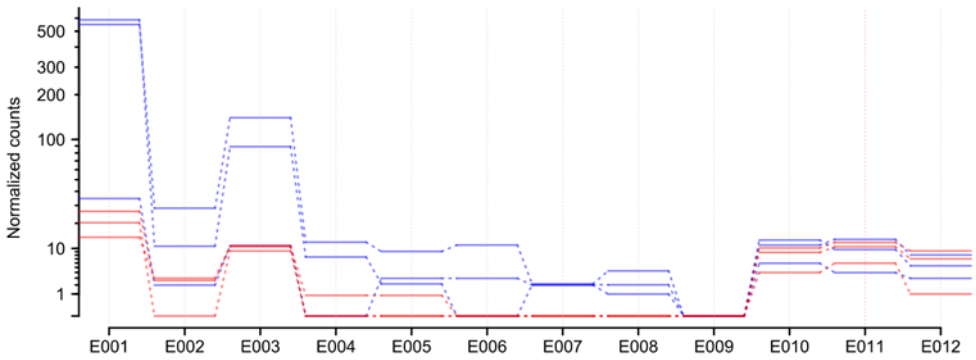

Figure 5.3.26 DEXSeq normalised counts in the *Sphk2* gene across individual samples.

DEXSeq plot of exon usage in the *Sphk2* gene in *Maf*$^{fl/fl}$*Cx3cr1*$^{Cre/+}$ (Blue line) and *Maf*$^{fl/fl}$*Cx3cr1*$^{+/+}$ (Red line).

5.3.5. Validation of RNA Sequencing of Naïve Peritoneal Macrophages Gene Discoveries

Differential genes identified through DESeq2, and edgeR were selected for validation based on being protein coding, have a p-value of <0.05 and a ±1log_2 fold change in at least one of the differential expression methods, when sex is included in the comparison matrix (summarised in Table 5.3.3).

Target	DESeq2		edgeR	
	Log_2 Fold Change	Adjusted P-Value	Log_2 Fold Change	Adjusted P-Value
Per3	2.089419	0.026839	2.1052125	1.22E-07
Creb5	1.725391	0.027082	1.7253906	0.027082
Cd300lf	1.118552	0.009727	1.1185516	0.0097269
Mrvi1	-1.12767	5.13E-12	-1.112107	1.68E-12
Dnm1	-1.13747	3.61E-05	-1.123607	4.81E-05
Ptprm	-1.24546	3.78E-13	-1.230884	3.83E-14
Maf	-7.56594	2.20E-16	-7.369870	1.85E-166
Dbp	NA	NA	3.6132277	0.0002330
Lyve1	NA	NA	-3.243814	0.0003427

Table 5.3.3 Summary of targets selected for validation of RNA sequencing data.

List of targets for validation by qPCR and flow cytometry with log_2 fold change and adjusted p-value from DESeq2 and edgeR analyses. Genes which did not meet the cut off (adjusted p-value <0.05 and ±1log_2 fold change) in one of the analyses had an NA applied.

5.3.5.1. Validation of Gene Discoveries by qPCR

To validate the differential gene discovery analysis qPCR was conducted on *Maf*$^{fl/fl}$*Cx3cr1*$^{+/+}$ and *Maf*$^{fl/fl}$*Cx3cr1*$^{Cre/+}$ peritoneal tissue resident macrophages, isolated by FACS as above (Figure 5.3.4A).

40-ΔCT indicated overall significance by Genotype, Targets and Genotype x Targets (p-value = <0.0001, ****), whilst Sex indicated no statistical significance when analysed by three-way ANOVA (Figure 5.3.27A). Tukey's multiple comparisons test indicated *Lyve1* to be statistically significant between male *Maf*$^{fl/fl}$*Cx3cr1*$^{+/+}$ and *Maf*$^{fl/fl}$*Cx3cr1*$^{Cre/+}$ mice (p-value = 0.0031, **) and *Maf* to be statistical significant between both female and male *Maf*$^{fl/fl}$*Cx3cr1*$^{+/+}$ and *Maf*$^{fl/fl}$*Cx3cr1*$^{Cre/+}$ mice (p-value = <0.0001, **** in both) (Figure 5.3.27A).

Whilst relative quantification of fold change gene expression indicates Targets (p-value = 0.0008, ***) and Genotype x Targets (p-value = 0.0010, **) being statistically significant when analysed by three-way ANOVA (Figure 5.3.27B). Tukey's multiple comparisons test demonstrated no statistical significance in any of the targets (Figure 5.3.27B).

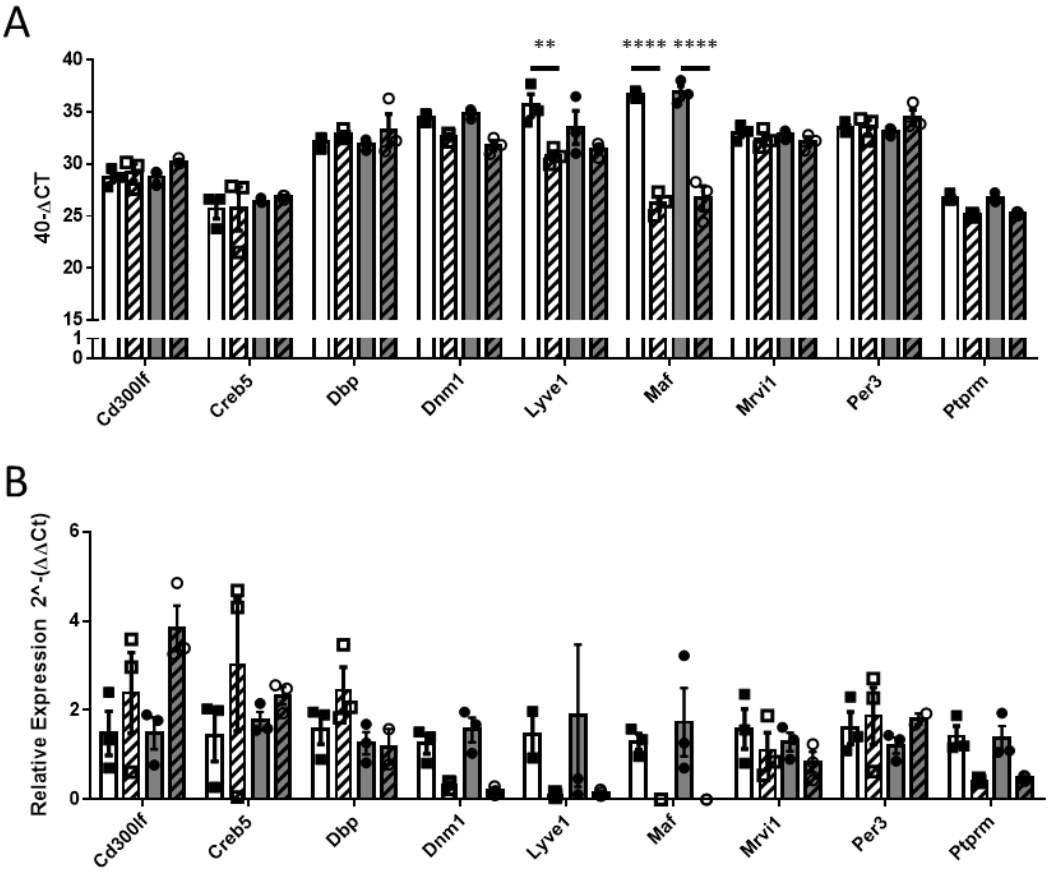

Figure 5.3.27 qPCR Validation of diffferential gene discoveries in naive peritoneal tissue resident macrphages.

A) 40-ΔCT values and B) relative quantification of fold change gene expression in *Maf$^{fl/fl}$Cx3cr1$^{+/+}$* mice (male (white), female (grey)) and *Maf$^{fl/fl}$Cx3cr1$^{Cre/+}$* (shaded) mice peritoneal tissue resident macrophages. Error bars indicate ± SEM (n=3). Mice were aged 6-8 weeks. All data was analysed using 3-way ANOVA with Tukey's multiple comparison test displayed on graphs (p-value = <0.01, ** and p-value = <0.0001, **).**

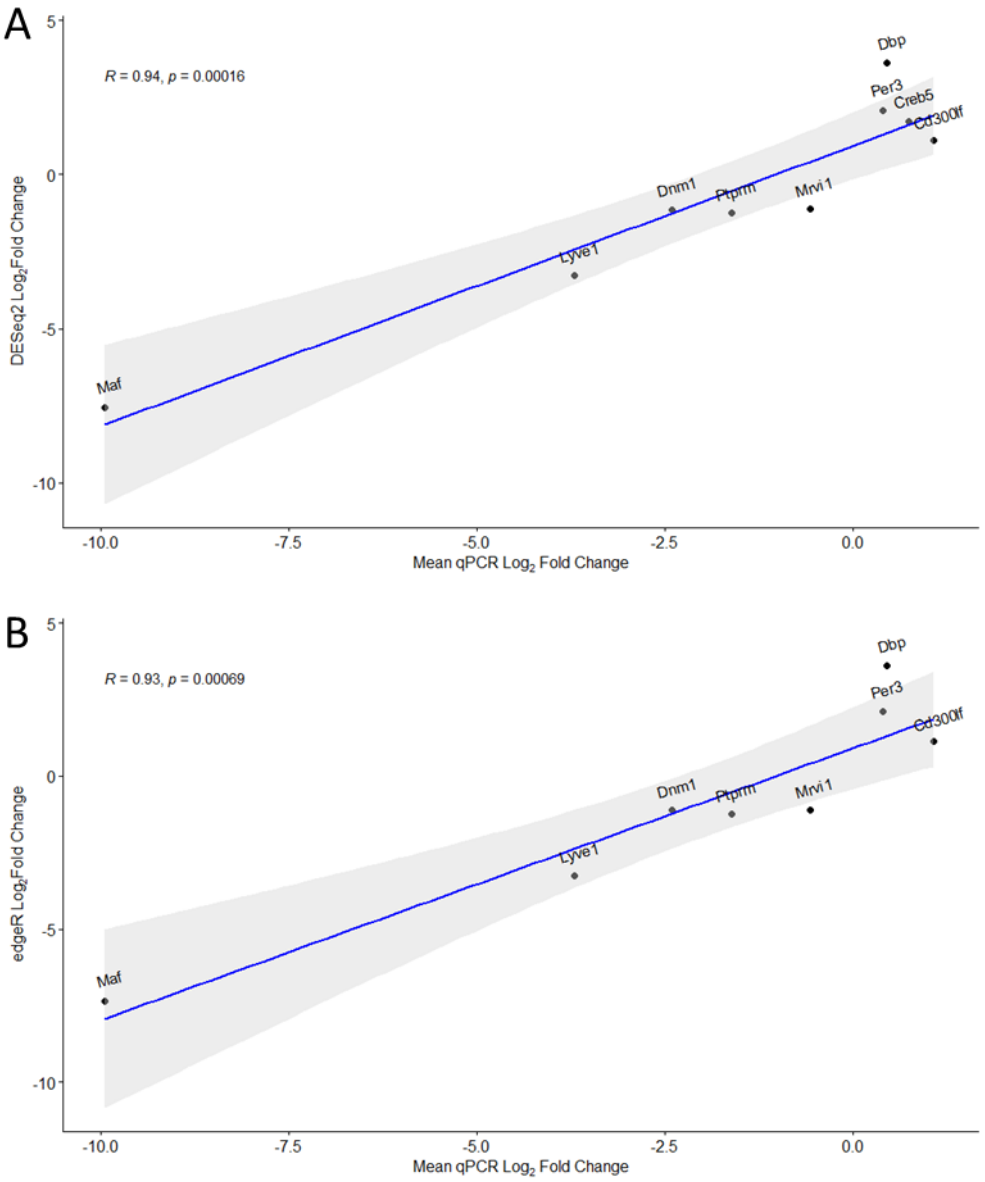

Figure 5.3.28 Pearson Correlation of Naïve Peritoneal Tissue Resident Macrophage RNA Sequencing log_2 fold change and qPCR log_2 fold change.

A) Correlation of DESeq2 analysis of *Maf*$^{fl/fl}$*Cx3cr1*$^{+/+}$ and *Maf*$^{fl/fl}$*Cx3cr1*$^{Cre/+}$ log_2 fold change against qPCR log_2 fold change based on relative quantification (2^(ΔΔCt) in Naïve Peritoneal Tissue Resident Macrophage. B) Correlation of edgeR analysis of *Maf*$^{fl/fl}$*Cx3cr1*$^{+/+}$and *Maf*$^{fl/fl}$*Cx3cr1*$^{Cre/+}$ log_2 fold change against qPCR log_2 fold change based on relative quantification (2^(ΔΔCt) in Naïve Peritoneal Tissue Resident Macrophage. Pearson correlation coefficient (R value and blue line) with coefficient interval (grey area) and p-value (p) are displayed on the graphs.

Correlation between the relative quantification of fold change against DESeq2 analysis (Figure 5.3.28A) and edgeR analysis (Figure 5.3.28B) log_2 fold change of *Maf*$^{fl/fl}$*Cx3cr1*$^{+/+}$and *Maf*$^{fl/fl}$*Cx3cr1*$^{Cre/+}$ naïve peritoneal tissue resident macrophages was investigated for further validation. DESeq2 analysis had a strong positive correlation coefficient of 0.9409275 (Figure 5.3.28A), and edgeR analysis had a strong positive correlation coefficient of 0.9336324 (Figure 5.3.28B), both of which were statistically significant (p-value = 0.00016 ***, and p-value = 0.00069 *** respectively).

5.3.5.2. Validation of Gene Discoveries by Flow Cytometry

To validate if the gene discoveries from RNA sequencing resulted in protein expression alterations, naïve peritoneal tissue resident macrophages from *Maf*$^{fl/fl}$*Cx3cr1*$^{+/+}$ and *Maf*$^{fl/fl}$*Cx3cr1*$^{Cre/+}$ mice were stained as in Figure 5.3.4A for flow cytometry analysis.

Of the tissue resident macrophage targets listed in Table 5.3.3 only previously published flow cytometry antibodies were available at the time for MAIR-V (the protein coded by *Cd300lf*), LYVE1 and MAF. Additionally recent publications have suggested a relationship between MAF and folate receptor 2 (FOLR2) expression (172,236), and therefore this was also investigated.

Tissue resident macrophages displayed no obvious difference in MAIR-V expression between *Maf*$^{fl/fl}$*Cx3cr1*$^{+/+}$ and *Maf*$^{fl/fl}$*Cx3cr1*$^{Cre/+}$ mice. Whereas both LYVE-1 and FOLR2 demonstrated a clear phenotypic reduction in expression in *Maf*$^{fl/fl}$*Cx3cr1*$^{Cre/+}$ mice when compared to *Maf*$^{fl/fl}$*Cx3cr1*$^{+/+}$ mice (Figure 5.3.29A).

When using a bisector gate on LYVE1 histogram of peritoneal tissue resident macrophages (Figure 5.3.29A), LYVE1^{high} population had a mean percentage of 13.82 % ± 3.74 (Mean ±SEM) in *Maf*$^{fl/fl}$*Cx3cr1*$^{+/+}$ and 0.44 % ±0.09 (Mean ± SEM) in *Maf*$^{fl/fl}$*Cx3cr1*$^{Cre/+}$ mice, and was statistically significance different when analysed with two-way ANOVA by genotype (p-value = <0.0001, ***) with Šidák's multiple comparison test (p-value = 0.0055, **) (Figure 5.3.29B).

Likewise FOLR2^{high} tissue resident macrophages had a mean percentage of 15.96 % ±4.26 (Mean ± SEM) and 1.46 % ±0.23 (Mean ±SEM) in *Maf*$^{fl/fl}$*Cx3cr1*$^{+/+}$ and *Maf*$^{fl/fl}$*Cx3cr1*$^{Cre/+}$ mice respectively. Šidák's multiple comparison test indicated statistical significance (p-value = 0.0028, **) between genotypes (Figure 5.3.29B). Whilst MAF was consistent, with reduction in protein expression between *Maf*$^{fl/fl}$*Cx3cr1*$^{Cre/+}$ and *Maf*$^{fl/fl}$*Cx3cr1*$^{+/+}$ mice (Figure 5.3.29A).

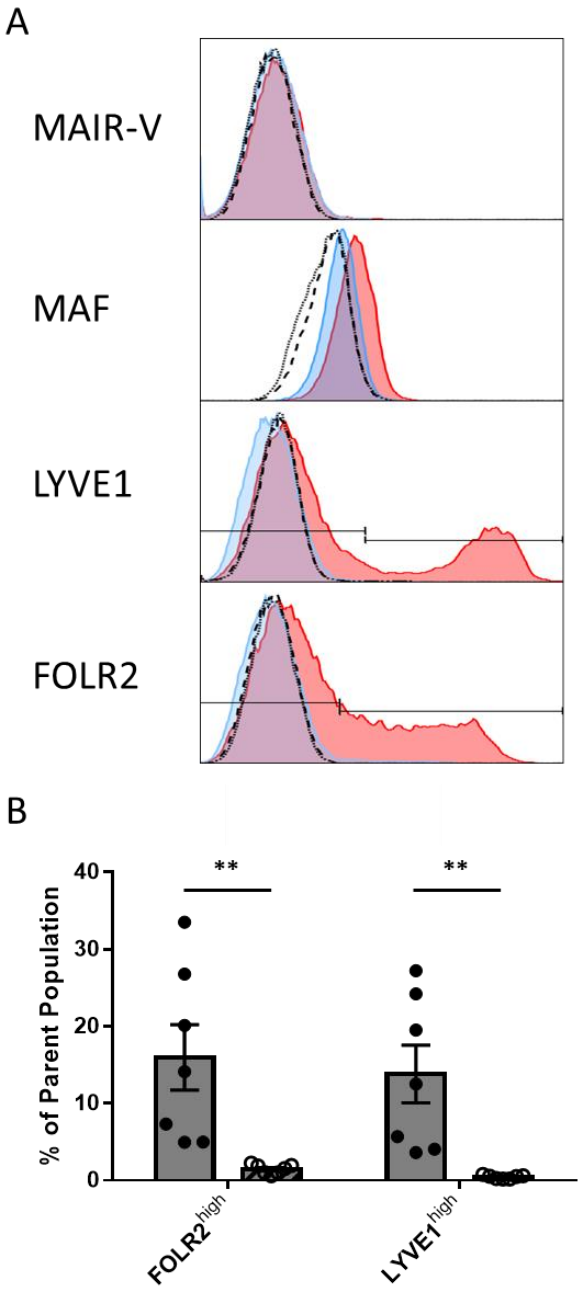

Figure 5.3.29 Flow cytometry validation of diffferential gene discoveries in naive peritoneal tissue resident macrphages markers identified from RNA Sequencing in *Maf*$^{fl/fl}$*Cx3cr1*$^{Cre/+}$ and *Maf*$^{fl/fl}$*Cx3cr1*$^{+/+}$ mice.

A) Representative flow cytometry histograms of diffferential gene discoveries. *Maf*$^{fl/fl}$*Cx3cr1*$^{+/+}$ (red), *Maf*$^{fl/fl}$*Cx3cr1*$^{Cre/+}$ (blue) and isotype controls (solid and dashed line respectively). Representative of n=7. B) Percentage of target expression as per bisector gates on histograms of *Maf*$^{fl/fl}$*Cx3cr1*$^{+/+}$ mice (grey) and *Maf*$^{fl/fl}$*Cx3cr1*$^{Cre/+}$ (shaded) mice. Data shown represents mean percentage ±SEM (n=7). Two-way ANOVA (Genotype, p-value = <0.0001, **). Šidák's multiple comparison indicated on graph (p-value = <0.005, **) All mice were female and aged 6-8 weeks.**

5.3.6. RNA Sequencing of Zymosan Treated Peritoneal Macrophage

Following 48 hr treatment with $2x10^6$ Zymosan particles delivered through intraperitoneal injection, peritoneal lavage was sorted (FACS Aria III), to obtain tissue resident macrophages ($CD11b^{high}$, $F4/80^{high}$, $Tim\text{-}4^{+}$) and inflammatory macrophages ($CD11b^{high}$ $F4/80^{low}$ $Tim4^{-}$).

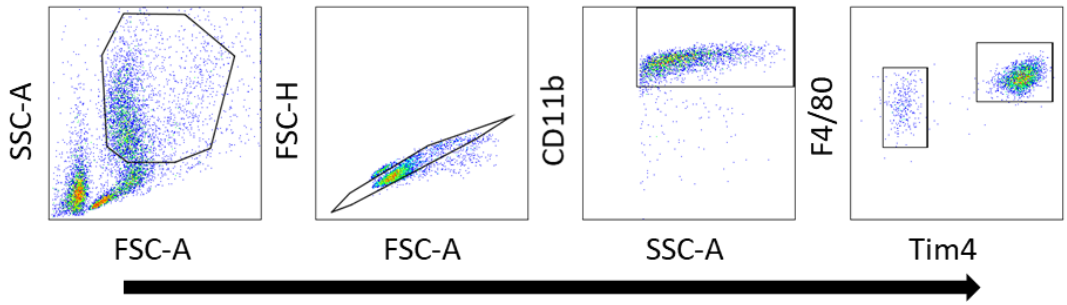

Figure 5.3.30 Determination of peritoneal tissue resident macrophages and inflammatory macrophages in *Maf$^{fl/fl}$Cx3cr1$^{Cre/+}$* and *Maf$^{fl/fl}$Cx3cr1$^{+/+}$* mice treated with Zymosan.

Gating strategy of peritoneal tissue resident macrophages and inflammatory macrophages with staining of CD11b, F4/80 and Tim-4.

5.3.6.1. Principal Component Analysis (PCA)

Exploratory data analysis of variance between samples and how they correlate through principal component analysis (PCA) of peritoneal tissue resident macrophages treated with zymosan particles for 48 hr indicate clear separation of *Maf$^{fl/fl}$Cx3cr1$^{Cre/+}$* and *Maf$^{fl/fl}$Cx3cr1$^{+/+}$* mice (Figure 5.3.31A). Whereas the inflammatory macrophages population from *Maf$^{fl/fl}$Cx3cr1$^{Cre/+}$* and *Maf$^{fl/fl}$Cx3cr1$^{+/+}$* display less variance (Figure 5.3.31B).

When tissue resident and inflammatory macrophages from zymosan treated mice are combined, those from *Maf$^{fl/fl}$Cx3cr1$^{+/+}$* mice display higher variance than those from *Maf$^{fl/fl}$Cx3cr1$^{Cre/+}$* mice (Figure 5.3.31C).

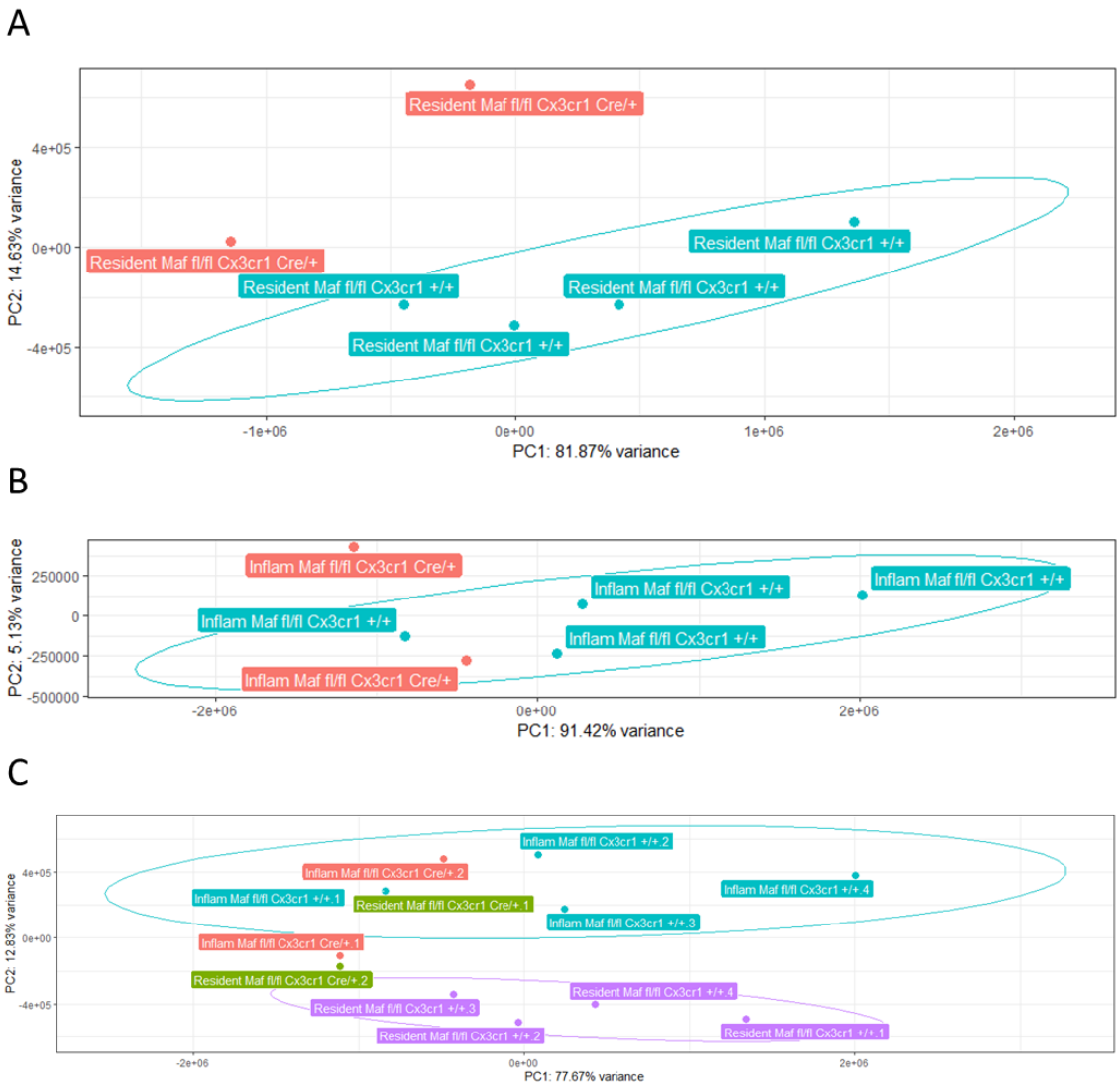

Figure 5.3.31 Principal component analysis (PCA) of RNA-sequencing samples.

A) Peritoneal tissue resident macrophages from *Maf*$^{fl/fl}$*Cx3cr1*$^{+/+}$ mice (Teal) and *Maf*$^{fl/fl}$*Cx3cr1*$^{Cre/+}$ (Red) mice treated with zymosan, with confidence ellipses by genotype where possible due to sample number. B) Peritoneal inflammatory macrophages from *Maf*$^{fl/fl}$*Cx3cr1*$^{+/+}$ mice (Teal) and *Maf*$^{fl/fl}$*Cx3cr1*$^{Cre/+}$ (Red) mice treated with zymosan, with confidence ellipses by genotype where possible due to sample number. C) Peritoneal tissue resident (*Maf*$^{fl/fl}$*Cx3cr1*$^{+/+}$ mice (Purple) and *Maf*$^{fl/fl}$*Cx3cr1*$^{Cre/+}$ (Green) mice) and inflammatory macrophages (*Maf*$^{fl/fl}$*Cx3cr1*$^{+/+}$ mice (Teal) and *Maf*$^{fl/fl}$*Cx3cr1*$^{Cre/+}$ (Red) mice) treated with zymosan, with confidence ellipses by genotype where possible due to sample number.

5.3.6.2. Gene Expression across Multiple Differential Expression Methods of Zymosan Treated Peritoneal Tissue Resident Macrophages

5.3.6.2.1. DESeq2 Differential Gene Expression Analysis

As DESeq2 analysis of *Maf*$^{fl/fl}$*Cx3cr1*$^{Cre/+}$ vs *Maf*$^{fl/fl}$*Cx3cr1*$^{+/+}$ peritoneal tissue resident macrophages following treatment with zymosan generated 5 differential gene discoveries with an adjusted p-value <0.05 (Figure 5.3.35A) (the full list of genes can be found in Appendix XII). Imposing a cut off ±1log$_2$ fold change did not result results in any change in differential gene discoveries (Figure 5.3.35B).

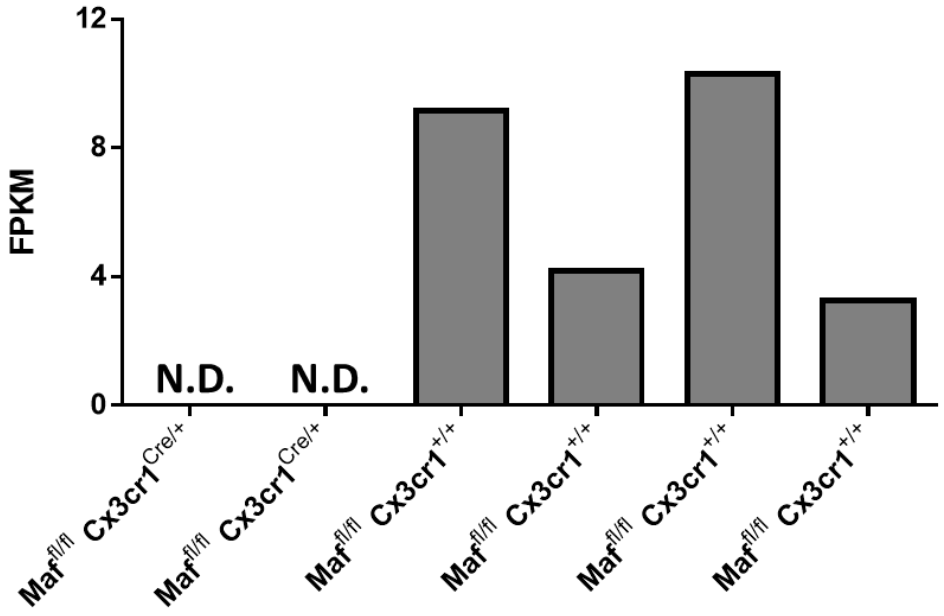

Figure 5.3.32 Fragments per kilobase of transcript per million (FPKM) mapped reads of *Maf* using DESeq2 differential gene expression analysis of zymosan treated tissue resident macrophages.

Female *Maf*$^{fl/fl}$*Cx3cr1*$^{+/+}$ mice (grey) and Female *Maf*$^{fl/fl}$*Cx3cr1*$^{Cre/+}$ (shaded) mice.

Maf expression determined by fragments per kilobase of transcript per million (FPKM) mapped reads indicated *Maf* to be undetectable in *Maf*$^{fl/fl}$*Cx3cr1*$^{Cre/+}$ mice and variable in *Maf*$^{fl/fl}$*Cx3cr1*$^{+/+}$ ranging from 3.24 to 10.28 FPKM (Figure 5.3.32). *Maf* was the most significantly changed gene between *Maf*$^{fl/fl}$*Cx3cr1*$^{Cre/+}$ and *Maf*$^{fl/fl}$*Cx3cr1*$^{+/+}$ zymosan treated peritoneal tissue resident macrophages, with a -12.80 log$_2$ fold change and an adjusted p-value 1.71E-11 (Figure 5.3.33A). Due to *Maf* being so markedly changed, the other gene changes are difficult to visualise graphically, therefore by removing *Maf* from the visualisation the other gene discoveries become clearer (Figure 5.3.33B).

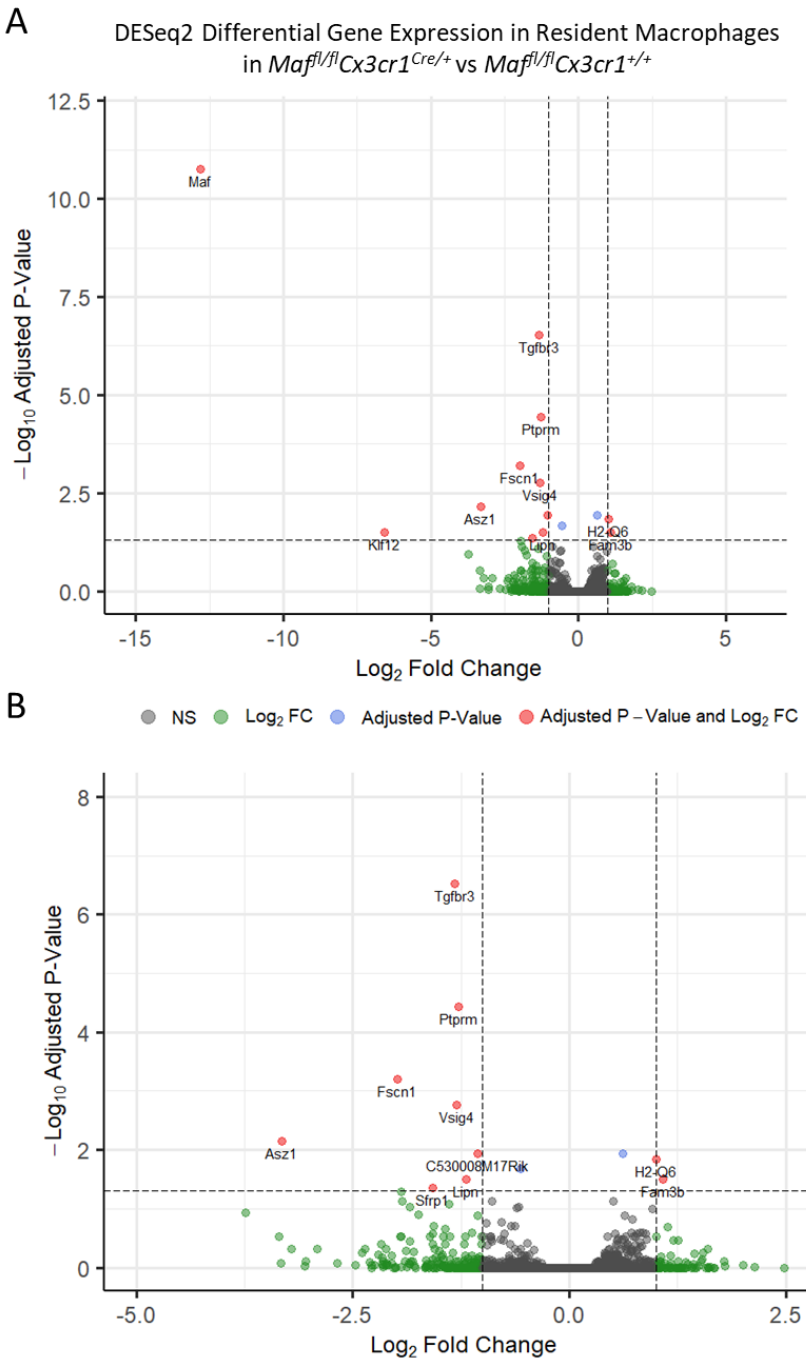

Figure 5.3.33 DESeq2 comparison of *Maf*$^{fl/fl}$*Cx3cr1*$^{Cre/+}$ vs *Maf*$^{fl/fl}$*Cx3cr1*$^{+/+}$ zymosan treated peritoneal tissue resident macrophages

RNA-Seq of zymosan treated *Maf*$^{fl/fl}$*Cx3cr1*$^{Cre/+}$ and *Maf*$^{fl/fl}$*Cx3cr1*$^{+/+}$ peritoneal tissue resident macrophages. A) Volcano plot of all gene discoveries using DESeq2 differential expression method. B) Volcano plot with *Maf* removed from the data set to improve visualisation of other significant genes. *Maf*$^{fl/fl}$*Cx3cr1*$^{Cre/+}$ (n=2) and *Maf*$^{fl/fl}$*Cx3cr1*$^{+/+}$ (n=4), with dashed lines representing cut off for adjusted p-value = 0.05 and ±log$_2$ fold change = 1.

5.3.6.2.2. edgeR Differential Gene Expression Analysis

edgeR comparison of *Maf*$^{fl/fl}$*Cx3cr1*$^{Cre/+}$ vs *Maf*$^{fl/fl}$*Cx3cr1*$^{+/+}$ peritoneal tissue resident macrophages generated 14 differential gene discoveries with an adjusted p-value <0.05 (Figure 5.3.35A) (the full list of genes can be found in Appendix XIII). Imposing a cut off ±1$\log_2$ fold change results in a reduction to 12 differential gene discoveries (Figure 5.3.35B).

Maf was the most significantly changed gene between *Maf*$^{fl/fl}$*Cx3cr1*$^{Cre/+}$ and *Maf*$^{fl/fl}$*Cx3cr1*$^{+/+}$ zymosan treated peritoneal tissue resident macrophages, with a -5.55 $\log_2$ fold change and an adjusted p-value 1.81E-33 (Figure 5.3.34A). Again, due to *Maf* being so significantly changed the other genes are difficult to visualise, and the removal of *Maf* from the visualisation allows other gene discoveries to become clearer (Figure 5.3.34B).

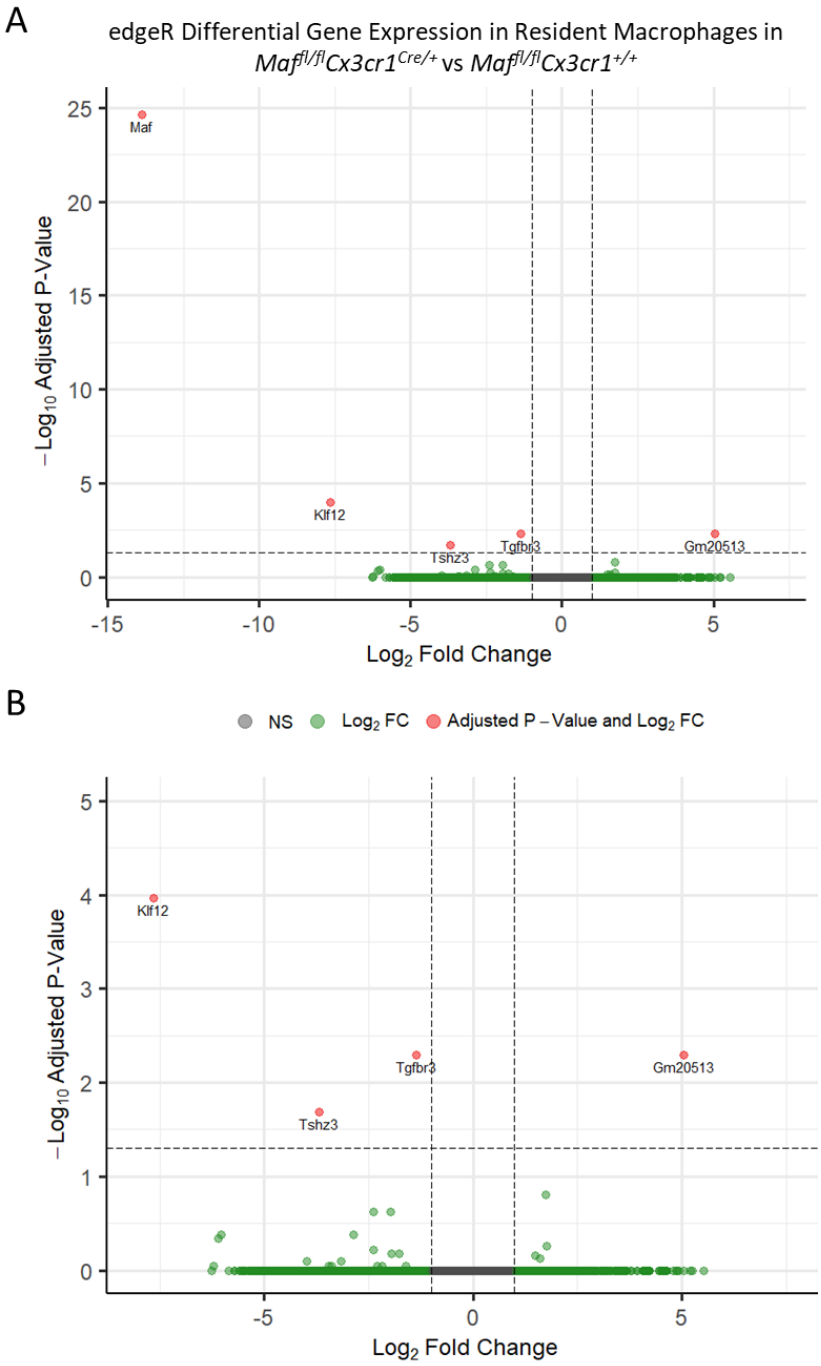

Figure 5.3.34 edgeR comparison of *Maf*$^{fl/fl}$*Cx3cr1*$^{Cre/+}$ vs *Maf*$^{fl/fl}$*Cx3cr1*$^{+/+}$ zymosan treated peritoneal tissue resident macrophages

RNA-Seq of zymosan treated *Maf*$^{fl/fl}$*Cx3cr1*$^{Cre/+}$ and *Maf*$^{fl/fl}$*Cx3cr1*$^{+/+}$ peritoneal tissue resident macrophages. A) Volcano plot of all gene discoveries using edgeR differential expression method. B) Volcano plot with *Maf* removed from the data set to improve visualisation of other significant genes. *Maf*$^{fl/fl}$*Cx3cr1*$^{Cre/+}$ (n=2) and *Maf*$^{fl/fl}$*Cx3cr1*$^{+/+}$ (n=4), with dashed lines representing cut off for adjusted p-value = 0.05 and ±log$_2$ fold change = 1.

Gene discoveries from peritoneal tissue resident macrophages after 48 hr zymosan treatment in *Maf*$^{fl/fl}$*Cx3cr1*$^{Cre/+}$ vs *Maf*$^{fl/fl}$*Cx3cr1*$^{+/+}$ mice resulted in 3 common genes which have an adjusted p-value of <0.05, with DESeq2 generating 11 and edgeR 2 unique differentially expressed genes (Figure 5.3.35A). Of those gene discoveries with an adjusted p-value of <0.05 and a ±1log$_2$ fold change common genes remained unchanged between the two differential expression methods (Figure 5.3.35B).

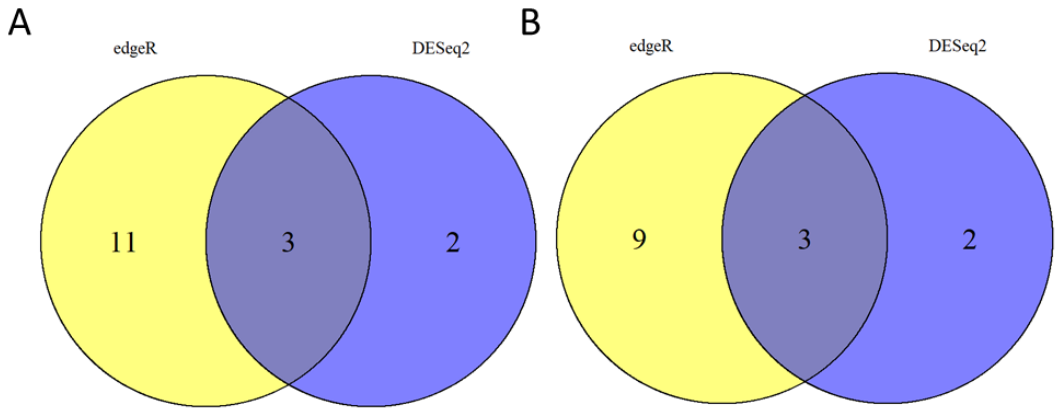

Figure 5.3.35 Venn diagram comparing between DESeq2 and edgeR differential expression methods in zymosan treated tissue resident macrophages

A) Venn Diagram comparing gene discoveries which are statistically significant (adjusted p-value <0.05) between DESeq2 and edgeR differential expression methods. B) Venn diagram comparing gene discoveries which are statistically significant (adjusted p-value <0.05) and have a ±1log$_2$ fold change between DESeq2 and edgeR differential expression methods.

5.3.6.2.3. Interaction Analysis of Naïve Vs Zymosan Treated Peritoneal Tissue Resident Macrophages

Utilising the previous RNA sequencing of female naïve tissue resident macrophages from *Maf*$^{fl/fl}$*Cx3cr1*$^{+/+}$ and *Maf*$^{fl/fl}$*Cx3cr1*$^{Cre/+}$ mice in section 5.3.4.1.3, allowed for comparison of naïve vs zymosan treated tissue resident macrophages in both genotypes through an interaction term contrast.

DESeq2 analysis highlighted only *Maf* to be differentially expressed between *Maf*$^{fl/fl}$*Cx3cr1*$^{+/+}$ and *Maf*$^{fl/fl}$*Cx3cr1*$^{Cre/+}$ in naïve and zymosan treatment, with a -8.81 $\log_2$ fold change and an adjusted p-value 7.20E-05 (Figure 5.3.36A). edgeR analysis highlighted *Maf* and *Tgfbr3* with -12.81 $\log_2$ fold change and an adjusted p-value 4.48E-11, and -1.33 $\log_2$ fold change and an adjusted p-value 3.14E-4 respectively (Figure 5.3.36B).

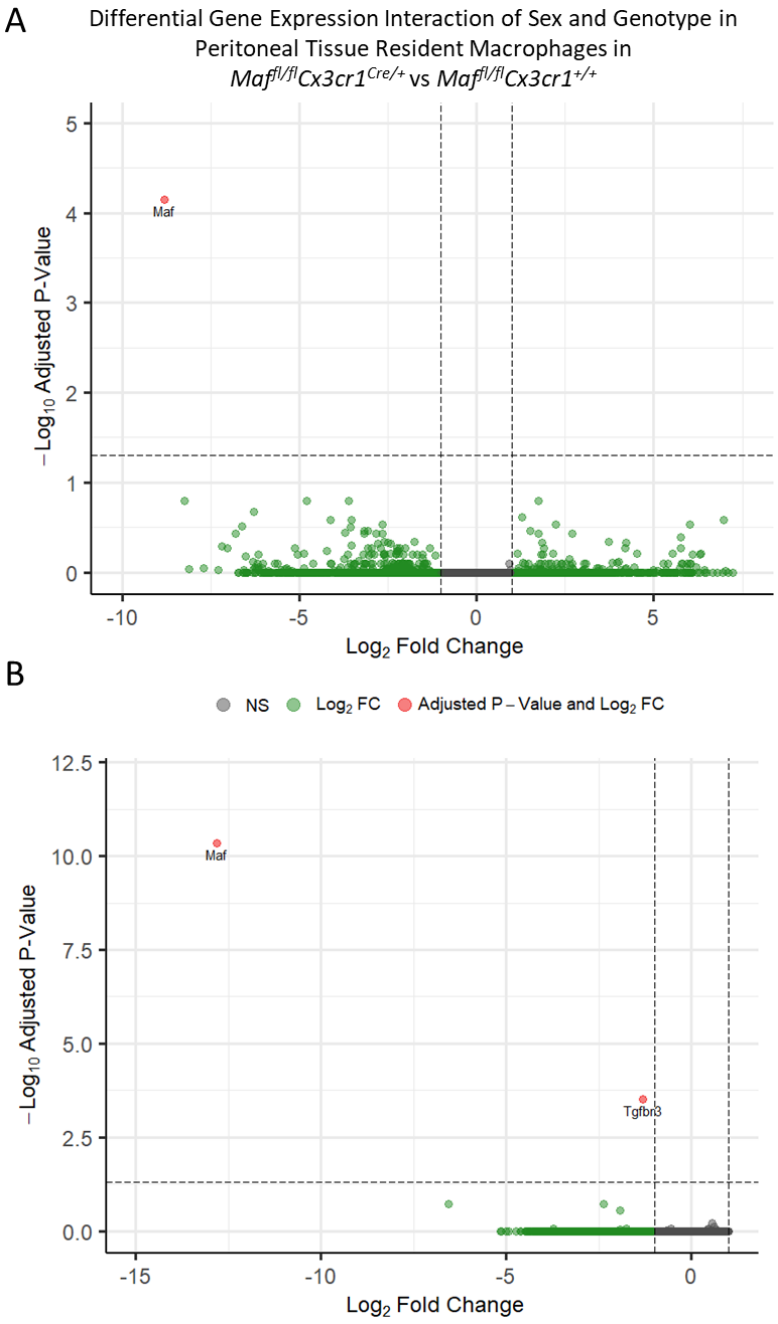

Figure 5.3.36 Interaction term comparison of *Maf*$^{fl/fl}$*Cx3cr1*$^{Cre/+}$ vs *Maf*$^{fl/fl}$*Cx3cr1*$^{+/+}$ in naïve and zymosan treated peritoneal tissue resident macrophages

RNA-Seq of naïve and zymosan treated *Maf*$^{fl/fl}$*Cx3cr1*$^{Cre/+}$ and *Maf*$^{fl/fl}$*Cx3cr1*$^{+/+}$ peritoneal tissue resident macrophages. A) Volcano plot of all gene discoveries using edgeR differential expression method, and B) using DESeq2 differential expression method. Naïve tissue resident macrophage *Maf*$^{fl/fl}$*Cx3cr1*$^{Cre/+}$ (n=2) and *Maf*$^{fl/fl}$*Cx3cr1*$^{+/+}$ (n=2), and zymosan treated tissue resident macrophage *Maf*$^{fl/fl}$*Cx3cr1*$^{Cre/+}$ (n=2) and *Maf*$^{fl/fl}$*Cx3cr1*$^{+/+}$ (n=4) from female mice. Dashed lines representing cut off for adjusted p-value = 0.05 and ±log$_2$ fold change = 1.

5.3.6.2.4. Differential Exon Usage

To determine splice variants within the RNA sequencing datasets, relative usage of exons between *Maf*$^{fl/fl}$*Cx3cr1*$^{Cre/+}$ and *Maf*$^{fl/fl}$*Cx3cr1*$^{+/+}$ zymosan treated peritoneal tissue resident macrophages generated 6 differential exons with an adjusted p-value <0.05 and a cut off ±1log$_2$ (Figure 5.3.37).

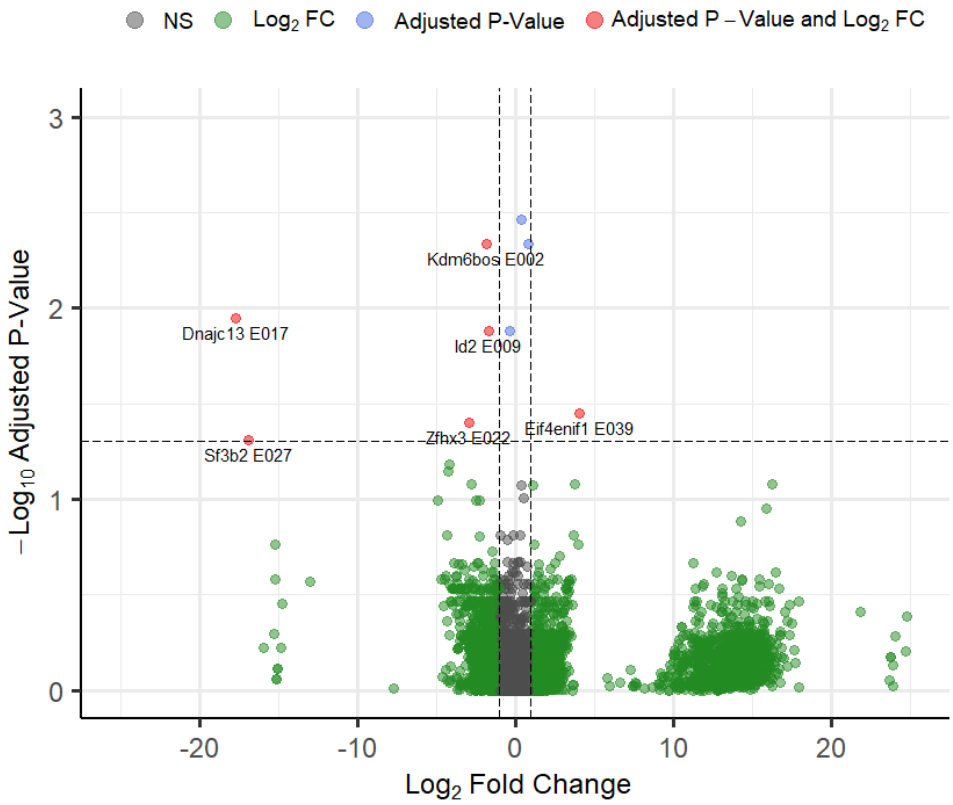

Figure 5.3.37 DEXSeq differential exon usage analysis of zymosan treated peritoneal tissue resident macrophages in *Maf*$^{fl/fl}$*Cx3cr1*$^{Cre/+}$ vs *Maf*$^{fl/fl}$*Cx3cr1*$^{+/+}$ mice

Volcano plot of DEXSeq differential exon usage analysis between *Maf*$^{fl/fl}$*Cx3cr1*$^{Cre/+}$ (n=2) vs *Maf*$^{fl/fl}$*Cx3cr1*$^{+/+}$ (n=4) mice, with dashed lines representing cut off for adjusted p-value = 0.05 and ±log$_2$ fold change = 1.

Genes with an adjusted p-value <0.05 and a cut off ±1log_2 are summarised in Table 5.3.4. Highlighted exons with p-value of <0.05 and transcripts of each gene (Figure 5.3.38-Figure 5.3.43) suggest an increase of differential transcript Zfhx3-201 in Zinc finger homeobox 3 (*Zfhx3*) (ENSMUSG00000038872) (Figure 5.3.38) and an increase of transcript Id2-202 in Inhibitor of DNA binding 2 (*Id2*) (ENSMUSG00000020644) (Figure 5.3.41) in *Maf*$^{fl/fl}$*Cx3cr1*$^{Cre/+}$ compared to *Maf*$^{fl/fl}$*Cx3cr1*$^{+/+}$.

Gene	Exon	Log_2 Fold Change	Adjusted P-Value
Zfhx3	22	2.90	0.040
Dnajc13	17	17.71	0.011
Sf3b2	27	16.90	0.049
Id2	9	1.687	0.013
Kdm6bos	2	1.824	0.005
Eif4enif1	39	-4.080	0.036

Table 5.3.4 Summary of genes with relative exon usage in zymosan treated peritoneal tissue resident macrophages *Maf*$^{fl/fl}$*Cx3cr1*$^{Cre/+}$ vs *Maf*$^{fl/fl}$*Cx3cr1*$^{+/+}$ mice with adjusted p-value of <0.05 and ±1 log_2 fold change.

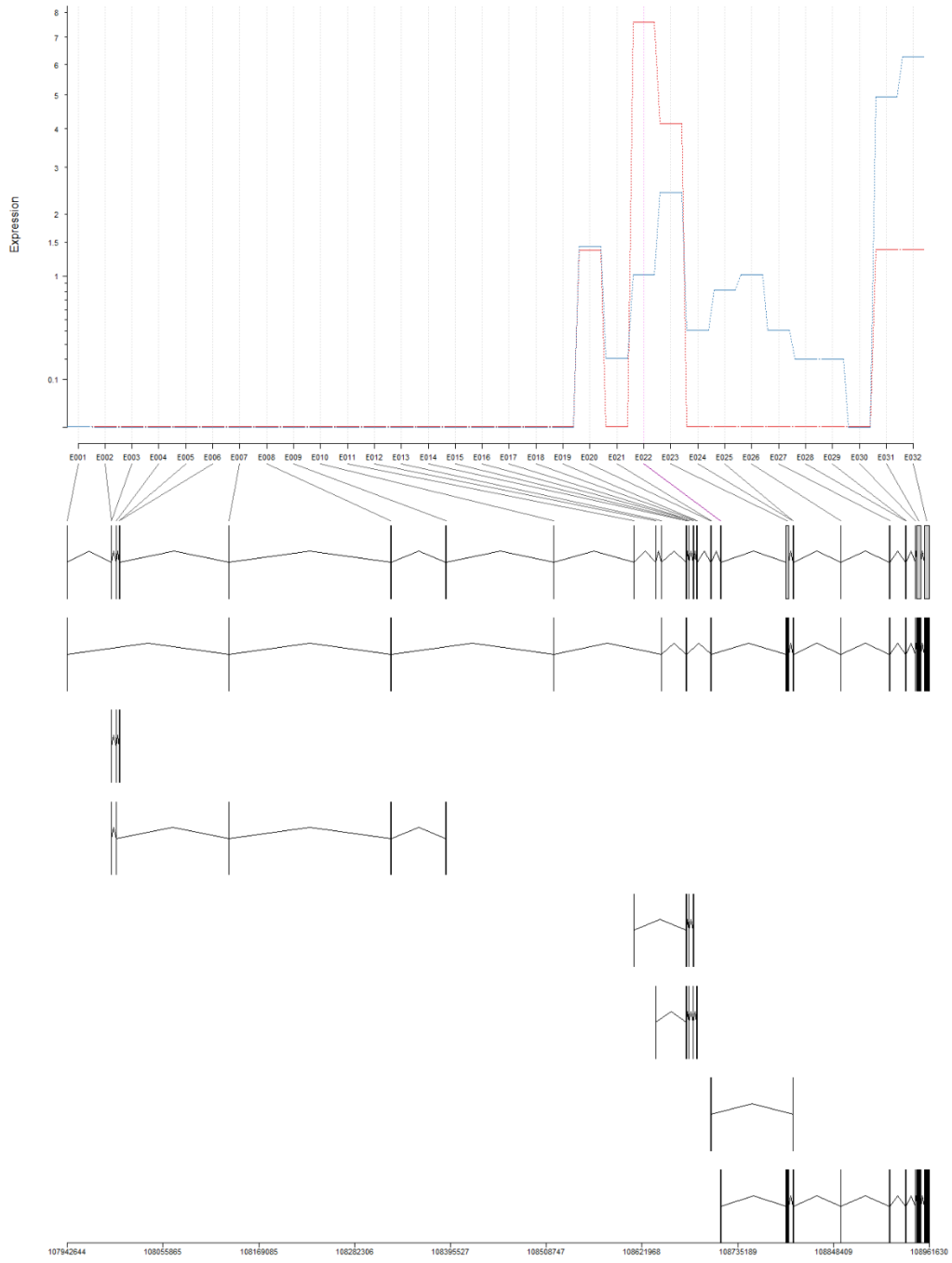

Figure 5.3.38 DEXSeq differential exon usage analysis of *Zfhx3* in zymosan treated peritoneal tissue resident macrophages in *Maf*$^{fl/fl}$*Cx3cr1*$^{Cre/+}$ vs *Maf*$^{fl/fl}$*Cx3cr1*$^{+/+}$ mice

DEXSeq plot of expression of exons in the *Zfhx3* gene in *Maf*$^{fl/fl}$*Cx3cr1*$^{Cre/+}$ (Blue line) (n=2) and *Maf*$^{fl/fl}$*Cx3cr1*$^{+/+}$ (Red line) (n=4). Differential exons highlighted in pink (p-value <0.05) and transcripts of *Zfhx3* gene in black below.

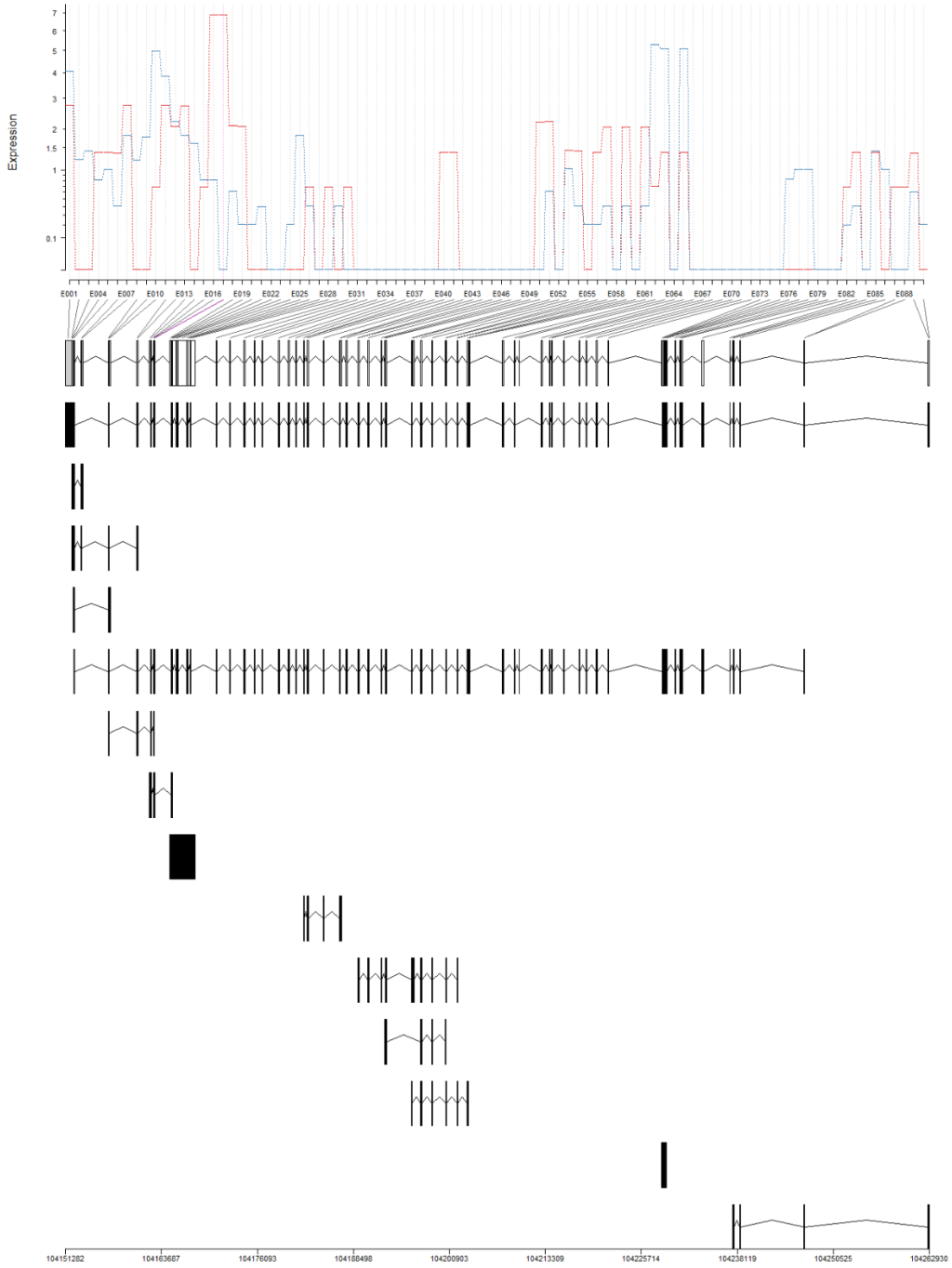

Figure 5.3.39 DEXSeq differential exon usage analysis of *Dnajc13* in zymosan treated peritoneal tissue resident macrophages in *Maf*$^{fl/fl}$*Cx3cr1*$^{Cre/+}$ vs *Maf*$^{fl/fl}$*Cx3cr1*$^{+/+}$ mice

DEXSeq plot of expression of exons in the *Dnajc13* gene in *Maf*$^{fl/fl}$*Cx3cr1*$^{Cre/+}$ (Blue line) (n=2) and *Maf*$^{fl/fl}$*Cx3cr1*$^{+/+}$ (Red line) (n=4). Differential exons highlighted in pink (p-value <0.05) and transcripts of *Dnajc13* gene in black below.

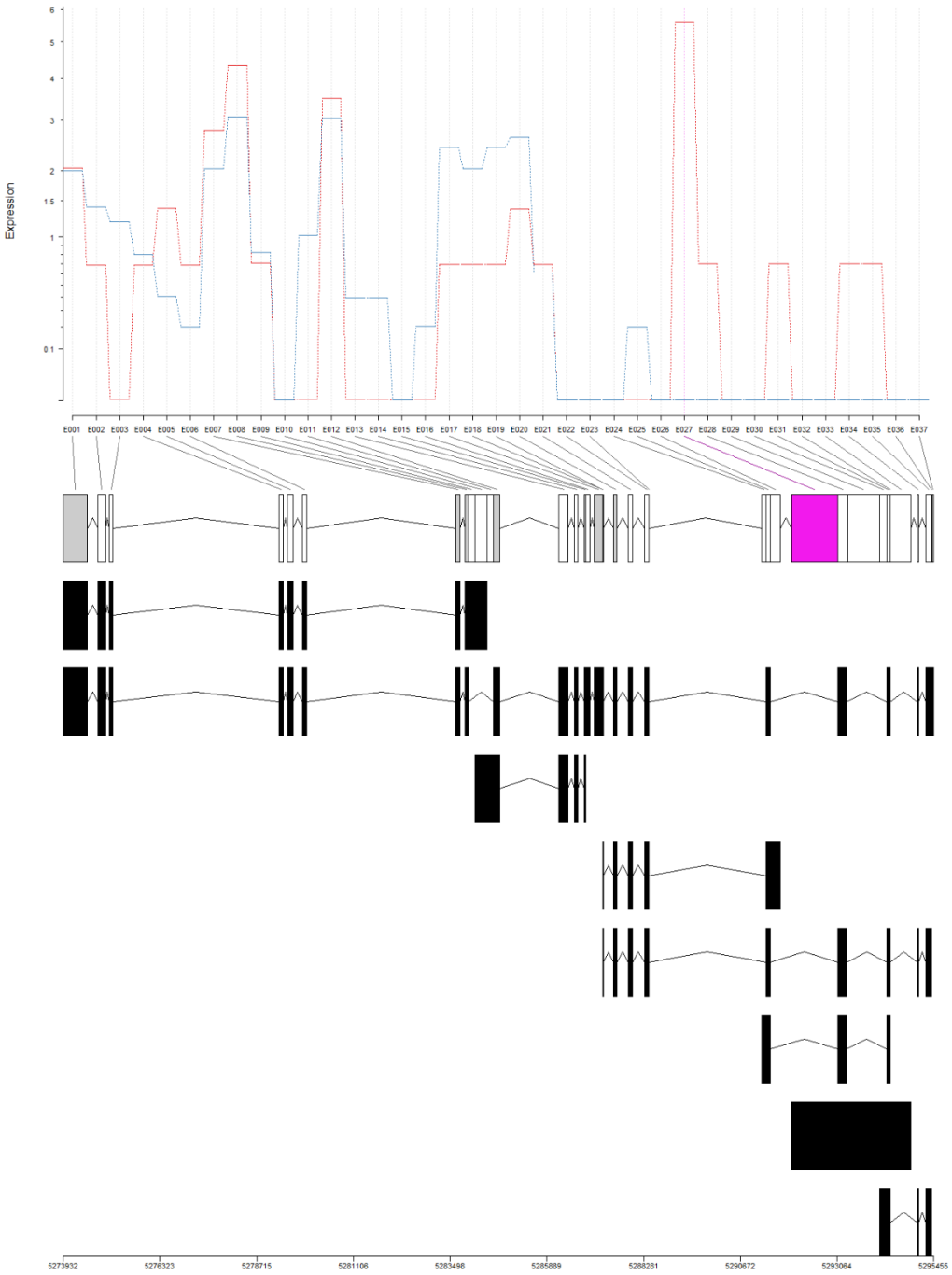

Figure 5.3.40 DEXSeq differential exon usage analysis of *Sf3b2* in zymosan treated peritoneal tissue resident macrophages in *Maf*$^{fl/fl}$*Cx3cr1*$^{Cre/+}$ vs *Maf*$^{fl/fl}$*Cx3cr1*$^{+/+}$ mice

DEXSeq plot of expression of exons in the *Sf3b2* gene in *Maf*$^{fl/fl}$*Cx3cr1*$^{Cre/+}$ (Blue line) (n=2) and *Maf*$^{fl/fl}$*Cx3cr1*$^{+/+}$ (Red line) (n=4). Differential exons highlighted in pink (p-value <0.05) and transcripts of *Sf3b2* gene in black below.

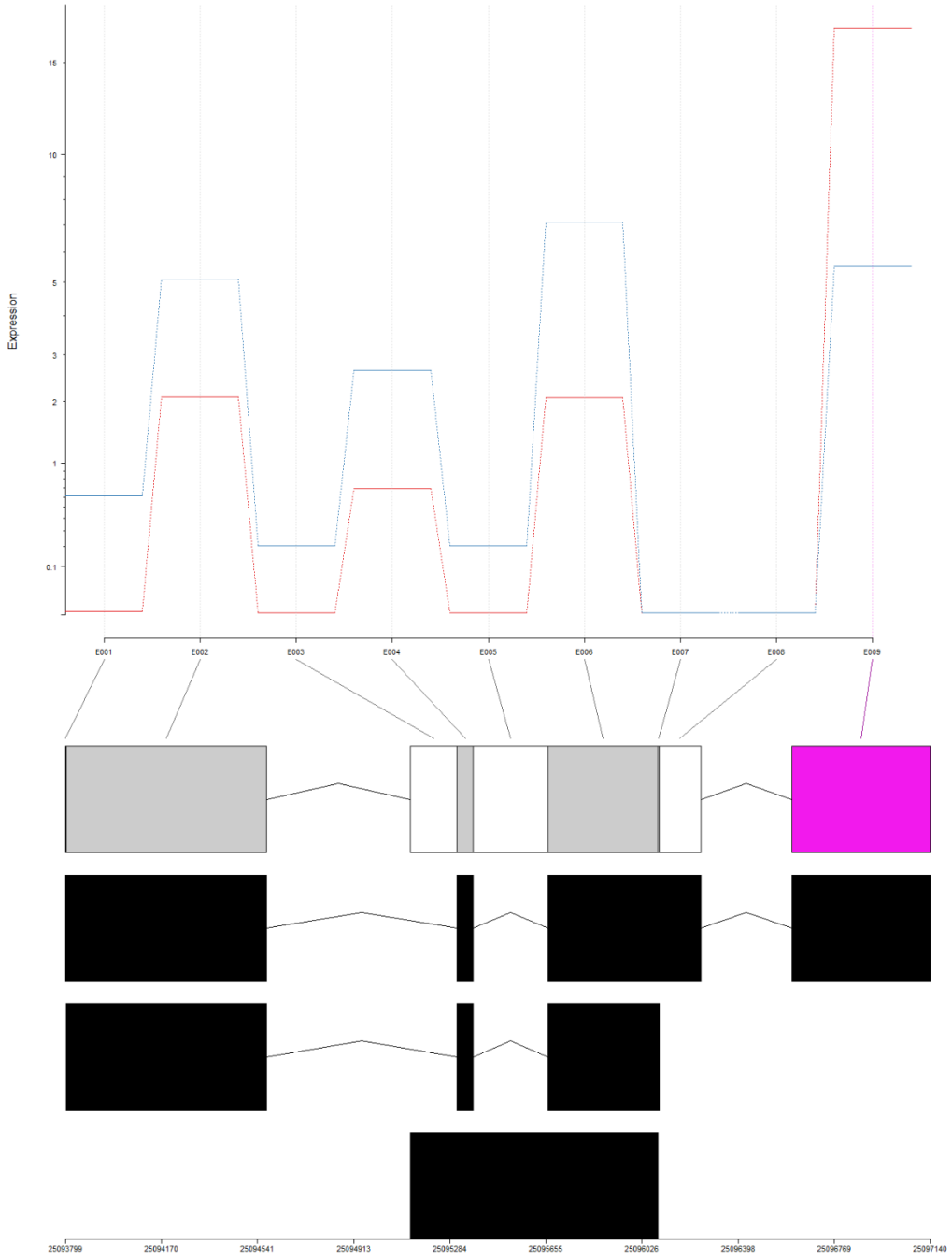

Figure 5.3.41 DEXSeq differential exon usage analysis of *Id2* in zymosan treated peritoneal tissue resident macrophages in *Maf*$^{fl/fl}$*Cx3cr1*$^{Cre/+}$ vs *Maf*$^{fl/fl}$*Cx3cr1*$^{+/+}$ mice

DEXSeq plot of expression of exons in the *Id2* gene in *Maf*$^{fl/fl}$*Cx3cr1*$^{Cre/+}$ (Blue line) (n=2) and *Maf*$^{fl/fl}$*Cx3cr1*$^{+/+}$ (Red line) (n=4). Differential exons highlighted in pink (p-value <0.05) and transcripts of *Id2* gene in black below.

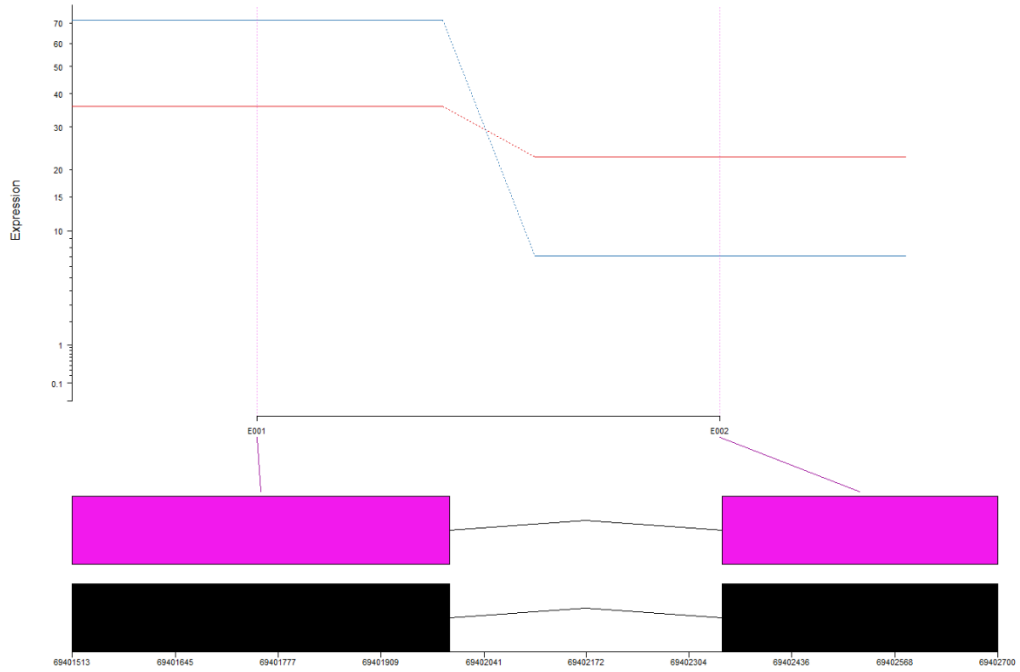

Figure 5.3.42 DEXSeq differential exon usage analysis of *Kdm6bos* in zymosan treated peritoneal tissue resident macrophages in *Maf*$^{fl/fl}$*Cx3cr1*$^{Cre/+}$ vs *Maf*$^{fl/fl}$*Cx3cr1*$^{+/+}$ mice

DEXSeq plot of expression of exons in the *Kdm6bos* gene in *Maf*$^{fl/fl}$*Cx3cr1*$^{Cre/+}$ (Blue line) (n=2) and *Maf*$^{fl/fl}$*Cx3cr1*$^{+/+}$ (Red line) (n=4). Differential exons highlighted in pink (p-value <0.05) and transcripts of *Kdm6bos* gene in black below.

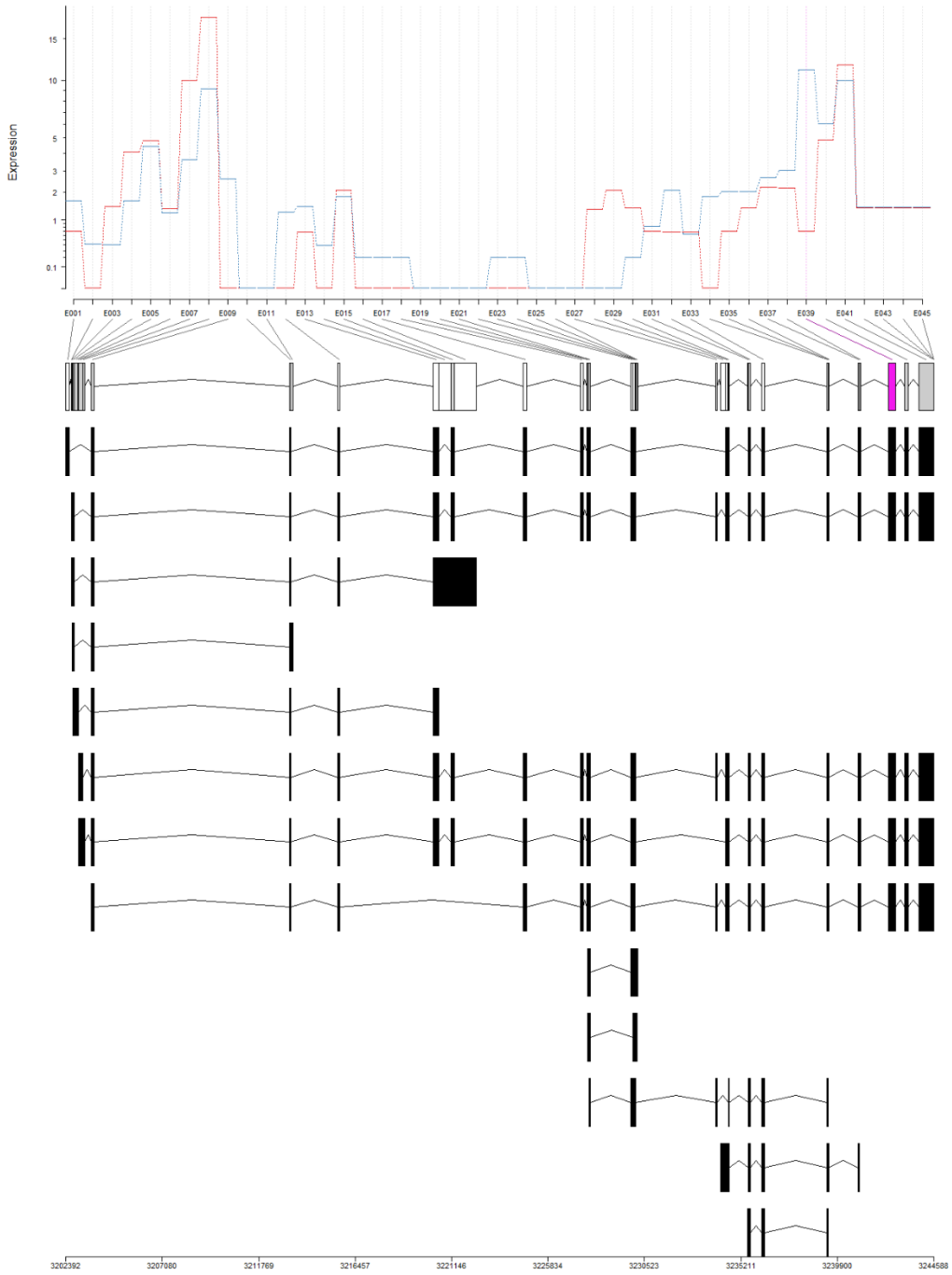

Figure 5.3.43 DEXSeq differential exon usage analysis of *Eif4enif1* in zymosan treated peritoneal tissue resident macrophages in *Maf*$^{fl/fl}$*Cx3cr1*$^{Cre/+}$ vs *Maf*$^{fl/fl}$*Cx3cr1*$^{+/+}$ mice

DEXSeq plot of expression of exons in the *Eif4enif1* gene in *Maf*$^{fl/fl}$*Cx3cr1*$^{Cre/+}$ (Blue line) (n=2) and *Maf*$^{fl/fl}$*Cx3cr1*$^{+/+}$ (Red line) (n=4). Differential exons highlighted in pink (p-value <0.05) and transcripts of *Eif4enif1* gene in black below.

5.3.6.3. Gene Expression across Multiple Differential Expression Methods of Inflammatory Peritoneal Macrophages

5.3.6.3.1. DESeq2 Differential Gene Expression Analysis

Gene discoveries from matched inflammatory macrophages of the same mice in section 5.3.6.2 in *Maf*$^{fl/fl}$*Cx3cr1*$^{Cre/+}$ vs *Maf*$^{fl/fl}$*Cx3cr1*$^{+/+}$ mice resulted 45 differential gene discoveries with DESeq2 that had an adjusted p-value <0.05 (Figure 5.3.46A) (the full list of genes can be found in Appendix XIV). Imposing a cut off ±1$\log_2$ fold change results in 43 differential gene discoveries (Figure 5.3.46B).

Maf was the most significantly changed gene between *Maf*$^{fl/fl}$*Cx3cr1*$^{Cre/+}$ and *Maf*$^{fl/fl}$*Cx3cr1*$^{+/+}$ peritoneal inflammatory macrophages, with a -5.06 $\log_2$ fold change and an adjusted p-value 13.68E-07 (Figure 5.3.44A). Due to *Maf* and *Lyve1* being so markedly changed, the other gene changes are difficult to visualise graphically therefore by removing *Maf* and *Lyve1* from the visualisation the other gene discoveries become clearer (Figure 5.3.44B).

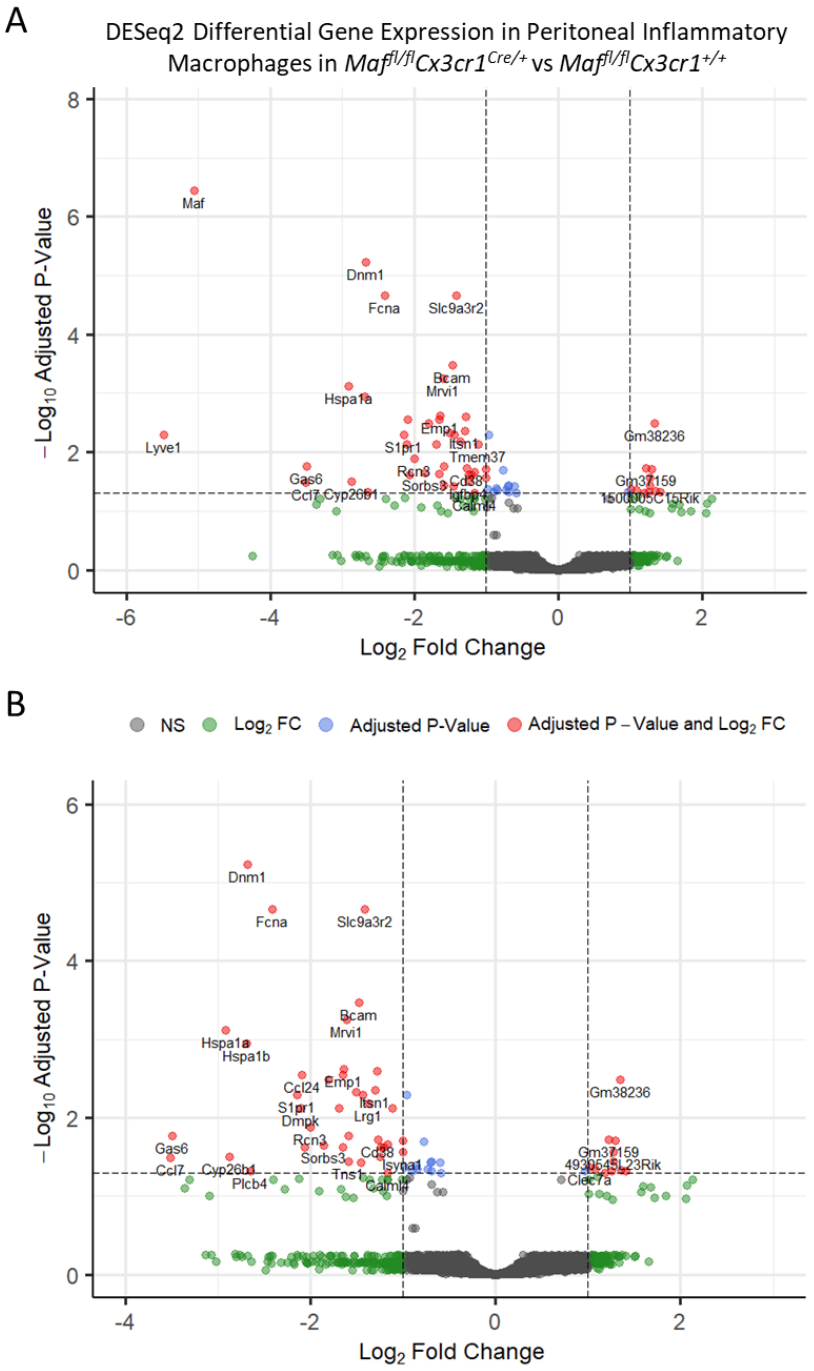

Figure 5.3.44 DESeq2 comparison of *Maf*$^{fl/fl}$*Cx3cr1*$^{Cre/+}$ vs *Maf*$^{fl/fl}$*Cx3cr1*$^{+/+}$ zymosan recruited peritoneal inflammatory macrophages

RNA-Seq of zymosan recuited *Maf*$^{fl/fl}$*Cx3cr1*$^{Cre/+}$ and *Maf*$^{fl/fl}$*Cx3cr1*$^{+/+}$ peritoneal inflammatory macrophages. A) Volcano plot of all gene discoveries using DESeq2 differential expression method. B) Volcano plot with *Maf* and *Lyve1* removed from the data set to improve visualisation of other significant genes. *Maf*$^{fl/fl}$*Cx3cr1*$^{Cre/+}$ (n=2) and *Maf*$^{fl/fl}$*Cx3cr1*$^{+/+}$ (n=4), with dashed lines representing cut off for adjusted p-value = 0.05 and $\log_2$ fold change = 1.

5.3.6.3.2. edgeR Differential Expression

edgeR comparison of *Maf*$^{fl/fl}$*Cx3cr1*$^{Cre/+}$ vs *Maf*$^{fl/fl}$*Cx3cr1*$^{+/+}$ peritoneal inflammatory macrophages generated 66 differential gene discoveries with an adjusted p-value <0.05 (Figure 5.3.46A) (the full list of genes can be found in Appendix XV). Imposing a cut off ±1log_2 fold change results in a reduction to 53 differential gene discoveries (Figure 5.3.46B).

Maf was the identified as the most significantly changed gene between *Maf*$^{fl/fl}$*Cx3cr1*$^{Cre/+}$ and *Maf*$^{fl/fl}$*Cx3cr1*$^{+/+}$ peritoneal inflammatory macrophages, with a -5.07 log_2 fold change and an adjusted p-value 1.08E-09 (Figure 5.3.45A). Again, due to *Maf* being so significantly changed the other genes are difficult to visualise, and the removal of *Maf* from the visualisation allows other gene discoveries to become clearer (Figure 5.3.45B).

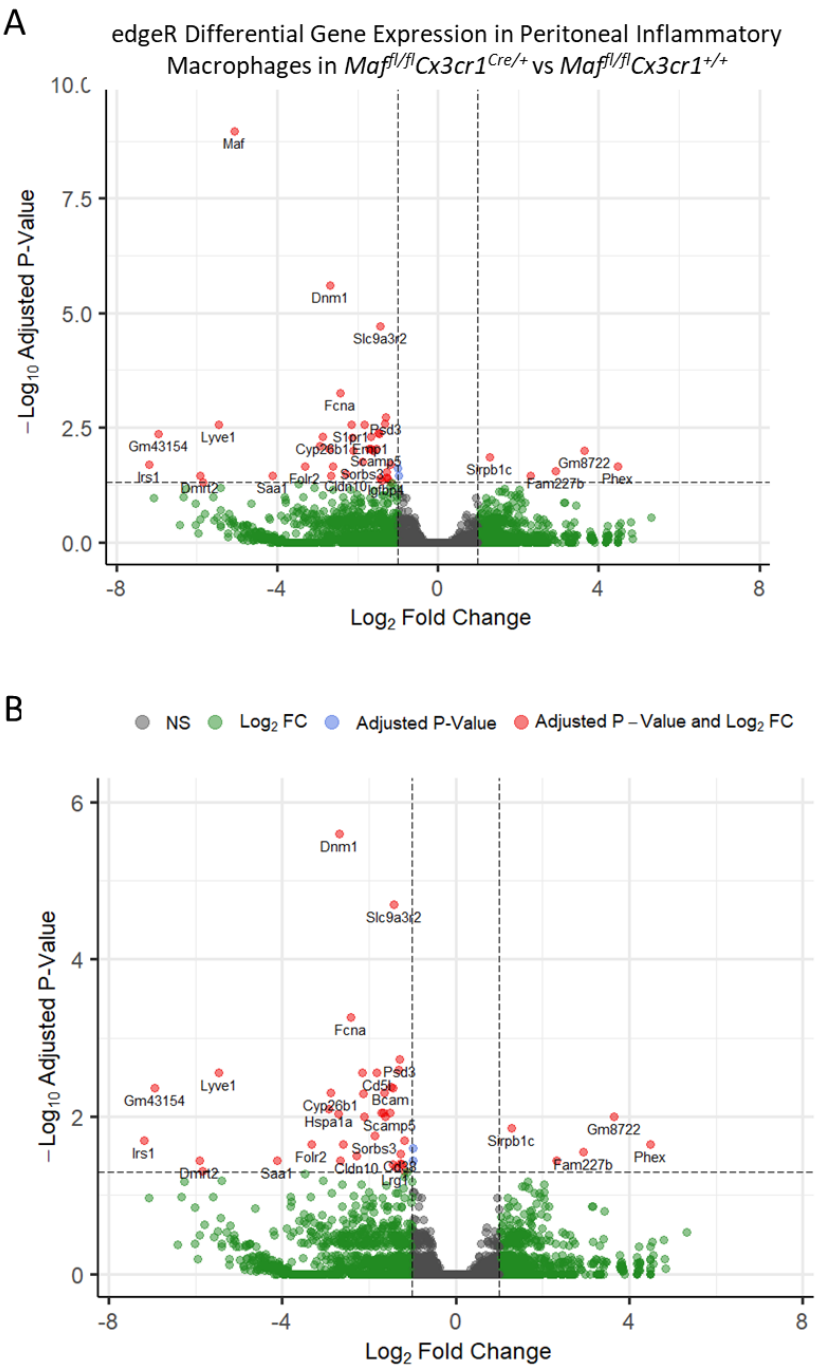

Figure 5.3.45 edgeR comparison of *Maf*$^{fl/fl}$*Cx3cr1*$^{Cre/+}$ vs *Maf*$^{fl/fl}$*Cx3cr1*$^{+/+}$ zymosan recruited peritoneal inflammatory macrophages

RNA-Seq of zymosan recuited *Maf*$^{fl/fl}$*Cx3cr1*$^{Cre/+}$ and *Maf*$^{fl/fl}$*Cx3cr1*$^{+/+}$ peritoneal inflammatory macrophages. A) Volcano plot of all gene discoveries using edgeR differential expression method. B) Volcano plot with *Maf* removed from the data set to improve visualisation of other significant genes. *Maf*$^{fl/fl}$*Cx3cr1*$^{Cre/+}$ (n=2) and *Maf*$^{fl/fl}$*Cx3cr1*$^{+/+}$ (n=4), with dashed lines representing cut off for adjusted p-value = 0.05 and ±log$_2$ fold change = 1.

Gene discoveries from peritoneal inflammatory macrophages after 48 hr zymosan treatment in *Maf*$^{fl/fl}$*Cx3cr1*$^{Cre/+}$ vs *Maf*$^{fl/fl}$*Cx3cr1*$^{+/+}$ mice resulted in 32 common genes which have an adjusted p-value of <0.05, with DESeq2 and edgeR generating 34 and 13 unique differentially expressed genes respectively (Figure 5.3.46A). Of those gene discoveries with an adjusted p-value of <0.05 and a ±1log$_2$ fold change, 30 common genes remain between the two differential expression methods (Figure 5.3.46B).

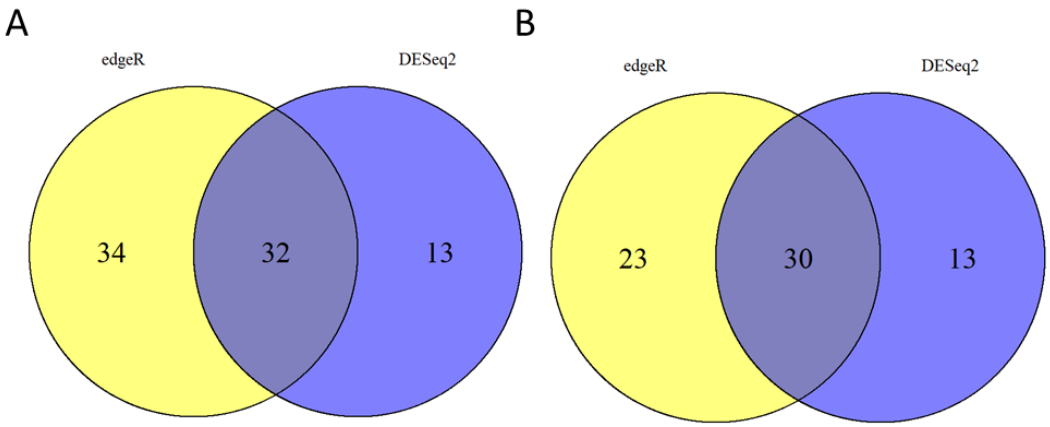

Figure 5.3.46 Venn diagram comparing between DESeq2 and edgeR differential expression methods in peritoneal inflammatory macrophages

A) Venn Diagram comparing gene discoveries which are statistically significant (adjusted p-value <0.05) between DESeq2 and edgeR differential expression methods. B) Venn diagram comparing gene discoveries which are statistically significant (adjusted p-value <0.05) and have a ±1log$_2$ fold change between DESeq2 and edgeR differential expression methods.

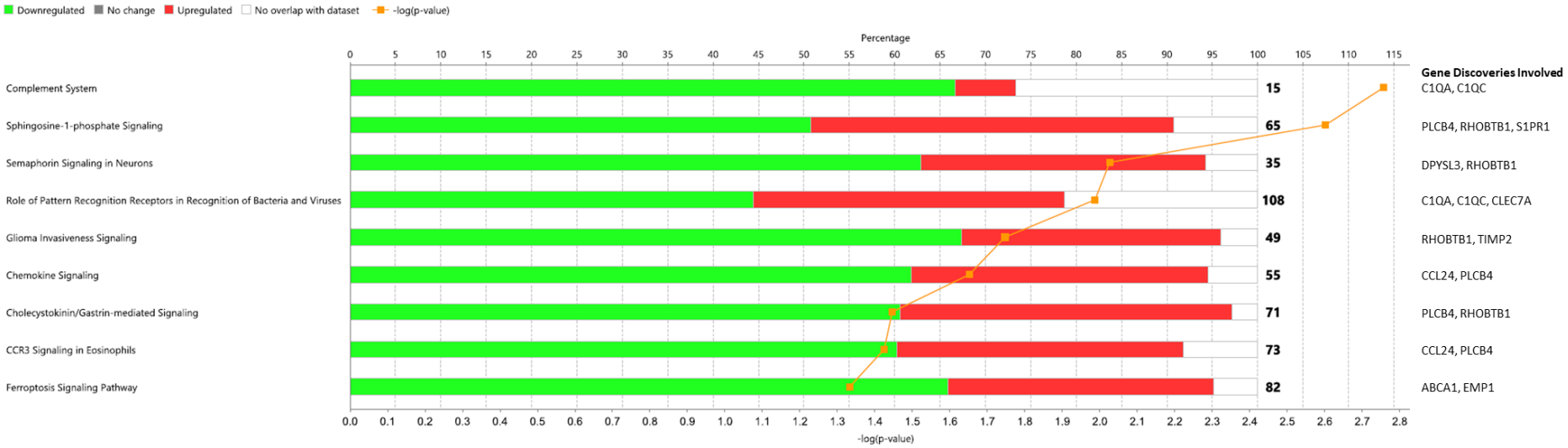

Figure 5.3.47 Canonical pathway analysis of DESeq2 differential gene expression analysis in inflammatory macrophages.

Canonical pathway analysis generated from Ingenuity Pathway Analysis (IPA) against those previously identified in all macrophages following DESeq2 differential gene expression method when sex is included in the model matrix. Percentage of genes in the analysis overlap with pathway (green = downregulated, red = upregulated, white = no overlap). Numbers in bold are the total number of genes involved in the pathway. Specific gene discoveries with adjusted p-value <0.05 involved in each pathway named, with-log p-value of each pathway indicated with orange line.

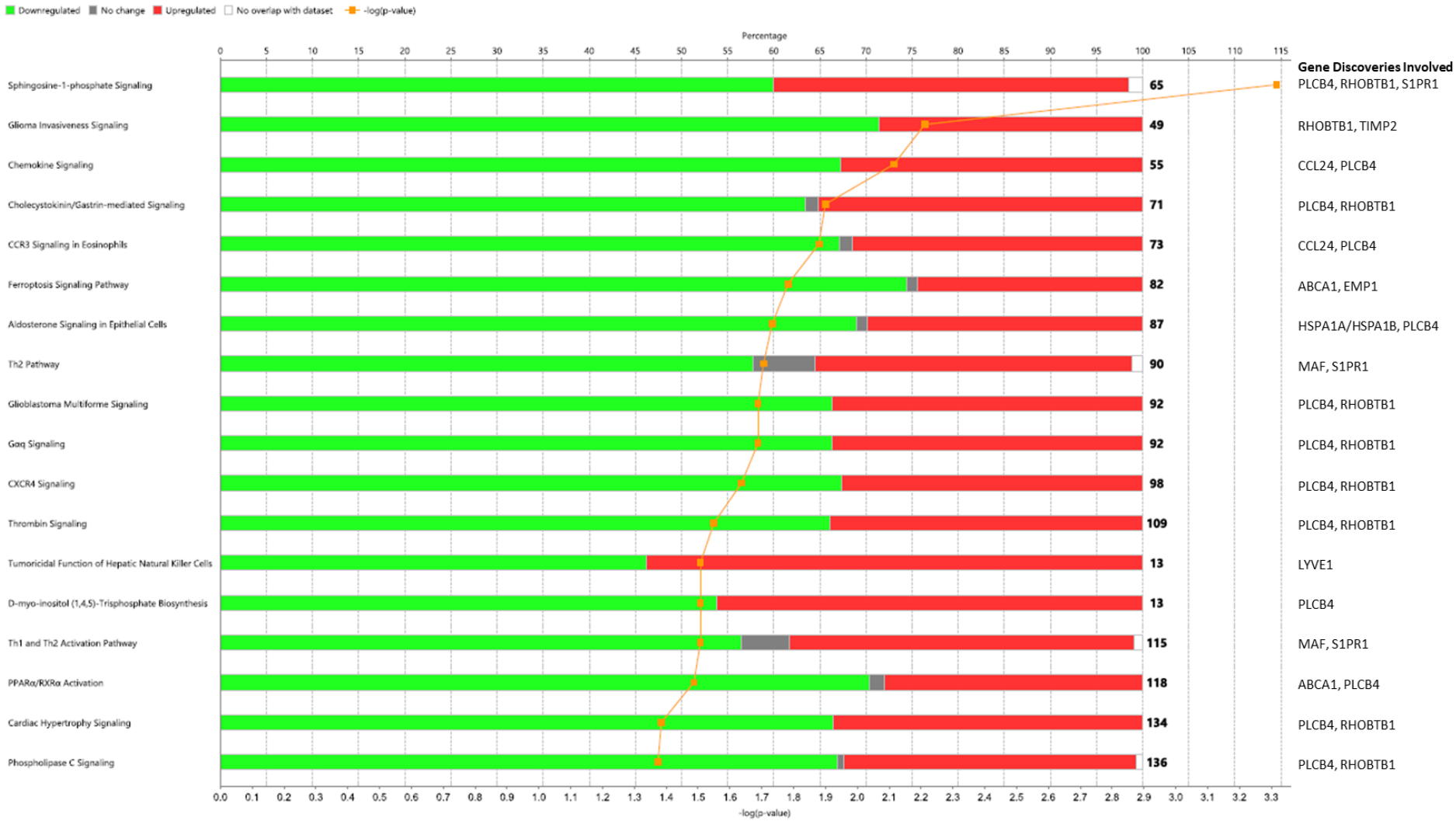

Figure 5.3.48 Canonical pathway analysis of edgeR differential gene expression analysis in inflammatory macrophages.

Canonical pathway analysis generated from Ingenuity Pathway Analysis (IPA) against those previously identified in all macrophages following edgeR differential gene expression method when sex is included in the model matrix. Percentage of genes in the analysis overlap with pathway (green = downregulated, red = upregulated, white = no overlap). Numbers in bold are the total number of genes involved in the pathway. Specific gene discoveries with adjusted p-value <0.05 involved in each pathway named, with-log p-value of each pathway indicated with orange line.

Canonical pathway analysis from IPA of the 45 gene discoveries from DESeq2 differential expression of inflammatory macrophages with an adjusted p-value of <0.05, highlighted several pathways of interest including the complement system, chemokine signalling and sphingoine-1-phosphate signalling (Figure 5.3.47). Analyses of the 66 edgeR differential gene discoveries as above, indicated several additional pathways including *Cxcr4* signalling and phospholipase-C signalling (Figure 5.3.48).

Upstream Regulators	DESeq2		
	Log_2 Fold Change	P-Value of Overlap	Targets in Dataset
Ppard	-0.009	2.99E-05	*C1qa,C1qc,Gas6*
Nr1h3	-0.326	0.000473	*Abca1, C1qa, Ccl7, Gas6*
Gata6	-1.044	0.000479	*Calml4, Lyve1, Sorbs3*
Ldlr	-0.071	0.000584	*Abca1, C1qa, Ccl7, Gas6*
Nr1h2	0.077	0.00252	*Abca1, Ccl7*
Rara	-0.123	0.00421	*Abca1*
Tardbp	-0.154	0.0084	*C1qa*
Rxra	-0.359	0.0084	*Abca1*
Cdkn2a	-1.22	0.0116	*Ccl24, Ccl7*
Parp1	-0.096	0.0126	*Abca1*
Plcg2	0.093	0.0179	*C1qa, Ccl7*
Il10ra	0.376	0.0187	*Gas6, S1pr1, Sirpb1*
Pkm	0.046	0.0209	*Abca1*
Mapk14	-0.043	0.0209	*Abca1*
Csf1	-0.995	0.0238	*Ccl7, Clec7a*
Alox15	-1.936	0.025	*Abca1*

Cd200	-1.29	0.0291	*Clec7a*
Cebpe	-0.203	0.0291	*Ccl7*
Irak1	-0.005	0.0291	*Abca1*
Nos2	-1.007	0.0332	*Ccl7*
Ifng		0.034	*Abca1, Ccl7, Clec7a*
Ppara	-3.54	0.0373	*Abca1*
Klf2	-0.392	0.0373	*Ccl7*
Ace	0.544	0.0413	*Ccl24*
Npc1	0.025	0.0494	*Abca1*
Il13	0.237	0.0494	*Abca1*

Table 5.3.5 Upstream regulators in DESeq2 differential gene expression analysis of inflammatory macrophages.

Upstream regulators identified in DESeq2 analysis with log2 fold change and p-value of overlap with each pathway. Genes with an adjusted p-value of <0.05 involved in each pathway are named.

Upstream Regulators	edgeR		
	Log_2 Fold Change	P-Value of Overlap	Targets in Dataset
Rara	-0.139	0.00242	*Abca1*
Gata6	-1.062	0.00353	*Lyve1,Sorbs3*
Il10ra	0.359	0.00396	*Folr2,S1pr1,Sirpb1*
Rxra	-0.376	0.00484	*Abca1*
Parp1	-0.112	0.00726	*Abca1*
Plm	0.03	0.0121	*Abca1*
Mapk14	-0.059	0.0121	*Abca1*
Alox15	-1.955	0.0145	*Abca1*
Irak1	-0.021	0.0169	*Abca1*
Ppara	-3.28	0.0216	*Abca1*
Ace	0.526	0.024	*Ccl24*
Npc1	0.01	0.0287	*Abca1*
Il13	0.203	0.0287	*Abca1*
Nr1h2	0.06	0.0428	*Abca1*

Table 5.3.6 Upstream regulators in edgeR differential gene expression analysis inflammatory macrophages.

Upstream regulators identified in edgeR analysis with log2 fold change and p-value of overlap with each pathway. Genes with an adjusted p-value of <0.05 involved in each pathway are named.

Several upstream regulators were identified using IPA from the DESeq2 analysis, with 10 of the 26 upstream regulators with a p-value of overlap <0.05 having more than one gene target highlighted (Table 5.3.5). These included peroxisome proliferator-activated receptor A (*Ppara*) and liver X receptors (LXRα and LXRβ encoded by *Nr1h3* and *Nr1h2* genes respectively) in addition to *Gata6* and *Il-10ra* (Table 5.3.5).

edgeR analysis highlighted 14 upstream regulators with a p-value of overlap <0.05 (Table 5.3.6). However the majority were associated to 1 gene discovery with an adjusted p-value of <0.05 associated, predominantly ATP-binding cassette (*Abca1*) (Table 5.3.6).

5.3.6.3.3. Differential Exon Usage

To determine splice variants within the RNA sequencing datasets, relative usage of exons between *Maf*$^{fl/fl}$*Cx3cr1*$^{Cre/+}$ and *Maf*$^{fl/fl}$*Cx3cr1*$^{+/+}$ zymosan treated peritoneal inflammatory macrophages generated 3 differential exons with an adjusted p-value <0.05 and a cut off ±1log$_2$ (Figure 5.3.49).

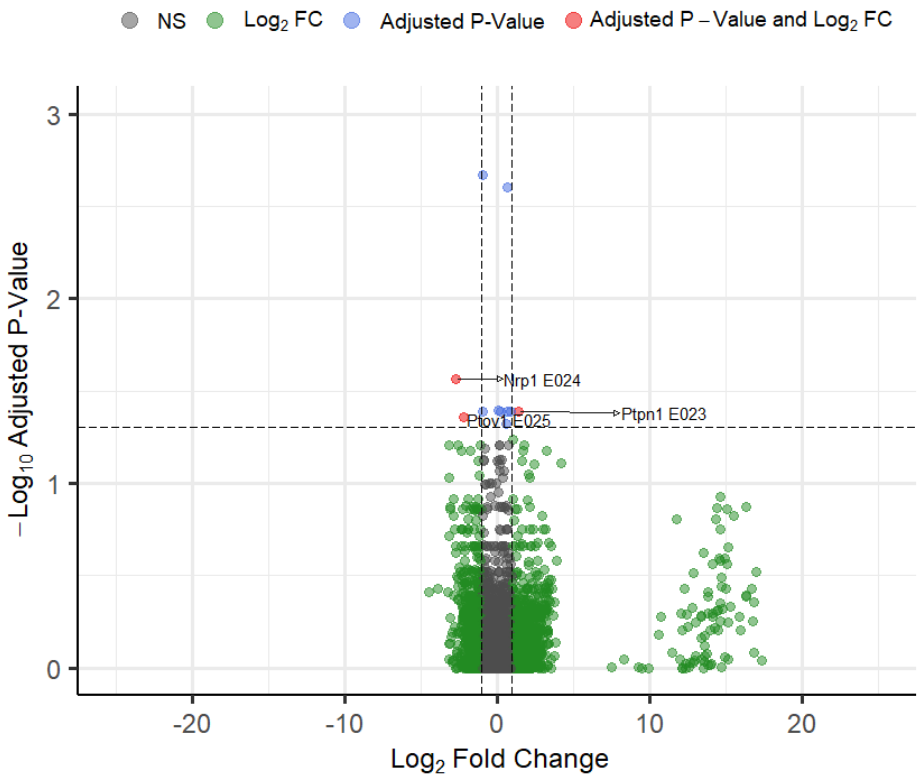

Figure 5.3.49 DEXSeq differential exon usage analysis of peritoneal inflammatory macrophages in *Maf*$^{fl/fl}$*Cx3cr1*$^{Cre/+}$ vs *Maf*$^{fl/fl}$*Cx3cr1*$^{+/+}$ mice

Volcano plot of DEXSeq differential exon usage analysis between *Maf*$^{fl/fl}$*Cx3cr1*$^{Cre/+}$ (n=2) vs *Maf*$^{fl/fl}$*Cx3cr1*$^{+/+}$ (n=4) mice, with dashed lines representing cut off for adjusted p-value = 0.05 and log$_2$ fold change = 1.

Prostate tumour over expressed gene 1 (*Ptov1*) (ENSMUSG00000038502) at exon 25 (Figure 5.3.50), Protein tyrosine phosphatase, non-receptor type 1 (*Ptpn1*) (ENSMUSG00000027540) at exon 23 (Figure 5.3.51) and Neuropilin 1 (*Nrp1*) ENSMUSG00000025810) at exon 24 (Figure 5.3.52) were identified as having statistically significantly changed usage with adjusted P-Values = 0.044, 0.041, 0.027 and log$_2$ fold changes = 2.189, -1.459, 2.707 between *Maf*$^{fl/fl}$*Cx3cr1*$^{Cre/+}$ and *Maf*$^{fl/fl}$*Cx3cr1*$^{+/+}$ mice respectively. However this did not elucidate any clear splice variant transcripts in these genes.

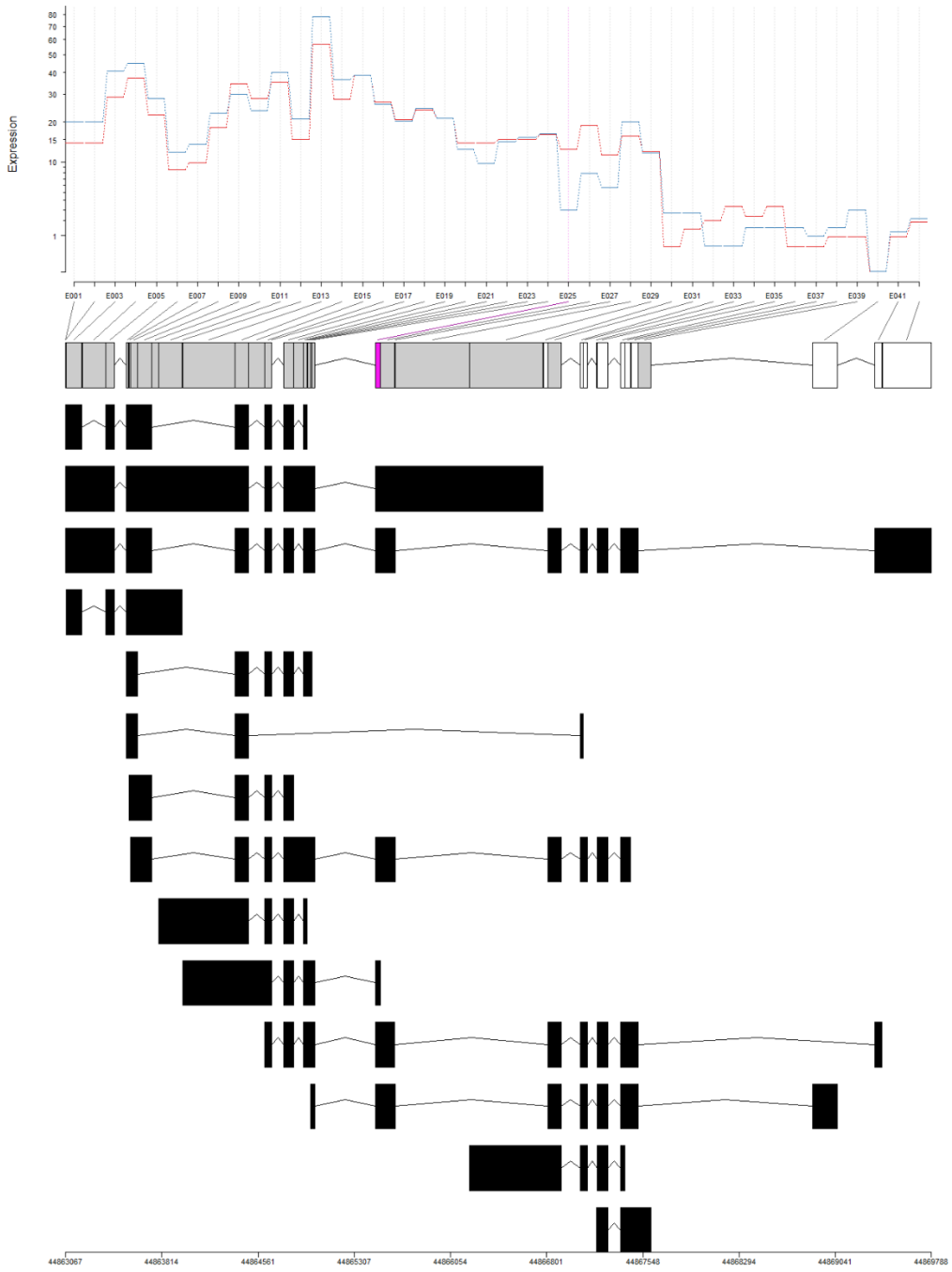

Figure 5.3.50 DEXSeq differential exon usage analysis of *Ptov1* in zymosan treated peritoneal inflammatory macrophages in *Maf*$^{fl/fl}$*Cx3cr1*$^{Cre/+}$ vs *Maf*$^{fl/fl}$*Cx3cr1*$^{+/+}$ mice

DEXSeq plot of expression of exons in the *Ptov1* gene in *Maf*$^{fl/fl}$*Cx3cr1*$^{Cre/+}$ (Blue line) (n=2) and *Maf*$^{fl/fl}$*Cx3cr1*$^{+/+}$ (Red line) (n=4). Differential exons highlighted in pink (p-value <0.05) and transcripts of *Ptov1* gene in black below.

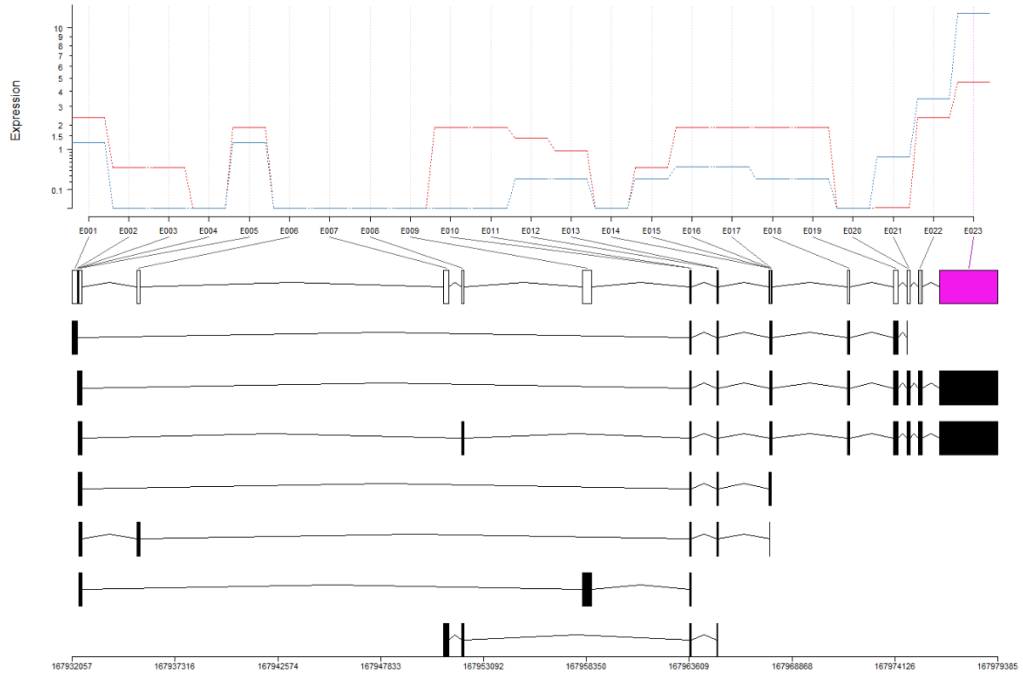

Figure 5.3.51 DEXSeq differential exon usage analysis of *Ptpn1* in zymosan treated peritoneal inflammatory macrophages in *Maf*$^{fl/fl}$*Cx3cr1*$^{Cre/+}$ vs *Maf*$^{fl/fl}$*Cx3cr1*$^{+/+}$ mice

DEXSeq plot of expression of exons in the *Ptpn1* gene in *Maf*$^{fl/fl}$*Cx3cr1*$^{Cre/+}$ (Blue line) (n=2) and *Maf*$^{fl/fl}$*Cx3cr1*$^{+/+}$ (Red line) (n=4). Differential exons highlighted in pink (p-value <0.05) and transcripts of *Ptpn1* gene in black below.

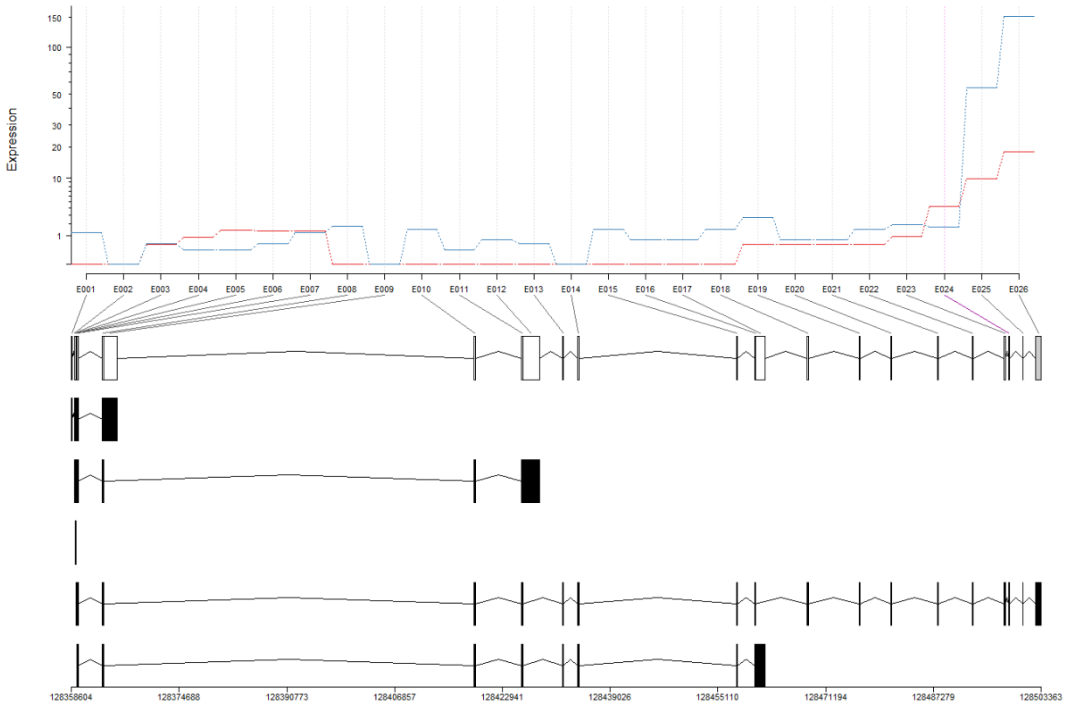

Figure 5.3.52 DEXSeq differential exon usage analysis of *Nrp1* in zymosan treated peritoneal inflammatory macrophages in *Maf*$^{fl/fl}$*Cx3cr1*$^{Cre/+}$ vs *Maf*$^{fl/fl}$*Cx3cr1*$^{+/+}$ mice

DEXSeq plot of expression of exons in the *Nrp1* gene in *Maf*$^{fl/fl}$*Cx3cr1*$^{Cre/+}$ (Blue line) (n=2) and *Maf*$^{fl/fl}$*Cx3cr1*$^{+/+}$ (Red line) (n=4). Differential exons highlighted in pink (p-value <0.05) and transcripts of *Nrp1* gene in black below.

5.3.7. Validation of RNA Sequencing of Zymosan Treated Peritoneal Macrophages Gene Discoveries

Differential genes identified through DESeq2 and edgeR were selected for validation based on being protein coding, have an adjusted p-value of <0.05 and a ±1log_2 fold change in at least one of the differential expression methods, summarised in Table 5.3.7 for zymosan treated peritoneal tissue resident macrophages and Table 5.3.8 for matched inflammatory macrophages.

Target	Resident DESeq2		Resident edgeR	
	Log_2 Fold Change	Adjusted P-Value	Log_2 Fold Change	Adjusted P-Value
Ptprm	-1.2764555	3.67E-05	NA	NA
Maf	-12.804101	1.71E-11	-13.877760	2.20E-25
Tgfbr3	-1.3245531	2.97E-07	NA	NA
H2-Q6	1.00524329	0.01464053	NA	NA
Klf12	-6.5682649	0.03173676	-7.6452401	0.00010865
Vsig4	-1.3033008	0.00174572	-1.3617065	0.00510816

Table 5.3.7 Summary of targets selected for validation of zymosan treated peritoneal tissue resident macrophage RNA sequencing data.

List of targets for validation by qPCR and Flow Cytometry for validation with log_2 fold change and Adjusted p-value from DESeq2 and edgeR analyses. Genes which did not meet the cut off (adjusted p-value <0.05 and have a ±1log_2 fold change) in one of the analyses had an NA applied.

Target	Inflammatory DESeq2		Inflammatory edgeR	
	Log_2 Fold Change	Adjusted P-Value	Log_2 Fold Change	Adjusted P-Value
Mrvi1	-1.6076099	0.00055498	-1.6222564	0.01008902
Dnm1	-2.6761509	5.83E-06	-2.6880586	2.52E-06
Maf	-5.0553070	3.68E-07	-5.0664076	1.08E-09
Lyve1	-5.4743881	0.00510194	-5.4596430	0.00273774
S1pr1	-2.1397604	0.00510194	-2.1564436	0.00273774
CD38	-1.2696856	0.01899230	-1.283228	0.02956580
Clec7a	1.01272715	0.04280789	NA	NA
Hspa1a/ Hspa1b	-2.9135240	0.0007659	-2.9309873	0.00808136
Folr2	NA	NA	-3.3144439	0.02249948

Table 5.3.8 Summary of targets selected for validation of zymosan treated peritoneal inflammatory macrophage RNA sequencing data.

List of targets for validation by qPCR and Flow Cytometry for validation with log_2 fold change and Adjusted p-value from DESeq2 and edgeR analyses. Genes which did not meet the cut off (adjusted p-value <0.05 and have a ±1log_2 fold change) in one of the analyses had an NA applied.

5.3.7.1. Validation of Gene Discoveries by qPCR

To validate the differential gene discovery analysis qPCR was conducted on *Maf*$^{fl/fl}$*Cx3cr1*$^{+/+}$ and *Maf*$^{fl/fl}$*Cx3cr1*$^{Cre/+}$ peritoneal macrophages after 48 hr treatment with zymosan as above in section 5.3.6, isolated by FACS as in Figure 5.3.30.

In tissue resident macrophages 40-ΔCT indicated overall significance by Genotype, Targets and Interaction (p-value = <0.0001, ****) when analysed by two-way ANOVA (A). Šidák's multiple comparisons test indicated *Klf12* and *Maf* to have high significance between genotypes (p-value = <0.0001, ****), as did *Vsig4* (p-value = 0.001, ***), *Ptprm* (p-value = 0.0011, **) and *Lyve1* (0.0032, **) (Figure 5.3.53A).

Whilst relative quantification of fold change gene expression indicates only Genotype being statistically significant (p-value = 0.0001, ***) when analysed by two-way ANOVA, Šidák's multiple comparisons test demonstrates no statistical significance (Figure 5.3.53B) in any of the targets.

In inflammatory macrophages 40-ΔCT indicated overall high significance by Genotype, Targets (p-value = <0.0001, ****) and Interaction (p-value = 0.0008, ***) when analysed by two-way ANOVA (Figure 5.3.53C). Šidák's multiple comparisons test indicated *Lyve1* and *Maf* to have high significance between genotypes (p-value = <0.0001, ****, and p-value = 0.0002, ***, respectively) (Figure 5.3.53C).

Relative quantification of fold change gene expression indicates genotype being statistically significant (p-value = 0.0269, *) when analysed by two-way ANOVA, Šidák's multiple comparisons test demonstrates no statistical significance (Figure 5.3.53D) between any of the targets.

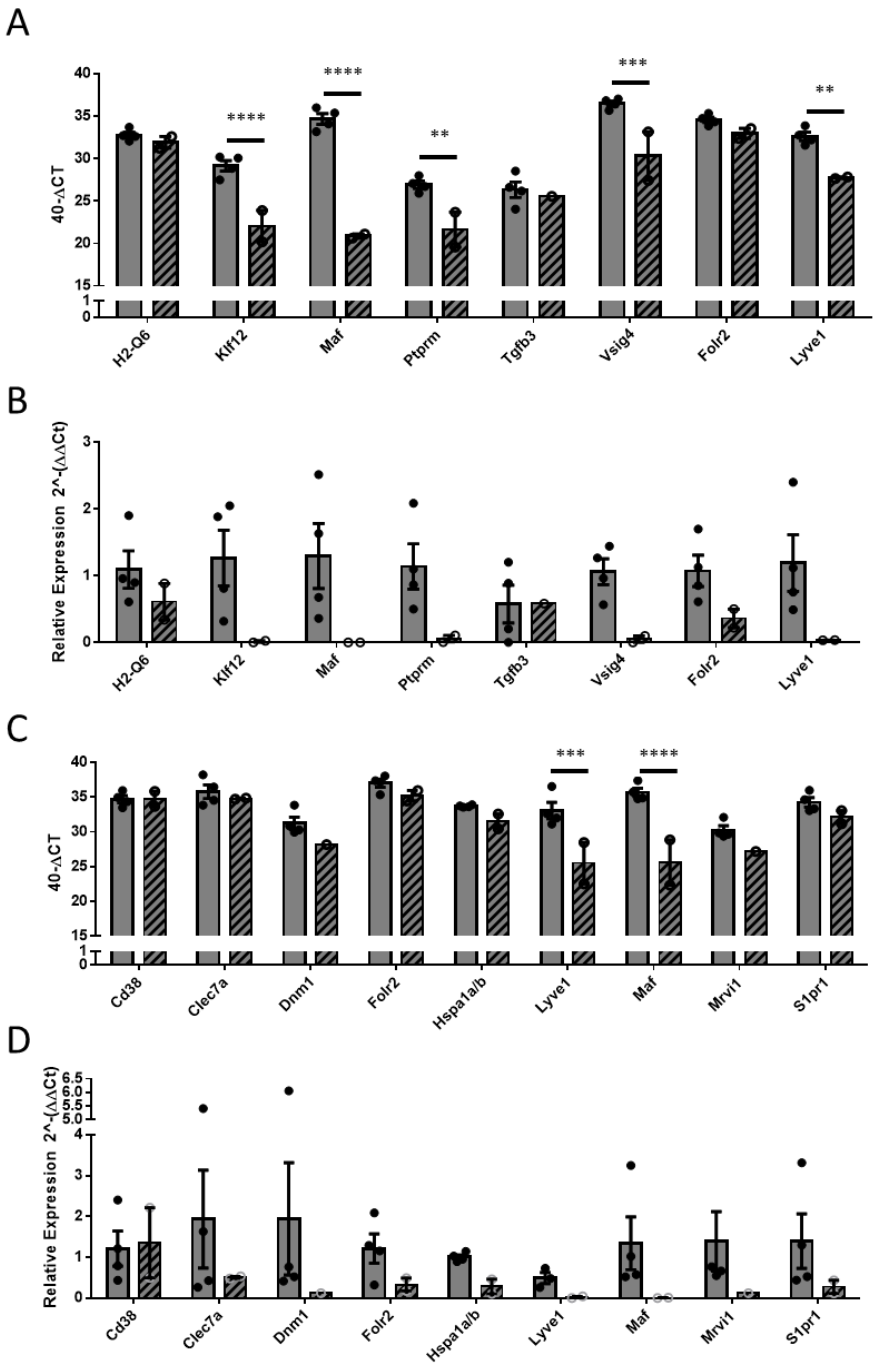

Figure 5.3.53 qPCR Validation of diffferential gene discoveries in Zymosan Treated peritoneal tissue resident macrophages and imflammatory macrphages.

A) 40-ΔCT values and B) relative quantification of fold change gene expression in *Maf*$^{fl/fl}$*Cx3cr1*$^{+/+}$ (n=4) and *Maf*$^{fl/fl}$*Cx3cr1*$^{Cre/+}$ (n=2) peritoneal tissue resident macrophages. C) 40-ΔCT values and D) relative quantification of fold change gene expression of matched peritoneal inflammatory macrophages from *Maf*$^{fl/fl}$*Cx3cr1*$^{+/+}$ (n=4) and *Maf*$^{fl/fl}$*Cx3cr1*$^{Cre/+}$ (n=2) mice. Error bars indicate ± SEM. Mice were all female, ages 6-8 weeks age.

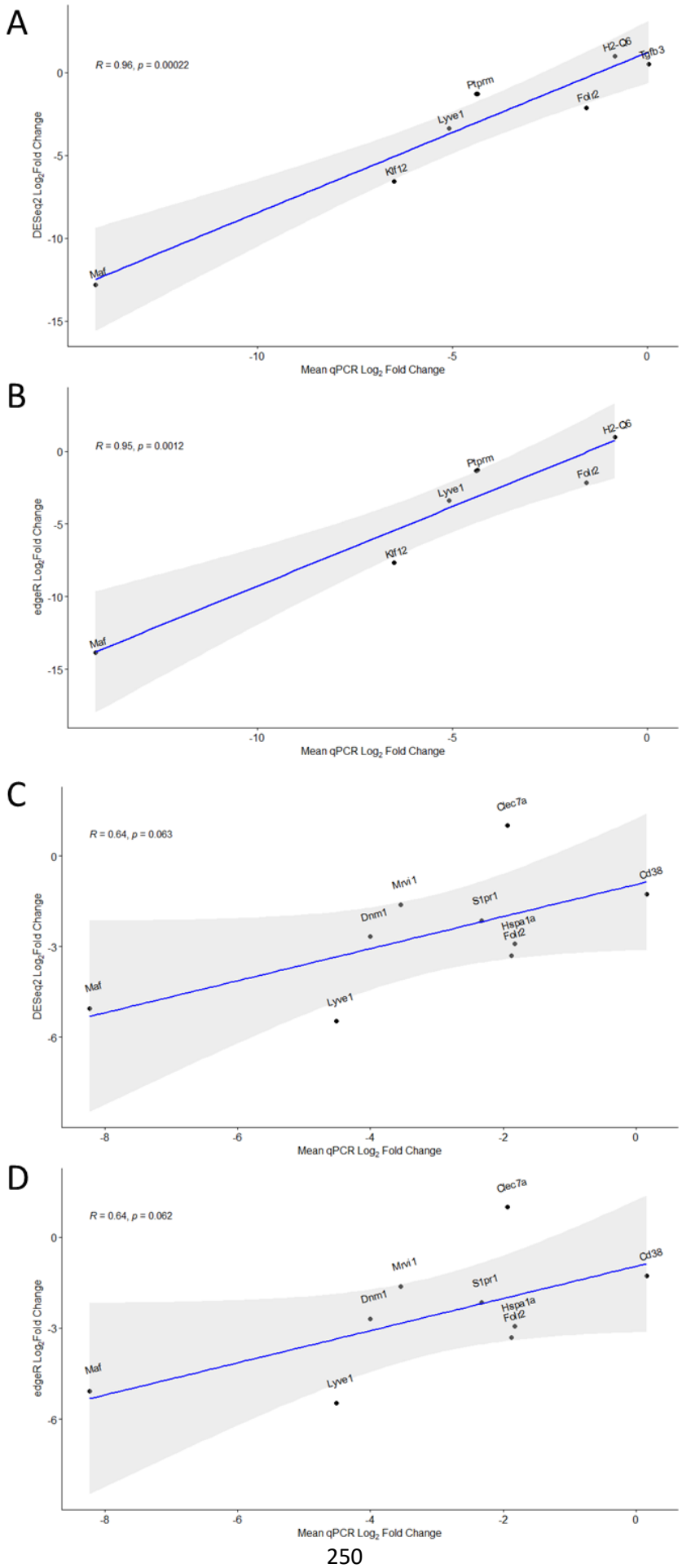
A
R = 0.96, p = 0.00022
DESeq2 Log2Fold Change
Mean qPCR Log2 Fold Change
H2-Q6
Tgfb3
Ptprm
Fcrl2
Lyve1
Klf12
Maf
B
R = 0.95, p = 0.0012
edgeR Log2Fold Change
Mean qPCR Log2 Fold Change
H2-Q6
Ptprm
Fcrl2
Lyve1
Klf12
Maf
C
R = 0.64, p = 0.063
DESeq2 Log2Fold Change
Mean qPCR Log2 Fold Change
Clec7a
Mrvi1
Cd38
S1pr1
Dnm1
Hspa1a
Fcrl2
Maf
Lyve1
D
R = 0.64, p = 0.062
edgeR Log2Fold Change
Mean qPCR Log2 Fold Change
Clec7a
Mrvi1
Cd38
S1pr1
Dnm1
Hspa1a
Fcrl2
Maf
Lyve1

Figure 5.3.54 Pearson Correlation of Zymosan treated Peritoneal Tissue Resident Macrophages and inflammatory macrophages RNA Sequencing Log_2 Fold Change and qPCR Log_2 Fold Change.

A) Correlation of DESeq2 analysis of *Maf*$^{fl/fl}$*Cx3cr1*$^{+/+}$and *Maf*$^{fl/fl}$*Cx3cr1*$^{Cre/+}$ zymosan treated peritoneal tissue resident macrophage Log_2 fold change against qPCR Log_2 fold change based on relative quantification (2^(ΔΔCt). B) Correlation of edgeR analysis of *Maf*$^{fl/fl}$*Cx3cr1*$^{+/+}$and *Maf*$^{fl/fl}$*Cx3cr1*$^{Cre/+}$ zymosan treated peritoneal tissue resident macrophage Log_2 fold change against qPCR Log_2 fold change based on relative quantification (2^(ΔΔCt). C) Correlation of DESeq2 analysis of *Maf*$^{fl/fl}$*Cx3cr1*$^{+/+}$and *Maf*$^{fl/fl}$*Cx3cr1*$^{Cre/+}$ zymosan treated peritoneal inflammatory macrophage Log_2 fold change against qPCR Log_2 fold change based on relative quantification (2^(ΔΔCt). D) Correlation of edgeR analysis of *Maf*$^{fl/fl}$*Cx3cr1*$^{+/+}$and *Maf*$^{fl/fl}$*Cx3cr1*$^{Cre/+}$ zymosan treated peritoneal inflammatory macrophage Log_2 fold change against qPCR Log_2 fold change based on relative quantification (2^(ΔΔCt). Pearson correlation coefficient (R value and blue line) with coefficient interval (grey area) and p-value displayed on graph (p)

RNA sequencing and qPCR generate relative gene expression through log_2 fold change. Therefore comparing log_2 fold change results from qPCR and RNA sequencing was considered to be the most relevant approach to validate differential gene discoveries. Correlation between the relative quantification of fold change against DESeq2 analysis (Figure 5.3.54A) and edgeR analysis (Figure 5.3.54B) log_2 fold change of *Maf*$^{fl/fl}$*Cx3cr1*$^{+/+}$and *Maf*$^{fl/fl}$*Cx3cr1*$^{Cre/+}$ zymosan peritoneal tissue resident macrophages, was investigated for further validation. DESeq2 analysis had a strong positive correlation coefficient of 0.95529 (Figure 5.3.54A), and edgeR analysis had a strong positive correlation coefficient of 0.9466636 (Figure 5.3.54B), both of which were statistically significant (p-value = 0.000216 ****, and p-value = 0.001226 *** respectively).

Correlation between the relative quantification of fold change against DESeq2 analysis (Figure 5.3.54C) and edgeR analysis (Figure 5.3.54D) log_2 fold change of *Maf*$^{fl/fl}$*Cx3cr1*$^{+/+}$and *Maf*$^{fl/fl}$*Cx3cr1*$^{Cre/+}$ and zymosan treated peritoneal inflammatory macrophages resulted in DESeq2 analysis having a moderate-strong positive correlation coefficient of 0.6413393 (Figure 5.3.54C), and edgeR analysis had a moderate-strong positive correlation coefficient of 0.641953 (Figure 5.3.54D). However neither correlations were statistically significant (p-value = 0.06265 NS, and p-value = 0.06232 NS respectively) (Figure 5.3.54C and Figure 5.3.54D).

5.3.7.2. Validation of Gene Discoveries by Flow Cytometry

To validate if the gene discoveries from RNA sequencing resulted in protein expression alterations, peritoneal tissue resident macrophages and inflammatory macrophages from *Maf*$^{fl/fl}$*Cx3cr1*$^{+/+}$ and *Maf*$^{fl/fl}$*Cx3cr1*$^{Cre/+}$ mice were stained as in Figure 5.3.30 for flow cytometry analysis.

Of the tissue resident macrophage targets listed in Table 5.3.7 only previously published flow cytometry antibodies were available at the time for major histocompatibility complex (MHC) H2, VSIG4 and MAF. Likewise for peritoneal inflammatory macrophages targets in Table 5.3.8 all but *Dynamin1* and *Clec7a* were investigated by flow cytometry. Due to *Maf* having been identified as having a role in *Il-10* control, major histocompatibility complex II (MHCII) was additionally targeted as it has been previously demonstrated in C57BL/6.Il10$^{-/-}$ (IL-10$^{-/-}$) mice to alter phenotype in peritoneal inflammatory macrophages (213).

Tissue resident macrophages displayed a small increase in MHC H2 expression whilst also demonstrating a small increase in the inflammatory macrophage population. VSIG4 demonstrated a reduction in expression in both macrophage populations. Utilising a bisector gate (Figure 5.3.55A), VSIG4^{high} tissue resident macrophages having a mean percentage of 98.03 % ±0.24 (Mean ± SEM) in *Maf*$^{fl/fl}$*Cx3cr1*$^{+/+}$ and 70.20 % ±12.70 (Mean ± SEM) in *Maf*$^{fl/fl}$*Cx3cr1*$^{Cre/+}$. Furthermore the VSIG4^{high} inflammatory macrophages had a mean percentage of 94.33 % ±0.90 (Mean ± SEM) in *Maf*$^{fl/fl}$*Cx3cr1*$^{+/+}$ and 61.93% ±13.77 (Mean ± SEM) in *Maf*$^{fl/fl}$*Cx3cr1*$^{Cre/+}$ mice (Figure 5.3.55B).

Analysis by two-way ANOVA indicated genotype, targets and interaction of the two factors to be statistically significant (p-value = 0.0279, *, p-value = 0.0007, *** and p-value = 0.0008, *** respectively) (Figure 5.3.55B). Šidák's multiple comparison test indicated statistical significance between genotypes in inflammatory macrophages (p-value = 0.0184, *) (Figure 5.3.55B). Whilst MAF was consistent, with reduction in protein expression in both tissue resident and inflammatory macrophages of *Maf*$^{fl/fl}$*Cx3cr1*$^{Cre/+}$ mice when compared to *Maf*$^{fl/fl}$*Cx3cr1*$^{+/+}$ mice.

CD38 expression was distinctively different in inflammatory macrophages in *Maf*$^{fl/fl}$*Cx3cr1*$^{Cre/+}$ and *Maf*$^{fl/fl}$*Cx3cr1*$^{+/+}$ mice with mean of CD38^{high} 77.53 % ±5.43 (Mean ±SEM) of and 60.13 % ±3.53 (Mean ±SEM) respectively (Figure 5.3.55B), and a small

reduction in tissue resident macrophages (Figure 5.3.55A). HSP70 (the protein encoded by *Hspa1a/b*) was expressed at low levels on inflammatory macrophages, however did suggest reduction in expression in both cell types in *Maf*$^{fl/fl}$*Cx3cr1*$^{Cre/+}$ compared to *Maf*$^{fl/fl}$*Cx3cr1*$^{+/+}$ mice (Figure 5.3.55A).

FOLR2 was increased in tissue resident macrophages whilst expression was heavily reduced in inflammatory macrophages, with FOLR2^{high} macrophages expressing a mean of 73.23 % ±3.76 (Mean ±SEM) and 29.10 % ±3.31 (Mean ±SEM) in *Maf*$^{fl/fl}$*Cx3cr1*$^{Cre/+}$ and *Maf*$^{fl/fl}$*Cx3cr1*$^{+/+}$ mice respectively (Figure 5.3.55B).

Additional targets of MHCII displayed increases in expression in both populations however this was more markedly evident in inflammatory macrophages, with a mean percentage of 51.00 % ±4.49 (Mean ±SEM) in *Maf*$^{fl/fl}$*Cx3cr1*$^{+/+}$ being MHCII^{high} and 73.67 % ±6.89 (Mean ±SEM) in *Maf*$^{fl/fl}$*Cx3cr1*$^{Cre/+}$ mice, however Šidák's multiple comparison did not indicate any statistical significance between genotypes (Figure 5.3.55B).

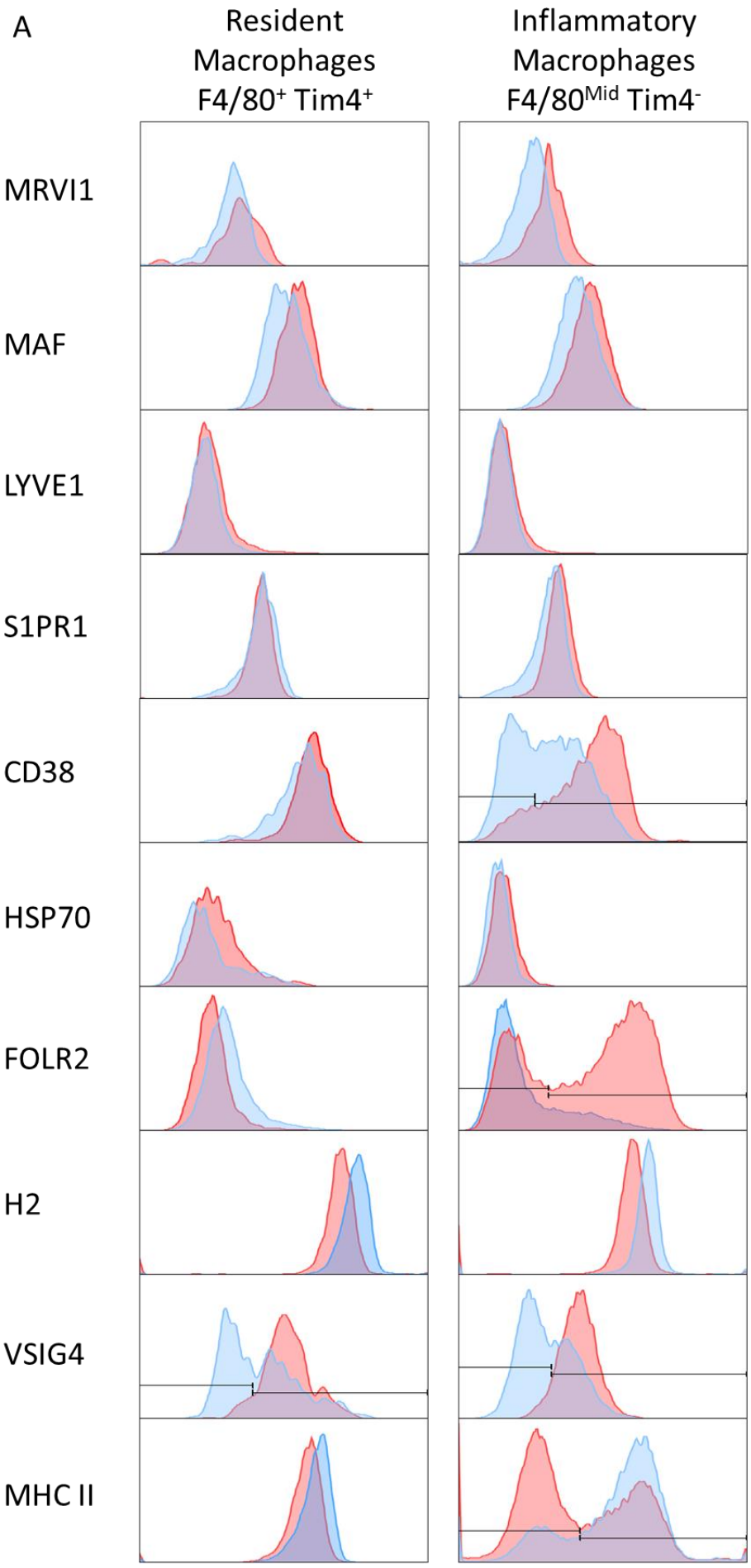
A
Resident Macrophages F4/80+ Tim4+
Inflammatory Macrophages F4/80Mid Tim4-
MRVI1
MAF
LYVE1
S1PR1
CD38
HSP70
FOLR2
H2
VSIG4
MHC II

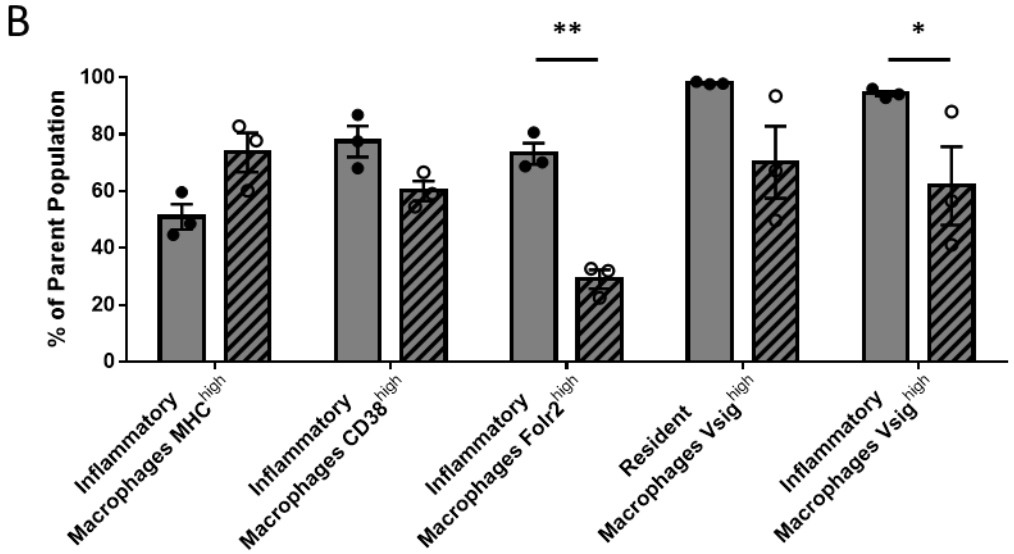

Figure 5.3.55 Flow cytometry validation of diffferential gene discoveries zymosan treated peritoneal tissue resident and inflammatory macrophages markers identified from RNA Sequencing in *Maf*$^{fl/fl}$*Cx3cr1*$^{Cre/+}$ and *Maf*$^{fl/fl}$*Cx3cr1*$^{+/+}$ mice.

A) Representative flow cytometry histograms of diffferential gene discoveries in *Maf*$^{fl/fl}$*Cx3cr1*$^{+/+}$ (red), *Maf*$^{fl/fl}$*Cx3cr1*$^{Cre/+}$ (blue), representative of n=3. B) % of target expression as per bisector gates on histograms of *Maf*$^{fl/fl}$*Cx3cr1*$^{+/+}$ mice (grey) and *Maf*$^{fl/fl}$*Cx3cr1*$^{Cre/+}$ (shaded) mice. Data shown represents mean percentage ± SEM (n=3). Two-way ANOVA with Šidák's multiple comparison indicated on graph (p-value = <0.005, ** and p-value = <0.05, *) All mice were female and aged 6-8 weeks.

5.4. Discussion

5.4.1. Validation of *Maf* Expression in Peritoneal Tissue Resident Macrophages

In *Maf*$^{fl/fl}$*Cx3cr1*$^{Cre/+}$ mice protein expression of MAF in peritoneal tissues resident macrophages display significant reduction between *Maf*$^{fl/fl}$*Cx3cr1*$^{+/+}$ and *Maf*$^{fl/fl}$*Cx3cr1*$^{Cre/+}$ mice (Figure 5.3.2). It is also important to note that the MAF antibody, which was validated in Chapter 3 of this thesis, maybe at least be partially specific, or specific but with high background which is not controlled for by the isotype control, explaining the residual MAF protein expression in *Maf*$^{fl/fl}$*Cx3cr1*$^{Cre/+}$ mice (Figure 5.3.2).

No significant differences were observed in the percentage of CD11b^{high}, F4/80^{high} and Tim-4^{+} tissue resident macrophages in total lavage (Figure 5.3.1B). Whilst absolute number suggested an increase in total number of peritoneal tissue resident macrophages in *Maf*$^{fl/fl}$*Cx3cr1*$^{Cre/+}$ mice when compared to *Maf*$^{fl/fl}$*Cx3cr1*$^{+/+}$ mice, this was not statistically significant (Figure 5.3.1C).

Furthermore among common myeloid markers other than CX3CR1 there was no observable differences (Figure 5.3.3). Reduction in CX3CR1 expression in *Maf*$^{fl/fl}$*Cx3cr1*$^{Cre/+}$ mice when compared to *Maf*$^{fl/fl}$*Cx3cr1*$^{+/+}$ mice is to be expected due to the genotype, where one of the *Cx3cr1* alleles is replaced with a gene encoding the constitutively active Cre recombinase (9). qPCR indicated significant deletion in both male and female *Maf*$^{fl/fl}$*Cx3cr1*$^{Cre/+}$ mice when compared to *Maf*$^{fl/fl}$*Cx3cr1*$^{+/+}$ mice (Figure 5.3.4), which was confirmed through FPKM of *Maf* in RNA-sequencing of peritoneal tissue resident macrophages (Figure 5.3.9).

It has been previously described that *Maf* is required for the expression of F4/80 in macrophages (104). This publication was conducted in *Maf* knockout (Maf$^{-/-}$) mice where foetal liver cells were adoptively transferred to another irradiated mouse line. However as these Maf$^{-/-}$ mice were embryonical lethal, what functional role *Maf* plays in F4/80 expression in adult macrophage could not be investigated at the time in this publication. It is evident from the data generated in this thesis that there is no difference in F4/80 expression on adult peritoneal tissue resident macrophages from *Maf*$^{fl/fl}$*Cx3cr1*$^{Cre/+}$ mice when compared to *Maf*$^{fl/fl}$*Cx3cr1*$^{+/+}$ mice (Figure 5.3.1 and Figure 5.3.3).

Overall phenotyping of peritoneal tissue resident macrophages, together with analysis of macrophage proportions of peritoneal lavage indicated the constitutively expressed *Cre* and subsequent loss of *Maf* in *Maf*$^{fl/fl}$*Cx3cr1*$^{Cre/+}$ mice, resulted in no overt abnormalities in tissue resident macrophages generation or phenotype under naïve conditions between *Maf*$^{fl/fl}$*Cx3cr1*$^{Cre/+}$ and *Maf*$^{fl/fl}$*Cx3cr1*$^{+/+}$ mice.

5.4.2. Generation and Time Course Assays Utilising MΦP Cell Lines

MΦPs were generated from both male and female *Maf*$^{fl/fl}$*Cx3cr1*$^{Cre/+}$ and *Maf*$^{fl/fl}$*Cx3cr1*$^{+/+}$ mice, as alternatives to the shRNA tested in Chapter 3. Both qPCR (Figure 5.3.6) and flow cytometry (Figure 5.3.5) determined statistically significant reduction of *Maf* expression at a genomic and protein level respectively. Therefore these cell lines could be utilised for *in vitro* assays such as for treatment with *E. Coli* LPS time course experiments (Figure 5.3.6 and Figure 5.3.7).

However no obvious differences were seen between genotypes in *Bhlhe40* (Figure 5.3.6), which has previously been identified as a possible repressor of *Maf* (229,235). Likewise common cytokines such as *Il-1b*, *Il-10* or *Tnf* did not indicate any differences between genotypes (Figure 5.3.7). Whereas *Il-6* did demonstrate a reduction in relative expression and a delay in activation, peaking at 6 hr in *Maf*$^{fl/fl}$*Cx3cr1*$^{Cre/+}$ cells and at 3 hr in *Maf*$^{fl/fl}$*Cx3cr1*$^{+/+}$ cells (Figure 5.3.7). *Il-12* did indicate a reduction in *Maf*$^{fl/fl}$*Cx3cr1*$^{Cre/+}$ cells; however its expression was very low in all cells (Figure 5.3.7).

Maf has repeatedly been demonstrated to play an important role in *Il-1 0* expression in tumour associated macrophages (TAMs) (157), RAW264.7 macrophage cell line (100,158,159) and in BMDMs (155,157). Predominantly siRNAs targeting *Maf* have been employed in these cells, and in the case of BMDMs always after differentiation. In the MΦP cell lines derived from *Maf*$^{fl/fl}$*Cx3cr1*$^{Cre/+}$ and *Maf*$^{fl/fl}$*Cx3cr1*$^{+/+}$ mice however there is no difference in *Il-10* expression by qPCR after stimulation with LPS (Figure 5.3.7), and *Maf* expression peaks at 6 hr (Figure 5.3.6) after the peak of Il-10 expression at 3 hr (Figure 5.3.7).

Furthermore many of these publications utilise the addition of IFN-γ to increase potency of the response to LPS (100,157,159). Inversely however it has been suggested that IFN-γ reduces the induction of *Il-10* by TLR activation such as LPS (237). Whether this additional stimulant would affect the role of *Maf* and *Il-10* in the MΦP cell lines is yet to be explored. Macrophage colony-stimulating factor (M-CSF) is required for the survival of these cells,

particularly the longer timepoints of 12 and 24 hr, and this could have acted as an additional stimuli effecting the production of cytokines. Finally using BMDMs derived from *Maf*$^{fl/fl}$*Cx3cr1*$^{Cre/+}$ and *Maf*$^{fl/fl}$*Cx3cr1*$^{+/+}$ mice may be a more appropriate model to confirm cytokine release studies as they have been a heavily utilised previously.

5.4.3. RNA Sequencing of Naïve Peritoneal Tissue Resident Macrophages

Utilising both edgeR vs DESeq2 differential expression methods, the majority of genes discovered with an adjusted p-value of <0.05, were common between the two methods, however both edgeR and DESeq2 generated unique discoveries (Figure 5.3.14A). PCA analysis indicated male *Maf*$^{fl/fl}$*Cx3cr1*$^{Cre/+}$ and *Maf*$^{fl/fl}$*Cx3cr1*$^{+/+}$ to have less variance than the female counterparts (Figure 5.3.15), and the male *Maf*$^{fl/fl}$*Cx3cr1*$^{+/+}$ mouse correlates closer with all three *Maf*$^{fl/fl}$*Cx3cr1*$^{+/+}$ mice (Figure 5.3.15).

Analysis of sex variations between the samples indicated few common genes which have an adjusted p-value of <0.05, with female mice generating 122 unique genes and male mice generating 68 (Figure 5.3.18A). However correlation and regression analysis of $\log_2$ fold change sex variations indicated moderate correlation with only *Maf* being both an outlier, based on Cook's distance, and high leverage/influence (Figure 5.3.18D). This suggest greater sample number would reduce background and increase statistical power in the comparison matrix (238,239).

The low *Maf* FPKM values of 4.43-4.71 for peritoneal tissue resident macrophage in *Maf*$^{fl/fl}$*Cx3cr1*$^{+/+}$ mice (Figure 5.3.9) may explain the small difference in ΔMFI of Maf protein expression between *Maf*$^{fl/fl}$*Cx3cr1*$^{Cre/+}$ and *Maf*$^{fl/fl}$*Cx3cr1*$^{+/+}$ mice (Figure 5.3.2). Furthermore this aligns with previous RNA-sequencing data obtained from ImmGen (http://rstats.immgen.org/Skyline/skyline.html), where murine peritoneal macrophages are indicated to be relatively low in *Maf* expression.

When including sex into the model for DESeq2 or edgeR, which have an adjusted p-value of <0.05, resulted in 97 shared gene discoveries, with edgeR generating 51 unique genes and DESeq2 generating 12 (Figure 5.3.21A).

Canonical pathway analysis with sex in the matrix highlighted several key macrophage pathways including phagosome formation. Multiple fatty acid signalling pathways were highlighted in canonical pathway analysis including eicosanoid, phospholipases and leukotriene pathways (and Figure 5.3.23). Furthermore differential exon usage analysis

utilising DEXSeq highlighted differential exon usages, with a p-value cut off of <0.05 and ±1log fold change, in sphingosine kinase gene *SphK2* E11 was identified across both sexes (Figure 5.3.24), and additionally *Sphk2* E10 (Figure 5.3.25) in female mice, however this could not be confirmed in male mice due to only sequencing a single pair of $Maf^{fl/fl}Cx3cr1^{Cre/+}$ and $Maf^{fl/fl}Cx3cr1^{+/+}$ mice.

Leukotriene C_4 synthase (*Ltc4s*) was identified in canonical pathway analysis as resulting in downregulation of the leukotriene biosynthesis in both DESeq2 () and edgeR (Figure 5.3.23). Leukotrienes are an important component of the immune response and have been demonstrated to be involved in inflammation and recruitment of other immune cells (240). Eicosanoids include prostaglandins and thromboxane, and prostaglandin E2 has been demonstrated to inhibit IL-10 production in regulatory T cells (Tr1) through cAMP signalling, also highlighted in DESeq2 differential gene expression canonical pathway analysis (), and inhibition of *Maf* expression (241). Investigation into lipidomic differences in these pathways and any downstream effects in the peritoneal cavity requires future work.

Whilst samples were collected at the same time circadian rhythm signalling pathways indicated differences due to $\log_2$ fold changes in *Per2*, *Per3* and *Creb5* (and Figure 5.3.23). Differences in expression were confirmed by qPCR, however neither *Per3* nor *Creb5* were statistically significant (Figure 5.3.27).

Circadian rhythm signalling has previously been demonstrated to modulate ≈8% of the expressed genes peritoneal macrophages (242). Stimulation with LPS at different time points highlight circadian rhythms in TNF-α and IL-6 secretion in *in vitro* culture, suggesting that macrophage-intrinsic circadian clock may govern cytokine release (242). Canonical clock genes such as *Cry2* and *Per3* were evident in both analyses when sex is included in the analysis matrix (and Figure 5.3.23), meanwhile *Per2*, *Nr1d1* and *Nr1d2* (also known as *Rev-Erbα* and *Rev-Erbβ* respectively) as well as the clock-controlled genes *Dbp* and *Nfil3* were highlighted in edgeR differential gene analysis with adjusted p-value of <0.05 (Figure 5.3.23). The exact nature of the role of *Maf* in circadian rhythm has yet to be investigated and is an area for future study.

Upstream regulators from DESeq2 analysis identified *Il10ra* and *Cited2* (Table 5.3.2A) with *Gata6* and *Csf1* also being identified as an upstream regulator in edgeR (Table 5.3.2B). As *Maf* has previously been identified in *Il-10* regulation and since Gata6-deficient peritoneal

tissue resident macrophages exhibited a 7.9 fold increase in *Maf* expression compared to wild type cells, this is consistent with previous data.

Validation of naïve RNA Sequencing was conducted in both male and female mice, to investigate if there were in fact sex specific difference as identified in RNA Sequencing analysis (Figure 5.3.22). qPCR indicated overall statistically significant difference by genotype when analysed by qPCR with both *Maf* and *Lyve1* demonstrating significant expression differences between $Maf^{fl/fl}Cx3cr1^{Cre/+}$ and $Maf^{fl/fl}Cx3cr1^{+/+}$ mice (Figure 5.3.27A). Correlation of DESeq2 and edgeR $\log_2$ fold change against that from qPCR indicated strong correlation in naïve tissue resident macrophages, further confirming the qPCR validation (Figure 5.3.28).

Protein expression of some of the selected targets along with the addition of folate receptor 2 based on recent publications (172,236) was confirmed by flow cytometry and indicated highly significant differences by genotype (Figure 5.3.29) for both LYVE1 and FOLR2.

In human tumour-associated macrophages, from multiple tumours, identified potential regulators of *FOLR2* gene expression including *MAF*, additionally *FOLR2* was found to correlate with *MAF* expression in breast carcinoma (236). *Folr2* and *Lyve1* have also been previously been identified as increased in gene expression in tissue resident peritoneal macrophages in *Bhlhe40* knockout mice, where *Maf* expression is also increased (243). A recent publication in the same $Maf^{fl/fl}$ mice in vasculature-associated adipose tissue macrophage (VAMs) resulted in loss of $CD206^{high}FOLR2^{+}$ macrophages in the large intestine in $Maf^{fl/fl}$ mice on multiple Cre lines including $Lyve1^{Cre/+}$, $LySM^{Cre/+}$ and $Csf1r^{Cre/+}$ mice (172).

In summary, both qPCR and flow cytometry validation across selected targets confirmed the naïve peritoneal tissue resident macrophage RNA sequencing gene expression discoveries at genomic and protein level. Increasing sample number would increase power, and fully elucidate if there were sex difference in peritoneal tissue resident macrophages. Future work in investigating the role of *Maf* in circadian rhythms and lipidomic analysis between mice would further validate the differential gene expression analysis. The data suggests expression of *Folr2* and *Lyve1* are regulated by *Maf* expression, and utilisation of the previously generated overexpression vectors in Chapter 3 could confirm this in peritoneal tissue resident macrophages.

5.4.4. RNA Sequencing of Peritoneal Tissue Resident Macrophages and Inflammatory Recruited Macrophages during Zymosan-Induced Inflammation

Following treatment with zymosan for 48 hr two populations of F4/80^{high} Tim4^{+} tissue resident macrophages and F4/80^{low} Tim4^{-} macrophages (Figure 5.3.30) were RNA sequenced. PCA analysis indicated clear variance of *Maf*$^{fl/fl}$*Cx3cr1*$^{Cre/+}$ and *Maf*$^{fl/fl}$*Cx3cr1*$^{+/+}$ mice in tissue resident macrophages (Figure 5.3.31A), but less so in inflammatory macrophages (Figure 5.3.31B). When tissue resident and inflammatory macrophages were combined, those from *Maf*$^{fl/fl}$*Cx3cr1*$^{+/+}$ mice display higher variance than those from *Maf*$^{fl/fl}$*Cx3cr1*$^{Cre/+}$ mice (Figure 5.3.31C).

Comparison of *Maf*$^{fl/fl}$*Cx3cr1*$^{+/+}$ and *Maf*$^{fl/fl}$*Cx3cr1*$^{Cre/+}$ tissue resident macrophages generated very few gene discoveries, with an adjusted p-value of <0.05 with only 3 genes common between both edgeR vs DESeq2 differential expression methods. However both edgeR and DESeq2 generated unique discoveries (Figure 5.3.35A). Differential gene analysis utilising only *Maf*$^{fl/fl}$*Cx3cr1*$^{+/+}$ mice expressing higher FPKM of *Maf* (>5) (Figure 5.3.9) could increase the genes discovered, however this would reduce the experimental power. Therefore increasing the sample number would increase statistical power and allow for additional analyses between high and low *Maf* expressing *Maf*$^{fl/fl}$*Cx3cr1*$^{+/+}$ mice to *Maf*$^{fl/fl}$*Cx3cr1*$^{Cre/+}$ mice, possibly elucidating additional *Maf* associated differential genes.

edgeR and DESeq2 differential gene analysis of zymosan treated inflammatory macrophages identified both *Maf* and *Lyve1* as being markedly changed (Figure 5.3.44A and Figure 5.3.45A). There were 32 common genes which have an adjusted p-value of <0.05, in both DESeq2 and edgeR differentially expressed analysis (Figure 5.3.46A). Of those gene discoveries with an adjusted p-value of <0.05 and a $\pm 1 \log_2$ fold change, 30 common genes remain between the two differential expression methods (Figure 5.3.46B).

Canonical pathway analysis of DESeq2 identified complement signalling, sphinogine-1-phosphate signalling (Figure 5.3.47) whilst edgeR additionally indicated phospholipase C signalling and *Ppara/Rxra* activation (Figure 5.3.48). *Ccl24* was identified as an important gene with a p-value of <0.05 in chemokine signalling and *Ccr3* signalling in both analyses (Figure 5.3.47 and Figure 5.3.48). Several upstream regulators were identified from the DESeq2 analysis, peroxisome proliferator-activated receptor A (*Ppara*) and liver X

receptors (LXRα and LXRβ encoded by *Nr1h3* and *Nr1h2* genes) in addition to previously identified *Gata6* and *Il-10ra* (Table 5.3.4).

Abca1 was identified in both analyses with a p-value of <0.05 (and) and is known to be an essential cholesterol transporter for LXR-mediated cholesterol efflux (244). LXRs have been demonstrated to inhibit inflammatory genes including IL-1b and IL-6 after stimulation with LPS (245). Furthermore both LXRs and PPARs have an important role in clearance of apoptotic cells by macrophages through *Tyro3*, *Axl* and *Mer*, and their ligands *Gas6* and Protein S (246), with *Gas6* being identified in DESeq2 analysis with a p-value of <0.05 (Figure 5.3.44). Additionally LXR activation includes retinoid acid receptor a (*Rara*) by direct binding and transactivation of the Rara promoter, highlighted as an upstream regulators in both analyses (Table 5.3.5 and Table 5.3.6), with both *C1qb* and *C1qc* identified in edgeR analysis (Figure 5.3.48).

Validation of the RNA sequence data from both tissue resident and inflammatory macrophage populations from zymosan induced mice was conducted by qPCR. When analysing a panel of 9 genes and overall statistically significant difference attributed to genotype was indicated between $Maf^{fl/fl}Cx3cr1^{Cre/+}$ and $Maf^{fl/fl}Cx3cr1^{+/+}$ mice (Figure 5.3.53). Correlation of DESeq2 and edgeR $\log_2$ fold change against that from qPCR indicated strong correlation in zymosan treated tissue resident macrophages and moderate-strong correlation in zymosan treated inflammatory macrophages, further confirming the qPCR validation (Figure 5.3.54). Whilst correlation of inflammatory DESeq2 and edgeR analyses demonstrated moderate-strong correlation, neither were deemed statistically significant, however additional sample number for validation could overcome this.

Flow cytometric validation indicated changed expression in CD38, FOLR2 in inflammatory macrophages, and VSIG4 in both populations (Figure 5.3.55). An alteration in MHCII expression on inflammatory macrophages between the two genotypes was consistent with previous findings in IL-$10^{-/-}$ mice (213). The consistent alteration in *Folr2* and *Lyve1* expression suggests *Maf* may directly regulates these targets across multiple macrophage populations, particularly when considering other studies in the literature.

5.4.5. Summary of Main Findings

In summary overall phenotyping of peritoneal tissue resident macrophages, together with analysis of macrophage proportions of peritoneal lavage indicated the constitutively expressed *Cre* and subsequent loss of *Maf* in *Maf*$^{fl/fl}$*Cx3cr1*$^{Cre/+}$ mice, resulted in no overt abnormalities in tissue resident macrophages generation or phenotype under naïve conditions between *Maf*$^{fl/fl}$*Cx3cr1*$^{Cre/+}$ and *Maf*$^{fl/fl}$*Cx3cr1*$^{+/+}$ mice.

RNA sequencing generated a number of differential gene discoveries, suggesting *Maf* may interact with the circadian rhythm signalling. Both qPCR and flow cytometric validation across selected targets confirmed the RNA sequence-based gene expression discoveries at genomic and protein level in tissue resident in naïve conditions. RNA sequencing also suggested possible sex variations, however increased sample number would increase power, and fully elucidate if there were sex difference in peritoneal tissue resident macrophages.

Following treatment with zymosan for 48 hr two populations of tissue resident macrophage and recruited inflammatory macrophages were RNA sequenced, suggesting the role of *Maf* in lipidomic mediated inflammatory response and apoptotic clearance through LXRs and PPARs, however this area requires further exploration. Zymosan treated peritoneal tissue resident macrophages displayed few differential gene discoveries whereas recruited inflammatory macrophages generated 10-fold more differentially regulated genes.

The variable *Maf* expression in zymosan treated peritoneal tissue resident macrophages from *Maf*$^{fl/fl}$*Cx3cr1*$^{+/+}$ mice may indicate that earlier time points could be beneficial in elucidating the role of *Maf* in mild immune challenge in tissue resident macrophages, with additional samples from the tested time point increasing statistical power and possibly allowing for additional gene discoveries.

5.4.5.1. Hypothesis of Findings

It is hypothesised that loss of the transcription factor *Maf* has a more important role in the regulation of monocyte derived macrophage than in tissue resident macrophages in the peritoneal cavity and may have a more substantial role in the resolution of inflammation rather than in naïve conditions.

Chapter 6

General Discussion

6.1. Summary of Main Findings

6.1.1. Development of a System to Explore Tissue Resident Macrophages

The aim of this thesis was to determine the role of select transcription factors in tissue resident macrophages and their effect on the tissue resident phenotype. Therefore it was fundamental to establish a system in which these transcription factors could be investigated, and a reliable validation method for these targets.

Utilising GFP and rCD2 reporter *Maf* overexpression lentiviruses, successfully enforced *Maf* expression was validated by qPCR in infected MØPs and BMDMs (Figure 3.3.4). Additionally protein expression was determined by flow cytometry, with two previously published MAF antibodies investigated (section 3.3.3). GFP reporter *Maf* overexpression lentivirus demonstrated a consistent statistically significant increase in *Maf* expression in infected MØPs, M-CSF differentiated MØPs and BMDMs, however only with the Thermo Fisher MAF antibody (section 3.3.3).

Additionally, determination of the nuclear localisation of MAF immunoreactivity by colocalization of with the DNA marker DAPI, demonstrated that the Thermo Fisher antibody was more specific to MAF compared with that of the BD Bioscience antibody (Figure 3.3.14). However the shRNA lentivirus which was developed prior to the thesis was shown to have no significant effect on *Maf* expression by qPCR or by flow cytometry in any of the infected MØPs, M-CSF differentiated MØPs and BMDMs cell types however this was not a concern due to alternatives for knockdown of *Maf* in MØPs and BMDMs could be generated from *Maf* knockout mice.

Whilst generation of overexpression lentivirus for *Mlf1* were demonstrated by qPCR to be successful (Figure 3.3.5), as there was no commercial flow cytometry antibody available for protein validation of MLF1, this thesis ultimately concentrated on the role of *Maf* in tissue resident macrophages. This validation system was then employed for the study of *Maf* in knockout mice. Generation of $Maf^{fl/fl}Cx3cr1^{Cre/+}$ and $Maf^{fl/fl}Cx3cr1^{CreERT/+}$ mice for this thesis through crossing of $Maf^{fl/fl}$ mice with $Cx3cr1^{Cre}$ and $Cx3cr1^{CreERT}$ mice resulted in mice homozygous for the *Maf* floxed allele and heterozygous for either $Cx3cr1^{Cre}$ or $Cx3cr1^{CreERT}$ or control mice with wildtype *Maf* and *Cx3cr1* expression in $Maf^{fl/fl}Cx3cr1^{+/+}$ mice.

MΦPs were generated from both male and female *Maf*$^{fl/fl}$*Cx3cr1*$^{Cre/+}$ and *Maf*$^{fl/fl}$*Cx3cr1*$^{+/+}$ mice, as alternatives to the shRNA lentivirus tested in Chapter 3. Both qPCR (Figure 5.3.6) and flow cytometry (Figure 5.3.5) determined statistically significant reduction of *Maf* expression at a genomic and protein level respectively. Therefore these cell lines could be utilised for *in vitro* assays such as for treatment with *E. Coli* LPS time course experiments (Figure 5.3.6 and Figure 5.3.7).

Pilot experiments to determine the efficacy of tamoxifen on knockdown of *Maf* in microglia from *Maf*$^{fl/fl}$*Cx3cr1*$^{CreERT/+}$ mice, either through intraperitoneal injection in corn oil (Figure 4.3.1) or tamoxifen-sucrose chow (Figure 4.3.2) were evaluated by flow cytometry. qPCR validation of *Maf* in Maf$^{fl/fl}$Cx3cr1$^{CreERT/+}$ microglia following three intraperitoneal injection of 200 mg/kg tamoxifen demonstrated statistically significant reduction in *Maf* expression when compared to those in *Maf*$^{fl/fl}$*Cx3cr1*$^{+/+}$mice ().

In the constitutive knockout context, protein expression of MAF was reduced in microglia from *Maf*$^{fl/fl}$*Cx3cr1*$^{Cre/+}$ mice when compared to *Maf*$^{fl/fl}$*Cx3cr1*$^{+/+}$mice (Figure 4.3.4). qPCR validation of *Maf* in *Maf*$^{fl/fl}$*Cx3cr1*$^{Cre/+}$ demonstrated statistically significant reduction in *Maf* expression when compared to *Maf*$^{fl/fl}$*Cx3cr1*$^{+/+}$ mice (Figure 4.3.6). Inducible knockout of *Maf* in microglia was analysed by qPCR from Maf$^{fl/fl}$Cx3cr1$^{CreERT/+}$ mice following treatment with tamoxifen (), which indicated some residual *Maf* expression, compared to the complete loss in *Maf*$^{fl/fl}$*Cx3cr1*$^{Cre/+}$ mice (Figure 4.3.6), when compared to *Maf*$^{fl/fl}$*Cx3cr1*$^{+/+}$ mice. Therefore all further work in this thesis focused on *Maf*$^{fl/fl}$*Cx3cr1*$^{Cre/+}$ mice rather than in Maf$^{fl/fl}$Cx3cr1$^{CreERT/+}$ mice, removing any possible side effects of tamoxifen and allowing both microglia and peritoneal tissue resident macrophages to be studied in the same animal, reducing the number of animals required for this thesis.

In *Maf*$^{fl/fl}$*Cx3cr1*$^{Cre/+}$ mice protein expression of MAF in peritoneal tissues resident macrophages displayed significant reduction between *Maf*$^{fl/fl}$*Cx3cr1*$^{+/+}$ and *Maf*$^{fl/fl}$*Cx3cr1*$^{Cre/+}$ mice (Figure 5.3.2). It is important to note that the MAF antibody, which was validated in Chapter 3 of this thesis, may at least be only partially specific, or specific but with high background which is not controlled for by the isotype control. This conclusion is supported by the correspondence of *Maf* ΔMFI with qPCR validation in constitutive *Maf*$^{fl/fl}$*Cx3cr1*$^{Cre/+}$ mice when compared to *Maf*$^{fl/fl}$*Cx3cr1*$^{+/+}$ mice.

In summary, this thesis resulted in the generation of validated full length *Maf* overexpression constructs in two reporter lentiviral vectors which can be further utilised for the study of the role of *Maf* in cells *in vitro* or *in vivo* instead of current truncated *Maf*

sequences (100,157–159). Additionally generation of validated MΦP cell lines from *Maf*$^{fl/fl}$*Cx3cr1*$^{Cre/+}$ and *Maf*$^{fl/fl}$*Cx3cr1*$^{+/+}$ mice which provide a constitutive knockout of *Maf* compared to the current siRNAs utilised (155–157).

More importantly this thesis has generated and validated conditional and constitutive *Maf* knockout mice lines for the study of the role of *Maf* in myeloid cells *in vivo* rather than the more common *in vitro* work with cells lines such as RAW264.7 cells (100,158,159) or *ex vivo* bone marrow derived cells infected with siRNAs (155,157).

6.1.2. Modified Phenotype in Maf$^{fl/fl}$Cx3cr1$^{Cre/+}$ and Maf$^{fl/fl}$Cx3cr1$^{+/+}$ Mice

Utilising the *Maf*$^{fl/fl}$*Cx3cr1*$^{Cre/+}$ and *Maf*$^{fl/fl}$*Cx3cr1*$^{+/+}$ mice generated in this thesis, the role of *Maf* on tissue resident macrophage phenotype, or any effects on generation or retention of these cells, could be investigated. Gross phenotyping of microglia indicated common myeloid markers displayed little change except for PU.1 (Figure 4.3.5) and indicated no overt abnormalities or phenotype under naïve conditions between *Maf*$^{fl/fl}$*Cx3cr1*$^{Cre/+}$ and *Maf*$^{fl/fl}$*Cx3cr1*$^{+/+}$ mice by flow cytometry. Whilst absolute number of microglia determined by flow cytometry (Figure 4.3.4) indicated no statistically significant differences, this does not consider the *in situ* 3D structure of the brain or any possible effects on total cell number obtained through tissue dissociation and cell isolation.

Immunofluorescent microscopy of coronal brain slices indicated a statistically significant increase in microglia number in *Maf*$^{fl/fl}$*Cx3cr1*$^{Cre/+}$ mice (Figure 4.3.8E), and consequently a reduction in distance between microglia across multiple regions of the brain, when compared to *Maf*$^{fl/fl}$*Cx3cr1*$^{+/+}$ mice (Figure 4.3.8G). With no apparent differences in area of coverage (Figure 4.3.8F), alluding to *Maf*$^{fl/fl}$*Cx3cr1*$^{Cre/+}$ microglia having altered ramifications, which would require further investigation through 3D morphological analysis. As the C3 area of the hippocampus demonstrated statistical significance, increased study of additional hippocampal regions along with increased sample number could further elucidate these results.

The reduction in proportion and absolute number of MHCII^{-} CD206^{high} BAMs was statistically significant, as was the increase in the proportion of MHCII^{+} CD206^{low} BAM population (Figure 4.3.7D). However absolute number of cells in BAM populations indicated only MHCII^{-} CD206^{high} BAMs to be statistically significant (Figure 4.3.7E), whilst

MHCII^{+} CD206^{low} BAM population was not significant, possibly due to low sample number. This loss of the MHCII^{+} CD206^{low} BAM population is concurrent with recent literature (172).

In peritoneal tissue resident macrophages, defined as CD11b^{high}, F4/80^{high} and Tim4^{+}, under steady state naïve conditions there were no significant differences in percentage of CD11b^{high}, F4/80^{high} and Tim-4^{+} tissue resident macrophages in peritoneal cavity lavage (Figure 5.3.1B). Whilst absolute number suggested an increase in total number of peritoneal tissue resident macrophages in *Maf*$^{fl/fl}$*Cx3cr1*$^{Cre/+}$ mice when compared to *Maf*$^{fl/fl}$*Cx3cr1*$^{+/+}$ mice, this was not statistically significant (Figure 5.3.1C).

To investigate gross phenotypic differences of peritoneal tissue resident macrophages in *Maf*$^{fl/fl}$*Cx3cr1*$^{Cre/+}$ and *Maf*$^{fl/fl}$*Cx3cr1*$^{+/+}$ mice, common myeloid markers were studied using flow cytometry (Figure 5.3.3). Among the 16 myeloid markers only CX3CR1 displayed any clear differences in protein expression, with *Maf*$^{fl/fl}$*Cx3cr1*$^{+/+}$ exhibiting higher expression than in *Maf*$^{fl/fl}$*Cx3cr1*$^{Cre/+}$ mice (Figure 5.3.3). This is expected due to the genotype of the mice.

In summary, the role of *Maf* in these two tissue resident macrophage populations, microglia and peritoneal CD11b^{high}, F4/80^{high} and Tim4^{+} macrophages, indicated *Maf* resulted in different phenotypic control. Compared to *Maf*$^{fl/fl}$*Cx3cr1*$^{+/+}$ mice, *Maf*$^{fl/fl}$*Cx3cr1*$^{Cre/+}$ mice exhibited a mild microgliosis under naïve conditions and a loss of the MHCII^{+} CD206^{low} BAM population. In contrast, peritoneal tissue resident macrophages showed no significant changes in overall phenotype or cell number under naïve conditions between *Maf*$^{fl/fl}$*Cx3cr1*$^{Cre/+}$ and *Maf*$^{fl/fl}$*Cx3cr1*$^{+/+}$ mice.

6.1.3. Does *Maf*-deficiency have a Significant Impact on Tissue Resident Macrophage Transcriptome

6.1.3.1. RNA Sequencing of Naïve Microglia in *Maf*$^{fl/fl}$*Cx3cr1*$^{Cre/+}$ and *Maf*$^{fl/fl}$*Cx3cr1*$^{+/+}$ Mice

RNA sequencing of *Maf*$^{fl/fl}$*Cx3cr1*$^{+/+}$and *Maf*$^{fl/fl}$*Cx3cr1*$^{Cre/+}$ microglia resulted in almost 2,000 differential gene expression discoveries by both DESeq2 and edgeR, with 1,581 common genes with an adjusted p-value of <0.05, and 770 of these common genes with a ±1$\log_2$ fold change between the two differential expression methods (Figure 4.3.18).

Overall a considerable number of key immune related genes were evident within both DESeq2 and edgeR datasets, with significant changes in chemokines, chemokine receptors, cytokines, the complement system, pattern recognition receptors and MHC expression, along with several upstream regulators indicating a proinflammatory polarisation of microglia in *Maf*$^{fl/fl}$*Cx3cr1*$^{Cre/+}$ mice when compared to *Maf*$^{fl/fl}$*Cx3cr1*$^{+/+}$ mice under steady state conditions.

Canonical pathway analysis in IPA highlighted IL-12 signalling and production pathway, with IL-10 signalling pathway additionally identified in the DESeq2 analysis (), however neither indicates a significant Z score (defined as ±2 by IPA). *Il10ra* was also identified as an upstream regulator and was significantly reduced in both DESeq2 and edgeR analysis with a Z-score of -6.823 and -6.605 respectively and a p-value of overlap of 4.71E-23 and 6.26E-25 respectively (Figure 4.3.14 and Figure 4.3.17).

Therefore the statistically significant changes in *Il-10* and its receptor subunits (*Il10ra* and *Il10rb*), and likewise IL-12 receptor subunits (*Il12rb1* and *Il12rb2*), align with the literature regarding the role of *Maf* a potent activator of interleukin-10 (*Il-10*) gene expression in macrophages, and suppression of *Il-12* gene transcription (105) in *in vitro* and *ex vivo* studies. Whilst the effect of loss of *Il-10* has been demonstrated to result in this more proinflammatory transcriptome previously (247), it has not been demonstrated to be due to the loss of *Maf* in microglia *in vivo*.

Whilst it is recognised that enzymatic isolation of microglia can result in a pseudo *ex vivo* activation signature. As the differential gene discovery analysis is relative between the *Maf*$^{fl/fl}$*Cx3cr1*$^{Cre/+}$ and *Maf*$^{fl/fl}$*Cx3cr1*$^{+/+}$ phenotypes, it indicates that loss of *Maf* expression in microglia results, at a minimum, in a more reactive transcriptome or at most a

prolonged proinflammatory primed transcriptome under naïve conditions, potentially through the loss of *Il-10* due to *Maf* as its predominant activator. Additionally the loss of *Il-10* expression, and an overall more proinflammatory primed transcriptome indicates further study is required to determine the role of *Maf* in neuroinflammation.

6.1.3.2. RNA Sequencing of Naïve Peritoneal Tissue Resident Macrophages in *$Maf^{fl/fl}Cx3cr1^{Cre/+}$ and $Maf^{fl/fl}Cx3cr1^{+/+}$ Mice*

Meanwhile, study of naïve peritoneal tissue resident macrophages by RNA sequencing possibly indicated sex variations between the samples with few common genes which have an adjusted p-value of <0.05, with female mice generating 122 unique genes and male mice generating 68 (Figure 5.3.18A). When including sex into the model for DESeq2 or edgeR, which have an adjusted p-value of <0.05, resulted in 97 shared gene discoveries, with edgeR generating 51 unique genes and DESeq2 generating 12 (Figure 5.3.21A). Of those common differential genes 16 had a $\pm 1 \log_2$ fold change, with edgeR generating 20 distinct genes and DESeq2 9 (Figure 5.3.21B). Increasing sample number would increase power, and fully elucidate if there were sex difference in peritoneal tissue resident macrophages. Additionally the increased power may prove useful in generating more differential gene discoveries in naïve peritoneal tissue resident macrophages and would at a minimum reduce biological "noise" in the RNA sequencing.

Canonical pathway analysis with sex in the matrix highlighted several key macrophage pathways including multiple fatty acid signalling pathways including eicosanoid, phospholipases and leukotriene pathways (and Figure 5.3.23). Investigation into lipidomic differences in these pathways and any downstream effects in the peritoneal cavity requires future work.

Of interest, whilst samples were collected at the same time of day, circadian rhythm signalling pathways indicated differences. Canonical clock genes such as *Cry2* and *Per3* were evident in both analyses when sex is included in the analysis matrix (and Figure 5.3.23), meanwhile *Per2*, *Nr1d1* and *Nr1d2* (also known as *Rev-Erbα* and *Rev-Erbβ* respectively) as well as the clock-controlled genes *Dbp* and *Nfil3* were highlighted in edgeR differential gene analysis (Figure 5.3.23). The exact nature of the role of *Maf* in circadian rhythm has yet to be investigated and is an area for future study.

Validation of naïve RNA Sequencing by qPCR indicated overall statistically significant difference by genotype when analysed 3-way ANOVA, with both *Maf* and *Lyve1*

demonstrating significant expression differences between *Maf*$^{fl/fl}$*Cx3cr1*$^{Cre/+}$ and *Maf*$^{fl/fl}$*Cx3cr1*$^{+/+}$ mice (Figure 5.3.27A). Correlation of DESeq2 and edgeR $\log_2$ fold change against qPCR fold change indicated strong correlation coefficient of 0.9409275 and 0.9336324 respectively (Figure 5.3.28) in naïve tissue resident macrophages, further confirming the qPCR validation (Figure 5.3.28).

Unlike in naïve microglia, in naïve peritoneal tissue resident macrophages did not display the same proinflammatory transcriptome. However a number of interesting potential future investigations have been unveiled, with *Maf*-deficiency highlighting interaction with several lipidomic pathways and clock genes. *Maf* has repeatedly been demonstrated to be tissue and cell specific, with differences in *Maf*-deficiency in microglia and naïve tissue resident macrophages transcriptome corresponding with this.

6.1.3.3. RNA Sequencing of Peritoneal Tissue Resident Macrophages and Inflammatory Recruited Macrophages during Zymosan-Induced Inflammation in *Maf*$^{fl/fl}$*Cx3cr1*$^{Cre/+}$ *and Maf*$^{fl/fl}$*Cx3cr1*$^{+/+}$ *Mice*

As *Maf* has previously been suggested to control the phenotypic switch of macrophages due being an activator of *Il-10*, and suppression of *Il-12* gene transcription, to try and elucidate what role *Maf* played in mild inflammation of the peritoneal cavity. Following intraperitoneal injection with zymosan for 48 hr two populations of CD11b^{high}, F4/80^{high}, Tim4^{+} tissue resident macrophages and recruited inflammatory, predominantly monocyte-derived, CD11b^{high} F4/80^{low} Tim4^{-} macrophages (Figure 5.3.30) were analysed by RNA sequencing. Comparison of *Maf*$^{fl/fl}$*Cx3cr1*$^{+/+}$ and *Maf*$^{fl/fl}$*Cx3cr1*$^{Cre/+}$ tissue resident macrophages generated very few gene discoveries, with an adjusted p-value of <0.05 with only 3 genes common between both edgeR vs DESeq2 differential expression methods.

Maf expression in control *Maf*$^{fl/fl}$*Cx3cr1*$^{+/+}$ mice tissue resident macrophages were variable and differential gene analysis utilising only those *Maf*$^{fl/fl}$*Cx3cr1*$^{+/+}$ mice expressing higher FPKM of *Maf* (>5 FPKM) (Figure 5.3.9) could increase the differential genes discovered, however this would reduce the overall experimental power. Therefore increasing the sample number would increase statistical power and allow for additional analyses between “high” and “low” *Maf* expressing *Maf*$^{fl/fl}$*Cx3cr1*$^{+/+}$ mice as determined by FPKM to *Maf*$^{fl/fl}$*Cx3cr1*$^{Cre/+}$ mice, possibly elucidating additional *Maf* associated differential genes. *Maf* expression has previously been demonstrated to change in mouse colon macrophages treated with either a dextran sodium sulphate-induced colitis or acetic acid–

induced colitis mucosal inflammation model (159). The variable *Maf* expression in zymosan treated tissue resident macrophages may indicate that *Maf* expression changes during response to inflammatory stimuli in the peritoneal cavity, and therefore earlier time points could prove of more interest to investigate the role of *Maf* in the response to inflammation in peritoneal tissue resident macrophages.

edgeR and DESeq2 differential gene analysis of zymosan recruited inflammatory macrophages identified 32 common genes which have an adjusted p-value of <0.05, in both DESeq2 and edgeR differentially expressed analysis (Figure 5.3.46A). Of those gene discoveries with an adjusted p-value of <0.05 and ±1$\log_2$ fold change, 30 common genes remain between the two differential expression methods (Figure 5.3.46B).

Validation of the RNA sequence data from both tissue resident and inflammatory macrophage populations from zymosan induced mice was conducted by qPCR. When analysing a panel of 9 genes and overall statistically significant difference attributed to genotype was indicated between $Maf^{fl/fl}Cx3cr1^{Cre/+}$ and $Maf^{fl/fl}Cx3cr1^{+/+}$ mice ().

Correlation of DESeq2 and edgeR $\log_2$ fold change against that from qPCR indicated strong correlation in zymosan treated tissue resident macrophages and moderate-strong correlation in zymosan treated inflammatory macrophages, further confirming the qPCR validation (Figure 5.3.54). Whilst correlation of inflammatory DESeq2 and edgeR analyses demonstrated moderate-strong correlation, neither were deemed statistically significant, however additional sample number for validation could overcome this.

Interestingly, under mild immune challenge with zymosan, peritoneal tissue resident macrophages and recruited inflammatory macrophages demonstrate very different transcriptomic changes between $Maf^{fl/fl}Cx3cr1^{Cre/+}$ and $Maf^{fl/fl}Cx3cr1^{+/+}$ mice. With tissue resident macrophages displaying little to no difference in transcriptome, whereas recruited inflammatory macrophages generated 10-fold more differentially regulated genes. This is suggestive of *Maf* having a more important role in regulation of monocyte derived macrophage transcriptome than in tissue resident macrophages in the peritoneal cavity.

However the number of differentially expressed genes between $Maf^{fl/fl}Cx3cr1^{Cre/+}$ and $Maf^{fl/fl}Cx3cr1^{+/+}$ mice is still very low in both macrophage populations for what is believed to be a master regulator. This could be partially due to zymosan eliciting an acute self-resolving inflammatory model, and whether a more chronic inflammatory model such as

thioglycolate-induced peritonitis would be beneficial requires further investigation. Additionally utilisation of thioglycolate-induced peritonitis, which has been demonstrated to be slower to resolve than that of zymosan-induced (248), and recruit many monocyte-derived inflammatory macrophages may allow capture of kinetics of activation, resolution of inflammation and repopulation of tissue resident macrophages in *Maf*$^{fl/fl}$*Cx3cr1*$^{Cre/+}$ and *Maf*$^{fl/fl}$*Cx3cr1*$^{+/+}$ mice, which has yet to be investigated.

6.2. *Maf* Regulates Alternatively Activated Macrophage Phenotype

Whilst RNA sequencing of naive microglia, peritoneal tissue resident macrophages under steady state naïve conditions and following zymosan-induced inflammation indicated difference in transcriptome, it became apparent that a number of the differential gene discoveries were common between analyses of these macrophage populations, suggestive of *Maf* specific regulation across multiple macrophage populations.

These include *Folr2*, encodes for folate receptor beta, a member of a family of reduced folate and folic acid receptors that also include folate receptor alpha, gamma and delta. Folate receptor beta has been suggested to be restricted to myeloid cells, and a marker for alternative anti-inflammatory activation of tissue resident and tumour associated macrophages (236,249). It has previously been suggested that potential regulators of *Folr2* could include *Spi1* (which encodes PU.1), *Maf* and *Nr1h3* (which encodes LXRa) in human tumour associated macrophages (TAMs) (236). Upstream regulator analysis of zymosan-recruited peritoneal inflammatory macrophages identified liver X receptors (LXRα and LXRβ encoded by *Nr1h3* and *Nr1h2* genes) in the DESeq2 analysis (Table 5.3.4).

Lyve1 was also identified across multiple RNA sequencing analyses in $Maf^{fl/fl}Cx3cr1^{Cre/+}$ and $Maf^{fl/fl}Cx3cr1^{+/+}$ mice macrophage populations. *Lyve1* (Lymphatic vessel endothelial hyaluronan receptor 1) has been demonstrated to be expressed on arterial resident macrophages, and binds hyaluronan expressed by smooth muscle, which has been demonstrated to sustain large blood vessel functional homeostasis through modulating collagen (250). $LYVE1^{+}$ tissue resident macrophage populations have also been demonstrated to exist in multiple tissues including the heart (251), lung (252), skeletal (253), mammary gland (254), adipose tissue (172) and the eye (255).

Lyve1 expressing adipose tissue resident macrophage have been indicated to be distinguishable from other macrophages due to their expression of ATP-binding cassette transporter G1 (*Abca1*) and the lack of *Nr1h3* expression (256). In zymosan-recruited inflammatory peritoneal macrophages both *Lyve1* and *Folr2* were identified in edgeR analysis with an adjusted p-value <0.05 and with $\log_2$ fold change of -5.459643 and -3.314444 respectively (). *Abca1* was also differentially expressed in these cells between $Maf^{fl/fl}Cx3cr1^{Cre/+}$ and $Maf^{fl/fl}Cx3cr1^{+/+}$ mice, with an adjusted p-value of <0.05 and a $\log_2$ fold change of -1.167818 and -1.183922 in DESeq2 and edgeR analyses respectively

(and). *Abca1* was also identified in peritoneal tissue resident macrophages treated with zymosan in the DESeq2 analysis, with a -0.561707 log_2 fold change (Figure 5.3.33). However neither *Lyve1* nor *Folr2* were identified in peritoneal tissue resident macrophages following zymosan induced inflammation by RNA sequencing and this was confirmed by flow cytometric validation (Figure 5.3.29).

Whilst *Folr2* is not identified in naïve peritoneal tissue resident macrophage RNA sequencing as being significantly different between *Maf* expressing and deficient cells, *Lyve1* was identified with an adjust p-value <0.05 and a -3.2438146 log_2 fold change between the two genotypes (Figure 5.3.20). However when validating protein expression of LYVE1 on naïve peritoneal tissue resident macrophages, FOLR2 was also investigated and displayed statistically significant reduction (Figure 5.3.29).

Lyve1 and *Folr2* were also identified in both edgeR and DESeq2 analyses of naïve microglia RNA sequencing (Figure 4.3.15 and Figure 4.3.12). However this may be evident of MHCII^{-} CD206^{high} BAM population contamination in the microglia RNA sequencing, as LYVE1 and FOLR2 have been demonstrated to be expressed by MHCII^{-} CD206^{high} BAMs and not MHCII^{+} CD206^{low} BAMs nor microglia (172). Additionally LYVE1 and FOLR2 protein expression has been utilised as differential expression markers for distinguishing microglia from BAMs (189,257). In BAMs and vascular-associated intestinal adipose tissue resident macrophages it has been indicated LYVE1 and FOLR2 protein expression is lost in *Maf*-deficient mice (172). This contamination could be overcome with employing single cell sequencing instead of bulk RNA, however this would result in reduced sequencing depth, or additional staining when employing FACS to better separate the microglial and BAM populations (Figure 4.3.7B).

The recent advancement in binary transgenic split Cre system in mice (258), has further demonstrated the BAM specificity of *Lyve1* expression, as utilised to generate *Lyve1*^{nCre}*Cx3cr1*^{cCre} animals exclusively targeting BAMs and not microglia, and likewise *Sall1*^{nCre}*Cx3cr1*^{cCre} mice specifically targeting microglia (258). Crossing of the *Maf*$^{fl/fl}$ mice onto these split Cre lines would allow investigation of what role *Maf* has in either BAMs or microglial independently of each other.

Hyaluronan receptor-like molecule stabilin-1 (encoded by *Stab1*), is a close relative of the hyaluronan receptor CD44 (259). *Stab1* has been shown to be induced in macrophages upon alternative activation (260), and Stabilin-1 expression on tumour associated macrophages has been demonstrated to positively correlate with LYVE-1 expression (261).

Stabilin-1 has been demonstrated to act as a phagocytic receptor on alternatively activated macrophages, mediating the clearance of apoptotic cells dependent on phosphatidylserine (262).

Liver sinusoidal endothelial cells are well-established to express *Lyve1* and *Stab1* (263), with *Maf* being identified as a regulator of their expression (260). *Stab1* was identified in naïve peritoneal tissue resident macrophages with a p-value <0.05, and a $\log_2$ fold change of -0.9508501 and -0.9642315 in edgeR and DESeq2 analysis respectively. Likewise in zymosan recruited inflammatory macrophages *Stab1* had a p-value of <0.05 and was reduced in both edgeR and DESeq2 analyses with a $\log_2$ fold change of -1.666519 and -1.652378 respectively.

MHCII expression has been inversely associated with that of LYVE1 on macrophages (252,253,264), which is concurrent with changes in MHCII expression through flow cytometric validation of zymosan-recruited inflammatory macrophages between *Maf*$^{fl/fl}$*Cx3cr1*$^{Cre/+}$ and *Maf*$^{fl/fl}$*Cx3cr1*$^{+/+}$ mice, and previous findings in *Il-10*$^{-/-}$ mice (213).

As previously discussed (in section 5.4.3), *Folr2* and *Lyve1* have also been previously been identified to increase in gene expression in tissue resident peritoneal macrophages in *Bhlhe40* knockout mice, where *Maf* expression is increased (243). Additionally *Stab1* and *Cd163* were highlighted in this study to also be increased, suggesting their transcriptional regulation by *Maf* (243).

As well as classically activated macrophages, alternatively activated macrophages have been demonstrated to be generated through stimulus with IL-10/M-CSF or a combination of with interleukin-4 and interleukin-13 (IL-4/IL-13) (265). *Lyve1*, *Folr2*, *Stab1*, and *Abca1* expression in macrophages corresponds to a group of genes identified to be associated with IL-10/M-CSF associated alternative activation pathway of macrophages (236,252,266–269). With the M-CSF encoding gene (*Csf1*) was identified as an upstream regulator in edgeR analysis of naïve peritoneal tissue resident macrophages (Table 5.3.2).

These alternative activated macrophages have been reported to express an immature phenotype associated with expression of a number of genes including *Cd163* (270). *Cd163* was identified to be reduced in the microglia RNA sequencing between *Maf*$^{fl/fl}$*Cx3cr1*$^{Cre/+}$ and *Maf*$^{fl/fl}$*Cx3cr1*$^{+/+}$ mice, in both edgeR and DESeq2 analyses, with an adjusted p-value of <0.05 and with a $\log_2$ fold change of -2.824617 and -2.8318043 respectively (and). Additionally *Cd163* had an adjusted p-value of <0.05 with a -0.8843006 $\log_2$ fold change in

edgeR analysis of naïve peritoneal tissue resident macrophages. CD163 expression has previously been correlated with MAF expression on alternatively activated human macrophages in non-small-cell lung cancer (271) and utilised combination staining in Crohn's disease (272) and in Hodgkin Lymphoma (273).

In summary several genes associated with IL-10/M-CSF alternative activation pathway of macrophages, have been demonstrated to be downregulated in *Maf*$^{fl/fl}$*Cx3cr1*$^{Cre/+}$ mice when compared to *Maf*$^{fl/fl}$*Cx3cr1*$^{+/+}$ mice, across multiple macrophage populations. Therefore it would be of interest to investigate how *Maf*-deficiency effects tissue resident macrophage and monocyte-derived inflammatory macrophages respond in an alternative activation of macrophages model, such as intraperitoneal injection IL-4/IL-13, or utilising a helminth model, which have been previously demonstrated to result in alternative macrophage activation (274).

6.3. Conclusion

Ultimately this thesis has resulted in the generation of several cell lines, *Maf* overexpression constructs for the study of the role of *Maf* and the creation of a conditional and constitutive cell-restricted *Maf* knockout mouse lines for the study of the role of *Maf* in myeloid cells.

The role of *Maf* was investigated in two tissue resident macrophage populations: microglia and peritoneal CD11b^{high}, F4/80^{high} and Tim4^{+} macrophages. Overall indicating *Maf* played different phenotypic control of these populations, with evidence of microgliosis in *Maf*$^{fl/fl}$*Cx3cr1*$^{Cre/+}$ under naïve conditions when compared to *Maf*$^{fl/fl}$*Cx3cr1*$^{+/+}$ mice and loss of the MHCII^{+} CD206^{low} BAM population. In contrast, no significant changes in overall phenotype or peritoneal tissue resident macrophages generation under naïve conditions between *Maf*$^{fl/fl}$*Cx3cr1*$^{Cre/+}$ and *Maf*$^{fl/fl}$*Cx3cr1*$^{+/+}$ mice.

Transcriptomic analysis of *Maf*$^{fl/fl}$*Cx3cr1*$^{Cre/+}$ and *Maf*$^{fl/fl}$*Cx3cr1*$^{+/+}$ mice indicated that loss of *Maf* expression in microglia resulted in a more reactive proinflammatory primed transcriptome under naïve conditions, potentially through the loss of *Il-10*, due to the role of *Maf* as its predominant activator. Unlike naïve microglia, naïve peritoneal tissue resident macrophages did not display the same proinflammatory transcriptome. However a number of possible future investigations have been disclosed, with *Maf*-deficiency highlighting interaction with several lipidomic pathways and clock genes. In zymosan-induced peritonitis *Maf* was suggested to play a more important role in regulation of monocyte derived macrophage transcriptome than that of tissue resident macrophages in the peritoneal cavity.

However across multiple transcriptomic analyses several genes associated with an IL-10/M-CSF alternative activation pathway of macrophages have been demonstrated to be downregulated in *Maf*$^{fl/fl}$*Cx3cr1*$^{Cre/+}$ mice, when compared to *Maf*$^{fl/fl}$*Cx3cr1*$^{+/+}$ mice. Therefore whilst the role of *Maf* in control tissue resident macrophage generation, and transcriptome has been demonstrated to be tissue and cell specific, there appears to be an overarching phenotype change through the loss of alternatively activated macrophage phenotype.

6.4. References

1. Gordon S. Elie Metchnikoff: Father of natural immunity. Eur J Immunol. 2008;38(12):3257–64.

2. van Furth R, Cohn ZA, Hirsch JG, Humphrey JH, Spector WG, Langevoort HL. The mononuclear phagocyte system: a new classification of macrophages, monocytes, and their precursor cells. Bull World Health Organ. 1972;46(6):845–52.

3. Fogg DK, Sibon C, Miled C, Jung S, Aucouturier P, Littman DR, et al. A Clonogenic Bone Marrow Progenitor Specific for Macrophages and Dendritic Cells. Science [Internet]. 2006 Jan 6 [cited 2022 Jan 12]; Available from: https://www.science.org/doi/abs/10.1126/science.1117729

4. Hettinger J, Richards DM, Hansson J, Barra MM, Joschko AC, Krijgsveld J, et al. Origin of monocytes and macrophages in a committed progenitor. Nat Immunol. 2013 Aug;14(8):821–30.

5. Moore MAS, Metcalf D. Ontogeny of the Haemopoietic System: Yolk Sac Origin of In Vivo and In Vitro Colony Forming Cells in the Developing Mouse Embryo*. Br J Haematol. 1970;18(3):279–96.

6. Ginhoux F, Greter M, Leboeuf M, Nandi S, See P, Gokhan S, et al. Fate Mapping Analysis Reveals That Adult Microglia Derive from Primitive Macrophages. Science [Internet]. 2010 Nov 5 [cited 2022 Jan 11]; Available from: https://www.science.org/doi/abs/10.1126/science.1194637

7. Schulz C, Perdiguero EG, Chorro L, Szabo-Rogers H, Cagnard N, Kierdorf K, et al. A Lineage of Myeloid Cells Independent of Myb and Hematopoietic Stem Cells. Science. 2012 Apr 6;336(6077):86–90.

8. Hashimoto D, Chow A, Noizat C, Teo P, Beasley M, Leboeuf M, et al. Tissue-Resident Macrophages Self-Maintain Locally throughout Adult Life with Minimal Contribution from Circulating Monocytes. Immunity. 2013 Apr;38(4):792–804.

9. Yona S, Kim KW, Wolf Y, Mildner A, Varol D, Breker M, et al. Fate Mapping Reveals Origins and Dynamics of Monocytes and Tissue Macrophages under Homeostasis. Immunity. 2013 Jan;38(1):79–91.

10. Bertrand JY, Jalil A, Klaine M, Jung S, Cumano A, Godin I. Three pathways to mature macrophages in the early mouse yolk sac. Blood. 2005 Nov 1;106(9):3004–11.

11. Perdiguero EG, Geissmann F. Development and maintainance of resident macrophages. Nat Immunol. 2016 Jan;17(1):2–8.

12. Takahashi K, Yamamura F, Naito M. Differentiation, Maturation, and Proliferation of Macrophages in the Mouse Yolk Sac: A Light-Microscopic, Enzyme-Cytochemical, Immunohistochemical, and Ultrastructural Study. J Leukoc Biol. 1989;45(2):87–96.

13. Naito M, Takahashi K, Nishikawa S Ichi. Development, Differentiation, and Maturation of Macrophages in the Fetal Mouse Liver. J Leukoc Biol. 1990;48(1):27–37.

14. Stremmel C, Schuchert R, Wagner F, Thaler R, Weinberger T, Pick R, et al. Yolk sac macrophage progenitors traffic to the embryo during defined stages of development. Nat Commun. 2018 Jan 8;9(1):75.

15. Chen MJ, Li Y, De Obaldia ME, Yang Q, Yzaguirre AD, Yamada-Inagawa T, et al. Erythroid/myeloid progenitors and hematopoietic stem cells originate from distinct populations of endothelial cells. Cell Stem Cell. 2011 Dec 2;9(6):541–52.

16. Hoeffel G, Chen J, Lavin Y, Low D, Almeida FF, See P, et al. C-Myb+ Erythro-Myeloid Progenitor-Derived Fetal Monocytes Give Rise to Adult Tissue-Resident Macrophages. Immunity. 2015 Apr 21;42(4):665–78.

17. Gomez Perdiguero E, Klapproth K, Schulz C, Busch K, Azzoni E, Crozet L, et al. Tissue-resident macrophages originate from yolk sac-derived erythro-myeloid progenitors. Nature. 2015 Feb 26;518(7540):547–51.

18. Kieusseian A, Brunet de la Grange P, Burlen-Defranoux O, Godin I, Cumano A. Immature hematopoietic stem cells undergo maturation in the fetal liver. Dev Camb Engl. 2012 Oct;139(19):3521–30.

19. de Bruijn MFTR, Speck NA, Peeters MCE, Dzierzak E. Definitive hematopoietic stem cells first develop within the major arterial regions of the mouse embryo. EMBO J. 2000 Jun 1;19(11):2465–74.

20. Frame JM, Fegan KH, Conway SJ, McGrath KE, Palis J. Definitive Hematopoiesis in the Yolk Sac Emerges from Wnt-Responsive Hemogenic Endothelium Independently of Circulation and Arterial Identity. Stem Cells Dayt Ohio. 2016 Feb;34(2):431–44.

21. Baker SJ, Ma'ayan A, Lieu YK, John P, Reddy MVR, Chen EY, et al. B-myb is an essential regulator of hematopoietic stem cell and myeloid progenitor cell development. Proc Natl Acad Sci U S A. 2014 Feb 25;111(8):3122–7.

22. Heinz S, Benner C, Spann N, Bertolino E, Lin YC, Laslo P, et al. Simple Combinations of Lineage-Determining Transcription Factors Prime cis-Regulatory Elements Required for Macrophage and B Cell Identities. Mol Cell. 2010 May 28;38(4):576–89.

23. Ghisletti S, Barozzi I, Mietton F, Polletti S, Santa FD, Venturini E, et al. Identification and Characterization of Enhancers Controlling the Inflammatory Gene Expression Program in Macrophages. Immunity. 2010 Mar 26;32(3):317–28.

24. Riel B van, Rosenbauer F. Epigenetic control of hematopoiesis: the PU.1 chromatin connection. Biol Chem. 2014 Nov 1;395(11):1265–74.

25. Hume DA, Yue X, Ross IL, Favot P, Lichanska A, Ostrowski MC. Regulation of CSF-1 receptor expression. Mol Reprod Dev. 1997;46(1):46–53.

26. Kierdorf K, Prinz M, Geissmann F, Gomez Perdiguero E. Development and function of tissue resident macrophages in mice. Semin Immunol. 2015 Dec;27(6):369–78.

27. Easley-Neal C, Foreman O, Sharma N, Zarrin AA, Weimer RM. CSF1R Ligands IL-34 and CSF1 Are Differentially Required for Microglia Development and Maintenance in White and Gray Matter Brain Regions. Front Immunol. 2019 Sep 20;10:2199.

28. Wang Y, Szretter KJ, Vermi W, Gilfillan S, Rossini C, Cella M, et al. IL-34 is a tissue-restricted ligand of CSF1R required for the development of Langerhans cells and microglia. Nat Immunol. 2012 Aug;13(8):753–60.

29. Kurotaki D, Sasaki H, Tamura T. Transcriptional control of monocyte and macrophage development. Int Immunol. 2017 Mar 1;29(3):97–107.

30. Lavin Y, Winter D, Blecher-Gonen R, David E, Keren-Shaul H, Merad M, et al. Tissue-Resident Macrophage Enhancer Landscapes Are Shaped by the Local Microenvironment. Cell. 2014 Dec 4;159(6):1312–26.

31. Li MO, Sarkisian MR, Mehal WZ, Rakic P, Flavell RA. Phosphatidylserine receptor is required for clearance of apoptotic cells. Science. 2003 Nov 28;302(5650):1560–3.

32. Muñoz-Espín D, Cañamero M, Maraver A, Gómez-López G, Contreras J, Murillo-Cuesta S, et al. Programmed cell senescence during mammalian embryonic development. Cell. 2013 Nov 21;155(5):1104–18.

33. Blair HC, Teitelbaum SL, Ghiselli R, Gluck S. Osteoclastic bone resorption by a polarized vacuolar proton pump. Science. 1989 Aug 25;245(4920):855–7.

34. Teitelbaum SL. Bone resorption by osteoclasts. Science. 2000 Sep 1;289(5484):1504–8.

35. Terpstra V, van Berkel TJ. Scavenger receptors on liver Kupffer cells mediate the in vivo uptake of oxidatively damaged red blood cells in mice. Blood. 2000 Mar 15;95(6):2157–63.

36. Forbes A, Pickell M, Foroughian M, Yao LJ, Lewis J, Veldhuizen R. Alveolar macrophage depletion is associated with increased surfactant pool sizes in adult rats. J Appl Physiol Bethesda Md 1985. 2007 Aug;103(2):637–45.

37. Dong Q, Wright JR. Degradation of surfactant protein D by alveolar macrophages. Am J Physiol. 1998 Jan;274(1):L97-105.

38. Leendertse M, Willems RJL, Giebelen IAJ, Roelofs JJTH, van Rooijen N, Bonten MJM, et al. Peritoneal macrophages are important for the early containment of Enterococcus faecium peritonitis in mice. Innate Immun. 2009 Feb 1;15(1):3–12.

39. Gosselin D, Link VM, Romanoski CE, Fonseca GJ, Eichenfield DZ, Spann NJ, et al. Environment Drives Selection and Function of Enhancers Controlling Tissue-Specific Macrophage Identities. Cell. 2014 Dec;159(6):1327–40.

40. Ganz T. Macrophages and Systemic Iron Homeostasis. J Innate Immun. 2012 Aug;4(5–6):446–53.

41. Karlsson MCI, Guinamard R, Bolland S, Sankala M, Steinman RM, Ravetch JV. Macrophages Control the Retention and Trafficking of B Lymphocytes in the Splenic Marginal Zone. J Exp Med. 2003 Jul 21;198(2):333–40.

42. Nissl F. Über einige Beziehungen zwischen Nervenzellerkrankungen und gliösen Erscheinungen bei verschiedenen Psychosen. Arch F Psychiatr. 1899;32:656–76.

43. del Rio-Hortega P. Microglia. Cytol Cell Pathol Nerv Syst. 1932;2:481–534.

44. De S, Van Deren D, Peden E, Hockin M, Boulet A, Titen S, et al. Two distinct ontogenies confer heterogeneity to mouse brain microglia. Dev Camb Engl. 2018 Jul 1;145(13):dev152306.

45. Saili KS, Zurlinden TJ, Schwab AJ, Silvin A, Baker NC, Sidney Hunter E, et al. Blood-Brain Barrier Development: Systems Modeling and Predictive Toxicology. Birth Defects Res. 2017 Dec 1;109(20):1680–710.

46. Elmore MRP, Lee RJ, West BL, Green KN. Characterizing Newly Repopulated Microglia in the Adult Mouse: Impacts on Animal Behavior, Cell Morphology, and Neuroinflammation. PLOS ONE. 2015 Apr 7;10(4):e0122912.

47. Mendes MS, Atlas J, Brehm Z, Ladron-de-Guevara A, McCall MN, Majewska AK. In vivo imaging of the kinetics of microglial self-renewal and maturation in the adult visual cortex [Internet]. 2020 Apr [cited 2022 Jan 15] p. 2020.03.05.977553. Available from: https://www.biorxiv.org/content/10.1101/2020.03.05.977553v2

48. Elmore MRP, Najafi AR, Koike MA, Dagher NN, Spangenberg EE, Rice RA, et al. CSF1 receptor signaling is necessary for microglia viability, which unmasks a cell that rapidly repopulates the microglia-depleted adult brain. Neuron. 2014 Apr 16;82(2):380–97.

49. Bruttger J, Karram K, Wörtge S, Regen T, Marini F, Hoppmann N, et al. Genetic Cell Ablation Reveals Clusters of Local Self-Renewing Microglia in the Mammalian Central Nervous System. Immunity. 2015 Jul 21;43(1):92–106.

50. Zhan L, Fan L, Kodama L, Sohn PD, Wong MY, Mousa GA, et al. A MAC2-positive progenitor-like microglial population is resistant to CSF1R inhibition in adult mouse brain. Stevens B, Bronner ME, Christian Bennett F, editors. eLife. 2020 Oct 15;9:e51796.

51. Mecha M, Rabadán M a., Peña-Melián A, Valencia M, Mondéjar T, Blanco M j. Expression of TGF-βs in the embryonic nervous system: Analysis of interbalance between isoforms. Dev Dyn. 2008;237(6):1709–17.

52. Butovsky O, Weiner HL. Microglial signatures and their role in health and disease. Nat Rev Neurosci. 2018 Oct;19(10):622–35.

53. Buttgereit A, Lelios I, Yu X, Vrohlings M, Krakoski NR, Gautier EL, et al. Sall1 is a transcriptional regulator defining microglia identity and function. Nat Immunol. 2016 Dec;17(12):1397–406.

54. Wiktor-Jedrzejczak W, Bartocci A, Ferrante AW, Ahmed-Ansari A, Sell KW, Pollard JW, et al. Total absence of colony-stimulating factor 1 in the macrophage-deficient osteopetrotic (op/op) mouse. Proc Natl Acad Sci. 1990 Jun;87(12):4828–32.

55. Galatro TF, Holtman IR, Lerario AM, Vainchtein ID, Brouwer N, Sola PR, et al. Transcriptomic analysis of purified human cortical microglia reveals age-associated changes. Nat Neurosci. 2017 Aug;20(8):1162–71.

56. Thion MS, Low D, Silvin A, Chen J, Grisel P, Schulte-Schrepping J, et al. Microbiome Influences Prenatal and Adult Microglia in a Sex-Specific Manner. Cell. 2018 Jan 25;172(3):500-516.e16.

57. Nimmerjahn A, Kirchhoff F, Helmchen F. Resting Microglial Cells Are Highly Dynamic Surveillants of Brain Parenchyma in Vivo. Science [Internet]. 2005 May 27 [cited 2022 Jan 15]; Available from: https://www.science.org/doi/abs/10.1126/science.1110647

58. Wake H, Moorhouse AJ, Jinno S, Kohsaka S, Nabekura J. Resting Microglia Directly Monitor the Functional State of Synapses In Vivo and Determine the Fate of Ischemic Terminals. J Neurosci. 2009 Apr 1;29(13):3974–80.

59. Giulian D, Li J, Bartel S, Broker J, Li X, Kirkpatrick J. Cell surface morphology identifies microglia as a distinct class of mononuclear phagocyte. J Neurosci. 1995 Nov 1;15(11):7712–26.

60. Belarbi K, Rosi S. Modulation of adult-born neurons in the inflamed hippocampus. Front Cell Neurosci [Internet]. 2013 [cited 2022 Jan 15];7. Available from: https://www.frontiersin.org/article/10.3389/fncel.2013.00145

61. Kierdorf K, Prinz M. Microglia in steady state. J Clin Invest. 2017 Sep 1;127(9):3201–9.

62. Fourgeaud L, Través PG, Tufail Y, Leal-Bailey H, Lew ED, Burrola PG, et al. TAM receptors regulate multiple features of microglial physiology. Nature. 2016 Apr 14;532(7598):240–4.

63. Tondo G, Perani D, Comi C. TAM Receptor Pathways at the Crossroads of Neuroinflammation and Neurodegeneration. Dis Markers. 2019 Sep 15;2019:e2387614.

64. Paolicelli RC, Bolasco G, Pagani F, Maggi L, Scianni M, Panzanelli P, et al. Synaptic Pruning by Microglia Is Necessary for Normal Brain Development. Science [Internet]. 2011 Sep 9 [cited 2022 Jan 15]; Available from: https://www.science.org/doi/abs/10.1126/science.1202529

65. Schafer DP, Lehrman EK, Kautzman AG, Koyama R, Mardinly AR, Yamasaki R, et al. Microglia Sculpt Postnatal Neural Circuits in an Activity and Complement-Dependent Manner. Neuron. 2012 May 24;74(4):691–705.

66. Perry VH, O'Connor V. C1q: the perfect complement for a synaptic feast? Nat Rev Neurosci. 2008 Nov;9(11):807–11.

67. Lauro C, Catalano M, Trettel F, Mainiero F, Ciotti MT, Eusebi F, et al. The Chemokine CX3CL1 Reduces Migration and Increases Adhesion of Neurons with Mechanisms Dependent on the β1 Integrin Subunit. J Immunol. 2006 Dec 1;177(11):7599–606.

68. Sierra A, Encinas JM, Deudero JJ, Chancey JH, Enikolopov G, Overstreet-Wadiche LS, et al. Microglia shape adult hippocampal neurogenesis through apoptosis-coupled phagocytosis. Cell Stem Cell. 2010 Oct 8;7(4):483–95.

69. Kettenmann H. The brain's garbage men. Nature. 2007 Apr;446(7139):987–9.

70. Wang WY, Tan MS, Yu JT, Tan L. Role of pro-inflammatory cytokines released from microglia in Alzheimer's disease. Ann Transl Med. 2015 Jun;3(10):136.

71. Yang S, Gao L, Lu F, Wang B, Gao F, Zhu G, et al. Transcription factor myocyte enhancer factor 2D regulates interleukin-10 production in microglia to protect neuronal cells from inflammation-induced death. J Neuroinflammation. 2015 Feb 20;12:33.

72. Ghosn EEB, Cassado AA, Govoni GR, Fukuhara T, Yang Y, Monack DM, et al. Two physically, functionally, and developmentally distinct peritoneal macrophage subsets. Proc Natl Acad Sci. 2010 Feb 9;107(6):2568–73.

73. Daems WT, De Bakker JM. Do Resident Macrophages Proliferate? Immunobiology. 1982 Jan 1;161(3):204–11.

74. Melnicoff MJ, Horan PK, Breslin EW, Morahan PS. Maintenance of Peritoneal Macrophages in the Steady State. J Leukoc Biol. 1988;44(5):367–75.

75. Sheng J, Ruedl C, Karjalainen K. Most Tissue-Resident Macrophages Except Microglia Are Derived from Fetal Hematopoietic Stem Cells. Immunity. 2015 Aug 18;43(2):382–93.

76. Cain DW, O'Koren EG, Kan MJ, Womble M, Sempowski GD, Hopper K, et al. Identification of a Tissue-Specific, C/EBP -Dependent Pathway of Differentiation for Murine Peritoneal Macrophages. J Immunol. 2013 Nov 1;191(9):4665–75.

77. Davies LC, Rosas M, Smith PJ, Fraser DJ, Jones SA, Taylor PR. A quantifiable proliferative burst of tissue macrophages restores homeostatic macrophage populations after acute inflammation. Eur J Immunol. 2011 Aug;41(8):2155–64.

78. Geissmann F, Jung S, Littman DR. Blood monocytes consist of two principal subsets with distinct migratory properties. Immunity. 2003;19(1):71–82.

79. Geissmann F, Manz MG, Jung S, Sieweke MH, Merad M, Ley K. Development of Monocytes, Macrophages, and Dendritic Cells. Science. 2010 Feb 5;327(5966):656–61.

80. Rosas M, Davies LC, Giles PJ, Liao CT, Kharfan B, Stone TC, et al. The Transcription Factor Gata6 Links Tissue Macrophage Phenotype and Proliferative Renewal. Science. 2014 May 9;344(6184):645–8.

81. Okabe Y, Medzhitov R. Tissue-Specific Signals Control Reversible Program of Localization and Functional Polarization of Macrophages. Cell. 2014 May;157(4):832–44.

82. Relevy NZ, Harats D, Harari A, Ben-Amotz A, Bitzur R, Rühl R, et al. Vitamin A-Deficient Diet Accelerated Atherogenesis in Apolipoprotein E−/− Mice and Dietary β-Carotene Prevents This Consequence. BioMed Res Int. 2015;2015:758723.

83. Ruiz-Alcaraz AJ, Carmona-Martínez V, Tristán-Manzano M, Machado-Linde F, Sánchez-Ferrer ML, García-Peñarrubia P, et al. Characterization of human peritoneal monocyte/macrophage subsets in homeostasis: Phenotype, GATA6,

phagocytic/oxidative activities and cytokines expression. Sci Rep. 2018 Aug 24;8:12794.

84. Cassado A dos A, Albuquerque JAT de, Sardinha LR, Buzzo C de L, Faustino L, Nascimento R, et al. Cellular Renewal and Improvement of Local Cell Effector Activity in Peritoneal Cavity in Response to Infectious Stimuli. PLOS ONE. 2011 Jul 22;6(7):e22141.

85. Barth MW, Hendrak JA, Melnicoff M. Review of the macrophage disapperance reaction. J Leukoc Biol. 1995;57(3):361–7.

86. Bain CC, Hawley CA, Garner H, Scott CL, Schridde A, Steers NJ, et al. Long-lived self-renewing bone marrow-derived macrophages displace embryo-derived cells to inhabit adult serous cavities. Nat Commun. 2016 Jun 13;7:ncomms11852.

87. Liu Z, Gu Y, Chakarov S, Bleriot C, Kwok I, Chen X, et al. Fate Mapping via Ms4a3-Expression History Traces Monocyte-Derived Cells. Cell. 2019 Sep 5;178(6):1509-1525.e19.

88. Louwe PA, Badiola Gomez L, Webster H, Perona-Wright G, Bain CC, Forbes SJ, et al. Recruited macrophages that colonize the post-inflammatory peritoneal niche convert into functionally divergent resident cells. Nat Commun. 2021 Mar 19;12(1):1770.

89. Huang W, Lu N, Eberspaecher H, de Crombrugghe B. A New Long Form of c-Maf Cooperates with Sox9 to Activate the Type II Collagen Gene. J Biol Chem. 2002 Dec 27;277(52):50668–75.

90. Yang Y, Cvekl A. Large Maf transcription factors: cousins of AP-1 proteins and important regulators of cellular differentiation. Einstein J Biol Med EJBM. 2007;23(1):2.

91. Sakai M, Serria MS, Ikeda H, Yoshida K, Imaki J, Nishi S. Regulation of c-maf gene expression by Pax6 in cultured cells. Nucleic Acids Res. 2001 Mar 1;29(5):1228–37.

92. Ring BZ, Cordes SP, Overbeek PA, Barsh GS. Regulation of mouse lens fiber cell development and differentiation by the Maf gene. Development. 2000 Jan 15;127(2):307–17.

93. Nishizawa M, Kataoka K, Goto N, FuJIWARA KT, Kawai S. v-maf, a viral oncogene that encodes a" leucine zipper" motif. Proc Natl Acad Sci. 1989;86(20):7711–5.

94. Blank V, Andrews NC. The Maf transcription factors: regulators of differentiation. Trends Biochem Sci. 1997 Nov;22(11):437–41.

95. Latchman D. Eukaryotic Transcription Factors [Internet]. 5th ed. Academic Press; 2008 [cited 2019 Apr 20]. Available from: https://www.elsevier.com/books/eukaryotic-transcription-factors/latchman/978-0-12-373983-4

96. Kerppola TK, Curran T. A conserved region adjacent to the basic domain is required for recognition of an extended DNA binding site by Maf/Nrl family proteins. Oncogene. 1994 Nov;9(11):3149–58.

97. Dlakić M, Grinberg AV, Leonard DA, Kerppola TK. DNA sequence-dependent folding determines the divergence in binding specificities between Maf and other bZIP proteins. EMBO J. 2001 Feb 15;20(4):828–40.

98. Gordon S, Taylor PR. Monocyte and macrophage heterogeneity. Nat Rev Immunol. 2005 Dec;5(12):953–64.

99. Daassi D, Hamada M, Jeon H, Imamura Y, Nhu Tran MT, Takahashi S. Differential expression patterns of MafB and c-Maf in macrophages invivo and invitro. Biochem Biophys Res Commun. 2016 Apr;473(1):118–24.

100. Cao S, Liu J, Song L, Ma X. The Protooncogene c-Maf Is an Essential Transcription Factor for IL-10 Gene Expression in Macrophages. J Immunol Baltim Md 1950. 2005 Mar 15;174(6):3484–92.

101. Holtman IR, Skola D, Glass CK. Transcriptional control of microglia phenotypes in health and disease. J Clin Invest. 2017 Jul 31;127(9):3220–9.

102. Lewis ND, Hill JD, Juchem KW, Stefanopoulos DE, Modis LK. RNA sequencing of microglia and monocyte-derived macrophages from mice with experimental autoimmune encephalomyelitis illustrates a changing phenotype with disease course. J Neuroimmunol. 2014 Dec 15;277(1):26–38.

103. Kusakabe M, Hasegawa K, Hamada M, Nakamura M, Ohsumi T, Suzuki H, et al. c-Maf plays a crucial role for the definitive erythropoiesis that accompanies erythroblastic island formation in the fetal liver. Blood. 2011 Aug 4;118(5):1374–85.

104. Nakamura M, Hamada M, Hasegawa K, Kusakabe M, Suzuki H, Greaves DR, et al. c-Maf is essential for the F4/80 expression in macrophages in vivo. Gene. 2009 Sep;445(1–2):66–72.

105. Cao S, Liu J, Chesi M, Bergsagel PL, Ho IC, Donnelly RP, et al. Differential Regulation of IL-12 and IL-10 Gene Expression in Macrophages by the Basic Leucine Zipper Transcription Factor c-Maf Fibrosarcoma. J Immunol. 2002 Nov 15;169(10):5715–25.

106. Aziz A, Soucie E, Sarrazin S, Sieweke MH. MafB/c-Maf Deficiency Enables Self-Renewal of Differentiated Functional Macrophages. Science. 2009 Nov 6;326(5954):867–71.

107. Kim JI, Li T, Ho IC, Grusby MJ, Glimcher LH. Requirement for the c-Maf transcription factor in crystallin gene regulation and lens development. Proc Natl Acad Sci. 1999;96(7):3781–5.

108. Hitzler JK, Witte DP, Jenkins NA, Copeland NG, Gilbert DJ, Naeve CW, et al. cDNA Cloning, Expression Pattern, and Chromosomal Localization of Mlf1, Murine Homologue of a Gene Involved in Myelodysplasia and Acute Myeloid Leukemia. Am J Pathol. 1999 Jul 1;155(1):53–9.

109. Yoneda-Kato, Look, Kirstein, Valentine, Raimondi, Cohen, et al. The t(3;5)(q25.1;q34) of myelodysplastic syndrome and acute myeloid leukemia produces a novel... - Abstract - Europe PMC. Oncogene. 1996;12(2):265–75.

110. Matsumoto N, Yoneda-Kato N, Iguchi T, Kishimoto Y, Kyo T, Sawada H, et al. Elevated MLF1 expression correlates with malignant progression from myelodysplastic syndrome. Leukemia. 2000 Oct;14(10):1757–65.

111. Yoneda-Kato N, Kato J ya. Shuttling Imbalance of MLF1 Results in p53 Instability and Increases Susceptibility to Oncogenic Transformation. Mol Cell Biol. 2008 Jan;28(1):422–34.

112. Winteringham LN, Endersby R, Kobelke S, McCulloch RK, Williams JH, Stillitano J, et al. Myeloid Leukemia Factor 1 Associates with a Novel Heterogeneous Nuclear Ribonucleoprotein U-like Molecule *. J Biol Chem. 2006 Dec 15;281(50):38791–800.

113. Lim R, Winteringham LN, Williams JH, McCulloch RK, Ingley E, Tiao JYH, et al. MADM, a Novel Adaptor Protein That Mediates Phosphorylation of the 14-3-3 Binding Site of Myeloid Leukemia Factor 1. J Biol Chem. 2002 Oct 25;277(43):40997–1008.

114. Hanissian SH, Akbar U, Teng B, Janjetovic Z, Hoffmann A, Hitzler JK, et al. cDNA cloning and characterization of a novel gene encoding the MLF1-interacting protein MLF1IP. Oncogene. 2004 Apr;23(20):3700–7.

115. Williams JH, Daly LN, Ingley E, Beaumont JG, Tilbrook PA, Lalonde JP, et al. HLS7, a hemopoietic lineage switch gene homologous to the leukemia-inducing gene MLF1. EMBO J. 1999;18(20):5559–66.

116. Sun Y, Fu A, Xu W, Chao JR, Moshiach S, Morris SW. Myeloid leukemia factor 1 interfered with Bcl-XL to promote apoptosis and its function was regulated by 14-3-3. J Physiol Biochem. 2015 Dec 1;71(4):807–21.

117. Winteringham LN, Kobelke S, Williams JH, Ingley E, Klinken SP. Myeloid Leukemia Factor 1 inhibits erythropoietin-induced differentiation, cell cycle exit and p27Kip1 accumulation. Oncogene. 2004 Jun;23(29):5105–9.

118. Bras S, Martin-Lannerée S, Gobert V, Augé B, Breig O, Sanial M, et al. Myeloid leukemia factor is a conserved regulator of RUNX transcription factor activity involved in hematopoiesis. Proc Natl Acad Sci. 2012 Mar 27;109(13):4986–91.

119. Dimerization with PEBP2β protects RUNX1/AML1 from ubiquitin–proteasome-mediated degradation. EMBO J. 2001 Feb 15;20(4):723–33.

120. Wende H, Lechner SG, Cheret C, Bourane S, Kolanczyk ME, Pattyn A, et al. The Transcription Factor c-Maf Controls Touch Receptor Development and Function. Science. 2012 Mar 16;335(6074):1373–6.

121. Schneider U, Schwenk HU, Bornkamm G. Characterization of EBV-genome negative “null” and “T” cell lines derived from children with acute lymphoblastic leukemia and leukemic transformed non-Hodgkin lymphoma. Int J Cancer. 1977;19(5):621–6.

122. DuBridge RB, Tang P, Hsia HC, Leong PM, Miller JH, Calos MP. Analysis of mutation in human cells by using an Epstein-Barr virus shuttle system. Mol Cell Biol. 1987 Jan 1;7(1):379–87.

123. Rosas M, Osorio F, Robinson MJ, Davies LC, Dierkes N, Jones SA, et al. Hoxb8 conditionally immortalised macrophage lines model inflammatory monocytic cells with important similarity to dendritic cells. Eur J Immunol. 2011 Feb 1;41(2):356–65.

124. Liu Z, Chen O, Wall JBJ, Zheng M, Zhou Y, Wang L, et al. Systematic comparison of 2A peptides for cloning multi-genes in a polycistronic vector. Sci Rep. 2017 May 19;7(1):2193.

125. Daniels RW, Rossano AJ, Macleod GT, Ganetzky B. Expression of Multiple Transgenes from a Single Construct Using Viral 2A Peptides in Drosophila. PLOS ONE. 2014 Jun 19;9(6):e100637.

126. Zhang G, Gurtu V, Kain SR. An Enhanced Green Fluorescent Protein Allows Sensitive Detection of Gene Transfer in Mammalian Cells. Biochem Biophys Res Commun. 1996 Oct 23;227(3):707–11.

127. King PD, Sadra A, Teng JM, Bell GM, Dupont B. CD2-mediated activation of the Tec-family tyrosine kinase ITK is controlled by proline-rich stretch-4 of the CD2 cytoplasmic tail. Int Immunol. 1998 Jul 1;10(7):1009–16.

128. Naldini L. Lentiviruses as gene transfer agents for delivery to non-dividing cells. Curr Opin Biotechnol. 1998 Oct 1;9(5):457–63.

129. Ramezani A, Hawley RG. Overview of the HIV-1 Lentiviral Vector System. Curr Protoc Mol Biol. 2002;60(1):16.21.1-16.21.15.

130. Burns JC, Friedmann T, Driever W, Burrascano M, Yee JK. Vesicular stomatitis virus G glycoprotein pseudotyped retroviral vectors: concentration to very high titer and efficient gene transfer into mammalian and nonmammalian cells. Proc Natl Acad Sci. 1993 Sep 1;90(17):8033–7.

131. Kozak M. Features in the 5′ non-coding sequences of rabbit α and β-globin mRNAs that affect translational efficiency. J Mol Biol. 1994 Jan 7;235(1):95–110.

132. Kozak M. Possible role of flanking nucleotides in recognition of the AUG initiator codon by eukaryotic ribosomes. Nucleic Acids Res. 1981 Oct 24;9(20):5233–52.

133. Son KK, Patel DH, Tkach D, Park A. Cationic liposome and plasmid DNA complexes formed in serum-free medium under optimum transfection condition are negatively charged. Biochim Biophys Acta BBA - Biomembr. 2000 Jun 1;1466(1):11–5.

134. Pear WS, Nolan GP, Scott ML, Baltimore D. Production of high-titer helper-free retroviruses by transient transfection. Proc Natl Acad Sci. 1993 Sep 15;90(18):8392–6.

135. Ipseiz N, Czubala MA, Bart VMT, Davies LC, Jenkins RH, Brennan P, et al. Effective In Vivo Gene Modification in Mouse Tissue-Resident Peritoneal Macrophages by Intraperitoneal Delivery of Lentiviral Vectors. Mol Ther - Methods Clin Dev. 2020 Mar 13;16:21–31.

136. Poznansky M, Lever A, Bergeron L, Haseltine W, Sodroski J. Gene transfer into human lymphocytes by a defective human immunodeficiency virus type 1 vector. J Virol. 1991 Jan;65(1):532–6.

137. Schroeder A, Mueller O, Stocker S, Salowsky R, Leiber M, Gassmann M, et al. The RIN: an RNA integrity number for assigning integrity values to RNA measurements. BMC Mol Biol. 2006 Jan 31;7(1):3.

138. Fabbro CD, Scalabrin S, Morgante M, Giorgi FM. An Extensive Evaluation of Read Trimming Effects on Illumina NGS Data Analysis. PLOS ONE. 2013 Dec 23;8(12):e85024.

139. Parekh S, Ziegenhain C, Vieth B, Enard W, Hellmann I. The impact of amplification on differential expression analyses by RNA-seq. Sci Rep. 2016 May 9;6(1):1–11.

140. Reference Atlas :: Allen Brain Atlas: Mouse Brain [Internet]. [cited 2021 Oct 31]. Available from: https://mouse.brain-map.org/static/atlas

141. Legland D, Arganda-Carreras I, Andrey P. MorphoLibJ: integrated library and plugins for mathematical morphology with ImageJ. Bioinformatics. 2016 Nov 15;32(22):3532–4.

142. Dobin A, Davis CA, Schlesinger F, Drenkow J, Zaleski C, Jha S, et al. STAR: ultrafast universal RNA-seq aligner. Bioinforma Oxf Engl. 2013 Jan 1;29(1):15–21.

143. Krueger F. Babraham Bioinformatics - Trim Galore! [Internet]. [cited 2021 Feb 17]. Available from: https://www.bioinformatics.babraham.ac.uk/projects/trim_galore/

144. Andrews S. Babraham Bioinformatics - FastQC A Quality Control tool for High Throughput Sequence Data [Internet]. [cited 2021 Feb 17]. Available from: https://www.bioinformatics.babraham.ac.uk/projects/fastqc/

145. Durinck S, Spellman PT, Birney E, Huber W. Mapping Identifiers for the Integration of Genomic Datasets with the R/Bioconductor package biomaRt. Nat Protoc. 2009;4(8):1184–91.

146. Love MI, Huber W, Anders S. Moderated estimation of fold change and dispersion for RNA-seq data with DESeq2. Genome Biol. 2014 Dec 5;15(12):550.

147. Anders S, Reyes A, Huber W. Detecting differential usage of exons from RNA-seq data. Genome Res. 2012 Oct;22(10):2008–17.

148. Robinson MD, McCarthy DJ, Smyth GK. edgeR: a Bioconductor package for differential expression analysis of digital gene expression data. Bioinformatics. 2010 Jan 1;26(1):139–40.

149. Marini F, Binder H. pcaExplorer: an R/Bioconductor package for interacting with RNA-seq principal components. BMC Bioinformatics. 2019 Jun 13;20(1):331.

150. Zeng Y, Yi R, Cullen BR. Recognition and cleavage of primary microRNA precursors by the nuclear processing enzyme Drosha. EMBO J. 2005 Jan 12;24(1):138–48.

151. Järve A, Müller J, Kim IH, Rohr K, MacLean C, Fricker G, et al. Surveillance of siRNA integrity by FRET imaging. Nucleic Acids Res. 2007 Sep;35(18):e124.

152. Bernstein E, Caudy AA, Hammond SM, Hannon GJ. Role for a bidentate ribonuclease in the initiation step of RNA interference. Nature. 2001 Jan;409(6818):363–6.

153. Paddison PJ, Caudy AA, Bernstein E, Hannon GJ, Conklin DS. Short hairpin RNAs (shRNAs) induce sequence-specific silencing in mammalian cells. Genes Dev. 2002 Apr 15;16(8):948–58.

154. Cullen BR. RNAi the natural way. Nat Genet. 2005 Nov;37(11):1163–5.

155. Wang Y, Luan C, Zhang G, Sun C. The transcription factor cMaf is targeted by mTOR, and regulates the inflammatory response via the TLR4 signaling pathway. Int J Mol Med. 2018 May 1;41(5):2935–42.

156. Zhang J, Zhao H, Feng Y, Xu X, Yang Y, Zhang P, et al. Topoisomerase 2 inhibitor etoposide promotes interleukin-10 production in LPS-induced macrophages via upregulating transcription factor Maf and activating PI3K/Akt pathway. Int Immunopharmacol. 2021 Dec 1;101:108264.

157. Liu M, Tong Z, Ding C, Luo F, Wu S, Wu C, et al. Transcription factor c-Maf is a checkpoint that programs macrophages in lung cancer. J Clin Invest. 2020 Apr 1;130(4):2081–96.

158. Tran MTN, Hamada M, Jeon H, Shiraishi R, Asano K, Hattori M, et al. MafB is a critical regulator of complement component C1q. Nat Commun. 2017 Nov 22;8(1):1700.

159. Kikuchi K, Iida M, Ikeda N, Moriyama S, Hamada M, Takahashi S, et al. Macrophages Switch Their Phenotype by Regulating Maf Expression during Different Phases of Inflammation. J Immunol. 2018 Jul 15;201(2):635–51.

160. Yoneda-Kato N, Tomoda K, Umehara M, Arata Y, Kato J ya. Myeloid leukemia factor 1 regulates p53 by suppressing COP1 via COP9 signalosome subunit 3. EMBO J. 2005 May 4;24(9):1739–49.

161. Nakamae I, Kato J ya, Yokoyama T, Ito H, Yoneda-Kato N. Myeloid leukemia factor 1 stabilizes tumor suppressor C/EBPα to prevent Trib1-driven acute myeloid leukemia. Blood Adv. 2017 Sep 1;1(20):1682–93.

162. Gobert V, Haenlin M, Waltzer L. Myeloid leukemia factor. Transcription. 2012 Sep 1;3(5):250–4.

163. Steitz T. A mechanism for all polymerases. Nature. 1998 Jan 15;391:231–2.

164. Ranu RS. Relief of DNA Polymerase Stop(s) Due to Severity of Secondary Structure of Single-Stranded DNA Template during DNA Sequencing. Anal Biochem. 1994 Feb 15;217(1):158–61.

165. Needleman-Wunsch alignment of two nucleotide sequences [Internet]. [cited 2021 Nov 2]. Available from: https://blast.ncbi.nlm.nih.gov/Blast.cgi?PAGE_TYPE=BlastSearch&PROG_DEF=blastn&BLAST_PROG_DEF=blastn&BLAST_SPEC=GlobalAln&LINK_LOC=BlastHomeLink

166. Kataoka K, Nishizawa M, Kawai S. Structure-function analysis of the maf oncogene product, a member of the b-Zip protein family. J Virol. 1993 Apr 1;67(4):2133–41.

167. Kawauchi S, Takahashi S, Nakajima O, Ogino H, Morita M, Nishizawa M, et al. Regulation of Lens Fiber Cell Differentiation by Transcription Factor c-Maf. J Biol Chem. 1999 Jul 2;274(27):19254–60.

168. Xu M, Pokrovskii M, Ding Y, Yi R, Au C, Harrison OJ, et al. c-MAF-dependent regulatory T cells mediate immunological tolerance to a gut pathobiont. Nature. 2018 Feb;554(7692):373–7.

169. Zuberbuehler MK, Parker ME, Wheaton JD, Espinosa JR, Salzler HR, Park E, et al. The transcription factor c-Maf is essential for the commitment of IL-17-producing γδ T cells. Nat Immunol. 2019 Jan;20(1):73–85.

170. Neumann C, Blume J, Roy U, Teh PP, Vasanthakumar A, Beller A, et al. c-Maf-dependent T reg cell control of intestinal T H 17 cells and IgA establishes host–microbiota homeostasis. Nat Immunol. 2019 Apr;20(4):471–81.

171. Andris F, Denanglaire S, Anciaux M, Hercor M, Hussein H, Leo O. The Transcription Factor c-Maf Promotes the Differentiation of Follicular Helper T Cells. Front Immunol [Internet]. 2017 Apr 27 [cited 2020 Apr 14];8. Available from: https://www.ncbi.nlm.nih.gov/pmc/articles/PMC5406410/

172. Silva HM, Kitoko JZ, Queiroz CP, Kroehling L, Matheis F, Yang KL, et al. c-MAF–dependent perivascular macrophages regulate diet-induced metabolic syndrome. Sci Immunol. 2021 Oct 1;6(64):eabg7506.

173. Bernardini G, Sciumè G, Santoni A. Differential chemotactic receptor requirements for NK cell subset trafficking into bone marrow. Front Immunol [Internet]. 2013 [cited 2020 May 21];4. Available from: https://www.frontiersin.org/articles/10.3389/fimmu.2013.00012/full

174. Jung S, Aliberti J, Graemmel P, Sunshine MJ, Kreutzberg GW, Sher A, et al. Analysis of Fractalkine Receptor CX3CR1 Function by Targeted Deletion and Green Fluorescent Protein Reporter Gene Insertion. Mol Cell Biol. 2000 Jun 1;20(11):4106–14.

175. Hall JD, Kurtz SL, Rigel NW, Gunn BM, Taft-Benz S, Morrison JP, et al. The impact of chemokine receptor CX3CR1 deficiency during respiratory infections with Mycobacterium tuberculosis or Francisella tularensis. Clin Exp Immunol. 2009 May;156(2):278–84.

176. Harrison JK, Jiang Y, Chen S, Xia Y, Maciejewski D, McNamara RK, et al. Role for neuronally derived fractalkine in mediating interactions between neurons and CX3CR1-expressing microglia. Proc Natl Acad Sci. 1998 Sep 1;95(18):10896–901.

177. Zhao XF, Alam MM, Liao Y, Huang T, Mathur R, Zhu X, et al. Targeting Microglia Using Cx3cr1-Cre Lines: Revisiting the Specificity. eNeuro [Internet]. 2019 Jul 1 [cited 2020 Apr 14];6(4). Available from: https://www.eneuro.org/content/6/4/ENEURO.0114-19.2019

178. Metzger D, Clifford J, Chiba H, Chambon P. Conditional site-specific recombination in mammalian cells using a ligand-dependent chimeric Cre recombinase. Proc Natl Acad Sci. 1995 Jul 18;92(15):6991–5.

179. Feil S, Valtcheva N, Feil R. Inducible Cre Mice. In: Wurst W, Kühn R, editors. Gene Knockout Protocols: Second Edition [Internet]. Totowa, NJ: Humana Press; 2009 [cited 2020 Apr 18]. p. 343–63. (Methods in Molecular Biology). Available from: https://doi.org/10.1007/978-1-59745-471-1_18

180. Valny M, Honsa P, Kirdajova D, Kamenik Z, Anderova M. Tamoxifen in the Mouse Brain: Implications for Fate-Mapping Studies Using the Tamoxifen-Inducible Cre-loxP System. Front Cell Neurosci [Internet]. 2016 Oct 20;10. Available from: https://www.ncbi.nlm.nih.gov/pmc/articles/PMC5071318/

181. Wang Y, Zhao Z, Yang W, Li L, Zhu F, Pei G, et al. Evaluation of the safety and tolerability of tamoxifen for ischemia-incited renal injury in mice. Am J Transl Res. 2018;10(7):2184–94.

182. Ye R, Wang QA, Tao C, Vishvanath L, Shao M, McDonald JG, et al. Impact of tamoxifen on adipocyte lineage tracing: Inducer of adipogenesis and prolonged nuclear translocation of Cre recombinase. Mol Metab. 2015 Nov 1;4(11):771–8.

183. Zhong ZA, Sun W, Chen H, Zhang H, Lay YAE, Lane NE, et al. Optimizing tamoxifen-inducible Cre/loxp system to reduce tamoxifen effect on bone turnover in long bones of young mice. Bone. 2015 Dec;81:614–9.

184. Tamoxifen diets for inducible Cre-LoxP systems [Internet]. Envigo; [cited 2020 Apr 21]. Available from: https://insights.envigo.com/hubfs/resources/data-sheets/10337-envigo-r227-tamoxifen-info-sheet-eu-final-web.pdf

185. Schurch NJ, Schofield P, Gierliński M, Cole C, Sherstnev A, Singh V, et al. How many biological replicates are needed in an RNA-seq experiment and which differential expression tool should you use? RNA. 2016 Jun 1;22(6):839–51.

186. P Value of 0? [Internet]. Available from: https://support.bioconductor.org/p/64787/#64792

187. Reyes A, Anders S, Weatheritt RJ, Gibson TJ, Steinmetz LM, Huber W. Drift and conservation of differential exon usage across tissues in primate species. Proc Natl Acad Sci. 2013 Sep 17;110(38):15377–82.

188. Ochocka N, Kaminska B. Microglia Diversity in Healthy and Diseased Brain: Insights from Single-Cell Omics. Int J Mol Sci. 2021 Mar 16;22(6):3027.

189. Mrdjen D, Pavlovic A, Hartmann FJ, Schreiner B, Utz SG, Leung BP, et al. High-Dimensional Single-Cell Mapping of Central Nervous System Immune Cells Reveals Distinct Myeloid Subsets in Health, Aging, and Disease. Immunity. 2018 Feb 20;48(2):380-395.e6.

190. Yang T, Guo R, Zhang F. Brain perivascular macrophages: Recent advances and implications in health and diseases. CNS Neurosci Ther. 2019;25(12):1318–28.

191. Kierdorf K, Masuda T, Jordão MJC, Prinz M. Macrophages at CNS interfaces: ontogeny and function in health and disease. Nat Rev Neurosci. 2019 Sep;20(9):547–62.

192. Zhong X, Bao Y, Wu Q, Xi X, Zhu W, Chen S, et al. Long noncoding RNA XIST knockdown relieves the injury of microglia cells after spinal cord injury by sponging miR-219-5p. Open Med. 2021 Jan 1;16(1):1090–100.

193. Zhao Q, Lu F, Su Q, Liu Z, Xia X, Yan Z, et al. Knockdown of long noncoding RNA XIST mitigates the apoptosis and inflammatory injury of microglia cells after spinal cord injury through miR-27a/Smurf1 axis. Neurosci Lett. 2020 Jan 10;715:134649.

194. Zhang M, Yang JK, Ma J. Regulation of the long noncoding RNA XIST on the inflammatory polarization of microglia in cerebral infarction. Exp Ther Med. 2021 Sep 1;22(3):1–10.

195. Armoskus C, Moreira D, Bollinger K, Jimenez O, Taniguchi S, Tsai HW. Identification of sexually dimorphic genes in the neonatal mouse cortex and hippocampus. Brain Res. 2014 May 8;1562:23–38.

196. Rusmini M, Griseri P, Matera I, Pontarini E, Ravazzolo R, Mavilio D, et al. Expression Variability and Function of the RET Gene in Adult Peripheral Blood Mononuclear Cells. J Cell Physiol. 2014;229(12):2027–37.

197. Rusmini M, Griseri P, Lantieri F, Matera I, Hudspeth KL, Roberto A, et al. Induction of RET Dependent and Independent Pro-Inflammatory Programs in Human Peripheral Blood Mononuclear Cells from Hirschsprung Patients. PLOS ONE. 2013 Mar 18;8(3):e59066.

198. Boniakowski AE, Kimball AS, Joshi A, Schaller M, Davis FM, denDekker A, et al. Macrophage chemokine receptor CCR2 plays a crucial role in macrophage recruitment and regulated inflammation in wound healing. Eur J Immunol. 2018 Sep;48(9):1445–55.

199. El Khoury J, Toft M, Hickman SE, Means TK, Terada K, Geula C, et al. Ccr2 deficiency impairs microglial accumulation and accelerates progression of Alzheimer-like disease. Nat Med. 2007 Apr;13(4):432–8.

200. Kunkle BW, Grenier-Boley B, Sims R, Bis JC, Damotte V, Naj AC, et al. Genetic meta-analysis of diagnosed Alzheimer's disease identifies new risk loci and implicates Aβ, tau, immunity and lipid processing. Nat Genet. 2019 Mar;51(3):414–30.

201. Naert G, Rivest S. CC Chemokine Receptor 2 Deficiency Aggravates Cognitive Impairments and Amyloid Pathology in a Transgenic Mouse Model of Alzheimer's Disease. J Neurosci. 2011 Apr 20;31(16):6208–20.

202. He J, Chen Y, Farzan M, Choe H, Ohagen A, Gartner S, et al. CCR3 and CCR5 are co-receptors for HIV-1 infection of microglia. Nature. 1997 Feb;385(6617):645–9.

203. Su W, Hopkins S, Nesser NK, Sopher B, Silvestroni A, Ammanuel S, et al. The p53 Transcription Factor Modulates Microglia Behavior through MicroRNA-Dependent Regulation of c-Maf. J Immunol. 2014 Jan 1;192(1):358–66.

204. Zhu C, Xu B, Sun X, Zhu Q, Sui Y. Targeting CCR3 to Reduce Amyloid-β Production, Tau Hyperphosphorylation, and Synaptic Loss in a Mouse Model of Alzheimer's Disease. Mol Neurobiol. 2017 Dec 1;54(10):7964–78.

205. Block ML, Hong JS. Chronic microglial activation and progressive dopaminergic neurotoxicity. Biochem Soc Trans. 2007 Oct 25;35(5):1127–32.

206. Ma X, Yan W, Zheng H, Du Q, Zhang L, Ban Y, et al. Regulation of IL-10 and IL-12 production and function in macrophages and dendritic cells. F1000Research [Internet]. 2015 Dec 17;4. Available from: http://www.ncbi.nlm.nih.gov/pmc/articles/PMC4754024/

207. Zhang HF, Wu MX, Lin YQ, Xie SL, Huang TC, Liu PM, et al. IL-33 promotes IL-10 production in macrophages: a role for IL-33 in macrophage foam cell formation. Exp Mol Med. 2017 Nov;49(11):e388–e388.

208. Dagher R, Copenhaver AM, Besnard V, Berlin A, Hamidi F, Maret M, et al. IL-33-ST2 axis regulates myeloid cell differentiation and activation enabling effective club cell regeneration. Nat Commun. 2020 Sep 22;11(1):4786.

209. Yang Z, Grinchuk V, Urban JF, Bohl J, Sun R, Notari L, et al. Macrophages as IL-25/IL-33-Responsive Cells Play an Important Role in the Induction of Type 2 Immunity. PLoS ONE. 2013 Mar 25;8(3):e59441.

210. Orecchioni M, Ghosheh Y, Pramod AB, Ley K. Macrophage Polarization: Different Gene Signatures in M1(LPS+) vs. Classically and M2(LPS–) vs. Alternatively Activated Macrophages. Front Immunol. 2019;10:1084.

211. Santambrogio L, Belyanskaya SL, Fischer FR, Cipriani B, Brosnan CF, Ricciardi-Castagnoli P, et al. Developmental plasticity of CNS microglia. Proc Natl Acad Sci U S A. 2001 May 22;98(11):6295–300.

212. Wolf Y, Shemer A, Levy-Efrati L, Gross M, Kim JS, Engel A, et al. Microglial MHC class II is dispensable for experimental autoimmune encephalomyelitis and cuprizone-induced demyelination. Eur J Immunol. 2018;48(8):1308–18.

213. Liao CT, Rosas M, Davies LC, Giles PJ, Tyrrell VJ, O'Donnell VB, et al. IL-10 differentially controls the infiltration of inflammatory macrophages and antigen-presenting cells during inflammation. Eur J Immunol. 2016;46(9):2222–32.

214. D'Souza AR, Minczuk M. Mitochondrial transcription and translation: overview. Essays Biochem. 2018 Jul 20;62(3):309–20.

215. Angajala A, Lim S, Phillips JB, Kim JH, Yates C, You Z, et al. Diverse Roles of Mitochondria in Immune Responses: Novel Insights Into Immuno-Metabolism. Front Immunol. 2018;9:1605.

216. Arumugam P, Chauhan M, Rajeev T, Chakraborty R, Shankaran D, Ramalingam S, et al. The mitochondrial gene CMPK2 functions as a rheostat for macrophage homeostasis in inflammation [Internet]. 2021 Nov [cited 2021 Dec 8] p. 2021.11.01.466732. Available from: https://www.biorxiv.org/content/10.1101/2021.11.01.466732v1

217. Kim H, Subbannayya Y, Humphries F, Skejsol A, Pinto SM, Giambelluca M, et al. UMP-CMP kinase 2 gene expression in macrophages is dependent on the IRF3-IFNAR signaling axis. PLOS ONE. 2021 Oct 27;16(10):e0258989.

218. Zhong Z, Liang S, Sanchez-Lopez E, He F, Shalapour S, Lin X jia, et al. New mitochondrial DNA synthesis enables NLRP3 inflammasome activation. Nature. 2018 Aug;560(7717):198–203.

219. Kierdorf K, Erny D, Goldmann T, Sander V, Schulz C, Perdiguero EG, et al. Microglia emerge from erythromyeloid precursors via Pu.1- and Irf8-dependent pathways. Nat Neurosci. 2013 Mar;16(3):273–80.

220. Taniguchi T, Ogasawara K, Takaoka A, Tanaka N. IRF Family of Transcription Factors as Regulators of Host Defense. Annu Rev Immunol. 2001;19(1):623–55.

221. Masuda T, Tsuda M, Yoshinaga R, Tozaki-Saitoh H, Ozato K, Tamura T, et al. IRF8 Is a Critical Transcription Factor for Transforming Microglia into a Reactive Phenotype. Cell Rep. 2012 Apr 19;1(4):334–40.

222. Zhao J, Kong HJ, Li H, Huang B, Yang M, Zhu C, et al. IRF-8/Interferon (IFN) Consensus Sequence-binding Protein Is Involved in Toll-like Receptor (TLR) Signaling and Contributes to the Cross-talk between TLR and IFN-γ Signaling Pathways*. J Biol Chem. 2006 Apr 14;281(15):10073–80.

223. Walker DG. Defining activation states of microglia in human brain tissue: an unresolved issue for Alzheimer's disease. Neuroimmunol Neuroinflammation. 2020 Jul 12;7(3):194–214.

224. Moraes L, Zanchin NIT, Cerutti JM. ABI3, a component of the WAVE2 complex, is potentially regulated by PI3K/AKT pathway. Oncotarget. 2017 Jun 29;8(40):67769–81.

225. Karahan H, Smith DC, Kim B, Dabin LC, Al-Amin MM, Wijeratne HRS, et al. Deletion of Abi3 gene locus exacerbates neuropathological features of Alzheimer's disease in a mouse model of Aβ amyloidosis. Sci Adv. 7(45):eabe3954.

226. Sims R, van der Lee SJ, Naj AC, Bellenguez C, Badarinarayan N, Jakobsdottir J, et al. Rare coding variants in PLCG2, ABI3, and TREM2 implicate microglial-mediated innate immunity in Alzheimer's disease. Nat Genet. 2017 Sep;49(9):1373–84.

227. Paris D, Ait-Ghezala G, Bachmeier C, Laco G, Beaulieu-Abdelahad D, Lin Y, et al. The spleen tyrosine kinase (Syk) regulates Alzheimer amyloid-β production and Tau hyperphosphorylation. J Biol Chem. 2014 Dec 5;289(49):33927–44.

228. Aschenbrenner D, Foglierini M, Jarrossay D, Hu D, Weiner HL, Kuchroo VK, et al. An immunoregulatory and tissue-residency program modulated by c-MAF in human T H 17 cells. Nat Immunol. 2018 Oct;19(10):1126.

229. Gabryšová L, O'Garra A. Regulating the regulator: Bhlhe40 directly keeps IL-10 in check. J Exp Med. 2018 Jul 2;215(7):1767–9.

230. Zhang H, Madi A, Yosef N, Chihara N, Awasthi A, Pot C, et al. An IL-27-Driven Transcriptional Network Identifies Regulators of IL-10 Expression across T Helper Cell Subsets. Cell Rep. 2020 Nov 24;33(8):108433.

231. Parker ME, Barrera A, Wheaton JD, Zuberbuehler MK, Allan DSJ, Carlyle JR, et al. c-Maf regulates the plasticity of group 3 innate lymphoid cells by restraining the type

1 program. J Exp Med [Internet]. 2019 Sep 30 [cited 2021 Jun 10];217(1). Available from: https://www.ncbi.nlm.nih.gov/pmc/articles/PMC7037249/

232. Imbratta C, Hussein H, Andris F, Verdeil G. c-MAF, a Swiss Army Knife for Tolerance in Lymphocytes. Front Immunol [Internet]. 2020 [cited 2020 Apr 14];11. Available from: https://www.frontiersin.org/articles/10.3389/fimmu.2020.00206/full

233. Tizian C, Lahmann A, Hölsken O, Cosovanu C, Kofoed-Branzk M, Heinrich F, et al. c-Maf restrains T-bet-driven programming of CCR6-negative group 3 innate lymphoid cells. Rath S, Withers D, editors. eLife. 2020 Feb 10;9:e52549.

234. Soucie EL, Weng Z, Geirsdottir L, Molawi K, Maurizio J, Fenouil R, et al. Lineage-specific enhancers activate self-renewal genes in macrophages and embryonic stem cells. Science. 2016 Feb 12;351(6274):aad5510–aad5510.

235. Yu F, Sharma S, Jankovic D, Gurram RK, Su P, Hu G, et al. The transcription factor Bhlhe40 is a switch of inflammatory versus antiinflammatory Th1 cell fate determination. J Exp Med. 2018 Jul 2;215(7):1813–21.

236. Samaniego R, Domínguez-Soto Á, Ratnam M, Matsuyama T, Sánchez-Mateos P, Corbí ÁL, et al. Folate Receptor β (FRβ) Expression in Tissue-Resident and Tumor-Associated Macrophages Associates with and Depends on the Expression of PU.1. Cells. 2020 Jun;9(6):1445.

237. Müller E, Christopoulos PF, Halder S, Lunde A, Beraki K, Speth M, et al. Toll-Like Receptor Ligands and Interferon-γ Synergize for Induction of Antitumor M1 Macrophages. Front Immunol. 2017;8:1383.

238. Liu Y, Zhou J, White KP. RNA-seq differential expression studies: more sequence or more replication? Bioinformatics. 2014 Feb 1;30(3):301–4.

239. Ching T, Huang S, Garmire LX. Power analysis and sample size estimation for RNA-Seq differential expression. RNA. 2014 Nov 1;20(11):1684–96.

240. Busse WW. Leukotrienes and Inflammation. Am J Respir Crit Care Med. 1998 Jun 1;157(6):S210–3.

241. Hooper KM, Kong W, Ganea D. Prostaglandin E2 inhibits Tr1 cell differentiation through suppression of c-Maf. PLOS ONE. 2017 Jun 12;12(6):e0179184.

242. Keller M, Mazuch J, Abraham U, Eom GD, Herzog ED, Volk HD, et al. A circadian clock in macrophages controls inflammatory immune responses. Proc Natl Acad Sci. 2009 Dec 15;106(50):21407–12.

243. Jarjour NN, Schwarzkopf EA, Bradstreet TR, Shchukina I, Lin CC, Huang SCC, et al. Bhlhe40 mediates tissue-specific control of macrophage proliferation in homeostasis and type 2 immunity. Nat Immunol. 2019 Jun;20(6):687.

244. Venkateswaran A, Laffitte BA, Joseph SB, Mak PA, Wilpitz DC, Edwards PA, et al. Control of cellular cholesterol efflux by the nuclear oxysterol receptor LXRα. Proc Natl Acad Sci. 2000 Oct 24;97(22):12097–102.

245. Joseph SB, Castrillo A, Laffitte BA, Mangelsdorf DJ, Tontonoz P. Reciprocal regulation of inflammation and lipid metabolism by liver X receptors. Nat Med. 2003 Feb;9(2):213–9.

246. Lemke G, Burstyn-Cohen T. TAM receptors and the clearance of apoptotic cells. Ann N Y Acad Sci. 2010;1209(1):23–9.

247. Laffer B, Bauer D, Wasmuth S, Busch M, Jalilvand TV, Thanos S, et al. Loss of IL-10 Promotes Differentiation of Microglia to a M1 Phenotype. Front Cell Neurosci. 2019;13:430.

248. Davies LC, Rosas M, Jenkins SJ, Liao CT, Scurr MJ, Brombacher F, et al. Distinct bone marrow-derived and tissue-resident macrophage lineages proliferate at key stages during inflammation. Nat Commun. 2013 May 21;4:1886.

249. Puig-Kröger A, Sierra-Filardi E, Domínguez-Soto A, Samaniego R, Corcuera MT, Gómez-Aguado F, et al. Folate Receptor β Is Expressed by Tumor-Associated Macrophages and Constitutes a Marker for M2 Anti-inflammatory/Regulatory Macrophages. Cancer Res. 2009 Dec 15;69(24):9395–403.

250. Lim HY, Lim SY, Tan CK, Thiam CH, Goh CC, Carbajo D, et al. Hyaluronan Receptor LYVE-1-Expressing Macrophages Maintain Arterial Tone through Hyaluronan-Mediated Regulation of Smooth Muscle Cell Collagen. Immunity. 2018 Aug;49(2):326-341.e7.

251. Bizou M, Itier R, Majdoubi M, Abbadi D, Pichery E, Dutaur M, et al. Cardiac macrophage subsets differentially regulate lymphatic network remodeling during pressure overload. Sci Rep. 2021 Aug 19;11(1):16801.

252. Schyns J, Bai Q, Ruscitti C, Radermecker C, De Schepper S, Chakarov S, et al. Non-classical tissue monocytes and two functionally distinct populations of interstitial macrophages populate the mouse lung. Nat Commun. 2019 Sep 3;10:3964.

253. Wang X, Sathe AA, Smith GR, Ruf-Zamojski F, Nair V, Lavine KJ, et al. Heterogeneous origins and functions of mouse skeletal muscle-resident macrophages. Proc Natl Acad Sci. 2020 Aug 25;117(34):20729–40.

254. Wang Y, Chaffee TS, LaRue RS, Huggins DN, Witschen PM, Ibrahim AM, et al. Tissue-resident macrophages promote extracellular matrix homeostasis in the mammary gland stroma of nulliparous mice. Rath S, Rothlin CV, Davis F, editors. eLife. 2020 Jun 1;9:e57438.

255. Xu H, Chen M, Reid DM, Forrester JV. LYVE-1–Positive Macrophages Are Present in Normal Murine Eyes. Invest Ophthalmol Vis Sci. 2007 May 1;48(5):2162–71.

256. Magalhaes MS, Smith P, Portman JR, Jackson-Jones LH, Bain CC, Ramachandran P, et al. Role of Tim4 in the regulation of ABCA1+ adipose tissue macrophages and post-prandial cholesterol levels. Nat Commun. 2021 Dec;12(1):4434.

257. Utz SG, See P, Mildenberger W, Thion MS, Silvin A, Lutz M, et al. Early Fate Defines Microglia and Non-parenchymal Brain Macrophage Development. Cell. 2020 Apr;181(3):557-573.e18.

258. Kim JS, Kolesnikov M, Peled-Hajaj S, Scheyltjens I, Xia Y, Trzebanski S, et al. A Binary Cre Transgenic Approach Dissects Microglia and CNS Border-Associated Macrophages. Immunity. 2021 Jan 12;54(1):176-190.e7.

259. Jackson DG. Biology of the lymphatic marker LYVE-1 and applications in research into lymphatic trafficking and lymphangiogenesis. APMIS. 2004;112(7–8):526–38.

260. Schledzewski K, Falkowski M, Moldenhauer G, Metharom P, Kzhyshkowska J, Ganss R, et al. Lymphatic endothelium-specific hyaluronan receptor LYVE-1 is expressed by stabilin-1+, F4/80+, CD11b+ macrophages in malignant tumours and wound healing tissue in vivo and in bone marrow cultures in vitro: implications for the assessment of lymphangiogenesis. J Pathol. 2006;209(1):67–77.

261. Mitrofanova I, Zavyalova M, Riabov V, Cherdyntseva N, Kzhyshkowska J. The effect of neoadjuvant chemotherapy on the correlation of tumor-associated macrophages with CD31 and LYVE-1. Immunobiology. 2018 Jun 1;223(6):449–59.

262. Park SY, Jung MY, Lee SJ, Kang KB, Gratchev A, Riabov V, et al. Stabilin-1 mediates phosphatidylserine-dependent clearance of cell corpses in alternatively activated macrophages. J Cell Sci. 2009 Sep 15;122(18):3365–73.

263. Desroches-Castan A, Tillet E, Ricard N, Ouarné M, Mallet C, Belmudes L, et al. Bone Morphogenetic Protein 9 Is a Paracrine Factor Controlling Liver Sinusoidal Endothelial Cell Fenestration and Protecting Against Hepatic Fibrosis. Hepatology. 2019;70(4):1392–408.

264. Chakarov S, Lim HY, Tan L, Lim SY, See P, Lum J, et al. Two distinct interstitial macrophage populations coexist across tissues in specific subtissular niches. Science [Internet]. 2019 Mar 15 [cited 2022 Jan 5]; Available from: https://www.science.org/doi/abs/10.1126/science.aau0964

265. Chávez-Galán L, Olleros ML, Vesin D, Garcia I. Much More than M1 and M2 Macrophages, There are also CD169+ and TCR+ Macrophages. Front Immunol [Internet]. 2015 [cited 2022 Jan 16];6. Available from: https://www.frontiersin.org/article/10.3389/fimmu.2015.00263

266. Dick SA, Macklin JA, Nejat S, Momen A, Clemente-Casares X, Althagafi MG, et al. Self-renewing resident cardiac macrophages limit adverse remodeling following myocardial infarction. Nat Immunol. 2019 Jan;20(1):29–39.

267. Pinto AR, Paolicelli R, Salimova E, Gospocic J, Slonimsky E, Bilbao-Cortes D, et al. An Abundant Tissue Macrophage Population in the Adult Murine Heart with a Distinct Alternatively-Activated Macrophage Profile. PLoS ONE. 2012 May 10;7(5):e36814.

268. Weinberger T, Esfandyari D, Messerer D, Percin G, Schleifer C, Thaler R, et al. Ontogeny of arterial macrophages defines their functions in homeostasis and inflammation. Nat Commun. 2020 Sep 11;11(1):4549.

269. Ma L, Dong F, Zaid M, Kumar A, Zha X. ABCA1 protein enhances Toll-like receptor 4 (TLR4)-stimulated interleukin-10 (IL-10) secretion through protein kinase A (PKA) activation. J Biol Chem. 2012 Nov 23;287(48):40502–12.

270. Porcheray F, Viaud S, Rimaniol AC, Léone C, Samah B, Dereuddre-Bosquet N, et al. Macrophage activation switching: an asset for the resolution of inflammation. Clin Exp Immunol. 2005 Dec 1;142(3):481–9.

271. Shen J, Sun X, Pan B, Cao S, Cao J, Che D, et al. IL-17 induces macrophages to M2-like phenotype via NF-κB. Cancer Manag Res. 2018 Oct 4;10:4217–28.

272. Barros MHM, Hauck F, Dreyer JH, Kempkes B, Niedobitek G. Macrophage Polarisation: an Immunohistochemical Approach for Identifying M1 and M2 Macrophages. PLOS ONE. 2013 Nov 15;8(11):e80908.

273. Gusak A, Fedorova L, Lepik K, Volkov N, Popova M, Moiseev I, et al. Immunosuppressive Microenvironment and Efficacy of PD-1 Inhibitors in Relapsed/Refractory Classic Hodgkin Lymphoma: Checkpoint Molecules Landscape and Macrophage Populations. Cancers. 2021 Jan;13(22):5676.

274. Rolot M, Dewals BG. Macrophage Activation and Functions during Helminth Infection: Recent Advances from the Laboratory Mouse. J Immunol Res. 2018 Jul 2;2018:2790627.

6.5. Appendixes

Appendix I

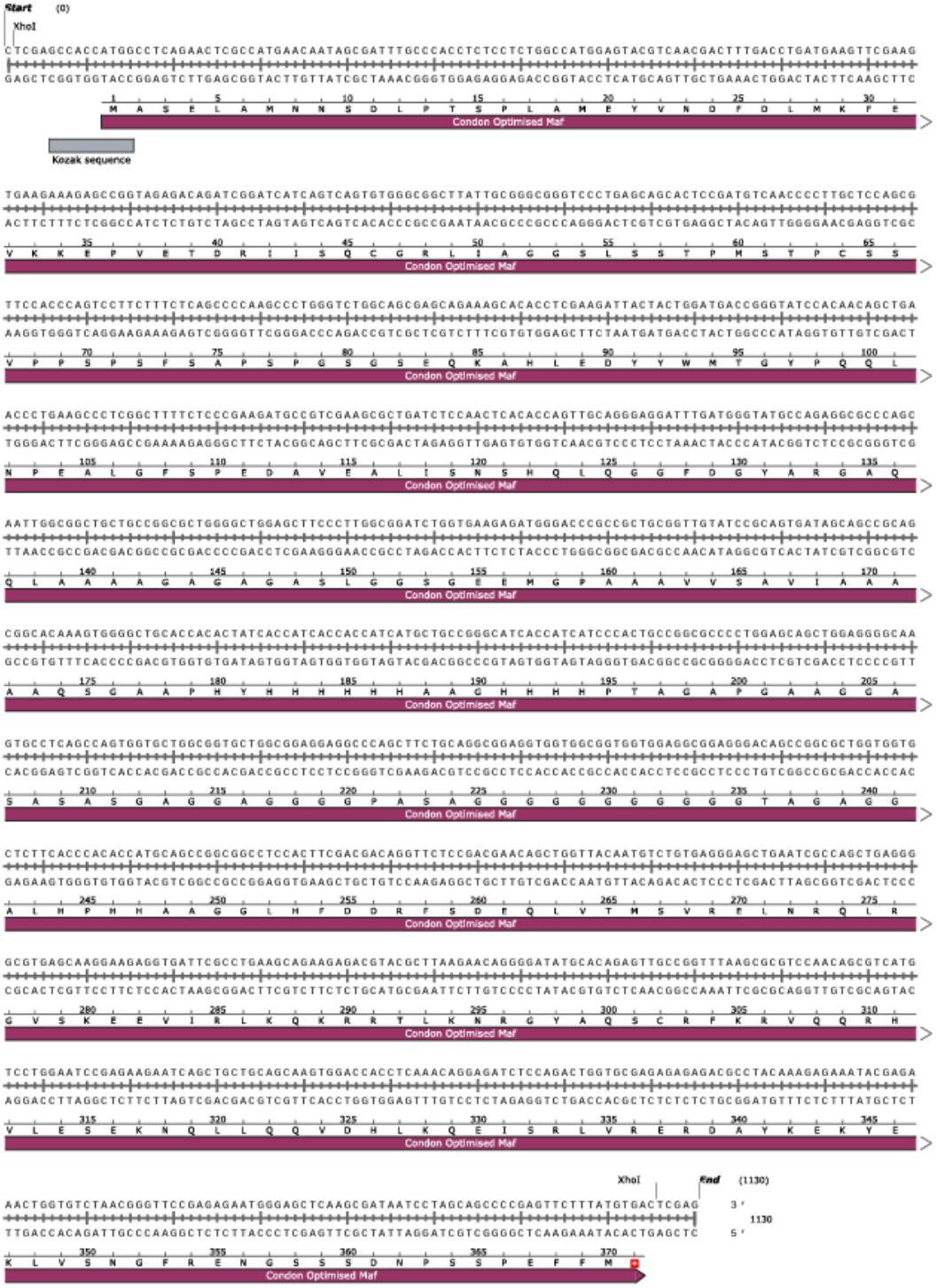

Appendix Ia Codon Optimised *Maf* sequence utilised for *Maf* Overexpression Cloning

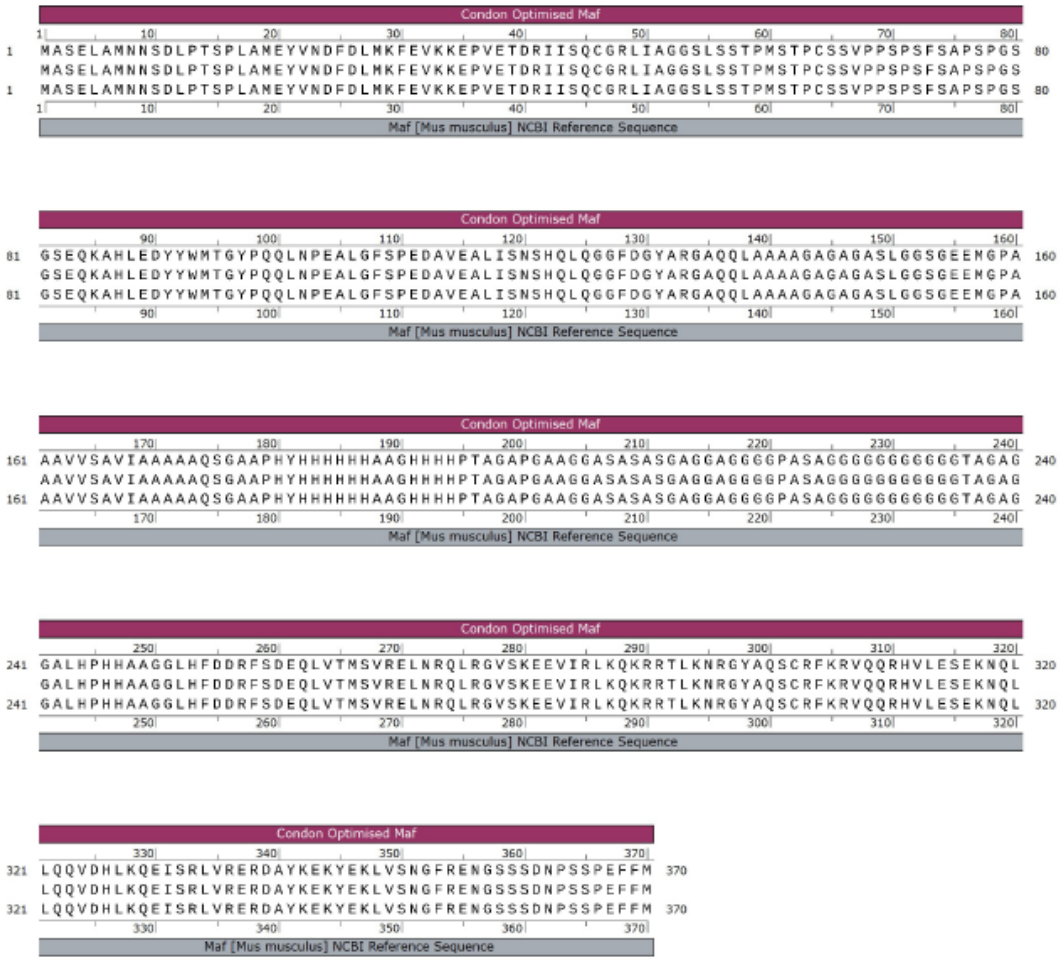

Appendix Ib Alignment of *Maf* Codon Optimised protein sequence with NCBI Reference Sequence for *Maf* in *Mus musculus*

Appendix II

Ensembl Gene ID	External Gene Name	log_2 Fold Change	Adjusted P-Value
ENSMUSG00000022311	Csmd3	-5.741278	1e-314
ENSMUSG00000015852	Fcrls	-3.357179	1.74E-271
ENSMUSG00000022150	Dab2	-3.219142	1.80E-231
ENSMUSG00000042286	Stab1	-2.519946	5.39E-181
ENSMUSG00000026712	Mrc1	-2.550286	5.51E-159
ENSMUSG00000026303	Mlph	-4.553465	2.50E-157
ENSMUSG00000031451	Gas6	-2.603117	1.80E-110
ENSMUSG00000052336	Cx3cr1	-1.329301	2.62E-109
ENSMUSG00000069833	Ahnak	-2.177321	7.20E-101
ENSMUSG00000020181	Nav3	-5.35778	1.95E-93
ENSMUSG00000020695	Mrc2	-2.572845	2.70E-88
ENSMUSG00000027435	Cd93	-2.866712	3.07E-87
ENSMUSG00000024371	C2	3.0339156	6.93E-80
ENSMUSG00000046245	Pilra	2.485957	8.41E-80
ENSMUSG00000000318	Clec10a	-4.772919	6.75E-68
ENSMUSG00000002602	Axl	1.5942372	3.73E-67
ENSMUSG00000039899	Fgl2	1.859097	2.38E-65
ENSMUSG00000022957	Itsn1	-1.866185	8.28E-62
ENSMUSG00000049538	Adamts16	-3.546448	2.08E-61
ENSMUSG00000028362	Tnfsf8	2.9106575	1.62E-60
ENSMUSG00000049313	Sorl1	1.1824917	2.60E-57
ENSMUSG00000009292	Trpm2	1.3860737	2.93E-57
ENSMUSG00000064351	mt-Co1	-1.035002	4.36E-57
ENSMUSG00000034656	Cacna1a	-1.326218	1.82E-56
ENSMUSG00000028214	Gem	-2.087538	1.82E-56
ENSMUSG00000003418	St8sia6	1.3843657	9.23E-55
ENSMUSG00000027200	Sema6d	-3.356184	2.70E-54
ENSMUSG00000015568	Lpl	-1.752523	6.58E-53
ENSMUSG00000004707	Ly9	1.5523714	6.24E-51
ENSMUSG00000073411	H2-D1	1.1625184	1.35E-48
ENSMUSG00000061232	H2-K1	1.1152492	5.46E-48
ENSMUSG00000033278	Ptprm	-1.788299	1.89E-47
ENSMUSG00000074305	Peak1	-1.533915	2.44E-47
ENSMUSG00000062960	Kdr	2.0713291	3.00E-47
ENSMUSG00000027358	Bmp2	-3.564775	3.36E-47
ENSMUSG00000040229	Gpr34	-1.011387	1.28E-46
ENSMUSG00000055413	H2-Q5	1.9151417	3.80E-46
ENSMUSG00000072720	Myo18b	-6.957094	1.82E-45
ENSMUSG00000074505	Fat3	-1.161076	1.74E-44
ENSMUSG00000032661	Oas3	2.5400152	1.96E-44
ENSMUSG00000036353	P2ry12	-0.900783	3.73E-44

ENSMUSG00000027962	Vcam1	2.0350706	1.09E-43
ENSMUSG00000000753	Serpinf1	-1.876555	2.16E-43
ENSMUSG00000043263	Ifi209	1.858083	2.16E-43
ENSMUSG00000026271	Gpr35	1.7505781	2.77E-43
ENSMUSG00000053062	Jam2	-1.606942	7.02E-43
ENSMUSG00000024529	Lox	1.8825747	1.12E-42
ENSMUSG00000030787	Lyve1	-7.83762	1.37E-42
ENSMUSG00000073599	Ecscr	-2.555552	3.93E-42
ENSMUSG00000040950	Mgl2	-2.223146	1.22E-41
ENSMUSG00000073489	Ifi204	1.539917	2.63E-40
ENSMUSG00000027580	Helz2	1.9570643	3.07E-40
ENSMUSG00000022122	Ednrb	-4.457134	3.18E-40
ENSMUSG00000027799	Nbea	-1.57384	3.19E-39
ENSMUSG00000028195	Ccn1	-1.958106	4.64E-39
ENSMUSG00000030117	Gdf3	3.9043948	7.05E-39
ENSMUSG00000043943	Naalad2	1.1304023	6.64E-38
ENSMUSG00000035493	Tgfbi	-1.184391	6.07E-37
ENSMUSG00000049436	Upk1b	-2.698578	8.02E-37
ENSMUSG00000031012	Cask	-1.509253	1.55E-36
ENSMUSG00000059089	Fcgr4	2.0130168	4.94E-36
ENSMUSG00000021719	Rgs7bp	-3.109476	2.56E-35
ENSMUSG00000086503	Xist	11.419784	1.60E-34
ENSMUSG00000024044	Epb41l3	1.3735304	1.21E-33
ENSMUSG00000024042	Sik1	1.2929103	2.62E-33
ENSMUSG00000032609	Klhdc8b	-1.60317	8.61E-33
ENSMUSG00000018217	Pmp22	-1.076414	1.62E-32
ENSMUSG00000031216	Stard8	-1.346074	3.20E-32
ENSMUSG00000029373	Pf4	-2.081317	8.04E-32
ENSMUSG00000049744	Arhgap15	1.8658165	1.17E-31
ENSMUSG00000074743	Thbd	-2.608742	1.59E-31
ENSMUSG00000052911	Lamb2	-1.784451	4.58E-31
ENSMUSG00000069515	Lyz1	2.5590912	5.23E-31
ENSMUSG00000024610	Cd74	-0.77587	1.37E-30
ENSMUSG00000048895	Cdk5r1	-1.452125	9.87E-30
ENSMUSG00000036381	P2ry14	3.6020343	1.93E-29
ENSMUSG00000042834	Nrep	-2.67902	2.07E-29
ENSMUSG00000029084	Cd38	-4.045738	2.77E-29
ENSMUSG00000030107	Usp18	2.0098122	8.20E-29
ENSMUSG00000028080	Lrba	-1.205519	1.94E-28
ENSMUSG00000030156	Cd69	2.0147451	4.73E-28
ENSMUSG00000030539	Sema4b	-1.63127	6.80E-28
ENSMUSG00000030577	Cd22	1.77031	7.37E-28
ENSMUSG00000023913	Pla2g7	-2.089583	2.01E-27
ENSMUSG00000062488	Ifit3b	2.2145946	3.70E-27
ENSMUSG00000022265	Ank	-1.280736	7.19E-27
ENSMUSG00000009418	Nav1	-1.604599	9.05E-27

ENSMUSG00000018459	Slc13a3	1.3934965	1.35E-26
ENSMUSG00000027514	Zbp1	2.1573007	1.87E-26
ENSMUSG00000019256	Ahr	-2.714038	2.52E-26
ENSMUSG00000046876	Atxn1	-2.176243	3.36E-26
ENSMUSG00000048126	Col6a3	-6.150749	3.36E-26
ENSMUSG00000034459	Ifit1	2.258935	3.63E-26
ENSMUSG00000031425	Plp1	-2.426158	5.00E-26
ENSMUSG00000079491	H2-T10	2.6862336	9.36E-26
ENSMUSG00000111118	Gm6545	2.9014297	1.06E-25
ENSMUSG00000029581	Fscn1	-0.729367	6.26E-25
ENSMUSG00000045092	S1pr1	-1.434194	7.39E-25
ENSMUSG00000031327	Chic1	3.2982712	1.04E-24
ENSMUSG00000032717	Mdfi	-3.55642	1.36E-24
ENSMUSG00000056313	Tcim	1.1686576	1.42E-24
ENSMUSG00000032517	Mobp	-2.780328	2.01E-24
ENSMUSG00000011256	Adam19	-2.778287	1.62E-23
ENSMUSG00000026104	Stat1	1.1781827	1.68E-23
ENSMUSG00000035914	Cd276	-1.944501	2.83E-23
ENSMUSG00000022994	Adcy6	-2.823949	3.06E-23
ENSMUSG00000030789	Itgax	1.191006	5.28E-23
ENSMUSG00000039959	Hip1	-1.472758	1.66E-22
ENSMUSG00000072966	Gprasp2	-2.646045	1.94E-22
ENSMUSG00000000957	Mmp14	1.0079781	2.43E-22
ENSMUSG00000074570	Cass4	-1.781093	4.92E-22
ENSMUSG00000088185	Scarna2	0.658301	7.33E-22
ENSMUSG00000060802	B2m	0.8205248	9.77E-22
ENSMUSG00000102975	Gm37347	1.7915284	1.05E-21
ENSMUSG00000067212	H2-T23	0.9686825	1.05E-21
ENSMUSG00000058427	Cxcl2	-1.367871	1.69E-21
ENSMUSG00000038775	Vill	2.1962627	2.55E-21
ENSMUSG00000035929	H2-Q4	1.048783	2.98E-21
ENSMUSG00000060586	H2-Eb1	-0.796713	3.48E-21
ENSMUSG00000028037	Ifi44	2.8933634	4.07E-21
ENSMUSG00000030104	Edem1	-0.695372	4.67E-21
ENSMUSG00000028976	Slc2a5	-0.844513	5.29E-21
ENSMUSG00000032640	Chsy1	-1.057127	5.81E-21
ENSMUSG00000027646	Src	0.9472364	7.71E-21
ENSMUSG00000041058	Wwp1	-1.092823	7.96E-21
ENSMUSG00000015340	Cybb	0.8884468	1.16E-20
ENSMUSG00000000732	Icosl	0.8574212	1.45E-20
ENSMUSG00000112148	Lilrb4a	-0.808275	1.75E-20
ENSMUSG00000029163	Emilin1	1.7366719	1.83E-20
ENSMUSG00000097899	Gm16894	2.418973	1.97E-20
ENSMUSG00000025993	Slc40a1	-0.815519	1.97E-20
ENSMUSG00000031709	Tbc1d9	0.822211	4.09E-20
ENSMUSG00000016206	H2-M3	1.0925577	4.21E-20

ENSMUSG00000035042	Ccl5	3.2795336	1.05E-19
ENSMUSG00000033083	Tbc1d4	-1.718503	1.38E-19
ENSMUSG00000069045	Ddx3y	-13.82826	1.66E-19
ENSMUSG00000021338	Carmil1	1.447646	2.19E-19
ENSMUSG00000036594	H2-Aa	-0.744717	2.25E-19
ENSMUSG00000023367	Tmem176a	0.7585498	3.51E-19
ENSMUSG00000049134	Nrap	-4.974514	5.12E-19
ENSMUSG00000020689	Itgb3	-1.104733	5.24E-19
ENSMUSG00000029401	Rilpl2	1.1873991	7.04E-19
ENSMUSG00000021676	Iqgap2	-2.372677	1.15E-18
ENSMUSG00000085337	Gm15964	1.7740992	1.37E-18
ENSMUSG00000026896	Ifih1	1.0248338	1.38E-18
ENSMUSG00000060519	Tor3a	0.86284	2.35E-18
ENSMUSG00000050022	Amz1	0.8546801	3.86E-18
ENSMUSG00000050530	Fam171a1	-3.953021	4.24E-18
ENSMUSG00000038400	Pmepa1	-0.793215	4.28E-18
ENSMUSG00000018819	Lsp1	0.9956353	5.00E-18
ENSMUSG00000024675	Ms4a4c	1.5720723	5.37E-18
ENSMUSG00000022537	Tmem44	-1.980825	6.16E-18
ENSMUSG00000032359	Ctsh	0.6785766	7.25E-18
ENSMUSG00000009376	Met	2.247746	1.02E-17
ENSMUSG00000079363	Gbp4	2.2068039	1.03E-17
ENSMUSG00000041762	Gpr155	-0.722342	1.13E-17
ENSMUSG00000040964	Arhgef10l	-1.189163	1.61E-17
ENSMUSG00000038894	Irs2	0.8295191	1.73E-17
ENSMUSG00000052609	Plekhg3	-2.196843	1.83E-17
ENSMUSG00000027315	Spint1	0.8483485	2.80E-17
ENSMUSG00000026222	Sp100	1.133002	2.90E-17
ENSMUSG00000024597	Slc12a2	-0.70496	3.19E-17
ENSMUSG00000000682	Cd52	0.9635714	3.52E-17
ENSMUSG00000023078	Cxcl13	4.1013617	3.77E-17
ENSMUSG00000036887	C1qa	0.6131927	3.84E-17
ENSMUSG00000069049	Eif2s3y	-12.9346	5.20E-17
ENSMUSG00000051439	Cd14	-0.646592	6.28E-17
ENSMUSG00000039953	Clstn1	-0.711681	6.73E-17
ENSMUSG00000018593	Sparc	-0.578822	6.92E-17
ENSMUSG00000027784	Ppm1l	-1.346251	8.42E-17
ENSMUSG00000028868	Wasf2	-0.617322	1.07E-16
ENSMUSG00000038642	Ctss	0.6715488	1.09E-16
ENSMUSG00000004317	Clcn5	-0.936252	1.16E-16
ENSMUSG00000021224	Numb	-0.699181	1.55E-16
ENSMUSG00000056673	Kdm5d	-12.73184	1.72E-16
ENSMUSG00000022353	Mtss1	-0.949074	2.27E-16
ENSMUSG00000005087	Cd44	1.2656315	2.29E-16
ENSMUSG00000040249	Lrp1	-0.502123	2.41E-16
ENSMUSG00000059810	Rgs3	-1.244874	2.88E-16

ENSMUSG00000035164	Zc3h12c	1.0914502	2.94E-16
ENSMUSG00000079164	Tlr5	-1.671053	3.25E-16
ENSMUSG00000073421	H2-Ab1	-0.717335	4.78E-16
ENSMUSG00000091649	Phf11b	1.5182787	5.12E-16
ENSMUSG00000024661	Fth1	0.5501878	5.96E-16
ENSMUSG00000028859	Csf3r	0.5572234	6.00E-16
ENSMUSG00000068457	Uty	-12.51888	6.28E-16
ENSMUSG00000029470	P2rx4	0.7449877	7.59E-16
ENSMUSG00000031995	St14	1.3278187	8.80E-16
ENSMUSG00000004891	Nes	-1.562109	9.89E-16
ENSMUSG00000032193	Ldlr	-1.478844	9.89E-16
ENSMUSG00000020400	Tnip1	1.1258767	1.21E-15
ENSMUSG00000017009	Sdc4	-1.3734	1.27E-15
ENSMUSG00000047126	Cltc	-0.531732	1.29E-15
ENSMUSG00000112023	Lilr4b	-0.917939	1.33E-15
ENSMUSG00000040339	Fam102b	-0.702865	1.34E-15
ENSMUSG00000047798	Cd300lf	3.2858718	2.75E-15
ENSMUSG00000029177	Cenpa	-1.663508	2.82E-15
ENSMUSG00000056608	Chd9	-0.598095	3.29E-15
ENSMUSG00000039497	Dse	-0.870087	3.34E-15
ENSMUSG00000025492	Ifitm3	1.0322335	3.46E-15
ENSMUSG00000020541	Tom1l1	-1.679082	3.53E-15
ENSMUSG00000076617	Ighm	-0.68485	4.41E-15
ENSMUSG00000025203	Scd2	-0.896446	4.84E-15
ENSMUSG00000026177	Slc11a1	0.6609551	6.31E-15
ENSMUSG00000021806	Nid2	-1.6521	6.37E-15
ENSMUSG00000053318	Slamf8	1.0842774	6.39E-15
ENSMUSG00000040829	Zmynd15	1.2583808	6.64E-15
ENSMUSG00000074896	Ifit3	2.4406662	6.72E-15
ENSMUSG00000002799	Jag2	-1.57508	7.94E-15
ENSMUSG00000040033	Stat2	0.9683552	8.14E-15
ENSMUSG00000038390	Gpr162	1.2846965	1.04E-14
ENSMUSG00000073555	Gm4951	1.5004529	1.09E-14
ENSMUSG00000032596	Uba7	0.7229992	1.11E-14
ENSMUSG00000040564	Apoc1	2.2660579	1.19E-14
ENSMUSG00000034413	Neurl1b	1.840472	1.23E-14
ENSMUSG00000006800	Sulf2	-1.204474	1.31E-14
ENSMUSG00000021756	Il6st	-0.527506	1.38E-14
ENSMUSG00000052776	Oas1a	1.3484708	1.52E-14
ENSMUSG00000039304	Tnfsf10	1.5685242	2.18E-14
ENSMUSG00000068245	Phf11d	1.1708568	2.30E-14
ENSMUSG00000040152	Thbs1	0.6852231	2.88E-14
ENSMUSG00000055435	Maf	-9.96517	3.10E-14
ENSMUSG00000026193	Fn1	-1.843056	3.36E-14
ENSMUSG00000028459	Cd72	1.1084834	3.62E-14
ENSMUSG00000041607	Mbp	-0.872184	3.62E-14

ENSMUSG00000029814	Igf2bp3	1.6219154	5.50E-14
ENSMUSG00000030830	Itgal	1.4045424	5.85E-14
ENSMUSG00000037849	Ifi206	1.5308107	6.07E-14
ENSMUSG00000032035	Ets1	-0.672456	9.18E-14
ENSMUSG00000028270	Gbp2	1.4185126	1.11E-13
ENSMUSG00000025151	Maged1	-0.868772	1.20E-13
ENSMUSG00000023349	Clec4n	-3.54944	1.52E-13
ENSMUSG00000039529	Atp8b1	-2.827255	1.81E-13
ENSMUSG00000063611	Gm10134	-1.244122	2.20E-13
ENSMUSG00000054072	Iigp1	1.6296744	2.20E-13
ENSMUSG00000037347	Chst7	-1.000136	2.47E-13
ENSMUSG00000056116	H2-T22	1.0532945	2.71E-13
ENSMUSG00000008845	Cd163	-2.831804	2.78E-13
ENSMUSG00000030747	Dgat2	1.697805	2.78E-13
ENSMUSG00000040296	Ddx58	0.9272302	2.81E-13
ENSMUSG00000021411	Pxdc1	1.0783229	2.94E-13
ENSMUSG00000037999	Arap2	-3.311936	3.03E-13
ENSMUSG00000017390	Aldoc	-2.045839	3.52E-13
ENSMUSG00000004562	Arhgef40	-0.6233	3.58E-13
ENSMUSG00000020900	Myh10	-1.266951	3.70E-13
ENSMUSG00000025150	Cbr2	-4.837649	3.94E-13
ENSMUSG00000086109	Gm13391	1.5483107	4.25E-13
ENSMUSG00000023961	Enpp4	1.0603545	4.49E-13
ENSMUSG00000000673	Haao	1.2464957	5.41E-13
ENSMUSG00000101389	Ms4a4a	-3.344107	5.55E-13
ENSMUSG00000072235	Tuba1a	-1.063574	7.02E-13
ENSMUSG00000003134	Tbc1d8	0.8019453	7.90E-13
ENSMUSG00000038886	Man2a2	-0.651637	8.30E-13
ENSMUSG00000104713	Gbp6	2.5131577	9.56E-13
ENSMUSG00000026483	Niban1	0.6780824	1.11E-12
ENSMUSG00000051652	Lrrc3	0.5790758	1.24E-12
ENSMUSG00000020053	Igf1	-1.440191	1.30E-12
ENSMUSG00000040552	C3ar1	-0.582395	1.39E-12
ENSMUSG00000016494	Cd34	0.6397274	1.66E-12
ENSMUSG00000017830	Dhx58	1.1103973	2.39E-12
ENSMUSG00000060550	H2-Q7	2.4015404	2.45E-12
ENSMUSG00000009585	Apobec3	0.6353882	2.45E-12
ENSMUSG00000097039	Pvt1	1.2080366	2.92E-12
ENSMUSG00000037661	Gpr160	0.8100757	2.95E-12
ENSMUSG00000020638	Cmpk2	1.5626393	3.01E-12
ENSMUSG00000031210	Gpr165	-1.6815	3.16E-12
ENSMUSG00000043953	Ccrl2	0.5783453	3.51E-12
ENSMUSG00000079017	Ifi27l2a	1.1614993	3.82E-12
ENSMUSG00000032577	Mapkapk3	0.8915592	3.89E-12
ENSMUSG00000043740	B430306N03Rik	1.2918202	4.27E-12
ENSMUSG00000012017	Scarf2	1.2053111	5.19E-12

ENSMUSG00000047945	Marcksl1	-0.939774	5.33E-12
ENSMUSG00000015766	Eps8	-1.225404	6.18E-12
ENSMUSG00000033066	Gas7	-1.07767	6.90E-12
ENSMUSG00000041849	Card6	0.8875646	1.02E-11
ENSMUSG00000049502	Dtx3l	0.6459323	1.09E-11
ENSMUSG00000048612	Myof	-1.369779	1.11E-11
ENSMUSG00000043671	Dpy19l3	-2.015986	1.22E-11
ENSMUSG00000066861	Oas1g	1.6227334	1.30E-11
ENSMUSG00000031990	Jam3	-3.015097	1.30E-11
ENSMUSG00000040274	Cdk6	-0.878518	1.46E-11
ENSMUSG00000005142	Man2b1	0.4716395	1.57E-11
ENSMUSG00000006611	Hfe	-0.735249	1.75E-11
ENSMUSG00000057914	Cacnb2	1.21796	1.86E-11
ENSMUSG00000034422	Parp14	0.6879571	2.05E-11
ENSMUSG00000090386	Mir99ahg	-1.033872	2.89E-11
ENSMUSG00000068220	Lgals1	-2.854902	2.92E-11
ENSMUSG00000025795	Rassf3	0.7148377	3.15E-11
ENSMUSG00000074622	Mafb	0.5056538	3.41E-11
ENSMUSG00000003882	Il7r	-0.880671	3.41E-11
ENSMUSG00000002233	Rhoc	-1.227652	3.76E-11
ENSMUSG00000020021	Fgd6	-1.588121	4.53E-11
ENSMUSG00000040061	Plcb2	0.5617605	4.74E-11
ENSMUSG00000037369	Kdm6a	0.661362	4.91E-11
ENSMUSG00000041827	Oasl1	3.4139219	4.95E-11
ENSMUSG00000040522	Tlr8	-1.528628	5.01E-11
ENSMUSG00000062078	Qk	-0.476002	5.71E-11
ENSMUSG00000016756	Cmah	-1.470073	5.80E-11
ENSMUSG00000040276	Pacsin1	-2.346781	6.77E-11
ENSMUSG00000058254	Tspan7	-0.687382	6.80E-11
ENSMUSG00000022098	Bmp1	-2.265326	6.90E-11
ENSMUSG00000022817	Itgb5	0.4160269	6.91E-11
ENSMUSG00000017631	Abr	0.5207535	6.97E-11
ENSMUSG00000035352	Ccl12	1.0264168	7.08E-11
ENSMUSG00000033685	Ucp2	0.5113948	7.53E-11
ENSMUSG00000018920	Cxcl16	0.6925141	7.73E-11
ENSMUSG00000073409	H2-Q6	2.9301945	7.94E-11
ENSMUSG00000024014	Pim1	-0.716984	8.12E-11
ENSMUSG00000031770	Herpud1	0.4930318	8.24E-11
ENSMUSG00000004558	Ndrg2	-2.070837	8.47E-11
ENSMUSG00000109245	Gm44860	0.5921895	8.88E-11
ENSMUSG00000031749	St3gal2	-0.663564	9.30E-11
ENSMUSG00000034957	Cebpa	0.4845535	9.39E-11
ENSMUSG00000033350	Chst2	1.0999799	9.51E-11
ENSMUSG00000046879	Irgm1	0.9031895	1.02E-10
ENSMUSG00000025887	Casp12	1.9745883	1.09E-10
ENSMUSG00000045932	Ifit2	2.4834338	1.12E-10

ENSMUSG00000033721	Vav3	-2.008527	1.15E-10
ENSMUSG00000027860	Vangl1	-3.859575	1.17E-10
ENSMUSG00000035208	Slfn8	0.7227518	1.24E-10
ENSMUSG00000075014	Gm10800	-2.428441	1.28E-10
ENSMUSG00000023274	Cd4	-3.495816	1.35E-10
ENSMUSG00000022906	Parp9	0.6786441	1.35E-10
ENSMUSG00000025044	Msr1	-1.006955	1.50E-10
ENSMUSG00000087006	Gm13889	-1.281612	1.60E-10
ENSMUSG00000022425	Enpp2	-1.317875	1.63E-10
ENSMUSG00000034438	Gbp8	2.7701533	1.83E-10
ENSMUSG00000006344	Ggt5	-0.923399	1.88E-10
ENSMUSG00000031613	Hpgd	-0.534851	2.60E-10
ENSMUSG00000032089	Il10ra	0.4503168	2.65E-10
ENSMUSG00000038679	Trps1	0.8453066	2.85E-10
ENSMUSG00000060227	Golm2	-2.541006	3.09E-10
ENSMUSG00000026786	Apbb1ip	-0.539882	3.09E-10
ENSMUSG00000000078	Klf6	-0.40845	3.80E-10
ENSMUSG00000024168	Tmem204	-1.652008	3.80E-10
ENSMUSG00000002957	Ap2a2	-0.596556	3.82E-10
ENSMUSG00000025324	Atp10a	1.9018827	4.06E-10
ENSMUSG00000022102	Dok2	-2.00507	4.12E-10
ENSMUSG00000078349	AW011738	1.229976	4.29E-10
ENSMUSG00000001627	Ifrd1	-0.550184	4.33E-10
ENSMUSG00000030256	Bhlhe41	0.4732276	4.51E-10
ENSMUSG00000021880	Rnase6	1.3031659	5.66E-10
ENSMUSG00000047867	Gimap6	-1.018266	6.08E-10
ENSMUSG00000024640	Psat1	-1.467426	6.27E-10
ENSMUSG00000039763	Dnajc28	0.9518235	6.48E-10
ENSMUSG00000029094	Afap1	-1.800916	6.71E-10
ENSMUSG00000037321	Tap1	0.7731897	7.11E-10
ENSMUSG00000032340	Neo1	-1.943872	8.76E-10
ENSMUSG00000073491	Ifi213	1.9200102	9.14E-10
ENSMUSG00000028234	Rps20	0.5451621	9.26E-10
ENSMUSG00000005958	Ephb3	-1.61949	9.37E-10
ENSMUSG00000026321	Tnfrsf11a	-0.507281	9.48E-10
ENSMUSG00000020424	Castor1	1.0167404	1.09E-09
ENSMUSG00000042770	Hebp1	0.9350986	1.12E-09
ENSMUSG00000037685	Atp8a1	0.4434083	1.12E-09
ENSMUSG00000096727	Psmb9	0.8578789	1.14E-09
ENSMUSG00000026829	Gbgt1	-1.266411	1.23E-09
ENSMUSG00000034353	Ramp1	-1.252008	1.39E-09
ENSMUSG00000030123	Plxnd1	-1.354021	1.59E-09
ENSMUSG00000079056	Kcnip3	0.8886062	1.59E-09
ENSMUSG00000007892	Rplp1	0.461137	1.64E-09
ENSMUSG00000014599	Csf1	-0.70686	1.88E-09
ENSMUSG00000019818	Cd164	-0.480716	2.09E-09

ENSMUSG00000020122	Egfr	-3.351667	2.61E-09
ENSMUSG00000024672	Ms4a7	-1.089735	2.74E-09
ENSMUSG00000022799	Arhgap31	-0.82875	2.79E-09
ENSMUSG00000035373	Ccl7	-2.118818	3.04E-09
ENSMUSG00000031138	F9	-1.428655	3.10E-09
ENSMUSG00000026317	Cln8	-0.561839	3.14E-09
ENSMUSG00000019866	Crybg1	1.4369906	3.22E-09
ENSMUSG00000026442	Nfasc	-2.303443	3.29E-09
ENSMUSG00000030122	Ptms	0.5271499	3.71E-09
ENSMUSG00000022014	Epsti1	0.7584125	3.98E-09
ENSMUSG00000001300	Efnb2	-2.233822	4.00E-09
ENSMUSG00000029298	Gbp9	0.7190635	4.32E-09
ENSMUSG00000075602	Ly6a	1.5615635	4.42E-09
ENSMUSG00000004814	Ccl24	-2.297972	4.98E-09
ENSMUSG00000074151	Nlrc5	1.7324646	5.19E-09
ENSMUSG00000015843	Rxrg	3.7911073	5.36E-09
ENSMUSG00000054404	Slfn5	0.8708817	5.94E-09
ENSMUSG00000025555	Farp1	-1.873885	6.06E-09
ENSMUSG00000038059	Smim3	0.6166394	6.26E-09
ENSMUSG00000045502	Hcar2	1.589078	6.37E-09
ENSMUSG00000015314	Slamf6	0.9462932	6.40E-09
ENSMUSG00000070738	Dgkd	-0.463249	6.74E-09
ENSMUSG00000033450	Tagap	0.4337381	6.80E-09
ENSMUSG00000030536	Iqgap1	-0.711371	6.80E-09
ENSMUSG00000063268	Parp10	0.717986	7.04E-09
ENSMUSG00000066800	Rnasel	-0.746585	7.22E-09
ENSMUSG00000013033	Adgrl1	-1.691904	7.50E-09
ENSMUSG00000030589	Rasgrp4	-1.319647	7.75E-09
ENSMUSG00000062661	Ncs1	-1.466221	7.75E-09
ENSMUSG00000052920	Prkg1	-1.947621	7.75E-09
ENSMUSG00000027803	Wwtr1	1.6616385	7.95E-09
ENSMUSG00000030701	Plekhb1	-1.895296	8.15E-09
ENSMUSG00000004730	Adgre1	-0.424373	8.29E-09
ENSMUSG00000031328	Flna	-0.476136	8.45E-09
ENSMUSG00000050138	Kcnk12	-1.100626	8.78E-09
ENSMUSG00000003283	Hck	0.4943198	9.03E-09
ENSMUSG00000045136	Tubb2b	-1.121753	9.40E-09
ENSMUSG00000054676	1600014C10Rik	0.7477153	9.95E-09
ENSMUSG00000029096	Htra3	-1.925678	1.05E-08
ENSMUSG00000032860	P2ry2	2.2764102	1.07E-08
ENSMUSG00000055809	Dnaaf3	1.1214274	1.10E-08
ENSMUSG00000029919	Hpgds	-0.41244	1.10E-08
ENSMUSG00000079298	Klrb1b	3.7539153	1.22E-08
ENSMUSG00000052160	Pld4	0.4476215	1.35E-08
ENSMUSG00000037921	Ddx60	0.8101358	1.44E-08
ENSMUSG00000001440	Kpnb1	-0.454559	1.50E-08

ENSMUSG00000039193	Nlrc4	-1.919773	1.57E-08
ENSMUSG00000027951	Adar	0.5995811	1.57E-08
ENSMUSG00000045817	Zfp36l2	0.3958176	1.59E-08
ENSMUSG00000043391	2510009E07Rik	-0.691154	1.62E-08
ENSMUSG00000000244	Tspan32	1.0044486	1.70E-08
ENSMUSG00000000594	Gm2a	0.5797081	1.74E-08
ENSMUSG00000021684	Pde8b	1.0187178	1.80E-08
ENSMUSG00000022575	Gsdmd	0.5031006	1.85E-08
ENSMUSG00000064370	mt-Cytb	-1.113027	1.85E-08
ENSMUSG00000037922	Bank1	-0.981883	1.95E-08
ENSMUSG00000024079	Eif2ak2	0.6711146	1.96E-08
ENSMUSG00000007891	Ctsd	0.3773914	1.97E-08
ENSMUSG00000025017	Pik3ap1	0.4285205	2.04E-08
ENSMUSG00000038170	Pde4dip	0.4942332	2.13E-08
ENSMUSG00000055322	Tns1	0.456417	2.19E-08
ENSMUSG00000063382	Bcl9l	-0.666544	2.40E-08
ENSMUSG00000013236	Ptprs	-0.527885	2.61E-08
ENSMUSG00000029798	Herc6	0.9026734	2.67E-08
ENSMUSG00000071042	Rasgrp3	-0.444981	2.72E-08
ENSMUSG00000071068	Treml2	1.2269947	2.90E-08
ENSMUSG00000114761	Gm47242	3.5243189	2.92E-08
ENSMUSG00000019843	Fyn	-1.016825	3.27E-08
ENSMUSG00000023341	Mx2	1.0746047	3.38E-08
ENSMUSG00000016256	Ctsz	0.4481551	3.45E-08
ENSMUSG00000017607	Tns4	1.2360593	3.52E-08
ENSMUSG00000025498	Irf7	1.8514274	4.04E-08
ENSMUSG00000026073	Il1r2	1.3498002	4.06E-08
ENSMUSG00000041439	Mfsd6	-2.559283	4.23E-08
ENSMUSG00000002625	Akap8l	0.4715252	4.41E-08
ENSMUSG00000048490	Nrip1	-0.44786	4.53E-08
ENSMUSG00000069793	Slfn9	1.1761531	4.70E-08
ENSMUSG00000039428	Tmem135	-0.506603	4.78E-08
ENSMUSG00000032306	Mpi	-0.855625	4.79E-08
ENSMUSG00000031838	Ifi30	0.6388274	5.11E-08
ENSMUSG00000031849	Comp	1.4798112	5.40E-08
ENSMUSG00000030201	Lrp6	-0.504697	5.71E-08
ENSMUSG00000052688	Rab7b	-1.0561	5.73E-08
ENSMUSG00000038034	Igsf8	0.7099961	5.82E-08
ENSMUSG00000087968	Gm25395	0.605283	5.89E-08
ENSMUSG00000026315	Serpinb8	-1.633241	5.97E-08
ENSMUSG00000102748	Pcdhgb2	-1.109108	5.97E-08
ENSMUSG00000054008	Ndst1	0.5952898	6.18E-08
ENSMUSG00000059326	Csf2ra	0.5182471	6.18E-08
ENSMUSG00000015839	Nfe2l2	0.4841195	6.66E-08
ENSMUSG00000057135	Scimp	1.4754369	6.66E-08
ENSMUSG00000032322	Pstpip1	1.0400359	6.68E-08

ENSMUSG00000016552	Foxred2	-1.982097	6.98E-08
ENSMUSG00000033306	Lpp	-0.798263	7.09E-08
ENSMUSG00000073902	Gvin3	0.5533057	7.23E-08
ENSMUSG00000020134	Peli1	0.4956466	7.24E-08
ENSMUSG00000030865	Chp2	-6.78286	7.40E-08
ENSMUSG00000021242	Npc2	0.4650718	7.40E-08
ENSMUSG00000039109	F13a1	-1.597477	7.58E-08
ENSMUSG00000102717	Gm37759	1.8284658	7.63E-08
ENSMUSG00000015143	Actn1	-1.061561	7.65E-08
ENSMUSG00000071537	Klrg2	1.4980717	8.06E-08
ENSMUSG00000024521	Pmaip1	0.5787847	8.36E-08
ENSMUSG00000004207	Psap	0.4198948	9.17E-08
ENSMUSG00000021556	Golm1	-0.384373	9.24E-08
ENSMUSG00000044708	Kcnj10	1.0463603	9.40E-08
ENSMUSG00000014418	Hps5	0.5143479	1.02E-07
ENSMUSG00000032690	Oas2	1.7938191	1.11E-07
ENSMUSG00000019467	Arhgef25	-2.833282	1.12E-07
ENSMUSG00000066191	Anks6	-0.858865	1.19E-07
ENSMUSG00000006360	Crip1	-1.556278	1.19E-07
ENSMUSG00000038843	Gcnt1	0.5698838	1.20E-07
ENSMUSG00000061808	Ttr	-1.025453	1.22E-07
ENSMUSG00000019970	Sgk1	-0.423278	1.26E-07
ENSMUSG00000029810	Tmem176b	0.4866344	1.27E-07
ENSMUSG00000040848	Sft2d2	-0.412362	1.28E-07
ENSMUSG00000075225	Ccdc162	-2.911147	1.39E-07
ENSMUSG00000030465	Psd3	-1.003254	1.43E-07
ENSMUSG00000040855	Reps2	-1.378368	1.49E-07
ENSMUSG00000051495	Irf2bp2	0.4012088	1.59E-07
ENSMUSG00000035311	Gnptab	0.653275	1.59E-07
ENSMUSG00000036362	P2ry13	-0.36555	1.65E-07
ENSMUSG00000026213	Stk11ip	0.5542404	1.66E-07
ENSMUSG00000039501	Znfx1	0.5275089	1.72E-07
ENSMUSG00000082088	Gm15753	1.9168368	1.75E-07
ENSMUSG00000007097	Atp1a2	-1.303024	1.79E-07
ENSMUSG00000059479	B3gnt8	1.2159943	1.88E-07
ENSMUSG00000030878	Cdr2	-1.976284	1.97E-07
ENSMUSG00000024397	Aif1	0.5255594	2.08E-07
ENSMUSG00000079227	Ccr5	-0.365373	2.23E-07
ENSMUSG00000049791	Fzd4	-0.811341	2.45E-07
ENSMUSG00000025283	Sat1	0.3426288	2.52E-07
ENSMUSG00000026536	Ifi211	1.3606157	2.64E-07
ENSMUSG00000039997	Ifi203	-0.956307	2.64E-07
ENSMUSG00000007207	Stx1a	-1.925627	2.79E-07
ENSMUSG00000016239	Lonrf3	-0.850513	2.81E-07
ENSMUSG00000044811	Cd300c2	0.4411501	2.85E-07
ENSMUSG00000034412	Tbc1d10a	0.7073836	3.02E-07

ENSMUSG00000047407	Tgif1	0.4228056	3.06E-07
ENSMUSG00000039853	Trim14	0.7196639	3.06E-07
ENSMUSG00000027457	Snph	-1.312157	3.20E-07
ENSMUSG00000044468	Tent5c	0.3923879	3.36E-07
ENSMUSG00000026600	Soat1	0.4345931	3.37E-07
ENSMUSG00000102289	Gm31258	-2.044676	3.41E-07
ENSMUSG00000035666	Gtf3c4	-0.572749	3.41E-07
ENSMUSG00000031137	Fgf13	-1.230304	3.45E-07
ENSMUSG00000069601	Ank3	-2.793004	3.60E-07
ENSMUSG00000025332	Kdm5c	0.4449991	3.82E-07
ENSMUSG00000036905	C1qb	0.3443723	3.90E-07
ENSMUSG00000063455	D630045J12Rik	-2.39436	4.16E-07
ENSMUSG00000038352	Arl5c	0.8755933	4.53E-07
ENSMUSG00000051043	Gprc5c	-2.999508	4.72E-07
ENSMUSG00000082292	Gm12250	1.2155395	5.30E-07
ENSMUSG00000019726	Lyst	0.4266359	5.41E-07
ENSMUSG00000063889	Crem	-1.115004	5.43E-07
ENSMUSG00000023191	P3h3	0.6910423	5.55E-07
ENSMUSG00000057335	Cep170	-0.42475	5.65E-07
ENSMUSG00000050965	Prkca	-0.636856	5.76E-07
ENSMUSG00000029822	Osbpl3	0.9538024	6.22E-07
ENSMUSG00000020572	Nampt	0.6160734	6.26E-07
ENSMUSG00000040037	Negr1	3.9048936	6.28E-07
ENSMUSG00000018965	Ywhah	0.3855466	6.44E-07
ENSMUSG00000031662	Snx20	0.4896659	6.50E-07
ENSMUSG00000040483	Xaf1	1.012164	6.54E-07
ENSMUSG00000042249	Grk3	0.8079568	7.08E-07
ENSMUSG00000060402	Chst8	-4.838551	7.12E-07
ENSMUSG00000022010	Tsc22d1	-0.748723	7.13E-07
ENSMUSG00000042190	Cmklr1	0.4528949	7.32E-07
ENSMUSG00000042589	Cux2	-2.202277	7.36E-07
ENSMUSG00000072612	Gm10382	0.4848507	7.39E-07
ENSMUSG00000064372	mt-Tp	-1.355177	7.62E-07
ENSMUSG00000016496	Cd274	0.7977622	8.21E-07
ENSMUSG00000032570	Atp2c1	-0.419572	8.24E-07
ENSMUSG00000096351	Samd11	-2.578528	8.60E-07
ENSMUSG00000027959	Sass6	0.9345753	8.83E-07
ENSMUSG00000034342	Cbl	-0.396218	9.17E-07
ENSMUSG00000061577	Adgrg5	3.2927067	9.65E-07
ENSMUSG00000027215	Cd82	0.4824612	9.95E-07
ENSMUSG00000039682	Lap3	0.4990897	1.02E-06
ENSMUSG00000047747	Rnf150	0.974809	1.03E-06
ENSMUSG00000038648	Creb3l2	-0.568454	1.05E-06
ENSMUSG00000005107	Slc2a9	0.9563894	1.06E-06
ENSMUSG00000022885	St6gal1	-0.515698	1.09E-06
ENSMUSG00000020282	Rhbdf1	-0.934637	1.10E-06

ENSMUSG00000115338	Pnp	-0.639985	1.15E-06
ENSMUSG00000052142	Rasal3	0.3741261	1.18E-06
ENSMUSG00000039208	Metrnl	-1.045283	1.19E-06
ENSMUSG00000024180	Pgap6	-1.675468	1.20E-06
ENSMUSG00000028565	Nfia	-0.611721	1.23E-06
ENSMUSG00000005611	Irag1	-3.01155	1.26E-06
ENSMUSG00000068606	Gm4841	2.0786034	1.32E-06
ENSMUSG00000025508	Rplp2	0.3994817	1.35E-06
ENSMUSG00000021708	Rasgrf2	1.1607391	1.36E-06
ENSMUSG00000056144	Trim34a	0.8568498	1.39E-06
ENSMUSG00000036908	Unc93b1	0.3259716	1.41E-06
ENSMUSG00000024334	H2-Oa	1.1227109	1.48E-06
ENSMUSG00000041695	Kcnj2	-0.435698	1.48E-06
ENSMUSG00000022216	Psme1	0.6015152	1.49E-06
ENSMUSG00000039954	Stk32a	6.265771	1.50E-06
ENSMUSG00000037972	Snn	-0.446924	1.51E-06
ENSMUSG00000022797	Tfrc	-1.050452	1.54E-06
ENSMUSG00000052942	Glis3	-3.06176	1.60E-06
ENSMUSG00000031342	Gpm6b	-1.342003	1.64E-06
ENSMUSG00000031497	Tnfsf13b	0.6449699	1.66E-06
ENSMUSG00000025207	Sema4g	-0.560372	1.66E-06
ENSMUSG00000032648	Pygm	-2.612197	1.69E-06
ENSMUSG00000042613	Pbxip1	0.4177177	1.74E-06
ENSMUSG00000026605	Cenpf	-1.785732	1.74E-06
ENSMUSG00000035448	Ccr3	-3.355191	1.75E-06
ENSMUSG00000028514	Usp24	-0.369493	1.82E-06
ENSMUSG00000041112	Elmo1	-0.38214	1.84E-06
ENSMUSG00000097352	C920009B18Rik	1.2823993	1.86E-06
ENSMUSG00000060935	Tmem263	-1.644264	1.90E-06
ENSMUSG00000030930	Chst15	0.6710679	1.98E-06
ENSMUSG00000006435	Neurl1a	0.6013249	2.03E-06
ENSMUSG00000002885	Adgre5	-1.230215	2.07E-06
ENSMUSG00000078920	Ifi47	1.2636656	2.11E-06
ENSMUSG00000079339	Ifit1bl1	2.8253691	2.16E-06
ENSMUSG00000038305	Spats2l	-3.316954	2.26E-06
ENSMUSG00000026921	Egfl7	-1.846413	2.56E-06
ENSMUSG00000038156	Spon1	1.9284296	2.58E-06
ENSMUSG00000052387	Trpm3	-2.107679	2.72E-06
ENSMUSG00000027698	Nceh1	0.6119307	2.74E-06
ENSMUSG00000034993	Vat1	-0.866409	2.74E-06
ENSMUSG00000099809	Gm18665	-8.370737	2.92E-06
ENSMUSG00000005533	Igf1r	-0.699515	2.95E-06
ENSMUSG00000098188	Sowahc	0.4145227	2.97E-06
ENSMUSG00000027375	Mal	-2.740966	3.06E-06
ENSMUSG00000052062	Pard3b	-1.139619	3.12E-06
ENSMUSG00000104108	Gm37876	-3.097761	3.24E-06

ENSMUSG00000029592	Usp30	0.7106856	3.30E-06
ENSMUSG00000028986	Klhl7	-0.632522	3.32E-06
ENSMUSG00000041075	Fzd7	-0.549407	3.32E-06
ENSMUSG00000034248	Slc25a37	-0.452971	3.33E-06
ENSMUSG00000025558	Dock9	-0.54948	3.33E-06
ENSMUSG00000042129	Rassf4	0.3664251	3.38E-06
ENSMUSG00000034906	Ncaph	-1.436691	3.49E-06
ENSMUSG00000030283	St8sia1	1.8189101	3.58E-06
ENSMUSG00000023328	Ache	-0.986755	3.66E-06
ENSMUSG00000041202	Pla2g2d	-1.02843	3.78E-06
ENSMUSG00000028273	Pdlim5	-0.611373	3.87E-06
ENSMUSG00000029816	Gpnmb	1.6901289	4.08E-06
ENSMUSG00000038332	Sesn1	-0.479846	4.17E-06
ENSMUSG00000036833	Pnpla7	0.3998465	4.23E-06
ENSMUSG00000022540	Rogdi	0.4929526	4.30E-06
ENSMUSG00000100060	Gm17944	2.5677925	4.42E-06
ENSMUSG00000091472	Gm3739	-1.421478	4.53E-06
ENSMUSG00000022180	Slc7a8	-0.394174	4.58E-06
ENSMUSG00000019961	Tmpo	0.4699358	4.60E-06
ENSMUSG00000085761	4930455G09Rik	3.3518501	4.61E-06
ENSMUSG00000073676	Hspe1	0.5212021	4.62E-06
ENSMUSG00000031431	Tsc22d3	0.4926192	4.79E-06
ENSMUSG00000026305	Lrrfip1	0.450729	4.82E-06
ENSMUSG00000027692	Tnik	1.7378098	4.88E-06
ENSMUSG00000033209	Ttc28	-0.436355	5.04E-06
ENSMUSG00000034118	Tpst1	1.1243485	5.07E-06
ENSMUSG00000056515	Rab31	-0.465696	5.11E-06
ENSMUSG00000030657	Xylt1	-0.841536	5.23E-06
ENSMUSG00000019302	Atp6v0a1	-0.475164	5.26E-06
ENSMUSG00000031217	Efnb1	-0.985977	5.29E-06
ENSMUSG00000021838	Samd4	-2.193641	5.34E-06
ENSMUSG00000026773	Pfkfb3	0.3404742	5.54E-06
ENSMUSG00000039137	Whrn	-0.535494	5.56E-06
ENSMUSG00000094796	BC147527	1.1382722	5.72E-06
ENSMUSG00000042677	Zc3h12a	0.5144077	5.83E-06
ENSMUSG00000007029	Vars	0.4295163	5.87E-06
ENSMUSG00000051212	Gpr183	-0.373495	6.05E-06
ENSMUSG00000023206	Il15ra	1.0166446	6.05E-06
ENSMUSG00000051586	Mical3	-0.731185	6.08E-06
ENSMUSG00000029605	Oas1b	1.3831357	6.17E-06
ENSMUSG00000028967	Errfi1	-0.598774	6.24E-06
ENSMUSG00000022855	Senp2	0.3881411	6.33E-06
ENSMUSG00000036896	C1qc	0.3646951	6.51E-06
ENSMUSG00000034330	Plcg2	0.3703649	6.55E-06
ENSMUSG00000044037	Als2cl	0.942455	6.61E-06
ENSMUSG00000037225	Fgf2	-1.214417	6.79E-06

ENSMUSG00000075015	Gm10801	-2.26333	6.85E-06
ENSMUSG00000027276	Jag1	-1.220717	6.90E-06
ENSMUSG00000037224	Zfyve28	0.8681458	7.07E-06
ENSMUSG00000034751	Mast4	-0.87927	7.07E-06
ENSMUSG00000079110	Capn3	0.3774651	7.25E-06
ENSMUSG00000029765	Plxna4	-0.445023	7.28E-06
ENSMUSG00000055675	Kbtbd11	-1.403145	7.33E-06
ENSMUSG00000090387	Gm17056	-1.047033	7.37E-06
ENSMUSG00000016477	E2f3	-0.795491	7.55E-06
ENSMUSG00000034652	Cd300a	0.4540011	7.99E-06
ENSMUSG00000005360	Slc1a3	0.6463021	8.34E-06
ENSMUSG00000021281	Tnfaip2	0.7867366	8.44E-06
ENSMUSG00000105771	2900064K03Rik	4.0023982	8.68E-06
ENSMUSG00000057841	Rpl32	0.3940954	8.85E-06
ENSMUSG00000056215	Lrguk	1.0649198	8.85E-06
ENSMUSG00000028073	Pear1	-1.215593	9.43E-06
ENSMUSG00000032194	Kank2	-1.087156	9.49E-06
ENSMUSG00000016933	Plcg1	-0.534593	9.51E-06
ENSMUSG00000060183	Cxcl11	4.2704637	9.70E-06
ENSMUSG00000036334	Igsf10	-1.320962	9.70E-06
ENSMUSG00000029204	Rhoh	0.4078892	9.83E-06
ENSMUSG00000022892	App	-0.367041	9.95E-06
ENSMUSG00000090877	Hspa1b	0.3689809	9.99E-06
ENSMUSG00000026656	Fcgr2b	0.4316316	1.00E-05
ENSMUSG00000052749	Trim30b	1.3473279	1.00E-05
ENSMUSG00000030447	Cyfip1	-0.312462	1.01E-05
ENSMUSG00000037706	Cd81	0.3369829	1.04E-05
ENSMUSG00000064341	mt-Nd1	-1.231157	1.10E-05
ENSMUSG00000033032	Afap1l1	-0.707653	1.10E-05
ENSMUSG00000045551	Fpr1	1.6312365	1.12E-05
ENSMUSG00000070327	Rnf213	1.0215799	1.14E-05
ENSMUSG00000097654	Gm26714	0.9797691	1.16E-05
ENSMUSG00000041642	Kif21b	-0.334841	1.17E-05
ENSMUSG00000053559	Smagp	-1.031212	1.19E-05
ENSMUSG00000028517	Plpp3	-2.375193	1.22E-05
ENSMUSG00000057596	Trim30d	0.4858379	1.23E-05
ENSMUSG00000022091	Sorbs3	-1.441715	1.25E-05
ENSMUSG00000064339	mt-Rnr2	-0.950535	1.26E-05
ENSMUSG00000036206	Sh3bp4	1.1970728	1.27E-05
ENSMUSG00000074825	Itpripl1	-0.465276	1.27E-05
ENSMUSG00000038274	Fau	0.4037123	1.28E-05
ENSMUSG00000020102	Slc16a7	-0.560902	1.31E-05
ENSMUSG00000104213	Ighd	-1.520805	1.32E-05
ENSMUSG00000100183	Gm28512	-2.441927	1.35E-05
ENSMUSG00000029380	Cxcl1	-1.142331	1.37E-05
ENSMUSG00000008668	Rps18	0.4221455	1.38E-05

ENSMUSG00000030352	Tspan9	-1.0823	1.41E-05
ENSMUSG00000019889	Ptprk	-3.656192	1.41E-05
ENSMUSG00000046330	Rpl37a	0.423844	1.43E-05
ENSMUSG00000043456	Zfp536	-1.401149	1.44E-05
ENSMUSG00000034445	Cyb561a3	0.4701154	1.44E-05
ENSMUSG00000017493	Igfbp4	-0.485527	1.47E-05
ENSMUSG00000027223	Mapk8ip1	-1.719241	1.49E-05
ENSMUSG00000058013	Septin11	-0.799329	1.50E-05
ENSMUSG00000033717	Adra2a	-2.341275	1.51E-05
ENSMUSG00000054675	Tmem119	0.3458082	1.51E-05
ENSMUSG00000019920	Lims1	-0.439055	1.51E-05
ENSMUSG00000118123	Gm50346	1.0447481	1.52E-05
ENSMUSG00000031665	Sall1	-0.313578	1.52E-05
ENSMUSG00000079138	Gm8818	-3.899241	1.53E-05
ENSMUSG00000109408	A930037H05Rik	1.0919023	1.53E-05
ENSMUSG00000022489	Pde1b	-0.571222	1.54E-05
ENSMUSG00000026249	Serpine2	0.4322582	1.55E-05
ENSMUSG00000053080	2700081O15Rik	-0.83321	1.59E-05
ENSMUSG00000070501	Ifi214	2.5324089	1.59E-05
ENSMUSG00000020573	Pik3cg	-0.340401	1.61E-05
ENSMUSG00000097705	Gm26740	0.9744961	1.62E-05
ENSMUSG00000026986	Hnmt	-0.974354	1.62E-05
ENSMUSG00000051790	Nlgn2	-1.327015	1.64E-05
ENSMUSG00000029501	Ankle2	0.4081709	1.65E-05
ENSMUSG00000032265	Tent5a	0.3798395	1.67E-05
ENSMUSG00000061983	Rps12	0.4002941	1.67E-05
ENSMUSG00000030798	Cd37	0.3951299	1.70E-05
ENSMUSG00000048806	Ifnb1	4.1583681	1.71E-05
ENSMUSG00000040907	Atp1a3	0.6693203	1.71E-05
ENSMUSG00000033542	Arhgef5	-2.630568	1.73E-05
ENSMUSG00000000365	Rnf17	1.5115523	1.74E-05
ENSMUSG00000049517	Rps23	0.3825363	1.74E-05
ENSMUSG00000030708	Dnajb13	0.7183996	1.82E-05
ENSMUSG00000028771	Ptpn12	-0.845663	1.83E-05
ENSMUSG00000000562	Adora3	0.5558698	1.83E-05
ENSMUSG00000001270	Ckb	-0.368894	1.84E-05
ENSMUSG00000031639	Tlr3	0.5236159	1.95E-05
ENSMUSG00000030786	Itgam	-0.410129	2.00E-05
ENSMUSG00000046841	Ckap4	-0.686966	2.00E-05
ENSMUSG00000002944	Cd36	-0.712102	2.02E-05
ENSMUSG00000034926	Dhcr24	-2.461234	2.03E-05
ENSMUSG00000024164	C3	1.4488237	2.15E-05
ENSMUSG00000020787	P2rx1	1.035353	2.18E-05
ENSMUSG00000023019	Gpd1	-1.41053	2.20E-05
ENSMUSG00000039943	Plcb4	-2.405818	2.20E-05
ENSMUSG00000017404	Rpl19	0.4340456	2.20E-05

ENSMUSG00000021451	Sema4d	0.3515834	2.25E-05
ENSMUSG00000006731	B4galnt1	0.6299325	2.29E-05
ENSMUSG00000046805	Mpeg1	0.2978921	2.34E-05
ENSMUSG00000021870	Slmap	-0.457543	2.34E-05
ENSMUSG00000028078	Dclk2	-1.29212	2.53E-05
ENSMUSG00000059248	Septin9	0.635975	2.59E-05
ENSMUSG00000036948	Map11	0.3934418	2.59E-05
ENSMUSG00000018923	Med11	0.7246173	2.62E-05
ENSMUSG00000006930	Hap1	1.5446624	2.65E-05
ENSMUSG00000020644	Id2	0.4816662	2.66E-05
ENSMUSG00000042826	Fgf11	-1.241075	2.67E-05
ENSMUSG00000035297	Cops4	-0.590194	2.69E-05
ENSMUSG00000017754	Pltp	-1.866834	2.70E-05
ENSMUSG00000031304	Il2rg	1.4558704	2.72E-05
ENSMUSG00000071064	Zfp827	-0.877274	2.74E-05
ENSMUSG00000053477	Tcf4	-0.376492	2.74E-05
ENSMUSG00000039982	Dtx4	-0.339223	2.76E-05
ENSMUSG00000031790	Mmp15	-2.406671	2.78E-05
ENSMUSG00000030525	Chrna7	3.7488051	2.84E-05
ENSMUSG00000073418	C4b	0.3430554	2.91E-05
ENSMUSG00000058145	Adamts17	-3.607764	3.00E-05
ENSMUSG00000015355	Cd48	0.548223	3.01E-05
ENSMUSG00000027544	Nfatc2	-0.486318	3.02E-05
ENSMUSG00000031586	Rbpms	0.6807404	3.03E-05
ENSMUSG00000089828	Gm16300	-7.849819	3.04E-05
ENSMUSG00000020641	Rsad2	1.7898516	3.07E-05
ENSMUSG00000066677	Ifi208	1.3065403	3.09E-05
ENSMUSG00000064367	mt-Nd5	-1.167014	3.20E-05
ENSMUSG00000000489	Pdgfb	0.3582712	3.21E-05
ENSMUSG00000058818	Pirb	0.5149892	3.22E-05
ENSMUSG00000030091	Nup210	0.739698	3.39E-05
ENSMUSG00000024769	Cdc42bpg	-1.826804	3.39E-05
ENSMUSG00000037418	Best1	0.4718405	3.40E-05
ENSMUSG00000024732	Ccdc86	0.5265971	3.41E-05
ENSMUSG00000026365	Cfh	-0.285977	3.41E-05
ENSMUSG00000110397	Gm45540	-0.706041	3.64E-05
ENSMUSG00000024948	Map4k2	-0.458237	3.72E-05
ENSMUSG00000062545	Tlr12	0.6130432	3.79E-05
ENSMUSG00000030345	Dyrk4	0.9440151	3.94E-05
ENSMUSG00000036875	Dna2	0.8880913	3.96E-05
ENSMUSG00000047735	Samd9l	0.5228338	3.97E-05
ENSMUSG00000042476	Abcb4	-0.583839	4.10E-05
ENSMUSG00000035458	Tnni3	1.1508576	4.12E-05
ENSMUSG00000058672	Tubb2a	-0.564848	4.16E-05
ENSMUSG00000098557	Kctd12	-0.308977	4.19E-05
ENSMUSG00000037625	Cldn11	-2.529055	4.19E-05

ENSMUSG00000000184	Ccnd2	0.7270897	4.27E-05
ENSMUSG00000076431	Sox4	-0.389325	4.40E-05
ENSMUSG00000074657	Kif5a	-1.359429	4.44E-05
ENSMUSG00000005583	Mef2c	-0.357745	4.46E-05
ENSMUSG00000031714	Gab1	-0.509147	4.57E-05
ENSMUSG00000030275	Etnk1	0.3690236	4.61E-05
ENSMUSG00000029657	Hsph1	0.3976956	4.69E-05
ENSMUSG00000045128	Rpl18a	0.3409326	4.80E-05
ENSMUSG00000024462	Gabbr1	-0.482326	4.96E-05
ENSMUSG00000038068	Rnf144b	-0.545159	5.00E-05
ENSMUSG00000044066	Cep68	-0.385646	5.11E-05
ENSMUSG00000074578	Zfas1	0.658295	5.38E-05
ENSMUSG00000004626	Stxbp2	0.3982093	5.54E-05
ENSMUSG00000039934	Gsap	0.4169218	5.55E-05
ENSMUSG00000022272	Myo10	0.9884338	5.56E-05
ENSMUSG00000073412	Lst1	0.7540362	5.69E-05
ENSMUSG00000004665	Cnn2	-0.871608	5.84E-05
ENSMUSG00000101059	Gm4017	-7.788259	5.95E-05
ENSMUSG00000092060	Bend4	-1.613626	5.96E-05
ENSMUSG00000042228	Lyn	0.2993775	5.99E-05
ENSMUSG00000031402	Mpp1	-0.595675	6.07E-05
ENSMUSG00000071226	Cecr2	-2.38694	6.12E-05
ENSMUSG00000037419	Endod1	-0.478089	6.25E-05
ENSMUSG00000038371	Sbf2	-0.403355	6.25E-05
ENSMUSG00000093930	Hmgcs1	-0.679119	6.39E-05
ENSMUSG00000050627	Gpd1l	0.4653886	6.58E-05
ENSMUSG00000117079	Gm41611	1.1027844	6.61E-05
ENSMUSG00000078350	Smim1	-1.403443	6.63E-05
ENSMUSG00000030691	Fchsd2	-0.386954	6.71E-05
ENSMUSG00000053644	Aldh7a1	-0.798344	6.88E-05
ENSMUSG00000001750	Tcirg1	0.3342073	7.03E-05
ENSMUSG00000048537	Phldb1	-0.793263	7.10E-05
ENSMUSG00000085084	4930570G19Rik	4.2505654	7.10E-05
ENSMUSG00000085133	B930095G15Rik	-2.880754	7.12E-05
ENSMUSG00000035150	Eif2s3x	0.5917104	7.27E-05
ENSMUSG00000027222	Pex16	0.8906166	7.40E-05
ENSMUSG00000058056	Palld	-3.274161	7.63E-05
ENSMUSG00000053799	Exoc6	0.4860979	7.64E-05
ENSMUSG00000090231	Cfb	3.1016462	7.81E-05
ENSMUSG00000020387	Jade2	0.4241948	7.82E-05
ENSMUSG00000073468	Sft2d1	-0.398411	7.82E-05
ENSMUSG00000046204	Pnma2	-3.111959	7.91E-05
ENSMUSG00000043415	Otud1	-0.513485	8.25E-05
ENSMUSG00000031389	Arhgap4	0.3203923	8.37E-05
ENSMUSG00000025037	Maoa	-1.496181	8.38E-05
ENSMUSG00000031785	Adgrg1	-0.346387	8.38E-05

ENSMUSG00000033577	Myo6	-0.898031	8.47E-05
ENSMUSG00000006333	Rps9	0.3367951	8.56E-05
ENSMUSG00000019558	Slc6a8	-1.566728	8.62E-05
ENSMUSG00000041120	Nbl1	-2.01857	8.62E-05
ENSMUSG00000030084	Plxna1	-0.894735	8.76E-05
ENSMUSG00000032589	Bsn	-1.106875	8.76E-05
ENSMUSG00000114996	Gm48958	-4.272971	8.78E-05
ENSMUSG00000110388	Gm30329	-0.858536	8.87E-05
ENSMUSG00000063804	Lin28b	-4.067816	8.89E-05
ENSMUSG00000056602	Fry	-0.517441	8.89E-05
ENSMUSG00000011179	Odc1	0.4226123	8.90E-05
ENSMUSG00000041538	H2-Ob	0.6009926	8.90E-05
ENSMUSG00000099974	Bcl2a1d	0.8885896	8.92E-05
ENSMUSG00000029561	Oasl2	1.4459142	9.11E-05
ENSMUSG00000042644	Itpr3	0.6189442	9.12E-05
ENSMUSG00000040722	Scamp5	-0.465131	9.31E-05
ENSMUSG00000005483	Dnajb1	0.8998531	9.58E-05
ENSMUSG00000065987	Cd209b	-6.91202	9.77E-05
ENSMUSG00000005656	Snx6	-0.485243	9.85E-05
ENSMUSG00000017057	Il13ra1	0.3412546	0.0001016
ENSMUSG00000021200	Asb2	0.4670446	0.0001019
ENSMUSG00000028793	Rnf19b	0.3524668	0.0001063
ENSMUSG00000035919	Bbs9	-0.66342	0.0001063
ENSMUSG00000028328	Tmod1	-1.929449	0.0001076
ENSMUSG00000031112	Stk26	-1.272545	0.000111
ENSMUSG00000071415	Rpl23	0.3860376	0.000112
ENSMUSG00000038058	Nod1	0.5697747	0.0001123
ENSMUSG00000045287	Rtn4rl1	-0.391649	0.0001131
ENSMUSG00000043795	Prr33	1.3790585	0.0001137
ENSMUSG00000097440	Gm6277	-0.770933	0.0001148
ENSMUSG00000027750	Postn	-1.085354	0.000116
ENSMUSG00000060477	Irak2	0.3817103	0.0001181
ENSMUSG00000000386	Mx1	1.6525307	0.0001181
ENSMUSG00000034613	Ppm1h	0.3699189	0.0001187
ENSMUSG00000038151	Prdm1	0.4696206	0.0001214
ENSMUSG00000035441	Myo1d	-1.783865	0.0001272
ENSMUSG00000062997	Rpl35	0.4857019	0.0001286
ENSMUSG00000007379	Dennd2c	-0.554656	0.0001299
ENSMUSG00000024338	Psmb8	0.5237159	0.00013
ENSMUSG00000079470	Utp14b	-1.224073	0.0001312
ENSMUSG00000006651	Aplp1	-1.609739	0.0001329
ENSMUSG00000021280	Exoc3l4	2.1611451	0.0001378
ENSMUSG00000022708	Zbtb20	-0.502032	0.0001378
ENSMUSG00000042684	Npl	-0.767866	0.0001378
ENSMUSG00000026979	Psd4	0.3970769	0.0001383
ENSMUSG00000111926	Gm46204	2.6119855	0.0001397

ENSMUSG00000002985	Apoe	0.2871171	0.0001415
ENSMUSG00000030165	Klrd1	-2.654083	0.0001455
ENSMUSG00000029076	Sdf4	0.3665575	0.0001484
ENSMUSG00000057440	Mpp7	0.4944151	0.0001534
ENSMUSG00000032666	1700025G04Rik	-1.741367	0.0001535
ENSMUSG00000037852	Cpe	-1.219689	0.0001605
ENSMUSG00000025871	4833439L19Rik	-0.477318	0.0001647
ENSMUSG00000024772	Ehd1	-0.675182	0.0001647
ENSMUSG00000074874	Ctla2b	1.3944286	0.0001658
ENSMUSG00000020589	Cyria	0.5911158	0.0001694
ENSMUSG00000039741	Bahcc1	-0.741429	0.0001711
ENSMUSG00000106807	Gm10441	-4.952619	0.000175
ENSMUSG00000026425	Srgap2	-0.29401	0.0001756
ENSMUSG00000031740	Mmp2	-0.583221	0.0001756
ENSMUSG00000085591	Gm13479	-1.163172	0.0001802
ENSMUSG00000030055	Rab43	0.6662381	0.0001802
ENSMUSG00000027995	Tlr2	0.420608	0.0001849
ENSMUSG00000053580	Tanc2	-0.283781	0.0001884
ENSMUSG00000009772	Nuak2	0.4982027	0.0001896
ENSMUSG00000020917	Acly	0.3126204	0.0001957
ENSMUSG00000009621	Vav2	0.3581753	0.000196
ENSMUSG00000060636	Rpl35a	0.3838209	0.0001979
ENSMUSG00000027639	Samhd1	0.336671	0.0001984
ENSMUSG00000015312	Gadd45b	-0.552631	0.0001985
ENSMUSG00000064289	Tank	0.5922422	0.0001987
ENSMUSG00000039713	Plekhg5	-0.504038	0.0002098
ENSMUSG00000022807	Osbpl11	-0.365554	0.0002098
ENSMUSG00000016529	Il10	-3.205811	0.0002148
ENSMUSG00000047810	Ccdc88b	0.3264607	0.0002293
ENSMUSG00000072889	Nfxl1	-0.38517	0.0002358
ENSMUSG00000041797	Abca9	-0.285338	0.0002451
ENSMUSG00000042529	Kcnj12	-7.371816	0.000247
ENSMUSG00000063605	Ccdc102a	0.9852136	0.0002472
ENSMUSG00000021362	Gcm2	4.1103697	0.0002477
ENSMUSG00000027562	Car2	-2.054547	0.0002485
ENSMUSG00000026519	Tmem63a	-0.380836	0.0002488
ENSMUSG00000061477	Rps7	0.3732858	0.0002503
ENSMUSG00000060675	Plaat3	1.1111225	0.0002507
ENSMUSG00000053550	Shisa7	1.2286101	0.0002547
ENSMUSG00000032725	Folr2	-3.79994	0.000257
ENSMUSG00000035342	Lzts2	-1.101072	0.000257
ENSMUSG00000020288	Ahsa2	0.6184317	0.0002588
ENSMUSG00000070939	Tgfbrap1	-0.397924	0.0002607
ENSMUSG00000025647	Shisa5	0.40525	0.0002661
ENSMUSG00000043822	Adamtsl5	-7.35661	0.0002775
ENSMUSG00000032336	Nptn	-0.340315	0.0002864

ENSMUSG00000018001	Cyth3	0.4726888	0.0002873
ENSMUSG00000006235	Epor	-2.760867	0.0002922
ENSMUSG00000104030	5330406M23Rik	0.6383768	0.0002985
ENSMUSG00000041736	Tspo	0.5746594	0.0002985
ENSMUSG00000028268	Gbp3	0.6536421	0.0003032
ENSMUSG00000034616	Ssh3	0.4362232	0.0003041
ENSMUSG00000027376	Prom2	1.2589726	0.0003091
ENSMUSG00000025511	Tspan4	-0.589957	0.0003133
ENSMUSG00000029309	Sparcl1	-1.004925	0.0003185
ENSMUSG00000040616	Tmem51	1.9777306	0.0003226
ENSMUSG00000062591	Tubb4a	-1.511478	0.000323
ENSMUSG00000026866	Kynu	1.4822567	0.0003267
ENSMUSG00000037731	Themis2	0.3564489	0.0003272
ENSMUSG00000021701	Plk2	-0.498373	0.000331
ENSMUSG00000029869	Ephb6	-4.372798	0.000337
ENSMUSG00000021185	Dglucy	0.5179	0.0003379
ENSMUSG00000026615	Eprs	-0.410982	0.0003386
ENSMUSG00000079445	B3gnt7	-1.592268	0.0003486
ENSMUSG00000037523	Mavs	0.4698081	0.0003505
ENSMUSG00000044042	Fmn1	-1.086828	0.0003505
ENSMUSG00000040111	Gramd1b	-0.682069	0.000355
ENSMUSG00000053398	Phgdh	-0.721147	0.0003621
ENSMUSG00000022439	Parvg	0.3672221	0.0003682
ENSMUSG00000063193	Cd300lb	-1.375996	0.0003687
ENSMUSG00000099398	Ms4a14	-1.672187	0.0003695
ENSMUSG00000028108	Ecm1	-1.785505	0.000379
ENSMUSG00000048154	Kmt2d	-0.27718	0.0003882
ENSMUSG00000085037	4933421O10Rik	0.4375188	0.0003888
ENSMUSG00000020100	Slc29a3	0.2859837	0.0003991
ENSMUSG00000097194	9330175E14Rik	1.3912539	0.000403
ENSMUSG00000002307	Daxx	0.6021882	0.0004042
ENSMUSG00000064349	mt-Tc	-0.909204	0.0004051
ENSMUSG00000084821	Gm15880	-2.213416	0.0004053
ENSMUSG00000041841	Rpl37	0.3749898	0.0004054
ENSMUSG00000020277	Pfkl	0.3898141	0.0004066
ENSMUSG00000059456	Ptk2b	0.3372107	0.0004127
ENSMUSG00000002325	Irf9	0.4050486	0.0004142
ENSMUSG00000010660	Plcd1	0.567527	0.000416
ENSMUSG00000036995	Asap3	-0.469417	0.0004174
ENSMUSG00000064373	Selenop	-0.3133	0.0004304
ENSMUSG00000032870	Smap2	-0.275098	0.0004362
ENSMUSG00000107723	Gm43964	1.1601239	0.0004413
ENSMUSG00000030744	Rps3	0.3030589	0.0004416
ENSMUSG00000021876	Rnase4	-0.333125	0.000449
ENSMUSG00000082402	Gm15621	1.46306	0.0004538
ENSMUSG00000020262	Adarb1	-1.255294	0.000459

ENSMUSG00000045322	Tlr9	0.3442954	0.0004675
ENSMUSG00000039765	Cc2d2a	-1.281871	0.0004686
ENSMUSG00000039013	Siglecf	-0.687898	0.0004703
ENSMUSG00000060938	Rpl26	0.3131817	0.0004864
ENSMUSG00000023169	Slc38a1	0.3325484	0.0004898
ENSMUSG00000002741	Ykt6	-0.411852	0.0005013
ENSMUSG00000020077	Srgn	0.436786	0.0005022
ENSMUSG00000026014	Raph1	-0.656329	0.0005045
ENSMUSG00000064345	mt-Nd2	-1.238348	0.000507
ENSMUSG00000048285	Frmd6	-1.084738	0.0005074
ENSMUSG00000037940	Inpp4b	0.4175087	0.0005092
ENSMUSG00000020128	Vps54	0.3808653	0.0005137
ENSMUSG00000022867	Usp25	0.3643022	0.0005148
ENSMUSG00000015829	Tnr	-2.603491	0.000516
ENSMUSG00000026548	Slamf9	0.5774298	0.0005161
ENSMUSG00000022982	Sod1	0.3861992	0.0005293
ENSMUSG00000038910	Plcl2	-0.304748	0.0005412
ENSMUSG00000027843	Ptpn22	1.1455911	0.0005412
ENSMUSG00000027254	Map1a	-1.665541	0.0005442
ENSMUSG00000041444	Arhgap32	-0.687269	0.0005454
ENSMUSG00000003541	Ier3	-0.461602	0.0005534
ENSMUSG00000038732	Mboat1	-1.993027	0.0005559
ENSMUSG00000063873	Slc24a3	-0.64975	0.0005561
ENSMUSG00000065232	Gm22973	1.1889456	0.0005573
ENSMUSG00000049401	Ogfr	0.4470678	0.0005643
ENSMUSG00000061186	Sfmbt2	-1.527917	0.0005736
ENSMUSG00000031488	Rab11fip1	1.2125913	0.0005825
ENSMUSG00000005089	Slc1a2	-0.960471	0.0005825
ENSMUSG00000001700	Gramd3	1.2543036	0.0006014
ENSMUSG00000076621	Ighj1	-1.286531	0.0006015
ENSMUSG00000025648	Pfkfb4	0.3839208	0.000609
ENSMUSG00000036585	Fgf1	-2.45974	0.0006174
ENSMUSG00000077391	Gm24336	0.8081764	0.000626
ENSMUSG00000029178	Klf3	-0.322158	0.000626
ENSMUSG00000032067	Pts	0.6097377	0.000626
ENSMUSG00000025026	Add3	-0.49611	0.0006268
ENSMUSG00000092277	Gm19684	5.2482523	0.0006268
ENSMUSG00000034707	Gns	0.2555936	0.0006325
ENSMUSG00000036949	Slc39a12	-3.723446	0.0006339
ENSMUSG00000007039	Ddah2	-0.787415	0.0006346
ENSMUSG00000024851	Pitpnm1	0.4392858	0.0006351
ENSMUSG00000033880	Lgals3bp	1.3465717	0.0006523
ENSMUSG00000057315	Arhgap24	0.8015096	0.0006533
ENSMUSG00000029419	Ajm1	-0.627012	0.0006631
ENSMUSG00000085759	1700061E18Rik	-2.493904	0.000664
ENSMUSG00000008682	Rpl10	0.2905213	0.000666

ENSMUSG00000048621	Gm6377	-1.171707	0.0006854
ENSMUSG00000107075	Gm43068	2.2171883	0.0006859
ENSMUSG00000050335	Lgals3	-0.827577	0.0006924
ENSMUSG00000023026	Dip2b	-0.269185	0.0006968
ENSMUSG00000004798	Ulk2	-0.342104	0.0006979
ENSMUSG00000039456	Morc3	0.3159037	0.0007026
ENSMUSG00000005871	Apc	-0.353997	0.0007053
ENSMUSG00000032202	Rab27a	0.4744938	0.000706
ENSMUSG00000109089	4833411C07Rik	1.0027917	0.000706
ENSMUSG00000023927	Satb1	-0.947169	0.0007177
ENSMUSG00000037649	H2-DMa	0.387112	0.0007177
ENSMUSG00000004267	Eno2	-1.542667	0.0007262
ENSMUSG00000022587	Ly6e	0.7088871	0.0007263
ENSMUSG00000026509	Capn2	-1.091995	0.0007414
ENSMUSG00000026535	Ifi202b	-4.635364	0.0007452
ENSMUSG00000032058	Ppp2r1b	-0.497422	0.0007463
ENSMUSG00000051906	Cd209f	-7.096188	0.000748
ENSMUSG00000029207	Apbb2	-0.504769	0.000748
ENSMUSG00000064337	mt-Rnr1	-1.065835	0.0007582
ENSMUSG00000019505	Ubb	0.3045324	0.0007698
ENSMUSG00000032434	Cmtm6	-0.291751	0.0007699
ENSMUSG00000052560	Cpne8	-6.402246	0.0007726
ENSMUSG00000102291	Gm37542	-2.44028	0.0007753
ENSMUSG00000091418	Gm3164	-3.18792	0.0008027
ENSMUSG00000025880	Smad7	0.3577153	0.0008126
ENSMUSG00000090105	Gm15890	0.7246563	0.0008126
ENSMUSG00000032184	Lysmd2	2.9128477	0.0008189
ENSMUSG00000006411	Nectin4	0.4854889	0.0008189
ENSMUSG00000004270	Lpcat3	-0.398386	0.000832
ENSMUSG00000026496	Parp1	0.3554315	0.0008321
ENSMUSG00000092591	Gm20429	5.175896	0.0008321
ENSMUSG00000005823	Gpr108	0.4317181	0.000835
ENSMUSG00000040612	Ildr2	0.919426	0.0008373
ENSMUSG00000095742		-0.82872	0.0008431
ENSMUSG00000024600	Slc27a6	-7.064425	0.0008446
ENSMUSG00000031447	Lamp1	0.2498628	0.0008446
ENSMUSG00000018417	Myo1b	0.3819636	0.0008649
ENSMUSG00000033436	Armcx2	-0.759828	0.0008777
ENSMUSG00000040785	Ttc3	-0.399193	0.0008777
ENSMUSG00000030282	Cmas	-0.479325	0.0008798
ENSMUSG00000035725	Prkx	-0.503435	0.0008891
ENSMUSG00000093674	Rpl41	0.3080806	0.0009
ENSMUSG00000027852	Nras	-0.38237	0.000906
ENSMUSG00000017713	Tha1	0.672798	0.0009366
ENSMUSG00000037295	Ldlrap1	0.5539438	0.000943
ENSMUSG00000011257	Pabpc4	-0.522472	0.0009784

ENSMUSG00000058600	Rpl30	0.3428431	0.000989
ENSMUSG00000026748	Plxdc2	-0.240376	0.0009969
ENSMUSG00000033917	Gde1	0.4674619	0.0010068
ENSMUSG00000001774	Chordc1	0.4169112	0.0010193
ENSMUSG00000007038	Neu1	0.4325872	0.0010388
ENSMUSG00000105504	Gbp5	0.6359307	0.0010565
ENSMUSG00000031214	Ophn1	-0.288623	0.0010565
ENSMUSG00000039007	Cpq	0.6578299	0.0010678
ENSMUSG00000061100	Retnla	-7.004297	0.001076
ENSMUSG00000032911	Cspg4	-2.353392	0.0010777
ENSMUSG00000044092	C130050O18Rik	0.7796604	0.0010824
ENSMUSG00000046006	Gapt	1.5357885	0.0011009
ENSMUSG00000036617	Etl4	-1.474679	0.0011173
ENSMUSG00000019763	Rmnd1	0.4903165	0.0011416
ENSMUSG00000087117	Gm11523	-7.040005	0.0011451
ENSMUSG00000027339	Rassf2	0.2679436	0.0011493
ENSMUSG00000027956	Tmem144	-0.619154	0.0011493
ENSMUSG00000072964	Bhlhb9	-0.904577	0.0011496
ENSMUSG00000024601	Isoc1	0.4504682	0.0011534
ENSMUSG00000096957	E230013L22Rik	0.663478	0.0011534
ENSMUSG00000022964	Tmem50b	0.3942253	0.0011543
ENSMUSG00000040710	St8sia4	-0.492603	0.0011593
ENSMUSG00000033033	Calhm2	0.4118073	0.0011708
ENSMUSG00000105742	Gm42748	-0.962115	0.0011803
ENSMUSG00000070034	Sp110	0.4372019	0.0011822
ENSMUSG00000034135	Sik3	0.4409329	0.0011837
ENSMUSG00000052151	Plpp2	0.970131	0.0011871
ENSMUSG00000045216	Hs6st1	0.3716393	0.001208
ENSMUSG00000032281	Acsbg1	-2.18124	0.001208
ENSMUSG00000038900	Rpl12	0.3050124	0.0012127
ENSMUSG00000020886	Dlg4	-0.62066	0.0012158
ENSMUSG00000029513	Prkab1	-0.406519	0.0012208
ENSMUSG00000097585	E230029C05Rik	0.4078508	0.0012208
ENSMUSG00000076619	Ighj3	-1.919187	0.0012218
ENSMUSG00000022114	Spry2	-2.501249	0.0012402
ENSMUSG00000047888	Tnrc6b	-0.345472	0.0012451
ENSMUSG00000035681	Kcnc2	-5.105386	0.0012537
ENSMUSG00000029553	Tfec	-1.605239	0.0012611
ENSMUSG00000028654	Mycl	-0.819189	0.0012646
ENSMUSG00000022139	Mbnl2	-0.333079	0.0012766
ENSMUSG00000058290	Espl1	-0.667315	0.0012879
ENSMUSG00000000791	Il12rb1	3.5154798	0.0012983
ENSMUSG00000072620	Slfn2	0.5299986	0.0013025
ENSMUSG00000026778	Prkcq	-1.882069	0.0013025
ENSMUSG00000042451	Mybph	1.0011463	0.0013166
ENSMUSG00000005610	Eif4g2	-0.252972	0.0013218

ENSMUSG00000097296	Gm26532	-0.730873	0.0013361
ENSMUSG00000025743	Sdc3	0.8752144	0.0013363
ENSMUSG00000085977	Gm5970	1.4363946	0.0013522
ENSMUSG00000056268	Dennd1b	0.3800352	0.0013657
ENSMUSG00000017781	Pitpna	-0.347038	0.0013901
ENSMUSG00000030187	Klra2	0.6313618	0.0013916
ENSMUSG00000026199	Ankzf1	0.4600474	0.0013916
ENSMUSG00000003974	Grm3	-3.1584	0.0014028
ENSMUSG00000023805	Synj2	0.5049082	0.0014264
ENSMUSG00000037234	Hook3	-0.349675	0.0014417
ENSMUSG00000108897	Gm44861	0.5067746	0.0014443
ENSMUSG00000032261	Sh3bgrl2	-2.142008	0.001447
ENSMUSG00000101191	Gm28809	0.6907401	0.0014519
ENSMUSG00000004996	Mri1	0.9791604	0.0014551
ENSMUSG00000051456	Hspb3	-0.864233	0.0014594
ENSMUSG00000024197	Plin3	0.6084062	0.00149
ENSMUSG00000021948	Prkcd	0.2721603	0.0015121
ENSMUSG00000102037	Bcl2a1a	0.6163343	0.0015186
ENSMUSG00000052727	Map1b	-1.11565	0.0015186
ENSMUSG00000029759	Pon3	0.3860759	0.0015239
ENSMUSG00000042726	Trafd1	0.3216019	0.001526
ENSMUSG00000062585	Cnr2	0.4882129	0.001526
ENSMUSG00000042429	Adora1	1.3708652	0.0015279
ENSMUSG00000002227	Mov10	0.4471836	0.0015399
ENSMUSG00000048347	Pcdhb18	-6.918055	0.0015686
ENSMUSG00000074361	C5ar2	0.3837743	0.0015934
ENSMUSG00000046442	Ppm1e	-0.97073	0.0016045
ENSMUSG00000067878	Map7d3	1.2280432	0.001609
ENSMUSG00000031647	Mfap3l	-2.089105	0.0016284
ENSMUSG00000062006	Rpl34	0.3167562	0.0016402
ENSMUSG00000030203	Dusp16	-0.479992	0.0016403
ENSMUSG00000028245	Nsmaf	0.344763	0.0016572
ENSMUSG00000044471	Lncpint	0.4032879	0.0016573
ENSMUSG00000003518	Dusp3	-0.414478	0.0016573
ENSMUSG00000036636	Clcn7	0.3404758	0.0016703
ENSMUSG00000022376	Adcy8	-5.045464	0.0016811
ENSMUSG00000026994	Galnt3	0.7347142	0.0016811
ENSMUSG00000006462	A530013C23Rik	0.7709262	0.0017091
ENSMUSG00000025503	Taldo1	0.3732229	0.0017171
ENSMUSG00000036564	Ndrg4	-1.446277	0.0017339
ENSMUSG00000027881	Prpf38b	0.3226137	0.0017655
ENSMUSG00000075595	Zfp652	-0.306185	0.0017717
ENSMUSG00000046364	Rpl27a	0.3219915	0.0017963
ENSMUSG00000039531	Zup1	0.3601623	0.0017969
ENSMUSG00000036957	Lrfn3	-2.599698	0.0018125
ENSMUSG00000023885	Thbs2	-2.701106	0.0018245

ENSMUSG00000025058	Tasl	0.5016106	0.0018256
ENSMUSG00000028546	Elavl4	-1.436355	0.0018408
ENSMUSG00000068735	Trp53i11	0.7186873	0.0018447
ENSMUSG00000021175	Cdca7l	1.6205947	0.0018526
ENSMUSG00000034484	Snx2	-0.352071	0.0019167
ENSMUSG00000052889	Prkcb	0.329254	0.0019167
ENSMUSG00000019916	P4ha1	0.3071131	0.0019454
ENSMUSG00000034101	Ctnnd1	-0.671571	0.0019656
ENSMUSG00000032549	Rab6b	-0.479625	0.001983
ENSMUSG00000032718	Mansc1	1.6361183	0.0019838
ENSMUSG00000076620	Ighj2	-1.811819	0.0020121
ENSMUSG00000110235	Gm5086	0.4146232	0.0020133
ENSMUSG00000025959	Klf7	-0.381686	0.0020507
ENSMUSG00000000127	Fer	-0.612162	0.0020615
ENSMUSG00000029322	Plac8	1.2694713	0.002073
ENSMUSG00000090582	Gm17024	-0.704156	0.0020768
ENSMUSG00000032076	Cadm1	0.2972029	0.0021156
ENSMUSG00000020798	Spns3	0.7628966	0.0021538
ENSMUSG00000074342	I830077J02Rik	0.4026366	0.002158
ENSMUSG00000040462	Os9	0.3267793	0.002158
ENSMUSG00000073590	3222401L13Rik	-0.712148	0.0021839
ENSMUSG00000022895	Ets2	-0.333795	0.0022
ENSMUSG00000104696	Gm42946	2.8866389	0.0022024
ENSMUSG00000021990	Spata13	0.2933264	0.0022041
ENSMUSG00000025967	Eef1b2	0.3280476	0.002217
ENSMUSG00000021699	Pde4d	-1.252565	0.0022273
ENSMUSG00000022893	Adamts1	-0.651007	0.0022318
ENSMUSG00000047146	Tet1	-0.775942	0.0022318
ENSMUSG00000062300	Nectin2	0.496392	0.0022889
ENSMUSG00000043323	Fbrsl1	0.3706772	0.0022956
ENSMUSG00000029528	Pxn	-0.308968	0.0023403
ENSMUSG00000029392	Rilpl1	0.4102203	0.0023447
ENSMUSG00000073680	Tmem88b	-3.448621	0.0023533
ENSMUSG00000037563	Rps16	0.2828927	0.0023546
ENSMUSG00000039005	Tlr4	0.305077	0.0023713
ENSMUSG00000042328	Hps4	0.2731523	0.0023745
ENSMUSG00000085875	Gm12905	0.5300158	0.0024118
ENSMUSG00000030541	Idh2	-0.367541	0.002415
ENSMUSG00000024451	Arap3	-0.280305	0.0024155
ENSMUSG00000003949	Hlf	-1.78892	0.0024225
ENSMUSG00000003484	Cyp4f18	0.7743135	0.0024268
ENSMUSG00000008658	Rbfox1	-1.982189	0.002438
ENSMUSG00000040212	Emp3	-0.614377	0.0024389
ENSMUSG00000020460	Rps27a	0.3002722	0.0025028
ENSMUSG00000028497	Hacd4	0.4228528	0.0025106
ENSMUSG00000040613	Apobec1	0.3554592	0.0025106

ENSMUSG00000029461	Fam168a	-0.348728	0.0025121
ENSMUSG00000026630	Batf3	0.6142977	0.0025208
ENSMUSG00000019810	Fuca2	0.3557431	0.0025216
ENSMUSG00000027674	Pex5l	-2.844819	0.0026179
ENSMUSG00000031278	Acsl4	-0.342164	0.0026986
ENSMUSG00000026357	Rgs18	-1.691302	0.0027099
ENSMUSG00000022887	Masp1	-1.194392	0.0027227
ENSMUSG00000001942	Siae	0.486264	0.002752
ENSMUSG00000034177	Rnf43	2.7733988	0.0027713
ENSMUSG00000055546	Timd4	-1.33067	0.002773
ENSMUSG00000028081	Rps3a1	0.2768826	0.0027961
ENSMUSG00000102418	Sh2d1b1	1.5256437	0.0028086
ENSMUSG00000026938	Fcna	-6.061349	0.0028621
ENSMUSG00000034731	Dgkh	-0.801061	0.0028636
ENSMUSG00000038260	Trpm4	-0.576591	0.0029074
ENSMUSG00000027318	Adam33	0.4815944	0.0029168
ENSMUSG00000103585	Pcdhgb4	-0.952941	0.0029293
ENSMUSG00000032554	Trf	0.2620506	0.0029571
ENSMUSG00000001783	Rtcb	0.3192259	0.0029586
ENSMUSG00000022285	Ywhaz	-0.300763	0.002987
ENSMUSG00000013523	Bcas1	-1.897077	0.0030074
ENSMUSG00000043467	Zbtb37	-0.425636	0.0030636
ENSMUSG00000039782	Cpeb2	-0.371189	0.0030901
ENSMUSG00000042804	Gpr153	-2.122595	0.0030901
ENSMUSG00000087289	4933424M12Rik	1.1701288	0.0030945
ENSMUSG00000056476	Med12l	-0.380033	0.0031339
ENSMUSG00000049723	Mmp12	-1.459259	0.0031386
ENSMUSG00000066170	E230001N04Rik	1.7175292	0.0031455
ENSMUSG00000030432	Rpl28	0.301477	0.0031822
ENSMUSG00000044456	Rin3	0.352241	0.0031934
ENSMUSG00000053835	H2-T24	0.4241967	0.0031934
ENSMUSG00000032462	Pik3cb	0.3258905	0.003201
ENSMUSG00000028645	Slc2a1	0.3824775	0.003201
ENSMUSG00000033948	Zswim5	-0.987599	0.003201
ENSMUSG00000016128	Stard13	-2.169127	0.0032138
ENSMUSG00000054203	Ifi205	2.8080181	0.0032241
ENSMUSG00000091549	Gm6548	0.6480118	0.0032649
ENSMUSG00000041571	Selenow	0.5618801	0.0032919
ENSMUSG00000028644	Ermap	0.498452	0.0032968
ENSMUSG00000056888	Glipr1	0.6961878	0.0033117
ENSMUSG00000020717	Pecam1	-0.596191	0.003319
ENSMUSG00000020932	Gfap	-1.451341	0.0033452
ENSMUSG00000067336	Bmpr2	-0.289184	0.0033567
ENSMUSG00000038271	Iffo1	-0.33422	0.0033605
ENSMUSG00000075122	Cd80	0.5703234	0.003376
ENSMUSG00000103851	Gm37606	-1.305971	0.0033896

ENSMUSG00000041645	Ddx24	0.3905608	0.0034042
ENSMUSG00000028680	Plk3	0.7595662	0.0034296
ENSMUSG00000018830	Myh11	-3.377211	0.0034296
ENSMUSG00000022378	Cyrib	0.2635837	0.0034296
ENSMUSG00000026848	Tor1b	0.3501196	0.0034999
ENSMUSG00000022791	Tnk2	-1.180189	0.0035523
ENSMUSG00000038028	Tigar	0.8604137	0.0035597
ENSMUSG00000026012	Cd28	-3.726708	0.003578
ENSMUSG00000025059	Gk	0.7088728	0.0035893
ENSMUSG00000053040	Aph1c	0.8241007	0.0036025
ENSMUSG00000036986	Pml	0.5187216	0.0036325
ENSMUSG00000017561	Crlf3	0.3077212	0.0036557
ENSMUSG00000058793	Cds2	-0.289028	0.0037292
ENSMUSG00000031504	Rab20	0.8099148	0.0037292
ENSMUSG00000028278	Rragd	-1.273447	0.0037482
ENSMUSG00000037692	Ahdc1	-0.41747	0.0037517
ENSMUSG00000028989	Angptl7	-1.27557	0.0037605
ENSMUSG00000026728	Vim	-0.450793	0.0037724
ENSMUSG00000033781	Asb13	0.5175637	0.0037777
ENSMUSG00000026074	Map4k4	-0.264106	0.0038153
ENSMUSG00000103144	Pcdhga1	-1.265703	0.0039015
ENSMUSG00000035354	Uvrag	0.3327958	0.0039099
ENSMUSG00000101167	Macroh2a3	2.4414117	0.0039099
ENSMUSG00000028399	Ptprd	-2.799467	0.003911
ENSMUSG00000066129	Kndc1	-2.247007	0.0039172
ENSMUSG00000026604	Ptpn14	-1.977592	0.0039557
ENSMUSG00000033208	S100b	-1.733557	0.0039637
ENSMUSG00000032238	Rora	-0.906856	0.0039658
ENSMUSG00000075254	Heg1	-1.314979	0.0039798
ENSMUSG00000039145	Camk1d	0.2882622	0.0040177
ENSMUSG00000102336	Gm37233	-0.472147	0.0040405
ENSMUSG00000037260	Hgsnat	-0.400293	0.0040616
ENSMUSG00000064348	mt-Tn	-0.89114	0.004068
ENSMUSG00000053063	Clec12a	-0.595837	0.0040982
ENSMUSG00000038733	Wdr26	-0.255581	0.0041176
ENSMUSG00000033871	Ppargc1b	1.0003391	0.0041204
ENSMUSG00000090881	Phf11	2.4696069	0.0042268
ENSMUSG00000110245	Gm20100	1.024783	0.0042336
ENSMUSG00000050002	Idnk	0.4820953	0.0042636
ENSMUSG00000039153	Runx2	-1.519934	0.0043998
ENSMUSG00000094628	Gm3252	-1.641455	0.0044148
ENSMUSG00000029826	Zc3hav1	0.3271324	0.0044305
ENSMUSG00000114329	Gm30489	-2.374731	0.0044383
ENSMUSG00000028610	Dmrtb1	0.9729116	0.004454
ENSMUSG00000061244	Exoc5	-0.397748	0.0044721
ENSMUSG00000046160	Olig1	-2.491773	0.00451

ENSMUSG00000032300	1700017B05Rik	0.2640522	0.004553
ENSMUSG00000092035	Peg10	-0.458321	0.0045628
ENSMUSG00000055110	A630012P03Rik	3.666661	0.0046167
ENSMUSG00000008496	Pou2f2	-0.361476	0.0046427
ENSMUSG00000022946	Dop1b	0.3802344	0.0046929
ENSMUSG00000114205	Gm7480	1.2843215	0.0047262
ENSMUSG00000033697	Arhgap39	0.2736726	0.0047529
ENSMUSG00000053049	Gm15413	4.269843	0.0047968
ENSMUSG00000028189	Ctbs	0.4367098	0.004814
ENSMUSG00000026466	Tor1aip1	0.2965759	0.004814
ENSMUSG00000103332	Pcdhga2	-1.405382	0.004814
ENSMUSG00000090272	Mndal	-0.554389	0.004814
ENSMUSG00000024533	Spire1	0.2998605	0.0048191
ENSMUSG00000026782	Abi2	-0.48721	0.0048191
ENSMUSG00000029490	Mfsd7a	0.7366336	0.0048564
ENSMUSG00000020682	Mmp28	-2.463193	0.0048751
ENSMUSG00000076618	Ighj4	-1.294004	0.0048751
ENSMUSG00000030149	Klrk1	1.9010416	0.0048751
ENSMUSG00000036661	Dennd3	1.085695	0.0048827
ENSMUSG00000041329	Atp1b2	-1.802076	0.0049646
ENSMUSG00000032547	Ryk	-0.63762	0.0050024
ENSMUSG00000056145	AI504432	-0.695955	0.0050115
ENSMUSG00000104292	Gm38042	0.635349	0.0050553
ENSMUSG00000037306	Man1c1	-0.245215	0.00509
ENSMUSG00000001424	Snd1	0.3049763	0.0051244
ENSMUSG00000032656	Marchf3	-1.19921	0.0051334
ENSMUSG00000045193	Cirbp	0.5216887	0.0051376
ENSMUSG00000022371	Col14a1	-0.753472	0.0051525
ENSMUSG00000025375	Aatk	0.5604968	0.0051525
ENSMUSG00000095186	Gm10718	-2.792229	0.005156
ENSMUSG00000035877	Zhx3	-0.574132	0.0051952
ENSMUSG00000037280	Galnt6	-1.172107	0.0051952
ENSMUSG00000030671	Pde3b	-0.30735	0.005202
ENSMUSG00000064141	Zfp69	0.4445868	0.005202
ENSMUSG00000028495	Rps6	0.2961309	0.0052022
ENSMUSG00000035212	Leprot	0.3063416	0.0052596
ENSMUSG00000033174	Mgll	-0.498986	0.0053022
ENSMUSG00000030310	Slc6a1	-2.320648	0.005335
ENSMUSG00000025008	Tctn3	0.6579207	0.0053473
ENSMUSG00000066440	Zfyve26	0.3052325	0.0053473
ENSMUSG00000022360	Atad2	0.474168	0.0053585
ENSMUSG00000025986	Slc39a10	-0.384703	0.0053667
ENSMUSG00000002265	Peg3	-1.858087	0.0053684
ENSMUSG00000018340	Anxa6	0.3926149	0.0053749
ENSMUSG00000060261	Gtf2i	-0.278197	0.0053843
ENSMUSG00000040797	Iqsec3	-6.560125	0.0053856

ENSMUSG00000054150	Syne3	-1.685973	0.0054341
ENSMUSG00000034892	Rps29	0.3410429	0.0054675
ENSMUSG00000105700	Gm42772	6.5277314	0.0054675
ENSMUSG00000027351	Spred1	-0.317762	0.0054675
ENSMUSG00000022987	Zfp641	0.812735	0.0054675
ENSMUSG00000054252	Fgfr3	-2.421681	0.0054965
ENSMUSG00000002059	Rab34	-0.800709	0.005522
ENSMUSG00000024805	Pcgf5	0.6573283	0.0055896
ENSMUSG00000037344	Slc12a9	0.288511	0.0056135
ENSMUSG00000031540	Kat6a	-0.249992	0.0056528
ENSMUSG00000047220	Iho1	-1.580185	0.0056561
ENSMUSG00000048022	Tmem229a	0.9095161	0.0057496
ENSMUSG00000026678	Rgs5	-1.358666	0.0057844
ENSMUSG00000097855	A930007I19Rik	0.5900595	0.0057903
ENSMUSG00000052428	Tmco1	0.3851279	0.0058404
ENSMUSG00000053560	Ier2	-0.286068	0.0058421
ENSMUSG00000030403	Vasp	0.26792	0.0058423
ENSMUSG00000025982	Sf3b1	0.2313128	0.0058664
ENSMUSG00000106639	Gm43121	0.7532171	0.0058786
ENSMUSG00000052384	Nrros	-0.36499	0.0058786
ENSMUSG00000079641	Rpl39	0.387999	0.0059837
ENSMUSG00000038507	Parp12	0.8123326	0.0060225
ENSMUSG00000042978	Sbk1	-1.106147	0.0060506
ENSMUSG00000039294	Cybc1	0.329936	0.0060506
ENSMUSG00000017737	Mmp9	-1.179397	0.0060513
ENSMUSG00000034297	Med13	-0.290055	0.0060539
ENSMUSG00000027522	Stx16	0.3144784	0.0060794
ENSMUSG00000006281	Tep1	0.3039089	0.0060875
ENSMUSG00000020721	Helz	-0.321631	0.0061015
ENSMUSG00000020154	Ptprb	-1.028153	0.0061892
ENSMUSG00000022351	Sqle	-1.202683	0.0061895
ENSMUSG00000050121	Opalin	-6.517744	0.0062295
ENSMUSG00000012640	Zfp715	-0.310866	0.0062497
ENSMUSG00000030265	Kras	-0.427143	0.0062785
ENSMUSG00000024308	Tapbp	0.2678188	0.0063303
ENSMUSG00000056724	Nbeal2	-0.296542	0.0063921
ENSMUSG00000032854	Ugt8a	-2.347265	0.0064161
ENSMUSG00000038366	Lasp1	-0.258037	0.0064745
ENSMUSG00000022295	Atp6v1c1	0.2855089	0.0065087
ENSMUSG00000026223	Itm2c	0.2410791	0.0065213
ENSMUSG00000037318	Traf3ip3	0.4003921	0.0065213
ENSMUSG00000027808	Serp1	0.327952	0.0065281
ENSMUSG00000035900	Gramd4	-0.626489	0.006529
ENSMUSG00000029417	Cxcl9	1.7776507	0.0066531
ENSMUSG00000040488	Ltbp4	-1.296314	0.0066865
ENSMUSG00000020522	Mfap3	-0.301944	0.00669

ENSMUSG00000032409	Atr	0.3621399	0.00669
ENSMUSG00000109713	Pvrig	1.127954	0.0067477
ENSMUSG00000045382	Cxcr4	0.477657	0.0067984
ENSMUSG00000071369	Map3k5	0.3113114	0.0068005
ENSMUSG00000000275	Trim25	0.4012722	0.0068691
ENSMUSG00000063458	Lrmda	0.7586276	0.0069313
ENSMUSG00000045268	Zfp691	0.3093967	0.0070852
ENSMUSG00000024140	Epas1	-1.0303	0.0070925
ENSMUSG00000048965	Mrgpre	-0.960351	0.0071199
ENSMUSG00000118183	Gm50345	0.7170457	0.0071858
ENSMUSG00000000740	Rpl13	0.2476853	0.0072317
ENSMUSG00000029009	Mthfr	0.3756346	0.0073101
ENSMUSG00000097325	Gm16897	1.0091209	0.0073101
ENSMUSG00000015222	Map2	-1.551824	0.0073101
ENSMUSG00000022453	Naga	0.3112207	0.0073824
ENSMUSG00000022148	Fyb	0.235714	0.0074171
ENSMUSG00000073771	Btbd19	0.4426582	0.0074264
ENSMUSG00000021453	Gadd45g	-0.442002	0.0074264
ENSMUSG00000040852	Plekhh2	-0.714475	0.0074391
ENSMUSG00000024608	Rps14	0.276716	0.0074885
ENSMUSG00000002007	Srpk3	-0.571328	0.0075299
ENSMUSG00000025372	Baiap2	0.6368106	0.0075516
ENSMUSG00000001249	Hpn	0.6936603	0.0075527
ENSMUSG00000020604	Arsg	-0.621446	0.0075697
ENSMUSG00000034855	Cxcl10	1.1708398	0.007604
ENSMUSG00000099881	2810013P06Rik	0.4886601	0.007604
ENSMUSG00000034575	Tent4a	0.4159677	0.007604
ENSMUSG00000043556	Fbxl7	-5.716953	0.007604
ENSMUSG00000021457	Syk	0.2391233	0.0076058
ENSMUSG00000036053	Fmnl2	0.370008	0.0076665
ENSMUSG00000031760	Mt3	-1.753482	0.0076712
ENSMUSG00000021666	Gfm2	-0.249725	0.0076933
ENSMUSG00000063354	Slc39a4	0.7895457	0.0077513
ENSMUSG00000041453	Rpl21	0.3109008	0.0077583
ENSMUSG00000049550	Clip1	-0.28947	0.0077743
ENSMUSG00000022586	Ly6i	2.5304016	0.0077933
ENSMUSG00000021061	Sptb	-1.924025	0.0079712
ENSMUSG00000022529	Zfp263	0.3384768	0.0079847
ENSMUSG00000056413	Adap1	0.4440471	0.0079929
ENSMUSG00000062328	Rpl17	0.2619619	0.0081671
ENSMUSG00000042333	Tnfrsf14	0.3946419	0.0082075
ENSMUSG00000030793	Pycard	-0.453005	0.0082121
ENSMUSG00000062098	Btbd3	-0.581826	0.0083083
ENSMUSG00000047215	Rpl9	0.2562652	0.0083458
ENSMUSG00000047843	Bri3	0.3840049	0.0083585
ENSMUSG00000113326	Gm47586	-2.292442	0.008401

ENSMUSG00000058756	Thra	-0.784282	0.008411
ENSMUSG00000041245	Wnk3	-3.017907	0.0084553
ENSMUSG00000057367	Birc2	0.3667955	0.0084619
ENSMUSG00000037300	Ttc13	-0.391176	0.0084762
ENSMUSG00000086370	Ftx	0.5810052	0.0084888
ENSMUSG00000051506	Wdfy4	0.248705	0.0085459
ENSMUSG00000000881	Dlg3	-0.552962	0.0085956
ENSMUSG00000104339	C130089K02Rik	0.6611768	0.0086014
ENSMUSG00000049999	Ppp1r3d	0.5772532	0.0086832
ENSMUSG00000020898	Ctc1	0.2712925	0.0087148
ENSMUSG00000071713	Csf2rb	0.2811799	0.0087342
ENSMUSG00000079481	Nhsl2	-0.698998	0.0088492
ENSMUSG00000037887	Dusp8	-1.071544	0.00889
ENSMUSG00000062373	Tmem65	0.3840997	0.0088939
ENSMUSG00000041720	Pi4ka	-0.308124	0.0089237
ENSMUSG00000020331	Hcn2	-1.89907	0.0089237
ENSMUSG00000031133	Arhgef6	-0.265932	0.0089237
ENSMUSG00000023845	Lnpep	0.2375213	0.0089804
ENSMUSG00000035692	Isg15	1.7189027	0.0089849
ENSMUSG00000026458	Ppfia4	0.2452792	0.0089849
ENSMUSG00000017670	Elmo2	-0.327511	0.0089869
ENSMUSG00000061143	Maml3	0.3822308	0.0091827
ENSMUSG00000029063	Nadk	0.3277757	0.0092703
ENSMUSG00000030162	Olr1	-1.143234	0.0093059
ENSMUSG00000022228	Zscan26	0.2781799	0.0093243
ENSMUSG00000037533	Rapgef6	-0.270036	0.0093299
ENSMUSG00000092528	Nlrp1c-ps	0.3214922	0.0093299
ENSMUSG00000022186	Oxct1	-0.262486	0.0093299
ENSMUSG00000023067	Cdkn1a	-0.385504	0.0093299
ENSMUSG00000039081	Zfp503	1.2264054	0.0093443
ENSMUSG00000040165	Cd209c	-6.437245	0.0093782
ENSMUSG00000112640	Gm32687	-6.437245	0.0093782
ENSMUSG00000025809	Itgb1	-0.231923	0.0093847
ENSMUSG00000044629	Cnrip1	-0.831986	0.0094609
ENSMUSG00000058446	Znrf2	0.3145247	0.0094617
ENSMUSG00000055421	Pcdh9	-2.582973	0.0094617
ENSMUSG00000062170	Fmr1nb	-2.945299	0.0094617
ENSMUSG00000022629	Kif21a	-2.713683	0.0094617
ENSMUSG00000036820	Amdhd2	0.3721997	0.0095256
ENSMUSG00000037552	Plekhg2	-0.514932	0.0095639
ENSMUSG00000031227	Magee1	-1.042959	0.009625
ENSMUSG00000006519	Cyba	0.3033953	0.0096341
ENSMUSG00000032118	Fez1	-1.846932	0.0096845
ENSMUSG00000037408	Cnnm4	0.4230223	0.0097627
ENSMUSG00000024013	Fgd2	0.2361118	0.0098529
ENSMUSG00000001348	Acp5	2.349664	0.009917

ENSMUSG00000106047	Gm42942	6.3384294	0.0099806
ENSMUSG00000036246	Gmip	0.2522583	0.0100018
ENSMUSG00000097149	G630030J09Rik	0.6112226	0.0101324
ENSMUSG00000030774	Pak1	0.3299443	0.0101561
ENSMUSG00000050549	Fam241a	1.1990628	0.0101799
ENSMUSG00000026109	Tmeff2	-3.803888	0.0103054
ENSMUSG00000020256	Aldh1l2	-1.451685	0.010471
ENSMUSG00000033790	Tubgcp5	-0.278483	0.0104776
ENSMUSG00000097571	Jpx	0.7823459	0.0104776
ENSMUSG00000087107	AI662270	-1.855435	0.0105059
ENSMUSG00000027199	Gatm	0.2590298	0.0105398
ENSMUSG00000031309	Rps6ka3	-0.345958	0.0105398
ENSMUSG00000046314	Stxbp6	-3.594422	0.0105398
ENSMUSG00000055717	Slain1	-2.845732	0.0106434
ENSMUSG00000029213	Commd8	-0.306858	0.0107187
ENSMUSG00000000290	Itgb2	0.2116928	0.0107206
ENSMUSG00000029299	Abcg3	0.6556914	0.0107212
ENSMUSG00000058881	Zfp516	0.3297303	0.0107298
ENSMUSG00000049119	Fam110b	-1.935518	0.0107898
ENSMUSG00000022475	Hdac7	0.7899269	0.0108238
ENSMUSG00000086841	2410006H16Rik	0.4253047	0.0108269
ENSMUSG00000034009	Rxfp1	-2.900818	0.010851
ENSMUSG00000028381	Ugcg	0.3449972	0.0108849
ENSMUSG00000008348	Ubc	0.2199585	0.0108897
ENSMUSG00000036438	Calm2	-0.264826	0.0109715
ENSMUSG00000001166	Oas1c	1.2992227	0.0109958
ENSMUSG00000095041		0.2329283	0.0110763
ENSMUSG00000031604	Msmo1	-0.570828	0.0110857
ENSMUSG00000040466	Blvrb	-0.650265	0.0110964
ENSMUSG00000108820	Gm44620	1.4421223	0.0111206
ENSMUSG00000032643	Fhl3	-0.59373	0.0111206
ENSMUSG00000037936	Scarb1	-0.602829	0.0111312
ENSMUSG00000026482	Rgl1	-0.322982	0.0112916
ENSMUSG00000111390	Gm48796	-2.603055	0.0113133
ENSMUSG00000005580	Adcy9	-0.4217	0.0113198
ENSMUSG00000026880	Stom	-0.490107	0.0114075
ENSMUSG00000089712	Gm15889	0.7614374	0.0114783
ENSMUSG00000028811	Yars	-0.400948	0.0115197
ENSMUSG00000070565	Rasal2	-0.423338	0.0116157
ENSMUSG00000035299	Mid1	-0.724523	0.0116484
ENSMUSG00000026958	Dpp7	0.3918367	0.0117656
ENSMUSG00000037742	Eef1a1	0.2034871	0.0117808
ENSMUSG00000069919	Hba-a1	-2.656081	0.0118363
ENSMUSG00000031320	Rps4x	0.22935	0.0118634
ENSMUSG00000025855	Prkar1b	0.7606472	0.0118715
ENSMUSG00000038023	Atp6v0a2	0.2763774	0.0120954

ENSMUSG00000028656	Cap1	-0.21475	0.0121113
ENSMUSG00000026933	Camsap1	-0.333219	0.0121265
ENSMUSG00000035713	Usp35	0.251631	0.012153
ENSMUSG00000115762	Gm34907	-2.538919	0.0121693
ENSMUSG00000032624	Eml4	-0.283149	0.0122357
ENSMUSG00000030307	Slc6a11	-2.168122	0.0123507
ENSMUSG00000002190	Clgn	-1.085563	0.0123542
ENSMUSG00000035004	Igsf6	0.3522194	0.0123542
ENSMUSG00000035829	Ppp1r26	-0.814941	0.0125293
ENSMUSG00000040537	Adam22	-0.815546	0.0125498
ENSMUSG00000042700	Sipa1l1	-0.333356	0.0125525
ENSMUSG00000039470	Zdhhc2	2.1051556	0.0125622
ENSMUSG00000103050	Gm38273	1.7214101	0.0126164
ENSMUSG00000079388	2610042L04Rik	-2.81229	0.0126796
ENSMUSG00000026991	Pkp4	-0.476095	0.0127913
ENSMUSG00000006576	Slc4a3	1.6619541	0.0128845
ENSMUSG00000026395	Ptprc	0.2295152	0.0129032
ENSMUSG00000054499	Dedd2	0.4945328	0.012906
ENSMUSG00000045658	Pid1	-0.364312	0.0129177
ENSMUSG00000024248	Cox7a2l	0.317547	0.0129177
ENSMUSG00000018398	Septin8	-0.428671	0.0129468
ENSMUSG00000029189	Sel1l3	-4.014552	0.0129709
ENSMUSG00000045917	Tmem268	0.3628262	0.0129841
ENSMUSG00000020399	Havcr2	0.2555452	0.0130211
ENSMUSG00000027224	Duoxa1	-2.656235	0.0130634
ENSMUSG00000064363	mt-Nd4	-1.142501	0.0130786
ENSMUSG00000112545	1300014J16Rik	0.7560484	0.0131488
ENSMUSG00000052698	Tln2	-0.318241	0.0131488
ENSMUSG00000035064	Eef2k	-0.259194	0.0132869
ENSMUSG00000100017	2410022M11Rik	0.7831219	0.0132906
ENSMUSG00000031939	Taf1d	0.2922971	0.0134321
ENSMUSG00000086291	Gm15513	0.7648726	0.0134697
ENSMUSG00000078763	Slfn1	0.9055921	0.013492
ENSMUSG00000049532	Sall2	-0.461531	0.013507
ENSMUSG00000022240	Ctnnd2	-0.587918	0.0135157
ENSMUSG00000054520	Sh3bp2	0.3407562	0.0135284
ENSMUSG00000028337	Coro2a	0.4647128	0.01359
ENSMUSG00000019082	Slc25a22	0.5639365	0.0136079
ENSMUSG00000026826	Nr4a2	-0.744609	0.0136265
ENSMUSG00000035824	Tk2	0.3105485	0.0137335
ENSMUSG00000027293	Ehd4	-0.253333	0.013832
ENSMUSG00000040747	Cd53	-0.204107	0.0138324
ENSMUSG00000030921	Trim30a	0.6882436	0.013929
ENSMUSG00000104034	2900092N22Rik	2.1767645	0.0140732
ENSMUSG00000028842	Ago3	-0.319286	0.0141525
ENSMUSG00000052270	Fpr2	0.9614269	0.0141786

ENSMUSG00000033192	Lpcat2	0.2506404	0.0141901
ENSMUSG00000015133	Lrrk1	0.2452202	0.0142178
ENSMUSG00000031154	Otud5	0.2729931	0.0142178
ENSMUSG00000022607	Ptk2	-0.88732	0.0142606
ENSMUSG00000000901	Mmp11	-1.369936	0.0142855
ENSMUSG00000059336	Slc14a1	-1.203765	0.0144309
ENSMUSG00000025997	Ikzf2	-0.571047	0.0144309
ENSMUSG00000031858	Mau2	0.2457325	0.0145332
ENSMUSG00000026489	Coq8a	0.6544994	0.0145723
ENSMUSG00000039427	Alg1	0.4052905	0.0146095
ENSMUSG00000027806	Tsc22d2	0.2602548	0.0146359
ENSMUSG00000073728	Tmem51os1	6.2187296	0.0146507
ENSMUSG00000022054	Nefm	-2.175428	0.014676
ENSMUSG00000018341	Il12rb2	0.9269421	0.0147377
ENSMUSG00000112095	A130077B15Rik	0.6354541	0.0147909
ENSMUSG00000021198	Unc79	-1.105081	0.0148329
ENSMUSG00000054843	Atrnl1	0.5138208	0.0148515
ENSMUSG00000050578	Mmp13	-6.298793	0.014862
ENSMUSG00000009927	Rps25	0.2631376	0.0151569
ENSMUSG00000034312	Iqsec1	-0.420156	0.015258
ENSMUSG00000014782	Plekhg4	4.5156319	0.015266
ENSMUSG00000030471	Zdhhc13	0.4223292	0.015279
ENSMUSG00000029538	Srsf9	0.3109057	0.0154441
ENSMUSG00000020458	Rtn4	-0.228063	0.0156353
ENSMUSG00000117613	Gm2629	-0.269947	0.0156671
ENSMUSG00000020840	Blmh	-0.402426	0.0156947
ENSMUSG00000039477	Tnrc18	-0.248123	0.0156981
ENSMUSG00000008734	Gprc5b	-2.027496	0.0157125
ENSMUSG00000049103	Ccr2	-1.332581	0.0158092
ENSMUSG00000117239	Gpr31c	2.0556781	0.0159239
ENSMUSG00000024045	Akap8	0.2484924	0.0160366
ENSMUSG00000038026	Kcnj9	0.9133904	0.0161123
ENSMUSG00000024750	Zfand5	-0.228436	0.0161647
ENSMUSG00000021365	Nedd9	0.5981311	0.0162591
ENSMUSG00000041654	Slc39a11	0.4862666	0.0163348
ENSMUSG00000036036	Zfp57	-2.118708	0.0163532
ENSMUSG00000056429	Tgoln1	0.2280249	0.0166991
ENSMUSG00000000628	Hk2	0.2437074	0.0168433
ENSMUSG00000030737	Slco2b1	-0.187987	0.0168537
ENSMUSG00000024378	Stard4	-0.967623	0.0169139
ENSMUSG00000027273	Snap25	-1.050466	0.0169279
ENSMUSG00000027078	Ube2l6	0.6458825	0.0169687
ENSMUSG00000064347	mt-Ta	-1.002723	0.0169687
ENSMUSG00000001763	Tspan33	0.6338154	0.0169687
ENSMUSG00000090733	Rps27	0.2835273	0.0169687
ENSMUSG00000111324	Gm31410	0.9521566	0.017006

ENSMUSG00000032827	Ppp1r9a	-0.234546	0.0170893
ENSMUSG00000038463	Olfml2b	-0.527972	0.0170893
ENSMUSG00000045095	Magi1	-0.446155	0.0170893
ENSMUSG00000029705	Cux1	-0.25582	0.0171188
ENSMUSG00000058325	Dock1	-0.296614	0.0172352
ENSMUSG00000036452	Arhgap26	-0.842846	0.0173126
ENSMUSG00000029033	Acap3	-0.597595	0.0173379
ENSMUSG00000031996	Aplp2	-0.250915	0.0173379
ENSMUSG00000063077	Kif1b	0.2625214	0.0174818
ENSMUSG00000010663	Fads1	-0.324733	0.0176562
ENSMUSG00000017740	Slc12a5	-1.403986	0.0176799
ENSMUSG00000045968	Teddm2	0.4659068	0.0182212
ENSMUSG00000025701	Alox5	0.3321561	0.0183
ENSMUSG00000087674	4930447M23Rik	-1.405461	0.0184159
ENSMUSG00000008393	Carhsp1	-0.549716	0.0185698
ENSMUSG00000102808	5430420F09Rik	0.9941698	0.0186747
ENSMUSG00000070044	Fam149a	0.618632	0.0186999
ENSMUSG00000025813	Homer2	-3.204569	0.0187011
ENSMUSG00000044667	Plppr4	0.6927385	0.0187213
ENSMUSG00000030986	Dhx32	-0.468293	0.0189419
ENSMUSG00000034449	Dhrs11	0.7722947	0.0190321
ENSMUSG00000090394	4930523C07Rik	1.0463756	0.0190724
ENSMUSG00000019996	Map7	-0.75981	0.0191332
ENSMUSG00000038527	C1rl	0.5781161	0.0191517
ENSMUSG00000063457	Rps15	0.2781361	0.0191566
ENSMUSG00000075010	AW112010	0.9523442	0.0194289
ENSMUSG00000040774	Cept1	0.3046457	0.0194987
ENSMUSG00000020733	Slc9a3r1	0.3471358	0.0195116
ENSMUSG00000022504	Ciita	-0.731129	0.0195282
ENSMUSG00000025085	Ablim1	-0.944539	0.019556
ENSMUSG00000006304	Arpc2	-0.234846	0.0196026
ENSMUSG00000037119	Fam91a1	0.2055136	0.0196168
ENSMUSG00000039361	Picalm	-0.213659	0.01972
ENSMUSG00000037664	Cdkn1c	-1.118765	0.01972
ENSMUSG00000046718	Bst2	0.945012	0.019727
ENSMUSG00000063450	Syne2	-0.583778	0.0197776
ENSMUSG00000020580	Rock2	-0.259496	0.019791
ENSMUSG00000036850	Mrpl41	0.5708075	0.0198009
ENSMUSG00000030402	Ppm1n	2.5636184	0.0199045
ENSMUSG00000022884	Eif4a2	0.2112519	0.0199064
ENSMUSG00000028152	Tspan5	-0.588075	0.0199064
ENSMUSG00000079197	Psme2	0.3628052	0.0199688
ENSMUSG00000106385	Gm42943	2.8313761	0.0200099
ENSMUSG00000017466	Timp2	-0.236123	0.0202083
ENSMUSG00000026424	Gpr37l1	-2.166072	0.0202611
ENSMUSG00000041390	Mdfic	-0.56117	0.0202611

ENSMUSG00000025270	Alas2	-2.484678	0.020291
ENSMUSG00000028463	Car9	1.4888687	0.0203337
ENSMUSG00000024679	Ms4a6d	0.3572445	0.0203892
ENSMUSG00000022037	Clu	-1.15357	0.0205207
ENSMUSG00000022051	Bnip3l	-0.3291	0.0205748
ENSMUSG00000029471	Camkk2	0.320642	0.0205748
ENSMUSG00000026565	Pou2f1	-0.342551	0.0205781
ENSMUSG00000086708	Gm15577	3.7609856	0.020596
ENSMUSG00000022667	Cd200r1	-0.563024	0.0206769
ENSMUSG00000030707	Coro1a	0.2223104	0.0207016
ENSMUSG00000086813	Gm13657	1.2697474	0.0207016
ENSMUSG00000007458	M6pr	0.231714	0.0208155
ENSMUSG00000033538	Casp4	0.4547219	0.0210194
ENSMUSG00000035413	Tmem98	-3.180021	0.0210412
ENSMUSG00000026930	Gpsm1	-0.465189	0.0210412
ENSMUSG00000017291	Taok1	-0.221719	0.021149
ENSMUSG00000071547	Nt5dc2	-0.750034	0.021149
ENSMUSG00000035273	Hpse	0.9785918	0.0211769
ENSMUSG00000073940	Hbb-bt	-2.703193	0.0212433
ENSMUSG00000024187	Fam234a	-0.418837	0.0214312
ENSMUSG00000038776	Ephx1	-0.520388	0.0216868
ENSMUSG00000015599	Ttbk1	-1.281793	0.0218937
ENSMUSG00000048852	Gm12185	0.8842785	0.0218937
ENSMUSG00000093661	Eif4e3	0.5671787	0.0222588
ENSMUSG00000083305	Gm13315	1.819733	0.0222757
ENSMUSG00000001751	Naglu	0.2672393	0.0223234
ENSMUSG00000051223	Bzw1	-0.265707	0.0224674
ENSMUSG00000028378	Ptgr1	0.5898413	0.0225239
ENSMUSG00000041633	Kctd12b	-0.820081	0.0225504
ENSMUSG00000037996	Slc24a2	-2.946103	0.0228895
ENSMUSG00000044807	Zfp354c	-0.908239	0.0228895
ENSMUSG00000074415	Mir100hg	-6.098796	0.0229041
ENSMUSG00000027900	Dram2	0.3052067	0.0229041
ENSMUSG00000049866	Arl4c	0.2173874	0.0230388
ENSMUSG00000079222		6.0667234	0.0230939
ENSMUSG00000052305	Hbb-bs	-2.621754	0.0231303
ENSMUSG00000079685	Ulbp1	0.7221904	0.0232047
ENSMUSG00000029675	Eln	-3.781837	0.0234414
ENSMUSG00000024097	Srsf7	0.2486176	0.0235201
ENSMUSG00000040128	Pnrc1	0.2215101	0.0235991
ENSMUSG00000076439	Mog	-2.117934	0.0236081
ENSMUSG00000029254	Stap1	-0.763385	0.0236618
ENSMUSG00000083651	Gm11524	-6.088319	NA
ENSMUSG00000031129	Slc9a9	-0.266241	0.0240439
ENSMUSG00000024425	Ndfip1	-0.273506	0.0240689
ENSMUSG00000038178	Slc43a2	-0.258702	0.0241232

ENSMUSG00000105873	Gm43708	-6.218394	0.0243362
ENSMUSG00000103885	Gm37006	1.5557502	0.0243645
ENSMUSG00000079523	Tmsb10	0.671383	0.0245875
ENSMUSG00000005043	Sgsh	0.4433993	0.0249528
ENSMUSG00000117964	Gm36043	0.6200171	0.0250825
ENSMUSG00000060181	Slc35e3	-0.512891	0.0251433
ENSMUSG00000037816	Fbxw17	0.5630118	0.0251813
ENSMUSG00000022451	Twf1	-0.394377	0.025183
ENSMUSG00000030269	Mtmr14	0.3964899	0.0253934
ENSMUSG00000056687	Gm11696	0.6676757	0.0254398
ENSMUSG00000091971	Hspa1a	0.2338786	0.0255177
ENSMUSG00000021596	Mctp1	-0.406677	0.0255517
ENSMUSG00000012848	Rps5	0.2316184	0.0255795
ENSMUSG00000026110	Mgat4a	-0.197254	0.0256132
ENSMUSG00000057522	Spop	0.2871576	0.0256246
ENSMUSG00000027878	Notch2	0.2105815	0.0256246
ENSMUSG00000019790	Stxbp5	-0.277576	0.0256427
ENSMUSG00000049521	Cdc42ep1	-2.277191	0.0258928
ENSMUSG00000028082	Sh3d19	-1.548193	0.0258928
ENSMUSG00000020415	Pttg1	0.5953426	0.0258928
ENSMUSG00000061887	Ssbp3	-0.438274	0.0261046
ENSMUSG00000027961	Lrrc39	-1.12753	0.0262006
ENSMUSG00000002603	Tgfb1	-0.218398	0.0262857
ENSMUSG00000024548	Setbp1	-1.249692	0.0262857
ENSMUSG00000022969	Il10rb	0.2954201	0.0262857
ENSMUSG00000006219	Fblim1	0.418875	0.0262857
ENSMUSG00000026589	Sec16b	-1.226799	0.0262857
ENSMUSG00000002395	Use1	0.3361989	0.0264325
ENSMUSG00000070390	Nlrp1b	0.2693624	0.026507
ENSMUSG00000001175	Calm1	-0.218	0.0265985
ENSMUSG00000046079	Lrrc8d	0.3120095	0.0266677
ENSMUSG00000014547	Wdfy2	-0.237617	0.0268348
ENSMUSG00000020700	Map3k3	0.2654971	0.0268693
ENSMUSG00000024620	Pdgfrb	-1.883005	0.0269181
ENSMUSG00000035673	Sbno2	0.2547952	0.0271384
ENSMUSG00000078945	Naip2	0.2427366	0.0271405
ENSMUSG00000049281	Scn3b	-6.040116	NA
ENSMUSG00000046031	Calhm6	1.0144466	0.0271859
ENSMUSG00000038486	Sv2a	-0.583788	0.0274425
ENSMUSG00000046634	Pkd1l1	6.2243439	0.02747
ENSMUSG00000023830	Igf2r	-0.65988	0.0275441
ENSMUSG00000022762	Ncam2	-4.375573	0.0275683
ENSMUSG00000020893	Per1	0.2538432	0.0275954
ENSMUSG00000048264	Dip2c	-0.508643	0.0276604
ENSMUSG00000022496	Tnfrsf17	-0.993594	0.0278203
ENSMUSG00000036707	Cab39	-0.257415	0.0278406

ENSMUSG00000012123	Crybg2	1.4779073	0.0278406
ENSMUSG00000053175	Bcl3	0.68483	0.0278793
ENSMUSG00000005442	Cic	-0.231315	0.0279725
ENSMUSG00000042390	Gatad2b	-0.278033	0.0281137
ENSMUSG00000093327	Mir5107	-0.991429	0.0282592
ENSMUSG00000062980	Cped1	1.7189025	0.0283606
ENSMUSG00000114864	Gm41071	0.869749	0.0283732
ENSMUSG00000038872	Zfhx3	-0.204186	0.0284303
ENSMUSG00000102854	C130023A14Rik	-1.203445	0.0285165
ENSMUSG00000026447	Pik3c2b	0.5120372	0.028612
ENSMUSG00000038172	Ttc39b	0.3035056	0.0286219
ENSMUSG00000069763	Tmem100	-0.662021	0.02863
ENSMUSG00000036304	Zdhhc23	-1.369255	0.0286346
ENSMUSG00000027525	Phactr3	-3.276643	0.0290195
ENSMUSG00000021130	Galnt16	-2.079068	0.0290893
ENSMUSG00000025656	Arhgef9	-1.218765	0.0291283
ENSMUSG00000057963	Itpk1	0.4077152	0.0291431
ENSMUSG00000020687	Cdc27	-0.342976	0.0291505
ENSMUSG00000029223	Uchl1	-1.827349	0.029218
ENSMUSG00000057863	Rpl36	0.3086512	0.0293045
ENSMUSG00000102419	Gm36940	-1.236659	0.029384
ENSMUSG00000110682	A530010L16Rik	1.7508261	0.0293863
ENSMUSG00000004892	Bcan	-1.263541	0.0294233
ENSMUSG00000035356	Nfkbiz	-0.200083	0.0294645
ENSMUSG00000023022	Lima1	-0.387246	0.0297699
ENSMUSG00000030291	Med21	0.4630627	0.0297798
ENSMUSG00000059493	Nhs	-5.230791	0.0300503
ENSMUSG00000031897	Psmb10	0.3531561	0.0300907
ENSMUSG00000012350	Ehf	3.1075497	0.0301263
ENSMUSG00000086360	Gm16214	1.6101858	0.0301586
ENSMUSG00000032267	Usp28	-0.523956	0.0301586
ENSMUSG00000022257	Laptm4b	0.4659213	0.0303448
ENSMUSG00000051065	Mb21d2	-2.674011	0.0304931
ENSMUSG00000055945	Prr18	-1.483409	0.0304931
ENSMUSG00000029233	Srd5a3	0.4574615	0.0305628
ENSMUSG00000110498	A630001O12Rik	0.8974664	0.0305854
ENSMUSG00000028063	Lmna	0.5908919	0.0308008
ENSMUSG00000025290	Rps24	0.2724427	0.0309632
ENSMUSG00000030826	Bcat2	0.4099486	0.03109
ENSMUSG00000030020	Prickle2	-2.020976	0.031273
ENSMUSG00000026339	Ccdc93	-0.228098	0.0312777
ENSMUSG00000060147	Serpinb6a	-0.852116	0.0312998
ENSMUSG00000006585	Cdt1	0.6690592	0.0312998
ENSMUSG00000021097	Clmn	-1.897069	0.0313065
ENSMUSG00000052310	Slc39a1	-0.280079	0.0313417
ENSMUSG00000087362	Gm13710	1.3641882	0.0313417

ENSMUSG00000031808	Slc27a1	0.3793867	0.0314591
ENSMUSG00000027009	Itga4	-0.448217	0.0314772
ENSMUSG00000097715	Gpr137b-ps	-0.308628	0.0315361
ENSMUSG00000010358	Ifi35	0.4799833	0.0318731
ENSMUSG00000050721	Plekho2	0.2925221	0.0320042
ENSMUSG00000041707	Tmem273	0.3442012	0.0320793
ENSMUSG00000063488	Zkscan7	0.6132379	0.0321221
ENSMUSG00000039116	Adgrg6	-2.835818	0.0322561
ENSMUSG00000035104	Eva1a	-0.752849	0.0323932
ENSMUSG00000021820	Camk2g	-0.359146	0.0325232
ENSMUSG00000004568	Arhgef18	0.318048	0.0326088
ENSMUSG00000039221	Rpl22l1	0.4488779	0.0326751
ENSMUSG00000078794	Dact3	-1.202121	0.0327059
ENSMUSG00000021624	Cd180	-0.300786	0.0327209
ENSMUSG00000022641	Bbx	0.3060204	0.0329342
ENSMUSG00000013419	Zfp651	-0.693299	0.0329599
ENSMUSG00000021311	Mtr	-0.236579	0.0329599
ENSMUSG00000036158	Prickle1	-0.785863	0.0330059
ENSMUSG00000064368	mt-Nd6	-0.676335	0.0330059
ENSMUSG00000111116	Gm48065	0.7878583	0.0330355
ENSMUSG00000061132	Blnk	0.2255637	0.0330639
ENSMUSG00000003992	Ssbp2	0.402029	0.0330962
ENSMUSG00000025212	Sfxn3	-0.494519	0.0331765
ENSMUSG00000097156	Gm3764	-3.805684	0.0334843
ENSMUSG00000039217	Il18	0.5628406	0.0336124
ENSMUSG00000049130	C5ar1	-0.379307	0.0337164
ENSMUSG00000032702	Kank1	-1.712254	0.0337164
ENSMUSG00000064350	mt-Ty	-0.932916	0.0337182
ENSMUSG00000108912	E230020D15Rik	-3.271398	0.0338316
ENSMUSG00000113165	Gm47863	0.5898501	0.0339732
ENSMUSG00000032086	Bace1	-0.542624	0.0340274
ENSMUSG00000055538	Zcchc24	-0.33848	0.0340812
ENSMUSG00000019832	Rab32	0.3534551	0.0340812
ENSMUSG00000056069	Otulinl	0.2224904	0.0340958
ENSMUSG00000068129	Cst7	0.7722573	0.0340958
ENSMUSG00000011158	Brf1	-0.290744	0.0340958
ENSMUSG00000021186	Fbln5	-4.238678	0.0340958
ENSMUSG00000009214	Mymk	-1.466179	0.0341697
ENSMUSG00000024896	Minpp1	0.4123838	0.0342372
ENSMUSG00000078853	Igtp	0.5049033	0.0342739
ENSMUSG00000064267	Hvcn1	0.3278607	0.0342994
ENSMUSG00000110626	Gm45805	0.975618	0.0343814
ENSMUSG00000110697	Gm31718	0.9703939	0.0345772
ENSMUSG00000034667	Xpot	-0.258306	0.0346011
ENSMUSG00000044626	Liph	0.4791514	0.0348166
ENSMUSG00000020300	Cpeb4	-0.29858	0.0348681

ENSMUSG00000010021	Kif19a	0.8158835	0.0348905
ENSMUSG00000103367	Gm38158	-0.478576	0.0350018
ENSMUSG00000070436	Serpinh1	-1.922234	0.0350758
ENSMUSG00000030287	Itpr2	0.2054116	0.035197
ENSMUSG00000024174	Pot1b	0.3749459	0.0352888
ENSMUSG00000091754	Gm3636	-0.794396	0.0352888
ENSMUSG00000103037	Pcdhgb1	-1.765644	0.035322
ENSMUSG00000026069	Il1rl1	-0.729464	0.0353495
ENSMUSG00000036745	Ttll7	-1.409789	0.0353863
ENSMUSG00000011831	Evi5	-0.322306	0.0353863
ENSMUSG00000028599	Tnfrsf1b	0.2059953	0.0353863
ENSMUSG00000109438	Gm45073	-3.074608	0.0354486
ENSMUSG00000025429	Pstpip2	-0.823082	0.0354486
ENSMUSG00000038204	Asb10	-0.880484	0.0354625
ENSMUSG00000032020	Ubash3b	-0.245645	0.0354625
ENSMUSG00000001280	Sp1	-0.222613	0.0354825
ENSMUSG00000090862	Rps13	0.2864519	0.035484
ENSMUSG00000090942	F830016B08Rik	0.9533052	0.0356025
ENSMUSG00000045038	Prkce	-0.489533	0.0356785
ENSMUSG00000015804	Med28	0.3922072	0.0358547
ENSMUSG00000066258	Trim12a	0.323241	0.0358547
ENSMUSG00000059291	Rpl11	0.2800099	0.0359837
ENSMUSG00000114980	4933432I03Rik	1.668882	0.0359837
ENSMUSG00000027569	Mrgbp	0.4626145	0.0361112
ENSMUSG00000096573	1700009J07Rik	1.3436687	0.0361112
ENSMUSG00000115230	AU022793	-0.959553	0.0364079
ENSMUSG00000030757	Zkscan2	-1.716764	0.0364563
ENSMUSG00000116029	Gm41414	5.9403597	NA
ENSMUSG00000111147	Gm33699	0.5403622	0.036493
ENSMUSG00000024677	Ms4a6b	-0.307513	0.0367358
ENSMUSG00000030088	Aldh1l1	1.0518278	0.0368377
ENSMUSG00000039234	Sec24d	-0.499132	0.036961
ENSMUSG00000085394	2210414B05Rik	5.8845922	NA
ENSMUSG00000009687	Fxyd5	-0.519677	0.037018
ENSMUSG00000025877	Hk3	-0.242007	0.0370504
ENSMUSG00000047139	Cd24a	-0.782357	0.0370859
ENSMUSG00000034641	Cd300ld	-1.047492	0.037193
ENSMUSG00000118265	Gm50211	0.5679004	0.0373252
ENSMUSG00000025318	Jph3	-0.741824	0.0373252
ENSMUSG00000020806	Rhbdf2	0.3850587	0.0374548
ENSMUSG00000023348	Trip6	0.3886458	0.0374957
ENSMUSG00000022951	Rcan1	-0.419672	0.0377206
ENSMUSG00000018899	Irf1	0.2995088	0.0377206
ENSMUSG00000108420	Gm45141	5.8931676	NA
ENSMUSG00000027858	Tspan2	-1.468537	0.037898
ENSMUSG00000010307	Tmem86a	0.238894	0.0379151

ENSMUSG00000038677	Scube3	-1.716768	0.0379151
ENSMUSG00000021589	Rhobtb3	-3.40854	0.0379451
ENSMUSG00000033579	Fa2h	-3.039053	0.0379451
ENSMUSG00000036218	Pdzrn4	-5.921014	NA
ENSMUSG00000033392	Clasp2	-0.207826	0.0383489
ENSMUSG00000059851	Kmt5c	0.3088836	0.0384978
ENSMUSG00000045594	Glb1	0.2727045	0.0385182
ENSMUSG00000067288	Rps28	0.2467947	0.0386135
ENSMUSG00000031029	Eif3f	0.2776782	0.0386683
ENSMUSG00000029456	Acad10	0.718947	0.0387864
ENSMUSG00000024978	Gpam	-0.380164	0.0387864
ENSMUSG00000039783	Kmo	-1.515672	0.0388104
ENSMUSG00000039512	Uhrf1bp1	0.2639572	0.0388285
ENSMUSG00000038807	Rap1gap2	0.3038658	0.0390488
ENSMUSG00000037747	Phyhipl	-2.147097	0.0390488
ENSMUSG00000042659	Arrdc4	0.3866412	0.0390661
ENSMUSG00000022332	Khdrbs3	-5.564156	0.0390661
ENSMUSG00000047098	Rnf31	0.2847933	0.0390661
ENSMUSG00000033767	Tmem131l	0.2438941	0.0390661
ENSMUSG00000056952	Tatdn2	0.2556181	0.039087
ENSMUSG00000078921	Tgtp2	1.7005099	0.0391714
ENSMUSG00000033855	Ston1	0.9881933	0.0392287
ENSMUSG00000032046	Abhd12	-0.194488	0.0395394
ENSMUSG00000020473	Aebp1	-1.731908	0.0396034
ENSMUSG00000096904	Lamtor3-ps	-1.880569	0.0398909
ENSMUSG00000040354	Mars1	-0.329115	0.0401713
ENSMUSG00000024507	Hsd17b4	0.260461	0.0404538
ENSMUSG00000020099	Unc5b	-1.645682	0.0407688
ENSMUSG00000026657	Frmd4a	0.2111935	0.0408293
ENSMUSG00000027447	Cst3	-0.160622	0.0408927
ENSMUSG00000015790	Surf1	0.4633774	0.0410227
ENSMUSG00000043895	S1pr2	-0.536578	0.0410419
ENSMUSG00000042688	Mapk6	-0.333892	0.0410419
ENSMUSG00000030538	Cib1	-0.559296	0.0412245
ENSMUSG00000034723	Tmx4	-0.220454	0.0412326
ENSMUSG00000060036	Rpl3	0.1906138	0.0412332
ENSMUSG00000019944	Rhobtb1	-0.290113	0.0413569
ENSMUSG00000042570	Mier2	0.3140551	0.0413586
ENSMUSG00000054293	P2ry10b	-0.553207	0.0414242
ENSMUSG00000041889	Shisa4	-2.76214	0.0416578
ENSMUSG00000084883	Ccdc85c	-0.486153	0.0418256
ENSMUSG00000058070	Eml1	-2.648108	0.0418687
ENSMUSG00000002279	Lmf1	0.3848439	0.0419258
ENSMUSG00000029156	Sgcb	0.4671224	0.0419258
ENSMUSG00000024298	Zfp871	-0.23275	0.0419258
ENSMUSG00000114784	Gm47754	1.3818955	0.0419667

ENSMUSG00000097729	2310015A10Rik	0.5225002	0.0420476
ENSMUSG00000020105	Lrig3	0.3935577	0.0420476
ENSMUSG00000022105	Rb1	-0.276767	0.0420476
ENSMUSG00000021779	Thrb	-2.748312	0.0420595
ENSMUSG00000102302	Gm38190	-0.62177	0.0421673
ENSMUSG00000037266	Rsrp1	0.1909634	0.0422057
ENSMUSG00000030147	Clec4b1	-1.82114	0.0422526
ENSMUSG00000041515	Irf8	0.1967641	0.0426374
ENSMUSG00000032060	Cryab	-1.561251	0.0427874
ENSMUSG00000034771	Tle2	-0.795566	0.04284
ENSMUSG00000015947	Fcgr1	0.2357191	0.0430038
ENSMUSG00000079457	Gm7609	2.417822	0.0430618
ENSMUSG00000003420	Fcgrt	-0.346732	0.0431767
ENSMUSG00000056999	Ide	-0.442195	0.0436276
ENSMUSG00000002249	Tead3	-0.888583	0.0437094
ENSMUSG00000039405	Prss23	-4.166049	0.043713
ENSMUSG00000041859	Mcm3	0.3076818	0.0437375
ENSMUSG00000029804	Herc3	0.547754	0.0439826
ENSMUSG00000025145	Lrrc45	0.3119809	0.0440445
ENSMUSG00000029385	Ccng2	-0.206779	0.0442964
ENSMUSG00000106426	Gm36211	-2.626977	0.0443565
ENSMUSG00000032369	Plscr1	0.7607523	0.0443595
ENSMUSG00000018169	Mfng	0.266379	0.0443595
ENSMUSG00000032399	Rpl4	0.1952327	0.0448446
ENSMUSG00000048960	Prex2	-1.54161	0.0451114
ENSMUSG00000090307	1700071M16Rik	-1.91018	0.0451114
ENSMUSG00000038523	1700003F12Rik	1.1085266	0.0451628
ENSMUSG00000020785	Camkk1	0.5682617	0.0453662
ENSMUSG00000024150	Mcfd2	0.2806758	0.0455398
ENSMUSG00000056501	Cebpb	0.919178	0.0457397
ENSMUSG00000040987	Mill2	-2.183653	0.0457418
ENSMUSG00000013089	Etv5	-0.223861	0.0457418
ENSMUSG00000097177	9330159M07Rik	0.9269671	0.0457418
ENSMUSG00000028019	Pdgfc	-5.06978	0.0460438
ENSMUSG00000030102	Itpr1	0.3887297	0.0460982
ENSMUSG00000114961	A930002C04Rik	-5.854479	NA
ENSMUSG00000026663	Atf6	0.2298153	0.0462206
ENSMUSG00000071176	Arhgef10	-1.301506	0.0465078
ENSMUSG00000031103	Elf4	0.2310004	0.0466523
ENSMUSG00000038893	Fam117a	0.6881296	0.0468407
ENSMUSG00000021047	Nova1	-0.562803	0.0469059
ENSMUSG00000019966	Kitl	-0.393766	0.0471093
ENSMUSG00000062647	Rpl7a	0.2027102	0.0477697
ENSMUSG00000035783	Acta2	-1.654928	0.0478185
ENSMUSG00000066415	Msl2	0.2364699	0.0478632
ENSMUSG00000023262	Acy1	-0.526953	0.0481002

ENSMUSG00000026721	Rabgap1l	-0.629425	0.0481327
ENSMUSG00000067203	H2-K2	0.3117668	0.0482674
ENSMUSG00000004709	Cd244a	0.9863889	0.0487513
ENSMUSG00000036192	Rorb	-3.222398	0.0489109
ENSMUSG00000091985	Gm17354	-1.064704	0.0494651
ENSMUSG00000043259	Fam13c	-1.873326	0.0494698
ENSMUSG00000074502	Ubtfl1	-1.561483	0.0499287
ENSMUSG00000021638	Ocln	0.9043321	0.049968
ENSMUSG00000022463	Srebf2	-0.301775	0.049968

Appendix II Differential Gene Discovories from DESeq2 analysis of Naïve Microglia

Appendix III

Canonical Pathways	-log (p-value)	z-score	Down	No Change	Up	No Overlap	P<0.05 Molecules
Phagosome Formation	16	-0.318	139/ 276 (50%)	0/ 276 (0%)	99/ 276 (36%)	38/ 276 (14%)	ADGRE1, ADGRE5, ADGRG1, ADGRG6, ADORA1, ADORA3, APBB1IP, C3, C3AR1, C5AR1, C5AR2, CCR2, CCR3, CCR5, CD14, CD36, CLIP1, CMKLR1, CNR2, CX3CR1, DOCK1, EDNRB, ELMO2, FCGR1A, FCGR2B, FCGR3A/ FCGR3B, FN1, FPR1, FPR2, FYN, GPR108, GPR155, GPR160, GPR183, GPR34, GPR35, HCAR2, HCK, ITGA4, ITGAL, ITGAM, ITGAX, ITGB1, ITGB2, ITGB3, ITGB5, ITPR1, ITPR2, LYN, MRC1, MRC2, MSR1, MYH10, MYO10, P2RY12, P2RY13, P2RY14, P2RY2, PAK1, PIK3C2B, PIK3CB, PIK3CG, PLA2G2D, PLA2G7, PLAAT3,

							PLCG2, PLD4, PRKCA, PRKCB, PRKCD, PTK2, PTK2B, ROCK2, S1PR1, S1PR2, SRC, SYK, TIMD4, TLN2, Tlr12, TLR2, TLR3, TLR4, TLR5, TLR8, TLR9, VAV2, VAV3, WASF2
Role of Pattern Recognition Receptors in Recognition of Bacteria and Viruses	9.49	3.024	33/ 108 (31%)	0/ 108 (0%)	57/ 108 (53%)	18/ 108 (17%)	C1QA, C1QB, C1QC, C3, C3AR1, C5AR1, CCL5, CLEC6A, DDX58, EIF2AK2, IFIH1, IFNB1, IL10, IL18, IRF7, MAVS, NLRC4, NOD1, OAS1, OAS2, OAS3, PIK3C2B, PIK3CB, PIK3CG, PLCG2, PRKCA, PRKCB, PRKCD, RNASEL, SYK, TGFB1, TLR2, TLR3, TLR4, TLR5, TLR8, TLR9, TNFSF10, TNFSF13B, TNFSF8
Granulocyte Adhesion and Diapedesis	8.41	N/ A	41/ 90 (46%)	0/ 90 (0%)	29/ 90 (32%)	20/ 90 (22%)	C5AR1, CCL2, CCL24, CCL5, Ccl7, CCR2, CCR3, CCR5, CSF3R, CXCL10, CXCL13, CXCL16, CXCL2, CXCL3, Cxcl9, CXCR4, FPR1, FPR2, IL18, IL1R2, IL1RL1, ITGA4, ITGAM,

							ITGB1, ITGB2, MMP12, MMP14, MMP2, MMP9, PECAM1, PF4, SDC3, SDC4, TNFRSF1B
Role of Hypercytokinemia/ Hyperchemokinemia in the Pathogenesis of Influenza	8.34	3.674	11/ 51 (22%)	0/ 51 (0%)	33/ 51 (65%)	7/ 51 (14%)	CCL2, CCL5, CXCL10, CXCL3, DDX58, EIF2AK2, IFIT2, IFIT3, IFNB1, IL10, IL18, IRF7, IRF9, OAS1, OAS2, OAS3, PYCARD, RSAD2, S1PR1, STAT1, STAT2, TLR3, TLR4, TLR9
Crosstalk between Dendritic Cells and Natural Killer Cells	7.19	2.065	18/ 53 (34%)	0/ 53 (0%)	26/ 53 (49%)	9/ 53 (17%)	ACTA2, CAMK2G, CD28, CD80, CSF2RB, FSCN1, HLA-DRB5, HLA-E, HLA-G, IFNB1, IL15RA, IL18, IL2RG, ITGAL, KLRD1, MICB, NECTIN2, TLN2, TLR3, TLR4, TLR9, TNFRSF1B, TNFSF10
Th1 and Th2 Activation Pathway	6.94	N/ A	51/ 115 (44%)	0/ 115 (0%)	46/ 115 (40%)	18/ 115 (16%)	BMPR2, CCR3, CCR5, CD274, CD28, CD4, CD80, CXCR4, HAVCR2, HLA-DMA, HLA-DOA, HLA-DQA1, HLA-DQB1, HLA-DRB5, ICOSLG/ LOC102723996, IL10, IL10RA, IL10RB, IL12RB1, IL12RB2, IL18, IL1RL1, IL2RG, IRF1, ITGB2,

							JAG1, JAG2, KLRD1, MAF, NOTCH2, PIK3C2B, PIK3CB, PIK3CG, S1PR1, STAT1, TGFB1, TIMD4
Agranulocyte Adhesion and Diapedesis	6.91	N/ A	44/ 88 (50%)	0/ 88 (0%)	26/ 88 (30%)	18/ 88 (20%)	ACTA2, C5AR1, CCL2, CCL24, CCL5, Ccl7, CCR2, CCR3, CCR5, CD34, CXCL10, CXCL13, CXCL16, CXCL2, CXCL3, Cxcl9, CXCR4, FN1, IL18, ITGA4, ITGB1, ITGB2, MMP12, MMP14, MMP2, MMP9, MYH10, MYO10, PECAM1, PF4, SDC4
Fcγ Receptor-mediated Phagocytosis in Macrophages and Monocytes	6.33	1.46	36/ 58 (62%)	0/ 58 (0%)	22/ 58 (38%)	0/ 58 (0%)	ACTA2, CBL, DOCK1, FCGR1A, FCGR3A/ FCGR3B, FYB1, FYN, HCK, LYN, PAK1, PIK3CG, PLD4, PRKCA, PRKCB, PRKCD, PTK2B, PXN, SRC, SYK, TLN2, VASP, VAV2, VAV3
Leukocyte Extravasation Signalling	6.32	-0.354	58/ 102 (57%)	0/ 102 (0%)	33/ 102 (32%)	11/ 102 (11%)	ACTA2, ACTN1, ARHGAP4, CD44, CXCR4, CYBA, CYBB, ITGA4, ITGAL, ITGAM, ITGB1, ITGB2, MMP12, MMP14, MMP2, MMP9, PECAM1, PIK3C2B, PIK3CB,

							PIK3CG, PLCG2, PRKCA, PRKCB, PRKCD, PTK2, PTK2B, PXN, ROCK2, SRC, TIMP2, VASP, VAV2, VAV3
Antigen Presentation Pathway	6.28	N/ A	7/ 25 (28%)	0/ 25 (0%)	16/ 25 (64%)	2/ 25 (8%)	B2M, CD74, CIITA, HLA-DMA, HLA-DOA, HLA-DQA1, HLA-DQB1, HLA-DRB5, HLA-E, HLA-G, NLRC5, PSMB9, TAP1, TAPBP
Breast Cancer Regulation by Stathmin1	5.87	-0.802	119/ 230 (52%)	0/ 230 (0%)	76/ 230 (33%)	35/ 230 (15%)	ADGRE1, ADGRE5, ADGRG1, ADGRG6, ADORA1, ADORA3, ARHGEF18, ARHGEF6, C3AR1, C5AR1, C5AR2, CAMK1D, CAMK2G, CCND2, CCR2, CCR3, CCR5, CDK6, CMKLR1, CNR2, CX3CR1, EDNRB, FPR1, FPR2, GPR108, GPR155, GPR160, GPR183, GPR34, GPR35, HCAR2, IGF1, MMP2, MMP9, P2RY12, P2RY13, P2RY14, P2RY2, PAK1, PDGFB, PDGFC, PIK3C2B, PIK3CB, PIK3CG, PLCB2,

							PLCB4, PPP1R3D, PPP2R1B, PRKCA, PRKCB, PRKCD, RPS6KA3, S1PR1, S1PR2, TGFB1, TUBA1A, TUBB2A
Actin Cytoskeleton Signalling	5.66	-1.877	74/ 118 (63%)	0/ 118 (0%)	42/ 118 (36%)	2/ 118 (2%)	ABI2, ACTA2, ACTN1, ARHGEF6, BAIAP2, CD14, CYFIP1, DOCK1, FGF1, FN1, IQGAP2, ITGA4, ITGAL, ITGAM, ITGAX, ITGB1, ITGB2, ITGB3, ITGB5, MYH10, MYO10, PAK1, PDGFB, PDGFC, PIK3C2B, PIK3CB, PIK3CG, PTK2, PXN, ROCK2, SSH3, TLN2, VAV2, VAV3, WASF2
Th2 Pathway	5.59	0.447	41/ 90 (46%)	0/ 90 (0%)	34/ 90 (38%)	15/ 90 (17%)	BMPR2, CCR3, CCR5, CD28, CD4, CD80, CXCR4, HLA-DMA, HLA-DOA, HLA-DQA1, HLA-DQB1, HLA-DRB5, ICOSLG/ LOC102723996, IL10, IL12RB1, IL12RB2, IL1RL1, IL2RG, ITGB2, JAG1, JAG2, MAF, NOTCH2, PIK3C2B, PIK3CB, PIK3CG, S1PR1, TGFB1, TIMD4

Complement System	5.58	1.633	4/ 15 (27%)	0/ 15 (0%)	7/ 15 (47%)	4/ 15 (27%)	C1QA, C1QB, C1QC, C2, C3, C3AR1, C5AR1, ITGAM, ITGAX, ITGB2
Communication between Innate and Adaptive Immune Cells	5.49	N/ A	15/ 51 (29%)	0/ 51 (0%)	28/ 51 (55%)	8/ 51 (16%)	B2M, CCL5, CD28, CD4, CD80, CXCL10, HLA-DRB5, HLA-E, HLA-G, IFNB1, IL10, IL18, Tlr12, TLR2, TLR3, TLR4, TLR5, TLR8, TLR9, TNFSF13B
Macropinocytosis Signalling	5.34	1.155	28/ 52 (54%)	0/ 52 (0%)	24/ 52 (46%)	0/ 52 (0%)	CD14, CSF1, ITGB1, ITGB2, ITGB3, ITGB5, MET, MRC1, PAK1, PDGFB, PDGFC, PIK3C2B, PIK3CB, PIK3CG, PLCG2, PRKCA, PRKCB, PRKCD, RAB34, SRC
Th1 Pathway	5.04	1.342	30/ 81 (37%)	0/ 81 (0%)	40/ 81 (49%)	11/ 81 (14%)	CCR5, CD274, CD28, CD4, CD80, HAVCR2, HLA-DMA, HLA-DOA, HLA-DQA1, HLA-DQB1, HLA-DRB5, ICOSLG/ LOC102723996, IL10, IL10RA, IL10RB, IL12RB1, IL12RB2, IL18, IRF1, ITGB2, KLRD1, NOTCH2, PIK3C2B, PIK3CB, PIK3CG, STAT1
Neuroinflammation Signalling Pathway	4.93	1.761	81/ 179 (45%)	0/ 179 (0%)	85/ 179 (47%)	13/ 179 (7%)	APP, B2M, BIRC2, BMPR2, CCL2, CCL5, CD200R1, CD80,

							CX3CR1, CXCL10, CYBB, HLA-DMA, HLA-DOA, HLA-DQA1, HLA-DQB1, HLA-DRB5, HLA-E, HLA-G, IDE, IFNB1, IL10, IL18, IRAK2, IRF7, MMP9, NAIP, NFE2L2, PIK3C2B, PIK3CB, PIK3CG, PLA2G2D, PLCG2, PYCARD, SLC1A2, SLC1A3, STAT1, SYK, TGFB1, Tlr12, TLR2, TLR3, TLR4, TLR5, TLR8, TLR9
Osteoarthritis Pathway	4.89	-1.732	66/ 132 (50%)	0/ 132 (0%)	48/ 132 (36%)	18/ 132 (14%)	ANKH, BMP2, BMPR2, CASP4, CEBPB, EPAS1, FN1, IL1R2, IL1RL1, ITGA4, ITGAL, ITGAM, ITGAX, ITGB1, ITGB2, ITGB3, ITGB5, JAG1, LRP1, MEF2C, MMP12, MMP9, NAMPT, PDGFC, PRKAB1, RUNX2, S1PR2, SDC4, SIK3, SMAD7, SP1, TCF4, TGFB1, TLR2, TLR4, TNFRSF1B
CREB Signalling in Neurons	4.85	-1.089	123/ 230 (53%)	0/ 230 (0%)	69/ 230 (30%)	38/ 230 (17%)	ADCY9, ADGRE1, ADGRE5, ADGRG1, ADGRG6, ADORA1,

							ADORA3, BMPR2, C3AR1, C5AR1, C5AR2, CACNA1A, CAMK2G, CCR2, CCR3, CCR5, CMKLR1, CNR2, CX3CR1, EDNRB, FPR1, FPR2, GPR108, GPR155, GPR160, GPR183, GPR34, GPR35, HCAR2, IGF1, IGF1R, ITPR1, ITPR2, KDR, P2RY12, P2RY13, P2RY14, P2RY2, PDGFB, PDGFRB, PIK3C2B, PIK3CB, PIK3CG, PLCB2, PLCB4, PLCG2, PLCL2, PRKCA, PRKCB, PRKCD, S1PR1, S1PR2, TGFB1, TNFRSF11A
Axonal Guidance Signalling	4.78	N/ A	133/ 220 (60%)	0/ 220 (0%)	67/ 220 (30%)	20/ 220 (9%)	ADAM22, ARHGEF6, BAIAP2, BMP1, BMP2, CXCR4, DOCK1, EFNB1, EPHB6, FYN, IGF1, ITGA4, ITGAL, ITGAM, ITGAX, ITGB1, ITGB2, ITGB3, ITGB5, ITSN1, LNPEP, MET, MMP12, MMP14, MMP2, MMP9, PAK1, PDGFB, PDGFC,

							PIK3C2B, PIK3CB, PIK3CG, PLCB2, PLCB4, PLCG2, PLCL2, PLXNA1, PLXND1, PRKCA, PRKCB, PRKCD, PTK2, PXN, RGS3, ROCK2, RTN4, SEMA6D, SRGAP2, TUBA1A, TUBB2A, UNC5B, VASP
T Helper Cell Differentiation	4.72	N/ A	17/ 52 (33%)	0/ 52 (0%)	23/ 52 (44%)	12/ 52 (23%)	CD28, CD80, HLA-DMA, HLA-DOA, HLA-DQA1, HLA-DQB1, HLA-DRB5, ICOSLG/ LOC102723996, IL10, IL10RA, IL10RB, IL12RB1, IL12RB2, IL18, IL2RG, IL6ST, STAT1, TGFB1, TNFRSF1B
Atherosclerosis Signalling	4.71	N/ A	33/ 70 (47%)	0/ 70 (0%)	23/ 70 (33%)	14/ 70 (20%)	ALOX5, APOE, CCL2, CCR2, CCR3, CD36, CLU, CSF1, CXCR4, IL18, ITGA4, ITGB2, LPL, LYZ, MMP9, MSR1, PDGFB, PDGFC, PLA2G2D, PLA2G7, PLAAT3, TGFB1, TNFRSF14
Sperm Motility	4.68	0.258	58/ 109 (53%)	0/ 109 (0%)	41/ 109 (38%)	10/ 109 (9%)	AATK, AXL, CSF2RA, DYRK4, FYN, HCK, IGF1R, ITPR1, ITPR2, KDR, LYN, MET, PDGFRB, PEAK1,

							PLA2G2D, PLA2G7, PLAAT3, PLCB2, PLCB4, PLCG2, PLCL2, PRKCA, PRKCB, PRKCD, PTK2, PTK2B, RYK, SLC12A2, SRC, SYK, TWF1
Caveolar-mediated Endocytosis Signalling	4.65	N/ A	21/ 44 (48%)	0/ 44 (0%)	23/ 44 (52%)	0/ 44 (0%)	ACTA2, B2M, CD48, FYN, HLA-E, HLA-G, ITGA4, ITGAL, ITGAM, ITGAX, ITGB1, ITGB2, ITGB3, ITGB5, ITSN1, PRKCA, SRC
TREM1 Signalling	4.64	0.894	23/ 57 (40%)	0/ 57 (0%)	34/ 57 (60%)	0/ 57 (0%)	CCL2, CIITA, CXCL3, FCGR2B, IL10, IL18, IL1RL1, ITGAX, ITGB1, NLRC4, NLRC5, NOD1, PLCG2, Tlr12, TLR2, TLR3, TLR4, TLR5, TLR8, TLR9
TEC Kinase Signalling	4.59	1.043	55/ 110 (50%)	0/ 110 (0%)	52/ 110 (47%)	3/ 110 (3%)	ACTA2, FYN, HCK, ITGA4, ITGAL, ITGAM, ITGAX, ITGB1, ITGB2, ITGB3, ITGB5, LYN, PAK1, PIK3C2B, PIK3CB, PIK3CG, PLCG2, PRKCA, PRKCB, PRKCD, PTK2, PTK2B, RHOBTB1, RHOC, SRC, STAT1, STAT2, TLR4, TNFSF10, VAV2, VAV3

IL-15 Production	4.58	1.528	29/ 62 (47%)	0/ 62 (0%)	30/ 62 (48%)	3/ 62 (5%)	AATK, AXL, CSF2RA, DYRK4, FYN, HCK, IFNB1, IGF1R, IRF1, KDR, LYN, MET, PDGFRB, PEAK1, PTK2, PTK2B, RYK, SRC, STAT1, SYK, TWF1
HGF Signalling	4.51	0.471	52/ 91 (57%)	0/ 91 (0%)	38/ 91 (42%)	1/ 91 (1%)	CDKN1A, DOCK1, ELF4, ETS1, ETS2, GAB1, ITGA4, ITGAL, ITGAM, ITGAX, ITGB1, ITGB2, ITGB3, ITGB5, MAP3K3, MAP3K5, MET, PAK1, PIK3C2B, PIK3CB, PIK3CG, PLCG2, PRKCA, PRKCB, PRKCD, PTK2, PXN
FAK Signalling	4.46	N/ A	46/ 77 (60%)	0/ 77 (0%)	30/ 77 (39%)	1/ 77 (1%)	ACTA2, ARHGAP26, ARHGEF6, CAPN2, DOCK1, FYN, ITGA4, ITGAL, ITGAM, ITGAX, ITGB1, ITGB2, ITGB3, ITGB5, PAK1, PIK3C2B, PIK3CB, PIK3CG, PLCG2, PTK2, PXN, SRC, TLN2, TNS1
Virus Entry via Endocytic Pathways	4.46	N/ A	36/ 63 (57%)	0/ 63 (0%)	27/ 63 (43%)	0/ 63 (0%)	ACTA2, AP2A2, B2M, CLTC, FYN, HLA-E, HLA-G, ITGB1, ITGB2, ITGB3, ITGB5, ITSN1, PIK3C2B, PIK3CB, PIK3CG, PLCG2, PRKCA,

							PRKCB, PRKCD, SRC, TFRC
EIF2 Signalling	4.36	3.3	47/ 118 (40%)	0/ 118 (0%)	70/ 118 (59%)	1/ 118 (1%)	ACTA2, AGO3, EIF2AK2, EIF2S3, EIF4G2, IGF1R, PIK3C2B, PIK3CB, PIK3CG, RPL10, RPL11, RPL13, RPL17, RPL18A, RPL19, RPL23, RPL27A, RPL28, RPL35, RPL35A, RPL37, RPL37A, RPS13, RPS14, RPS16, RPS23, RPS24, RPS27A, RPS29, RPS3, RPS4Y1, RPS5
CDC42 Signalling	4.34	0	43/ 83 (52%)	0/ 83 (0%)	38/ 83 (46%)	2/ 83 (2%)	ARHGEF6, B2M, BAIAP2, CLIP1, EXOC5, EXOC6, HLA-DMA, HLA-DOA, HLA-DQA1, HLA-DQB1, HLA-DRB5, HLA-E, HLA-G, IQGAP2, ITGA4, ITGAL, ITGAM, ITGAX, ITGB1, ITGB2, ITGB3, ITGB5, PAK1, SRC, VAV2
T Cell Exhaustion Signalling Pathway	4.33	1.706	49/ 103 (48%)	0/ 103 (0%)	48/ 103 (47%)	6/ 103 (6%)	BMPR2, CD274, CD28, CD80, HAVCR2, HLA-DMA, HLA-DOA, HLA-DQA1, HLA-DQB1, HLA-DRB5, HLA-E, HLA-G, IL10, IL10RA, IL10RB, IL12RB1, IL12RB2, IRF9, KDR, PIK3C2B, PIK3CB, PIK3CG,

							PLCG2, PPP2R1B, PRDM1, STAT1, STAT2, TGFB1, TNFRSF14
Systemic Lupus Erythematosus In B Cell Signalling Pathway	4.32	1.852	68/ 172 (40%)	0/ 172 (0%)	86/ 172 (50%)	18/ 172 (10%)	BLNK, CBL, CCND2, CD22, FCGR2B, FYN, GAB1, HCK, IFIH1, IFIT2, IFIT3, IFNB1, IL10, IL18, IL6ST, IRF7, IRF9, LILRB3, LILRB4, LYN, MAP4K4, MAVS, PIK3AP1, PIK3C2B, PIK3CB, PIK3CG, PLCG2, PRKCA, PRKCB, PRKCD, SRC, STAT1, STAT2, SYK, SYNJ2, TGFB1, TLR3, TLR8, TLR9, TNFSF10, TNFSF13B, TNFSF8
Altered T Cell and B Cell Signalling in Rheumatoid Arthritis	4.27	N/ A	23/ 60 (38%)	0/ 60 (0%)	26/ 60 (43%)	11/ 60 (18%)	CD28, CD80, CSF1, CXCL13, HLA-DMA, HLA-DOA, HLA-DQA1, HLA-DQB1, HLA-DRB5, IL10, IL18, TGFB1, Tlr12, TLR2, TLR3, TLR4, TLR5, TLR8, TLR9, TNFSF13B
PI3K Signalling in B Lymphocytes	4.24	1.633	48/ 89 (54%)	0/ 89 (0%)	40/ 89 (45%)	1/ 89 (1%)	ATF6, BLNK, C3, CAMK2G, CBL, CD180, CD81, FCGR2B, FYN, IRS2, ITPR1, ITPR2, LYN, PIK3AP1, PIK3CB,

							PIK3CG, PLCB2, PLCB4, PLCG2, PLCL2, PRKCB, PTPRC, SYK, TLR4, VAV2, VAV3
B Cell Development	4.18	N/ A	6/ 13 (46%)	0/ 13 (0%)	6/ 13 (46%)	1/ 13 (8%)	CD80, HLA-DMA, HLA-DOA, HLA-DQA1, HLA-DQB1, HLA-DRB5, IL7R, PTPRC
Dendritic Cell Maturation	4.03	1.976	42/ 117 (36%)	0/ 117 (0%)	64/ 117 (55%)	11/ 117 (9%)	B2M, CD80, FCGR1A, FCGR2B, FCGR3A/ FCGR3B, FSCN1, HLA-DMA, HLA-DOA, HLA-DQA1, HLA-DQB1, HLA-DRB5, HLA-E, HLA-G, IFNB1, IL10, IL18, IRF8, PIK3C2B, PIK3CB, PIK3CG, PLCB2, PLCB4, PLCG2, PLCL2, STAT1, STAT2, TLR2, TLR3, TLR4, TLR9, TNFRSF1B
Paxillin Signalling	3.99	-1	40/ 72 (56%)	0/ 72 (0%)	32/ 72 (44%)	0/ 72 (0%)	ACTA2, ACTN1, ARHGEF6, DOCK1, ITGA4, ITGAL, ITGAM, ITGAX, ITGB1, ITGB2, ITGB3, ITGB5, PAK1, PIK3C2B, PIK3CB, PIK3CG, PTK2, PTK2B, PTPN12, PXN, SRC, TLN2
Calcium-induced T Lymphocyte Apoptosis	3.95	0	17/ 28 (61%)	0/ 28 (0%)	9/ 28 (32%)	2/ 28 (7%)	CAPN2, CD4, HLA-DMA, HLA-DOA, HLA-DQA1,

							HLA-DQB1, HLA-DRB5, ITPR1, ITPR2, PRKCA, PRKCB, PRKCD
Role of Macrophages, Fibroblasts and Endothelial Cells in Rheumatoid Arthritis	3.93	N/ A	87/ 184 (47%)	0/ 184 (0%)	82/ 184 (45%)	15/ 184 (8%)	C5AR1, CAMK2G, CCL2, CCL5, CEBPA, CEBPB, CSF1, FCGR1A, FCGR3A/ FCGR3B, FN1, IL10, IL18, IL1R2, IL1RL1, IL6ST, IRAK2, LRP1, PDGFB, PDGFC, PIK3C2B, PIK3CB, PIK3CG, PLCB2, PLCB4, PLCG2, PLCL2, PRKCA, PRKCB, PRKCD, ROCK2, RYK, SRC, TCF4, TGFB1, Tlr12, TLR2, TLR3, TLR4, TLR5, TLR8, TLR9, TNFRSF1B, TNFSF13B
Hepatic Fibrosis / Hepatic Stellate Cell Activation	3.86	N/ A	64/ 130 (49%)	0/ 130 (0%)	41/ 130 (32%)	25/ 130 (19%)	ACTA2, CCL2, CCL5, CCR5, CD14, COL6A3, CSF1, CXCL3, EDNRB, FGF1, FN1, IGF1, IGF1R, IL10, IL10RA, IL1R2, IL1RL1, KDR, KLF6, MET, MMP2, MMP9, MYH10, MYO10, PDGFB, PDGFC, PDGFRB, SMAD7, STAT1, TGFB1, TIMP2, TLR4, TNFRSF1B
NUR77 Signalling in T Lymphocytes	3.84	0.333	23/ 50 (46%)	0/ 50 (0%)	24/ 50 (48%)	3/ 50 (6%)	B2M, CD28, CD80, HDAC7,

							HLA-DMA, HLA-DOA, HLA-DQA1, HLA-DQB1, HLA-DRB5, HLA-E, HLA-G, MAP3K3, PRKCA, PRKCB, PRKCD, RPS6KA3, TNFSF10
Clathrin-mediated Endocytosis Signalling	3.83	N/ A	66/ 104 (63%)	0/ 104 (0%)	31/ 104 (30%)	7/ 104 (7%)	ACTA2, AP2A2, APOE, CBL, CLTC, CLU, DAB2, FGF1, HIP1, IGF1, ITGB1, ITGB2, ITGB3, ITGB5, LDLR, LDLRAP1, LYZ, MET, NUMB, PDGFB, PDGFC, PICALM, PIK3C2B, PIK3CB, PIK3CG, RPS27A, SRC, TFRC
Chemokine Signalling	3.79	0	36/ 55 (65%)	0/ 55 (0%)	17/ 55 (31%)	2/ 55 (4%)	CAMK1D, CAMK2G, CCL2, CCL24, CCL5, CCR3, CCR5, CXCR4, PIK3CG, PLCB2, PLCB4, PLCG2, PRKCA, PRKCB, PTK2, PTK2B, ROCK2, SRC
ERK/ MAPK Signalling	3.63	-0.408	76/ 128 (59%)	0/ 128 (0%)	49/ 128 (38%)	3/ 128 (2%)	DOCK1, ELF4, ETS1, ETS2, FYN, ITGA4, ITGAL, ITGAM, ITGAX, ITGB1, ITGB2, ITGB3, ITGB5, PAK1, PIK3C2B, PIK3CB, PIK3CG, PLA2G2D, PLCG2, PPP1R3D, PPP2R1B, PRKCA, PRKCB,

							PRKCD, PTK2, PTK2B, PXN, SRC, STAT1, TLN2, YWHAH, YWHAZ
MSP-RON Signalling Pathway	3.61	N/ A	12/ 30 (40%)	0/ 30 (0%)	15/ 30 (50%)	3/ 30 (10%)	ACTA2, CCL2, CCR2, CSF1, CSF2RB, ITGAM, ITGB2, PIK3C2B, PIK3CB, PIK3CG, TLR2, TLR4
Regulation of Cellular Mechanics by Calpain Protease	3.49	-1.633	29/ 53 (55%)	0/ 53 (0%)	21/ 53 (40%)	3/ 53 (6%)	ACTN1, CAPN2, CCND2, CDK6, ITGA4, ITGAL, ITGAM, ITGAX, ITGB1, ITGB2, ITGB3, ITGB5, PTK2, PXN, RB1, SRC, TLN2
Phospholipase C Signalling	3.47	0	77/ 136 (57%)	0/ 136 (0%)	56/ 136 (41%)	3/ 136 (2%)	ADCY9, AHNAK, ARHGEF18, ARHGEF6, BLNK, FCGR2B, FYN, HDAC7, ITGA4, ITGAL, ITGAM, ITGAX, ITGB1, ITGB2, ITGB3, ITGB5, ITPR1, ITPR2, LYN, MEF2C, PLA2G2D, PLCB2, PLCB4, PLCG2, PLD4, PRKCA, PRKCB, PRKCD, RHOBTB1, RHOC, RPS6KA3, SRC, SYK
Allograft Rejection Signalling	3.43	N/ A	9/ 27 (33%)	0/ 27 (0%)	10/ 27 (37%)	8/ 27 (30%)	B2M, CD28, CD80, HLA-DMA, HLA-DOA, HLA-DQA1, HLA-DQB1, HLA-DRB5, HLA-E, HLA-G, IL10

Coronavirus Pathogenesis Pathway	3.37	-4.243	49/ 132 (37%)	0/ 132 (0%)	78/ 132 (59%)	5/ 132 (4%)	CCL2, CCL5, CCR2, DDX58, EEF1A1, HDAC7, IFNB1, IRF7, IRF9, KPNB1, MAVS, OAS1, OAS2, OAS3, PYCARD, RB1, RPS13, RPS14, RPS16, RPS23, RPS24, RPS27A, RPS29, RPS3, RPS4Y1, RPS5, STAT1, STAT2, TGFB1, TLR3, TRIM25, ZC3HAV1
Cardiac Hypertrophy Signalling (Enhanced)	3.32	0.143	143/ 285 (50%)	0/ 285 (0%)	115/ 285 (40%)	27/ 285 (9%)	ADCY9, ATF6, BMPR2, CACNA1A, CAMK2G, CSF2RB, CYBB, EDNRB, FGF1, GDE1, HDAC7, IGF1, IGF1R, IL10RA, IL10RB, IL12RB1, IL12RB2, IL13RA1, IL15RA, IL18, IL1R2, IL1RL1, IL2RG, IL6ST, IL7R, ITGA4, ITGAL, ITGAM, ITGAX, ITGB1, ITGB2, ITGB3, ITGB5, ITPR1, ITPR2, MAP3K3, MAP3K5, MAPKAPK3, MEF2C, PDE3B, PIK3C2B, PIK3CB, PIK3CG, PLCB2, PLCB4, PLCG2,

							PLCL2, PRKCA, PRKCB, PRKCD, PTK2, RCAN1, ROCK2, TGFB1, TNFRSF1B, TNFSF10, TNFSF13B, TNFSF8
Autoimmune Thyroid Disease Signalling	3.26	N/ A	8/ 24 (33%)	0/ 24 (0%)	9/ 24 (38%)	7/ 24 (29%)	CD28, CD80, HLA-DMA, HLA-DOA, HLA-DQA1, HLA-DQB1, HLA-DRB5, HLA-E, HLA-G, IL10
PI3K/ AKT Signalling	3.18	-0.632	63/ 124 (51%)	0/ 124 (0%)	58/ 124 (47%)	3/ 124 (2%)	CDKN1A, CSF2RB, GAB1, IL10RA, IL10RB, IL12RB1, IL12RB2, IL13RA1, IL15RA, IL1R2, IL1RL1, IL2RG, IL6ST, IL7R, ITGA4, ITGAL, ITGAM, ITGAX, ITGB1, ITGB2, ITGB3, ITGB5, LIMS1, MAP3K5, PIK3CB, PIK3CG, PPP2R1B, SYNJ2, YWHAH, YWHAZ
LXR/ RXR Activation	3.07	-1.5	25/ 62 (40%)	0/ 62 (0%)	30/ 62 (48%)	7/ 62 (11%)	APOE, C3, CCL2, CD14, CD36, CLU, IL18, IL1R2, IL1RL1, LDLR, LPL, LYZ, MMP9, MSR1, SERPINF1, TLR3, TLR4, TNFRSF1B
Integrin Signalling	3.06	-0.962	82/ 126 (65%)	0/ 126 (0%)	43/ 126 (34%)	1/ 126 (1%)	ACTA2, ACTN1, ARHGAP26, CAPN2, DOCK1, FYN, ITGA4, ITGAL, ITGAM,

							ITGAX, ITGB1, ITGB2, ITGB3, ITGB5, LIMS1, NEDD9, PAK1, PDGFB, PIK3C2B, PIK3CB, PIK3CG, PLCG2, PTK2, PXN, RHOBTB1, RHOC, SRC, TLN2, TSPAN2, VASP
Pulmonary Healing Signalling Pathway	3.02	0.962	61/ 110 (55%)	0/ 110 (0%)	34/ 110 (31%)	15/ 110 (14%)	BMPR2, CHRNA7, CXCR4, FYN, HCK, IDH2, JAG1, KDR, LYN, MMP12, MMP14, MMP2, MMP9, NOTCH2, PDGFC, PECAM1, PRKAB1, PRKCA, PRKCB, PRKCD, SRC, TCF4, TGFB1, THBS1, TLR2, TLR4, TNFRSF1B
Role of PKR in Interferon Induction and Antiviral Response	2.96	2.524	35/ 84 (42%)	0/ 84 (0%)	45/ 84 (54%)	4/ 84 (5%)	DDX58, EIF2AK2, FCGR1A, HSPA1A/ HSPA1B, IFIH1, IFNB1, IL18, IRF1, IRF9, MAVS, MSR1, NLRP1, PDGFB, PDGFC, PDGFRB, PYCARD, SP1, STAT1, STAT2, TLR3, TLR4, TLR9
Semaphorin Neuronal Repulsive Signalling Pathway	2.96	-1.342	50/ 84 (60%)	0/ 84 (0%)	33/ 84 (39%)	1/ 84 (1%)	BCAN, CD44, CSPG4, FARP1, FYN, ITGA4, ITGAL, ITGAM, ITGAX, ITGB1, ITGB2, ITGB3, ITGB5, PAK1,

							PIK3C2B, PIK3CB, PIK3CG, PLCG2, PLXNA1, PLXND1, ROCK2, SEMA6D
Graft-versus-Host Disease Signalling	2.94	N/ A	11/ 26 (42%)	0/ 26 (0%)	10/ 26 (38%)	5/ 26 (19%)	CD28, CD80, HLA-DMA, HLA-DOA, HLA-DQA1, HLA-DQB1, HLA-DRB5, HLA-E, HLA-G, IL18
Interferon Signalling	2.94	3	5/ 26 (19%)	0/ 26 (0%)	19/ 26 (73%)	2/ 26 (8%)	IFIT1, IFIT3, IFITM3, IFNB1, IRF1, IRF9, OAS1, STAT1, STAT2, TAP1
Natural Killer Cell Signalling	2.87	1.512	50/ 118 (42%)	0/ 118 (0%)	61/ 118 (52%)	7/ 118 (6%)	B2M, CD48, FCGR3A/ FCGR3B, FYN, HLA-E, HLA-G, HSPA1A/ HSPA1B, IL12RB1, IL12RB2, IL18, ITGAL, ITGB1, KLRD1, MAP3K3, MAP3K5, MICB, NECTIN2, PAK1, PIK3C2B, PIK3CB, PIK3CG, PLCG2, PTK2B, PXN, SYK, TNFSF10, VAV2, VAV3
Sphingosine-1-phosphate Signalling	2.81	-0.728	38/ 65 (58%)	0/ 65 (0%)	26/ 65 (40%)	1/ 65 (2%)	ADCY9, CASP4, PDGFB, PDGFC, PDGFRB, PIK3C2B, PIK3CB, PIK3CG, PLCB2, PLCB4, PLCG2, PLCL2, PTK2, PTK2B, RHOBTB1, RHOC, S1PR1, S1PR2

G-Protein Coupled Receptor Signalling	2.77	-0.674	149/ 281 (53%)	0/ 281 (0%)	99/ 281 (35%)	33/ 281 (12%)	ADCY9, ADGRE1, ADGRE5, ADGRG1, ADGRG6, ADORA1, ADORA3, C3AR1, C5AR1, C5AR2, CAMK2G, CCR2, CCR3, CCR5, CMKLR1, CNR2, CX3CR1, EDNRB, FPR1, FPR2, FYN, GDE1, GPR108, GPR155, GPR160, GPR183, GPR34, GPR35, GRK3, HCAR2, MAP3K3, MAP3K5, MEF2C, P2RY12, P2RY13, P2RY14, P2RY2, PAK1, PDE3B, PIK3C2B, PIK3CB, PIK3CG, PLCB2, PLCB4, PLCG2, PRKCA, PRKCB, PTK2, PTK2B, PXN, RGS18, ROCK2, S1PR1, S1PR2, SRC
STAT3 Pathway	2.7	0	48/ 93 (52%)	0/ 93 (0%)	38/ 93 (41%)	7/ 93 (8%)	BMPR2, CDKN1A, CSF2RB, IGF1, IGF1R, IL10RA, IL10RB, IL12RB1, IL12RB2, IL13RA1, IL15RA, IL1R2, IL1RL1, IL2RG, IL6ST, IL7R, KDR, PDGFB, PDGFRB, PIM1, SRC, TGFB1, TNFRSF11A

PAK Signalling	2.67	-0.832	39/ 72 (54%)	0/ 72 (0%)	33/ 72 (46%)	0/ 72 (0%)	ARHGEF6, ITGA4, ITGAL, ITGAM, ITGAX, ITGB1, ITGB2, ITGB3, ITGB5, PAK1, PDGFB, PDGFC, PDGFRB, PIK3C2B, PIK3CB, PIK3CG, PTK2, PTK2B, PXN
T Cell Receptor Signalling	2.66	0.962	58/ 116 (50%)	0/ 116 (0%)	51/ 116 (44%)	7/ 116 (6%)	B2M, CBL, CD28, CD4, CD80, FYB1, FYN, HLA-DMA, HLA-DOA, HLA-DQA1, HLA-DQB1, HLA-DRB5, HLA-E, HLA-G, ICOSLG/ LOC102723996, ITGAL, ITGB1, ITGB2, PIK3C2B, PIK3CB, PIK3CG, PTK2B, PTPN22, PTPRC, TCF4, VAV2, VAV3
Regulation of eIF4 and p70S6K Signalling	2.64	0	54/ 105 (51%)	0/ 105 (0%)	51/ 105 (49%)	0/ 105 (0%)	AGO3, EIF2S3, EIF4G2, ITGA4, ITGAL, ITGAM, ITGAX, ITGB1, ITGB2, ITGB3, ITGB5, PIK3C2B, PIK3CB, PIK3CG, PPP2R1B, RPS13, RPS14, RPS16, RPS23, RPS24, RPS27A, RPS29, RPS3, RPS4Y1, RPS5
CTLA4 Signalling in Cytotoxic T Lymphocytes	2.62	N/ A	24/ 47 (51%)	0/ 47 (0%)	22/ 47 (47%)	1/ 47 (2%)	AP2A2, B2M, CD28, CD80, CLTC, FYN, HLA-E, HLA-G, PIK3C2B, PIK3CB, PIK3CG,

							PPP2R1B, PTPN22, SYK
IL-12 Signalling and Production in Macrophages	2.58	N/ A	34/ 84 (40%)	0/ 84 (0%)	42/ 84 (50%)	8/ 84 (10%)	APOE, CEBPB, CLU, IL10, IL12RB1, IL12RB2, IL18, IRF1, IRF8, LYZ, MAF, PIK3C2B, PIK3CB, PIK3CG, PRKCA, PRKCB, PRKCD, STAT1, TGFB1, TLR2, TLR4
Ephrin A Signalling	2.46	N/ A	14/ 25 (56%)	0/ 25 (0%)	10/ 25 (40%)	1/ 25 (4%)	FYN, PAK1, PIK3C2B, PIK3CB, PIK3CG, PTK2, ROCK2, VAV2, VAV3
VDR/ RXR Activation	2.44	-0.302	22/ 44 (50%)	0/ 44 (0%)	13/ 44 (30%)	9/ 44 (20%)	CCL5, CD14, CDKN1A, CEBPA, CEBPB, CXCL10, IL1RL1, PRKCA, PRKCB, PRKCD, RUNX2, SP1, THBD
Glioblastoma Multiforme Signalling	2.42	0.688	51/ 92 (55%)	0/ 92 (0%)	38/ 92 (41%)	3/ 92 (3%)	CCND2, CDK6, CDKN1A, IGF1, IGF1R, ITPR1, ITPR2, PDGFB, PDGFC, PDGFRB, PIK3C2B, PIK3CB, PIK3CG, PLCB2, PLCB4, PLCG2, PLCL2, PRKCD, RB1, RHOBTB1, RHOC, SRC
Glioma Signalling	2.41	0	45/ 81 (56%)	0/ 81 (0%)	35/ 81 (43%)	1/ 81 (1%)	CAMK1D, CAMK2G, CCND2, CDK6, CDKN1A, HDAC7, IDH2, IGF1, IGF1R, PDGFB, PDGFC, PDGFRB, PIK3C2B, PIK3CB,

							PIK3CG, PLCG2, PRKCA, PRKCB, PRKCD, RB1
Role of NFAT in Regulation of the Immune Response	2.4	1.043	64/ 115 (56%)	0/ 115 (0%)	49/ 115 (43%)	2/ 115 (2%)	BLNK, CD28, CD4, CD80, FCGR1A, FCGR2B, FCGR3A/ FCGR3B, FYN, HLA-DMA, HLA-DOA, HLA-DQA1, HLA-DQB1, HLA-DRB5, ITPR1, ITPR2, KPNB1, LYN, MEF2C, PIK3C2B, PIK3CB, PIK3CG, PLCB2, PLCB4, PLCG2, RCAN1, SYK
CXCR4 Signalling	2.39	0.655	60/ 98 (61%)	0/ 98 (0%)	38/ 98 (39%)	0/ 98 (0%)	ADCY9, CD4, CXCR4, DOCK1, ELMO2, ITPR1, ITPR2, LYN, PAK1, PIK3C2B, PIK3CB, PIK3CG, PLCB2, PLCB4, PRKCA, PRKCB, PRKCD, PTK2, PXN, RHOBTB1, RHOC, ROCK2, SRC
Pyroptosis Signalling Pathway	2.38	2	25/ 60 (42%)	0/ 60 (0%)	30/ 60 (50%)	5/ 60 (8%)	CASP4, GBP2, GSDMD, IL18, NAIP, NLRC4, NLRP1, PYCARD, Tlr12, TLR2, TLR3, TLR4, TLR5, TLR8, TLR9, TNFRSF1B
Phospholipases	2.33	0	12/ 26 (46%)	0/ 26 (0%)	11/ 26 (42%)	3/ 26 (12%)	LPL, PLA2G2D, PLA2G7, PLAAT3, PLCB2, PLCB4, PLCG2, PLCL2, PLD4

PKCθ Signalling in T Lymphocytes	2.32	0	43/ 88 (49%)	0/ 88 (0%)	39/ 88 (44%)	6/ 88 (7%)	CACNA1A, CAMK2G, CD28, CD4, CD80, FYN, HLA-DMA, HLA-DOA, HLA-DQA1, HLA-DQB1, HLA-DRB5, ITPR1, ITPR2, MAP3K3, MAP3K5, PIK3C2B, PIK3CB, PIK3CG, PLCG2, VAV2, VAV3
B Cell Receptor Signalling	2.29	1.225	59/ 117 (50%)	0/ 117 (0%)	57/ 117 (49%)	1/ 117 (1%)	APBB1IP, BCL2A1, BLNK, CAMK2G, CD22, ETS1, FCGR2B, GAB1, LYN, MAP3K3, MAP3K5, MEF2C, PIK3AP1, PIK3C2B, PIK3CB, PIK3CG, PLCG2, POU2F2, PRKCB, PTK2, PTK2B, PTPRC, SYK, SYNJ2, VAV2, VAV3
Systemic Lupus Erythematosus In T Cell Signalling Pathway	2.27	0	74/ 129 (57%)	0/ 129 (0%)	46/ 129 (36%)	9/ 129 (7%)	B2M, CASP4, CBL, CD28, CD44, CD80, CREM, HLA-DMA, HLA-DOA, HLA-DQA1, HLA-DQB1, HLA-DRB5, HLA-E, HLA-G, ICOSLG/ LOC102723996, IL10, ITGAL, ITPR1, PIK3C2B, PIK3CB, PIK3CG, PPP2R1B, PTK2, RHOBTB1, RHOC, ROCK2, SP1, SYK
TR/ RXR Activation	2.25	N/ A	22/ 41 (54%)	0/ 41 (0%)	18/ 41 (44%)	1/ 41 (2%)	COL6A3, LDLR, PDE3B, PIK3C2B,

							PIK3CB, PIK3CG, SCARB1, SLC2A1, SREBF2, THRA, THRB, UCP2
Ephrin B Signalling	2.25	-0.905	30/ 41 (73%)	0/ 41 (0%)	11/ 41 (27%)	0/ 41 (0%)	CBL, CXCR4, EFNB1, EPHB6, ITSN1, PAK1, PTK2, PXN, RGS3, ROCK2, VAV2, VAV3
MSP-RON Signalling In Cancer Cells Pathway	2.22	-0.447	46/ 84 (55%)	0/ 84 (0%)	34/ 84 (40%)	4/ 84 (5%)	ACTA2, CSF2RB, ELF4, ETS1, ETS2, ITGB1, MET, PDGFC, PIK3C2B, PIK3CB, PIK3CG, PTK2, PTK2B, RPS6KA3, SP1, SRC, ST14, TCF4, YWHAH, YWHAZ
ILK Signalling	2.21	-1.606	67/ 107 (63%)	0/ 107 (0%)	35/ 107 (33%)	5/ 107 (5%)	ACTA2, ACTN1, ARHGEF6, BMP2, DOCK1, FN1, IRS2, ITGB1, ITGB2, ITGB3, ITGB5, LIMS1, MMP9, MYH10, MYO10, PDGFC, PIK3C2B, PIK3CB, PIK3CG, PPP2R1B, PTK2, PXN, RHOBTB1, RHOC
Neuropathic Pain Signalling In Dorsal Horn Neurons	2.21	1.291	31/ 57 (54%)	0/ 57 (0%)	20/ 57 (35%)	6/ 57 (11%)	CAMK1D, CAMK2G, ITPR1, ITPR2, PIK3C2B, PIK3CB, PIK3CG, PLCB2, PLCB4, PLCG2, PLCL2, PRKCA, PRKCB, PRKCD, SRC
ICOS-ICOSL Signalling in T Helper Cells	2.19	0	31/ 68 (46%)	0/ 68 (0%)	31/ 68 (46%)	6/ 68 (9%)	CAMK2G, CD28, CD4, CD80, HLA-DMA, HLA-DOA, HLA-DQA1, HLA-

							DQB1, HLA-DRB5, ICOSLG/ LOC102723996, IL2RG, ITPR1, ITPR2, PIK3C2B, PIK3CB, PIK3CG, PTPRC
Growth Hormone Signalling	2.16	1.265	23/ 42 (55%)	0/ 42 (0%)	18/ 42 (43%)	1/ 42 (2%)	CEBPA, IGF1, IGF1R, PIK3C2B, PIK3CB, PIK3CG, PLCG2, PRKCA, PRKCB, PRKCD, RPS6KA3, STAT1
p70S6K Signalling	2.15	2	45/ 74 (61%)	0/ 74 (0%)	28/ 74 (38%)	1/ 74 (1%)	EEF2K, IL2RG, LYN, PIK3C2B, PIK3CB, PIK3CG, PLCB2, PLCB4, PLCG2, PLCL2, PPP2R1B, PRKCA, PRKCB, PRKCD, SRC, SYK, YWHAH, YWHAZ
Iron homeostasis Signalling pathway	2.15	N/ A	36/ 74 (49%)	0/ 74 (0%)	33/ 74 (45%)	5/ 74 (7%)	ATP6V0A1, ATP6V0A2, ATP6V1C1, BMP1, BMP2, BMPR2, CD163, EPAS1, FTH1, HFE, LRP1, PDGFB, PDGFRB, SLC11A1, SLC25A37, SLC40A1, TCIRG1, TFRC
Necroptosis Signalling Pathway	2.13	2.065	27/ 80 (34%)	0/ 80 (0%)	46/ 80 (57%)	7/ 80 (9%)	AXL, BIRC2, CAMK2G, CAPN2, CYBB, EIF2AK2, IFNB1, IRF9, PELI1, PLA2G2D, PYCARD, RB1, STAT1, STAT2, TLR3, TLR4,

							TNFRSF1B, TNFSF10, TSPO
Role of Osteoblasts, Osteoclasts and Chondrocytes in Rheumatoid Arthritis	2.09	N/ A	64/ 121 (53%)	0/ 121 (0%)	44/ 121 (36%)	13/ 121 (11%)	BIRC2, BMP1, BMP2, BMPR2, CBL, CSF1, IGF1, IL10, IL18, IL1R2, IL1RL1, ITGB3, LRP1, MAP3K5, MMP14, NAIP, PIK3C2B, PIK3CB, PIK3CG, PTK2B, RUNX2, SRC, TCF4, TGFB1, TNFRSF11A, TNFRSF1B
Primary Immunodeficiency Signalling	2.07	N/ A	7/ 19 (37%)	0/ 19 (0%)	9/ 19 (47%)	3/ 19 (16%)	BLNK, CD4, CIITA, IL2RG, IL7R, PTPRC, TAP1
14-3-3-mediated Signalling	2.03	0.832	47/ 76 (62%)	0/ 76 (0%)	29/ 76 (38%)	0/ 76 (0%)	CBL, GFAP, MAP3K5, PIK3C2B, PIK3CB, PIK3CG, PLCB2, PLCB4, PLCG2, PLCL2, PRKCA, PRKCB, PRKCD, SRC, TUBA1A, TUBB2A, YWHAH, YWHAZ
Factors Promoting Cardiogenesis in Vertebrates	2.02	-1.807	41/ 65 (63%)	0/ 65 (0%)	17/ 65 (26%)	7/ 65 (11%)	BMP1, BMP2, BMPR2, CAMK2G, LRP1, MEF2C, PLCB2, PLCB4, PLCG2, PLCL2, PRKCA, PRKCB, PRKCD, ROCK2, TCF4, TGFB1
Cholecystokinin/ Gastrin-mediated Signalling	1.99	0	50/ 71 (70%)	0/ 71 (0%)	21/ 71 (30%)	0/ 71 (0%)	CREM, IL18, ITPR1, ITPR2, MEF2C, PLCB2, PLCB4, PRKCA, PRKCB, PRKCD, PTK2, PTK2B,

							PXN, RHOBTB1, RHOC, ROCK2, SRC
Gustation Pathway	1.96	0	30/ 66 (45%)	0/ 66 (0%)	20/ 66 (30%)	16/ 66 (24%)	ADCY9, CACNA1A, CD36, ITPR1, ITPR2, LPL, LRRC8D, P2RX1, P2RX4, P2RY12, P2RY13, P2RY14, P2RY2, PDE3B, PLCB2, TRPM4
IL-8 Signalling	1.95	0.392	70/ 136 (51%)	0/ 136 (0%)	60/ 136 (44%)	6/ 136 (4%)	CCND2, CYBB, IRAK2, ITGAM, ITGAX, ITGB2, ITGB3, KDR, LASP1, MAP4K4, MMP2, MMP9, PDGFC, PIK3C2B, PIK3CB, PIK3CG, PLCB2, PLD4, PRKCA, PRKCB, PRKCD, PTK2, PTK2B, RHOBTB1, RHOC, ROCK2, SRC, VASP
NF-κB Signalling	1.95	1.4	56/ 124 (45%)	0/ 124 (0%)	60/ 124 (48%)	8/ 124 (6%)	BMP2, BMPR2, EIF2AK2, IGF1R, IL18, IL1R2, KDR, MAP3K3, MAP4K4, PDGFRB, PELI1, PIK3C2B, PIK3CB, PIK3CG, PLCG2, PRKCB, TANK, TLR2, TLR3, TLR4, TLR5, TLR8, TLR9, TNFRSF11A, TNFRSF1B, TNFSF13B

PD-1, PD-L1 cancer immunotherapy pathway	1.93	-0.5	27/ 72 (38%)	0/ 72 (0%)	35/ 72 (49%)	10/ 72 (14%)	B2M, CD274, CD28, CD80, HLA-DMA, HLA-DOA, HLA-DQA1, HLA-DQB1, HLA-DRB5, HLA-E, HLA-G, IL2RG, PIK3C2B, PIK3CB, PIK3CG, TGFB1, TNFRSF1B
RHOGDI Signalling	1.92	0.832	59/ 95 (62%)	0/ 95 (0%)	35/ 95 (37%)	1/ 95 (1%)	ACTA2, ARHGAP4, ARHGEF18, ARHGEF6, CD44, ITGA4, ITGAL, ITGAM, ITGAX, ITGB1, ITGB2, ITGB3, ITGB5, MYH10, PAK1, PRKCA, RHOBTB1, RHOC, ROCK2, SRC, WASF2
Tumour Microenvironment Pathway	1.91	-1.225	58/ 113 (51%)	0/ 113 (0%)	39/ 113 (35%)	16/ 113 (14%)	CCL2, CD274, CD44, CSF1, CSPG4, CXCR4, FGF1, FN1, HLA-E, HLA-G, IGF1, IL10, ITGB3, MMP12, MMP14, MMP2, MMP9, PDGFB, PDGFC, PIK3C2B, PIK3CB, PIK3CG, SLC2A1, TGFB1
Ephrin Receptor Signalling	1.91	-1.155	72/ 113 (64%)	0/ 113 (0%)	37/ 113 (33%)	4/ 113 (4%)	CXCR4, EFNB1, EPHB6, FGF1, FYN, ITGA4, ITGAL, ITGAM, ITGAX, ITGB1, ITGB2, ITGB3, ITGB5, ITSN1, MAP4K4, PAK1, PDGFB, PDGFC,

							PIK3CG, PTK2, PXN, RGS3, ROCK2, SRC
RAC Signalling	1.88	-0.258	53/ 96 (55%)	0/ 96 (0%)	40/ 96 (42%)	3/ 96 (3%)	ABI2, BAIAP2, CD44, CDK5R1, CYBB, CYFIP1, IQGAP2, ITGA4, ITGAL, ITGAM, ITGAX, ITGB1, ITGB2, ITGB3, ITGB5, PAK1, PIK3C2B, PIK3CB, PIK3CG, PTK2, PTK2B
GP6 Signalling Pathway	1.85	0.258	43/ 79 (54%)	0/ 79 (0%)	24/ 79 (30%)	12/ 79 (15%)	APBB1IP, COL6A3, FYB1, FYN, ITGB3, ITPR1, LYN, PIK3C2B, PIK3CB, PIK3CG, PLCG2, PRKCA, PRKCB, PRKCD, PTK2, SYK, VAV2, VAV3
GM-CSF Signalling	1.79	2.111	27/ 52 (52%)	0/ 52 (0%)	25/ 52 (48%)	0/ 52 (0%)	BCL2A1, CAMK2G, CSF2RA, CSF2RB, ETS1, HCK, LYN, PIK3C2B, PIK3CB, PIK3CG, PIM1, PRKCB, STAT1
Epithelial Adherens Junction Signalling	1.78	1.789	65/ 92 (71%)	0/ 92 (0%)	26/ 92 (28%)	1/ 92 (1%)	BAIAP2, BMPR2, FGF1, FRMD6, FYN, IGF1R, MET, MYH10, NECTIN2, NOTCH2, PAK1, PPP2R1B, PRKAB1, ROCK2, SRC, TCF4, TNS1, VAV2, YWHAH, YWHAZ
Neuregulin Signalling	1.77	0.707	43/ 69 (62%)	0/ 69 (0%)	24/ 69 (35%)	2/ 69 (3%)	CDK5R1, DLG4, ERRFI1, ITGA4, ITGAL, ITGAM,

							ITGAX, ITGB1, ITGB2, ITGB3, ITGB5, PLCG2, PRKCA, PRKCB, PRKCD, SRC
VEGF Signalling	1.77	-0.258	41/ 69 (59%)	0/ 69 (0%)	25/ 69 (36%)	3/ 69 (4%)	ACTA2, ACTN1, EIF2S3, KDR, PDGFC, PIK3C2B, PIK3CB, PIK3CG, PLCG2, PRKCA, PRKCB, PTK2, PTK2B, PXN, ROCK2, SRC
Synaptogenesis Signalling Pathway	1.74	-0.192	90/ 135 (67%)	0/ 135 (0%)	42/ 135 (31%)	3/ 135 (2%)	ADCY9, AP2A2, APOE, CADM1, CAMK2G, CLASP2, DLG4, EFNB1, EPHB6, FARP1, FYN, HCK, ITPR1, ITSN1, LRP1, LYN, PAK1, PIK3C2B, PIK3CB, PIK3CG, PLCG2, PRKCD, SRC, STXBP2, STXBP5, THBS1, YKT6
Production of Nitric Oxide and Reactive Oxygen Species in Macrophages	1.73	2.711	56/ 117 (48%)	0/ 117 (0%)	54/ 117 (46%)	7/ 117 (6%)	APOE, CLU, CYBA, CYBB, IRF1, IRF8, LYZ, MAP3K3, MAP3K5, PIK3C2B, PIK3CB, PIK3CG, PLCG2, PPP1R3D, PPP2R1B, PRKCA, PRKCB, PRKCD, RHOBTB1, RHOC, STAT1, TLR2, TLR4, TNFRSF1B
Dermatan Sulphate Biosynthesis (Late Stages)	1.68	0.447	5/ 13 (38%)	0/ 13 (0%)	6/ 13 (46%)	2/ 13 (15%)	CHST15, CHST2, CHST7, DSE, NDST1

Protein Kinase A Signalling	1.67	0.539	107/ 187 (57%)	0/ 187 (0%)	73/ 187 (39%)	7/ 187 (4%)	ADCY9, ADD3, AKAP8, CAMK2G, CDC27, CREM, DUSP16, DUSP3, GDE1, ITPR1, ITPR2, MYH10, PDE3B, PLCB2, PLCB4, PLCG2, PLCL2, PPP1R3D, PRKCA, PRKCB, PRKCD, PTK2, PTK2B, PTPN12, PTPN22, PTPRC, PTPRM, PXN, ROCK2, TCF4, TGFB1, UBASH3B, VASP, YWHAH, YWHAZ
Signalling by Rho Family GTPases	1.67	-0.894	80/ 143 (56%)	0/ 143 (0%)	59/ 143 (41%)	4/ 143 (3%)	ACTA2, ARHGEF18, ARHGEF6, BAIAP2, CLIP1, CYBB, CYFIP1, GFAP, ITGA4, ITGAL, ITGAM, ITGAX, ITGB1, ITGB2, ITGB3, ITGB5, PAK1, PIK3C2B, PIK3CB, PIK3CG, PTK2, PTK2B, RHOBTB1, RHOC, ROCK2, SEPTIN11, SEPTIN8, SEPTIN9
Activation of IRF by Cytosolic Pattern Recognition Receptors	1.66	2.714	15/ 43 (35%)	0/ 43 (0%)	27/ 43 (63%)	1/ 43 (2%)	DDX58, IFIH1, IFIT2, IFNB1, IL10, IRF7, IRF9, MAVS, STAT1, STAT2, TANK
Toll-like Receptor Signalling	1.66	0.905	23/ 54 (43%)	0/ 54 (0%)	29/ 54 (54%)	2/ 54 (4%)	CD14, EIF2AK2, IL18, IL1RL1, IRAK2, MAP4K4,

							RPS27A, TLR2, TLR3, TLR4, TLR5, TLR8, TLR9
Endothelin-1 Signalling	1.64	1.091	54/ 101 (53%)	0/ 101 (0%)	40/ 101 (40%)	7/ 101 (7%)	ADCY9, CASP4, EDNRB, GAB1, ITPR1, ITPR2, PIK3C2B, PIK3CB, PIK3CG, PLA2G2D, PLA2G7, PLAAT3, PLCB2, PLCB4, PLCG2, PLCL2, PLD4, PRKCA, PRKCB, PRKCD, SRC
Cellular Effects of Sildenafil (Viagra)	1.62	N/ A	30/ 49 (61%)	0/ 49 (0%)	15/ 49 (31%)	4/ 49 (8%)	ACTA2, ADCY9, CACNA1A, ITPR1, ITPR2, MYH10, MYO10, PDE3B, PLCB2, PLCB4, PLCG2, PLCL2
MSP-RON Signalling In Macrophages Pathway	1.62	0.258	33/ 66 (50%)	0/ 66 (0%)	29/ 66 (44%)	4/ 66 (6%)	CIITA, HLA-DMA, HLA-DOA, HLA-DQA1, HLA-DQB1, HLA-DRB5, IL10, ITGAM, ITGB2, PIK3C2B, PIK3CB, PIK3CG, ST14, STAT1, TLR4
HIF1α Signalling	1.61	0.2	70/ 126 (56%)	0/ 126 (0%)	42/ 126 (33%)	14/ 126 (11%)	CAMK1D, CAMK2G, CCNG2, CDKN1A, CYBB, HK2, HSPA1A/ HSPA1B, IGF1, KDR, MET, MMP12, MMP14, MMP2, MMP9, PDGFB, PDGFC, PIK3C2B, PIK3CB, PIK3CG, PLCG2, PRKCA,

							PRKCB, PRKCD, SLC2A1, TGFB1
Inflammasome pathway	1.61	0.816	7/ 18 (39%)	0/ 18 (0%)	11/ 18 (61%)	0/ 18 (0%)	IL18, NAIP, NLRC4, NLRP1, PYCARD, TLR4
Role of NFAT in Cardiac Hypertrophy	1.61	-0.209	74/ 120 (62%)	0/ 120 (0%)	40/ 120 (33%)	6/ 120 (5%)	ADCY9, CACNA1A, CAMK1D, CAMK2G, HDAC7, IGF1, IGF1R, IL6ST, ITPR1, ITPR2, MEF2C, PIK3C2B, PIK3CB, PIK3CG, PLCB2, PLCB4, PLCG2, PLCL2, PRKCA, PRKCB, PRKCD, RCAN1, SRC, TGFB1
Synaptic Long Term Depression	1.6	0.243	46/ 78 (59%)	0/ 78 (0%)	23/ 78 (29%)	9/ 78 (12%)	CACNA1A, IGF1, IGF1R, ITPR1, ITPR2, LYN, PLA2G2D, PLA2G7, PLAAT3, PLCB2, PLCB4, PLCG2, PLCL2, PPP2R1B, PRKCA, PRKCB, PRKCD
Dopamine-DARPP32 Feedback in cAMP Signalling	1.6	0.258	49/ 78 (63%)	0/ 78 (0%)	24/ 78 (31%)	5/ 78 (6%)	ADCY9, CACNA1A, CAMKK1, CAMKK2, CREM, ITPR1, ITPR2, KCNJ2, PLCB2, PLCB4, PLCG2, PLCL2, PPP1R3D, PPP2R1B, PRKCA, PRKCB, PRKCD
FcγRIIB Signalling in B Lymphocytes	1.59	1.89	22/ 44 (50%)	0/ 44 (0%)	19/ 44 (43%)	3/ 44 (7%)	BLNK, CACNA1A, FCGR2B, ITPR1, ITPR2, LYN, PIK3C2B, PIK3CB,

							PIK3CG, PLCG2, SYK
Molecular Mechanisms of Cancer	1.55	N/ A	140/ 256 (55%)	0/ 256 (0%)	106/ 256 (41%)	10/ 256 (4%)	ADCY9, ARHGEF18, ARHGEF6, ATR, BIRC2, BMP1, BMP2, BMPR2, CAMK2G, CBL, CCND2, CDK6, CDKN1A, DAXX, FYN, GAB1, HDAC7, ITGA4, ITGAL, ITGAM, ITGAX, ITGB1, ITGB2, ITGB3, ITGB5, LRP1, MAP3K5, NAIP, PAK1, PIK3C2B, PIK3CB, PIK3CG, PLCB2, PLCB4, PRKCA, PRKCB, PRKCD, PTK2, RB1, RHOBTB1, RHOC, SMAD7, SRC, TCF4, TGFB1
CD28 Signalling in T Helper Cells	1.55	1.155	42/ 79 (53%)	0/ 79 (0%)	34/ 79 (43%)	3/ 79 (4%)	CD28, CD4, CD80, FYN, HLA-DMA, HLA-DOA, HLA-DQA1, HLA-DQB1, HLA-DRB5, ITPR1, ITPR2, PAK1, PIK3C2B, PIK3CB, PIK3CG, PTPRC, SYK
Type II Diabetes Mellitus Signalling	1.55	0.577	36/ 85 (42%)	0/ 85 (0%)	43/ 85 (51%)	6/ 85 (7%)	ACSL4, CACNA1A, CD36, CEBPB, IRS2, ITPR1, ITPR2, MAP3K5, NSMAF, PIK3C2B, PIK3CB, PIK3CG, PRKAB1,

							PRKCA, PRKCB, PRKCD, SLC27A1, TNFRSF1B
Chondroitin Sulphate Biosynthesis (Late Stages)	1.53	0.447	5/ 14 (36%)	0/ 14 (0%)	6/ 14 (43%)	3/ 14 (21%)	CHST15, CHST2, CHST7, CHSY1, NDST1
GPCR-Mediated Nutrient Sensing in Enteroendocrine Cells	1.52	0.302	24/ 45 (53%)	0/ 45 (0%)	15/ 45 (33%)	6/ 45 (13%)	ADCY9, CACNA1A, ITPR1, ITPR2, PLCB2, PLCB4, PLCG2, PLCL2, PRKCA, PRKCB, PRKCD
Hepatic Fibrosis Signalling Pathway	1.51	-0.324	130/ 251 (52%)	0/ 251 (0%)	98/ 251 (39%)	23/ 251 (9%)	ACTA2, BMPR2, CACNA1A, CCL2, CCL5, CEBPB, CYBB, FTH1, IL18, IL1R2, IL1RL1, IRAK2, IRS2, ITGA4, ITGAL, ITGAM, ITGAX, ITGB1, ITGB2, ITGB3, ITGB5, KDR, LRP1, PDGFB, PDGFC, PDGFRB, PIK3C2B, PIK3CB, PIK3CG, PLCG2, PRKCA, PRKCB, PRKCD, PTK2, RHOBTB1, RHOC, ROCK2, SMAD7, SP1, TCF4, TFRC, TGFB1, TLR4, TNFRSF1B
PTEN Signalling	1.5	1.387	60/ 98 (61%)	0/ 98 (0%)	33/ 98 (34%)	5/ 98 (5%)	BMPR2, CBL, CDKN1A, IGF1R, ITGA4, ITGAL, ITGAM, ITGAX, ITGB1, ITGB2, ITGB3, ITGB5, KDR, PDGFRB, PIK3CB, PIK3CG, PTK2, SYNJ2,

							TNFRSF11A, YWHAH
mTOR Signalling	1.49	0.905	64/ 123 (52%)	0/ 123 (0%)	55/ 123 (45%)	4/ 123 (3%)	EIF4G2, PDGFC, PIK3C2B, PIK3CB, PIK3CG, PLD4, PPP2R1B, PRKAB1, PRKCA, PRKCB, PRKCD, RHOBTB1, RHOC, RPS13, RPS14, RPS16, RPS23, RPS24, RPS27A, RPS29, RPS3, RPS4Y1, RPS5, RPS6KA3
Pathogenesis of Multiple Sclerosis	1.46	N/ A	3/ 6 (50%)	0/ 6 (0%)	3/ 6 (50%)	0/ 6 (0%)	CCL5, CCR5, CXCL10
Semaphorin Signalling in Neurons	1.45	N/ A	26/ 35 (74%)	0/ 35 (0%)	8/ 35 (23%)	1/ 35 (3%)	FYN, ITGB1, MET, PAK1, PLXNA1, PTK2, RHOBTB1, RHOC, ROCK2
OX40 Signalling Pathway	1.45	N/ A	12/ 35 (34%)	0/ 35 (0%)	19/ 35 (54%)	4/ 35 (11%)	B2M, CD4, HLA-DMA, HLA-DOA, HLA-DQA1, HLA-DQB1, HLA-DRB5, HLA-E, HLA-G
IL-10 Signalling	1.43	N/ A	28/ 52 (54%)	0/ 52 (0%)	23/ 52 (44%)	1/ 52 (2%)	BLVRB, CCR5, CD14, FCGR2B, IL10, IL10RA, IL10RB, IL18, IL1R2, IL1RL1, MAP4K4, SP1
PDGF Signalling	1.42	1.387	34/ 58 (59%)	0/ 58 (0%)	24/ 58 (41%)	0/ 58 (0%)	EIF2AK2, PDGFB, PDGFC, PDGFRB, PIK3C2B, PIK3CB, PIK3CG, PLCG2, PRKCA, PRKCB, SRC, STAT1, SYNJ2
Role of JAK1 and JAK3 in γc Cytokine Signalling	1.39	N/ A	20/ 47 (43%)	0/ 47 (0%)	24/ 47 (51%)	3/ 47 (6%)	BLNK, IL15RA, IL2RG, IL7R, IRS2, PIK3C2B, PIK3CB,

							PIK3CG, PTK2B, STAT1, SYK
Melatonin Signalling	1.38	0.333	26/ 36 (72%)	0/ 36 (0%)	10/ 36 (28%)	0/ 36 (0%)	CAMK2G, PLCB2, PLCB4, PLCG2, PLCL2, PRKCA, PRKCB, PRKCD, RORA
Insulin Secretion Signalling Pathway	1.37	0.784	71/ 139 (51%)	0/ 139 (0%)	62/ 139 (45%)	6/ 139 (4%)	ADCY9, AGO3, CACNA1A, CAMK2G, EIF2S3, EIF4G2, FYN, HCK, ITPR1, ITPR2, LYN, PIK3C2B, PIK3CB, PIK3CG, PLCB2, PLCB4, PLCG2, PLCL2, PRKCA, PRKCB, PRKCD, SLC2A1, SRC, STAT1, STAT2, YKT6
Actin Nucleation by ARP-WASP Complex	1.37	-0.816	38/ 59 (64%)	0/ 59 (0%)	21/ 59 (36%)	0/ 59 (0%)	BAIAP2, ITGA4, ITGAL, ITGAM, ITGAX, ITGB1, ITGB2, ITGB3, ITGB5, RHOBTB1, RHOC, ROCK2, VASP
Phagosome Maturation	1.37	N/ A	37/ 89 (42%)	0/ 89 (0%)	46/ 89 (52%)	6/ 89 (7%)	ATP6V0A1, ATP6V0A2, ATP6V1C1, B2M, CTSD, CTSS, CTSZ, CYBB, HLA-DRB5, HLA-E, HLA-G, LAMP1, RAB7B, TAP1, TCIRG1, TUBA1A, TUBB2A, YKT6
HOTAIR Regulatory Pathway	1.37	0	50/ 89 (56%)	0/ 89 (0%)	29/ 89 (33%)	10/ 89 (11%)	AGO3, ATXN1, CD44, CDKN1A, IRF1, MET, MMP12, MMP14, MMP2, MMP9, PIK3C2B,

							PIK3CB, PIK3CG, RHOC, ROCK2, TCF4, TGFB1, TLR4
Fc Epsilon RI Signalling	1.36	0.258	42/ 71 (59%)	0/ 71 (0%)	26/ 71 (37%)	3/ 71 (4%)	FYN, GAB1, LYN, PIK3C2B, PIK3CB, PIK3CG, PLA2G2D, PLCG2, PRKCA, PRKCB, PRKCD, SYK, SYNJ2, VAV2, VAV3
Systemic Lupus Erythematosus Signalling	1.35	N/ A	51/ 108 (47%)	0/ 108 (0%)	52/ 108 (48%)	5/ 108 (5%)	CBL, CD22, CD28, CD80, CREM, FCGR1A, FCGR2B, FCGR3A/ FCGR3B, HLA-E, HLA-G, IL10, IL18, LYN, PIK3C2B, PIK3CB, PIK3CG, PLCG2, PRPF38B, PTPRC, TLR9, TNFSF13B
Notch Signalling	1.32	-0.447	13/ 26 (50%)	0/ 26 (0%)	11/ 26 (42%)	2/ 26 (8%)	DTX4, JAG1, JAG2, MAML3, MFNG, NOTCH2, NUMB
Thrombin Signalling	1.31	0.688	63/ 109 (58%)	0/ 109 (0%)	45/ 109 (41%)	1/ 109 (1%)	ADCY9, ARHGEF6, CAMK1D, CAMK2G, ITPR1, ITPR2, PIK3C2B, PIK3CB, PIK3CG, PLCB2, PLCB4, PLCG2, PLCL2, PRKCA, PRKCB, PRKCD, PTK2, RHOBTB1, RHOC, ROCK2, SRC
eNOS Signalling	1.31	0.577	36/ 72 (50%)	0/ 72 (0%)	28/ 72 (39%)	8/ 72 (11%)	ADCY9, CHRNA7, HSPA1A/ HSPA1B, ITPR1, ITPR2, KDR,

							PDGFC, PIK3C2B, PIK3CB, PIK3CG, PLCG2, PRKAB1, PRKCA, PRKCB, PRKCD
Dermatan Sulphate Biosynthesis	1.3	0	8/ 21 (38%)	0/ 21 (0%)	10/ 21 (48%)	3/ 21 (14%)	CHST15, CHST2, CHST7, CHSY1, DSE, NDST1

Appendix III Cannonical Pathway Analysis from IPA of DESeq2 analysis of Naïve Microglia

Appendix IV

Upstream Regulator	Expr Log Ratio	Predicted Activation State	Activation z-score	p-value Overlap	Target Molecules in Dataset
IFNG		Activated	4.179	9.69E-26	C2, CARD6, CCL5, Ccl7, CCND2, CCR2, CCR5, CD274, CD44, CD74, CD80, CDKN1A, CHST7, CIITA, CLEC10A, CMPK2, CSF1, CXCL10, CXCL2, Cxcl9, CXCR4, CYRIA, DAXX, DDX58, ENDOD1, FCGR2B, FGF1, FMNL2, FN1, GBP2, HCAR2, HCK, HIP1, HK2, HLA-DOA, HLA-DQA1, HLA-DQB1, HLA-DRB5, ICOSLG/LOC102723996, IFI16, IFI44, IFIH1, IFIT1B, IFIT2, IFIT3, IFNB1, IFRD1, IGF1, IL10, IL13RA1, IRF1, IRF8, ITGAL, ITPR1, LDLR, Ly6a (includes others), MARCKSL1, MRC1, OAS1, OAS3, OASL, P2RY14, PDGFC, PFKFB3, PIM1, PML, PRDM1, RB1, Retnla, RSAD2, SAMHD1, SLC2A1, STAT1, TAP1, TGFB1, THBS1, TLR9, XAF1
IL10RA	0.45	Inhibited	-6.823	4.71E-23	ADD3, ALOX5, ANKH, B3GNT7, BMP2, C3, CA2, CALHM6, CCL5, Cd24a, CD300LF, CD34, CD36, CLCN7, CLEC12A, COL14A1, CSF3R, CST7, Cxcl9, EDNRB, F13A1, FN1, FOLR2, GAS6, GBP2, GSAP, HCAR2, HPSE, IFI16, IL12RB1, IL15RA, IL2RG, IRF1, IRF7, KITLG, Ly6a (includes others), NAMPT, NLRC5, NOD1, NPL, OLR1, PARVG, PF4, PLAAT3, PSMB9, REPS2, Retnla, RGS18, RNF213, RSAD2, S1PR1, SAMHD1, SLAMF6, SLAMF8, SLC2A1, SLCO2B1, SPARC, STARD8, STAT1, TAP1, TFEC, TLR2, TNFRSF14, TRPM2, ZC3H12C
CITED2	-0.12	Inhibited	-5.113	1.52E-20	B2M, BBX, C3, C5AR1, CALHM6, CD274, CD80, CLEC10A, CMPK2, CPEB4, CXCL10, CXCL2, CXCL3, Cxcl9, CYBB, CYRIA, DAXX, DDX58, DTX3L, ENDOD1, FCGR2B, FCGR3A/FCGR3B, FMNL2, GBP2, HCAR2, IFI16, IFI44, IFIH1, IFIT1B, IFIT2, IFIT3, IFNB1, IFRD1, IL13RA1, IRF1, IRF8, IRF9, ITGA4, KLF6, KYNU, LPL, MED13, MRC1, MTMR14, NAMPT, OAS1, OAS3, OASL, P2RY14, PARP14, PDGFC, PFKFB3, PIM1, PLAC8, Retnla, RSAD2, SLAMF8, TAGAP, TOR1AIP1, TTC39B, XAF1
PTGER4	-0.124	Inhibited	-4.942	3.98E-18	CCL2, Ccl7, CCNG2, CDK6, CMPK2, CXCL10, Cxcl9, CXCR4, CYBB, CYRIA, DAXX, DDX58, GAB1, GBP2, GLIS3, HAVCR2, HCAR2, HERC6, IFI16, IFIH1, IFIT1B, IFIT2, IL18, IRF1, IRF7, OLR1, PARP14, PDGFB, RASSF2, RNASEL, RNF144B, RNF213, RSAD2, S1PR1, SLAMF8, SLFN5, ST6GAL1, ST8SIA4, TAGAP, TBC1D4, TLR8, TNFSF10, TOR3A, USP18, XAF1
IFNB1	4.158		1.785	1.55E-14	CCL2, CCL5, Cd24a, CD274, CDKN1A, CMPK2, CXCL10, CXCL2, CXCL3, DAXX, DDX3Y, DDX58, GBP2, HMGCS1, ICOSLG/LOC102723996, IFI16, IFIH1, IFIT1B, IFIT2, IFIT3, IL10, IL18, IRF1,

					IRF7, NOD1, PRDM1, RNASE4, RSAD2, SQLE, STARD4, STAT1, STAT2, THBS1, USP18
NFAT5	-0.064	Inhibited	-3.343	2.16E-14	CCR3, CD74, CIITA, Cxcl9, DAXX, HLA-DMA, HLA-DQA1, HLA-DQB1, HLA-DRB5, IFI16, IFIT1B, IFIT2, IFIT3, IFNB1, IRF1, RSAD2, STAT1, TNFSF10
CSF1	-0.707		-1.834	6.55E-11	APOE, APP, AXL, C5AR1, CAPN2, CBL, CCL2, Ccl7, CCR2, CD163, CD74, CDKN1A, CTSD, GAS7, GPNMB, GPR34, ICOSLG/LOC102723996, IL10, ITGA4, ITGAX, ITGB1, LAMP1, LPL, P2RY12, Retnla, SPARC, TGFB1, TNFRSF11A
MYD88	-0.035	Activated	2.926	3.06E-10	CASP4, CCL5, CD200R1, CLEC10A, CMPK2, CXCL10, CXCL13, CXCL2, CXCL3, Cxcl9, EDNRB, ETS2, FPR1, FPR2, IFIT1B, IFIT2, IFNB1, IL10, IL18, IRF1, IRF8, ITGAX, ITPR2, JAG1, MET, MMP14, MRC1, OASL, PILRA, RSAD2, SAMHD1, SCARB1, TFEC, TLR2, TSC22D1
MEF2A	-0.067	Activated	3.649	8.83E-09	CXCL10, Cxcl9, GBP2, IFI44, IFIT1B, IFIT2, IFIT3, IFNB1, IRF1, IRF7, NLRC5, NOD1, OAS1, RSAD2
TICAM1	0.25		1.448	1.42E-08	CASP4, CCL5, CMPK2, CXCL10, CXCL13, CXCL2, CXCL3, EDNRB, ETS2, FPR1, FPR2, ICOSLG/LOC102723996, IFIT1B, IFIT2, IFNB1, IRF1, ITPR2, JAG1, MET, OASL, PILRA, RSAD2, SAMHD1, TFEC, TLR2, TSC22D1
COP1	0.035	Inhibited	-2.744	9.35E-08	APOE, C3, CCL5, CEBPB, CXCL10, CXCL3, FPR1, FPR2, FTH1, GPNMB, IFI16, ITGAX
TGFBR2	-0.017		0.2	9.53E-08	ADGRE1, CX3CR1, ITGAM, MRC1, MSR1, P2RY12, PTPRC, TIMD4
LDLR	-1.479			1.46E-07	APOE, C1QA, CCL2, CCL5, Ccl7, CCR2, CCR3, CCR5, CD274, CD36, CD4, CDKN1A, CX3CR1, FCGR1A, FGL2, FPR1, FPR2, GAS6, GATM, IL10, IL12RB1, IRF7, ITGB3, LSP1, LYZ, MMP14, MMP2, MMP9, MSR1, NOD1, SCARB1, TAP1
NR1H3	-0.485		0.332	1.56E-06	APOE, ARL4C, C1QA, CCL2, CCL5, Ccl7, CCR2, CCR3, CCR5, CD274, CD4, CDKN1A, CX3CR1, CXCL10, FCGR1A, FGL2, FPR1, FPR2, GAS6, IL10, IL12RB1, IRF7, ITGAL, ITGB3, LSP1, LYZ, MMP9, NOD1, TAP1
QKI	-0.476		-0.632	2.64E-06	CD36, CTSS, FYN, HIP1, HLA-DOA, HLA-DQA1, HLA-DQB1, ITGAM, ITGAX, TAP1
IFNAR1	0.05	Activated	2.036	4.16E-06	CCL5, CIITA, CXCL10, EIF2AK2, HMGCS1, IFNB1, IL18, OAS1, OAS2, OAS3, RSAD2, SQLE, SREBF2
STAT1	1.178	Activated	3.241	5.48E-06	C3, CCL5, CXCL10, Cxcl9, GBP2, IFIT1B, IFNB1, IGF1, IL18, IRF1, PPARGC1B, PSME1, TLR9, TRAFD1
IRF3	0.126	Activated	2.805	1.08E-05	CCL5, CXCL10, DDX58, IFIH1, IFIT1B, IFIT2, IFNB1, RSAD2
MAP3K8	0.237		0	2.01E-05	ADORA3, BMP1, CCR2, CCR5, CDK5R1, CIITA, CXCL2, DOK2, FSCN1, GAB1, GPR160, HIP1, IFNB1, IGF1R, IL10, PPARGC1B, RGS3, SESN1, SNN, SPATS2L, TSPAN33

RGS10	-0.001			2.23E-05	CCL2, Ccl7, CCR3, CXCL10, CXCL2, IL10, IL10RA, IL10RB, IL18, IL1R2, IL6ST, ITGAM, ITGB2, PF4, Retnla, TGFB1, TNFRSF1B
IRF1	0.3	Activated	2.191	2.81E-05	CCL5, CXCL16, GBP2, IFNB1, IL12RB1, IL12RB2, MAP4K4, MMP9, PML, SAMHD1, TLR3, TLR9
PPARG	0.108		1.08	7.18E-05	APOE, C3, CD36, CDK6, CXCL3, HEBP1, IFNB1, LPL, MCTP1, MMP9, PF4, PID1, RAB20, Retnla, RNF144B, SGK1, TLR4, TNFSF10
IL4	-0.787		-1.884	7.55E-05	CD44, CHST7, CIITA, CLEC10A, CXCL10, IGF1, IL10, KLF6, LPL, MRC1, Retnla, TFRC, TGFB1, TNFRSF11A
TBK1	0.164		1.963	0.00012	CXCL10, IFI16, IFNB1, IRF7, RSAD2, USP18
STING1	-0.119		1.492	0.000234	CCL5, CXCL10, CXCL2, Cxcl9, GAS7, IFI16, IFIT1B, IFNB1, IL10, OASL
NR3C1	-0.181	Inhibited	-2.804	0.000257	CCL5, CXCL10, Cxcl9, HCAR2, IFIT1B, IFIT2, IFNB1, OASL
ITGB8	0.676		-0.132	0.000311	APOE, ITGB5, P2RY12, TMEM119
HIF1A	-0.033		0.609	0.000331	CCR2, CCR5, CSF1, CXCL2, HK2, MMP2, PFKFB3, SLC2A1, TFRC
IRF8	0.197		1.587	0.000454	CBL, CCL5, CXCL16, DAB2, MAP4K4, MMP9, PML, TLR9
TREM2	0.038		-0	0.000537	AXL, CD36, CST7, CXCL2, IRF8, ITGAX, LGALS1, LGALS3, LOX, LPL, SULF2
TNF	-0.244		0.749	0.000592	Acp5, CA2, CCL5, CD44, CSF1, CXCL10, CXCL13, CXCL2, CXCL3, Cxcl9, FPR1, GBP2, IL10, MMP9, TGFB1
TYROBP	0.18			0.000762	IL10RA, IL13RA1, IL18, IRF8, ITGAM, ITGAX, NPC2, NRROS, SFT2D2, TCIRG1, TNFRSF1B
IRF2	-0.048		-1.254	0.00175	CLEC10A, HK2, PFKFB3, Retnla, TLR3, TLR4, TLR5
TLR2	0.421		0.347	0.00231	CCL5, CXCL2, CXCL3, Cxcl9, CYBB, HLA-DQA1, HLA-DRB5, IFNB1, IL10, IRF1, Retnla, SLC40A1, TSPAN33
ITGB5	0.416			0.00234	IL10, MMP2, MMP9
TNFRSF1B	0.206			0.00234	ITGB5, MMP9, SRC
IRF9	0.405			0.00234	IFIT2, IFNB1, IL18
IL13	-1.62			0.00246	IL10, MRC1, Retnla, TFRC, TGFB1, TNFRSF11A
PLAU	-0.001		0.333	0.00252	CCR5, FCGR1A, HLA-DMA, MMP12, OAS1, OAS3, PLK3, Retnla, SLC2A1
MAPKAPK2	0.119		-1.746	0.00276	CXCL2, CXCL3, IFNB1, IL10, MRC1, MSR1, Retnla
CX3CR1	-1.329		0	0.00326	CD14, CD36, IGF1, MSR1, TGFB1
CDKN2A	1.78	Activated	2.309	0.00356	C3, CCL2, CCL24, CCL5, Ccl7, CXCL10, CXCL13, Cxcl9, IL1R2, IL2RG, TLR4, TNFRSF1B
NLRP3	0.049			0.00373	CXCL2, IL18, MRC1, MSR1
TAZ	0.2		0.632	0.004	CCL5, CD80, CXCL2, CXCL3, CXCR4, FN1, MRC1, PDE3B, ST6GAL1, THBS1
ACE	-1.193		-1	0.00581	CCL2, CCL24, CCL5, CEBPB, Retnla
TGFB1	-0.218	Inhibited	-2	0.00581	CD44, ITGAM, ITGAX, ITGB1, ITGB2
NFE2L2	0.484		-0.954	0.00631	CCL5, CXCL10, CXCL2, CXCL3, IFNB1, SCARB1
GATA6	-0.383		0.915	0.0069	ATP6V0A1, ATP6V0A2, ATP6V1C1, CD163, CLEC10A, CXCL13, IL10, LYVE1, MRC1, SORBS3, STARD13
ITGB2	0.212		0	0.00779	BCL2A1, CXCL10, CXCL2, CXCL3

CEBPE	-0.01		-1.214	0.00779	Ccl7, CD14, IL10, IL18
MAPK7	0.049	Activated	2	0.00779	CXCL10, Cxcl9, IFNB1, NOD1
PPP2CA	-0.135			0.00844	Cxcl9, IFNB1, IRF7
CCR3	-3.355			0.00844	CCL5, CCR2, CCR5
SMURF1	-0.192			0.00844	CXCL10, Cxcl9, IRF1
CLEC4E	-0.23			0.00844	CXCL2, CXCL3, IL10
PPARD	0.286		1.067	0.00935	C1QA, C1QB, C1QC, GAS6, MRC1, THBS1
TFEC	-1.605			0.0095	BBX, COL6A3, CSF3R, F13A1, IGF1R
TLR4	0.305		-0.114	0.0129	CCL5, CD200R1, CDK6, CXCL10, CXCL2, CXCL3, HLA-DQA1, IFNB1, IL10, IL18, IRF1, ITGAM, SCARB1, TSPAN33
TLR7	-0.171		-0.873	0.0133	BCL2A1, CXCL2, CXCL3, ETS2, IFNB1, IL10
RORA	-0.907	Inhibited	-2	0.0139	CXCL10, Cxcl9, IL18, TLR3
G6PC3	-0.009			0.0177	CYBA, CYBB
TARDBP	0.038			0.0177	C1QA, C1QB
WNT5A	-0.176			0.0177	CD14, IFNB1
STAT2	0.968			0.0177	CIITA, IRF1
IL2	1.707			0.0177	Ly6a (includes others), PECAM1
TREX1				0.0177	IFI44, USP18
IL6	-0.026			0.0177	CD36, IFNB1
TLR3	0.524		0.937	0.0183	CCL5, CXCL10, CXCL2, CXCL3, IFNB1, TSPAN33
MAVS	0.47			0.019	CCL5, CXCL10, IFNB1
MAPKAPK3	0.892	Inhibited	-2	0.0225	CXCL2, CXCL3, IFNB1, IL10
BACH1	-0.066		1	0.0225	CEBPB, IGF1, IL10, SLC40A1
NR1H2	0.076		0.092	0.0244	APOE, CCL5, Ccl7, CXCL10, ITGAL, MMP9
NFKB1	0.169		-0.294	0.0244	CSF2RA, CXCL3, IFNB1, IL10, Retnla, STAT1
CEBPB	0.919		0.777	0.0259	BLNK, CCND2, CIRBP, CXCL3, HSD17B4, IRF9, LYN, PRKCD, SERP1, SLC12A2, TMEM50B
CYBB	0.888		1	0.0336	CCL5, CXCL10, CXCL3, IFNB1
IRAK3	0.621		0	0.0336	BCL2A1, CCR2, CXCL2, ETS2
BCL2L11	-0.183			0.0343	CD274, CD36, NOD1
SPI1	-0.117			0.0343	ADGRE1, ITGAM, TLR4
IL1A	0.097			0.0343	Acp5, CA2, MMP9
IRAK4	-0.063		-0.651	0.0392	CXCL2, IDE, IFNB1, IL10, IRF7
ZFP36	0.089			0.0405	CXCL2, CXCL3, IFNB1, IL10, PNRC1, PRDM1
EPAS1	-1.03			0.0483	CCR2, CCR5
STAT4	0.1			0.0483	DDX58, IFNB1
TRIM3	-0.02			0.0483	IFIT1B, IFNB1
SYK	0.239			0.0483	CXCL10, Cxcl9
PTGS2	-0.122			0.0483	CXCL3, PIK3CG
TNFRSF1A	0.077			0.0483	ITGB5, SRC
RHOB	-0.061			0.0483	ITGB2, ITGB3

Appendix IV Upstream Regulator Analysis from IPA of DESeq2 analysis of Naïve Microglia

Appendix V

Ensembl Gene ID	External Gene Name	log_2 Fold Change	Adjusted P-Value
ENSMUSG00000022311	Csmd3	-5.73756	1e-314
ENSMUSG00000064339	mt-Rnr2	-0.95058	1e-314
ENSMUSG00000069045	Ddx3y	-14.3626	1e-314
ENSMUSG00000086503	Xist	11.37509	4.69E-305
ENSMUSG00000055435	Maf	-10.1058	6.65E-245
ENSMUSG00000069049	Eif2s3y	-13.469	8.92E-243
ENSMUSG00000056673	Kdm5d	-13.2663	8.92E-243
ENSMUSG00000026303	Mlph	-4.54769	2.52E-225
ENSMUSG00000068457	Uty	-13.0533	8.69E-207
ENSMUSG00000072720	Myo18b	-6.92072	2.15E-131
ENSMUSG00000020181	Nav3	-5.3512	1.18E-116
ENSMUSG00000027435	Cd93	-2.8625	5.06E-112
ENSMUSG00000031451	Gas6	-2.60216	2.22E-107
ENSMUSG00000024371	C2	3.034803	5.42E-107
ENSMUSG00000030787	Lyve1	-7.79074	5.24E-101
ENSMUSG00000069833	Ahnak	-2.17586	6.81E-101
ENSMUSG00000000318	Clec10a	-4.76457	1.08E-97
ENSMUSG00000020695	Mrc2	-2.57233	9.95E-91
ENSMUSG00000046245	Pilra	2.48564	1.19E-90
ENSMUSG00000049538	Adamts16	-3.53837	1.63E-88
ENSMUSG00000027200	Sema6d	-3.35103	2.13E-79
ENSMUSG00000028362	Tnfsf8	2.909422	3.38E-78
ENSMUSG00000022957	Itsn1	-1.86483	2.47E-76
ENSMUSG00000022150	Dab2	-3.22027	9.89E-72
ENSMUSG00000015852	Fcrls	-3.35633	3.94E-71
ENSMUSG00000039899	Fgl2	1.859491	3.94E-71
ENSMUSG00000025150	Cbr2	-4.8851	2.99E-70
ENSMUSG00000028214	Gem	-2.08774	2.71E-65
ENSMUSG00000022122	Ednrb	-4.44245	1.11E-64
ENSMUSG00000064351	mt-Co1	-1.03438	4.48E-62
ENSMUSG00000027358	Bmp2	-3.56202	1.09E-61
ENSMUSG00000062960	Kdr	2.073122	2.14E-61
ENSMUSG00000048126	Col6a3	-6.10633	7.78E-61
ENSMUSG00000030117	Gdf3	3.901679	1.70E-60
ENSMUSG00000015568	Lpl	-1.75224	1.76E-60
ENSMUSG00000000753	Serpinf1	-1.87434	6.03E-60
ENSMUSG00000055413	H2-Q5	1.915576	6.03E-60
ENSMUSG00000024529	Lox	1.88288	4.34E-59
ENSMUSG00000073599	Ecscr	-2.55418	5.88E-58
ENSMUSG00000053062	Jam2	-1.60576	3.98E-57
ENSMUSG00000040950	Mgl2	-2.21788	2.63E-55

ENSMUSG00000023078	Cxcl13	4.095953	3.05E-55
ENSMUSG00000047798	Cd300lf	3.28067	1.15E-54
ENSMUSG00000026271	Gpr35	1.75043	1.40E-54
ENSMUSG00000033278	Ptprm	-1.78559	2.92E-54
ENSMUSG00000074305	Peak1	-1.5319	1.44E-53
ENSMUSG00000032661	Oas3	2.538636	1.95E-53
ENSMUSG00000079298	Klrb1b	3.741895	3.09E-52
ENSMUSG00000074896	Ifit3	2.440317	7.48E-52
ENSMUSG00000027962	Vcam1	2.034841	6.35E-50
ENSMUSG00000027799	Nbea	-1.57264	1.32E-49
ENSMUSG00000008845	Cd163	-2.82462	1.65E-49
ENSMUSG00000021719	Rgs7bp	-3.10005	1.24E-48
ENSMUSG00000060550	H2-Q7	2.402278	7.22E-48
ENSMUSG00000043263	Ifi209	1.858784	8.46E-48
ENSMUSG00000040037	Negr1	3.887799	1.86E-47
ENSMUSG00000042286	Stab1	-2.51933	4.19E-47
ENSMUSG00000029084	Cd38	-4.03766	2.56E-46
ENSMUSG00000049436	Upk1b	-2.69037	5.51E-46
ENSMUSG00000029373	Pf4	-2.07686	5.06E-45
ENSMUSG00000036381	P2ry14	3.598048	5.06E-45
ENSMUSG00000052911	Lamb2	-1.78272	1.94E-44
ENSMUSG00000069515	Lyz1	2.557478	2.11E-44
ENSMUSG00000059089	Fcgr4	2.01384	1.15E-43
ENSMUSG00000028195	Ccn1	-1.95556	2.28E-43
ENSMUSG00000042834	Nrep	-2.67875	7.39E-43
ENSMUSG00000027580	Helz2	1.956714	1.54E-42
ENSMUSG00000031012	Cask	-1.507	2.13E-42
ENSMUSG00000074743	Thbd	-2.59973	2.28E-42
ENSMUSG00000032609	Klhdc8b	-1.60381	2.55E-42
ENSMUSG00000045932	Ifit2	2.483066	1.18E-41
ENSMUSG00000024044	Epb41l3	1.374355	2.92E-41
ENSMUSG00000041827	Oasl1	3.410965	1.51E-40
ENSMUSG00000026712	Mrc1	-2.55019	1.83E-40
ENSMUSG00000062488	Ifit3b	2.214979	2.09E-40
ENSMUSG00000023913	Pla2g7	-2.08494	2.76E-39
ENSMUSG00000030156	Cd69	2.01463	5.39E-39
ENSMUSG00000052336	Cx3cr1	-1.32843	5.73E-39
ENSMUSG00000073489	Ifi204	1.540126	1.51E-38
ENSMUSG00000048895	Cdk5r1	-1.45152	1.77E-38
ENSMUSG00000079491	H2-T10	2.683036	2.15E-38
ENSMUSG00000032717	Mdfi	-3.54388	3.07E-38
ENSMUSG00000031216	Stard8	-1.34409	3.69E-38
ENSMUSG00000030539	Sema4b	-1.62756	1.88E-37
ENSMUSG00000019256	Ahr	-2.70796	8.83E-37
ENSMUSG00000009418	Nav1	-1.60389	2.25E-36
ENSMUSG00000031327	Chic1	3.292775	5.40E-36

ENSMUSG00000034459	Ifit1	2.257824	5.59E-36
ENSMUSG00000030577	Cd22	1.769405	1.60E-35
ENSMUSG00000073491	Ifi213	1.9204	2.44E-35
ENSMUSG00000046876	Atxn1	-2.16951	3.05E-35
ENSMUSG00000035493	Tgfbi	-1.18313	5.98E-35
ENSMUSG00000111118	Gm6545	2.897402	6.53E-35
ENSMUSG00000018459	Slc13a3	1.394345	1.30E-34
ENSMUSG00000022265	Ank	-1.27997	1.71E-34
ENSMUSG00000075014	Gm10800	-2.4268	2.55E-34
ENSMUSG00000045092	S1pr1	-1.43281	7.31E-34
ENSMUSG00000049744	Arhgap15	1.866937	1.32E-33
ENSMUSG00000022994	Adcy6	-2.81782	5.85E-33
ENSMUSG00000039959	Hip1	-1.47197	1.11E-32
ENSMUSG00000028080	Lrba	-1.20357	5.67E-32
ENSMUSG00000035914	Cd276	-1.94255	8.98E-32
ENSMUSG00000011256	Adam19	-2.76844	1.14E-31
ENSMUSG00000049134	Nrap	-4.94709	2.02E-31
ENSMUSG00000024042	Sik1	1.293791	2.07E-31
ENSMUSG00000030107	Usp18	2.009282	2.90E-31
ENSMUSG00000072966	Gprasp2	-2.63719	3.51E-31
ENSMUSG00000074570	Cass4	-1.77993	1.69E-30
ENSMUSG00000074151	Nlrc5	1.73208	2.22E-30
ENSMUSG00000097899	Gm16894	2.415602	1.00E-29
ENSMUSG00000073409	H2-Q6	2.930155	1.89E-29
ENSMUSG00000022332	Khdrbs3	-5.71345	2.82E-29
ENSMUSG00000027514	Zbp1	2.156645	5.13E-29
ENSMUSG00000025498	Irf7	1.850281	7.09E-29
ENSMUSG00000028037	Ifi44	2.890075	2.03E-28
ENSMUSG00000029163	Emilin1	1.737768	2.09E-28
ENSMUSG00000050530	Fam171a1	-3.9327	2.91E-28
ENSMUSG00000038775	Vill	2.198019	4.23E-28
ENSMUSG00000085337	Gm15964	1.774235	6.13E-28
ENSMUSG00000102975	Gm37347	1.791094	1.17E-27
ENSMUSG00000033083	Tbc1d4	-1.71831	1.76E-27
ENSMUSG00000045502	Hcar2	1.587916	2.72E-27
ENSMUSG00000021338	Carmil1	1.447242	3.63E-27
ENSMUSG00000035042	Ccl5	3.271047	4.53E-27
ENSMUSG00000031425	Plp1	-2.42586	5.81E-27
ENSMUSG00000022537	Tmem44	-1.97902	6.24E-27
ENSMUSG00000032640	Chsy1	-1.05561	4.62E-26
ENSMUSG00000032517	Mobp	-2.78043	9.00E-26
ENSMUSG00000021676	Iqgap2	-2.36196	9.09E-26
ENSMUSG00000024675	Ms4a4c	1.571241	1.50E-25
ENSMUSG00000031494	Cd209a	-4.87018	5.76E-25
ENSMUSG00000039109	F13a1	-1.59377	7.08E-25
ENSMUSG00000026104	Stat1	1.178369	9.31E-25

ENSMUSG00000052609	Plekhg3	-2.18737	3.07E-24
ENSMUSG00000009376	Met	2.24451	3.92E-24
ENSMUSG00000030865	Chp2	-6.598	5.10E-24
ENSMUSG00000041058	Wwp1	-1.09076	2.20E-23
ENSMUSG00000016206	H2-M3	1.093423	4.26E-23
ENSMUSG00000020541	Tom1l1	-1.67845	5.27E-23
ENSMUSG00000027784	Ppm1l	-1.3425	5.36E-23
ENSMUSG00000040964	Arhgef10l	-1.18612	9.78E-23
ENSMUSG00000079363	Gbp4	2.205644	1.76E-22
ENSMUSG00000020689	Itgb3	-1.10316	1.78E-22
ENSMUSG00000056313	Tcim	1.170313	1.81E-22
ENSMUSG00000002799	Jag2	-1.57524	2.56E-22
ENSMUSG00000004891	Nes	-1.56329	2.58E-22
ENSMUSG00000000957	Mmp14	1.008691	2.84E-22
ENSMUSG00000040564	Apoc1	2.263516	8.04E-22
ENSMUSG00000058427	Cxcl2	-1.36689	1.17E-21
ENSMUSG00000029814	Igf2bp3	1.622106	1.90E-21
ENSMUSG00000029401	Rilpl2	1.188469	1.98E-21
ENSMUSG00000079164	Tlr5	-1.66675	2.92E-21
ENSMUSG00000032193	Ldlr	-1.4791	3.12E-21
ENSMUSG00000026896	Ifih1	1.025245	3.13E-21
ENSMUSG00000029177	Cenpa	-1.66011	3.23E-21
ENSMUSG00000034413	Neurl1b	1.841937	3.23E-21
ENSMUSG00000021806	Nid2	-1.65088	4.19E-21
ENSMUSG00000035164	Zc3h12c	1.091582	5.87E-21
ENSMUSG00000020400	Tnip1	1.126297	5.87E-21
ENSMUSG00000064337	mt-Rnr1	-1.0661	7.07E-21
ENSMUSG00000004317	Clcn5	-0.93508	8.71E-21
ENSMUSG00000027646	Src	0.947898	1.09E-20
ENSMUSG00000030747	Dgat2	1.697547	1.77E-20
ENSMUSG00000002602	Axl	1.594627	1.86E-20
ENSMUSG00000018819	Lsp1	0.996168	2.60E-20
ENSMUSG00000000682	Cd52	0.964112	3.66E-20
ENSMUSG00000039529	Atp8b1	-2.82181	5.96E-20
ENSMUSG00000017390	Aldoc	-2.04074	1.38E-19
ENSMUSG00000031995	St14	1.327957	1.57E-19
ENSMUSG00000022353	Mtss1	-0.94715	1.80E-19
ENSMUSG00000035929	H2-Q4	1.049135	2.13E-19
ENSMUSG00000104713	Gbp6	2.509383	2.18E-19
ENSMUSG00000068245	Phf11d	1.170691	2.19E-19
ENSMUSG00000020641	Rsad2	1.789954	2.64E-19
ENSMUSG00000039304	Tnfsf10	1.568263	3.19E-19
ENSMUSG00000025492	Ifitm3	1.032253	3.26E-19
ENSMUSG00000063611	Gm10134	-1.24305	3.54E-19
ENSMUSG00000039954	Stk32a	6.103265	3.58E-19
ENSMUSG00000091649	Phf11b	1.517812	3.61E-19

ENSMUSG00000024164	C3	1.449621	4.24E-19
ENSMUSG00000073555	Gm4951	1.499531	4.98E-19
ENSMUSG00000006800	Sulf2	-1.20138	6.70E-19
ENSMUSG00000053318	Slamf8	1.084043	7.90E-19
ENSMUSG00000020053	Igf1	-1.43989	8.01E-19
ENSMUSG00000017754	Pltp	-1.85451	8.31E-19
ENSMUSG00000054072	Iigp1	1.629422	1.08E-18
ENSMUSG00000028270	Gbp2	1.418724	1.11E-18
ENSMUSG00000086109	Gm13391	1.547031	1.35E-18
ENSMUSG00000023349	Clec4n	-3.5511	1.94E-18
ENSMUSG00000037347	Chst7	-0.99793	2.06E-18
ENSMUSG00000000386	Mx1	1.652562	2.70E-18
ENSMUSG00000004707	Ly9	1.552921	2.95E-18
ENSMUSG00000017009	Sdc4	-1.37311	3.39E-18
ENSMUSG00000101389	Ms4a4a	-3.33562	3.66E-18
ENSMUSG00000037999	Arap2	-3.28756	3.80E-18
ENSMUSG00000039497	Dse	-0.86898	4.44E-18
ENSMUSG00000000673	Haao	1.246215	4.57E-18
ENSMUSG00000021411	Pxdc1	1.078015	5.15E-18
ENSMUSG00000005087	Cd44	1.266023	5.95E-18
ENSMUSG00000031990	Jam3	-3.00282	8.48E-18
ENSMUSG00000050022	Amz1	0.855436	1.01E-17
ENSMUSG00000028459	Cd72	1.108039	1.25E-17
ENSMUSG00000023961	Enpp4	1.062228	1.54E-17
ENSMUSG00000040829	Zmynd15	1.259638	1.56E-17
ENSMUSG00000056116	H2-T22	1.052941	1.73E-17
ENSMUSG00000029561	Oasl2	1.446882	1.81E-17
ENSMUSG00000015766	Eps8	-1.22272	3.45E-17
ENSMUSG00000020900	Myh10	-1.26282	5.28E-17
ENSMUSG00000038390	Gpr162	1.284884	5.36E-17
ENSMUSG00000012017	Scarf2	1.204721	5.36E-17
ENSMUSG00000099809	Gm18665	-8.90777	6.24E-17
ENSMUSG00000037849	Ifi206	1.529894	7.89E-17
ENSMUSG00000048612	Myof	-1.36587	8.37E-17
ENSMUSG00000003418	St8sia6	1.385634	8.53E-17
ENSMUSG00000030830	Itgal	1.404082	9.34E-17
ENSMUSG00000020021	Fgd6	-1.5835	9.46E-17
ENSMUSG00000073411	H2-D1	1.163011	1.13E-16
ENSMUSG00000027860	Vangl1	-3.85204	1.15E-16
ENSMUSG00000059810	Rgs3	-1.24295	1.57E-16
ENSMUSG00000026222	Sp100	1.133288	2.33E-16
ENSMUSG00000052776	Oas1a	1.347723	2.36E-16
ENSMUSG00000097039	Pvt1	1.20712	2.69E-16
ENSMUSG00000065987	Cd209b	-6.59812	2.80E-16
ENSMUSG00000032577	Mapkapk3	0.892617	2.96E-16
ENSMUSG00000112023	Lilr4b	-0.91601	2.98E-16

ENSMUSG00000020638	Cmpk2	1.5606	2.98E-16
ENSMUSG00000002233	Rhoc	-1.22683	3.04E-16
ENSMUSG00000043740	B430306N03Rik	1.290723	3.75E-16
ENSMUSG00000033721	Vav3	-1.99902	4.00E-16
ENSMUSG00000047945	Marcksl1	-0.9393	4.00E-16
ENSMUSG00000025151	Maged1	-0.86669	4.30E-16
ENSMUSG00000031210	Gpr165	-1.67902	4.60E-16
ENSMUSG00000090386	Mir99ahg	-1.03135	4.63E-16
ENSMUSG00000057914	Cacnb2	1.217995	7.00E-16
ENSMUSG00000040276	Pacsin1	-2.34054	7.53E-16
ENSMUSG00000032690	Oas2	1.793367	7.67E-16
ENSMUSG00000004558	Ndrg2	-2.07315	8.64E-16
ENSMUSG00000025887	Casp12	1.974854	1.13E-15
ENSMUSG00000043671	Dpy19l3	-2.01729	1.20E-15
ENSMUSG00000026193	Fn1	-1.84042	1.60E-15
ENSMUSG00000068220	Lgals1	-2.85874	1.63E-15
ENSMUSG00000072235	Tuba1a	-1.06098	1.97E-15
ENSMUSG00000033066	Gas7	-1.07424	2.23E-15
ENSMUSG00000079017	Ifi27l2a	1.161923	4.52E-15
ENSMUSG00000024640	Psat1	-1.46473	5.43E-15
ENSMUSG00000041607	Mbp	-0.87119	5.83E-15
ENSMUSG00000024168	Tmem204	-1.6539	6.45E-15
ENSMUSG00000025044	Msr1	-1.00422	6.45E-15
ENSMUSG00000064370	mt-Cytb	-1.11281	8.10E-15
ENSMUSG00000022102	Dok2	-1.99667	8.24E-15
ENSMUSG00000016756	Cmah	-1.46388	9.46E-15
ENSMUSG00000033350	Chst2	1.099365	1.05E-14
ENSMUSG00000041849	Card6	0.889178	1.09E-14
ENSMUSG00000009292	Trpm2	1.386653	1.35E-14
ENSMUSG00000021880	Rnase6	1.302155	1.35E-14
ENSMUSG00000060402	Chst8	-4.75021	1.46E-14
ENSMUSG00000017830	Dhx58	1.110312	1.80E-14
ENSMUSG00000029094	Afap1	-1.80395	2.02E-14
ENSMUSG00000023274	Cd4	-3.46554	2.05E-14
ENSMUSG00000015843	Rxrg	3.763728	2.72E-14
ENSMUSG00000061232	H2-K1	1.115782	2.95E-14
ENSMUSG00000037661	Gpr160	0.810661	3.02E-14
ENSMUSG00000022098	Bmp1	-2.25986	3.28E-14
ENSMUSG00000019866	Crybg1	1.436921	4.04E-14
ENSMUSG00000040522	Tlr8	-1.52233	4.57E-14
ENSMUSG00000005958	Ephb3	-1.61353	4.57E-14
ENSMUSG00000025324	Atp10a	1.901412	4.58E-14
ENSMUSG00000031138	F9	-1.42821	4.58E-14
ENSMUSG00000006344	Ggt5	-0.92247	4.73E-14
ENSMUSG00000006611	Hfe	-0.73394	5.23E-14
ENSMUSG00000025203	Scd2	-0.89475	5.41E-14

ENSMUSG00000034656	Cacna1a	-1.3252	5.69E-14
ENSMUSG00000047867	Gimap6	-1.01732	6.04E-14
ENSMUSG00000039763	Dnajc28	0.953498	6.41E-14
ENSMUSG00000034438	Gbp8	2.766907	6.83E-14
ENSMUSG00000040033	Stat2	0.968687	6.90E-14
ENSMUSG00000003882	Il7r	-0.87803	8.07E-14
ENSMUSG00000026442	Nfasc	-2.30346	1.09E-13
ENSMUSG00000034353	Ramp1	-1.25355	1.15E-13
ENSMUSG00000075602	Ly6a	1.561575	1.33E-13
ENSMUSG00000032340	Neo1	-1.93448	1.41E-13
ENSMUSG00000079056	Kcnip3	0.890018	2.90E-13
ENSMUSG00000013033	Adgrl1	-1.68921	3.17E-13
ENSMUSG00000066861	Oas1g	1.621994	3.27E-13
ENSMUSG00000060227	Golm2	-2.54797	3.88E-13
ENSMUSG00000040296	Ddx58	0.927442	5.24E-13
ENSMUSG00000087006	Gm13889	-1.27948	6.11E-13
ENSMUSG00000040274	Cdk6	-0.8761	6.54E-13
ENSMUSG00000027803	Wwtr1	1.659166	7.35E-13
ENSMUSG00000030701	Plekhb1	-1.88865	8.22E-13
ENSMUSG00000024014	Pim1	-0.71556	1.07E-12
ENSMUSG00000042770	Hebp1	0.935641	1.10E-12
ENSMUSG00000015314	Slamf6	0.946043	1.51E-12
ENSMUSG00000114761	Gm47242	3.500287	2.05E-12
ENSMUSG00000089828	Gm16300	-8.3885	2.11E-12
ENSMUSG00000004814	Ccl24	-2.28618	2.14E-12
ENSMUSG00000050138	Kcnk12	-1.0975	2.16E-12
ENSMUSG00000017607	Tns4	1.237248	2.19E-12
ENSMUSG00000078349	AW011738	1.229096	2.35E-12
ENSMUSG00000096727	Psmb9	0.857804	2.36E-12
ENSMUSG00000022425	Enpp2	-1.31589	3.42E-12
ENSMUSG00000035373	Ccl7	-2.12254	3.58E-12
ENSMUSG00000038642	Ctss	0.671906	3.58E-12
ENSMUSG00000052920	Prkg1	-1.94137	3.89E-12
ENSMUSG00000045136	Tubb2b	-1.12287	3.89E-12
ENSMUSG00000075225	Ccdc162	-2.89721	4.30E-12
ENSMUSG00000022014	Epsti1	0.75923	5.10E-12
ENSMUSG00000025555	Farp1	-1.865	5.42E-12
ENSMUSG00000019467	Arhgef25	-2.829	5.68E-12
ENSMUSG00000038679	Trps1	0.845822	6.35E-12
ENSMUSG00000058254	Tspan7	-0.68638	6.46E-12
ENSMUSG00000062661	Ncs1	-1.46008	6.68E-12
ENSMUSG00000001300	Efnb2	-2.22412	6.71E-12
ENSMUSG00000026829	Gbgt1	-1.2619	7.20E-12
ENSMUSG00000019843	Fyn	-1.01489	8.69E-12
ENSMUSG00000025795	Rassf3	0.716225	9.23E-12
ENSMUSG00000039193	Nlrc4	-1.90813	9.24E-12

ENSMUSG00000030123	Plxnd1	-1.35153	9.54E-12
ENSMUSG00000057135	Scimp	1.474991	1.06E-11
ENSMUSG00000029096	Htra3	-1.91929	1.06E-11
ENSMUSG00000030589	Rasgrp4	-1.31563	1.17E-11
ENSMUSG00000020122	Egfr	-3.34487	1.29E-11
ENSMUSG00000102717	Gm37759	1.825619	1.36E-11
ENSMUSG00000066800	Rnasel	-0.7459	1.41E-11
ENSMUSG00000000244	Tspan32	1.005915	1.44E-11
ENSMUSG00000074505	Fat3	-1.16005	1.48E-11
ENSMUSG00000102748	Pcdhgb2	-1.1052	1.83E-11
ENSMUSG00000022906	Parp9	0.679331	2.16E-11
ENSMUSG00000020424	Castor1	1.016009	2.36E-11
ENSMUSG00000024672	Ms4a7	-1.08565	2.48E-11
ENSMUSG00000031749	St3gal2	-0.66224	2.68E-11
ENSMUSG00000061577	Adgrg5	3.271667	3.47E-11
ENSMUSG00000054676	1600014C10Rik	0.748053	4.29E-11
ENSMUSG00000032860	P2ry2	2.272703	4.66E-11
ENSMUSG00000038305	Spats2l	-3.30423	4.84E-11
ENSMUSG00000035352	Ccl12	1.025975	4.99E-11
ENSMUSG00000049313	Sorl1	1.1837	5.75E-11
ENSMUSG00000007097	Atp1a2	-1.29767	6.11E-11
ENSMUSG00000069601	Ank3	-2.7738	6.12E-11
ENSMUSG00000021684	Pde8b	1.019729	6.27E-11
ENSMUSG00000016552	Foxred2	-1.97149	6.45E-11
ENSMUSG00000041439	Mfsd6	-2.54107	7.13E-11
ENSMUSG00000051043	Gprc5c	-2.98712	7.71E-11
ENSMUSG00000006360	Crip1	-1.55214	7.83E-11
ENSMUSG00000055809	Dnaaf3	1.122055	8.24E-11
ENSMUSG00000031137	Fgf13	-1.22609	8.47E-11
ENSMUSG00000037922	Bank1	-0.97826	8.91E-11
ENSMUSG00000071537	Klrg2	1.495768	9.18E-11
ENSMUSG00000026073	Il1r2	1.349063	9.37E-11
ENSMUSG00000026315	Serpinb8	-1.6371	1.15E-10
ENSMUSG00000036353	P2ry12	-0.89975	1.16E-10
ENSMUSG00000030878	Cdr2	-1.96658	1.19E-10
ENSMUSG00000043943	Naalad2	1.131756	1.24E-10
ENSMUSG00000082088	Gm15753	1.916951	1.34E-10
ENSMUSG00000046879	Irgm1	0.903242	1.45E-10
ENSMUSG00000052688	Rab7b	-1.05357	1.52E-10
ENSMUSG00000052560	Cpne8	-6.09326	1.53E-10
ENSMUSG00000031849	Comp	1.479977	1.63E-10
ENSMUSG00000032322	Pstpip1	1.039212	1.65E-10
ENSMUSG00000007207	Stx1a	-1.92824	1.67E-10
ENSMUSG00000019889	Ptprk	-3.64284	1.69E-10
ENSMUSG00000037369	Kdm6a	0.662603	1.71E-10
ENSMUSG00000063268	Parp10	0.718261	1.79E-10

ENSMUSG00000032306	Mpi	-0.85587	1.89E-10
ENSMUSG00000079138	Gm8818	-3.82369	2.04E-10
ENSMUSG00000106807	Gm10441	-4.79941	2.05E-10
ENSMUSG00000044708	Kcnj10	1.045242	2.06E-10
ENSMUSG00000085761	4930455G09Rik	3.325828	2.08E-10
ENSMUSG00000037921	Ddx60	0.810671	2.35E-10
ENSMUSG00000079339	Ifit1bl1	2.811192	2.38E-10
ENSMUSG00000029798	Herc6	0.902005	2.46E-10
ENSMUSG00000027457	Snph	-1.3086	2.49E-10
ENSMUSG00000066191	Anks6	-0.85665	2.56E-10
ENSMUSG00000029298	Gbp9	0.719789	2.60E-10
ENSMUSG00000085084	4930570G19Rik	4.184871	2.84E-10
ENSMUSG00000030465	Psd3	-1.00288	3.33E-10
ENSMUSG00000040855	Reps2	-1.37134	4.07E-10
ENSMUSG00000064341	mt-Nd1	-1.23095	4.07E-10
ENSMUSG00000063382	Bcl9l	-0.66516	4.38E-10
ENSMUSG00000049791	Fzd4	-0.81144	4.62E-10
ENSMUSG00000021708	Rasgrf2	1.161895	5.62E-10
ENSMUSG00000039853	Trim14	0.720699	5.62E-10
ENSMUSG00000102289	Gm31258	-2.03243	5.79E-10
ENSMUSG00000032648	Pygm	-2.59302	5.91E-10
ENSMUSG00000033306	Lpp	-0.79676	5.98E-10
ENSMUSG00000059479	B3gnt8	1.214814	6.23E-10
ENSMUSG00000069919	Hba-a1	-2.65097	6.96E-10
ENSMUSG00000035448	Ccr3	-3.32734	7.02E-10
ENSMUSG00000024180	Pgap6	-1.66954	7.78E-10
ENSMUSG00000024334	H2-Oa	1.124176	8.34E-10
ENSMUSG00000026536	Ifi211	1.358015	8.75E-10
ENSMUSG00000114996	Gm48958	-4.20198	8.95E-10
ENSMUSG00000082292	Gm12250	1.213465	9.04E-10
ENSMUSG00000064372	mt-Tp	-1.3504	9.78E-10
ENSMUSG00000017737	Mmp9	-1.17362	9.83E-10
ENSMUSG00000016239	Lonrf3	-0.84728	1.01E-09
ENSMUSG00000049502	Dtx3l	0.646857	1.02E-09
ENSMUSG00000040229	Gpr34	-1.01042	1.09E-09
ENSMUSG00000039208	Metrnl	-1.04498	1.18E-09
ENSMUSG00000024079	Eif2ak2	0.671894	1.20E-09
ENSMUSG00000063889	Crem	-1.10995	1.29E-09
ENSMUSG00000100060	Gm17944	2.562841	1.31E-09
ENSMUSG00000104108	Gm37876	-3.05741	1.32E-09
ENSMUSG00000058145	Adamts17	-3.57203	1.35E-09
ENSMUSG00000027959	Sass6	0.936328	1.37E-09
ENSMUSG00000060935	Tmem263	-1.63928	1.37E-09
ENSMUSG00000047747	Rnf150	0.976463	1.40E-09
ENSMUSG00000105771	2900064K03Rik	3.969568	1.54E-09
ENSMUSG00000030789	Itgax	1.191447	1.57E-09

ENSMUSG00000063455	D630045J12Rik	-2.38962	1.70E-09
ENSMUSG00000071068	Treml2	1.225726	1.77E-09
ENSMUSG00000092591	Gm20429	5.032441	1.95E-09
ENSMUSG00000063804	Lin28b	-4.00131	1.98E-09
ENSMUSG00000023191	P3h3	0.691774	2.05E-09
ENSMUSG00000015143	Actn1	-1.05786	2.22E-09
ENSMUSG00000016496	Cd274	0.799391	2.33E-09
ENSMUSG00000022010	Tsc22d1	-0.74672	2.41E-09
ENSMUSG00000020282	Rhbdf1	-0.93372	2.52E-09
ENSMUSG00000042589	Cux2	-2.19252	2.55E-09
ENSMUSG00000029822	Osbpl3	0.95452	2.55E-09
ENSMUSG00000052062	Pard3b	-1.13614	2.55E-09
ENSMUSG00000018217	Pmp22	-1.07489	2.80E-09
ENSMUSG00000031342	Gpm6b	-1.33575	3.07E-09
ENSMUSG00000030525	Chrna7	3.729465	3.19E-09
ENSMUSG00000101059	Gm4017	-8.32524	3.25E-09
ENSMUSG00000069793	Slfn9	1.176039	3.62E-09
ENSMUSG00000035311	Gnptab	0.654391	3.70E-09
ENSMUSG00000092277	Gm19684	5.08928	3.85E-09
ENSMUSG00000052942	Glis3	-3.02564	3.90E-09
ENSMUSG00000005107	Slc2a9	0.955715	3.92E-09
ENSMUSG00000049103	Ccr2	-1.32695	4.09E-09
ENSMUSG00000026921	Egfl7	-1.84072	4.20E-09
ENSMUSG00000021838	Samd4	-2.19549	4.45E-09
ENSMUSG00000050965	Prkca	-0.63534	4.80E-09
ENSMUSG00000052387	Trpm3	-2.10765	4.87E-09
ENSMUSG00000068606	Gm4841	2.072997	4.87E-09
ENSMUSG00000043391	2510009E07Rik	-0.68932	5.04E-09
ENSMUSG00000023328	Ache	-0.98456	5.06E-09
ENSMUSG00000035692	Isg15	1.716959	5.45E-09
ENSMUSG00000070501	Ifi214	2.522394	5.86E-09
ENSMUSG00000030283	St8sia1	1.815123	6.81E-09
ENSMUSG00000027692	Tnik	1.737408	7.30E-09
ENSMUSG00000056144	Trim34a	0.857331	7.93E-09
ENSMUSG00000042529	Kcnj12	-7.91165	7.97E-09
ENSMUSG00000078920	Ifi47	1.2619	8.30E-09
ENSMUSG00000054404	Slfn5	0.870997	8.32E-09
ENSMUSG00000030536	Iqgap1	-0.70961	8.70E-09
ENSMUSG00000005611	Irag1	-2.97876	8.84E-09
ENSMUSG00000022799	Arhgap31	-0.8287	8.87E-09
ENSMUSG00000100183	Gm28512	-2.44155	9.12E-09
ENSMUSG00000034855	Cxcl10	1.167581	9.69E-09
ENSMUSG00000090387	Gm17056	-1.04532	1.00E-08
ENSMUSG00000023206	Il15ra	1.015955	1.10E-08
ENSMUSG00000064367	mt-Nd5	-1.16702	1.10E-08
ENSMUSG00000035681	Kcnc2	-4.94033	1.13E-08

ENSMUSG00000038034	Igsf8	0.710177	1.14E-08
ENSMUSG00000097352	C920009B18Rik	1.285865	1.15E-08
ENSMUSG00000041202	Pla2g2d	-1.02895	1.16E-08
ENSMUSG00000002957	Ap2a2	-0.59547	1.19E-08
ENSMUSG00000033542	Arhgef5	-2.61647	1.27E-08
ENSMUSG00000023341	Mx2	1.074339	1.33E-08
ENSMUSG00000030930	Chst15	0.671489	1.41E-08
ENSMUSG00000029869	Ephb6	-4.29232	1.41E-08
ENSMUSG00000039943	Plcb4	-2.3976	1.51E-08
ENSMUSG00000091472	Gm3739	-1.41567	1.52E-08
ENSMUSG00000034993	Vat1	-0.86316	1.56E-08
ENSMUSG00000038352	Arl5c	0.874857	1.57E-08
ENSMUSG00000096351	Samd11	-2.57861	1.58E-08
ENSMUSG00000038156	Spon1	1.924579	1.58E-08
ENSMUSG00000037225	Fgf2	-1.21442	1.59E-08
ENSMUSG00000021362	Gcm2	4.037158	1.80E-08
ENSMUSG00000031217	Efnb1	-0.98649	1.83E-08
ENSMUSG00000043822	Adamtsl5	-7.89844	1.84E-08
ENSMUSG00000032194	Kank2	-1.08338	1.99E-08
ENSMUSG00000043456	Zfp536	-1.39766	1.99E-08
ENSMUSG00000073940	Hbb-bt	-2.69555	2.14E-08
ENSMUSG00000097654	Gm26714	0.981511	2.15E-08
ENSMUSG00000033880	Lgals3bp	1.346284	2.26E-08
ENSMUSG00000094796	BC147527	1.138376	2.38E-08
ENSMUSG00000033717	Adra2a	-2.32582	2.44E-08
ENSMUSG00000016529	Il10	-3.17713	2.57E-08
ENSMUSG00000036206	Sh3bp4	1.19705	2.61E-08
ENSMUSG00000022091	Sorbs3	-1.44464	2.61E-08
ENSMUSG00000028073	Pear1	-1.21622	2.61E-08
ENSMUSG00000058626	Capn11	-4.59348	2.63E-08
ENSMUSG00000054008	Ndst1	0.596507	2.78E-08
ENSMUSG00000070327	Rnf213	1.021627	2.81E-08
ENSMUSG00000035666	Gtf3c4	-0.57185	2.87E-08
ENSMUSG00000036334	Igsf10	-1.31824	2.91E-08
ENSMUSG00000044037	Als2cl	0.942602	2.94E-08
ENSMUSG00000028517	Plpp3	-2.35455	2.96E-08
ENSMUSG00000115338	Pnp	-0.63771	2.98E-08
ENSMUSG00000055675	Kbtbd11	-1.39744	3.15E-08
ENSMUSG00000027276	Jag1	-1.21668	3.26E-08
ENSMUSG00000046204	Pnma2	-3.06265	3.36E-08
ENSMUSG00000038648	Creb3l2	-0.56752	3.37E-08
ENSMUSG00000027698	Nceh1	0.612604	3.45E-08
ENSMUSG00000048806	Ifnb1	4.100578	3.47E-08
ENSMUSG00000034751	Mast4	-0.87676	3.50E-08
ENSMUSG00000029592	Usp30	0.710742	3.70E-08
ENSMUSG00000097705	Gm26740	0.976282	4.09E-08

ENSMUSG00000028986	Klhl7	-0.63199	4.23E-08
ENSMUSG00000027223	Mapk8ip1	-1.71607	4.33E-08
ENSMUSG00000053559	Smagp	-1.02816	4.37E-08
ENSMUSG00000034412	Tbc1d10a	0.708204	4.47E-08
ENSMUSG00000025270	Alas2	-2.47703	4.48E-08
ENSMUSG00000090231	Cfb	3.082678	4.48E-08
ENSMUSG00000104213	Ighd	-1.51447	4.48E-08
ENSMUSG00000051586	Mical3	-0.72869	4.53E-08
ENSMUSG00000026213	Stk11ip	0.555188	4.68E-08
ENSMUSG00000029816	Gpnmb	1.686376	4.92E-08
ENSMUSG00000051790	Nlgn2	-1.32551	4.92E-08
ENSMUSG00000118123	Gm50346	1.044368	5.15E-08
ENSMUSG00000038507	Parp12	0.812451	5.18E-08
ENSMUSG00000024521	Pmaip1	0.579651	5.74E-08
ENSMUSG00000071226	Cecr2	-2.37136	5.74E-08
ENSMUSG00000032725	Folr2	-3.73317	5.97E-08
ENSMUSG00000029605	Oas1b	1.379999	6.11E-08
ENSMUSG00000026317	Cln8	-0.56069	6.66E-08
ENSMUSG00000020572	Nampt	0.61661	6.66E-08
ENSMUSG00000030352	Tspan9	-1.08391	7.19E-08
ENSMUSG00000061808	Ttr	-1.02427	7.39E-08
ENSMUSG00000028565	Nfia	-0.61043	7.77E-08
ENSMUSG00000024769	Cdc42bpg	-1.8233	8.00E-08
ENSMUSG00000026986	Hnmt	-0.96986	8.51E-08
ENSMUSG00000030657	Xylt1	-0.83816	8.53E-08
ENSMUSG00000034926	Dhcr24	-2.45778	8.72E-08
ENSMUSG00000023019	Gpd1	-1.40583	8.97E-08
ENSMUSG00000036949	Slc39a12	-3.63694	9.35E-08
ENSMUSG00000042826	Fgf11	-1.23887	1.00E-07
ENSMUSG00000060183	Cxcl11	4.217891	1.03E-07
ENSMUSG00000085133	B930095G15Rik	-2.87665	1.04E-07
ENSMUSG00000026535	Ifi202b	-4.53985	1.17E-07
ENSMUSG00000028771	Ptpn12	-0.84418	1.18E-07
ENSMUSG00000022376	Adcy8	-4.92444	1.20E-07
ENSMUSG00000030345	Dyrk4	0.944714	1.22E-07
ENSMUSG00000056215	Lrguk	1.063401	1.23E-07
ENSMUSG00000058013	Septin11	-0.79676	1.26E-07
ENSMUSG00000042249	Grk3	0.807452	1.27E-07
ENSMUSG00000028967	Errfi1	-0.59751	1.28E-07
ENSMUSG00000025207	Sema4g	-0.55896	1.30E-07
ENSMUSG00000034906	Ncaph	-1.42938	1.51E-07
ENSMUSG00000021281	Tnfaip2	0.788551	1.55E-07
ENSMUSG00000052305	Hbb-bs	-2.6188	1.56E-07
ENSMUSG00000037224	Zfyve28	0.870889	1.61E-07
ENSMUSG00000053080	2700081O15Rik	-0.83032	1.62E-07
ENSMUSG00000051906	Cd209f	-7.63764	1.66E-07

ENSMUSG00000030165	Klrd1	-2.62464	1.66E-07
ENSMUSG00000026605	Cenpf	-1.77669	1.69E-07
ENSMUSG00000046718	Bst2	0.944635	1.70E-07
ENSMUSG00000039997	Ifi203	-0.95384	1.70E-07
ENSMUSG00000040483	Xaf1	1.011687	1.78E-07
ENSMUSG00000024600	Slc27a6	-7.60625	1.80E-07
ENSMUSG00000016477	E2f3	-0.79188	1.87E-07
ENSMUSG00000064345	mt-Nd2	-1.23859	2.02E-07
ENSMUSG00000031497	Tnfsf13b	0.64531	2.03E-07
ENSMUSG00000111926	Gm46204	2.605743	2.11E-07
ENSMUSG00000060802	B2m	0.821022	2.20E-07
ENSMUSG00000031790	Mmp15	-2.39313	2.31E-07
ENSMUSG00000037625	Cldn11	-2.50952	2.31E-07
ENSMUSG00000000365	Rnf17	1.514756	2.36E-07
ENSMUSG00000109408	A930037H05Rik	1.090025	2.36E-07
ENSMUSG00000022797	Tfrc	-1.05001	2.57E-07
ENSMUSG00000029380	Cxcl1	-1.14521	2.59E-07
ENSMUSG00000006930	Hap1	1.540458	2.65E-07
ENSMUSG00000045551	Fpr1	1.630779	2.80E-07
ENSMUSG00000028078	Dclk2	-1.2882	2.83E-07
ENSMUSG00000031586	Rbpms	0.682275	2.96E-07
ENSMUSG00000091418	Gm3164	-3.13726	3.03E-07
ENSMUSG00000006235	Epor	-2.7224	3.05E-07
ENSMUSG00000026938	Fcna	-5.74778	3.19E-07
ENSMUSG00000018923	Med11	0.724851	3.20E-07
ENSMUSG00000022272	Myo10	0.988049	3.49E-07
ENSMUSG00000034118	Tpst1	1.12255	3.69E-07
ENSMUSG00000074657	Kif5a	-1.36102	3.80E-07
ENSMUSG00000071064	Zfp827	-0.875	3.93E-07
ENSMUSG00000092060	Bend4	-1.61508	4.16E-07
ENSMUSG00000006435	Neurl1a	0.602613	4.17E-07
ENSMUSG00000041075	Fzd7	-0.54868	4.31E-07
ENSMUSG00000117079	Gm41611	1.10462	4.42E-07
ENSMUSG00000028273	Pdlim5	-0.61094	4.55E-07
ENSMUSG00000059248	Septin9	0.636917	4.98E-07
ENSMUSG00000061100	Retnla	-7.54604	5.00E-07
ENSMUSG00000000791	Il12rb1	3.459862	5.07E-07
ENSMUSG00000000184	Ccnd2	0.727292	5.90E-07
ENSMUSG00000074578	Zfas1	0.659262	6.04E-07
ENSMUSG00000006731	B4galnt1	0.62986	6.13E-07
ENSMUSG00000079470	Utp14b	-1.22345	6.13E-07
ENSMUSG00000078350	Smim1	-1.40165	6.27E-07
ENSMUSG00000069917	Hba-a2	-2.68839	6.51E-07
ENSMUSG00000027222	Pex16	0.890238	8.04E-07
ENSMUSG00000078921	Tgtp2	1.702782	8.10E-07
ENSMUSG00000058056	Palld	-3.28383	8.25E-07

ENSMUSG00000005533	Igf1r	-0.69687	8.45E-07
ENSMUSG00000003974	Grm3	-3.15106	8.49E-07
ENSMUSG00000022885	St6gal1	-0.51465	8.56E-07
ENSMUSG00000030091	Nup210	0.740695	9.06E-07
ENSMUSG00000033032	Afap1l1	-0.70452	9.32E-07
ENSMUSG00000037852	Cpe	-1.21815	9.40E-07
ENSMUSG00000028328	Tmod1	-1.91377	9.59E-07
ENSMUSG00000035458	Tnni3	1.150587	9.59E-07
ENSMUSG00000027562	Car2	-2.05383	1.01E-06
ENSMUSG00000075015	Gm10801	-2.255	1.02E-06
ENSMUSG00000027750	Postn	-1.08526	1.02E-06
ENSMUSG00000046841	Ckap4	-0.68391	1.03E-06
ENSMUSG00000014418	Hps5	0.51537	1.04E-06
ENSMUSG00000036585	Fgf1	-2.45917	1.04E-06
ENSMUSG00000052749	Trim30b	1.345342	1.07E-06
ENSMUSG00000042677	Zc3h12a	0.515795	1.13E-06
ENSMUSG00000016933	Plcg1	-0.53322	1.15E-06
ENSMUSG00000066677	Ifi208	1.306878	1.27E-06
ENSMUSG00000043795	Prr33	1.375727	1.28E-06
ENSMUSG00000015829	Tnr	-2.60444	1.30E-06
ENSMUSG00000036887	C1qa	0.613808	1.30E-06
ENSMUSG00000053049	Gm15413	4.18292	1.34E-06
ENSMUSG00000073412	Lst1	0.754736	1.34E-06
ENSMUSG00000085759	1700061E18Rik	-2.49598	1.43E-06
ENSMUSG00000022489	Pde1b	-0.57074	1.49E-06
ENSMUSG00000031304	Il2rg	1.452858	1.50E-06
ENSMUSG00000025037	Maoa	-1.48812	1.54E-06
ENSMUSG00000093930	Hmgcs1	-0.67665	1.54E-06
ENSMUSG00000031402	Mpp1	-0.59403	1.56E-06
ENSMUSG00000002885	Adgre5	-1.22605	1.58E-06
ENSMUSG00000041120	Nbl1	-2.01604	1.67E-06
ENSMUSG00000027375	Mal	-2.72767	1.76E-06
ENSMUSG00000035441	Myo1d	-1.77995	1.80E-06
ENSMUSG00000104696	Gm42946	2.865232	1.80E-06
ENSMUSG00000053644	Aldh7a1	-0.79681	1.83E-06
ENSMUSG00000102291	Gm37542	-2.43922	1.89E-06
ENSMUSG00000048537	Phldb1	-0.7896	1.97E-06
ENSMUSG00000067212	H2-T23	0.969333	1.97E-06
ENSMUSG00000084821	Gm15880	-2.20532	1.98E-06
ENSMUSG00000110388	Gm30329	-0.85935	2.00E-06
ENSMUSG00000026012	Cd28	-3.65599	2.01E-06
ENSMUSG00000073680	Tmem88b	-3.43893	2.04E-06
ENSMUSG00000022216	Psme1	0.601774	2.08E-06
ENSMUSG00000023885	Thbs2	-2.68298	2.13E-06
ENSMUSG00000035919	Bbs9	-0.66173	2.17E-06
ENSMUSG00000020787	P2rx1	1.03417	2.19E-06

ENSMUSG00000053550	Shisa7	1.228118	2.23E-06
ENSMUSG00000033577	Myo6	-0.89394	2.30E-06
ENSMUSG00000042684	Npl	-0.76719	2.34E-06
ENSMUSG00000033355	Rtp4	1.154936	2.35E-06
ENSMUSG00000043556	Fbxl7	-5.40907	2.35E-06
ENSMUSG00000032184	Lysmd2	2.884366	2.49E-06
ENSMUSG00000035297	Cops4	-0.59031	2.57E-06
ENSMUSG00000005483	Dnajb1	0.899784	2.59E-06
ENSMUSG00000087117	Gm11523	-7.58435	2.64E-06
ENSMUSG00000040616	Tmem51	1.969558	2.72E-06
ENSMUSG00000028108	Ecm1	-1.77795	2.74E-06
ENSMUSG00000025558	Dock9	-0.54794	2.74E-06
ENSMUSG00000002944	Cd36	-0.7093	2.79E-06
ENSMUSG00000024732	Ccdc86	0.527255	2.99E-06
ENSMUSG00000035150	Eif2s3x	0.592223	3.00E-06
ENSMUSG00000020102	Slc16a7	-0.55883	3.02E-06
ENSMUSG00000031112	Stk26	-1.26571	3.14E-06
ENSMUSG00000063605	Ccdc102a	0.98464	3.21E-06
ENSMUSG00000048347	Pcdhb18	-7.45866	3.24E-06
ENSMUSG00000042476	Abcb4	-0.58281	3.25E-06
ENSMUSG00000030084	Plxna1	-0.89658	3.25E-06
ENSMUSG00000032911	Cspg4	-2.34092	3.27E-06
ENSMUSG00000042644	Itpr3	0.619298	3.27E-06
ENSMUSG00000110397	Gm45540	-0.70362	3.28E-06
ENSMUSG00000005360	Slc1a3	0.647204	3.30E-06
ENSMUSG00000032666	1700025G04Rik	-1.73125	3.31E-06
ENSMUSG00000027674	Pex5l	-2.8139	3.50E-06
ENSMUSG00000039682	Lap3	0.500056	3.55E-06
ENSMUSG00000035342	Lzts2	-1.09718	3.73E-06
ENSMUSG00000040907	Atp1a3	0.669049	3.86E-06
ENSMUSG00000058818	Pirb	0.516044	4.22E-06
ENSMUSG00000006651	Aplp1	-1.60524	4.44E-06
ENSMUSG00000030055	Rab43	0.667562	4.46E-06
ENSMUSG00000058672	Tubb2a	-0.56259	4.50E-06
ENSMUSG00000039741	Bahcc1	-0.73872	4.51E-06
ENSMUSG00000107723	Gm43964	1.159182	4.60E-06
ENSMUSG00000074874	Ctla2b	1.391137	4.77E-06
ENSMUSG00000041538	H2-Ob	0.603141	4.83E-06
ENSMUSG00000007379	Dennd2c	-0.5542	4.96E-06
ENSMUSG00000060519	Tor3a	0.863772	5.08E-06
ENSMUSG00000047735	Samd9l	0.523284	5.50E-06
ENSMUSG00000027254	Map1a	-1.66528	6.17E-06
ENSMUSG00000020589	Cyria	0.591174	6.56E-06
ENSMUSG00000055110	A630012P03Rik	3.614168	6.57E-06
ENSMUSG00000024772	Ehd1	-0.67263	6.57E-06
ENSMUSG00000044703	Phf11a	2.124746	6.75E-06

ENSMUSG00000057596	Trim30d	0.486571	6.85E-06
ENSMUSG00000097440	Gm6277	-0.76993	6.92E-06
ENSMUSG00000031714	Gab1	-0.50803	7.22E-06
ENSMUSG00000037419	Endod1	-0.47709	7.47E-06
ENSMUSG00000085591	Gm13479	-1.16468	7.61E-06
ENSMUSG00000039765	Cc2d2a	-1.28287	7.79E-06
ENSMUSG00000024462	Gabbr1	-0.48113	8.31E-06
ENSMUSG00000025993	Slc40a1	-0.814	8.35E-06
ENSMUSG00000060675	Plaat3	1.11226	8.68E-06
ENSMUSG00000064289	Tank	0.59274	8.75E-06
ENSMUSG00000038058	Nod1	0.569945	8.88E-06
ENSMUSG00000017493	Igfbp4	-0.48401	8.96E-06
ENSMUSG00000024338	Psmb8	0.524037	9.10E-06
ENSMUSG00000063193	Cd300lb	-1.36779	9.15E-06
ENSMUSG00000024222	Fkbp5	0.892796	9.24E-06
ENSMUSG00000026866	Kynu	1.478424	9.27E-06
ENSMUSG00000001700	Gramd3	1.255387	9.35E-06
ENSMUSG00000027315	Spint1	0.849449	9.65E-06
ENSMUSG00000038732	Mboat1	-1.97398	9.92E-06
ENSMUSG00000079445	B3gnt7	-1.58218	1.03E-05
ENSMUSG00000004267	Eno2	-1.53744	1.04E-05
ENSMUSG00000030708	Dnajb13	0.720764	1.06E-05
ENSMUSG00000028399	Ptprd	-2.76793	1.09E-05
ENSMUSG00000021280	Exoc3l4	2.154809	1.10E-05
ENSMUSG00000018593	Sparc	-0.57806	1.13E-05
ENSMUSG00000038068	Rnf144b	-0.54478	1.15E-05
ENSMUSG00000040111	Gramd1b	-0.68059	1.15E-05
ENSMUSG00000029309	Sparcl1	-0.99871	1.15E-05
ENSMUSG00000028976	Slc2a5	-0.84401	1.18E-05
ENSMUSG00000099974	Bcl2a1d	0.887207	1.19E-05
ENSMUSG00000004665	Cnn2	-0.8696	1.21E-05
ENSMUSG00000032261	Sh3bgrl2	-2.12672	1.21E-05
ENSMUSG00000064349	mt-Tc	-0.90422	1.22E-05
ENSMUSG00000034177	Rnf43	2.762825	1.24E-05
ENSMUSG00000036875	Dna2	0.888012	1.25E-05
ENSMUSG00000007039	Ddah2	-0.78724	1.26E-05
ENSMUSG00000050335	Lgals3	-0.82699	1.27E-05
ENSMUSG00000031740	Mmp2	-0.58368	1.28E-05
ENSMUSG00000038400	Pmepa1	-0.79206	1.29E-05
ENSMUSG00000000562	Adora3	0.556132	1.31E-05
ENSMUSG00000031709	Tbc1d9	0.822998	1.34E-05
ENSMUSG00000048285	Frmd6	-1.08128	1.36E-05
ENSMUSG00000031488	Rab11fip1	1.214509	1.36E-05
ENSMUSG00000020288	Ahsa2	0.618747	1.37E-05
ENSMUSG00000048621	Gm6377	-1.16957	1.40E-05
ENSMUSG00000046160	Olig1	-2.49371	1.41E-05

ENSMUSG00000000732	Icosl	0.858383	1.41E-05
ENSMUSG00000082402	Gm15621	1.461772	1.51E-05
ENSMUSG00000041736	Tspo	0.574942	1.51E-05
ENSMUSG00000022540	Rogdi	0.493653	1.51E-05
ENSMUSG00000020262	Adarb1	-1.25142	1.53E-05
ENSMUSG00000112148	Lilrb4a	-0.80715	1.59E-05
ENSMUSG00000024610	Cd74	-0.77495	1.59E-05
ENSMUSG00000032281	Acsbg1	-2.19019	1.62E-05
ENSMUSG00000032589	Bsn	-1.1088	1.62E-05
ENSMUSG00000054203	Ifi205	2.774104	1.65E-05
ENSMUSG00000014782	Plekhg4	4.34582	1.66E-05
ENSMUSG00000062591	Tubb4a	-1.51364	1.66E-05
ENSMUSG00000050627	Gpd1l	0.466266	1.66E-05
ENSMUSG00000044042	Fmn1	-1.0801	1.72E-05
ENSMUSG00000090881	Phf11	2.448573	1.73E-05
ENSMUSG00000039013	Siglecf	-0.68759	1.73E-05
ENSMUSG00000015340	Cybb	0.889808	1.77E-05
ENSMUSG00000066129	Kndc1	-2.22451	1.79E-05
ENSMUSG00000042804	Gpr153	-2.11695	1.80E-05
ENSMUSG00000019558	Slc6a8	-1.56964	1.80E-05
ENSMUSG00000036957	Lrfn3	-2.61477	1.81E-05
ENSMUSG00000028268	Gbp3	0.654099	1.81E-05
ENSMUSG00000022114	Spry2	-2.46359	1.95E-05
ENSMUSG00000109089	4833411C07Rik	1.004487	1.95E-05
ENSMUSG00000041444	Arhgap32	-0.6862	1.98E-05
ENSMUSG00000054252	Fgfr3	-2.40605	2.03E-05
ENSMUSG00000010660	Plcd1	0.56792	2.04E-05
ENSMUSG00000064363	mt-Nd4	-1.14287	2.06E-05
ENSMUSG00000088185	Scarna2	0.659088	2.06E-05
ENSMUSG00000104030	5330406M23Rik	0.639803	2.07E-05
ENSMUSG00000015355	Cd48	0.548353	2.08E-05
ENSMUSG00000026014	Raph1	-0.65555	2.10E-05
ENSMUSG00000027376	Prom2	1.255614	2.21E-05
ENSMUSG00000039713	Plekhg5	-0.50218	2.21E-05
ENSMUSG00000046006	Gapt	1.536748	2.28E-05
ENSMUSG00000061186	Sfmbt2	-1.52445	2.31E-05
ENSMUSG00000062545	Tlr12	0.612908	2.33E-05
ENSMUSG00000025511	Tspan4	-0.59021	2.42E-05
ENSMUSG00000005656	Snx6	-0.48337	2.58E-05
ENSMUSG00000095742		-0.82528	2.64E-05
ENSMUSG00000046314	Stxbp6	-3.6112	2.74E-05
ENSMUSG00000027544	Nfatc2	-0.48572	2.80E-05
ENSMUSG00000026109	Tmeff2	-3.69577	2.87E-05
ENSMUSG00000038151	Prdm1	0.471212	2.95E-05
ENSMUSG00000029419	Ajm1	-0.62584	2.95E-05
ENSMUSG00000021185	Dglucy	0.518656	2.95E-05

ENSMUSG00000029189	Sel1l3	-3.93252	2.95E-05
ENSMUSG00000053799	Exoc6	0.487193	3.02E-05
ENSMUSG00000030310	Slc6a1	-2.29018	3.16E-05
ENSMUSG00000002307	Daxx	0.602893	3.16E-05
ENSMUSG00000041245	Wnk3	-2.9667	3.23E-05
ENSMUSG00000076621	Ighj1	-1.27788	3.24E-05
ENSMUSG00000044092	C130050O18Rik	0.779178	3.27E-05
ENSMUSG00000022629	Kif21a	-2.68669	3.28E-05
ENSMUSG00000024210	Ip6k3	3.175518	3.31E-05
ENSMUSG00000032067	Pts	0.609426	3.41E-05
ENSMUSG00000052727	Map1b	-1.11393	3.50E-05
ENSMUSG00000025871	4833439L19Rik	-0.47576	3.54E-05
ENSMUSG00000023927	Satb1	-0.94117	3.65E-05
ENSMUSG00000027843	Ptpn22	1.145927	3.72E-05
ENSMUSG00000055421	Pcdh9	-2.56171	3.94E-05
ENSMUSG00000026305	Lrrfip1	0.451787	3.98E-05
ENSMUSG00000026509	Capn2	-1.09441	4.07E-05
ENSMUSG00000038332	Sesn1	-0.47857	4.13E-05
ENSMUSG00000076619	Ighj3	-1.92622	4.18E-05
ENSMUSG00000039137	Whrn	-0.53414	4.24E-05
ENSMUSG00000074825	Itpripl1	-0.46423	4.24E-05
ENSMUSG00000040797	Iqsec3	-7.10419	4.56E-05
ENSMUSG00000063873	Slc24a3	-0.64637	4.65E-05
ENSMUSG00000020682	Mmp28	-2.41733	4.68E-05
ENSMUSG00000072964	Bhlhb9	-0.90342	4.87E-05
ENSMUSG00000050121	Opalin	-7.06175	4.87E-05
ENSMUSG00000079388	2610042L04Rik	-2.79259	4.89E-05
ENSMUSG00000022586	Ly6i	2.504955	5.05E-05
ENSMUSG00000022708	Zbtb20	-0.5	5.27E-05
ENSMUSG00000003949	Hlf	-1.7832	5.29E-05
ENSMUSG00000021701	Plk2	-0.49747	5.29E-05
ENSMUSG00000105700	Gm42772	7.134836	5.37E-05
ENSMUSG00000090105	Gm15890	0.727261	5.43E-05
ENSMUSG00000036617	Etl4	-1.4672	5.45E-05
ENSMUSG00000105742	Gm42748	-0.95718	5.69E-05
ENSMUSG00000038894	Irs2	0.830124	5.71E-05
ENSMUSG00000060586	H2-Eb1	-0.7957	5.73E-05
ENSMUSG00000107075	Gm43068	2.207375	5.76E-05
ENSMUSG00000031647	Mfap3l	-2.06382	5.76E-05
ENSMUSG00000042451	Mybph	0.999439	5.96E-05
ENSMUSG00000056602	Fry	-0.51536	5.96E-05
ENSMUSG00000051456	Hspb3	-0.86028	5.99E-05
ENSMUSG00000057315	Arhgap24	0.802276	6.01E-05
ENSMUSG00000026778	Prkcq	-1.86394	6.02E-05
ENSMUSG00000101167	Macroh2a3	2.42363	6.09E-05
ENSMUSG00000097194	9330175E14Rik	1.38696	6.30E-05

ENSMUSG00000067878	Map7d3	1.226875	6.30E-05
ENSMUSG00000029553	Tfec	-1.59213	6.30E-05
ENSMUSG00000024661	Fth1	0.550926	6.47E-05
ENSMUSG00000113326	Gm47586	-2.29866	6.48E-05
ENSMUSG00000015312	Gadd45b	-0.55285	6.49E-05
ENSMUSG00000115762	Gm34907	-2.5297	6.63E-05
ENSMUSG00000111390	Gm48796	-2.56045	6.98E-05
ENSMUSG00000030149	Klrk1	1.898854	7.03E-05
ENSMUSG00000009772	Nuak2	0.498402	7.13E-05
ENSMUSG00000027224	Duoxa1	-2.64116	7.30E-05
ENSMUSG00000003134	Tbc1d8	0.80301	7.40E-05
ENSMUSG00000101191	Gm28809	0.691716	7.40E-05
ENSMUSG00000065232	Gm22973	1.187142	7.42E-05
ENSMUSG00000040957	Cables1	-0.85509	7.80E-05
ENSMUSG00000032202	Rab27a	0.475226	7.86E-05
ENSMUSG00000031639	Tlr3	0.524425	7.99E-05
ENSMUSG00000046442	Ppm1e	-0.96814	8.14E-05
ENSMUSG00000096957	E230013L22Rik	0.663218	8.39E-05
ENSMUSG00000004207	Psap	0.420386	8.47E-05
ENSMUSG00000037418	Best1	0.473176	8.49E-05
ENSMUSG00000055717	Slain1	-2.87174	8.50E-05
ENSMUSG00000102418	Sh2d1b1	1.525831	8.61E-05
ENSMUSG00000032854	Ugt8a	-2.34395	8.74E-05
ENSMUSG00000021175	Cdca7l	1.613638	8.98E-05
ENSMUSG00000053398	Phgdh	-0.7219	9.08E-05
ENSMUSG00000037523	Mavs	0.470165	9.18E-05
ENSMUSG00000039007	Cpq	0.65986	9.19E-05
ENSMUSG00000017713	Tha1	0.671954	9.20E-05
ENSMUSG00000052151	Plpp2	0.967601	9.27E-05
ENSMUSG00000036564	Ndrg4	-1.44998	9.28E-05
ENSMUSG00000011257	Pabpc4	-0.52232	9.42E-05
ENSMUSG00000106047	Gm42942	6.948215	9.66E-05
ENSMUSG00000018001	Cyth3	0.47296	9.67E-05
ENSMUSG00000029207	Apbb2	-0.50318	0.000102789
ENSMUSG00000027956	Tmem144	-0.61633	0.000102789
ENSMUSG00000099398	Ms4a14	-1.66183	0.000103274
ENSMUSG00000024948	Map4k2	-0.45687	0.000103274
ENSMUSG00000085977	Gm5970	1.437842	0.000107463
ENSMUSG00000028546	Elavl4	-1.42906	0.000112036
ENSMUSG00000102037	Bcl2a1a	0.616011	0.000113431
ENSMUSG00000013523	Bcas1	-1.88398	0.000113898
ENSMUSG00000066170	E230001N04Rik	1.712569	0.000114535
ENSMUSG00000085037	4933421O10Rik	0.439036	0.000115494
ENSMUSG00000035725	Prkx	-0.50134	0.0001164
ENSMUSG00000055546	Timd4	-1.32961	0.000116956
ENSMUSG00000018830	Myh11	-3.35726	0.000119117

ENSMUSG00000005089	Slc1a2	-0.9552	0.000124166
ENSMUSG00000006411	Nectin4	0.486292	0.000126473
ENSMUSG00000019763	Rmnd1	0.491218	0.00012741
ENSMUSG00000076620	Ighj2	-1.81717	0.000128171
ENSMUSG00000020798	Spns3	0.763347	0.000130125
ENSMUSG00000026604	Ptpn14	-1.97979	0.000133283
ENSMUSG00000068735	Trp53i11	0.717525	0.000134851
ENSMUSG00000037295	Ldlrap1	0.553496	0.000135105
ENSMUSG00000023805	Synj2	0.50532	0.00013664
ENSMUSG00000029470	P2rx4	0.745889	0.000139209
ENSMUSG00000114329	Gm30489	-2.33675	0.000140431
ENSMUSG00000016128	Stard13	-2.14902	0.000144291
ENSMUSG00000042429	Adora1	1.367271	0.000150773
ENSMUSG00000036995	Asap3	-0.46858	0.000156248
ENSMUSG00000035413	Tmem98	-3.13845	0.000156347
ENSMUSG00000034616	Ssh3	0.436799	0.00015675
ENSMUSG00000021061	Sptb	-1.91111	0.000159392
ENSMUSG00000029322	Plac8	1.267094	0.000160314
ENSMUSG00000008658	Rbfox1	-1.98233	0.000162127
ENSMUSG00000049401	Ogfr	0.447412	0.000162498
ENSMUSG00000105504	Gbp5	0.635349	0.000163269
ENSMUSG00000040249	Lrp1	-0.50119	0.000163691
ENSMUSG00000004996	Mri1	0.976508	0.000164868
ENSMUSG00000007891	Ctsd	0.378231	0.00016712
ENSMUSG00000024601	Isoc1	0.451178	0.000167782
ENSMUSG00000040612	Ildr2	0.922817	0.000167782
ENSMUSG00000034009	Rxfp1	-2.86285	0.000167893
ENSMUSG00000033917	Gde1	0.469136	0.00016951
ENSMUSG00000020886	Dlg4	-0.61722	0.000170576
ENSMUSG00000041762	Gpr155	-0.72146	0.000170733
ENSMUSG00000103585	Pcdhgb4	-0.94928	0.000171203
ENSMUSG00000025743	Sdc3	0.875347	0.000175623
ENSMUSG00000073590	3222401L13Rik	-0.70914	0.000176371
ENSMUSG00000033436	Armcx2	-0.75908	0.000177349
ENSMUSG00000033871	Ppargc1b	1.002018	0.000178151
ENSMUSG00000002265	Peg3	-1.84305	0.000178151
ENSMUSG00000032058	Ppp2r1b	-0.49706	0.000178385
ENSMUSG00000030282	Cmas	-0.4773	0.000180457
ENSMUSG00000043415	Otud1	-0.51195	0.00018131
ENSMUSG00000006462	A530013C23Rik	0.772127	0.000183775
ENSMUSG00000094628	Gm3252	-1.63385	0.000188281
ENSMUSG00000025058	Tasl	0.502982	0.000188827
ENSMUSG00000037940	Inpp4b	0.418509	0.000191168
ENSMUSG00000020331	Hcn2	-1.8785	0.000197725
ENSMUSG00000028654	Mycl	-0.81402	0.000199532
ENSMUSG00000021699	Pde4d	-1.24517	0.000199786

ENSMUSG00000030402	Ppm1n	2.553443	0.00020355
ENSMUSG00000028610	Dmrtb1	0.971837	0.00020355
ENSMUSG00000030187	Klra2	0.633726	0.000203809
ENSMUSG00000034101	Ctnnd1	-0.67221	0.000204653
ENSMUSG00000062585	Cnr2	0.488914	0.000209213
ENSMUSG00000025059	Gk	0.708979	0.000210326
ENSMUSG00000090582	Gm17024	-0.70499	0.000211112
ENSMUSG00000059493	Nhs	-4.9356	0.000211488
ENSMUSG00000106385	Gm42943	2.82013	0.000214168
ENSMUSG00000026199	Ankzf1	0.460774	0.000214168
ENSMUSG00000038028	Tigar	0.861627	0.000222241
ENSMUSG00000003484	Cyp4f18	0.775396	0.000222281
ENSMUSG00000039934	Gsap	0.417975	0.000222973
ENSMUSG00000034135	Sik3	0.441552	0.00022784
ENSMUSG00000025813	Homer2	-3.09705	0.000228094
ENSMUSG00000029581	Fscn1	-0.72829	0.000230322
ENSMUSG00000028989	Angptl7	-1.27147	0.000237122
ENSMUSG00000058290	Espl1	-0.66558	0.000237826
ENSMUSG00000110245	Gm20100	1.023468	0.000237892
ENSMUSG00000039953	Clstn1	-0.71093	0.000242641
ENSMUSG00000085875	Gm12905	0.530311	0.000243689
ENSMUSG00000023367	Tmem176a	0.75985	0.00024416
ENSMUSG00000000127	Fer	-0.61252	0.000251061
ENSMUSG00000021200	Asb2	0.467642	0.000251061
ENSMUSG00000021186	Fbln5	-4.14041	0.000256331
ENSMUSG00000062300	Nectin2	0.49679	0.000257563
ENSMUSG00000002227	Mov10	0.447604	0.000259265
ENSMUSG00000077391	Gm24336	0.808407	0.000260815
ENSMUSG00000033948	Zswim5	-0.98416	0.000260815
ENSMUSG00000030203	Dusp16	-0.47909	0.000267876
ENSMUSG00000026357	Rgs18	-1.68267	0.000267946
ENSMUSG00000095186	Gm10718	-2.7749	0.000269266
ENSMUSG00000114205	Gm7480	1.283262	0.000270692
ENSMUSG00000041329	Atp1b2	-1.79126	0.000275958
ENSMUSG00000063696	Gm8730	5.924297	0.000276798
ENSMUSG00000024197	Plin3	0.608997	0.000280301
ENSMUSG00000038260	Trpm4	-0.57456	0.000280686
ENSMUSG00000022791	Tnk2	-1.174	0.000281199
ENSMUSG00000039153	Runx2	-1.50684	0.000281262
ENSMUSG00000093861	Igkv1-110	-9.05768	0.000282272
ENSMUSG00000103332	Pcdhga2	-1.3964	0.000283834
ENSMUSG00000030307	Slc6a11	-2.1797	0.00029042
ENSMUSG00000027525	Phactr3	-3.23814	0.000290532
ENSMUSG00000047146	Tet1	-0.77107	0.000297331
ENSMUSG00000021224	Numb	-0.69821	0.000297331
ENSMUSG00000087289	4933424M12Rik	1.170472	0.00029946

ENSMUSG00000070034	Sp110	0.437783	0.00029946
ENSMUSG00000040165	Cd209c	-6.98595	0.000305045
ENSMUSG00000112640	Gm32687	-6.98595	0.00030509
ENSMUSG00000036594	H2-Aa	-0.74416	0.00030514
ENSMUSG00000053040	Aph1c	0.825992	0.000308026
ENSMUSG00000001774	Chordc1	0.417492	0.00030887
ENSMUSG00000056888	Glipr1	0.697047	0.000311791
ENSMUSG00000036661	Dennd3	1.085647	0.00031289
ENSMUSG00000073728	Tmem51os1	6.844106	0.000327873
ENSMUSG00000040212	Emp3	-0.61288	0.000330293
ENSMUSG00000032359	Ctsh	0.679389	0.000344684
ENSMUSG00000117239	Gpr31c	2.04385	0.00034942
ENSMUSG00000047220	Iho1	-1.58084	0.000355043
ENSMUSG00000033033	Calhm2	0.413245	0.000359384
ENSMUSG00000062997	Rpl35	0.486368	0.000369535
ENSMUSG00000020077	Srgn	0.437213	0.000369827
ENSMUSG00000036036	Zfp57	-2.13253	0.000372164
ENSMUSG00000028278	Rragd	-1.26806	0.000375518
ENSMUSG00000022887	Masp1	-1.1922	0.000377268
ENSMUSG00000097156	Gm3764	-3.6836	0.000378312
ENSMUSG00000037280	Galnt6	-1.16867	0.00037871
ENSMUSG00000106639	Gm43121	0.753949	0.000393632
ENSMUSG00000037321	Tap1	0.773631	0.000394081
ENSMUSG00000097296	Gm26532	-0.72754	0.00039506
ENSMUSG00000008734	Gprc5b	-1.99733	0.000403739
ENSMUSG00000032035	Ets1	-0.67146	0.000403739
ENSMUSG00000075122	Cd80	0.570364	0.000404706
ENSMUSG00000002741	Ykt6	-0.41108	0.000405403
ENSMUSG00000005823	Gpr108	0.432323	0.000406362
ENSMUSG00000022371	Col14a1	-0.75095	0.00040699
ENSMUSG00000004270	Lpcat3	-0.39718	0.00041013
ENSMUSG00000026548	Slamf9	0.577271	0.000415615
ENSMUSG00000032547	Ryk	-0.636	0.000422267
ENSMUSG00000103144	Pcdhga1	-1.26151	0.00042601
ENSMUSG00000072844	G530011O06Rik	-1.01472	0.000428583
ENSMUSG00000032718	Mansc1	1.634839	0.000437874
ENSMUSG00000091549	Gm6548	0.649794	0.000443029
ENSMUSG00000001348	Acp5	2.345137	0.000451012
ENSMUSG00000105290	Gm43528	4.721895	0.000452029
ENSMUSG00000003541	Ier3	-0.46137	0.000458728
ENSMUSG00000030104	Edem1	-0.69425	0.000476412
ENSMUSG00000026994	Galnt3	0.735791	0.000482173
ENSMUSG00000028644	Ermap	0.498612	0.000483963
ENSMUSG00000051065	Mb21d2	-2.68637	0.000485697
ENSMUSG00000042978	Sbk1	-1.1079	0.000496122
ENSMUSG00000022987	Zfp641	0.811744	0.000496153

ENSMUSG00000041571	Selenow	0.562505	0.000499108
ENSMUSG00000020717	Pecam1	-0.59321	0.000503113
ENSMUSG00000097325	Gm16897	1.009933	0.000512259
ENSMUSG00000033781	Asb13	0.517287	0.000515511
ENSMUSG00000022054	Nefm	-2.15396	0.000523205
ENSMUSG00000006576	Slc4a3	1.656796	0.000524887
ENSMUSG00000022893	Adamts1	-0.6496	0.000526005
ENSMUSG00000104292	Gm38042	0.637096	0.000528288
ENSMUSG00000064348	mt-Tn	-0.88768	0.000531443
ENSMUSG00000032118	Fez1	-1.849	0.000535128
ENSMUSG00000031760	Mt3	-1.7356	0.000547385
ENSMUSG00000022587	Ly6e	0.709111	0.000549968
ENSMUSG00000039405	Prss23	-4.0091	0.000568788
ENSMUSG00000022351	Sqle	-1.19849	0.000577542
ENSMUSG00000021589	Rhobtb3	-3.27465	0.000578204
ENSMUSG00000026630	Batf3	0.613466	0.000579156
ENSMUSG00000039116	Adgrg6	-2.81041	0.000580215
ENSMUSG00000032238	Rora	-0.90435	0.000584774
ENSMUSG00000073421	H2-Ab1	-0.71688	0.000586393
ENSMUSG00000033208	S100b	-1.72398	0.000591427
ENSMUSG00000033579	Fa2h	-2.99738	0.000597773
ENSMUSG00000029490	Mfsd7a	0.736043	0.000610651
ENSMUSG00000103851	Gm37606	-1.29723	0.000616359
ENSMUSG00000108912	E230020D15Rik	-3.26241	0.000616777
ENSMUSG00000057440	Mpp7	0.496142	0.000627494
ENSMUSG00000025026	Add3	-0.49455	0.000636792
ENSMUSG00000076618	Ighj4	-1.29752	0.00066196
ENSMUSG00000103050	Gm38273	1.722949	0.000662818
ENSMUSG00000050002	Idnk	0.482397	0.000665381
ENSMUSG00000026678	Rgs5	-1.36139	0.000672594
ENSMUSG00000056145	AI504432	-0.69347	0.000672594
ENSMUSG00000030020	Prickle2	-2.00327	0.000692239
ENSMUSG00000109713	Pvrig	1.126421	0.000703648
ENSMUSG00000110235	Gm5086	0.416019	0.000721954
ENSMUSG00000029392	Rilpl1	0.411071	0.000724889
ENSMUSG00000056501	Cebpb	0.921077	0.000725239
ENSMUSG00000108897	Gm44861	0.509036	0.000726083
ENSMUSG00000075254	Heg1	-1.31231	0.000729143
ENSMUSG00000037996	Slc24a2	-2.91322	0.000755711
ENSMUSG00000108820	Gm44620	1.437409	0.000767616
ENSMUSG00000001942	Siae	0.488308	0.000776641
ENSMUSG00000001249	Hpn	0.692618	0.000783644
ENSMUSG00000043467	Zbtb37	-0.42411	0.000790491
ENSMUSG00000041889	Shisa4	-2.73639	0.000790707
ENSMUSG00000002059	Rab34	-0.79713	0.000794424
ENSMUSG00000032656	Marchf3	-1.1977	0.000796066

ENSMUSG00000087107	AI662270	-1.83257	0.000797144
ENSMUSG00000118183	Gm50345	0.715852	0.00080766
ENSMUSG00000074342	I830077J02Rik	0.403514	0.000838042
ENSMUSG00000025375	Aatk	0.561694	0.000841188
ENSMUSG00000026424	Gpr37l1	-2.17686	0.000846325
ENSMUSG00000022982	Sod1	0.387334	0.000852112
ENSMUSG00000037887	Dusp8	-1.06785	0.000861504
ENSMUSG00000003518	Dusp3	-0.41297	0.00087557
ENSMUSG00000028189	Ctbs	0.437949	0.000891255
ENSMUSG00000039470	Zdhhc2	2.085985	0.00089543
ENSMUSG00000079222		6.693397	0.000916222
ENSMUSG00000032596	Uba7	0.72378	0.000933414
ENSMUSG00000026483	Niban1	0.679499	0.000942027
ENSMUSG00000029223	Uchl1	-1.83127	0.000942189
ENSMUSG00000024805	Pcgf5	0.659079	0.000946154
ENSMUSG00000034731	Dgkh	-0.79783	0.000947632
ENSMUSG00000029513	Prkab1	-0.4051	0.000947632
ENSMUSG00000024597	Slc12a2	-0.70423	0.000950293
ENSMUSG00000027852	Nras	-0.3811	0.000956179
ENSMUSG00000025008	Tctn3	0.659332	0.000962802
ENSMUSG00000109438	Gm45073	-3.10929	0.000963623
ENSMUSG00000033174	Mgll	-0.4968	0.000984679
ENSMUSG00000050549	Fam241a	1.198359	0.000986389
ENSMUSG00000035877	Zhx3	-0.57134	0.000987873
ENSMUSG00000022762	Ncam2	-4.2611	0.000997751
ENSMUSG00000045382	Cxcr4	0.479066	0.000998719
ENSMUSG00000039081	Zfp503	1.222839	0.001012956
ENSMUSG00000072889	Nfxl1	-0.38401	0.001018228
ENSMUSG00000097855	A930007I19Rik	0.590544	0.001018873
ENSMUSG00000040339	Fam102b	-0.70163	0.001035708
ENSMUSG00000062980	Cped1	1.714121	0.001047601
ENSMUSG00000110682	A530010L16Rik	1.746608	0.001060088
ENSMUSG00000020256	Aldh1l2	-1.4568	0.001069061
ENSMUSG00000104339	C130089K02Rik	0.663619	0.001069574
ENSMUSG00000037260	Hgsnat	-0.39933	0.001072851
ENSMUSG00000074415	Mir100hg	-6.64707	0.001073768
ENSMUSG00000035208	Slfn8	0.723291	0.0010828
ENSMUSG00000058756	Thra	-0.78543	0.001084374
ENSMUSG00000102336	Gm37233	-0.47142	0.001090654
ENSMUSG00000054150	Syne3	-1.68934	0.001091305
ENSMUSG00000036192	Rorb	-3.12144	0.001108967
ENSMUSG00000031227	Magee1	-1.03906	0.001108967
ENSMUSG00000001166	Oas1c	1.301974	0.001114156
ENSMUSG00000015222	Map2	-1.54935	0.001118267
ENSMUSG00000026782	Abi2	-0.48585	0.001118267
ENSMUSG00000047126	Cltc	-0.53066	0.001128634

ENSMUSG00000097149	G630030J09Rik	0.612303	0.001128634
ENSMUSG00000021130	Galnt16	-2.04201	0.001139262
ENSMUSG00000083651	Gm11524	-6.63822	0.001145066
ENSMUSG00000086708	Gm15577	3.655523	0.001145163
ENSMUSG00000029759	Pon3	0.387075	0.001148021
ENSMUSG00000025503	Taldo1	0.374364	0.001166057
ENSMUSG00000028680	Plk3	0.759567	0.001178571
ENSMUSG00000064141	Zfp69	0.446446	0.001199903
ENSMUSG00000021779	Thrb	-2.68405	0.001200746
ENSMUSG00000086479	Gm16014	-3.95252	0.001204939
ENSMUSG00000050578	Mmp13	-6.8427	0.001204939
ENSMUSG00000021097	Clmn	-1.88955	0.001216452
ENSMUSG00000049119	Fam110b	-1.93858	0.001221156
ENSMUSG00000044629	Cnrip1	-0.83309	0.00124569
ENSMUSG00000056476	Med12l	-0.37873	0.001262696
ENSMUSG00000014599	Csf1	-0.70587	0.00126301
ENSMUSG00000063458	Lrmda	0.762292	0.001263971
ENSMUSG00000040852	Plekhh2	-0.7148	0.001269285
ENSMUSG00000012350	Ehf	3.044038	0.001283404
ENSMUSG00000024851	Pitpnm1	0.439775	0.001285623
ENSMUSG00000072620	Slfn2	0.52969	0.001287317
ENSMUSG00000022475	Hdac7	0.791922	0.001290033
ENSMUSG00000048965	Mrgpre	-0.96242	0.001293771
ENSMUSG00000029299	Abcg3	0.658019	0.001298477
ENSMUSG00000092035	Peg10	-0.4559	0.001302944
ENSMUSG00000080763	Gm12341	4.507153	0.001306953
ENSMUSG00000031504	Rab20	0.810407	0.001307453
ENSMUSG00000038173	Enpp6	-4.55452	0.001308236
ENSMUSG00000070939	Tgfbrap1	-0.39686	0.001330844
ENSMUSG00000040466	Blvrb	-0.65052	0.001347142
ENSMUSG00000076617	Ighm	-0.68425	0.001350074
ENSMUSG00000053835	H2-T24	0.42449	0.001350074
ENSMUSG00000000881	Dlg3	-0.55113	0.001376385
ENSMUSG00000049999	Ppp1r3d	0.576999	0.001425598
ENSMUSG00000073771	Btbd19	0.444197	0.001426991
ENSMUSG00000032549	Rab6b	-0.4798	0.001433466
ENSMUSG00000062098	Btbd3	-0.58134	0.001433466
ENSMUSG00000074361	C5ar2	0.38456	0.001433466
ENSMUSG00000056268	Dennd1b	0.38142	0.001445875
ENSMUSG00000028463	Car9	1.489596	0.001445875
ENSMUSG00000045193	Cirbp	0.522765	0.001446523
ENSMUSG00000098132	Rassf10	-4.01024	0.001450905
ENSMUSG00000089712	Gm15889	0.762253	0.001456347
ENSMUSG00000028019	Pdgfc	-4.76698	0.00145999
ENSMUSG00000022360	Atad2	0.475384	0.001481903
ENSMUSG00000025648	Pfkfb4	0.384742	0.001491244

ENSMUSG00000028497	Hacd4	0.424335	0.001497663
ENSMUSG00000097571	Jpx	0.784904	0.001499949
ENSMUSG00000076439	Mog	-2.10445	0.001503564
ENSMUSG00000029304	Spp1	-1.08623	0.001534986
ENSMUSG00000024810	Il33	-2.41252	0.001539645
ENSMUSG00000083305	Gm13315	1.822926	0.001550036
ENSMUSG00000035900	Gramd4	-0.62451	0.00156252
ENSMUSG00000002190	Clgn	-1.0802	0.001566923
ENSMUSG00000022964	Tmem50b	0.395105	0.001573644
ENSMUSG00000027318	Adam33	0.481288	0.001573644
ENSMUSG00000078763	Slfn1	0.903632	0.001582303
ENSMUSG00000090272	Mndal	-0.55132	0.001600698
ENSMUSG00000049521	Cdc42ep1	-2.22921	0.001607876
ENSMUSG00000104034	2900092N22Rik	2.179334	0.001613805
ENSMUSG00000037936	Scarb1	-0.60169	0.001615924
ENSMUSG00000040987	Mill2	-2.15384	0.001619276
ENSMUSG00000054256	Msi1	-3.26	0.001668119
ENSMUSG00000025959	Klf7	-0.3801	0.001681172
ENSMUSG00000040785	Ttc3	-0.39761	0.00169018
ENSMUSG00000114255	Gm10734	4.493314	0.001705827
ENSMUSG00000038677	Scube3	-1.70234	0.001729069
ENSMUSG00000063354	Slc39a4	0.787807	0.001729069
ENSMUSG00000052428	Tmco1	0.386322	0.001742299
ENSMUSG00000030541	Idh2	-0.36634	0.00174585
ENSMUSG00000049281	Scn3b	-6.58865	0.001754106
ENSMUSG00000037692	Ahdc1	-0.41531	0.001771121
ENSMUSG00000009585	Apobec3	0.636542	0.001779059
ENSMUSG00000020932	Gfap	-1.45013	0.00178633
ENSMUSG00000070436	Serpinh1	-1.89257	0.00178633
ENSMUSG00000040152	Thbs1	0.686321	0.001797926
ENSMUSG00000106426	Gm36211	-2.57475	0.001797926
ENSMUSG00000087142	Gm12454	3.373271	0.001832763
ENSMUSG00000058070	Eml1	-2.57357	0.001857914
ENSMUSG00000044471	Lncpint	0.404815	0.00185855
ENSMUSG00000000416	Cttnbp2	-3.93896	0.001867541
ENSMUSG00000036452	Arhgap26	-0.83841	0.001885253
ENSMUSG00000026489	Coq8a	0.654723	0.001901505
ENSMUSG00000026177	Slc11a1	0.661669	0.00194139
ENSMUSG00000038886	Man2a2	-0.65002	0.00194806
ENSMUSG00000034575	Tent4a	0.4168	0.001962107
ENSMUSG00000032702	Kank1	-1.69145	0.001976138
ENSMUSG00000062170	Fmr1nb	-2.9254	0.001976703
ENSMUSG00000057337	Chst3	-3.61588	0.001987128
ENSMUSG00000061451	Tmem151a	-3.08602	0.002014253
ENSMUSG00000018920	Cxcl16	0.693605	0.002044296
ENSMUSG00000019775	Rgs17	-4.54123	0.002054204

ENSMUSG00000039531	Zup1	0.361196	0.002061441
ENSMUSG00000051439	Cd14	-0.64559	0.002061441
ENSMUSG00000100017	2410022M11Rik	0.784648	0.002069696
ENSMUSG00000002007	Srpk3	-0.5688	0.002134657
ENSMUSG00000030793	Pycard	-0.45322	0.00213921
ENSMUSG00000002325	Irf9	0.405775	0.002156935
ENSMUSG00000040537	Adam22	-0.81753	0.002169426
ENSMUSG00000111324	Gm31410	0.953959	0.002193373
ENSMUSG00000030638	Sh3gl3	-4.50959	0.002223111
ENSMUSG00000029417	Cxcl9	1.772427	0.00225933
ENSMUSG00000020591	Ntsr2	-2.36124	0.002264292
ENSMUSG00000086291	Gm15513	0.765604	0.002270634
ENSMUSG00000031604	Msmo1	-0.57016	0.002297607
ENSMUSG00000007038	Neu1	0.432966	0.002307153
ENSMUSG00000036218	Pdzrn4	-6.46875	0.002309897
ENSMUSG00000027273	Snap25	-1.04834	0.00231939
ENSMUSG00000053063	Clec12a	-0.59246	0.002345175
ENSMUSG00000112545	1300014J16Rik	0.759242	0.002351679
ENSMUSG00000025372	Baiap2	0.636828	0.002374522
ENSMUSG00000085394	2210414B05Rik	6.503792	0.002395624
ENSMUSG00000114310	Gm48602	-3.23044	0.002428738
ENSMUSG00000018417	Myo1b	0.382817	0.002430593
ENSMUSG00000026728	Vim	-0.44874	0.002430593
ENSMUSG00000021913	Ogdhl	-3.03611	0.002459678
ENSMUSG00000086370	Ftx	0.582612	0.002459678
ENSMUSG00000042333	Tnfrsf14	0.395787	0.002462372
ENSMUSG00000020154	Ptprb	-1.02605	0.002476641
ENSMUSG00000049723	Mmp12	-1.45619	0.002476641
ENSMUSG00000020099	Unc5b	-1.64823	0.002492013
ENSMUSG00000047843	Bri3	0.385309	0.002511384
ENSMUSG00000026615	Eprs	-0.40979	0.002515873
ENSMUSG00000113771	Gm36529	-2.75283	0.002515873
ENSMUSG00000025986	Slc39a10	-0.38374	0.002532841
ENSMUSG00000021365	Nedd9	0.59987	0.002556642
ENSMUSG00000032643	Fhl3	-0.59242	0.002561644
ENSMUSG00000028082	Sh3d19	-1.54405	0.002573837
ENSMUSG00000058589	Anks1b	-2.17213	0.002623972
ENSMUSG00000039830	Olig2	-2.99021	0.002626731
ENSMUSG00000087674	4930447M23Rik	-1.39195	0.002636949
ENSMUSG00000094763	Gm1647	1.87792	0.002671341
ENSMUSG00000054499	Dedd2	0.495163	0.00269145
ENSMUSG00000020128	Vps54	0.381938	0.002761849
ENSMUSG00000044667	Plppr4	0.693423	0.002824584
ENSMUSG00000070044	Fam149a	0.619844	0.002824584
ENSMUSG00000086841	2410006H16Rik	0.425815	0.002860373
ENSMUSG00000024378	Stard4	-0.96747	0.002862167

ENSMUSG00000041633	Kctd12b	-0.81906	0.002878833
ENSMUSG00000025997	Ikzf2	-0.57054	0.002892457
ENSMUSG00000048852	Gm12185	0.885289	0.002903878
ENSMUSG00000037300	Ttc13	-0.39016	0.002926813
ENSMUSG00000039782	Cpeb2	-0.37057	0.002948585
ENSMUSG00000029033	Acap3	-0.59766	0.002948585
ENSMUSG00000024421	Lama3	-2.08376	0.002948585
ENSMUSG00000043259	Fam13c	-1.88747	0.002963223
ENSMUSG00000048022	Tmem229a	0.910169	0.002974372
ENSMUSG00000028337	Coro2a	0.465755	0.002974372
ENSMUSG00000040488	Ltbp4	-1.28892	0.00298951
ENSMUSG00000036986	Pml	0.518345	0.00300375
ENSMUSG00000030162	Olr1	-1.13461	0.003012781
ENSMUSG00000026826	Nr4a2	-0.7456	0.003040847
ENSMUSG00000025902	Sox17	-1.89989	0.003046349
ENSMUSG00000060913	Trim55	2.802216	0.003047557
ENSMUSG00000116029	Gm41414	6.579124	0.003083483
ENSMUSG00000112095	A130077B15Rik	0.638742	0.003085908
ENSMUSG00000035829	Ppp1r26	-0.81734	0.003109098
ENSMUSG00000024620	Pdgfrb	-1.85153	0.003111106
ENSMUSG00000070565	Rasal2	-0.42146	0.003124851
ENSMUSG00000018341	Il12rb2	0.925028	0.003136306
ENSMUSG00000034422	Parp14	0.68853	0.003141412
ENSMUSG00000024548	Setbp1	-1.24482	0.003153809
ENSMUSG00000063760	Rnf217	-2.09468	0.003188627
ENSMUSG00000045216	Hs6st1	0.372765	0.003190716
ENSMUSG00000018398	Septin8	-0.42804	0.003191565
ENSMUSG00000035273	Hpse	0.980353	0.003206348
ENSMUSG00000022607	Ptk2	-0.88113	0.003222028
ENSMUSG00000075010	AW112010	0.952231	0.003222139
ENSMUSG00000037408	Cnnm4	0.423374	0.00326042
ENSMUSG00000035783	Acta2	-1.63905	0.00326042
ENSMUSG00000000901	Mmp11	-1.37359	0.003265854
ENSMUSG00000036850	Mrpl41	0.571425	0.003265854
ENSMUSG00000038059	Smim3	0.618113	0.003327143
ENSMUSG00000029675	Eln	-3.75438	0.003340633
ENSMUSG00000037747	Phyhipl	-2.16482	0.003362899
ENSMUSG00000059336	Slc14a1	-1.20524	0.003440873
ENSMUSG00000032409	Atr	0.362968	0.003448209
ENSMUSG00000017740	Slc12a5	-1.40147	0.003451305
ENSMUSG00000024140	Epas1	-1.02689	0.003505329
ENSMUSG00000030265	Kras	-0.42635	0.003517044
ENSMUSG00000037552	Plekhg2	-0.512	0.003532876
ENSMUSG00000041654	Slc39a11	0.486519	0.003646598
ENSMUSG00000026880	Stom	-0.48737	0.003667775
ENSMUSG00000114980	4933432I03Rik	1.662374	0.003683341

ENSMUSG00000025656	Arhgef9	-1.21498	0.003706048
ENSMUSG00000004562	Arhgef40	-0.6218	0.003706048
ENSMUSG00000028378	Ptgr1	0.590972	0.003731038
ENSMUSG00000037318	Traf3ip3	0.400665	0.003749445
ENSMUSG00000056966	Gjc3	-1.72761	0.003758599
ENSMUSG00000056004	Elapor2	-6.31105	0.003819654
ENSMUSG00000035299	Mid1	-0.72709	0.003840515
ENSMUSG00000012123	Crybg2	1.474359	0.003881163
ENSMUSG00000008393	Carhsp1	-0.54896	0.003919324
ENSMUSG00000018340	Anxa6	0.39286	0.003937394
ENSMUSG00000022037	Clu	-1.15629	0.003963113
ENSMUSG00000030317	Timp4	-2.68797	0.0039865
ENSMUSG00000028859	Csf3r	0.558091	0.0039865
ENSMUSG00000102808	5430420F09Rik	0.99801	0.004039421
ENSMUSG00000044807	Zfp354c	-0.90314	0.004039851
ENSMUSG00000039427	Alg1	0.406477	0.004051741
ENSMUSG00000033900	Map9	-1.79776	0.004090033
ENSMUSG00000079685	Ulbp1	0.722948	0.004092265
ENSMUSG00000028811	Yars	-0.39908	0.00410622
ENSMUSG00000073591	Pcdhb22	-1.31113	0.004110908
ENSMUSG00000029461	Fam168a	-0.34768	0.004153573
ENSMUSG00000038527	C1rl	0.57938	0.004157924
ENSMUSG00000022946	Dop1b	0.380866	0.004164794
ENSMUSG00000061244	Exoc5	-0.39656	0.004171096
ENSMUSG00000096573	1700009J07Rik	1.343289	0.004190272
ENSMUSG00000022817	Itgb5	0.417124	0.004201641
ENSMUSG00000034449	Dhrs11	0.772293	0.00422251
ENSMUSG00000064347	mt-Ta	-1.00282	0.004230598
ENSMUSG00000025855	Prkar1b	0.760402	0.004283516
ENSMUSG00000019996	Map7	-0.75521	0.004290378
ENSMUSG00000049532	Sall2	-0.45871	0.004310352
ENSMUSG00000114864	Gm41071	0.87069	0.004372539
ENSMUSG00000086813	Gm13657	1.265515	0.004380689
ENSMUSG00000030471	Zdhhc13	0.424121	0.004407283
ENSMUSG00000026589	Sec16b	-1.22811	0.004407283
ENSMUSG00000045095	Magi1	-0.44519	0.004427484
ENSMUSG00000017781	Pitpna	-0.34594	0.004427484
ENSMUSG00000105873	Gm43708	-6.76888	0.00443458
ENSMUSG00000028645	Slc2a1	0.382907	0.004451723
ENSMUSG00000020473	Aebp1	-1.73249	0.004451723
ENSMUSG00000028868	Wasf2	-0.61656	0.004525922
ENSMUSG00000108420	Gm45141	6.501485	0.004571853
ENSMUSG00000105096	Gbp10	4.409273	0.004586173
ENSMUSG00000048960	Prex2	-1.53683	0.004643027
ENSMUSG00000114784	Gm47754	1.377705	0.004648859
ENSMUSG00000074603	Gm10729	1.612386	0.00465389

ENSMUSG00000036053	Fmnl2	0.370521	0.004669561
ENSMUSG00000016494	Cd34	0.6408	0.004723283
ENSMUSG00000009214	Mymk	-1.44955	0.004723333
ENSMUSG00000074502	Ubtfl1	-1.55782	0.004798148
ENSMUSG00000020604	Arsg	-0.61791	0.004820526
ENSMUSG00000041645	Ddx24	0.391696	0.004833618
ENSMUSG00000056413	Adap1	0.444061	0.004853116
ENSMUSG00000026848	Tor1b	0.351025	0.004923586
ENSMUSG00000074622	Mafb	0.506332	0.004942929
ENSMUSG00000067818	Myl9	-2.40142	0.00496445
ENSMUSG00000057367	Birc2	0.368175	0.004995114
ENSMUSG00000005580	Adcy9	-0.41928	0.005024802
ENSMUSG00000071547	Nt5dc2	-0.74901	0.005051043
ENSMUSG00000022667	Cd200r1	-0.5605	0.005063633
ENSMUSG00000091745	Gm17098	6.335282	0.005075995
ENSMUSG00000034336	Ina	-2.74555	0.005094995
ENSMUSG00000022496	Tnfrsf17	-0.99206	0.005112769
ENSMUSG00000038143	Stox2	-1.99158	0.005154621
ENSMUSG00000111116	Gm48065	0.788023	0.00518044
ENSMUSG00000027961	Lrrc39	-1.12384	0.005198413
ENSMUSG00000020840	Blmh	-0.40111	0.005244778
ENSMUSG00000071280	Gm10322	-4.40115	0.005244778
ENSMUSG00000031838	Ifi30	0.640141	0.005244778
ENSMUSG00000040710	St8sia4	-0.4908	0.005253873
ENSMUSG00000087968	Gm25395	0.606431	0.005267637
ENSMUSG00000106539	Gm43670	2.51107	0.00532351
ENSMUSG00000026991	Pkp4	-0.47491	0.005330443
ENSMUSG00000117964	Gm36043	0.61932	0.005339466
ENSMUSG00000045968	Teddm2	0.465874	0.005346155
ENSMUSG00000036745	Ttll7	-1.40432	0.005353868
ENSMUSG00000029254	Stap1	-0.75881	0.005385007
ENSMUSG00000028245	Nsmaf	0.345777	0.005397776
ENSMUSG00000071550	Cfap44	-3.80776	0.005452953
ENSMUSG00000022529	Zfp263	0.33955	0.005473934
ENSMUSG00000053175	Bcl3	0.68581	0.005506651
ENSMUSG00000032537	Ephb1	-2.81541	0.005580154
ENSMUSG00000019810	Fuca2	0.356531	0.005613579
ENSMUSG00000030757	Zkscan2	-1.70757	0.005630823
ENSMUSG00000030921	Trim30a	0.688131	0.005708275
ENSMUSG00000097451	Rian	-2.3266	0.005715442
ENSMUSG00000052364	B630019K06Rik	-2.66244	0.005748353
ENSMUSG00000025020	Slit1	-2.38585	0.005771226
ENSMUSG00000027858	Tspan2	-1.45223	0.005786469
ENSMUSG00000054843	Atrnl1	0.51577	0.005873977
ENSMUSG00000056608	Chd9	-0.59717	0.005893573
ENSMUSG00000021198	Unc79	-1.09853	0.005927733

ENSMUSG00000056687	Gm11696	0.668212	0.005969629
ENSMUSG00000103037	Pcdhgb1	-1.73649	0.005998928
ENSMUSG00000062373	Tmem65	0.384815	0.006038944
ENSMUSG00000030994	D7Ertd443e	-1.66102	0.006053541
ENSMUSG00000037664	Cdkn1c	-1.11805	0.006082145
ENSMUSG00000022240	Ctnnd2	-0.58384	0.006187987
ENSMUSG00000114961	A930002C04Rik	-6.4033	0.006208142
ENSMUSG00000020396	Nefh	-2.72016	0.006223392
ENSMUSG00000055945	Prr18	-1.48198	0.006252127
ENSMUSG00000020176	Grb10	-1.96835	0.006361893
ENSMUSG00000037031	Tspan15	-3.97709	0.006362216
ENSMUSG00000086360	Gm16214	1.606618	0.00638378
ENSMUSG00000050447	Lypd6	-3.08518	0.006492596
ENSMUSG00000070802	Pnmal2	-1.67878	0.006529039
ENSMUSG00000005142	Man2b1	0.472537	0.006585574
ENSMUSG00000064340	mt-Tl1	-1.66259	0.00658897
ENSMUSG00000015599	Ttbk1	-1.28652	0.006602858
ENSMUSG00000024665	Fads2	-1.66125	0.006622616
ENSMUSG00000091754	Gm3636	-0.79197	0.006650611
ENSMUSG00000008496	Pou2f2	-0.36075	0.006650611
ENSMUSG00000028152	Tspan5	-0.58411	0.00665451
ENSMUSG00000034312	Iqsec1	-0.41769	0.006678716
ENSMUSG00000038776	Ephx1	-0.51907	0.006678716
ENSMUSG00000069763	Tmem100	-0.66134	0.006678716
ENSMUSG00000097906	Gm9625	4.321126	0.006684808
ENSMUSG00000030200	Bcl2l14	3.387424	0.006684808
ENSMUSG00000019082	Slc25a22	0.564275	0.006703941
ENSMUSG00000042371	Slc5a10	-1.82036	0.006751046
ENSMUSG00000052270	Fpr2	0.963158	0.006760992
ENSMUSG00000097585	E230029C05Rik	0.409127	0.006775152
ENSMUSG00000079481	Nhsl2	-0.69475	0.006973266
ENSMUSG00000021453	Gadd45g	-0.44225	0.006976781
ENSMUSG00000006585	Cdt1	0.668894	0.00697868
ENSMUSG00000036169	Sostdc1	-6.30541	0.006999157
ENSMUSG00000044548	Dact1	-1.85346	0.007015203
ENSMUSG00000030208	Emp1	-1.93657	0.007059612
ENSMUSG00000039217	Il18	0.563656	0.007109162
ENSMUSG00000085860	2410003L11Rik	1.685381	0.007182207
ENSMUSG00000045917	Tmem268	0.363312	0.007182207
ENSMUSG00000033538	Casp4	0.455609	0.00718457
ENSMUSG00000036304	Zdhhc23	-1.35414	0.007194739
ENSMUSG00000028381	Ugcg	0.346352	0.00728856
ENSMUSG00000079641	Rpl39	0.388633	0.007348377
ENSMUSG00000026958	Dpp7	0.393012	0.007348377
ENSMUSG00000006219	Fblim1	0.419338	0.007388661
ENSMUSG00000032060	Cryab	-1.55527	0.007389356

ENSMUSG00000039783	Kmo	-1.49776	0.007435262
ENSMUSG00000111544	4930534H03Rik	6.272	0.007463506
ENSMUSG00000013419	Zfp651	-0.69289	0.007463506
ENSMUSG00000034641	Cd300ld	-1.04518	0.007564765
ENSMUSG00000003545	Fosb	-0.67077	0.007564765
ENSMUSG00000064350	mt-Ty	-0.92908	0.007598303
ENSMUSG00000026447	Pik3c2b	0.512916	0.007666693
ENSMUSG00000004892	Bcan	-1.26118	0.007716951
ENSMUSG00000036820	Amdhd2	0.372412	0.007771371
ENSMUSG00000113165	Gm47863	0.590958	0.007786121
ENSMUSG00000078202	Nrarp	-1.89953	0.007805373
ENSMUSG00000097278	Gm26650	-1.91512	0.00781741
ENSMUSG00000061143	Maml3	0.384163	0.007827697
ENSMUSG00000022044	Stmn4	-2.9103	0.007936882
ENSMUSG00000026463	Atp2b4	-1.89753	0.007951541
ENSMUSG00000109721	Gm45280	2.814233	0.00797374
ENSMUSG00000110697	Gm31718	0.968799	0.008092715
ENSMUSG00000090394	4930523C07Rik	1.047525	0.008101639
ENSMUSG00000022818	Cyp2ab1	-3.71154	0.008170516
ENSMUSG00000041390	Mdfic	-0.55994	0.008176441
ENSMUSG00000023830	Igf2r	-0.65562	0.008176441
ENSMUSG00000041380	Htr2c	-2.1072	0.008222449
ENSMUSG00000036636	Clcn7	0.341516	0.008343913
ENSMUSG00000040613	Apobec1	0.356383	0.008389504
ENSMUSG00000063488	Zkscan7	0.613618	0.008389504
ENSMUSG00000055430	Nap1l5	-1.55742	0.008398412
ENSMUSG00000035104	Eva1a	-0.75229	0.008398412
ENSMUSG00000010021	Kif19a	0.817002	0.008398412
ENSMUSG00000030986	Dhx32	-0.46845	0.008403637
ENSMUSG00000019874	Fabp7	-2.22006	0.008427086
ENSMUSG00000005043	Sgsh	0.443786	0.00850187
ENSMUSG00000103885	Gm37006	1.55927	0.00850187
ENSMUSG00000109245	Gm44860	0.593223	0.008508293
ENSMUSG00000061887	Ssbp3	-0.43672	0.008518756
ENSMUSG00000057963	Itpk1	0.408537	0.008555534
ENSMUSG00000068323	Slc4a5	-2.15698	0.008596517
ENSMUSG00000024187	Fam234a	-0.41844	0.008648704
ENSMUSG00000102854	C130023A14Rik	-1.20729	0.008661269
ENSMUSG00000060181	Slc35e3	-0.51019	0.008687154
ENSMUSG00000040016	Ptger3	-1.742	0.008756139
ENSMUSG00000033685	Ucp2	0.512585	0.008770014
ENSMUSG00000027951	Adar	0.600404	0.00879404
ENSMUSG00000026930	Gpsm1	-0.46356	0.008795294
ENSMUSG00000038486	Sv2a	-0.58157	0.008823379
ENSMUSG00000070661	Rnf186	2.42859	0.008904532
ENSMUSG00000024679	Ms4a6d	0.35771	0.009051488

ENSMUSG00000099881	2810013P06Rik	0.491052	0.009079838
ENSMUSG00000059352	Gm10064	6.295361	0.009079838
ENSMUSG00000111147	Gm33699	0.541062	0.009080413
ENSMUSG00000002808	Epdr1	-3.4359	0.009122537
ENSMUSG00000044456	Rin3	0.353116	0.009158118
ENSMUSG00000017670	Elmo2	-0.32643	0.009219996
ENSMUSG00000030523	Trpm1	-6.32829	0.009250478
ENSMUSG00000115230	AU022793	-0.96172	0.009307102
ENSMUSG00000058881	Zfp516	0.33083	0.009400565
ENSMUSG00000025666	Tmem47	-2.1521	0.009412035
ENSMUSG00000025429	Pstpip2	-0.82581	0.009415185
ENSMUSG00000045658	Pid1	-0.36408	0.009594521
ENSMUSG00000027078	Ube2l6	0.644967	0.009594521
ENSMUSG00000102252	Snrpn	-1.53453	0.009628545
ENSMUSG00000093327	Mir5107	-0.98336	0.009750884
ENSMUSG00000002324	Rec8	1.453773	0.009750884
ENSMUSG00000022257	Laptm4b	0.466327	0.009785649
ENSMUSG00000038463	Olfml2b	-0.52635	0.009801206
ENSMUSG00000032086	Bace1	-0.53946	0.009820187
ENSMUSG00000071176	Arhgef10	-1.29949	0.009823524
ENSMUSG00000023067	Cdkn1a	-0.38493	0.009825314
ENSMUSG00000031444	F10	-2.92548	0.009891007
ENSMUSG00000027581	Stmn3	-1.84593	0.010032413
ENSMUSG00000083161	Gm11427	-2.01797	0.01006302
ENSMUSG00000084989	Crocc2	6.336001	0.01006302
ENSMUSG00000009687	Fxyd5	-0.51799	0.010085585
ENSMUSG00000022451	Twf1	-0.39222	0.010099231
ENSMUSG00000001120	Pcbp3	-1.86997	0.010135738
ENSMUSG00000029321	Slc10a6	-4.27669	0.010139993
ENSMUSG00000037166	Ppp1r14a	-3.15663	0.010151729
ENSMUSG00000037816	Fbxw17	0.562944	0.010151729
ENSMUSG00000102419	Gm36940	-1.23392	0.01023641
ENSMUSG00000110498	A630001O12Rik	0.898735	0.010311769
ENSMUSG00000037736	Limch1	-1.685	0.010311948
ENSMUSG00000026069	Il1rl1	-0.72841	0.010420135
ENSMUSG00000060147	Serpinb6a	-0.84567	0.010476139
ENSMUSG00000026255	Efhd1	-2.68104	0.010476139
ENSMUSG00000043592	Unc5cl	1.39459	0.010517027
ENSMUSG00000039221	Rpl22l1	0.450773	0.010517027
ENSMUSG00000030376	Slc8a2	-1.74622	0.010517321
ENSMUSG00000103160	C130012C08Rik	1.668325	0.01052771
ENSMUSG00000003934	Efnb3	-1.79999	0.010583783
ENSMUSG00000079457	Gm7609	2.384331	0.010586472
ENSMUSG00000005672	Kit	-1.88427	0.010586472
ENSMUSG00000022504	Ciita	-0.72647	0.010641805
ENSMUSG00000038523	1700003F12Rik	1.108253	0.010647392

ENSMUSG00000030088	Aldh1l1	1.054004	0.010667704
ENSMUSG00000030291	Med21	0.46358	0.010780837
ENSMUSG00000022790	Igsf11	-2.43544	0.010782596
ENSMUSG00000032451	Trim42	3.065542	0.010859506
ENSMUSG00000026565	Pou2f1	-0.34092	0.010934721
ENSMUSG00000020857	Nme2	2.122989	0.011064028
ENSMUSG00000035354	Uvrag	0.334096	0.011114585
ENSMUSG00000073902	Gvin3	0.554556	0.011116827
ENSMUSG00000020733	Slc9a3r1	0.348791	0.011131569
ENSMUSG00000029009	Mthfr	0.376001	0.011131569
ENSMUSG00000027347	Rasgrp1	-1.82054	0.011158917
ENSMUSG00000046031	Calhm6	1.014206	0.011243015
ENSMUSG00000037738	Nek5	-2.91872	0.011264768
ENSMUSG00000030538	Cib1	-0.55944	0.011264768
ENSMUSG00000023022	Lima1	-0.38579	0.011264768
ENSMUSG00000090307	1700071M16Rik	-1.87855	0.011343517
ENSMUSG00000029456	Acad10	0.717064	0.011519247
ENSMUSG00000030147	Clec4b1	-1.80784	0.011581404
ENSMUSG00000046240	Hepacam	-2.2903	0.011604988
ENSMUSG00000024896	Minpp1	0.414123	0.011738205
ENSMUSG00000002249	Tead3	-0.88557	0.011771079
ENSMUSG00000025085	Ablim1	-0.93953	0.011780672
ENSMUSG00000063821	Dupd1	-4.20297	0.011912872
ENSMUSG00000034833	Tespa1	2.385325	0.011917297
ENSMUSG00000110626	Gm45805	0.9787	0.011995908
ENSMUSG00000030269	Mtmr14	0.396329	0.012018457
ENSMUSG00000114997	Gm49038	-3.21768	0.012019706
ENSMUSG00000052889	Prkcb	0.330386	0.012075296
ENSMUSG00000051652	Lrrc3	0.580044	0.012151579
ENSMUSG00000026610	Esrrg	1.657783	0.012197029
ENSMUSG00000046634	Pkd1l1	6.826514	0.012232705
ENSMUSG00000106944	Gm43843	-3.56583	0.01229548
ENSMUSG00000040552	C3ar1	-0.58144	0.01229548
ENSMUSG00000100975	Gm28875	-3.56583	0.01229548
ENSMUSG00000043953	Ccrl2	0.579168	0.012303729
ENSMUSG00000096904	Lamtor3-ps	-1.88529	0.01244423
ENSMUSG00000115186	Gm49417	-1.88422	0.01244423
ENSMUSG00000092556	Olfr755-ps1	1.631928	0.012694179
ENSMUSG00000039234	Sec24d	-0.49956	0.012715644
ENSMUSG00000032267	Usp28	-0.52198	0.012771089
ENSMUSG00000111539	Gm48372	-2.96189	0.012956453
ENSMUSG00000062209	Erbb4	-3.65621	0.013175281
ENSMUSG00000031517	Gpm6a	-1.63876	0.013212604
ENSMUSG00000020721	Helz	-0.32054	0.013356237
ENSMUSG00000043895	S1pr2	-0.5364	0.013356237
ENSMUSG00000054293	P2ry10b	-0.55167	0.013428418

ENSMUSG00000095589	Ighv1-55	-6.994	0.013428418
ENSMUSG00000106211	Gm42842	-2.22798	0.013677678
ENSMUSG00000001627	Ifrd1	-0.54916	0.01383008
ENSMUSG00000017144	Rnd3	-1.83692	0.01383008
ENSMUSG00000025355	Mmp19	-1.08921	0.01383008
ENSMUSG00000023262	Acy1	-0.5256	0.013943749
ENSMUSG00000030826	Bcat2	0.409719	0.014060317
ENSMUSG00000022619	Mapk8ip2	-2.49919	0.014060317
ENSMUSG00000028234	Rps20	0.546356	0.014104442
ENSMUSG00000039110	Mycbpap	1.117339	0.014121607
ENSMUSG00000031897	Psmb10	0.354302	0.014170187
ENSMUSG00000002395	Use1	0.337643	0.01421168
ENSMUSG00000078794	Dact3	-1.20081	0.014342363
ENSMUSG00000030806	Stx1b	-1.47058	0.01435674
ENSMUSG00000038843	Gcnt1	0.57076	0.01435674
ENSMUSG00000038026	Kcnj9	0.912152	0.014409534
ENSMUSG00000096988	A930029G22Rik	1.460845	0.014409534
ENSMUSG00000032462	Pik3cb	0.326833	0.01447726
ENSMUSG00000040055	Gjb6	-2.49159	0.014519865
ENSMUSG00000069792	Wfdc17	-1.03727	0.014532876
ENSMUSG00000079523	Tmsb10	0.670645	0.014637126
ENSMUSG00000020687	Cdc27	-0.34235	0.014661988
ENSMUSG00000021820	Camk2g	-0.35792	0.014729766
ENSMUSG00000024302	Dtna	-1.65124	0.014736511
ENSMUSG00000029245	Epha5	-1.83392	0.014831108
ENSMUSG00000032369	Plscr1	0.762116	0.014842426
ENSMUSG00000038204	Asb10	-0.87939	0.01489556
ENSMUSG00000023348	Trip6	0.389601	0.014929306
ENSMUSG00000040061	Plcb2	0.563019	0.015096308
ENSMUSG00000038893	Fam117a	0.686694	0.015197706
ENSMUSG00000059921	Unc5c	-4.19171	0.015223755
ENSMUSG00000052566	Hook2	0.608444	0.015231912
ENSMUSG00000027954	Efna1	2.429905	0.015258231
ENSMUSG00000090592	Gm17571	2.919297	0.015320382
ENSMUSG00000093661	Eif4e3	0.565944	0.015346473
ENSMUSG00000051517	Arhgef39	0.794247	0.015434558
ENSMUSG00000095127	Ighv1-82	7.221261	0.015466507
ENSMUSG00000097177	9330159M07Rik	0.926072	0.015475232
ENSMUSG00000021596	Mctp1	-0.40421	0.015481698
ENSMUSG00000021552	Gkap1	0.631032	0.015530501
ENSMUSG00000019124	Scrn1	-1.89278	0.015835839
ENSMUSG00000020415	Pttg1	0.595878	0.015851755
ENSMUSG00000061972	Olfr99	1.250515	0.015871682
ENSMUSG00000021047	Nova1	-0.56399	0.015947795
ENSMUSG00000036158	Prickle1	-0.78751	0.015947795
ENSMUSG00000022899	Slc15a2	-1.57583	0.016025347

ENSMUSG00000027524	Edn3	-2.60328	0.01608379
ENSMUSG00000084497	Gm22107	0.932307	0.01608391
ENSMUSG00000025932	Eya1	-6.13961	0.016339004
ENSMUSG00000047515	BC049715	0.758699	0.016339004
ENSMUSG00000015790	Surf1	0.464815	0.016365102
ENSMUSG00000071722	Spin4	-3.16423	0.016467627
ENSMUSG00000041707	Tmem273	0.344669	0.016468288
ENSMUSG00000109291	Gm2814	1.623671	0.01653526
ENSMUSG00000040289	Hey1	-1.79283	0.016581567
ENSMUSG00000045515	Pou3f3	-1.99924	0.016588445
ENSMUSG00000054000	Tusc1	1.052517	0.016599147
ENSMUSG00000035824	Tk2	0.311405	0.016684575
ENSMUSG00000024248	Cox7a2l	0.318707	0.016689895
ENSMUSG00000020151	Ptprr	-6.17155	0.016800393
ENSMUSG00000099876	Gm29650	-6.17155	0.016800393
ENSMUSG00000026721	Rabgap1l	-0.62485	0.01684672
ENSMUSG00000030268	Bcat1	-2.92777	0.01684672
ENSMUSG00000115529	9630013A20Rik	-4.35367	0.017188209
ENSMUSG00000036782	Klhl13	-1.06304	0.017259866
ENSMUSG00000051497	Kcnj16	-3.00772	0.017275305
ENSMUSG00000029156	Sgcb	0.468691	0.0174665
ENSMUSG00000004709	Cd244a	0.984893	0.017495169
ENSMUSG00000079197	Psme2	0.363009	0.017575107
ENSMUSG00000020600	Slc7a15	-1.78363	0.01766127
ENSMUSG00000097729	2310015A10Rik	0.524786	0.017680553
ENSMUSG00000052031	Tagap1	0.603979	0.017713403
ENSMUSG00000002341	Ncan	-1.68915	0.017778712
ENSMUSG00000085282	Gm15663	-4.13235	0.017814762
ENSMUSG00000030255	Sspn	-1.55013	0.017839834
ENSMUSG00000036905	C1qb	0.345153	0.017839834
ENSMUSG00000048899	Rimkla	-6.13305	0.017923354
ENSMUSG00000031520	Vegfc	-6.13305	0.01794813
ENSMUSG00000026933	Camsap1	-0.332	0.017957471
ENSMUSG00000090942	F830016B08Rik	0.94963	0.018001655
ENSMUSG00000012640	Zfp715	-0.30987	0.018146177
ENSMUSG00000013236	Ptprs	-0.52721	0.018196626
ENSMUSG00000025212	Sfxn3	-0.49407	0.01825161
ENSMUSG00000032356	Rasgrf1	1.545526	0.018270074
ENSMUSG00000081008	Gm13314	2.137384	0.018323769
ENSMUSG00000091985	Gm17354	-1.06018	0.018323769
ENSMUSG00000031808	Slc27a1	0.381432	0.018336522
ENSMUSG00000010358	Ifi35	0.479693	0.018478619
ENSMUSG00000091694	Apol11b	-4.35087	0.018506481
ENSMUSG00000047797	Gjb1	-3.28571	0.018506481
ENSMUSG00000042659	Arrdc4	0.387731	0.018686224
ENSMUSG00000026830	Ermn	-1.80562	0.018827701

ENSMUSG00000042700	Sipa1l1	-0.33262	0.018827701
ENSMUSG00000029804	Herc3	0.546238	0.018859593
ENSMUSG00000003992	Ssbp2	0.401594	0.018875233
ENSMUSG00000118265	Gm50211	0.570445	0.018891637
ENSMUSG00000027522	Stx16	0.315479	0.018918658
ENSMUSG00000108184	Gm44198	0.717631	0.018956947
ENSMUSG00000024174	Pot1b	0.37621	0.018969343
ENSMUSG00000000594	Gm2a	0.580462	0.01905348
ENSMUSG00000018451	6330403K07Rik	-2.08928	0.019079391
ENSMUSG00000019779	Frk	-6.04931	0.019345359
ENSMUSG00000068699	Flnc	-6.0493	0.019360628
ENSMUSG00000055538	Zcchc24	-0.33772	0.019360628
ENSMUSG00000023032	Slc4a8	-1.64465	0.019360628
ENSMUSG00000019832	Rab32	0.353501	0.019592269
ENSMUSG00000021756	Il6st	-0.52655	0.019601723
ENSMUSG00000027569	Mrgbp	0.462479	0.019627772
ENSMUSG00000002279	Lmf1	0.385732	0.01972274
ENSMUSG00000028602	Tnfrsf8	1.067936	0.019751136
ENSMUSG00000029403	Cdkl2	-2.35798	0.019840234
ENSMUSG00000045038	Prkce	-0.4861	0.01986789
ENSMUSG00000028063	Lmna	0.590782	0.019945834
ENSMUSG00000040774	Cept1	0.305741	0.019968753
ENSMUSG00000022296	Baalc	-2.01532	0.02019712
ENSMUSG00000027661	Slc2a10	-3.3294	0.020233284
ENSMUSG00000104900	4930596I21Rik	2.048366	0.0202625
ENSMUSG00000027894	Slc6a17	-2.76185	0.02030022
ENSMUSG00000039492	Ccdc27	-6.26839	0.020362852
ENSMUSG00000028864	Hgf	-0.69579	0.02056755
ENSMUSG00000035004	Igsf6	0.353038	0.020597054
ENSMUSG00000015804	Med28	0.394617	0.020781995
ENSMUSG00000103367	Gm38158	-0.47917	0.020938605
ENSMUSG00000044626	Liph	0.47907	0.020947999
ENSMUSG00000024924	Vldlr	-2.89749	0.020987667
ENSMUSG00000029471	Camkk2	0.321104	0.021058715
ENSMUSG00000059970	Hspa2	0.644965	0.021059626
ENSMUSG00000068129	Cst7	0.76986	0.021070656
ENSMUSG00000025701	Alox5	0.333783	0.021435135
ENSMUSG00000033255	Gm5134	1.028378	0.021563253
ENSMUSG00000083210	Gm14869	-2.57635	0.021826416
ENSMUSG00000050050	Ccdc158	2.094827	0.021847432
ENSMUSG00000062082	Cd200r4	0.965822	0.021847432
ENSMUSG00000045268	Zfp691	0.310277	0.021860615
ENSMUSG00000000275	Trim25	0.401794	0.021860615
ENSMUSG00000021217	Tshz3	-4.21059	0.021875416
ENSMUSG00000102302	Gm38190	-0.61898	0.021888407
ENSMUSG00000055963	Triqk	-2.39337	0.021950492

ENSMUSG00000097633	Gm16617	-0.90379	0.022045106
ENSMUSG00000112053	Gm46328	0.985403	0.022069891
ENSMUSG00000113645	Gm47076	-2.95263	0.022524093
ENSMUSG00000047238	Mageh1	-1.67167	0.022548024
ENSMUSG00000029826	Zc3hav1	0.328038	0.022665764
ENSMUSG00000036560	Lgi4	0.757104	0.022741788
ENSMUSG00000044156	Hepacam2	-1.94671	0.022761515
ENSMUSG00000020105	Lrig3	0.395705	0.022809416
ENSMUSG00000001763	Tspan33	0.634148	0.022814433
ENSMUSG00000018500	Adora2b	-3.64622	0.022907229
ENSMUSG00000041556	Fbxo2	-2.31426	0.022907229
ENSMUSG00000034488	Edil3	-1.87295	0.022933221
ENSMUSG00000003863	Ppfia3	-1.93154	0.022933221
ENSMUSG00000048264	Dip2c	-0.50538	0.022934498
ENSMUSG00000030774	Pak1	0.330609	0.022990921
ENSMUSG00000090877	Hspa1b	0.369511	0.023358667
ENSMUSG00000118436	Gm32880	-6.05577	0.023403798
ENSMUSG00000091786	Gm8425	-3.20163	0.023640957
ENSMUSG00000034957	Cebpa	0.485662	0.023820048
ENSMUSG00000022636	Alcam	-0.77771	0.023829038
ENSMUSG00000056947	Mab21l1	-2.44232	0.023882443
ENSMUSG00000062078	Qk	-0.47489	0.023882443
ENSMUSG00000028842	Ago3	-0.31768	0.024076716
ENSMUSG00000039428	Tmem135	-0.5056	0.024106396
ENSMUSG00000022453	Naga	0.312059	0.024216077
ENSMUSG00000105293	Gm42843	-2.06255	0.024216077
ENSMUSG00000102617	Gm37842	-1.35648	0.024221807
ENSMUSG00000013921	Clip3	-1.39529	0.024257975
ENSMUSG00000071369	Map3k5	0.312574	0.024420743
ENSMUSG00000002985	Apoe	0.287776	0.024625273
ENSMUSG00000087362	Gm13710	1.367209	0.024685718
ENSMUSG00000036867	Smad6	0.675119	0.02470508
ENSMUSG00000055022	Cntn1	-1.96833	0.024877857
ENSMUSG00000118233	Gm30381	-4.17129	0.024877857
ENSMUSG00000090958	Lrrc32	-2.86943	0.024916908
ENSMUSG00000024978	Gpam	-0.37788	0.024978671
ENSMUSG00000026786	Apbb1ip	-0.53883	0.025058206
ENSMUSG00000022055	Nefl	-1.88951	0.025135301
ENSMUSG00000047139	Cd24a	-0.7767	0.025363055
ENSMUSG00000063450	Syne2	-0.58113	0.025365173
ENSMUSG00000102732	Gm37342	1.19622	0.025495364
ENSMUSG00000103165	Gm37560	0.837325	0.025529566
ENSMUSG00000030102	Itpr1	0.388327	0.0256684
ENSMUSG00000004568	Arhgef18	0.319176	0.025834355
ENSMUSG00000058325	Dock1	-0.2955	0.025882193
ENSMUSG00000032220	Myo1e	-0.37135	0.025887048

ENSMUSG00000090990	Gm17197	-5.97409	0.026064198
ENSMUSG00000103094	Gm37558	0.450501	0.026311081
ENSMUSG00000025318	Jph3	-0.73869	0.026311081
ENSMUSG00000068196	Col8a1	-2.48519	0.026311081
ENSMUSG00000063882	Uqcrh	0.384502	0.026311081
ENSMUSG00000049100	Pcdh10	-2.419	0.026311081
ENSMUSG00000033318	Gstt2	0.631119	0.026311081
ENSMUSG00000022641	Bbx	0.30756	0.026401375
ENSMUSG00000097715	Gpr137b-ps	-0.30769	0.026659775
ENSMUSG00000021219	Rgs6	-2.8114	0.026702201
ENSMUSG00000037681	Esyt3	-3.43749	0.026728716
ENSMUSG00000021591	Glrx	0.456634	0.02676802
ENSMUSG00000021638	Ocln	0.902952	0.026962276
ENSMUSG00000020609	Apob	-5.95277	0.027000349
ENSMUSG00000019863	Qrsl1	0.615464	0.027065964
ENSMUSG00000010663	Fads1	-0.32388	0.027091153
ENSMUSG00000090957	Gm7535	2.483964	0.027139227
ENSMUSG00000020474	Polm	0.408274	0.027147738
ENSMUSG00000025950	Idh1	-0.39419	0.027150682
ENSMUSG00000034771	Tle2	-0.7949	0.027227815
ENSMUSG00000028763	Hspg2	-1.2281	0.027227815
ENSMUSG00000031309	Rps6ka3	-0.34474	0.027288469
ENSMUSG00000041729	Coro2b	-1.82006	0.027351389
ENSMUSG00000039485	Tspyl4	-1.45109	0.027372027
ENSMUSG00000084883	Ccdc85c	-0.48276	0.027457145
ENSMUSG00000017718	Afmid	0.950111	0.02753933
ENSMUSG00000038172	Ttc39b	0.304522	0.027644098
ENSMUSG00000013584	Aldh1a2	-1.95181	0.027984534
ENSMUSG00000085715	Tsix	3.150037	0.028341858
ENSMUSG00000041720	Pi4ka	-0.30683	0.028426348
ENSMUSG00000072553	Gm525	6.061046	0.028749584
ENSMUSG00000022724	Riox2	0.521042	0.028795627
ENSMUSG00000106224	Gm43823	1.170018	0.029196171
ENSMUSG00000021872	Rnase10	-1.96561	0.029376016
ENSMUSG00000005045	Chd5	-1.28426	0.029456349
ENSMUSG00000029682	Spam1	1.802046	0.029525652
ENSMUSG00000020264	Slc36a2	-1.25062	0.029622371
ENSMUSG00000104266	Gm37748	1.765912	0.029622371
ENSMUSG00000032232	Cgnl1	-1.4292	0.029838765
ENSMUSG00000029538	Srsf9	0.311828	0.029961611
ENSMUSG00000052160	Pld4	0.448303	0.029961611
ENSMUSG00000060594	Layn	-0.62834	0.030052775
ENSMUSG00000026482	Rgl1	-0.32216	0.030052775
ENSMUSG00000039167	Adgrl4	-1.08503	0.030092634
ENSMUSG00000102989	Gm38318	0.934696	0.030210042
ENSMUSG00000020134	Peli1	0.496747	0.030293832

ENSMUSG00000022575	Gsdmd	0.504201	0.030740144
ENSMUSG00000066258	Trim12a	0.323926	0.030876614
ENSMUSG00000024397	Aif1	0.526742	0.030928805
ENSMUSG00000037071	Scd1	-1.51388	0.030950756
ENSMUSG00000031480	Thsd1	-0.95086	0.03105457
ENSMUSG00000029063	Nadk	0.328689	0.031168821
ENSMUSG00000098055	Gm26947	-1.27697	0.031190898
ENSMUSG00000053211	Zfy1	-6.76798	0.031190898
ENSMUSG00000025582	Nptx1	-2.25287	0.031262519
ENSMUSG00000015981	Stk32c	-2.47897	0.031367519
ENSMUSG00000020806	Rhbdf2	0.384667	0.031440645
ENSMUSG00000018581	Dnah11	-2.5135	0.031551638
ENSMUSG00000030110	Ret	-4.10375	0.031573595
ENSMUSG00000029722	Agfg2	0.490226	0.031730391
ENSMUSG00000056737	Capg	-0.39995	0.032137688
ENSMUSG00000038060	Dlec1	1.039715	0.032152182
ENSMUSG00000029233	Srd5a3	0.460131	0.032231286
ENSMUSG00000059022	Kcp	-0.70083	0.032255447
ENSMUSG00000059851	Kmt5c	0.309477	0.032289044
ENSMUSG00000102752	Gm7694	-0.50765	0.03236521
ENSMUSG00000097073	9430037G07Rik	1.45054	0.032536003
ENSMUSG00000017631	Abr	0.521929	0.032649649
ENSMUSG00000032089	Il10ra	0.451192	0.032653063
ENSMUSG00000041598	Cdc42ep4	-0.40208	0.032653063
ENSMUSG00000103138	Gm2238	1.301951	0.032653063
ENSMUSG00000057863	Rpl36	0.309101	0.032653063
ENSMUSG00000018570	2810408A11Rik	-2.4233	0.032686569
ENSMUSG00000105983	Gm42770	5.933017	0.032710936
ENSMUSG00000027845	Dclre1b	0.456576	0.032710936
ENSMUSG00000031613	Hpgd	-0.53376	0.032710936
ENSMUSG00000001020	S100a4	-4.03675	0.032766333
ENSMUSG00000022217	Emc9	0.641758	0.032839439
ENSMUSG00000072582	Ptrh2	-0.45451	0.032947825
ENSMUSG00000020629	Adi1	0.443697	0.032971798
ENSMUSG00000002983	Relb	0.358231	0.033007342
ENSMUSG00000027900	Dram2	0.306319	0.033007342
ENSMUSG00000115387	Gm49244	2.044872	0.033007342
ENSMUSG00000042688	Mapk6	-0.33176	0.033085305
ENSMUSG00000118068	Gm50275	0.730037	0.033169698
ENSMUSG00000031662	Snx20	0.491006	0.03324548
ENSMUSG00000042401	Crtac1	-5.87221	0.033269434
ENSMUSG00000039601	Rcan2	-1.68703	0.03349869
ENSMUSG00000041313	Slc7a1	-0.42619	0.033552078
ENSMUSG00000102673	Gm37437	1.916665	0.033601386
ENSMUSG00000034687	Fras1	-3.08544	0.033610409
ENSMUSG00000020732	Rab37	1.2495	0.033610409

ENSMUSG00000016256	Ctsz	0.448793	0.033857959
ENSMUSG00000028194	Ddah1	-1.70231	0.033867026
ENSMUSG00000064366	mt-Tl2	-1.51013	0.034059998
ENSMUSG00000041859	Mcm3	0.308748	0.034236383
ENSMUSG00000029778	Adcyap1r1	-1.74396	0.03426361
ENSMUSG00000103897	Pcdhga8	-0.97368	0.034314924
ENSMUSG00000033295	Ptprf	-2.01907	0.034451552
ENSMUSG00000019966	Kitl	-0.39087	0.034451552
ENSMUSG00000097572	Gm26797	1.504664	0.034585516
ENSMUSG00000025494	Sigirr	1.171861	0.034621515
ENSMUSG00000017615	Tnfaip1	-0.3082	0.034816949
ENSMUSG00000025145	Lrrc45	0.312594	0.034878189
ENSMUSG00000020227	Irak3	0.623145	0.034901728
ENSMUSG00000057522	Spop	0.288072	0.035020552
ENSMUSG00000014543	Klra17	1.698672	0.035035989
ENSMUSG00000038807	Rap1gap2	0.305185	0.035035989
ENSMUSG00000066043	Phactr4	-0.38857	0.035084806
ENSMUSG00000102644	Thap6	-0.52879	0.035084806
ENSMUSG00000030087	Klf15	-1.57498	0.035084806
ENSMUSG00000062773	Tex101	3.037396	0.035084806
ENSMUSG00000114412	4930405A10Rik	1.310828	0.035139359
ENSMUSG00000041020	Map7d2	-2.75748	0.035175809
ENSMUSG00000045827	Serpinb9	0.50619	0.035284402
ENSMUSG00000031939	Taf1d	0.293336	0.035305803
ENSMUSG00000000253	Gmpr	-0.45631	0.035499354
ENSMUSG00000005824	Tnfsf14	2.126532	0.035702376
ENSMUSG00000107402	4732416N19Rik	0.746507	0.035883145
ENSMUSG00000092528	Nlrp1c-ps	0.322312	0.036055671
ENSMUSG00000100154	Gm29052	-3.4276	0.036283778
ENSMUSG00000030201	Lrp6	-0.50339	0.036322659
ENSMUSG00000020785	Camkk1	0.568062	0.03641216
ENSMUSG00000031078	Cttn	-1.76272	0.036832509
ENSMUSG00000061576	Dpp6	1.511525	0.036945579
ENSMUSG00000030122	Ptms	0.528132	0.037020635
ENSMUSG00000026421	Csrp1	-0.63873	0.037048981
ENSMUSG00000062380	Tubb3	-1.71879	0.037086975
ENSMUSG00000042570	Mier2	0.314533	0.037136883
ENSMUSG00000052724	Gm9888	0.515128	0.037275489
ENSMUSG00000114553	Gm7644	1.761827	0.037370542
ENSMUSG00000102152	Gm37475	-5.88735	0.037498425
ENSMUSG00000035239	Neu3	1.014867	0.037541851
ENSMUSG00000022051	Bnip3l	-0.32769	0.037688134
ENSMUSG00000101678	Gm29609	1.434271	0.037688134
ENSMUSG00000052281	Tspan32os	1.936819	0.037818115
ENSMUSG00000038456	Dennd2a	0.484168	0.037861524
ENSMUSG00000024677	Ms4a6b	-0.3058	0.037927902

ENSMUSG00000032883	Acsl3	-0.68698	0.037927902
ENSMUSG00000074063	Osgin1	0.865376	0.037954122
ENSMUSG00000104153	Gm38105	2.195633	0.038016191
ENSMUSG00000070271	Gm13268	1.914028	0.038110711
ENSMUSG00000072437	Nanos1	-0.52814	0.038236575
ENSMUSG00000089417	Gm22009	0.665517	0.038255408
ENSMUSG00000113866	Gm47450	-4.10315	0.038340472
ENSMUSG00000053279	Aldh1a1	-1.24291	0.038484782
ENSMUSG00000100627	A830008E24Rik	0.465884	0.03851137
ENSMUSG00000016763	Scube1	-0.88984	0.038773371
ENSMUSG00000092349	Smim40	2.561939	0.038802616
ENSMUSG00000019944	Rhobtb1	-0.28888	0.038807575
ENSMUSG00000040354	Mars1	-0.32864	0.038807575
ENSMUSG00000034686	Prr7	-1.53587	0.03912523
ENSMUSG00000049252	Lrp1b	-2.75028	0.039140491
ENSMUSG00000059326	Csf2ra	0.519469	0.039213676
ENSMUSG00000072874	Gm6116	3.364788	0.039213676
ENSMUSG00000116702	Gm6553	1.758826	0.039414511
ENSMUSG00000117390	Gm50080	1.259289	0.03941705
ENSMUSG00000060924	Csmd1	-3.39293	0.03941705
ENSMUSG00000044674	Fzd1	-3.39293	0.03941705
ENSMUSG00000105987	AI506816	-0.35436	0.039860984
ENSMUSG00000053702	Nebl	-1.31076	0.039916997
ENSMUSG00000082143	Gm12864	4.01476	0.039934881
ENSMUSG00000056267	Cep70	0.504498	0.03997405
ENSMUSG00000086290	Snhg12	0.404332	0.04027138
ENSMUSG00000097191	Mm2pr	2.939847	0.040608681
ENSMUSG00000051747	Ttn	-1.2291	0.040885378
ENSMUSG00000025068	Gsto1	0.467197	0.040913204
ENSMUSG00000098207	Arl14	5.856285	0.040913204
ENSMUSG00000094930	Igkv6-25	6.417191	0.040914399
ENSMUSG00000097081	Gm10425	1.553792	0.040970734
ENSMUSG00000026321	Tnfrsf11a	-0.5064	0.041069378
ENSMUSG00000116226	Gm49502	-1.56575	0.041099768
ENSMUSG00000029053	Prkcz	0.89029	0.041184093
ENSMUSG00000011831	Evi5	-0.3203	0.041208504
ENSMUSG00000109499	Gm44864	1.613187	0.041355336
ENSMUSG00000028496	Mllt3	0.580705	0.041402652
ENSMUSG00000087222	E030042O20Rik	0.514023	0.041402652
ENSMUSG00000036062	Phf24	-2.11949	0.041405284
ENSMUSG00000046562	Unc119b	-0.39135	0.041508866
ENSMUSG00000058897	Col25a1	-2.01154	0.041576941
ENSMUSG00000019970	Sgk1	-0.42214	0.041576941
ENSMUSG00000040717	Il17rd	-2.99892	0.041628532
ENSMUSG00000097127	Gm26886	-2.99892	0.041628532
ENSMUSG00000072612	Gm10382	0.485561	0.041940269

ENSMUSG00000022231	Sema5a	-2.4718	0.042066385
ENSMUSG00000047098	Rnf31	0.285514	0.042066385
ENSMUSG00000032556	Bfsp2	-2.98699	0.042211926
ENSMUSG00000039781	Cep131	0.489872	0.042488031
ENSMUSG00000028461	Ccdc107	0.480636	0.042501536
ENSMUSG00000029338	Antxr2	0.408463	0.042902182
ENSMUSG00000070407	Hs3st3b1	0.616416	0.042906854
ENSMUSG00000090894	Olfr110	-0.74006	0.042906854
ENSMUSG00000027009	Itga4	-0.4456	0.042906854
ENSMUSG00000048677	Tpcn2	0.331856	0.0431767
ENSMUSG00000037434	Slc30a1	0.384302	0.0431767
ENSMUSG00000030161	Gabarapl1	-0.43558	0.043179548
ENSMUSG00000101249	Gm29216	-1.47564	0.043249223
ENSMUSG00000032679	Cd59a	2.11417	0.043249223
ENSMUSG00000020300	Cpeb4	-0.29715	0.043678035
ENSMUSG00000022463	Srebf2	-0.30046	0.043855961
ENSMUSG00000038170	Pde4dip	0.495518	0.043930762
ENSMUSG00000006386	Tek	-1.57493	0.043954296
ENSMUSG00000027459	Fam110a	-0.43381	0.044072162
ENSMUSG00000032373	Car12	-2.15939	0.044301383
ENSMUSG00000109812	Gm45640	0.598641	0.04434766
ENSMUSG00000001128	Cfp	-0.54434	0.044400909
ENSMUSG00000067203	H2-K2	0.311966	0.044667559
ENSMUSG00000109568	Gm45074	-5.78672	0.045022006
ENSMUSG00000117503	Gm7527	2.133082	0.045269139
ENSMUSG00000047415	Gpr68	1.19108	0.045269139
ENSMUSG00000023033	Scn8a	-2.53839	0.045368579
ENSMUSG00000023009	Nckap5l	-0.30503	0.045370292
ENSMUSG00000063660	Olfr98	3.913203	0.045472205
ENSMUSG00000096842	Gm10736	0.809695	0.04547365
ENSMUSG00000073676	Hspe1	0.522406	0.04547365
ENSMUSG00000045180	Shroom2	-2.00175	0.045521188
ENSMUSG00000052310	Slc39a1	-0.27905	0.045628529
ENSMUSG00000046805	Mpeg1	0.298646	0.045689319
ENSMUSG00000117430	Gm49968	-0.75919	0.046116806
ENSMUSG00000003410	Elavl3	-1.46337	0.046388845
ENSMUSG00000087213	2810408I11Rik	3.395067	0.046454043
ENSMUSG00000095440	Fignl2	0.630959	0.046527771
ENSMUSG00000090257	Gm4524	-0.68997	0.046596988
ENSMUSG00000087485	Gm13383	2.228441	0.046858484
ENSMUSG00000106579	Gm42771	6.013246	0.046877884
ENSMUSG00000022951	Rcan1	-0.41955	0.04714789
ENSMUSG00000014226	Cacybp	0.343745	0.04714789
ENSMUSG00000112009	Gm48591	1.147031	0.047352774
ENSMUSG00000027173	Depdc7	0.525998	0.047472696
ENSMUSG00000060961	Slc4a4	-1.29213	0.047546674

ENSMUSG00000028542	Slc6a9	0.986338	0.047576923
ENSMUSG00000033615	Cplx1	-1.54032	0.047589502
ENSMUSG00000107647	Gm44445	1.614139	0.047908668
ENSMUSG00000116589	Gm31323	-3.35501	0.048038651
ENSMUSG00000037826	Ppm1k	0.356936	0.048100904
ENSMUSG00000048100	Taf13	0.460279	0.048202476
ENSMUSG00000070524	Fcrlb	1.180007	0.048250936
ENSMUSG00000097387	4930563E18Rik	2.162487	0.048319
ENSMUSG00000114859	Gm47735	3.859854	0.048770363
ENSMUSG00000057969	Sema3b	-2.40534	0.048770363
ENSMUSG00000026566	Mpzl1	-1.19613	0.048806282
ENSMUSG00000079036	Alkbh1	0.396668	0.048845649
ENSMUSG00000037997	Parp11	0.38907	0.048845649
ENSMUSG00000033855	Ston1	0.990299	0.048845649
ENSMUSG00000039501	Znfx1	0.528118	0.048845649
ENSMUSG00000073402	Gm8909	5.768141	0.048852627
ENSMUSG00000039774	Galnt12	-0.39672	0.048976451
ENSMUSG00000027420	Bfsp1	1.983078	0.049037665
ENSMUSG00000106662	Gm43034	1.197655	0.049060703
ENSMUSG00000031788	Kifc3	-0.53459	0.049104883
ENSMUSG00000027215	Cd82	0.48385	0.049498482

Appendix V Differential Gene Discovories from edgeR analysis of Naïve Microglia

Appendix VI

Canonical Pathways	-log (p-value)	z-score	Down	No Change	Up	No Overlap	P<0.05 Molecules
Phagosome Formation	10.1	-1.213	153/ 276 (55%)	11/ 276 (4%)	111/ 276 (40%)	1/ 276 (0%)	ADGRE5, ADGRG6, ADORA1, ADORA2B, ADORA3, APBB1IP, C3, C3AR1, C5AR2, CCR2, CCR3, CD14, CD36, CNR2, CX3CR1, DOCK1, EDNRB, ELMO2, FCGR3A/ FCGR3B, FN1, FPR1, FPR2, FYN, FZD1, GPR108, GPR155, GPR160, GPR34, GPR35, GPR68, HCAR2, ITGA4, ITGAL, ITGAX, ITGB3, ITGB5, ITPR1, MRC1, MRC2, MSR1, MYH10, MYO10, P2RY12, P2RY14, P2RY2, PAK1, PIK3C2B, PIK3CB, PLA2G2D, PLA2G7, PLAAT3, PLD4, PRKCA, PRKCB, PTGER3, PTK2, RASGRP1, S1PR1, S1PR2, SRC, TIMD4, Tlr12, TLR3, TLR5, TLR8, TTN, VAV3, WASF2
Role of Hypercytokinemia/ Hyperchemokinemia in the Pathogenesis of Influenza	9.1	3.128	14/ 51 (27%)	4/ 51 (8%)	33/ 51 (65%)	0/ 51 (0%)	CCL2, CCL5, CXCL10, CXCL3, DDX58, EIF2AK2, IFIT2, IFIT3, IFNB1, IL10, IL18, IL33, IRF7, IRF9, OAS1, OAS2, OAS3, PYCARD, RSAD2, S1PR1, STAT1, STAT2, TLR3
Role of Pattern Recognition Receptors in Recognition of Bacteria and Viruses	7.53	2.683	36/ 108 (33%)	11/ 108 (10%)	61/ 108 (56%)	0/ 108 (0%)	C1QA, C1QB, C3, C3AR1, CCL5, CLEC6A, DDX58, EIF2AK2, IFIH1, IFNB1, IL10, IL18, IL33, IRF7, MAVS, NLRC4, NOD1, OAS1, OAS2, OAS3, PIK3C2B, PIK3CB,

							PRKCA, PRKCB, RELB, RNASEL, TLR3, TLR5, TLR8, TNFSF10, TNFSF13B, TNFSF14, TNFSF8
Granulocyte Adhesion and Diapedesis	7.25	N/A	49/ 90 (54%)	10/ 90 (11%)	31/ 90 (34%)	0/ 90 (0%)	CCL2, CCL24, CCL5, Ccl7, CCR2, CCR3, CSF3R, CXCL10, CXCL13, CXCL16, CXCL2, CXCL3, Cxcl9, CXCR4, FPR1, FPR2, IL18, IL1R2, IL1RL1, IL33, ITGA4, MMP12, MMP14, MMP2, MMP9, PECAM1, PF4, SDC3, SDC4
Agranulocyte Adhesion and Diapedesis	6.89	N/A	51/ 88 (58%)	9/ 88 (10%)	28/ 88 (32%)	0/ 88 (0%)	ACTA2, CCL2, CCL24, CCL5, Ccl7, CCR2, CCR3, CD34, CXCL10, CXCL13, CXCL16, CXCL2, CXCL3, Cxcl9, CXCR4, FN1, IL18, IL33, ITGA4, MMP12, MMP14, MMP2, MMP9, MYH10, MYO10, PECAM1, PF4, SDC4
Atherosclerosis Signalling	6.05	N/A	33/ 70 (47%)	6/ 70 (9%)	31/ 70 (44%)	0/ 70 (0%)	ALOX5, APOE, CCL2, CCR2, CCR3, CD36, CLU, CSF1, CXCR4, IL18, IL33, ITGA4, LPL, LYZ, MMP9, MSR1, PDGFC, PLA2G2D, PLA2G7, PLAAT3, RELB, TNFRSF14, TNFSF14
Breast Cancer Regulation by Stathmin1	5.75	-0.429	133/ 230 (58%)	11/ 230 (5%)	86/ 230 (37%)	0/ 230 (0%)	ADGRE5, ADGRG6, ADORA1, ADORA2B, ADORA3, ARHGEF18, C3AR1, C5AR2, CAMK2G, CCND2, CCR2, CCR3, CDK6, CNR2, CX3CR1, EDNRB, FPR1, FPR2, FZD1, GPR108, GPR155, GPR160, GPR34, GPR35, GPR68, HCAR2, HGF, IGF1, MMP2,

							MMP9, P2RY12, P2RY14, P2RY2, PAK1, PDGFC, PIK3C2B, PIK3CB, PLCB2, PLCB4, PPP1R3D, PPP2R1B, PRKCA, PRKCB, PTGER3, RPS6KA3, S1PR1, S1PR2, TUBA1A, TUBB2A, VEGFC
Crosstalk between Dendritic Cells and Natural Killer Cells	5.74	1.291	17/ 53 (32%)	6/ 53 (11%)	30/ 53 (57%)	0/ 53 (0%)	ACTA2, CAMK2G, CD28, CD80, FSCN1, HLA-DRB5, HLA-E, HLA-G, IFNB1, IL15RA, IL18, IL2RG, ITGAL, KLRD1, MICB, NECTIN2, RELB, TLR3, TNFSF10
Antigen Presentation Pathway	5.37	N/A	7/ 25 (28%)	1/ 25 (4%)	17/ 25 (68%)	0/ 25 (0%)	B2M, CD74, CIITA, HLA-DOA, HLA-DQA1, HLA-DQB1, HLA-DRB5, HLA-E, HLA-G, NLRC5, PSMB9, TAP1
Communication between Innate and Adaptive Immune Cells	5.36	N/A	15/ 51 (29%)	5/ 51 (10%)	30/ 51 (59%)	1/ 51 (2%)	B2M, CCL5, CD28, CD4, CD80, CXCL10, HLA-DRB5, HLA-E, HLA-G, IFNB1, IL10, IL18, IL33, Tlr12, TLR3, TLR5, TLR8, TNFSF13B
LXR/ RXR Activation	4.61	-0.775	26/ 62 (42%)	4/ 62 (6%)	32/ 62 (52%)	0/ 62 (0%)	APOE, C3, CCL2, CD14, CD36, CLU, IL18, IL1R2, IL1RL1, IL33, LDLR, LPL, LYZ, MMP9, MSR1, RELB, SCD, SERPINF1, TLR3
IL-15 Production	4.61	0	31/ 62 (50%)	0/ 62 (0%)	31/ 62 (50%)	0/ 62 (0%)	AATK, AXL, CSF2RA, DYRK4, ERBB4, FYN, IFNB1, IGF1R, KDR, MET, PDGFRB, PEAK1, PTK2, RELB, RYK, SRC, STAT1, TEK, TWF1
Th1 and Th2 Activation Pathway	4.38	N/A	55/ 115 (48%)	10/ 115 (9%)	49/ 115 (43%)	1/ 115 (1%)	CCR3, CD274, CD28, CD4, CD80, CXCR4, HLA-DOA, HLA-DQA1, HLA-DQB1, HLA-DRB5, ICOSLG/ LOC102723996, IL10, IL10RA, IL12RB1, IL12RB2, IL18,

							IL1RL1, IL2RG, IL33, JAG1, JAG2, KLRD1, MAF, PIK3C2B, PIK3CB, S1PR1, STAT1, TIMD4
Altered T Cell and B Cell Signalling in Rheumatoid Arthritis	4.26	N/A	22/ 60 (37%)	6/ 60 (10%)	31/ 60 (52%)	1/ 60 (2%)	CD28, CD80, CSF1, CXCL13, HLA-DOA, HLA-DQA1, HLA-DQB1, HLA-DRB5, IL10, IL18, IL33, RELB, SPP1, Tlr12, TLR3, TLR5, TLR8, TNFSF13B
Hepatic Fibrosis / Hepatic Stellate Cell Activation	4.18	N/A	72/ 130 (55%)	8/ 130 (6%)	50/ 130 (38%)	0/ 130 (0%)	ACTA2, CCL2, CCL5, CD14, COL25A1, COL6A3, COL8A1, CSF1, CXCL3, EDNRB, FGF1, FN1, HGF, IGF1, IGF1R, IL10, IL10RA, IL1R2, IL1RL1, KDR, MET, MMP2, MMP9, MYH10, MYO10, PDGFC, PDGFRB, RELB, STAT1, VEGFC
Th2 Pathway	4.05	-0.258	45/ 90 (50%)	8/ 90 (9%)	36/ 90 (40%)	1/ 90 (1%)	CCR3, CD28, CD4, CD80, CXCR4, HLA-DOA, HLA-DQA1, HLA-DQB1, HLA-DRB5, ICOSLG/ LOC102723996, IL10, IL12RB1, IL12RB2, IL1RL1, IL2RG, IL33, JAG1, JAG2, MAF, PIK3C2B, PIK3CB, S1PR1, TIMD4
Caveolar-mediated Endocytosis Signalling	3.74	N/A	21/ 44 (48%)	0/ 44 (0%)	23/ 44 (52%)	0/ 44 (0%)	ACTA2, B2M, CD48, FYN, HLA-E, HLA-G, ITGA4, ITGAL, ITGAX, ITGB3, ITGB5, ITSN1, PRKCA, SRC
CREB Signalling in Neurons	3.72	-0.905	143/ 230 (62%)	10/ 230 (4%)	77/ 230 (33%)	0/ 230 (0%)	ADCY9, ADGRE5, ADGRG6, ADORA1, ADORA2B, ADORA3, C3AR1, C5AR2, CACNA1A, CAMK2G, CCR2, CCR3, CNR2, CX3CR1, EDNRB, FPR1, FPR2, FZD1, GPR108, GPR155,

							GPR160, GPR34, GPR35, GPR68, HCAR2, HGF, IGF1, IGF1R, ITPR1, KDR, P2RY12, P2RY14, P2RY2, PDGFRB, PIK3C2B, PIK3CB, PLCB2, PLCB4, PRKCA, PRKCB, PTGER3, S1PR1, S1PR2, TNFRSF11A
Dermatan Sulfate Biosynthesis (Late Stages)	3.72	0.378	6/ 13 (46%)	1/ 13 (8%)	6/ 13 (46%)	0/ 13 (0%)	CHST15, CHST2, CHST3, CHST7, DSE, HS3ST3B1, NDST1
Graft-versus-Host Disease Signalling	3.57	N/A	11/ 26 (42%)	2/ 26 (8%)	12/ 26 (46%)	1/ 26 (4%)	CD28, CD80, HLA-DOA, HLA-DQA1, HLA-DQB1, HLA-DRB5, HLA-E, HLA-G, IL18, IL33
Sperm Motility	3.54	-0.632	64/ 109 (59%)	1/ 109 (1%)	44/ 109 (40%)	0/ 109 (0%)	AATK, AXL, CSF2RA, DYRK4, ERBB4, FYN, IGF1R, ITPR1, KDR, MET, PDGFRB, PEAK1, PLA2G2D, PLA2G7, PLAAT3, PLCB2, PLCB4, PRKCA, PRKCB, PTK2, RYK, SLC12A2, SRC, TEK, TWF1
TREM1 Signalling	3.48	-0.258	22/ 57 (39%)	0/ 57 (0%)	35/ 57 (61%)	0/ 57 (0%)	CCL2, CIITA, CXCL3, IL10, IL18, IL1RL1, ITGAX, NLRC4, NLRC5, NOD1, RELB, SIGIRR, Tlr12, TLR3, TLR5, TLR8
Clathrin-mediated Endocytosis Signalling	3.46	N/A	67/ 104 (64%)	4/ 104 (4%)	33/ 104 (32%)	0/ 104 (0%)	ACTA2, AP2A2, APOE, CLTC, CLU, CTTN, DAB2, FGF1, HIP1, IGF1, ITGB3, ITGB5, LDLR, LDLRAP1, LYZ, MET, MYO1E, NUMB, PDGFC, PIK3C2B, PIK3CB, SRC, TFRC, VEGFC
Chondroitin Sulfate Biosynthesis (Late Stages)	3.46	0.378	7/ 14 (50%)	1/ 14 (7%)	6/ 14 (43%)	0/ 14 (0%)	CHST15, CHST2, CHST3, CHST7, CHSY1, HS3ST3B1, NDST1
T Helper Cell Differentiation	3.44	N/A	21/ 52 (40%)	5/ 52 (10%)	25/ 52 (48%)	1/ 52 (2%)	CD28, CD80, HLA-DOA, HLA-DQA1, HLA-DQB1, HLA-DRB5, ICOSLG/ LOC102723996,

							IL10, IL10RA, IL12RB1, IL12RB2, IL18, IL2RG, IL6ST, STAT1
Macropinocytosis Signalling	3.44	0.632	28/ 52 (54%)	0/ 52 (0%)	24/ 52 (46%)	0/ 52 (0%)	CD14, CSF1, HGF, ITGB3, ITGB5, MET, MRC1, PAK1, PDGFC, PIK3C2B, PIK3CB, PRKCA, PRKCB, RAB34, SRC
Allograft Rejection Signalling	3.41	N/A	9/ 27 (33%)	5/ 27 (19%)	12/ 27 (44%)	1/ 27 (4%)	B2M, CD28, CD80, HLA-DOA, HLA-DQA1, HLA-DQB1, HLA-DRB5, HLA-E, HLA-G, IL10
Osteoarthritis Pathway	3.29	-1.706	69/ 132 (52%)	9/ 132 (7%)	53/ 132 (40%)	1/ 132 (1%)	ANKH, BMP2, CASP4, CEBPB, EPAS1, FN1, FZD1, IL1R2, IL1RL1, ITGA4, ITGAL, ITGAX, ITGB3, ITGB5, JAG1, LRP1, MMP12, MMP9, NAMPT, PDGFC, PRKAB1, RELB, RUNX2, S1PR2, SDC4, SIK3, SPP1, VEGFC
Tumor Microenvironment Pathway	3.29	-1.633	61/ 113 (54%)	7/ 113 (6%)	45/ 113 (40%)	0/ 113 (0%)	CCL2, CD274, CD44, CSF1, CSPG4, CXCR4, FGF1, FN1, HGF, HLA-E, HLA-G, IGF1, IL10, ITGB3, MMP12, MMP14, MMP2, MMP9, PDGFC, PIK3C2B, PIK3CB, RELB, SLC2A1, SPP1, VEGFC
Axonal Guidance Signalling	3.26	N/A	137/ 220 (62%)	7/ 220 (3%)	76/ 220 (35%)	0/ 220 (0%)	ADAM22, BAIAP2, BMP1, BMP2, CXCR4, DOCK1, EFNB1, EFNB3, EPHB6, FYN, FZD1, IGF1, ITGA4, ITGAL, ITGAX, ITGB3, ITGB5, ITSN1, MET, MMP12, MMP14, MMP2, MMP9, PAK1, PDGFC, PIK3C2B, PIK3CB, PLCB2, PLCB4, PLXNA1, PLXND1, PRKCA, PRKCB, PTK2, RGS3, SEMA6D, SLIT1, TUBA1A, TUBB2A, UNC5B, VEGFC

Leukocyte Extravasation Signalling	3.19	-0.218	61/ 102 (60%)	5/ 102 (5%)	36/ 102 (35%)	0/ 102 (0%)	ACTA2, ACTN1, CD44, CTTN, CXCR4, CYBB, EDIL3, ITGA4, ITGAL, MMP12, MMP14, MMP2, MMP9, PECAM1, PIK3C2B, PIK3CB, PRKCA, PRKCB, PTK2, RASGRP1, SRC, TIMP4, VAV3
Autoimmune Thyroid Disease Signalling	3.16	N/A	8/ 24 (33%)	4/ 24 (17%)	11/ 24 (46%)	1/ 24 (4%)	CD28, CD80, HLA-DOA, HLA-DQA1, HLA-DQB1, HLA-DRB5, HLA-E, HLA-G, IL10
NUR77 Signalling in T Lymphocytes	3.1	-0.378	23/ 50 (46%)	1/ 50 (2%)	25/ 50 (50%)	1/ 50 (2%)	B2M, CD28, CD80, HDAC7, HLA-DOA, HLA-DQA1, HLA-DQB1, HLA-DRB5, HLA-E, HLA-G, PRKCA, PRKCB, RPS6KA3, TNFSF10
LPS/ IL-1 Mediated Inhibition of RXR Function	3.09	-0.816	49/ 110 (45%)	5/ 110 (5%)	56/ 110 (51%)	0/ 110 (0%)	ACSL3, ALDH1A1, ALDH1A2, ALDH1L1, ALDH1L2, ALDH7A1, APOE, CD14, CHST15, CHST2, CHST3, CHST7, GSTO1, HMGCS1, HS3ST3B1, IL18, IL1R2, IL1RL1, IL33, MAOA, NDST1, PPARGC1B, SCARB1, SLC27A1
Actin Cytoskeleton Signalling	2.99	-1	72/ 118 (61%)	1/ 118 (1%)	45/ 118 (38%)	0/ 118 (0%)	ABI2, ACTA2, ACTN1, BAIAP2, CD14, DOCK1, FGF1, FN1, IQGAP2, ITGA4, ITGAL, ITGAX, ITGB3, ITGB5, MYH10, MYO10, PAK1, PDGFC, PIK3C2B, PIK3CB, PTK2, SSH3, TTN, VAV3, WASF2
Virus Entry via Endocytic Pathways	2.95	N/A	35/ 63 (56%)	0/ 63 (0%)	28/ 63 (44%)	0/ 63 (0%)	ACTA2, AP2A2, B2M, CLTC, FYN, HLA-E, HLA-G, ITGB3, ITGB5, ITSN1, PIK3C2B, PIK3CB, PRKCA, PRKCB, SRC, TFRC
Systemic Lupus Erythematosus In B	2.95	1.768	70/ 172 (41%)	11/ 172 (6%)	91/ 172 (53%)	0/ 172 (0%)	CCND2, CD22, FYN, GAB1, IFIH1, IFIT2,

Cell Signalling Pathway							IFIT3, IFNB1, IL10, IL18, IL33, IL6ST, IRF7, IRF9, LILRB3, LILRB4, MAVS, PIK3C2B, PIK3CB, PRKCA, PRKCB, RASGRP1, RELB, SRC, STAT1, STAT2, SYNJ2, TLR3, TLR8, TNFSF10, TNFSF13B, TNFSF14, TNFSF8
Neuroinflammation Signalling Pathway	2.95	1.3	83/ 179 (46%)	6/ 179 (3%)	90/ 179 (50%)	0/ 179 (0%)	B2M, BIRC2, CCL2, CCL5, CD200R1, CD80, CX3CR1, CXCL10, CYBB, FZD1, HLA-DOA, HLA-DQA1, HLA-DQB1, HLA-DRB5, HLA-E, HLA-G, IFNB1, IL10, IL18, IRAK3, IRF7, MMP9, PIK3C2B, PIK3CB, PLA2G2D, PYCARD, RELB, SLC1A2, SLC1A3, STAT1, Tlr12, TLR3, TLR5, TLR8
Dermatan Sulfate Biosynthesis	2.92	0	10/ 21 (48%)	1/ 21 (5%)	10/ 21 (48%)	0/ 21 (0%)	CHST15, CHST2, CHST3, CHST7, CHSY1, DSE, HS3ST3B1, NDST1
Interferon Signalling	2.87	2.828	4/ 26 (15%)	1/ 26 (4%)	20/ 26 (77%)	1/ 26 (4%)	IFIT1, IFIT3, IFITM3, IFNB1, IRF9, OAS1, STAT1, STAT2, TAP1
B Cell Development	2.8	N/A	6/ 13 (46%)	0/ 13 (0%)	7/ 13 (54%)	0/ 13 (0%)	CD80, HLA-DOA, HLA-DQA1, HLA-DQB1, HLA-DRB5, IL7R
T Cell Exhaustion Signalling Pathway	2.75	2	50/ 103 (49%)	2/ 103 (2%)	50/ 103 (49%)	1/ 103 (1%)	CD274, CD28, CD80, HLA-DOA, HLA-DQA1, HLA-DQB1, HLA-DRB5, HLA-E, HLA-G, IL10, IL10RA, IL12RB1, IL12RB2, IRF9, KDR, PIK3C2B, PIK3CB, PPP2R1B, PRDM1, STAT1, STAT2, TNFRSF14
Activation of IRF by Cytosolic Pattern Recognition Receptors	2.72	2.714	14/ 43 (33%)	0/ 43 (0%)	29/ 43 (67%)	0/ 43 (0%)	DDX58, IFIH1, IFIT2, IFNB1, IL10, IRF7, IRF9, MAVS, RELB, STAT1, STAT2, TANK
VDR/ RXR Activation	2.63	-0.333	23/ 44 (52%)	5/ 44 (11%)	16/ 44 (36%)	0/ 44 (0%)	CCL5, CD14, CDKN1A, CEBPA,

							CEBPB, CXCL10, IL1RL1, PRKCA, PRKCB, RUNX2, SPP1, THBD
Calcium-induced T Lymphocyte Apoptosis	2.62	-1	17/ 28 (61%)	0/ 28 (0%)	10/ 28 (36%)	1/ 28 (4%)	CAPN2, CD4, HLA-DOA, HLA-DQA1, HLA-DQB1, HLA-DRB5, ITPR1, PRKCA, PRKCB
G-Protein Coupled Receptor Signalling	2.61	-0.438	162/ 281 (58%)	9/ 281 (3%)	110/ 281 (39%)	0/ 281 (0%)	ADCY9, ADGRE5, ADGRG6, ADORA1, ADORA2B, ADORA3, C3AR1, C5AR2, CAMK2G, CCR2, CCR3, CNR2, CX3CR1, EDNRB, FPR1, FPR2, FYN, FZD1, GDE1, GPR108, GPR155, GPR160, GPR34, GPR35, GPR68, GRK3, HCAR2, MAP3K5, P2RY12, P2RY14, P2RY2, PAK1, PIK3C2B, PIK3CB, PLCB2, PLCB4, PRKCA, PRKCB, PTGER3, PTK2, RASGRP1, RELB, RGS18, S1PR1, S1PR2, SRC, TTN
Th1 Pathway	2.54	1.5	31/ 81 (38%)	6/ 81 (7%)	43/ 81 (53%)	1/ 81 (1%)	CD274, CD28, CD4, CD80, HLA-DOA, HLA-DQA1, HLA-DQB1, HLA-DRB5, ICOSLG/ LOC102723996, IL10, IL10RA, IL12RB1, IL12RB2, IL18, KLRD1, PIK3C2B, PIK3CB, STAT1
Xenobiotic Metabolism CAR Signalling Pathway	2.51	-0.5	39/ 69 (57%)	2/ 69 (3%)	28/ 69 (41%)	0/ 69 (0%)	ALDH1A1, ALDH1A2, ALDH1L1, ALDH1L2, ALDH7A1, CHST15, CHST2, CHST3, CHST7, GSTO1, HS3ST3B1, NDST1, PPP2R1B, PRKCA, PRKCB, SRC
Chondroitin Sulfate Biosynthesis	2.51	0.378	9/ 19 (47%)	1/ 19 (5%)	9/ 19 (47%)	0/ 19 (0%)	CHST15, CHST2, CHST3, CHST7, CHSY1, HS3ST3B1, NDST1

Xenobiotic Metabolism PXR Signalling Pathway	2.46	0.243	43/ 76 (57%)	2/ 76 (3%)	31/ 76 (41%)	0/ 76 (0%)	ALDH1A1, ALDH1A2, ALDH1L1, ALDH1L2, ALDH7A1, CAMK2G, CHST15, CHST2, CHST3, CHST7, GSTO1, HS3ST3B1, MAOA, NDST1, PPP1R3D, PRKCA, PRKCB
CDC42 Signalling	2.42	0.447	42/ 83 (51%)	0/ 83 (0%)	40/ 83 (48%)	1/ 83 (1%)	B2M, BAIAP2, EXOC5, EXOC6, HLA-DOA, HLA-DQA1, HLA-DQB1, HLA-DRB5, HLA-E, HLA-G, IQGAP2, ITGA4, ITGAL, ITGAX, ITGB3, ITGB5, PAK1, SRC
Complement System	2.42	2	7/ 15 (47%)	0/ 15 (0%)	8/ 15 (53%)	0/ 15 (0%)	C1QA, C1QB, C2, C3, C3AR1, ITGAX
TEC Kinase Signalling	2.38	-0.258	54/ 110 (49%)	1/ 110 (1%)	54/ 110 (49%)	1/ 110 (1%)	ACTA2, FYN, ITGA4, ITGAL, ITGAX, ITGB3, ITGB5, PAK1, PIK3C2B, PIK3CB, PRKCA, PRKCB, PTK2, RELB, RHOBTB1, RHOC, RND3, SRC, STAT1, STAT2, TNFSF10, VAV3
CTLA4 Signalling in Cytotoxic T Lymphocytes	2.37	N/A	24/ 47 (51%)	0/ 47 (0%)	22/ 47 (47%)	1/ 47 (2%)	AP2A2, B2M, CD28, CD80, CLTC, FYN, HLA-E, HLA-G, PIK3C2B, PIK3CB, PPP2R1B, PTPN22
ILK Signalling	2.19	-1.5	65/ 107 (61%)	1/ 107 (1%)	40/ 107 (37%)	1/ 107 (1%)	ACTA2, ACTN1, BMP2, DOCK1, FN1, IRS2, ITGB3, ITGB5, MMP9, MYH10, MYO10, PDGFC, PIK3C2B, PIK3CB, PPP2R1B, PTK2, RELB, RHOBTB1, RHOC, RND3, VEGFC
Role of Macrophages, Fibroblasts and Endothelial Cells in Rheumatoid Arthritis	2.19	N/A	90/ 184 (49%)	7/ 184 (4%)	87/ 184 (47%)	0/ 184 (0%)	CAMK2G, CCL2, CCL5, CEBPA, CEBPB, CSF1, FCGR3A/ FCGR3B, FN1, FZD1, IL10, IL18, IL1R2, IL1RL1, IL33, IL6ST, IRAK3, LRP1, PDGFC, PIK3C2B, PIK3CB, PLCB2,

							PLCB4, PRKCA, PRKCB, RYK, SRC, Tlr12, TLR3, TLR5, TLR8, TNFSF13B, VEGFC
Role of RIG1-like Receptors in Antiviral Innate Immunity	2.14	2.646	4/ 27 (15%)	0/ 27 (0%)	22/ 27 (81%)	1/ 27 (4%)	DDX58, IFIH1, IFNB1, IRF7, MAVS, RELB, TANK, TRIM25
Histamine Degradation	2.14	-2	5/ 8 (63%)	0/ 8 (0%)	3/ 8 (38%)	0/ 8 (0%)	ALDH1A1, ALDH1A2, ALDH7A1, HNMT
Dendritic Cell Maturation	2.05	1.279	42/ 117 (36%)	3/ 117 (3%)	71/ 117 (61%)	1/ 117 (1%)	B2M, CD80, FCGR3A/ FCGR3B, FSCN1, HLA-DOA, HLA-DQA1, HLA-DQB1, HLA-DRB5, HLA-E, HLA-G, IFNB1, IL10, IL18, IL33, PIK3C2B, PIK3CB, PLCB2, PLCB4, RELB, STAT1, STAT2, TLR3
HGF Signalling	1.99	0.277	52/ 91 (57%)	0/ 91 (0%)	39/ 91 (43%)	0/ 91 (0%)	CDKN1A, DOCK1, ETS1, GAB1, HGF, ITGA4, ITGAL, ITGAX, ITGB3, ITGB5, MAP3K5, MET, PAK1, PIK3C2B, PIK3CB, PRKCA, PRKCB, PTK2
Sphingosine-1-phosphate Signalling	1.97	-1.387	37/ 65 (57%)	0/ 65 (0%)	27/ 65 (42%)	1/ 65 (2%)	ADCY9, CASP4, PDGFC, PDGFRB, PIK3C2B, PIK3CB, PLCB2, PLCB4, PTK2, RHOBTB1, RHOC, RND3, S1PR1, S1PR2
Integrin Signalling	1.96	-0.894	80/ 126 (63%)	1/ 126 (1%)	45/ 126 (36%)	0/ 126 (0%)	ACTA2, ACTN1, ARHGAP26, CAPN2, CTTN, DOCK1, FYN, ITGA4, ITGAL, ITGAX, ITGB3, ITGB5, NEDD9, PAK1, PIK3C2B, PIK3CB, PTK2, RHOBTB1, RHOC, RND3, SRC, TSPAN2, TTN
OX40 Signalling Pathway	1.92	N/A	11/ 35 (31%)	1/ 35 (3%)	22/ 35 (63%)	1/ 35 (3%)	B2M, CD4, HLA-DOA, HLA-DQA1, HLA-DQB1, HLA-DRB5, HLA-E, HLA-G, RELB
Gustation Pathway	1.91	-0.535	38/ 66 (58%)	4/ 66 (6%)	24/ 66 (36%)	0/ 66 (0%)	ADCY9, CACNA1A, CD36, ITPR1, LPL, P2RX1, P2RX4, P2RY12, P2RY14, P2RY2, PLCB2,

							SCN3B, SCN8A, TRPM4
TR/ RXR Activation	1.91	N/A	22/ 41 (54%)	1/ 41 (2%)	18/ 41 (44%)	0/ 41 (0%)	COL6A3, LDLR, PIK3C2B, PIK3CB, SCARB1, SLC2A1, SREBF2, THRA, THRB, UCP2
Ascorbate Recycling (Cytosolic)	1.91	N/A	0/ 2 (0%)	0/ 2 (0%)	2/ 2 (100%)	0/ 2 (0%)	GLRX, GSTO1
STAT3 Pathway	1.89	-0.707	53/ 93 (57%)	1/ 93 (1%)	39/ 93 (42%)	0/ 93 (0%)	CDKN1A, HGF, IGF1, IGF1R, IL10RA, IL12RB1, IL12RB2, IL15RA, IL1R2, IL1RL1, IL2RG, IL6ST, IL7R, KDR, PDGFRB, PIM1, SRC, TNFRSF11A
Inhibition of Matrix Metalloproteases	1.89	0.447	15/ 24 (63%)	4/ 24 (17%)	5/ 24 (21%)	0/ 24 (0%)	HSPG2, LRP1, MMP12, MMP14, MMP2, MMP9, TIMP4
Necroptosis Signalling Pathway	1.87	2	30/ 80 (38%)	3/ 80 (4%)	46/ 80 (57%)	1/ 80 (1%)	AXL, BIRC2, CAMK2G, CAPN2, CYBB, EIF2AK2, IFNB1, IRF9, PELI1, PLA2G2D, PYCARD, STAT1, STAT2, TLR3, TNFSF10, TSPO
Airway Pathology in Chronic Obstructive Pulmonary Disease	1.85	N/A	16/ 48 (33%)	14/ 48 (29%)	18/ 48 (38%)	0/ 48 (0%)	CCL2, CXCL3, FGF1, IL18, IL33, MMP2, MMP9, TNFSF10, TNFSF13B, TNFSF14, TNFSF8
Systemic Lupus Erythematosus In T Cell Signalling Pathway	1.84	-0.209	73/ 129 (57%)	3/ 129 (2%)	51/ 129 (40%)	2/ 129 (2%)	B2M, CASP4, CD28, CD44, CD80, CREM, HLA-DOA, HLA-DQA1, HLA-DQB1, HLA-DRB5, HLA-E, HLA-G, ICOSLG/ LOC102723996, IL10, ITGAL, ITPR1, PIK3C2B, PIK3CB, PPP2R1B, PTK2, RHOBTB1, RHOC, RND3
Chemokine Signalling	1.8	0	35/ 55 (64%)	0/ 55 (0%)	20/ 55 (36%)	0/ 55 (0%)	CAMK2G, CCL2, CCL24, CCL5, CCR3, CXCR4, PLCB2, PLCB4, PRKCA, PRKCB, PTK2, SRC
ICOS-ICOSL Signalling in T Helper Cells	1.8	0	31/ 68 (46%)	2/ 68 (3%)	34/ 68 (50%)	1/ 68 (1%)	CAMK2G, CD28, CD4, CD80, HLA-DOA, HLA-DQA1, HLA-DQB1, HLA-DRB5, ICOSLG/ LOC102723996, IL2RG, ITPR1,

							PIK3C2B, PIK3CB, RELB
Glioma Invasiveness Signalling	1.78	-0.632	32/ 49 (65%)	0/ 49 (0%)	17/ 49 (35%)	0/ 49 (0%)	CD44, ITGB3, MMP2, MMP9, PIK3C2B, PIK3CB, PTK2, RHOBTB1, RHOC, RND3, TIMP4
Phospholipases	1.69	0	13/ 26 (50%)	0/ 26 (0%)	13/ 26 (50%)	0/ 26 (0%)	LPL, PLA2G2D, PLA2G7, PLAAT3, PLCB2, PLCB4, PLD4
FAK Signalling	1.68	N/A	46/ 77 (60%)	1/ 77 (1%)	30/ 77 (39%)	0/ 77 (0%)	ACTA2, ARHGAP26, CAPN2, DOCK1, FYN, ITGA4, ITGAL, ITGAX, ITGB3, ITGB5, PAK1, PIK3C2B, PIK3CB, PTK2, SRC
Semaphorin Neuronal Repulsive Signalling Pathway	1.68	-1.807	49/ 84 (58%)	0/ 84 (0%)	35/ 84 (42%)	0/ 84 (0%)	BCAN, CD44, CSPG4, FARP1, FYN, ITGA4, ITGAL, ITGAX, ITGB3, ITGB5, PAK1, PIK3C2B, PIK3CB, PLXNA1, PLXND1, SEMA6D
CXCR4 Signalling	1.67	0.5	59/ 98 (60%)	0/ 98 (0%)	39/ 98 (40%)	0/ 98 (0%)	ADCY9, CD4, CXCR4, DOCK1, ELMO2, ITPR1, PAK1, PIK3C2B, PIK3CB, PLCB2, PLCB4, PRKCA, PRKCB, PTK2, RHOBTB1, RHOC, RND3, SRC
Cardiac Hypertrophy Signalling (Enhanced)	1.66	-0.174	147/ 285 (52%)	12/ 285 (4%)	126/ 285 (44%)	0/ 285 (0%)	ADCY9, CACNA1A, CAMK2G, CYBB, EDNRB, FGF1, FZD1, GDE1, HDAC7, IGF1, IGF1R, IL10RA, IL12RB1, IL12RB2, IL15RA, IL18, IL1R2, IL1RL1, IL2RG, IL33, IL6ST, IL7R, ITGA4, ITGAL, ITGAX, ITGB3, ITGB5, ITPR1, MAP3K5, MAPKAPK3, PIK3C2B, PIK3CB, PLCB2, PLCB4, PRKCA, PRKCB, PTK2, RCAN1, RELB, TNFSF10, TNFSF13B, TNFSF14, TNFSF8
Heparan Sulfate Biosynthesis (Late Stages)	1.64	0.816	9/ 21 (43%)	2/ 21 (10%)	10/ 21 (48%)	0/ 21 (0%)	CHST15, CHST2, CHST3, CHST7,

							HS3ST3B1, NDST1
FXR/ RXR Activation	1.63	N/A	25/ 45 (56%)	6/ 45 (13%)	14/ 45 (31%)	0/ 45 (0%)	ABCB4, APOE, C3, CLU, IL18, IL33, LPL, SCARB1, SERPINF1, VLDLR
Glioblastoma Multiforme Signalling	1.63	-0.535	50/ 92 (54%)	0/ 92 (0%)	42/ 92 (46%)	0/ 92 (0%)	CCND2, CDK6, CDKN1A, FZD1, IGF1, IGF1R, ITPR1, PDGFC, PDGFRB, PIK3C2B, PIK3CB, PLCB2, PLCB4, RHOBTB1, RHOC, RND3, SRC
Role of Osteoblasts, Osteoclasts and Chondrocytes in Rheumatoid Arthritis	1.61	N/A	67/ 121 (55%)	7/ 121 (6%)	47/ 121 (39%)	0/ 121 (0%)	BIRC2, BMP1, BMP2, CSF1, FZD1, IGF1, IL10, IL18, IL1R2, IL1RL1, IL33, ITGB3, LRP1, MAP3K5, MMP14, PIK3C2B, PIK3CB, RUNX2, SPP1, SRC, TNFRSF11A
Paxillin Signalling	1.6	0	40/ 72 (56%)	0/ 72 (0%)	32/ 72 (44%)	0/ 72 (0%)	ACTA2, ACTN1, DOCK1, ITGA4, ITGAL, ITGAX, ITGB3, ITGB5, PAK1, PIK3C2B, PIK3CB, PTK2, PTPN12, SRC
PD-1, PD-L1 cancer immunotherapy pathway	1.6	-0.535	29/ 72 (40%)	4/ 72 (6%)	38/ 72 (53%)	1/ 72 (1%)	B2M, CD274, CD28, CD80, HLA-DOA, HLA-DQA1, HLA-DQB1, HLA-DRB5, HLA-E, HLA-G, IL2RG, PIK3C2B, PIK3CB, RASGRP1
Phospholipase C Signalling	1.59	-1.069	75/ 136 (55%)	1/ 136 (1%)	59/ 136 (43%)	1/ 136 (1%)	ADCY9, AHNAK, ARHGEF18, FYN, HDAC7, ITGA4, ITGAL, ITGAX, ITGB3, ITGB5, ITPR1, PLA2G2D, PLCB2, PLCB4, PLD4, PRKCA, PRKCB, RELB, RHOBTB1, RHOC, RND3, RPS6KA3, SRC
Tryptophan Degradation X (Mammalian, via Tryptamine)	1.58	-2	6/ 11 (55%)	0/ 11 (0%)	5/ 11 (45%)	0/ 11 (0%)	ALDH1A1, ALDH1A2, ALDH7A1, MAOA
Putrescine Degradation III	1.58	-2	7/ 11 (64%)	0/ 11 (0%)	4/ 11 (36%)	0/ 11 (0%)	ALDH1A1, ALDH1A2, ALDH7A1, MAOA
Regulation of Cellular Mechanics by Calpain Protease	1.54	-1	30/ 53 (57%)	2/ 53 (4%)	21/ 53 (40%)	0/ 53 (0%)	ACTN1, CAPN2, CCND2, CDK6, ITGA4, ITGAL,

							ITGAX, ITGB3, ITGB5, PTK2, SRC
Amyotrophic Lateral Sclerosis Signalling	1.51	0	35/ 67 (52%)	3/ 67 (4%)	29/ 67 (43%)	0/ 67 (0%)	BIRC2, CACNA1A, CAPN2, IGF1, NEFH, NEFL, PAK1, PDGFC, PIK3C2B, PIK3CB, SLC1A2, SOD1, VEGFC
PKCθ Signalling in T Lymphocytes	1.5	-0.832	42/ 88 (48%)	1/ 88 (1%)	44/ 88 (50%)	1/ 88 (1%)	CACNA1A, CAMK2G, CD28, CD4, CD80, FYN, HLA-DOA, HLA-DQA1, HLA-DQB1, HLA-DRB5, ITPR1, MAP3K5, PIK3C2B, PIK3CB, RELB, VAV3
Glioma Signalling	1.5	-1	45/ 81 (56%)	0/ 81 (0%)	36/ 81 (44%)	0/ 81 (0%)	CAMK2G, CCND2, CDK6, CDKN1A, HDAC7, IDH1, IDH2, IGF1, IGF1R, PDGFC, PDGFRB, PIK3C2B, PIK3CB, PRKCA, PRKCB
PI3K/ AKT Signalling	1.5	0	62/ 124 (50%)	1/ 124 (1%)	61/ 124 (49%)	0/ 124 (0%)	CDKN1A, GAB1, IL10RA, IL12RB1, IL12RB2, IL15RA, IL1R2, IL1RL1, IL2RG, IL6ST, IL7R, ITGA4, ITGAL, ITGAX, ITGB3, ITGB5, MAP3K5, PIK3CB, PPP2R1B, RELB, SYNJ2
NF-κB Signalling	1.5	0.894	59/ 124 (48%)	2/ 124 (2%)	62/ 124 (50%)	1/ 124 (1%)	BMP2, EIF2AK2, IGF1R, IL18, IL1R2, IL33, IRAK3, KDR, PDGFRB, PELI1, PIK3C2B, PIK3CB, PRKCB, RELB, SIGIRR, TANK, TLR3, TLR5, TLR8, TNFRSF11A, TNFSF13B
Toll-like Receptor Signalling	1.49	-0.333	22/ 54 (41%)	1/ 54 (2%)	31/ 54 (57%)	0/ 54 (0%)	CD14, EIF2AK2, IL18, IL1RL1, IL33, IRAK3, RELB, SIGIRR, TLR3, TLR5, TLR8
Ephrin B Signalling	1.48	-1	29/ 41 (71%)	0/ 41 (0%)	12/ 41 (29%)	0/ 41 (0%)	CXCR4, EFNB1, EFNB3, EPHB6, ITSN1, PAK1, PTK2, RGS3, VAV3
Pulmonary Healing Signalling Pathway	1.48	-0.688	67/ 110 (61%)	5/ 110 (5%)	38/ 110 (35%)	0/ 110 (0%)	CHRNA7, CXCR4, FYN, FZD1, IDH2, JAG1, KDR, MMP12, MMP14, MMP2,

							MMP9, PDGFC, PECAM1, PRKAB1, PRKCA, PRKCB, SRC, THBS1, VEGFC
Oleate Biosynthesis II (Animals)	1.47	N/A	3/ 3 (100%)	0/ 3 (0%)	0/ 3 (0%)	0/ 3 (0%)	SCD, Scd2
Semaphorin Signalling in Neurons	1.46	N/A	25/ 35 (71%)	0/ 35 (0%)	10/ 35 (29%)	0/ 35 (0%)	FYN, MET, PAK1, PLXNA1, PTK2, RHOBTB1, RHOC, RND3
Natural Killer Cell Signalling	1.46	1.147	48/ 118 (41%)	4/ 118 (3%)	66/ 118 (56%)	0/ 118 (0%)	B2M, CD48, FCGR3A/ FCGR3B, FYN, HLA-E, HLA-G, IL12RB1, IL12RB2, IL18, ITGAL, KLRD1, MAP3K5, MICB, NECTIN2, PAK1, PIK3C2B, PIK3CB, RELB, TNFSF10, VAV3
Dopamine Degradation	1.44	-2	6/ 12 (50%)	1/ 12 (8%)	5/ 12 (42%)	0/ 12 (0%)	ALDH1A1, ALDH1A2, ALDH7A1, MAOA
Xenobiotic Metabolism Signalling	1.43	N/A	71/ 141 (50%)	3/ 141 (2%)	67/ 141 (48%)	0/ 141 (0%)	AHR, ALDH1A1, ALDH1A2, ALDH1L1, ALDH1L2, ALDH7A1, CAMK2G, CHST15, CHST2, CHST3, CHST7, GSTO1, HS3ST3B1, MAF, MAOA, MAP3K5, NDST1, PIK3C2B, PIK3CB, PPP2R1B, PRKCA, PRKCB, RELB
Growth Hormone Signalling	1.42	1.134	23/ 42 (55%)	0/ 42 (0%)	18/ 42 (43%)	1/ 42 (2%)	CEBPA, IGF1, IGF1R, PIK3C2B, PIK3CB, PRKCA, PRKCB, RPS6KA3, STAT1
Role of MAPK Signalling in Inhibiting the Pathogenesis of Influenza	1.4	1.265	26/ 49 (53%)	1/ 49 (2%)	22/ 49 (45%)	0/ 49 (0%)	CCL2, CCL5, CXCL10, EIF2AK2, IFNB1, MAP3K5, PLA2G2D, PLA2G7, PLAAT3, RPS6KA3
IL-12 Signalling and Production in Macrophages	1.38	N/A	34/ 84 (40%)	5/ 84 (6%)	45/ 84 (54%)	0/ 84 (0%)	APOE, CEBPB, CLU, IL10, IL12RB1, IL12RB2, IL18, LYZ, MAF, PIK3C2B, PIK3CB, PRKCA, PRKCB, RELB, STAT1
Role of PKR in Interferon Induction and Antiviral Response	1.38	2.309	35/ 84 (42%)	2/ 84 (2%)	47/ 84 (56%)	0/ 84 (0%)	DDX58, EIF2AK2, IFIH1, IFNB1, IL18, IRF9, MAVS, MSR1, PDGFC, PDGFRB,

							PYCARD, RELB, STAT1, STAT2, TLR3
IL-8 Signalling	1.35	0.218	70/ 136 (51%)	2/ 136 (1%)	64/ 136 (47%)	0/ 136 (0%)	CCND2, CYBB, IRAK3, ITGAX, ITGB3, KDR, MMP2, MMP9, PDGFC, PIK3C2B, PIK3CB, PLCB2, PLD4, PRKCA, PRKCB, PTK2, RHOBTB1, RHOC, RND3, SRC, TEK, VEGFC
Type II Diabetes Mellitus Signalling	1.34	0.333	38/ 85 (45%)	1/ 85 (1%)	46/ 85 (54%)	0/ 85 (0%)	ACSL3, CACNA1A, CD36, CEBPB, IRS2, ITPR1, MAP3K5, NSMAF, PIK3C2B, PIK3CB, PRKAB1, PRKCA, PRKCB, RELB, SLC27A1
Antioxidant Action of Vitamin C	1.33	-0.378	25/ 57 (44%)	0/ 57 (0%)	32/ 57 (56%)	0/ 57 (0%)	CSF2RA, GLRX, GSTO1, PLA2G2D, PLA2G7, PLAAT3, PLCB2, PLCB4, PLD4, RELB, SLC2A1
Cholecystokinin/ Gastrin-mediated Signalling	1.33	-0.577	49/ 71 (69%)	0/ 71 (0%)	22/ 71 (31%)	0/ 71 (0%)	CREM, IL18, IL33, ITPR1, PLCB2, PLCB4, PRKCA, PRKCB, PTK2, RHOBTB1, RHOC, RND3, SRC
Fatty Acid α-oxidation	1.3	N/A	5/ 8 (63%)	0/ 8 (0%)	3/ 8 (38%)	0/ 8 (0%)	ALDH1A1, ALDH1A2, ALDH7A1

Appendix VI Cannonical Pathway Analysis from IPA of edgeR analysis of Naïve Microglia

Appendix VII

Upstream Regulator	Expr Log Ratio	Predicted Activation State	Activation z-score	p-value Overlap	Target Molecules in Dataset
IL10RA	0.451	Inhibited	-6.605	6.26E-25	ADD3, ALOX5, ANKH, B3GNT7, BMP2, C3, CA2, CALHM6, CCL5, Cd24a, CD300LF, CD34, CD36, CLCN7, CLEC12A, CLEC4M, COL14A1, CSF3R, CST7, Cxcl9, EDNRB, F13A1, FN1, FOLR2, GAS6, GBP2, GSAP, HCAR2, HPSE, IFI16, IL12RB1, IL15RA, IL2RG, IRF7, KITLG, Ly6a (includes others), NAMPT, NLRC5, NOD1, NPL, OLR1, PF4, PLAAT3, PSMB9, REPS2, Retnla, RGS18, RNF213, RSAD2, S1PR1, SERPINB9, SLAMF6, SLAMF8, SLC2A1, SPARC, STARD8, STAT1, TAP1, TFEC, TNFRSF14, TRPM2, ZC3H12C
IFNG	0	Activated	3.274	9.57E-24	ADORA2B, C2, CARD6, CCL5, Ccl7, CCND2, CCR2, CD274, CD44, CD74, CD80, CDKN1A, CHST3, CHST7, CIITA, CLEC10A, CMPK2, CSF1, CXCL10, CXCL2, Cxcl9, CXCR4, CYRIA, DAXX, DDX58, ENDOD1, FGF1, FMNL2, FN1, GBP2, HCAR2, HIP1, HLA-DOA, HLA-DQA1, HLA-DQB1, HLA-DRB5, ICOSLG/LOC102723996, IFI16, IFI44, IFIH1, IFIT1B, IFIT2, IFIT3, IFNB1, IFRD1, IGF1, IL10, ITGAL, ITPR1, LDLR, Ly6a (includes others), MARCKSL1, MRC1, OAS1, OAS3, OASL, P2RY14, PDGFC, PIM1, PML, PRDM1, Retnla, RSAD2, RTP4, SLC2A1, STAT1, TAP1, THBS1, XAF1
PTGER4	-0.122	Inhibited	-5.162	1.33E-17	CCL2, Ccl7, CDK6, CMPK2, CXCL10, Cxcl9, CXCR4, CYBB, CYRIA, DAXX, DDX58, GAB1, GBP2, GLIS3, HCAR2, HERC6, HGF, IFI16, IFIH1, IFIT1B, IFIT2, IL18, IRF7, OLR1, PARP14, RNASEL, RNF144B, RNF213, RSAD2, RTP4, S1PR1, SLAMF8, SLFN5, ST6GAL1, ST8SIA4, TBC1D4, TLR8, TNFSF10, TOR3A, USP18, XAF1
CITED2	-0.12	Inhibited	-5.057	1.78E-17	B2M, BBX, C3, CALHM6, CD274, CD80, CLEC10A, CMPK2, CPEB4, CXCL10, CXCL2, CXCL3, Cxcl9, CYBB, CYRIA, DAXX, DDX58, DTX3L, ENDOD1, FCGR3A/FCGR3B, FMNL2, GBP2, HCAR2, IFI16, IFI44, IFIH1, IFIT1B, IFIT2, IFIT3, IFNB1, IFRD1, IRF9, ITGA4, KYNU, LPL, MRC1, MTMR14, NAMPT, OAS1, OAS3, OASL, P2RY14, PARP14, PDGFC, PIM1, PLAC8, Retnla, RSAD2, RTP4, SLAMF8, TTC39B, XAF1
IFNB1	4.101		1.785	6.08E-17	CCL2, CCL5, Cd24a, CD274, CDKN1A, CMPK2, CXCL10, CXCL2, CXCL3, DAXX, DDX3Y, DDX58, GBP2, HMGCS1, ICOSLG/LOC102723996, IFI16, IFIH1, IFIT1B, IFIT2, IFIT3, IL10, IL18, IRF7, NOD1, NPTX1, PRDM1, RND3, RSAD2, SQLE, STARD4, STAT1, STAT2, THBS1, USP18

NFAT5	-0.063	Inhibited	-3.494	1.47E-12	CCR3, CD74, CIITA, Cxcl9, DAXX, HLA-DQA1, HLA-DQB1, HLA-DRB5, IFI16, IFIT1B, IFIT2, IFIT3, IFNB1, RSAD2, STAT1, TNFSF10
MYD88	-0.035	Activated	2.561	5.45E-09	CASP4, CCL5, CD200R1, CLEC10A, CMPK2, CXCL10, CXCL13, CXCL2, CXCL3, Cxcl9, EDNRB, FPR1, FPR2, IFIT1B, IFIT2, IFNB1, IL10, IL18, ITGAX, JAG1, MET, MMP14, MRC1, OASL, PILRA, RELB, RSAD2, SCARB1, TFEC, TSC22D1
LDLR	-1.479			7.7E-09	APOE, C1QA, CCL2, CCL5, Ccl7, CCR2, CCR3, CD274, CD36, CD4, CDKN1A, CX3CR1, FGL2, FPR1, FPR2, GAS6, IL10, IL12RB1, IRF7, ITGB3, LSP1, LYZ, MMP14, MMP2, MMP9, MSR1, NOD1, SCARB1, SCD, TAP1, TNFSF14
CSF1	-0.706		-1.501	1.09E-08	APOE, AXL, CAPN2, CCL2, Ccl7, CCR2, CD163, CD74, CDKN1A, CTSD, GAS7, GPNMB, GPR34, ICOSLG/LOC102723996, IL10, ITGA4, ITGAX, LPL, P2RY12, Retnla, SPARC, SPP1, TNFRSF11A
COP1	0.036	Inhibited	-2.744	1.19E-08	APOE, C3, CCL5, CEBPB, CXCL10, CXCL3, FPR1, FPR2, FTH1, GPNMB, IFI16, ITGAX
MEF2A	-0.066	Activated	3.512	1.31E-08	CXCL10, Cxcl9, GBP2, IFI44, IFIT1B, IFIT2, IFIT3, IFNB1, IRF7, NLRC5, NOD1, OAS1, RSAD2
QKI	-0.475		-0.905	2.66E-08	CD36, CLEC4M, CTSS, FYN, HIP1, HLA-DOA, HLA-DQA1, HLA-DQB1, ITGAX, SCD, TAP1
TICAM1	0.249		1.174	2.44E-07	CASP4, CCL5, CMPK2, CXCL10, CXCL13, CXCL2, CXCL3, EDNRB, FPR1, FPR2, ICOSLG/LOC102723996, IFIT1B, IFIT2, IFNB1, JAG1, MET, OASL, PILRA, RELB, RSAD2, TFEC, TSC22D1
NR1H3	-0.476		0.027	4.85E-07	APOE, C1QA, CCL2, CCL5, Ccl7, CCR2, CCR3, CD274, CD4, CDKN1A, CX3CR1, CXCL10, FGL2, FPR1, FPR2, GAS6, IL10, IL12RB1, IRF7, ITGAL, ITGB3, LSP1, LYZ, MMP9, NOD1, SCD, TAP1
IFNAR1	0.051	Activated	2.036	5.16E-07	CCL5, CIITA, CXCL10, EIF2AK2, HMGCS1, IFNB1, IL18, OAS1, OAS2, OAS3, RSAD2, SQLE, SREBF2
PPARG	0.094		0.515	1.28E-06	APOE, C3, CD36, CDK6, CXCL3, FZD1, HEBP1, IDH1, IFNB1, LPL, MCTP1, MMP9, PF4, PID1, RAB20, Retnla, RNF144B, SGK1, TNFSF10
IRF3	0.127	Activated	2.805	2.71E-06	CCL5, CXCL10, DDX58, IFIH1, IFIT1B, IFIT2, IFNB1, RSAD2
STING1	-0.118		1.117	6.57E-06	CCL5, CXCL10, CXCL2, Cxcl9, GAS7, IFI16, IFIT1B, IFNB1, IL10, IL33, OASL
MAP3K8	0.238		0	1.89E-05	ADORA3, BMP1, CCR2, CDK5R1, CIITA, CXCL2, DOK2, FSCN1, GAB1, GPR160, HIP1, IFNB1, IGF1R, IL10, PPARGC1B, RGS3, SESN1, SPATS2L, TSPAN33
TBK1	0.165		1.963	4.23E-05	CXCL10, IFI16, IFNB1, IRF7, RSAD2, USP18
IL4	-0.799	Inhibited	-2.442	5.07E-05	CD44, CHST3, CHST7, CIITA, CLEC10A, CXCL10, IGF1, IL10, LPL, MRC1, Retnla, TFRC, TNFRSF11A
NR3C1	-0.18	Inhibited	-2.804	7.03E-05	CCL5, CXCL10, Cxcl9, HCAR2, IFIT1B, IFIT2, IFNB1, OASL
STAT1	1.178	Activated	2.768	0.000155	C3, CCL5, CXCL10, Cxcl9, GBP2, IFIT1B, IFNB1, IGF1, IL18, PPARGC1B, PSME1

TNF	-0.246		0.443	0.000308	Acp5, CA2, CCL5, CD44, CSF1, CXCL10, CXCL13, CXCL2, CXCL3, Cxcl9, FPR1, GBP2, IL10, MMP9
TLR2	0.421		0.347	0.000418	CCL5, CXCL2, CXCL3, Cxcl9, CYBB, HLA-DQA1, HLA-DRB5, IFNB1, IL10, IL33, Retnla, SLC40A1, TSPAN33
TREM2	0.039		0.268	0.000543	AXL, CD36, CST7, CXCL2, ITGAX, LGALS1, LGALS3, LOX, LPL, SULF2
TGFBR2	-0.016		0.492	0.0007	CX3CR1, MRC1, MSR1, P2RY12, TIMD4
MAPKAPK2	0.12		-1.746	0.000939	CXCL2, CXCL3, IFNB1, IL10, MRC1, MSR1, Retnla
IRF1	0.3	Activated	2.138	0.000964	CCL5, CXCL16, GBP2, IFNB1, IL12RB1, IL12RB2, MMP9, PML, TLR3
TAZ	0.201		0.632	0.00101	ALDH1A2, CCL5, CD80, CXCL2, CXCL3, CXCR4, FN1, MRC1, ST6GAL1, THBS1
ITGB5	0.417			0.00136	IL10, MMP2, MMP9
TNFRSF1B	0.207			0.00136	ITGB5, MMP9, SRC
IRF9	0.406			0.00136	IFIT2, IFNB1, IL18
BACH1	-0.064		1.342	0.00143	CEBPB, IGF1, IL10, SLC40A1, SPP1
NLRP3	0.05			0.00188	CXCL2, IL18, MRC1, MSR1
RGS10	-0			0.00235	CCL2, Ccl7, CCR3, CXCL10, CXCL2, IL10, IL10RA, IL18, IL1R2, IL6ST, PF4, Retnla
NFE2L2	0.485		-0.954	0.00251	CCL5, CXCL10, CXCL2, CXCL3, IFNB1, SCARB1
ACE	-1.202		-1	0.0026	CCL2, CCL24, CCL5, CEBPB, Retnla
ITGB2	0.213		0	0.004	BCL2A1, CXCL10, CXCL2, CXCL3
CEBPE	-0.002		-1.214	0.004	Ccl7, CD14, IL10, IL18
MAPK7	0.048	Activated	2	0.004	CXCL10, Cxcl9, IFNB1, NOD1
TFEC	-1.592			0.00434	BBX, COL6A3, CSF3R, F13A1, IGF1R
PPP2CA	-0.133			0.005	Cxcl9, IFNB1, IRF7
ITGB8	0.669			0.005	APOE, ITGB5, P2RY12
CLEC4E	-0.225			0.005	CXCL2, CXCL3, IL10
IL13	-1.558			0.00676	IL10, MRC1, Retnla, TFRC, TNFRSF11A
RORA	-0.904	Inhibited	-2	0.00731	CXCL10, Cxcl9, IL18, TLR3
TLR3	0.524		0.937	0.00774	CCL5, CXCL10, CXCL2, CXCL3, IFNB1, TSPAN33
CDKN2A	1.756		1.897	0.00851	C3, CCL2, CCL24, CCL5, Ccl7, CXCL10, CXCL13, Cxcl9, IL1R2, IL2RG
NR1H2	0.078		0.092	0.0105	APOE, CCL5, Ccl7, CXCL10, ITGAL, MMP9
NFKB1	0.17		-0.294	0.0105	CSF2RA, CXCL3, IFNB1, IL10, Retnla, STAT1
MAVS	0.47			0.0115	CCL5, CXCL10, IFNB1
CX3CR1	-1.328		-0.577	0.012	CD14, CD36, IGF1, MSR1
MAPKAPK3	0.893	Inhibited	-2	0.012	CXCL2, CXCL3, IFNB1, IL10
TARDBP	0.04			0.0123	C1QA, C1QB
WNT5A	-0.144			0.0123	CD14, IFNB1
IL2	1.47			0.0123	Ly6a (includes others), PECAM1
TREX1	0			0.0123	IFI44, USP18
IL6	-0.024			0.0123	CD36, IFNB1
PLAU	-0.001		-0.378	0.0129	MMP12, OAS1, OAS3, PLK3, RELB, Retnla, SLC2A1
HIF1A	-0.032		-0.647	0.014	CCR2, CSF1, CXCL2, MMP2, SLC2A1, TFRC
TLR4	0.306		-0.557	0.018	CCL5, CD200R1, CDK6, CXCL10, CXCL2, CXCL3, HLA-DQA1, IFNB1, IL10, IL18, SCARB1, TSPAN33
CYBB	0.89		1	0.0183	CCL5, CXCL10, CXCL3, IFNB1

PPARD	0.286		0.776	0.0193	C1QA, C1QB, GAS6, MRC1, THBS1
BCL2L11	-0.182			0.0211	CD274, CD36, NOD1
IL1A	0.097			0.0211	Acp5, CA2, MMP9
TLR7	-0.17		-0.485	0.0256	BCL2A1, CXCL2, CXCL3, IFNB1, IL10
IRF8	0.198		1.457	0.0256	CCL5, CXCL16, DAB2, MMP9, PML
APOE	0.288			0.0256	CD36, CD80, IL10, TNFRSF14, TNFSF14
TLR9	0.346		0.391	0.0256	CCL5, CXCL2, IFNB1, IL10, RAB7B
HMOX1	-0.167		-1.067	0.0263	CXCL10, IL10, MRC1, TNFSF14
TIRAP	-0.282			0.0339	CXCL10, IFNB1, IL10
IRAK1	0.019			0.0339	IFNB1, IL10, RELB
STAT4	0.093			0.0342	DDX58, IFNB1
TRIM3	-0.02			0.0342	IFIT1B, IFNB1
SYK	0.24			0.0342	CXCL10, Cxcl9
TNFRSF1A	0.079			0.0342	ITGB5, SRC
FCGR2A	-0.01		-1	0.036	CXCL10, FCGR3A/FCGR3B, MARCKSL1, RASGRP1
BCL6	0.024		0.555	0.0417	Ccl7, CSF1, CXCL3, IL10, IL18
GATA6	-0.397		1.292	0.0466	CD163, CLEC10A, CXCL13, IL10, LYVE1, MRC1, SORBS3, STARD13
EIF4EBP1	-0.186		-1.091	0.0476	CCL5, CEBPB, CXCL10, IL10
EIF4EBP2	-0.195		-1.091	0.0476	CCL5, CEBPB, CXCL10, IL10
KDM6B	-0.056			0.0498	CCL5, ITGAL, OASL
MSR1	-1.004			0.0498	CCL5, CXCL10, IL10
IRF4	-0.238			0.0498	CIITA, CXCL3, IL10
TICAM2	-0.274			0.0498	ICOSLG/LOC102723996, IFNB1, MMP14
AXL	1.595			0.0498	IL10, IL18, Retnla
MERTK	0.134			0.0498	IL10, IL18, Retnla
NOS2	0.176			0.0498	Ccl7, CXCL2, CXCL3
CCR6	0.309			0.0498	CXCL10, IL10, MMP12

Appendix VII Upstream Regulator Analysis from IPA of edgeR analysis of Naïve Microglia

Appendix VIII

Ensembl Gene ID	External Gene Name	log_2 Fold Change	Adjusted P-Value
ENSMUSG00000055435	Maf	-7.426402313	6.65E-64
ENSMUSG00000005611	Mrvi1	-1.123015676	1.09E-12
ENSMUSG00000118423	Lrrc70	-1.258910251	3.29E-12
ENSMUSG00000068606	Gm4841	1.831703769	5.91E-11
ENSMUSG00000033278	Ptprm	-1.230865783	1.21E-08
ENSMUSG00000074677	Sirpb1c	1.169592823	2.76E-07
ENSMUSG00000045165	AI467606	-0.701885307	1.31E-06
ENSMUSG00000017754	Pltp	-0.844327381	1.31E-06
ENSMUSG00000042286	Stab1	-0.966480515	2.89E-06
ENSMUSG00000022180	Slc7a8	-0.946737166	3.51E-06
ENSMUSG00000010796	Asz1	-3.402471225	8.08E-06
ENSMUSG00000053062	Jam2	-0.708353018	9.84E-06
ENSMUSG00000036019	Tmtc2	-2.425587679	9.98E-06
ENSMUSG00000028976	Slc2a5	1.902440206	1.15E-05
ENSMUSG00000025330	Padi4	-0.802164284	1.50E-05
ENSMUSG00000090942	F830016B08Rik	1.030215438	1.70E-05
ENSMUSG00000010797	Wnt2	-0.564763014	2.31E-05
ENSMUSG00000044206	Vsig4	-0.643045389	6.31E-05
ENSMUSG00000039982	Dtx4	-0.941662963	0.000156
ENSMUSG00000029287	Tgfbr3	-0.9002809	0.000221
ENSMUSG00000073678	Pgap1	0.654243329	0.000265
ENSMUSG00000085977	Gm5970	0.924653545	0.000279
ENSMUSG00000090084	Srpx	-2.446454439	0.000295
ENSMUSG00000054072	Iigp1	1.391805291	0.000574
ENSMUSG00000055541	Lair1	0.745242311	0.000963
ENSMUSG00000039191	Rbpj	-0.542039511	0.000963
ENSMUSG00000039629	Strip2	0.912287529	0.001294
ENSMUSG00000035493	Tgfbi	-0.491384426	0.001294
ENSMUSG00000017670	Elmo2	-0.728749856	0.001708
ENSMUSG00000022623	Shank3	-0.81265396	0.001957
ENSMUSG00000013089	Etv5	-0.584789403	0.002137
ENSMUSG00000024772	Ehd1	-0.554981073	0.002772
ENSMUSG00000000682	Cd52	0.671849432	0.002772
ENSMUSG00000037894	H2az1	0.472194339	0.002772
ENSMUSG00000044827	Tlr1	0.768367617	0.003103
ENSMUSG00000043391	2510009E07Rik	-0.616358406	0.003103
ENSMUSG00000032289	Thsd4	-1.574852303	0.003202
ENSMUSG00000026825	Dnm1	-1.102782716	0.003503
ENSMUSG00000073555	Gm4951	0.688742354	0.004019
ENSMUSG00000073902	Gm1966	0.453531244	0.004205
ENSMUSG00000027692	Tnik	0.691162433	0.004742

ENSMUSG00000038843	Gcnt1	0.982962788	0.004742
ENSMUSG00000066026	Dhrs3	-0.520601964	0.004902
ENSMUSG00000059588	Calcrl	0.466421829	0.005188
ENSMUSG00000025150	Cbr2	-1.282052998	0.005313
ENSMUSG00000005373	Mlxipl	-0.632585323	0.007424
ENSMUSG00000092021	Gbp11	1.544471067	0.007424
ENSMUSG00000040855	Reps2	0.764974229	0.007424
ENSMUSG00000051177	Plcb1	-0.606944181	0.007664
ENSMUSG00000095609	Gm21188	-0.678495696	0.007664
ENSMUSG00000045092	S1pr1	-0.501176128	0.007664
ENSMUSG00000034647	Ankrd12	0.735240038	0.007827
ENSMUSG00000042364	Snx18	-0.55173536	0.007928
ENSMUSG00000036158	Prickle1	-0.893188493	0.008375
ENSMUSG00000032737	Inppl1	-0.543540457	0.009673
ENSMUSG00000047798	Cd300lf	1.175595856	0.009846
ENSMUSG00000031101	Sash3	-0.419720891	0.009873
ENSMUSG00000090307	1700071M16Rik	-1.039953361	0.009873
ENSMUSG00000059824	Dbp	3.953598454	0.010045
ENSMUSG00000114422	Gm30411	-1.98725382	0.010389
ENSMUSG00000014846	Tppp3	-0.770438133	0.011052
ENSMUSG00000022102	Dok2	-0.580491461	0.014023
ENSMUSG00000036381	P2ry14	0.58919914	0.015581
ENSMUSG00000028011	Tdo2	0.940370964	0.016006
ENSMUSG00000053007	Creb5	1.679075023	0.016992
ENSMUSG00000046410	Kcnk6	-0.546828024	0.016992
ENSMUSG00000071324	Armc2	-1.099454199	0.016992
ENSMUSG00000028957	Per3	2.302029117	0.016992
ENSMUSG00000051495	Irf2bp2	-0.432503217	0.016992
ENSMUSG00000049130	C5ar1	-0.507598793	0.01727
ENSMUSG00000068742	Cry2	1.188253694	0.017524
ENSMUSG00000055322	Tns1	-1.007238567	0.018452
ENSMUSG00000029108	Pcdh7	-2.016739282	0.018616
ENSMUSG00000114608	Gm36161	-0.86744831	0.021387
ENSMUSG00000060181	Slc35e3	-0.641534122	0.023837
ENSMUSG00000022270	Retreg1	-0.541423826	0.025702
ENSMUSG00000001761	Smo	-0.908365744	0.027068
ENSMUSG00000020604	Arsg	-0.40939459	0.027068
ENSMUSG00000021477	Ctsl	-0.430586477	0.02752
ENSMUSG00000000562	Adora3	1.160553006	0.02752
ENSMUSG00000030678	Maz	-0.399748613	0.027602
ENSMUSG00000062939	Stat4	-0.634376199	0.027732
ENSMUSG00000054626	Xlr	0.769055485	0.027732
ENSMUSG00000017493	Igfbp4	-0.67669579	0.027894
ENSMUSG00000029925	Tbxas1	-0.553329651	0.028567
ENSMUSG00000029833	Trim24	0.449396694	0.031652
ENSMUSG00000006235	Epor	1.200540877	0.037869

ENSMUSG00000013584	Aldh1a2	-0.808314419	0.039753
ENSMUSG00000034993	Vat1	-0.468680695	0.04234
ENSMUSG00000026991	Pkp4	-0.507917826	0.042851
ENSMUSG00000045664	Cdc42ep2	-0.694934376	0.043715
ENSMUSG00000103546	Gm37666	0.888606236	0.043921
ENSMUSG00000060147	Serpinb6a	-0.663457111	0.046571
ENSMUSG00000104955	1700016F12Rik	1.381641573	0.046571
ENSMUSG00000030208	Emp1	-0.643483398	0.048328
ENSMUSG00000059089	Fcgr4	0.570675671	0.048328
ENSMUSG00000002504	Slc9a3r2	-0.586044452	0.049775
ENSMUSG00000040430	Pitpnc1	-0.59877788	0.049785

Appendix VIII Differential Gene Discovories from DESeq2 analysis of Naïve Peritoneal Tissue Resident Macrophages

Appendix IX

Ensembl Gene ID	External Gene Name	log_2 Fold Change	Adjusted P-Value
ENSMUSG00000055435	Maf	-7.37272	6.88E-162
ENSMUSG00000005611	Mrvi1	-1.10789	2.21E-11
ENSMUSG00000118423	AC154328.1	-1.2442	1.39E-10
ENSMUSG00000068606	Gm4841	1.846217	2.29E-10
ENSMUSG00000033278	Ptprm	-1.21684	2.44E-08
ENSMUSG00000028957	Per3	2.31546	2.76E-07
ENSMUSG00000074677	Sirpb1c	1.183668	2.77E-07
ENSMUSG00000028976	Slc2a5	1.909862	4.51E-07
ENSMUSG00000059824	Dbp	3.963076	4.51E-07
ENSMUSG00000042286	Stab1	-0.95367	1.20E-06
ENSMUSG00000022180	Slc7a8	-0.93174	4.02E-06
ENSMUSG00000090942	F830016B08Rik	1.046331	1.07E-05
ENSMUSG00000022389	Tef	2.062098	1.21E-05
ENSMUSG00000045165	AI467606	-0.68644	1.96E-05
ENSMUSG00000017754	Pltp	-0.82917	7.84E-05
ENSMUSG00000053062	Jam2	-0.69272	7.96E-05
ENSMUSG00000029581	Fscn1	-1.67286	9.52E-05
ENSMUSG00000034438	Gbp8	2.455952	0.000144
ENSMUSG00000020889	Nr1d1	1.961019	0.00019
ENSMUSG00000114422	Gm30411	-1.95119	0.00019
ENSMUSG00000039982	Dtx4	-0.92577	0.00019
ENSMUSG00000021775	Nr1d2	1.384774	0.000208
ENSMUSG00000073678	Pgap1	0.670226	0.000306
ENSMUSG00000029287	Tgfbr3	-0.88508	0.000336
ENSMUSG00000085977	Gm5970	0.938701	0.000371
ENSMUSG00000044206	Vsig4	-0.62898	0.000395
ENSMUSG00000025150	Cbr2	-1.26423	0.000447
ENSMUSG00000055541	Lair1	0.759054	0.000557
ENSMUSG00000010797	Wnt2	-0.5496	0.000557
ENSMUSG00000044337	Ackr3	-1.47756	0.000576
ENSMUSG00000054072	Iigp1	1.406993	0.000848
ENSMUSG00000039629	Strip2	0.92762	0.001107
ENSMUSG00000092021	Gbp11	1.553418	0.001171
ENSMUSG00000000682	Cd52	0.686568	0.001349
ENSMUSG00000055866	Per2	2.999086	0.00138
ENSMUSG00000017670	Elmo2	-0.71323	0.001553
ENSMUSG00000073555	Gm4951	0.704906	0.001739
ENSMUSG00000030787	Lyve1	-3.13134	0.001793
ENSMUSG00000022623	Shank3	-0.79873	0.002195
ENSMUSG00000038843	Gcnt1	0.997234	0.002518
ENSMUSG00000040855	Reps2	0.778501	0.002919

ENSMUSG00000039191	Rbpj	-0.52764	0.003074
ENSMUSG00000044827	Tlr1	0.783189	0.003706
ENSMUSG00000027692	Tnik	0.706601	0.00378
ENSMUSG00000034647	Ankrd12	0.749189	0.004265
ENSMUSG00000026825	Dnm1	-1.08881	0.004464
ENSMUSG00000013089	Etv5	-0.56918	0.005646
ENSMUSG00000043391	2510009E07Rik	-0.60185	0.005921
ENSMUSG00000059588	Calcrl	0.482109	0.007367
ENSMUSG00000047798	Cd300lf	1.186447	0.008238
ENSMUSG00000036381	P2ry14	0.605354	0.009536
ENSMUSG00000095609	Gm21188	-0.66384	0.010345
ENSMUSG00000022114	Spry2	-1.08507	0.010661
ENSMUSG00000042364	Snx18	-0.53797	0.010661
ENSMUSG00000037894	H2afz	0.487735	0.011353
ENSMUSG00000051177	Plcb1	-0.59281	0.011739
ENSMUSG00000036158	Prickle1	-0.87934	0.013324
ENSMUSG00000006235	Epor	1.214314	0.013752
ENSMUSG00000014846	Tppp3	-0.75726	0.014738
ENSMUSG00000045092	S1pr1	-0.48662	0.015975
ENSMUSG00000028011	Tdo2	0.954173	0.01642
ENSMUSG00000032737	Inppl1	-0.52897	0.016458
ENSMUSG00000090307	1700071M16Rik	-1.02305	0.016734
ENSMUSG00000103546	Gm37666	0.900619	0.017221
ENSMUSG00000022102	Dok2	-0.56547	0.017647
ENSMUSG00000068742	Cry2	1.201916	0.024097
ENSMUSG00000049130	C5ar1	-0.49277	0.024097
ENSMUSG00000046410	Kcnk6	-0.5335	0.025446
ENSMUSG00000054626	Xlr	0.781688	0.027362
ENSMUSG00000001761	Smo	-0.89126	0.027614
ENSMUSG00000114608	Gm36161	-0.85325	0.027614
ENSMUSG00000005373	Mlxipl	-0.6182	0.030287
ENSMUSG00000060181	Slc35e3	-0.6277	0.030287
ENSMUSG00000017493	Igfbp4	-0.6593	0.032367
ENSMUSG00000029925	Tbxas1	-0.54048	0.032367
ENSMUSG00000073902	Gm1966	0.468492	0.032367
ENSMUSG00000031101	Sash3	-0.405	0.032367
ENSMUSG00000104955	1700016F12Rik	1.398217	0.032801
ENSMUSG00000059089	Fcgr4	0.584124	0.034708
ENSMUSG00000021728	Emb	0.619545	0.034708
ENSMUSG00000029833	Trim24	0.464666	0.040344
ENSMUSG00000024772	Ehd1	-0.54115	0.042671
ENSMUSG00000025511	Tspan4	0.651128	0.043071
ENSMUSG00000025330	Padi4	-0.78697	0.043933
ENSMUSG00000013584	Aldh1a2	-0.79294	0.044294
ENSMUSG00000060147	Serpinb6a	-0.65091	0.044367
ENSMUSG00000020644	Id2	0.507392	0.045572

ENSMUSG00000087838	Gm23954	0.980282	0.046014
ENSMUSG00000073739	Gm16287	-0.85495	0.046014
ENSMUSG00000062939	Stat4	-0.61973	0.046906
ENSMUSG00000002504	Slc9a3r2	-0.57145	0.048226
ENSMUSG00000022203	Efs	0.735155	0.048752
ENSMUSG00000118361	Gm50237	1.180057	0.048752
ENSMUSG00000055116	Arntl	-1.55356	0.048991
ENSMUSG00000021477	Ctsl	-0.41632	0.049037

Appendix IX Differential Gene Discovories from edgeR analysis of Naïve Peritoneal Tissue Resident Macrophages

Appendix X

Ensembl Gene ID	External Gene Name	log_2 Fold Change	Adjusted P-Value
ENSMUSG00000055435	Maf	-7.369870462	1.85E-166
ENSMUSG00000033278	Ptprm	-1.23088438	3.83E-14
ENSMUSG00000118423	AC154328.1	-1.240711283	1.57E-12
ENSMUSG00000005611	Mrvi1	-1.112107421	1.68E-12
ENSMUSG00000068606	Gm4841	1.874784981	3.63E-12
ENSMUSG00000042286	Stab1	-0.950850121	1.33E-08
ENSMUSG00000074677	Sirpb1c	1.182273887	1.33E-08
ENSMUSG00000022180	Slc7a8	-0.952214261	6.59E-08
ENSMUSG00000028957	Per3	2.105212578	1.22E-07
ENSMUSG00000028976	Slc2a5	1.876163484	3.81E-07
ENSMUSG00000017754	Pltp	-0.817650332	7.12E-07
ENSMUSG00000090942	F830016B08Rik	1.036053047	1.33E-06
ENSMUSG00000045165	AI467606	-0.684337928	2.82E-06
ENSMUSG00000073555	Gm4951	0.716373781	4.58E-06
ENSMUSG00000055116	Arntl	-1.947398352	6.32E-06
ENSMUSG00000053062	Jam2	-0.693354207	3.33E-05
ENSMUSG00000017670	Elmo2	-0.743179174	3.33E-05
ENSMUSG00000044206	Vsig4	-0.634534689	3.33E-05
ENSMUSG00000026825	Dnm1	-1.123607167	4.81E-05
ENSMUSG00000025330	Padi4	-0.801124856	4.81E-05
ENSMUSG00000020889	Nr1d1	1.689181997	8.13E-05
ENSMUSG00000022389	Tef	1.855810305	0.000103364
ENSMUSG00000114422	Gm30411	-2.010685427	0.000148872
ENSMUSG00000039982	Dtx4	-0.93203039	0.00015103
ENSMUSG00000010797	Wnt2	-0.550474352	0.000151073
ENSMUSG00000073678	Pgap1	0.665760466	0.000151073
ENSMUSG00000034438	Gbp8	2.600804297	0.000177967
ENSMUSG00000029287	Tgfbr3	-0.880144445	0.000228412
ENSMUSG00000085977	Gm5970	0.937225372	0.000233055
ENSMUSG00000059824	Dbp	3.613227755	0.000233055
ENSMUSG00000021775	Nr1d2	1.267594608	0.000277959
ENSMUSG00000038843	Gcnt1	1.037925714	0.000314157
ENSMUSG00000021728	Emb	0.600833315	0.000314157
ENSMUSG00000030787	Lyve1	-3.243814551	0.00034272
ENSMUSG00000036381	P2ry14	0.603331	0.000348129
ENSMUSG00000055541	Lair1	0.759568273	0.000358145
ENSMUSG00000054072	Iigp1	1.446053065	0.000407727
ENSMUSG00000029581	Fscn1	-1.598940334	0.000420217
ENSMUSG00000042364	Snx18	-0.534349253	0.000517883
ENSMUSG00000025150	Cbr2	-1.26466004	0.000517883
ENSMUSG00000040855	Reps2	0.76523558	0.000533142

ENSMUSG00000039191	Rbpj	-0.531660433	0.000790776
ENSMUSG00000039629	Strip2	0.924681155	0.000790776
ENSMUSG00000034647	Ankrd12	0.720501469	0.000790776
ENSMUSG00000000682	Cd52	0.682989734	0.000818475
ENSMUSG00000051177	Plcb1	-0.593507802	0.000893246
ENSMUSG00000092021	Gbp11	1.487942698	0.000893246
ENSMUSG00000044827	Tlr1	0.785792224	0.001153859
ENSMUSG00000059588	Calcrl	0.485818764	0.001357685
ENSMUSG00000043391	2510009E07Rik	-0.590567401	0.001397225
ENSMUSG00000005373	Mlxipl	-0.595910672	0.001451937
ENSMUSG00000044337	Ackr3	-1.404017846	0.001641303
ENSMUSG00000037894	H2afz	0.48570149	0.002001984
ENSMUSG00000022623	Shank3	-0.801348816	0.002014198
ENSMUSG00000019987	Arg1	-1.42893867	0.002458582
ENSMUSG00000045092	S1pr1	-0.49377803	0.002811837
ENSMUSG00000013089	Etv5	-0.570360699	0.00283338
ENSMUSG00000047798	Cd300lf	1.13098115	0.003020231
ENSMUSG00000002504	Slc9a3r2	-0.570548014	0.003093633
ENSMUSG00000027692	Tnik	0.705567784	0.003170836
ENSMUSG00000045502	Hcar2	0.674952639	0.003378527
ENSMUSG00000024772	Ehd1	-0.547621278	0.003512125
ENSMUSG00000095609	Gm21188	-0.667045042	0.00395578
ENSMUSG00000064373	Selenop	-0.512140967	0.004204782
ENSMUSG00000030707	Coro1a	0.627468901	0.004261819
ENSMUSG00000040026	Saa3	-0.908308947	0.00428114
ENSMUSG00000032737	Inppl1	-0.532789424	0.00428114
ENSMUSG00000019564	Arid3a	-0.621987029	0.00440237
ENSMUSG00000073902	Gm1966	0.470771231	0.005393225
ENSMUSG00000049130	C5ar1	-0.500461059	0.005696152
ENSMUSG00000024501	Dpysl3	-0.510429406	0.005864191
ENSMUSG00000104955	1700016F12Rik	1.358071053	0.006558432
ENSMUSG00000035273	Hpse	-0.510025544	0.007302912
ENSMUSG00000106951	5930430L01Rik	0.880630748	0.007504979
ENSMUSG00000035493	Tgfbi	-0.479377814	0.007580396
ENSMUSG00000029925	Tbxas1	-0.523852263	0.008612483
ENSMUSG00000023992	Trem2	-0.69175229	0.00897867
ENSMUSG00000000248	Clec2g	-1.919979363	0.009923236
ENSMUSG00000046410	Kcnk6	-0.528372178	0.01009136
ENSMUSG00000103546	Gm37666	0.915568195	0.010411223
ENSMUSG00000027360	Hdc	0.427934045	0.010609867
ENSMUSG00000034993	Vat1	-0.45809161	0.010609867
ENSMUSG00000022114	Spry2	-1.074272116	0.010671951
ENSMUSG00000014846	Tppp3	-0.757590915	0.010896683
ENSMUSG00000060181	Slc35e3	-0.631697899	0.011799946
ENSMUSG00000090307	1700071M16Rik	-0.997034876	0.012372942
ENSMUSG00000022899	Slc15a2	3.65010743	0.012372942

ENSMUSG00000022102	Dok2	-0.565260856	0.012372942
ENSMUSG00000066026	Dhrs3	-0.495281335	0.01270598
ENSMUSG00000054626	Xlr	0.789998833	0.013019742
ENSMUSG00000035954	Dock4	0.477812074	0.013134538
ENSMUSG00000028011	Tdo2	0.970259298	0.013134538
ENSMUSG00000006235	Epor	1.201820558	0.013134538
ENSMUSG00000036158	Prickle1	-0.852957247	0.013206923
ENSMUSG00000068742	Cry2	1.069544028	0.013660887
ENSMUSG00000051495	Irf2bp2	-0.42165781	0.013660887
ENSMUSG00000013584	Aldh1a2	-0.792116579	0.013660887
ENSMUSG00000025511	Tspan4	0.612949759	0.014108513
ENSMUSG00000017493	Igfbp4	-0.676069629	0.014122757
ENSMUSG00000001761	Smo	-0.912374171	0.014176778
ENSMUSG00000031101	Sash3	-0.40540398	0.015107168
ENSMUSG00000024140	Epas1	-0.500651167	0.015107168
ENSMUSG00000060147	Serpinb6a	-0.654987806	0.016626984
ENSMUSG00000028480	Glipr2	-0.619501637	0.016693894
ENSMUSG00000087150	BC064078	-0.861291009	0.016693894
ENSMUSG00000026991	Pkp4	-0.498276529	0.018080321
ENSMUSG00000020644	Id2	0.512847812	0.019147532
ENSMUSG00000008845	Cd163	-0.884300566	0.019147532
ENSMUSG00000059089	Fcgr4	0.592705232	0.019488357
ENSMUSG00000114608	Gm36161	-0.853926578	0.020392499
ENSMUSG00000029833	Trim24	0.462998478	0.021845661
ENSMUSG00000035441	Myo1d	0.495572078	0.022894586
ENSMUSG00000026581	Sell	0.653125088	0.025206528
ENSMUSG00000038807	Rap1gap2	-0.418410068	0.026522799
ENSMUSG00000040564	Apoc1	0.688683719	0.027021421
ENSMUSG00000021477	Ctsl	-0.417079879	0.027506304
ENSMUSG00000042616	Oscp1	0.483657047	0.02774176
ENSMUSG00000087838	Gm23954	0.962058559	0.02774176
ENSMUSG00000020377	Ltc4s	-0.43937308	0.02774176
ENSMUSG00000034764	1700006J14Rik	0.736893419	0.02774176
ENSMUSG00000060568	Fam78b	-0.451579558	0.029220001
ENSMUSG00000022203	Efs	0.739579152	0.029220001
ENSMUSG00000032691	Nlrp3	-0.699546252	0.029220001
ENSMUSG00000045664	Cdc42ep2	-0.694993608	0.029260052
ENSMUSG00000016382	Pls3	0.601244419	0.029260052
ENSMUSG00000098973	Mir6236	-0.930939224	0.029309152
ENSMUSG00000086150	Bach2os	-1.002011806	0.029309152
ENSMUSG00000034265	Zdhhc14	-0.516843101	0.030016464
ENSMUSG00000062939	Stat4	-0.614601143	0.030636639
ENSMUSG00000030208	Emp1	-0.633326068	0.03474505
ENSMUSG00000087805	Gm27926	-4.813774961	0.034753412
ENSMUSG00000027712	Anxa5	-0.647687587	0.035663103
ENSMUSG00000046562	Unc119b	-0.441125298	0.036746718

ENSMUSG00000030678	Maz	-0.383810828	0.037159137
ENSMUSG00000020604	Arsg	-0.394207649	0.037597356
ENSMUSG00000073739	Gm16287	-0.856098118	0.037597356
ENSMUSG00000020212	Mdm1	-0.605960305	0.037597356
ENSMUSG00000035891	Cerk	-0.496315832	0.04089649
ENSMUSG00000089417	Gm22009	0.416881533	0.04089649
ENSMUSG00000022220	Adcy4	0.580437962	0.041348562
ENSMUSG00000056749	Nfil3	-0.856019686	0.041668498
ENSMUSG00000022270	Retreg1	-0.526656547	0.041786288
ENSMUSG00000042487	Leo1	-0.801793843	0.042204996
ENSMUSG00000055866	Per2	2.857613646	0.042204996
ENSMUSG00000030257	Srgap3	-0.439819663	0.04262507
ENSMUSG00000039735	Fnbp1l	0.537815003	0.043024389
ENSMUSG00000118361	Gm50237	1.123104646	0.045987532
ENSMUSG00000021879	Dnah12	-0.445944105	0.04999822

Appendix X Differential Gene Discovories from edgeR analysis when sex is included in the matrix of Naïve Peritoneal Tissue Resident Macrophages

Appendix XI

Ensembl Gene ID	External Gene Name	log_2 Fold Change	Adjusted P-Value
ENSMUSG00000055435	Maf	-7.565943543	2.20E-16
ENSMUSG00000033278	Ptprm	-1.245455995	3.78E-13
ENSMUSG00000068606	Gm4841	1.858963876	5.13E-12
ENSMUSG00000005611	Mrvi1	-1.127668193	5.13E-12
ENSMUSG00000118423	Lrrc70	-1.255695126	1.33E-11
ENSMUSG00000025330	Padi4	-0.816346183	2.47E-08
ENSMUSG00000042286	Stab1	-0.964231488	2.47E-08
ENSMUSG00000017754	Pltp	-0.831732855	7.85E-08
ENSMUSG00000022180	Slc7a8	-0.966918089	1.18E-07
ENSMUSG00000074677	Sirpb1c	1.168612472	1.18E-07
ENSMUSG00000045165	AI467606	-0.700227574	1.16E-06
ENSMUSG00000090942	F830016B08Rik	1.019832418	9.08E-06
ENSMUSG00000073555	Gm4951	0.701227434	1.63E-05
ENSMUSG00000044206	Vsig4	-0.648899397	1.83E-05
ENSMUSG00000017670	Elmo2	-0.758104077	3.58E-05
ENSMUSG00000010796	Asz1	-3.414962446	3.58E-05
ENSMUSG00000036019	Tmtc2	-2.521284585	3.58E-05
ENSMUSG00000026825	Dnm1	-1.137469459	3.61E-05
ENSMUSG00000053062	Jam2	-0.708960086	4.97E-05
ENSMUSG00000010797	Wnt2	-0.565712285	5.35E-05
ENSMUSG00000028976	Slc2a5	1.868403375	9.00E-05
ENSMUSG00000090084	Srpx	-2.514195259	0.000132542
ENSMUSG00000039982	Dtx4	-0.948796832	0.000206403
ENSMUSG00000073678	Pgap1	0.650153774	0.000480812
ENSMUSG00000005373	Mlxipl	-0.611839014	0.000480812
ENSMUSG00000038843	Gcnt1	1.025519772	0.000589301
ENSMUSG00000042364	Snx18	-0.548723273	0.000686681
ENSMUSG00000029287	Tgfbr3	-0.894707135	0.000722855
ENSMUSG00000039191	Rbpj	-0.546528104	0.000736932
ENSMUSG00000064373	Selenop	-0.526182922	0.000974427
ENSMUSG00000035493	Tgfbi	-0.494636213	0.001011195
ENSMUSG00000024772	Ehd1	-0.561974942	0.001011195
ENSMUSG00000036381	P2ry14	0.587691822	0.001011195
ENSMUSG00000021728	Emb	0.586443654	0.001423126
ENSMUSG00000043391	2510009E07Rik	-0.606045404	0.001423126
ENSMUSG00000085977	Gm5970	0.922767239	0.001607052
ENSMUSG00000051177	Plcb1	-0.608018937	0.001702909
ENSMUSG00000066026	Dhrs3	-0.510621918	0.001776729
ENSMUSG00000055541	Lair1	0.745744889	0.001840098
ENSMUSG00000034647	Ankrd12	0.705857264	0.002703331
ENSMUSG00000045092	S1pr1	-0.508666863	0.002799297

ENSMUSG00000040855	Reps2	0.75138598	0.002871755
ENSMUSG00000037894	H2az1	0.470235438	0.002895723
ENSMUSG00000039629	Strip2	0.908813524	0.003026445
ENSMUSG00000059588	Calcrl	0.470728727	0.0031681
ENSMUSG00000000682	Cd52	0.667784473	0.003520086
ENSMUSG00000013089	Etv5	-0.585910819	0.004399705
ENSMUSG00000027692	Tnik	0.689225396	0.004484839
ENSMUSG00000073902	Gm1966	0.455341482	0.004489729
ENSMUSG00000002504	Slc9a3r2	-0.584595972	0.004489729
ENSMUSG00000024501	Dpysl3	-0.525400265	0.005215317
ENSMUSG00000049130	C5ar1	-0.51543656	0.005215317
ENSMUSG00000051495	Irf2bp2	-0.436408644	0.005215317
ENSMUSG00000032289	Thsd4	-1.543335639	0.005926159
ENSMUSG00000044827	Tlr1	0.770727733	0.006245383
ENSMUSG00000095609	Gm21188	-0.681758114	0.007339838
ENSMUSG00000032737	Inppl1	-0.547464194	0.009547659
ENSMUSG00000047798	Cd300lf	1.118551626	0.009726944
ENSMUSG00000035273	Hpse	-0.524402218	0.009956146
ENSMUSG00000029925	Tbxas1	-0.537905241	0.009999036
ENSMUSG00000090307	1700071M16Rik	-1.015622499	0.010697424
ENSMUSG00000019564	Arid3a	-0.637644912	0.012269513
ENSMUSG00000036158	Prickle1	-0.868900354	0.012269513
ENSMUSG00000030707	Coro1a	0.612458237	0.012670393
ENSMUSG00000045502	Hcar2	0.661250971	0.013642282
ENSMUSG00000022102	Dok2	-0.579606764	0.014677371
ENSMUSG00000068742	Cry2	1.05472135	0.015075074
ENSMUSG00000028011	Tdo2	0.954255318	0.01631954
ENSMUSG00000014846	Tppp3	-0.771005718	0.01631954
ENSMUSG00000046410	Kcnk6	-0.542255532	0.01631954
ENSMUSG00000114422	Gm30411	-2.076691564	0.01688071
ENSMUSG00000031101	Sash3	-0.420083537	0.01688071
ENSMUSG00000034993	Vat1	-0.472586525	0.01688071
ENSMUSG00000017493	Igfbp4	-0.6926761	0.01688071
ENSMUSG00000071324	Armc2	-1.069131817	0.01688071
ENSMUSG00000055322	Tns1	-1.02629456	0.01688071
ENSMUSG00000013584	Aldh1a2	-0.808199752	0.017568047
ENSMUSG00000092021	Gbp11	1.47416081	0.018810536
ENSMUSG00000024140	Epas1	-0.514574113	0.020021127
ENSMUSG00000025150	Cbr2	-1.282849548	0.020427856
ENSMUSG00000060147	Serpinb6a	-0.667608928	0.020429762
ENSMUSG00000023992	Trem2	-0.708073638	0.021226224
ENSMUSG00000027360	Hdc	0.413132765	0.021700077
ENSMUSG00000060181	Slc35e3	-0.645651293	0.025200294
ENSMUSG00000038807	Rap1gap2	-0.432821007	0.025200294
ENSMUSG00000025511	Tspan4	0.59756429	0.026116969
ENSMUSG00000104955	1700016F12Rik	1.340413337	0.026116969

ENSMUSG00000028957	Per3	2.08941888	0.026838623
ENSMUSG00000053007	Creb5	1.725390686	0.027082087
ENSMUSG00000114608	Gm36161	-0.86734007	0.03051028
ENSMUSG00000021477	Ctsl	-0.431344161	0.031282264
ENSMUSG00000020377	Ltc4s	-0.453616129	0.032428783
ENSMUSG00000028480	Glipr2	-0.634409503	0.033983933
ENSMUSG00000023913	Pla2g7	-0.438437165	0.037121124
ENSMUSG00000035891	Cerk	-0.511205697	0.037121124
ENSMUSG00000020604	Arsg	-0.409510958	0.038801697
ENSMUSG00000026991	Pkp4	-0.513052907	0.038832927
ENSMUSG00000026581	Sell	0.63773065	0.038832927
ENSMUSG00000001761	Smo	-0.93031205	0.039047339
ENSMUSG00000030678	Maz	-0.399259281	0.03920088
ENSMUSG00000017466	Timp2	-0.406066367	0.03931556
ENSMUSG00000040564	Apoc1	0.671786222	0.039817888
ENSMUSG00000035954	Dock4	0.46260914	0.040694408
ENSMUSG00000020644	Id2	0.499258023	0.043778349
ENSMUSG00000052681	Rap1b	-0.370354599	0.045330578
ENSMUSG00000045664	Cdc42ep2	-0.709536323	0.045375541
ENSMUSG00000046562	Unc119b	-0.455990041	0.048379503
ENSMUSG00000059089	Fcgr4	0.578054839	0.048379503
ENSMUSG00000060568	Fam78b	-0.46587915	0.049189887

Appendix XI Differential Gene Discovories from DESeq2 analysis when sex is included in the matrix of Naïve Peritoneal Tissue Resident Macrophages

Appendix XII

Ensembl Gene ID	External Gene Name	log_2 Fold Change	Adjusted P-Value
ENSMUSG00000055435	Maf	-13.87776009	2.20E-25
ENSMUSG00000072294	Klf12	-7.645240139	0.000108649
ENSMUSG00000029287	Tgfbr3	-1.361706449	0.00510816
ENSMUSG00000092415	Gm20513	5.039129868	0.00510816
ENSMUSG00000021217	Tshz3	-3.694589561	0.020708627

Appendix XII Differential Gene Discovories from DESeq2 analysis in Zymosan treated Peritoneal Tissue Resident Macrophages

Appendix XIII

Ensembl Gene ID	External Gene Name	log_2 Fold Change	Adjusted P-Value
ENSMUSG00000055435	Maf	-12.80410169	1.71E-11
ENSMUSG00000029287	Tgfbr3	-1.324553129	2.97E-07
ENSMUSG00000033278	Ptprm	-1.27645555	3.67E-05
ENSMUSG00000029581	Fscn1	-1.988240536	0.000639353
ENSMUSG00000044206	Vsig4	-1.303300805	0.001745728
ENSMUSG00000010796	Asz1	-3.315810942	0.007078151
ENSMUSG00000036377	C530008M17Rik	-1.06008814	0.011506666
ENSMUSG00000029162	Khk	0.618562206	0.011506666
ENSMUSG00000073409	H2-Q6	1.00524329	0.014640539
ENSMUSG00000015243	Abca1	-0.561707007	0.021074231
ENSMUSG00000072294	Klf12	-6.568264877	0.031736768
ENSMUSG00000024770	Lipn	-1.192715431	0.031736768
ENSMUSG00000022938	Fam3b	1.085818596	0.031934238
ENSMUSG00000031548	Sfrp1	-1.578214675	0.043634413
ENSMUSG00000067219	Nipal1	-1.945154732	0.051618928

Appendix XIII Differential Gene Discovories from edgeR analysis in Zymosan treated Peritoneal Tissue Resident Macrophages

Appendix XIV

Ensembl Gene ID	External Gene Name	log_2 Fold Change	Adjusted P-Value
ENSMUSG00000055435	Maf	-5.055307032	3.68E-07
ENSMUSG00000026825	Dnm1	-2.676150933	5.83E-06
ENSMUSG00000002504	Slc9a3r2	-1.409906254	2.17E-05
ENSMUSG00000026938	Fcna	-2.406665917	2.17E-05
ENSMUSG00000002980	Bcam	-1.472767121	0.000335434
ENSMUSG00000005611	Mrvi1	-1.607609904	0.00055498
ENSMUSG00000091971	Hspa1a	-2.91352396	0.000765895
ENSMUSG00000090877	Hspa1b	-2.686523779	0.00113188
ENSMUSG00000030208	Emp1	-1.640407064	0.002411463
ENSMUSG00000030465	Psd3	-1.281035643	0.002530819
ENSMUSG00000042286	Stab1	-1.652378077	0.002839308
ENSMUSG00000004814	Ccl24	-2.089450473	0.002839308
ENSMUSG00000103747	Gm38236	1.344216664	0.003226258
ENSMUSG00000015854	Cd5l	-1.80524005	0.003258469
ENSMUSG00000022957	Itsn1	-1.294583853	0.004396999
ENSMUSG00000040722	Scamp5	-1.506085599	0.004702463
ENSMUSG00000020773	Trim47	-1.438030005	0.005101941
ENSMUSG00000030787	Lyve1	-5.474388099	0.005101941
ENSMUSG00000045092	S1pr1	-2.139760421	0.005101941
ENSMUSG00000019944	Rhobtb1	-0.961415115	0.005101941
ENSMUSG00000037095	Lrg1	-1.368257356	0.006549532
ENSMUSG00000006445	Epha2	-1.694236854	0.007494188
ENSMUSG00000030409	Dmpk	-2.10636995	0.007494188
ENSMUSG00000050777	Tmem37	-1.111747866	0.007494188
ENSMUSG00000019539	Rcn3	-1.995861088	0.013063324
ENSMUSG00000024501	Dpysl3	-1.591197892	0.017089602
ENSMUSG00000031451	Gas6	-3.493972174	0.017089602
ENSMUSG00000103233	Gm37159	1.220685793	0.018992304
ENSMUSG00000029084	Cd38	-1.269685559	0.018992304
ENSMUSG00000010047	Hyal2	-1.002550868	0.019672846
ENSMUSG00000074677	Sirpb1c	1.294949373	0.019672846
ENSMUSG00000022353	Mtss1	-0.773644282	0.020400955
ENSMUSG00000015243	Abca1	-1.16781783	0.022056534
ENSMUSG00000022091	Sorbs3	-1.853642842	0.022376239
ENSMUSG00000014453	Blk	-1.652543876	0.023884118
ENSMUSG00000016024	Lbp	-1.238924836	0.024029674
ENSMUSG00000089542	Gm25835	-1.204239238	0.024029674
ENSMUSG00000024206	Rfx2	-2.066462244	0.024029674
ENSMUSG00000085247	4930545L23Rik	1.271569542	0.027368908
ENSMUSG00000019139	Isyna1	-1.000556948	0.027483154
ENSMUSG00000017493	Igfbp4	-1.248010041	0.031886321

ENSMUSG00000063415	Cyp26b1	-2.870449113	0.031886321
ENSMUSG00000035373	Ccl7	-3.510189479	0.032468666
ENSMUSG00000000204	Slfn4	-0.691374946	0.036343588
ENSMUSG00000104888	1500005C15Rik	1.273954145	0.036343588
ENSMUSG00000055322	Tns1	-1.583932924	0.036343588
ENSMUSG00000003746	Man1a	-0.60282251	0.037753723
ENSMUSG00000036887	C1qa	-0.70532717	0.037753723
ENSMUSG00000028121	Bcar3	-1.458402226	0.037753723
ENSMUSG00000053559	Smagp	-0.857962866	0.040688039
ENSMUSG00000017466	Timp2	-0.977682149	0.042461119
ENSMUSG00000079293	Clec7a	1.012727153	0.042807893
ENSMUSG00000086804	Gm43154	-6.224344927	NA
ENSMUSG00000036896	C1qc	-0.728497707	0.044714928
ENSMUSG00000046546	Fam43a	-0.846688591	0.044714928
ENSMUSG00000103546	Gm37666	1.082311419	0.044714928
ENSMUSG00000118339	4930592I03Rik	1.352955878	0.046033482
ENSMUSG00000055980	Irs1	-6.43810362	0.048117073
ENSMUSG00000003420	Fcgrt	-0.895772524	0.048117073
ENSMUSG00000034751	Mast4	1.255731174	0.048117073
ENSMUSG00000098851	Mir6353	1.412376772	0.048117073
ENSMUSG00000044162	Tnip3	0.968633001	0.048117073
ENSMUSG00000039943	Plcb4	-2.648275846	0.048117073
ENSMUSG00000040430	Pitpnc1	-0.692747821	0.048117073
ENSMUSG00000032246	Calml4	-1.168174116	0.049961786
ENSMUSG00000099241	Gm18852	1.186896373	0.049961786
ENSMUSG00000020823	Sec14l1	-0.586499783	0.049961786

Appendix XIV Differential Gene Discovories from DESeq2 analysis in Zymosan-recruited Inflammatory Macrophages

Appendix XV

Ensembl Gene ID	External Gene Name	log_2 Fold Change	Adjusted P-Value
ENSMUSG00000055435	Maf	-5.066407597	1.08E-09
ENSMUSG00000026825	Dnm1	-2.688058566	2.52E-06
ENSMUSG00000002504	Slc9a3r2	-1.426201263	1.99E-05
ENSMUSG00000026938	Fcna	-2.420735972	0.000550232
ENSMUSG00000030465	Psd3	-1.297447916	0.001871472
ENSMUSG00000022957	Itsn1	-1.310296128	0.002558529
ENSMUSG00000015854	Cd5l	-1.820544649	0.002737743
ENSMUSG00000030787	Lyve1	-5.459642967	0.002737743
ENSMUSG00000045092	S1pr1	-2.156443635	0.002737743
ENSMUSG00000002980	Bcam	-1.490085229	0.004196835
ENSMUSG00000020773	Trim47	-1.454348767	0.004359588
ENSMUSG00000086804	Gm43154	-6.952301088	0.004359588
ENSMUSG00000063415	Cyp26b1	-2.872980546	0.004972049
ENSMUSG00000030208	Emp1	-1.654308559	0.004972049
ENSMUSG00000030409	Dmpk	-2.122983943	0.005171314
ENSMUSG00000091971	Hspa1a	-2.93098728	0.00808136
ENSMUSG00000040722	Scamp5	-1.520459022	0.008999087
ENSMUSG00000006445	Epha2	-1.710406583	0.008999087
ENSMUSG00000042286	Stab1	-1.666519411	0.008999087
ENSMUSG00000090877	Hspa1b	-2.705041361	0.009307218
ENSMUSG00000005611	Mrvi1	-1.622256367	0.01008902
ENSMUSG00000081164	Gm8722	3.648635604	0.01008902
ENSMUSG00000004814	Ccl24	-2.105905531	0.01008902
ENSMUSG00000074677	Sirpb1c	1.279996785	0.013979921
ENSMUSG00000022091	Sorbs3	-1.870120482	0.017484452
ENSMUSG00000055980	Irs1	-7.174493835	0.020296654
ENSMUSG00000015243	Abca1	-1.183921901	0.020296654
ENSMUSG00000025150	Cbr2	-2.602031381	0.022208351
ENSMUSG00000057457	Phex	4.47970828	0.022499481
ENSMUSG00000032725	Folr2	-3.314443895	0.022499481
ENSMUSG00000017466	Timp2	-0.99469408	0.024865988
ENSMUSG00000027209	Fam227b	2.93843106	0.027788586
ENSMUSG00000029084	Cd38	-1.283228483	0.029565801
ENSMUSG00000022132	Cldn10	-2.287653096	0.03172976
ENSMUSG00000074115	Saa1	-4.112970292	0.036194473
ENSMUSG00000048138	Dmrt2	-5.906801965	0.036194473
ENSMUSG00000039943	Plcb4	-2.661637443	0.036251372
ENSMUSG00000065573	Mir350	2.31519616	0.036251372
ENSMUSG00000019944	Rhobtb1	-0.977964651	0.036251372
ENSMUSG00000017493	Igfbp4	-1.262072911	0.038916212
ENSMUSG00000034487	Poglut3	-1.445490177	0.040705953

ENSMUSG00000016024	Lbp	-1.25365261	0.040705953
ENSMUSG00000037095	Lrg1	-1.383078488	0.043939828
ENSMUSG00000026482	Rgl1	-1.17535186	0.049495557
ENSMUSG00000023931	Efhb	-5.83776009	0.049495557

Appendix XV Differential Gene Discovories from edgeR analysis in Zymosan-recruited Inflammatory Macrophages